Fakultät für Chemie

Fachgebiet Molekulare Katalyse

Synthesis and Characterisation of *N*-Heterocyclic Carbene Complexes of Rare Earth and Coinage Metals

Julia Rieb

Vollständiger Abdruck der von der Fakultät für Chemie der Technischen Universität München zur Erlangung des akademischen Grades eines Doktors der Naturwissenschaften genehmigten Dissertation.

Vorsitzende(r): Prof. Dr.-Ing. Kai-Olaf Hinrichsen

Prüfende/-r der Dissertation:

1. Prof. Dr. Fritz E. Kühn

2. Prof. Polly L. Arnold, Ph. D.

Die Dissertation wurde am 08.02.2017 bei der Technischen Universität München eingereicht und durch die Fakultät für Chemie am 10.03.2017 angenommen.

„Inmitten der Schwierigkeiten liegt die Möglichkeit.“

Albert Einstein

Acknowledgements

This thesis would not have been possible without the support of many people.

First of all, I would like to express my greatest gratitude to **Prof. Dr. F. E. Kühn** and **Prof. Dr. Polly L. Arnold** for giving me the opportunity to pursue interesting projects. I am grateful for their advice, continuous support and invaluable scientific input. My special thank goes to **Prof. Dr. Polly L. Arnold** and **Prof. Dr. Jason Love** for welcoming me in their lab in Edinburgh.

Furthermore, I am very grateful to **Dr. Alexander Pöthig** for his scientific support in the seminars and for recording and solving of some of the crystal structures. Moreover, I would like to sincerely thank **Christian Jandl** for recording and solving of the crystal structures as well as for being an extraordinary helpful colleague.

I want to sincerely thank **Dr. Max McMullon** who offered me invaluable assistance with the REE project and helped me to find my way around in Edinburgh.

A special thank is to **David Mayer** for conducting computational calculations and to **Bruno Dominelli** for taking over some of the synthetic work on the Gold project. I also wish to thank **Jonas Drechsel** and **Dr. Wolfgang Heydenreuter** for conducting cytotoxicity tests and **Prof. Dr. Stephan A. Sieber** for graciously agreeing to cooperate on this project.

I would like to express deepest gratitude to all **co-workers** in the research groups in Munich and Edinburgh as well. Without their help and advice this study would be not that successful. Many thanks for the great work atmosphere, help with the equipment, general willingness to discuss chemistry topics with me and fun we had during these three years. Especially I would like to thank my lab mates **Christian Jandl, Dr. Andrea Schmidt** and **Dr. Manuela Hollering** for creating a great work atmosphere in the lab.

My thanks also go to my lab students, **Andreas Hinterberger**, **Tim Kratky**, **Joachim Preinl**, **Julia Kröger** and **Jonas Schlagintweit** for experimental support and scientific input.

Special thanks to **all employees** and **staff** for their work to keep this business running; especially **Jürgen Kudermann, Maria Weindl, Martin Schellerer** and **Dr. Marcus Drees**.

For the encouragement and financial support, I would like to thank TUM Institute of Advanced Studies and TUM Graduate School.

At last but not the least, I wish to express my love and greatest gratitude to my **beloved family** and **Florian Mayr**; for their understanding and endless love through the duration of my doctorate program.

Abstract

Application of *N*-heterocyclic carbenes (NHCs) in coordination chemistry has been a rapidly expanding field since the isolation of the first thermally stable NHC.[1] During the last 25 years the number of reported NHC complexes for a plethora of elements grew quickly and many of the compounds show very promising behaviour for a variety of applications (e.g. catalysis, material sciences, design of new metal-based drugs etc.).[2] Among others, the NHC complexes with electropositive early transition metals attracted attention due to good stabilizing properties of the NHC ligands, which are capable of supporting e.g. unusually high oxidation states.[3] Especially donor-functionalised polydentate NHC ligands proved to provide additional stability due to robust attachment to the metal centre.[4] This offers an exciting possibility of the participation of labile NHC ligands in transformations on the metal centre, as its complete dissociation is impeded in tethered NHC complexes. Using this approach an unusual Frustrated Lewis acid/base type of reactivity has been recently reported with rare earth metal (REE) NHC complexes. Herby highly interesting C–Si and C–C bond formations as well C–H activations have been observed.[5]

This thesis focuses on various synthetic approaches for the preparation of complexes of REE with novel and literature known donor-functionalised bis- and mono(NHC) ligands aimed on further exploration of the frustrated Lewis acid/base type of reactivity. Firstly, the ligand precursors have been investigated towards their reactivity with various alkali metal bases in order to probe the possibility of using corresponding alkali metal NHC adducts in salt elimination reactions with rare earth precursors. The second approach utilizes a direct reaction of the pro-ligands with REE compounds capable of acting as internal base.

Using the second method, the first example of a negatively charged carbon-bridged anionic dicarbene cerium(III) complex is reported. The hexanuclear Ce *N*-heterocyclic dicarbene (NHDC) complex is synthesized *via* a reaction of 3-(3,5-di-*tert*-butyl-2-hydroxyphenyl)-1-methylimidazolium bromide with Li[Ce{N(*i*-Pr)$_2$}$_4$](THF) in benzene. This novel synthetic route offers further possibility for the preparation of other lanthanide complexes with bridging anionic dicarbene moieties. Such compounds are extremely rare and predicted to have unusual magnetic behaviour[6] and reactivity.[5, 7]

Also other tested *N*-(3,5-di-*tert*-butyl-2-hydroxyphenyl) and *N*-(3,5-di-*tert*-butyl-2-hydroxybenzyl) functionalised mono(NHC) ligands show good preliminary results concerning their propensity to form targeted cerium(III) NHC compounds using both reaction procedures described above. Hereby strong evidence for the formation of desired cerium organo compounds has been observed by NMR spectroscopy. However, the high air-sensitivity and paramagnetic nature of these molecules often complicate definitive characterization.

Therefore, the exact molecular structure of the obtained compounds remains uncertain. Further experiments towards isolation, crystallization and characterization of all products are ongoing.

Although bridge functionalised bis(imidazolium) salts readily form alkali metal NHC adducts, the utilization of these compounds in two-step procedures is often unsuccessful due to their thermal instability. The treatment of 1,1'-(2-hydroxyethane-1-1-diyl), 1,1'-(2-hydroxypropane-1,3-diyl) and 1,1'-(prop-1-ene-1,3-diyl) bridge functionalised *N*-mesityl substituted bis(imidazolium) salts with alkali metal bases followed by a transfer to a REE precursor frequently yields substituted imidazoles eliminated due to decomposition of the bridge. Generally, the same type of reactivity is observed directly with REE amides or alkyls acting as internal base. It is conceivable that the synthesis of REE bis(NHC) complexes with a donor-functionalised bridge poses additional difficulty due to vulnerability of the linker chain in such harsh reaction conditions.

Unfortunately, methylene and (ethane-1,2-diyl) bridged *N*-furanyl substituted bis(imidazolium) bromides yield diamagnetic decomposition products in reactions with REE precursors as well. For the methylene bridged compounds the 1,2-shift of the *N*-substituents is observed. However, due to the longer linker in (ethane-1,2-diyl) bridged *N*-furanyl functionalised bis(imidazolium) salts the deprotonation yields corresponding tetraazafulvalenes as products of formal dimerization of the NHCs. Therefore, by treating the corresponding bis(imidazolium) bromide with alkali metal bis(trimethylsilyl)amides the tetraazafulvalene 1,10-bis(5-(*tert*-butyl)furan-2-yl)-2,3,8,9-tetramethyl-1,5,6,10-tetrahydro-diimidazo[1,2-a:2',1'-c]pyrazine could be also readily isolated, characterised and further applied in reactions showing its potential as organic electron donor.

The last chapter of this thesis focuses on dinuclear coinage metal complexes. In the literature silver NHCs are mainly used as transmetallation agents but also gained importance in their own right as photoluminescent materials[8] as well as antimicrobial and antitumor agents.[8b, 9] Au(I) NHCs exhibit very interesting luminescent properties[10], show high potential for applications in catalysis[11] and medicinal chemistry[12].

In this work the formation of different conformers of dinuclear silver(I) and gold(I) 1,1'-(2-hydroxyethane-1,1-diyl)-bridge-functionalised bis(NHC) complexes with various wingtip substituents (R = methyl, isopropyl and mesityl) has been studied. The ratio of anti/syn isomers strongly depends both on wingtip substituents and the metal centre. Moreover, the reaction temperature plays a significant role during the transmetallation process for the ratio of gold(I) conformers, which are further affected by purification procedures. The 1,1'-(2-hydroxyethane-1,1-diyl)-bridge-functionalised bis(NHC) complexes of Au(I) have been applied in a standard MTT assay performed for screening the antiproliferative activity against human lung and liver

cancer cells. An application of sterically hindered mesityl wingtip substituents shows hereby the best results. Likely, the fine-tuning of lipophilicity and conformational isomerism are crucial for designing gold bis(NHC) based anti-cancer drugs. Moreover, first preliminary results aimed on modification of the 1,1'-(2-hydroxyethane-1-1-diyl) bridge of corresponding Au(I) complexes are presented.

Finally, novel dinuclear 1,1'-(prop-1-ene-1,3-diyl)-bridge functionalised bis(NHC) complexes of Ag(I) and Au(II) were readily isolated and fully characterised. Due to rigidity of the bridge these compounds exhibit interesting folded structures in the solid state. Furthermore, first tentative experiments towards post-synthetic modification of the bridge are discussed as well.

Zusammenfassung

Seit der Isolierung des ersten stabilen *N*-heterozyklischen Carbens (NHC)[1] ist die Anwendung von NHCs ein sich rasant entwickelndes Feld in der metallorganischen Chemie. Aufgrund der vielversprechenden Anwendungen in der Katalyse, medizinischen Chemie und den Materialwissenschaften wurde eine Fülle neuartiger NHC-Komplexe vieler Elemente in den letzten 25 Jahren synthetisiert.[2] Dabei erregten die NHC-Komplexe elektropositiver früher Übergangsmetalle große Aufmerksamkeit, weil NHCs z. B. aufgrund ihrer exzellenten Donor-Eigenschaften in der Lage sind, ungewöhnlich hohe Oxidationszahlen zu stabilisieren.[3] Besonders Donor-funktionalisierte polydentate NHC-Liganden bewährten sich hiermit besonders durch die Möglichkeit einer zusätzlichen Stabilisierung.[4] Dadurch wird die komplette Dissoziation des Liganden erheblich erschwert, was eine interessante Möglichkeit der Partizipation der labilen NHC-Einheit an Reaktionen am Metallzentrum bietet. Mit diesem Ansatz wurden kürzlich mit NHC-Komplexen der Seltenen Erden (REE) eine Reihe ungewöhnlicher Transformationen basierend auf einem frustrierten Lewis Säure/Base Reaktivitätstyp beschrieben. Zum Beispiel ermöglichen diese Verbindungen u.a. den Zugang zu neuartigen C–Si und C–C Bindungsformationen sowie C–H Aktivierungen.[5]

Mit dem Ziel, diese ungewöhnliche Reaktivität weiter zu untersuchen behandelt diese Arbeit zwei synthetische Ansätze, die den Zugang zu NHC-Komplexen der Seltenen Erden bieten. Hierfür wurden sowohl diverse neuartige als auch in der Literatur bekannte Mono- und Bis(imidazolium) Salze auf deren Reaktivität mit Alkalimetall-Basen untersucht, um die entsprechenden Alkalimetall-NHC-Addukte in Salzeliminierungsreaktionen mit verschiedenen Seltenerdmetall-Verbindungen einzusetzen. Bei der zweiten Methode wurden Seltenerdmetall-Vorstufen, welche als interne Base agieren können, in einer direkten Reaktion mit Proliganden verwendet.

Die zweite Herangehensweise ermöglichte hierbei die Isolierung des ersten bekannten Cer(III) Komplexes mit negativ geladenem kohlenstoffverbrückten Dicarben (NHDC)-Liganden. Der sechskernige Komplex ist direkt durch die Reaktion von 3-(3,5-Di-*tert*-butyl-2-hydroxyphenyl)-1-methylimidazolium Bromid mit Li[Ce{N(*i*-Pr)$_2$}$_4$](THF) in Benzol isoliert worden. Diese neuartige Syntheseroute bietet den Zugang zu weiteren Lanthanoid-NHDC-Komplexen, welche extrem selten sind sowie ungewöhnliche magnetische Eigenschaften[6] und Reaktivitäten[5, 7] besitzen sollen.

Auch andere getestete *N*-(3,5-di-*tert*-butyl-2-hydroxyphenyl) und *N*-(3,5-di-*tert*-butyl-2-hydroxybenzyl) funktionalisierte NHC-Liganden zeigen gute vorläufige Ergebnisse in Bezug auf die Bildung gewünschter Ce(III)-Verbindungen. Allerdings ist die eindeutige Strukturbestimmung durch den Paramagnetismus und die Luftempfindlichkeit der

Verbindungen enorm erschwert. Deshalb ist die exakte Struktur dieser Komplexe weiterhin nicht gesichert. Weitere Experimente zur Isolierung und Kristallisation der Produkte sind im Gange.

Obwohl Bis(imidazolium) Salze mit funktionalisierten Brücken leicht Alkalimetall-NHC-Addukte bilden, ist der Nutzen dieser Verbindungen in Zwei-Schritt-Reaktionen mit Seltenerdmetall-Vorstufen oft limitiert durch deren thermische Instabilität. Die Reaktion der 1,1'-(2-hydroxyethane-1-1-diyl)-, 1,1'-(2-hydroxypropane-1,3-diyl)- und 1,1'-(prop-1-ene-1,3-diyl)-Brücken-funktionalisierten Bis(imidazolium) Salze mit Alkalimetall-Basen und der anschließende Transfer zu einer REE-Vorstufe ergibt oftmals substituierte Imidazole aufgrund der Zersetzung der Brücke. Die gleiche Reaktivität ist mit REE-Amiden und Alkylen, die als interne Basen fungieren, zu beobachten. Es ist denkbar, dass, im Vergleich zu Mono(NHC)-Komplexen, die Synthese der REE-bis(NHC)-Komplexe mit Donor-funktionalisierten Brücken eine zusätzliche Schwierigkeit unter solch harschen Reaktionsbedingungen aufweist.

Leider reagieren auch die Methylen- und Ethylen-verbrückten *N*-furanyl-substituierten Bis(imidazolium) Salze unter Ausbildung diverser diamagnetischer Zersetzungsprodukte mit Alkalimetall-Basen und Seltenerdmetall-Vorstufen. Für die Methylen-verbrückten Verbindungen beobachtet man 1,2-Umlagerungen der *N*-Substituenten. Aufgrund der längeren Brücke reagieren dagegen die Ethylen-verbrückten Analogons unter Dimerisierung der NHCs zu Tetraazafulvalenen. Somit konnte der Tetraazafulvalen 10-Bis(5-(*tert*-butyl)furan-2-yl)-2,3,8,9-tetramethyl-1,5,6,10-tetrahydro-diimidazo[1,2-a:2',1'-c]pyrazin isoliert, charakterisiert und als potenzieller organischer Elektron-Donor in verschieden Reaktionen eingesetzt werden.

Das letzte Kapitel dieser Arbeit beschäftigt sich mit dinuklearen NHC-Komplexen der Münzmetalle. In der Literatur werden Silber-NHCs meist als Transmetallierungsreagenzien eingesetzt, dennoch gewannen diese Verbindungen an Relevanz als photolumineszente,[8] antimikrobielle und antitumorale Substanzen.[8b, 9] Au(I)-NHCs zeigen ebenfalls interessante lumineszente Eigenschaften[10] und haben hohes Potential für katalytische Anwendungen[11] sowie in der medizinischen Chemie.[12]

In dieser Arbeit wurden dinukleare Ag(I)- und Au(I)-1,1'-(2-hydroxyethane-1,1-diyl)-funktionalisierten bis(NHC)-Komplexe mit verschiedenen *N*-Substituenten (R = Methyl, Isopropyl, Mesityl) untersucht. Das Verhältnis der anti/syn Isomere dieser Komplexe zueinander ist stark von den *N*-Substituenten und Metallzentren abhängig. Außerdem beeinflusst die Reaktionstemperatur während der Transmetallierung von Ag zu Au sowie die jeweiligen Aufreinigungsschritte sehr stark das Verhältnis der Isomere im Endprodukt. Darüber hinaus wurden die 1,1'-(2-hydroxyethane-1,1-diyl)-Brücken-funktionalisierte bis(NHC)-Komplexe von Au(I) in einem Standard-MTT-Assay auf die antiproliferativen Eigenschaften

gegen humane Lungen- und Leber-Krebszellen getestet, wobei in dieser Testreihe der *N*-Mesityl substituierte Komplex die besten Ergebnisse zeigt. Es liegt nahe, dass die Feinabstimmung der Lipophilie und Konformation dabei entscheidend ist. Außerdem werden erste vorläufige Ergebnisse in Bezug auf die post-synthetische Modifizierung des 1,1'-(2-hydroxyethane-1,1-diyl)-Brücken-funktionalisierten *N*-methyl-substituierten Au(I)-bis(NHC)-Komplexes präsentiert.

Zuletzt wurden neuartige dinukleare Ag(I) und Au(I) 1,1'-(prop-1-ene-1,3-diyl)-Brücken-funktionalisierte bis(NHC)-Komplexe, die aufgrund der Starrheit der Brücke interessante gefaltete Strukturen im Festkörper aufweisen, isoliert und charakterisiert. Erste vorläufige Experimente zur post-synthetischen Modifizierung werden anschließend ebenfalls vorgestellt.

List of Abbreviations

18-crown-6	1,4,7,10,13,16-hexaoxacyclooctadecane
acac	acetylacetonate
*a*NHC	abnormal *N*-heterocyclic carbene
Ar	generic aryl group
9-BBN	9-borabicyclo[3.3.1]nonane
Bn	benzyl, $CH_2C_6H_5$
C_C	carbenic carbene
COD	cyclooctadiene
COT	organic cation transporter
Cp	cyclopentadienyl, C_5H_5
Cp*	pentamethyl cyclopentadienyl, C_5Me_5
Cy	cyclohexyl
d	day(s)
DCM	dichloromethane
DFT	density functional theory
Dipp	2,6-(*i*-Pr)-C_6H_3, 2,6-diisopropylphenyl
DLC	delocalized large cations
DME	dimethoxyethane
DMF	dimethylformamide
DMSO	dimethylsulfoxide
EA	elemental analysis
EG	ethylene glycol, ethane-1,2-diol
eq.	equivalents
ESR	electron spin resonance
Et	ethyl
Et_2O	diethyl ether
EtOH	ethanol
EXAFS	extended X-Ray absorption fine structure

h	hour(s)
HOMO	highest occupied molecular orbital
^{H}IDipp	1,3-bis(2,6-diisopropylphenyl)imidazol-2-ylidene
^{H}I(*i*-Pr)	1,3-bis(isopropyl)imidazol-2-ylidene
^{H}IMe	1,3-bis(methyl)imidazol-2-ylidene
^{H}IMes	1,3-bis(mesityl)imidazol-2-ylidene
^{H}I(*t*-Bu)	1,3-bis(*tert*-butyl)imidazol-2-ylidene
IC_{50}	half maximal inhibitory concentration
i-Pr	isopropyl
LC	ligand centred
LDA	lithium diisopropylamide
LUMO	lowest occupied molecular orbital
M	metal
Me	methyl
MeCN	acetonitrile
^{Me}I(*i*-Pr)	1,3-bis(isopropyl)-4,5-dimethylimidazol-2-ylidene
^{Me}IMe	1,3-bis(methyl)-4,5-dimethylimidazol-2-ylidene
MeOH	methanol
Mes	mesityl, 2,4,6-trimethylphenyl, 2,4,6-Me-C_6H_2,
N''	$N(SiMe_3)_2$
$N^{i\text{-Pr}}$	diisopropylamide
NBS	*N*-bromosuccinimide
n-Bu	*n*-butyl
NHC	*N*-heterocyclic carbene
NHDC	*N*-heterocyclic dicarbene
n-Pr	*n*-propyl
OTf	triflate
Ph	phenyl

PTC	phase transfer catalysis
R	generic alkyl group
REE	rare earth elements, rare earth metals
ROP	ring opening polymerization
RT	room temperature
SAXS	small-angle X-ray scattering
SC-XRD	single crystal X-Ray diffraction
SMD	solvation model density
t-Bu	*tert*-butyl
THD	tris-(2,2,6,6-tetramethylheptane-3,5-dionato)
THF	tetrahydrofuran
THT	tetrahydrothiophene
$TIME^{Me}$	[1,1,1-tris(3-methylimidazolium-1-yl)methyl]-ethane
TMEDA	tetramethyldiamine
TMP	2,2,6,6-tetramethylpiperidide
TMS	trimethylsilyl
TrxR	thioredoxin reductases
UV	ultraviolet

Nuclear Magnetic Resonance spectroscopic data

$^{13}C\{^{1}H\}$	proton decoupled ^{13}C NMR experiment
δ	chemical shift in ppm
br	broad
COSY	2D correlation spectroscopy
d	doublet
dd	doublet of doublets
DOSY	diffusion ordered spectroscopy
dt	doublet of triplets

hept	heptet
HSQC	heteronuclear single quantum coherence
Hz	hertz
^{x}J	coupling constant over x bonds
INEPT	insensitive nuclei enhanced by polarization transfer
m	multiplet
NMR	nuclear magnetic resonance
NOESY	nuclear Overhauser effect spectroscopy
p	pentet
q	quartet
s	singlet
sept	septet
t	triplet
tt	triplet of triplets
virt	virtual
VT	variable temperature

Mass spectroscopic data

ESI	electrospray ionization
FAB	fast atom bombardment
m/z	mass to charge ratio
M^+	molecular ion
MS	mass spectrometry

Table of Contents

Chapter 1

Introduction

1.1 *N*-Heterocyclic Carbenes

Carbenes have been known as fascinating and elusive compounds since the middle of the nineteenth century.[13] Although numerous attempts to isolate the most primitive members of this compound class, methylene and its relatives, have failed[13c], a "carbenic reactivity" of these compounds have been repeatedly described since 1950s in organic chemistry.[14]

Carbenes have been introduced as ligands in metal complexes by Fischer in 1964[15] and since then intensively investigated. Although no strangers in organometallic chemistry, free carbenes remained elusive until 1988, when Bertrand published the isolation of the first free carbene stabilized by silicon and phosphorus substituents.[16] Finally, in 1991, inspired by pioneering work on metal *N*-heterocyclic carbene (NHC) complexes by Wanzlick[17] and Öfele[18] in the 1960s and 1970s, Arduengo prepared 1,3-di(adamantyl)imidazol-2-ylidene, the first free, "bottleable" carbene incorporated into a nitrogen containing heterocycle.[1]

The isolation of a free NHC reignited the interest of the chemists in these compounds resulting in an explosion of the number of reported metal NHC complexes across the periodic table.[2a, 19] Nowadays, NHCs aren't laboratory curiosities and emerging alternatives to phosphines anymore. They firmly established themselves as powerful tools in organic and metalorganic chemistry and are applied in a plethora of commercially interesting transformations, medicinal and material chemistry.[2b-d, 20]

1.1.1 Definition and Properties of NHCs

Carbene is a divalent carbon centre with a six-electron valence shell, which can exhibit either linear or bent geometry (Figure 1.1.1, **a**).[19a, 19b] In the first case **A**, the non-bonding electrons singly occupy two degenerate, mutually orthogonal p-orbitals (p_x, p_y), while binding to the substituents is achieved *via* a sp-hybridized carbon centre. This geometry implies a triplet state ($^3B_1$). The majority of carbenes, however, consists of a sp^2-hybridized carbon atom with more energetically stabilized bent geometry (**B** and **C**, Figure 1.1.1, **a**).

Concerning the multiplicity of bent carbenes both singlet or triplet states are possible. Firstly, the non-bonding electrons can either occupy the two empty orbitals with a parallel spin leading to a triplet ground state ($\sigma^1p_\pi^1$, $^3B_1$, **B**). A more stable solution is the occupation of σ orbital with antiparallel spin orientation ($\sigma^2p_\pi^0$, $^1A_1$, **C**). The excited singlet states ($\sigma^1p_\pi^1$, $^1B_1$) and ($\sigma^0p_\pi^2$, $^1A_1$) aren't generally of high importance and therefore will be not discussed here.

The multiplicity of the ground state is an important feature for understanding the properties and reactivity of carbenes.[21] Singlet carbenes with a lone pair have ambiphilic character due to existence of a filled and an empty orbital. Triplet carbenes, on the other hand, are nucleophilic,

behave themselves as diradicals and therefore have an increased propensity for dimerization. Due to higher intrinsic stability of singlet carbenes, this compound class is predominantly applied in modern carbene chemistry.[22]

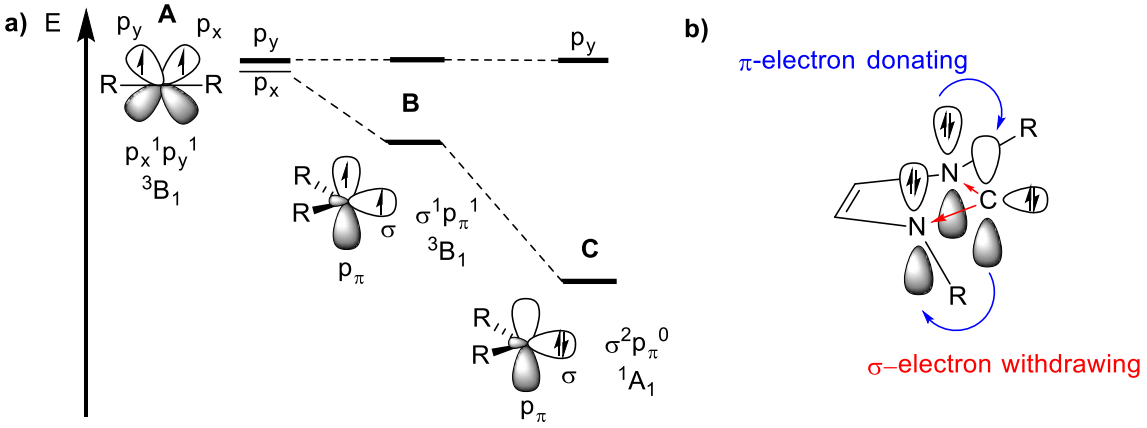

Figure 1.1.1. a). Frontier orbitals and possible electron configurations of carbenes.[19b] **b).** Ground state electronic structure of imidazol-2-ylidenes.[20]

So how can the electronic state of carbenes be controlled since it is so crucial for the reactivity? Similar to crystal field theory, the singlet ground state is favoured by larger σ-p_π separation.[19a, 19b] According to DFT calculation an energy difference of at least 2 eV is necessary to induce a singlet ground state, a value below 1.5 eV leads to a triplet state.[23] The stabilization of the singlet ground state can be achieved in different ways since the orbital energy separation is heavily dependent on steric and electronic properties of the substituents on the carbene carbon. On the one hand, placing σ-withdrawing, generally more electronegative substituents in the direct proximity of the carbene centre results in stabilization by pull-pull (inductive) ability lowering the relative energy of non-bonding σ-orbital.[24] On the other hand, mesomeric effects play a crucial role and can be achieved by application of π-donors (X) or π-acceptors (Z) as α-substituents.[19a, 19b, 23, 25]

The linear or almost linear (Z,Z) and (X,Z) carbenes will be not discussed here; for examples and the information on their electronic structure an interested reader is advised to read some excellent review articles.[19a, 19b] The (X,X)-carbenes however are predicted to be bent molecules in singlet ground state.[22] The donation of π-electrons into p_π-orbital of a carbene raises its relative energy, therefore leading to more stabilization by increasing the HOMO-LUMO gap. The most important singlet (X,X) carbenes with the double stabilization though σ-withdrawing and π-donating substituents are *N*-heterocyclic carbenes (NHCs), where this situation is achieved by a virtue of placing the carbene carbon between two nitrogens by simultaneously enforcing a bent geometry though incorporation into a cyclic structure (Figure 1.1.1, **b**)[20]. By donation of the substituents' lone pair into an empty p_y-orbital of carbene centre

the carbene−nitrogen bonds acquire partial double-bond character, which is reflected for imidazol-2-ylidenes by a C2−N bond distance falling between corresponding imidazolium salt and saturated NCH_2N-analogue.[1, 22]

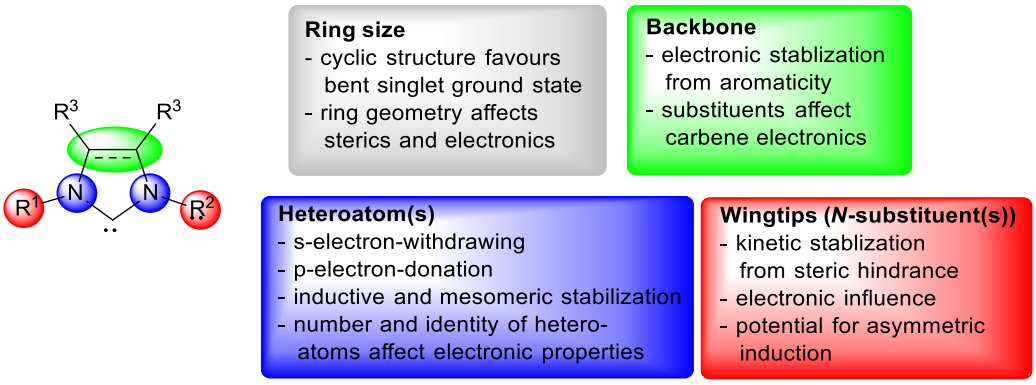

Figure 1.1.2. Illustration of structural features which influence the properties of NHCs.[20]

The influence on the electronic situation in NHCs is not only limited to heteroatoms, also the wingtips (*N*-Substituents) affect the electronics, e.g. by a greater degree of σ-donation. Consequently, the NHCs with alkyl wingtip-substituents have higher nucleophilic properties as their aryl-substituted analogues.[22] Moreover, the backbone substituents (C4 and C5 positions) have also high potential for electronic "fine-tuning". For instance, Arduengo *et al.* were able to isolate an exceptionally stable carbene by replacing the backbone hydrogens with chlorine atoms, which contributed to the stability of NHC with additional σ-withdrawing and π-donating abilities.[26] The backbone of NHCs is also important in another context: although the concept of aromaticity in carbenes is far less important than in their imidazolium precursors, due to their partial aromaticity imidazol-2-ylidenes are more thermodynamically stable by about 25 $kcal \cdot mol^{-1}$ than their saturated analogues, which are, therefore, more prone to dimerization.[27] Furthermore, the steric hindrance, especially produced by *N*-substituents, can kinetically stabilize many types of carbenes and prevent them e.g. from dimerization as well.[19a, 20] A good summary on all factors and structural elements affecting the stability and reactivity of NHCs in given in Figure 1.1.2. For more in-depth understanding of the bonding situation in NHCs a comprehensive overview on quantification of the parameters and factors defining electronic and steric situation in these compounds can be found in literature.[22]

Nowadays, due to numerous structural and electronic modifications the portfolio of selectable NHCs is huge and extremely versatile (for some important classes see Figure 1.1.3).[4, 8b, 19b, 22] Although the vast majority of NHCs is derived from five-membered heterocycles containing two nitrogen atoms, the so-called "ring-expanding" alternatives have been also reported, e.g. based on triazine, tetrahydropyrimidine and others.[19b], [19a, 22] Also a substitution of nitrogen by various heteroatoms is accessible, for example though the use of oxygen, sulphur or

phosphorus.[19a, 19b, 22] Moreover, the requirement of at least two nitrogens for stabilization of the carbene is not obligatory as a series of cyclic alkyl (amino)carbenes containing only one nitrogen atom have been also intensively investigated.[28] Additionally, there is also a possibility of generation of so-called mesoionic or “abnormal” carbenes, which are normally more nucleophilic than neutral NHCs.[28c, 29] Also remote NHCs, where the carbene is not directly bonded to a heteroatom, are known.[28c]

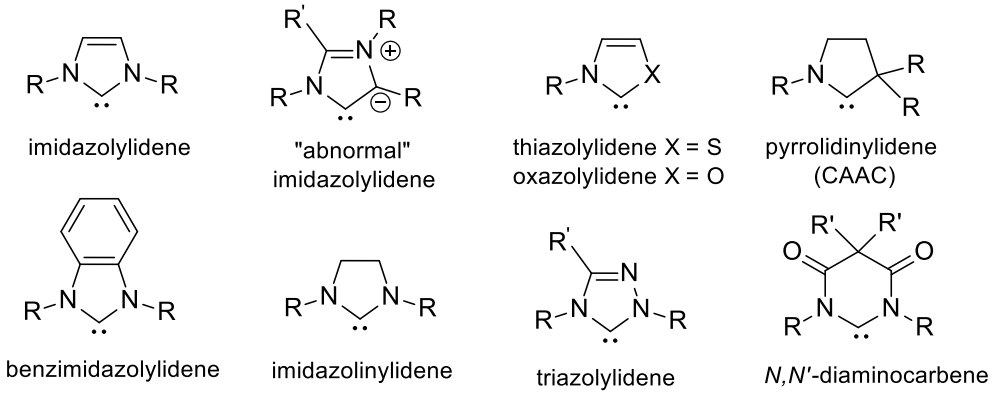

Figure 1.1.3. Molecular structures of some of the most common classes of NHCs.[20]

In conclusion, due to their electronic structure NHCs are considered as nucleophilic compounds. Consequently, they have strong propensity to act as σ-donors and bind to a wide range of metals and non-metals.[20] Their stability, generally strong binding mode as well as the possibility for “fine-tuning” of electronics and sterics make them very attractive tools in organometallic chemistry. Additionally, also one of the most attractive features of the carbenes is the relatively easy preparation of structurally diverse analogues, which can be studied in comparative investigations.[20]

1.1.2 Generation of Imidazol-2-ylidenes

Since this work focusses on the coordination chemistry of ”classical” five-membered NHCs with unsaturated backbone, this section discusses synthetic procedures leading to formation of NHCs derived from imidazol-2-ylidenes. For an overview of synthetic methods for the preparation of other classes of free NHCs, which are beyond the scope of this work, comprehensive review articles are highly recommended at this point.[2a, 2b, 19a, 19b, 28c]

The generation of imidazol-2-ylidenes is mostly achieved by deprotonation of corresponding imidazolium salts using alkali-metal bases such as MH, M(O*t*-Bu) or MN" (N" = $N(SiMe_3)_2$).[19b] Access to these pro-NHCs is feasible on different synthetic routes, of which the most widely applied are collected in Scheme 1.1.1.[19b] A very straightforward approach is the alkylation of imidazole *via* a nucleophilic substitution reaction (**a**).[30] By using a Brønsted base an

imidazolide is generated *in situ* and then treated with one equivalent of an alkyl- or aryl halide. Subsequently, the obtained 1-alkylimidazole can be further alkylated by addition of another equivalent of the same (**a**) or a different (**b**) organohalide. This strategy allows the synthesis of imidazolium salts with asymmetric or symmetric *N*-substitution pattern. A considerable disadvantage, however, is the fact that only primary alkyl halides react satisfactorily in this procedure. In case of the secondary and tertiary organohalides yields are substantially reduced due to undesired elimination reactions. Also the synthetic possibilities for 1-arylimidazoles are limited.[19b]

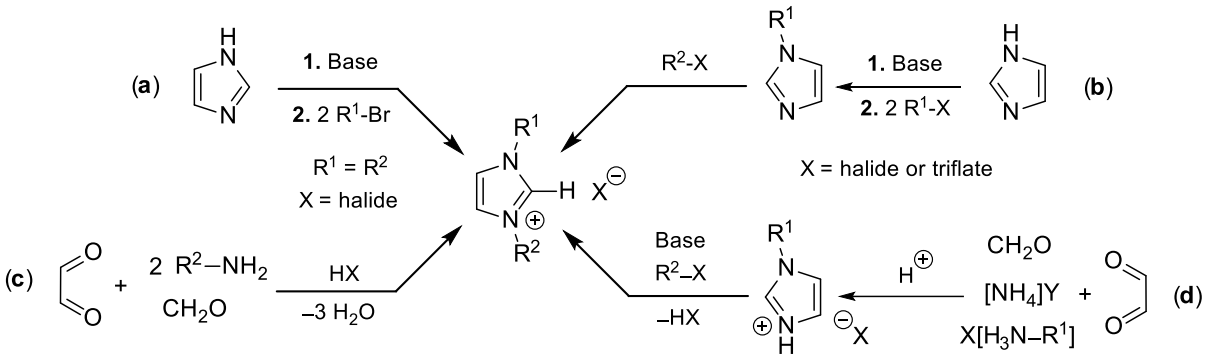

Scheme 1.1.1. Strategies for the preparations of asymmetric and symmetric imidazolium salts.[19b]

This drawback can be circumvented by building up the desired heterocycle in a multi-component one pot reaction using glyoxal, formaldehyde and two equivalents of a primary amine in presence of an acid (**c**).[31] Also a combination of both routes is possible and leads to an asymmetric substitution pattern (**d**).[32] The one-pot reaction is especially of advantage for the preparation of imidazolium salts bearing aromatic, very bulky or functionalised *N,N'*-substituents.[33] Furthermore, the introduction of different aryl-substituents can be also achieved by Ullman-type coupling reactions catalysed by copper.[34]

In the last 20 years there was also considerable interest in polydentate or donor-functionalised NHC ligands, which can be generally build up by the same methods described above. A comprehensive overview of reported variety of pro-ligands based on imidazol-2-ylidenes can be given by a number of review articles.[4, 8b, 19b] Some examples of polydentate NHC ligands will be discussed later in this thesis.

Another interesting approach for direct access to carbenes is possible though reductive desulfurization of imidazolin-2-thiones by metallic potassium.[35] The cyclic thioureas are synthesized by a condensation of α-hydroxyketones, e. g. 3-hydroxy-2-butanone, with suitable *N,N'*-substituted thiourea derivatives. However, this method is less frequently used in comparison to deprotonation of azolium salts described above. The two most common routes leading to preparation of imidazol-2-ylidenes are visualised in Scheme 1.1.2.

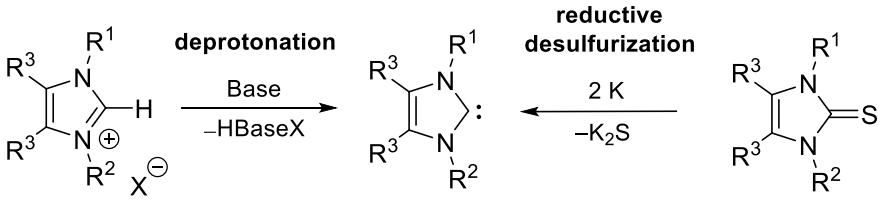

Scheme 1.1.2. Methods applied for generation of unsaturated *N*-heterocyclic carbenes.[19b]

The generation of free carbenes can be conveniently monitored by ^{13}C NMR spectroscopy, since the formation of imidazol-2-ylidenes is visible though the shift of the NCN resonance from approximately 140-150 ppm for imidazolium cations to 210-220 ppm for free NHCs.[19b]

1.1.3 Reactivity and Stability of Free Imidazol-2-ylidenes

1.1.3.1 Carbene Dimerization

The dimerization process for singlet free carbenes is believed to proceed *via* nonleast motion pathway. Hereby, in-plane σ lone pair of one carbene attacks the vacant out-of-plane p_π-orbital of the other carbene (Scheme 1.1.3, a).[36] Therefore, due to involvement of energetically high lying p_π-orbital one expects significant activation barrier for this reaction. Indeed, for aromatic 1,2,4-triazol-3-ylidenes this value was estimated to be 19.4 kcal·mol^{-1}.[37] However, by analysing the kinetics of dimerization of carbenes derived from aromatic *N*-heterocycles Chen and Jordann suggested that formal dimerization in fact proceeds by nucleophilic attack of a carbene upon its conjugated acid.[38] A subsequent elimination of the remaining proton in **3** would result in formally dimerized carbene **4** (Scheme 1.1.3, **b**). Unfortunately, in many cases it is not clear what kind of mechanism is involved.

Normally, in comparison to their saturated analogues, imidazol-2-ylidenes are remarkably resistant to dimerization[19b], which was first observed be Wanzlick for *N,N'*-phenylimidazolin-2-ylidene.[39] According to a model of Carter and Goddard[36a, 40], the strength of the C=C bond for dimerized carbenes should correspond to canonical C=C double bond (e.g. of ethylene 172 kcal·mol^{-1}) minus the sum of the singlet-triplet energy difference for both carbenes involved in the process. Therefore, since the energy gap between these states in unsaturated NHCs amounts to approximately 85 kcal·mol^{-1},[41] the C=C bond strength for the resulting tetraazafulvalene (dimerized carbene) is expected to be only ≈ 2 kcal·mol^{-1}.[42] Such small value is partially due to the loss of aromaticity in case of dimerization. A significantly smaller singlet-triplet gap for saturated NHC (≈ 69 kcal·mol^{-1})[41] would therefore energetically favour the formation of entetraamines, if the kinetic factors are not taken into consideration.

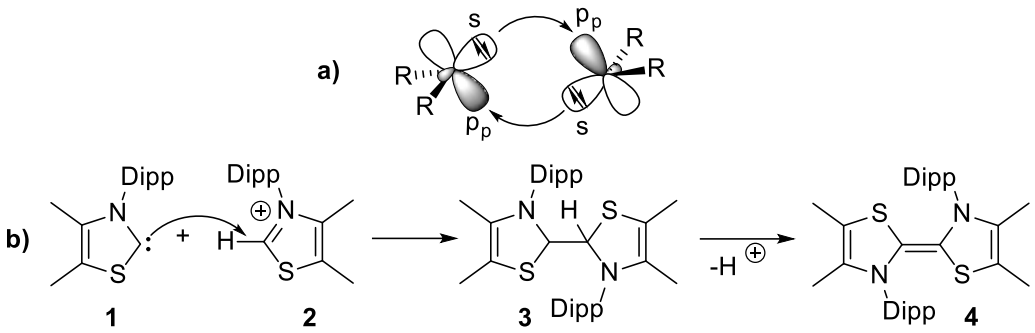

Scheme 1.1.3. a) "True" dimerization of singlet carbenes by nonleast motion pathway; **b)** Mechanism for the formal dimerization proceeding by an nucleophilic attack of carbene on thiazolium salt.

Since the bond strength for tetraazafulvalenes is quite weak, depending on the substituents and the conditions, a formed tetraazafulvalene can also dissociate to free NHCs.[43] Although initially postulated equilibrium between the free carbene *N,N'*-phenylimidazolidin-2-ylidene and its dimer mentioned above could not be confirmed and only entetraamine is always formed[44], this dimerization equilibrium is named the Wanzlick equilibrium after its proposer.

A first convincing experimental evidence for the weakness of the bonds in tetraazafulvalenes was provided by Chen and Taton.[42a-c] The deprotonation of doubly propylene bridged imidazolium salt **5** yields the doubly bridged tetraazafulvalene **6** (Scheme 1.1.4). Also the reduction of **7** in liquid ammonia produces this stable dimer. On the other hand, the deprotonation of its butylene analogue **8** results in formation of bis(imidazol-2-ylidene) **9** (Scheme 1.1.4). Besides these double bridged examples, where the dimerization process is undoubtedly favourable due to entropic reasons, up to 2012 the isolation of (mono)bridged or even less non-bridged tetraazafulvalenes proved to be very challenging.[42c, 45]

Finally, Murphy developed an approach to facilitate the dimerization of (mono)propylene bridged imidazol-2-ylidenes by using Thorpe-Ingold effect[46] from *gem*-dimethyl group on the middle carbon of the bridge.[47] Therefore, the deprotonation of **10a** with NaH in liquid ammonia affords almost 1:1 mixture of tetraazafulvalene **11a** and (bis)carbene **12a** (Scheme 1.1.5). Interestingly, this equilibrium can be further shifted exclusively to **11b** by replacing the backbone protons by methyl-groups in starting material. For imidazol-2-ylidenes without the benefit of Thorpe-Ingold effect (**10c**) an alternative approach *via* Birch reduction of **13c** is successful, yielding a metastable dimerized NHC **11c**, which then converts to (bis)carbene **12c** within hours in solution (Scheme 1.1.5). The precarious existence of non-bridged tetraazafulvalenes with a few minutes of half-life is also observed after a reduction with sodium of respective annulated disalt.[47]

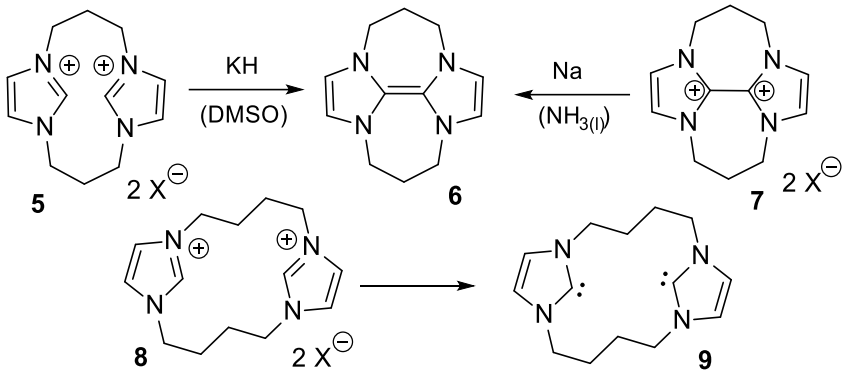

Scheme 1.1.4. Formation of double bridged tetraazafulvalenes *vs.* bis(carbenes).

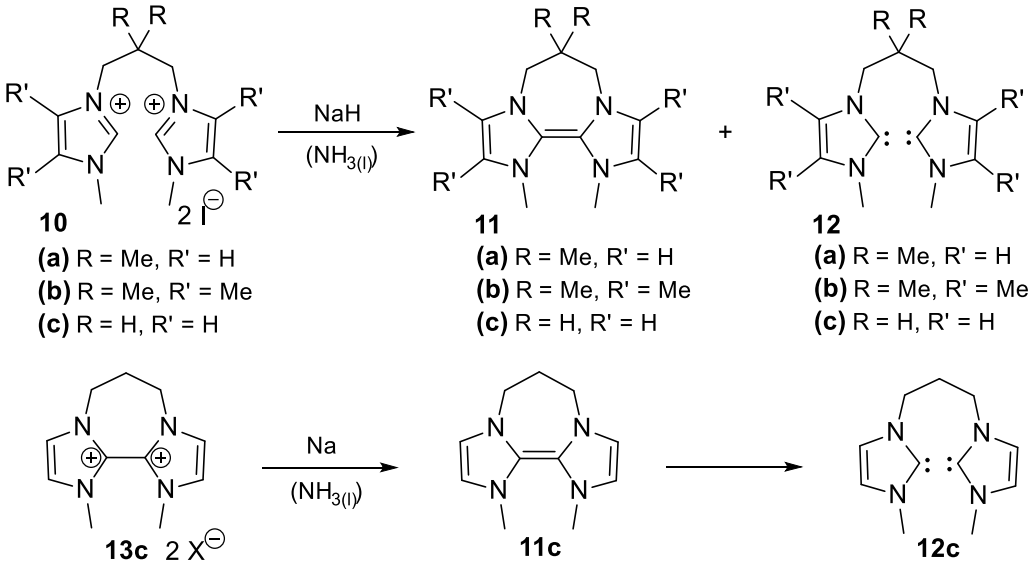

Scheme 1.1.5. Preparation of (mono)bridged tetraazafulvalenes.[47]

1.1.3.2 1,2-Migration Reactions

1,2-Migration is a universal reaction for singlet carbenes, which proceeds through a unimolecular concerted mechanism (Scheme 1.1.6, **a**).[48] However, in imidazol-2-ylidenes 1,2-hydrogen shift cannot proceed *via* intramolecular process in the plane of the ring since it would imply the crossing of two orbitals with the same symmetry.[19a] The theoretical studies on an alternative mechanism, which involves an interaction of N–H bond with out of plane π-orbital of the carbene, showed that imidazol-2-ylidenes would be kinetically stable towards this reaction due to high activation barrier (Scheme 1.1.6, **b**).[41, 49] The reason for it would be the required deformation of the ring and therefore loss of aromaticity.

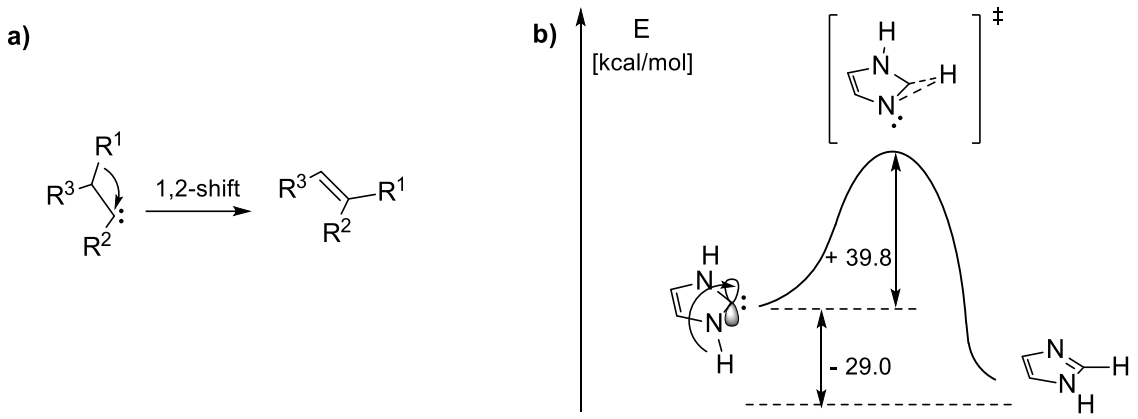

Scheme 1.1.6. a). Schematic representation of 1,2-migration occurring in singlet carbenes. **b).** Energy diagram for the calculated out of plane 1,2-shift of hydrogen for imidazol-2-ylidenes.[49]

But since this kind of reactivity has been repeatedly observed for aromatic carbenes[50], an alternative mechanism must take place. Indeed, by investigating the 1,2-shift behaviour of other aromatic NHCs such as 1,2,4-triazol-5-ylidenes Bertrand and co-workers were able to prove the intermolecular nature of this reaction by conducting cross-over experiment with carbenes bearing different substituents.[51] They proposed a nucleophilic attack of formed carbene **15** on a wingtip substituent of the starting material **14** (Scheme 1.1.7). A subsequent attack of the liberated nitrogen of **17** on the wingtip substituent of the intermediate azolium salt **16** ultimately would yield the observed rearrangement product **18**. It is possible that for imidazol-2-ylidenes the same mechanism takes hold.

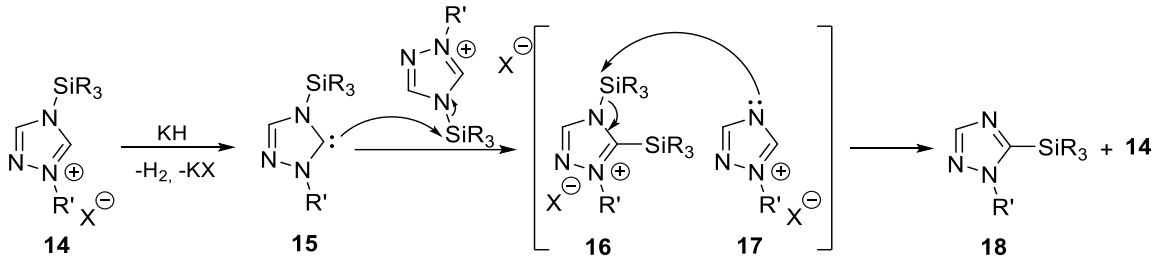

Scheme 1.1.7. Proposed intermolecular mechanism for 1,2-alkylmigration for aromatic NHCs.

1.1.3.3 Other Reactions

Other reactions of free singlet aromatic *N*-heterocyclic carbenes are less important for this work, but it should be mentioned, that these compounds have known to undergo addition to carbon–carbon double bonds and carbonyl-derivatives, inset into polarized bonds and form Lewis-acid adducts with main group elements.[19a, 20] The propensity of NHCs to react with carbon-electrophiles lead also to numerous applications as organocatalysts.[20, 52] Hereby, the vast majority of the reactions is initiated though nucleophilic attack on the carbonyl-group. This

leads to an umpolung of the carbonyl-group resulting in generation of transient carbon nucleophile, which can then be used in transesterification or polymerization reactions.

1.2 Alkali Metal NHC Adducts

In organometallic chemistry, an obtained free carbene can be subsequently transferred to the actual metal of interest. Also the usage of metal complexes, which can be utilised for transmetallation, is very popular. For middle-to late transition metal complexes the application of silver(I) NHC complexes as transfer reagents proved to be a convenient methodology.[9a, 53] Unfortunately, this procedure is also connected with some disadvantages and limitations.[54] Besides the high costs and the light sensitivity of some Ag NHCs, the lability of these compounds is not sufficiently high for more electropositive early transition metals to compete with the silver cation for the soft NHC ligand.[54] In this case the deprotonation of azolium salts with an alkali metal base is preferred resulting in aforementioned free carbenes or much more labile Group I NHC adducts,[19b, 19e] which are nowadays recognized as effective and less costly transmetallation reagents compared to their silver counterparts.[54]

1.2.1 Structural Survey

Chemists have begun with the characterization of Group 1 NHC adducts, predominantly Li compounds, in the middle of the 90s[19e], shortly after discovery of stable NHCs.[1] The first report on alkali metal NHC species dates back to 1995, when Boche and co-workers described the synthesis of bimetallic Li complex containing two 4-*tert*-butylthiazol-2-ylidenes and two bridging glyme moieties by deprotonation of 4-*tert*-butylthiazole with MeLi (**19**, Scheme 1.2.1, **a**).[55] **19** exhibits rather long metal–carbon distances (2.531(5) Å on average) and asymmetrical bounding of Li to NHCs. A couple of years later Arduengo reported the reaction of 1,3-di-*tert*-butylimidazol-2-ylidene with 1,2,4-tris(trimethylsilyl)cyclopentadienide lithium yielding **20**, the first example of Li-NHC where Li is only coordinated to carbon centres.[56] Subsequently, the first sodium and potassium NHCs (**21**) supported by 1,3-diisopropyl-3,4,5,6-tetrahydropyrimid-2-ylidene[57] and a couple of other dimeric Li NHC adducts have been described in the 90s,[50b, 57] but only after the turn of the millennia the bulk of reported alkali metal NHC compounds started to emerge.

In 2009 Hofmann reported access to mono- and bimetallic lithium complexes bearing bulky bidentate, anionic bis(3-*tert*-butylimidazol-2-ylidene)dimethylborate NHC ligands *via* deprotonation of the respective precursor **22a-b** with *n*-BuLi (Scheme 1.2.1, **b**).[58] While the crystals of **23a'** are composed of the bimetallic dimers, only monomeric species **23a** is found in solution. However, by replacing the substituents on the boron by phenyl- instead of methyl-groups, the monomeric form **23b** is also obtained in the solid state due large substituents precluding the formation of dimers. Notably, the Li–C distance in **23a'** with a value of 2.056 Å is the shortest lithium–carbene bond known to date.

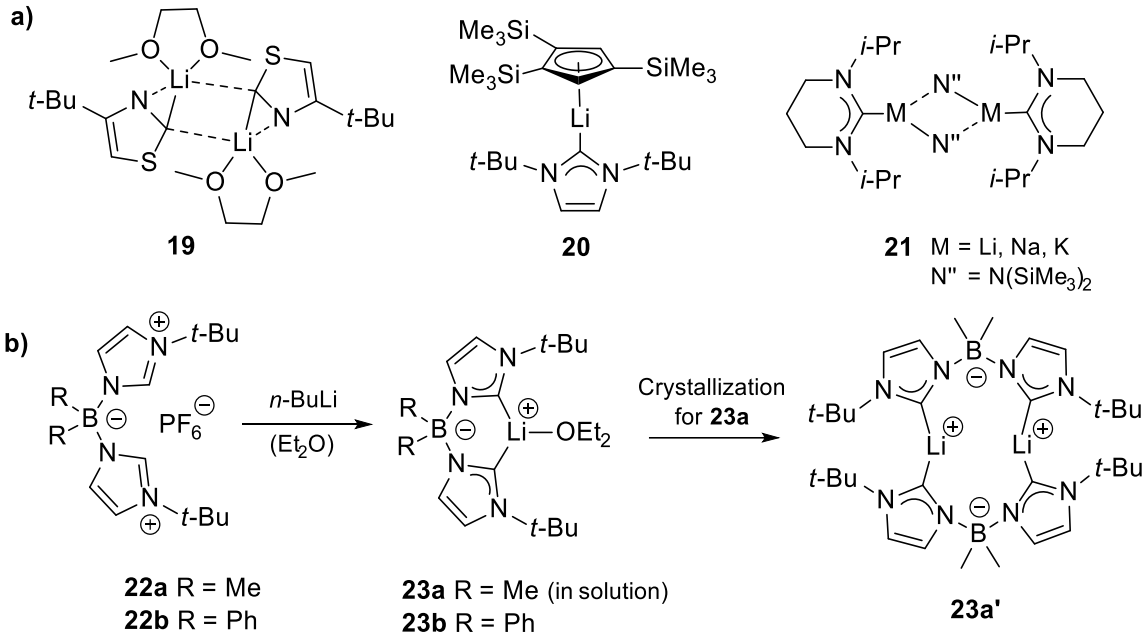

Scheme 1.2.1. a). Early alkali metal NHC complexes. **b).** Borate functionalised bis(NHC) adducts of Li.

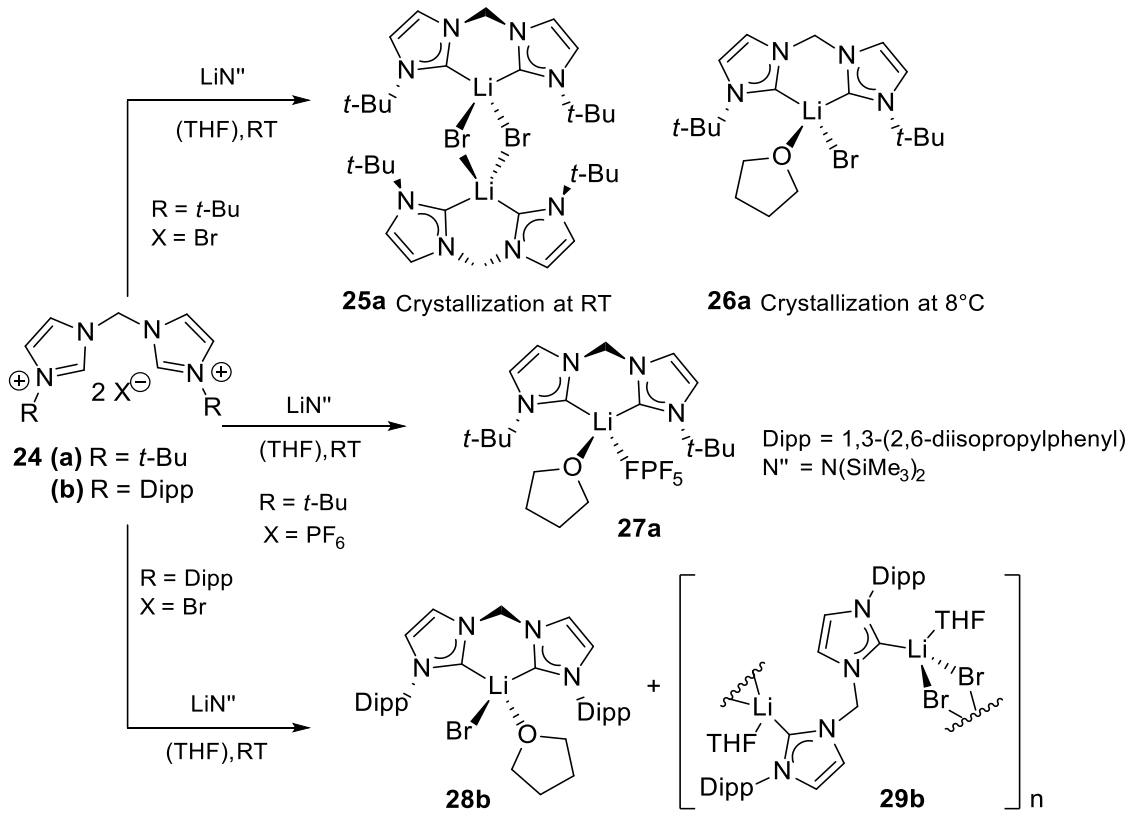

Scheme 1.2.2. Structure of neutral lithium bis(NHC) adducts reported by Hofmann.[59]

Lithium complexes of neutral bis(NHC) ligands were reported only recently by Hofmann who described the deprotonation of bis(imidazolium) bromides of the type **24** with an excess of LiN" in THF at RT (Scheme 1.2.2).[59] Depending on the crystallization method and the *N*-

substituents monomeric, dimeric or polymeric structures are obtained. Furthermore, using corresponding bis(imidazolium) hexafluorophosphate a rare Li bis(NHC) monomer **27a** with the hexafluorophosphate anion coordinated to Li *via* fluorine atom can be prepared.

A bis(carbene) adducts of lithium can be also accessed with (mono)carbenes by addition of 1,3-bis(2,6-diisopropylphenyl)imidazol-2-ylidene (^{H}IDipp) to a 1:1 mixture of Li[N(SiMe$_3$)$_2$] and Mg[N(SiMe$_3$)$_2$]$_2$.[60] The bulky substituents can efficiently stabilize Li centre producing lithium magnesiate salt **30** (Scheme 1.2.3, **a**). Furthermore, this synthetic protocol could be extended to heavier alkali and alkali earth metals. More recently, using similar principle, He*via* and co-workers were also able to generate sodium bis(NHC) compound **32** by the reaction of homoleptic sodium ferrate **31** with ^{H}IDipp (Scheme 1.2.3, **b**).[61]

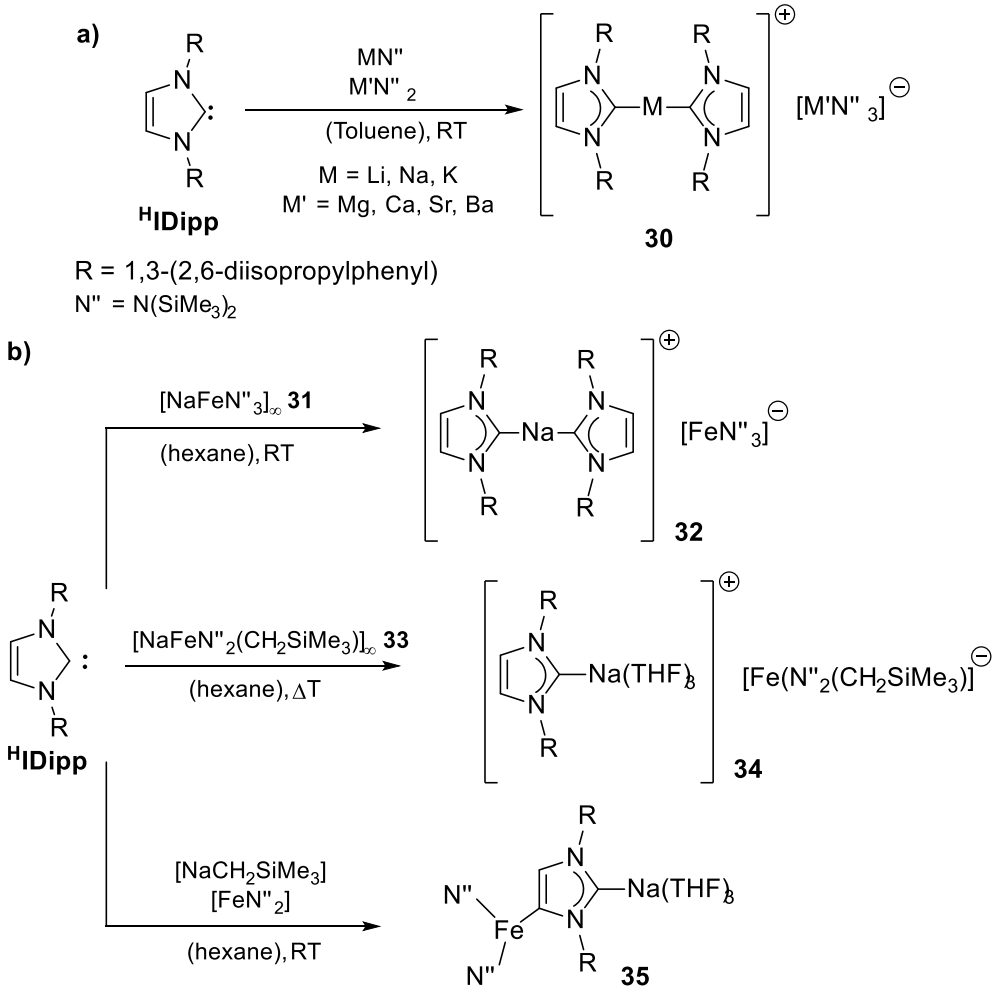

Scheme 1.2.3. Stabilization of alkali metal cations by a bulky (mono)NHC ligand and alkali earth metallates (**a**) or ferrates (**b**).

By using a slightly different, heteroleptic sodium ferrate **33** only (mono)NHC adduct **34**, which is additionally stabilized by THF molecules, is obtained (Scheme 1.2.3, **b**). Interestingly, although the heteroleptic sodium ferrate **33** is prepared by a reaction of FeN"$_2$ and

$NaCH_2SiMe_3$, in contrast to the reaction mentioned above, the subjection of ^{H}IDipp to a simple mixture of $NaCH_2SiMe_3$ and $FeN"_2$ yields heteroleptic ferrate **35** (Scheme 1.2.3, **b**), which can be further transformed into neutral abnormal Fe NHC complex by electrophilic interception with MeOTf.

In the past decades another approach for stabilization of highly Lewis acidic centres with NHCs became very popular. The application of polydentate donor-functionalised (mostly anionic tethered) NHCs increased a number of isolable early transition metals as well as Group I NHC adducts by promoting a robust attachment to the metal centres. One of the first groups to use this method was the group of Arnold, who were able to isolate a dimeric NHC lithium bromide adduct **38** by a stepwise deprotonation of respective alkylammonium imidazolium bromide **36** with *n*-BuLi (Scheme 1.2.4).[62]

The first anionic *N*-bonded alkali metal NHC was also reported by Arnold and co-workers shortly after.[63] Compound **40** can be readily obtained by deprotonation of the carbene precursor **39**, previously formed by a conversion of the same alkylammonium imidazolium bromide **36** with KH (Scheme 1.2.4). A few years later the same group described also the synthesis of tridentate amido-functionalised bis(NHC) attached to lithium, whose formation was confirmed by characteristic shifts in ^{13}C NMR spectra as well as elemental analysis.[64]

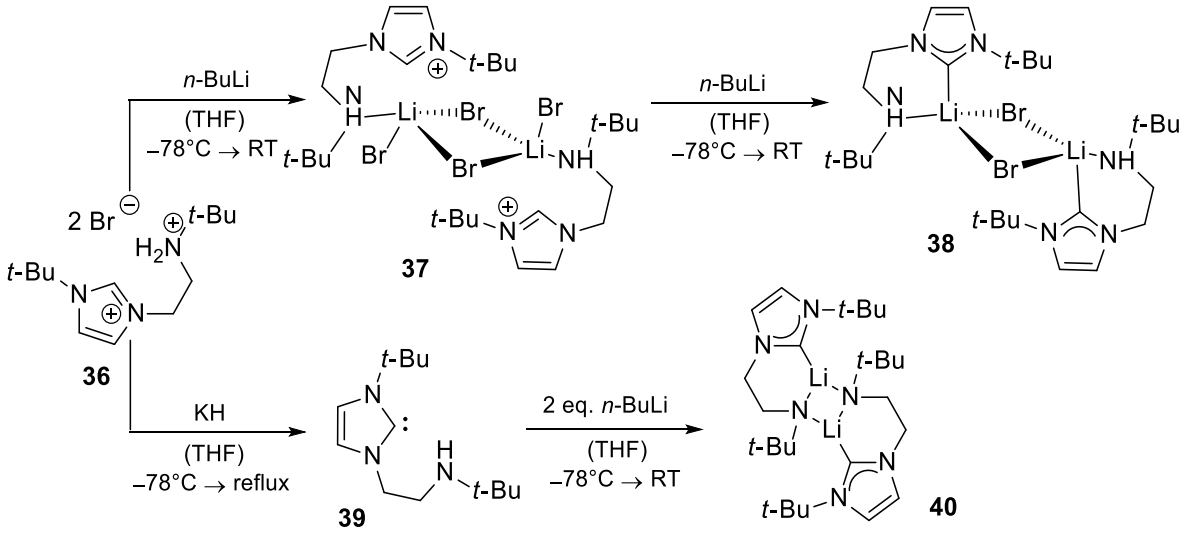

Scheme 1.2.4. Lithium amino- and amido-tethered NHC complexes.

Another possibility of anionic tethering by a negatively charged oxygen was also explored by Arnold's group at the same time as amido-functionalised complexes. The conversion of alkoxy-tethered NHC precursor **41** into their corresponding alkali metal NHC adducts is readily accomplished by sequential treatment with Group I bases (Scheme 1.2.5, left).[65] One the one hand, the deprotonation of **41** with two equivalents of LiN" in THF affords the bimetallic complex

43b, which is dimeric in its crystalline form containing a tetrameric lithium cage moiety (Scheme 1.2.5, right).[65a] Within this cage each Li_3-unit is capped by one of the two participating iodide.

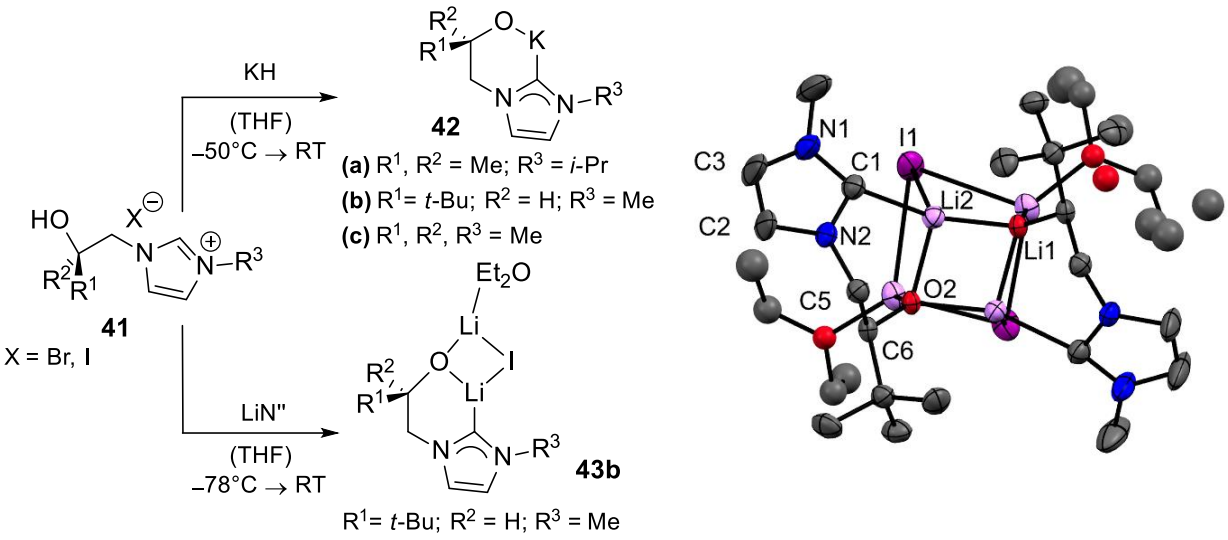

Scheme 1.2.5. Synthesis of alkali metal complexes with alkoxy-functionalised NHCs (left); Displacement ellipsoid drawing of **43b** with ellipsoids at 50 % probability (right). Hydrogen atoms are omitted for clarity.

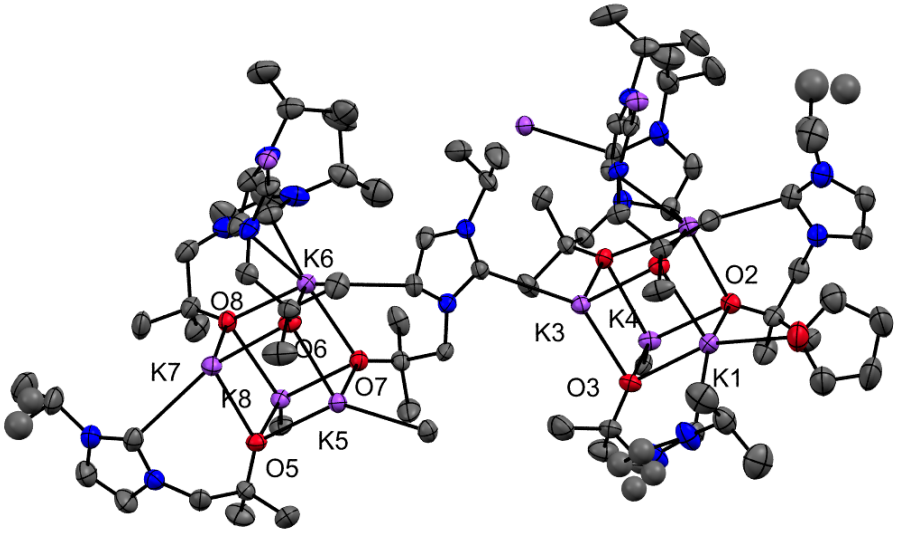

Figure 1.2.1. ORTEP style representation of **42b** with ellipsoids at 50 % probability. Hydrogen atoms are omitted for clarity.

On the other hand, a treatment of **41** with 2.0 eq. (or excess) of KH in THF generates the monomeric and monometallic species **42b**, which crystallises out as a tetrameric aggregate containing cube-shaped K_4O_4-clusters (Figure 1.2.1).[65b] Hence, each metal centre shows a four-coordinate binding mode to three anionic oxygen atoms. Furthermore, two of these entities are bridged by a NHC ligand *via* normal and abnormal fashion. The average

potassium–carbene bond lengths are, as expected, longer than the corresponding lithium analogues. All potassium-adducts **42a-c** have proven to be thermally and relatively air-stable compounds rendering them excellent transfer reagents for the synthesis of other early transition metal NHC complexes. This stability is actually a quite remarkable feature as the isolation of heavier alkali metal NHC complexes is usually impeded by 1,2-migration of the *N*-substituents.[66]

Downing *et al*. prepared NHC ligands with another pendant anionic tethers, indenyl and fluorenyl moieties, which can be deprotonated with 2 eq. of KN".[67] The solid state structure of corresponding fluorenyl-functionalised K NHC comprises of polymeric zigzag chains with K and bridging fluorenyl-moieties. Each potassium centre is sandwiched by two phenyl rings and additionally coordinated to NHC. Furthermore, the same group also synthesized pincer-like hybrid P-N-NHC ligand and reported its successful deprotonation with LiN" and KN".[68]

More recently, a lot of progress have been reported in the chemistry of Group I adducts of NHCs with anionic backbone functionalization and abnormal NHCs, which are considered as key intermediates for the access to unusual metal-carbene complexes.[19e] By the way, due to stronger coordinating nature of these ligands the structural characterization of its alkali metal adducts is much easier than with neutral NHC moieties. Although this approach is quite new, already the number of reported complexes is very high.[69] Some highlights of a very diverse coordination behaviour of these ligands are discussed below; for a more comprehensive overview an interested reader is advised to turn to some recent review articles.[69-70]

Braunstein isolated the pro-ligand **44a** featuring an amido moiety at the backbone in 2013 (Scheme 1.2.6).[71] The lithium NHC adduct **45a** is obtained by deprotonation of Dipp-functionalised precursor with $LiCH_2SiMe_3$. In subsequent studies the formation alkali metal adducts with the precursor series **44a-d**, derived from the pioneering study mentioned above, was more intensively investigated.[72] Hereby, the structures of the products strongly depends on the reaction conditions, *N*-substituents and the metal base (Scheme 1.2.6).

The first Li abnormal NHC (*a*NHC) compound was reported by Bertrand in 2009.[29] Hereby the corresponding ligand precursor 1,3-bis(Dipp)-2,4-diphenyl-imidazole is deprotonated with lithium diisopylamide (LDA) resulting in coordination of lithium at C5 position. Interestingly, by attempting to extend this procedure to potassium by using $K[N(SiMe_3)_2]$, only the free carbene was observed, indicating the higher propensity of heavier alkali metal bases for generating free carbenes instead of alkali metal NHC adducts.[19e]

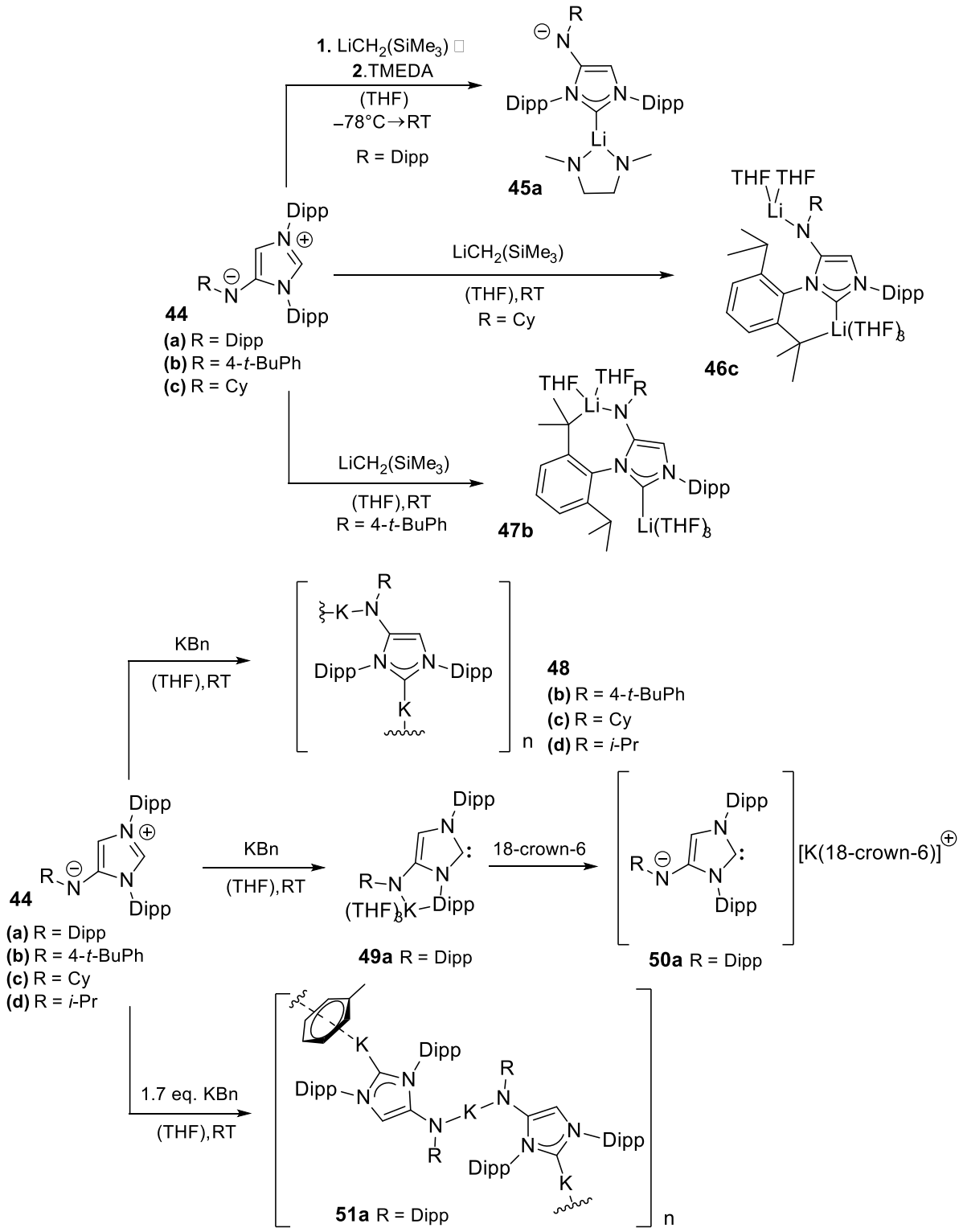

Scheme 1.2.6. Formation of Li and K NHC adducts with anionic backbone-amido-functionalised NHCs.

Robinson and co-workers also showed that 1,3-di(2,6-isopropylphenyl)imidazole could be readily deprotonated at C2 and C5 positions resulting in formation of polymeric anionic dicarbene lithium salt.[73] Subsequent reactivity studies with different Lewis acids and electrophiles were also conducted, showing a preference for the reaction at more electron

donating and sterically more opened C5 position, although some reagent such as CO_2 and BH_3 can react with both C2 and C5 positions.[73-74]

The access to *a*NHC adducts of heavier alkali metals analogues have also been investigated, e.g. *via* salt metathesis reaction from Li to K.[75] In the reactivity studies of these novel compounds a preferable attack of Lewis acids at C5 position was demonstrated similar to the previously mentioned Li compounds. Also sodium mediated zincations and magnesiations of ^{H}IDipp were recently described by treatment of ^{H}IDipp with TMP (TMP = 2,2,6,6-tetramethylpiperidide)-stabilized sodium zincate and sodium magnesiate species.[76]

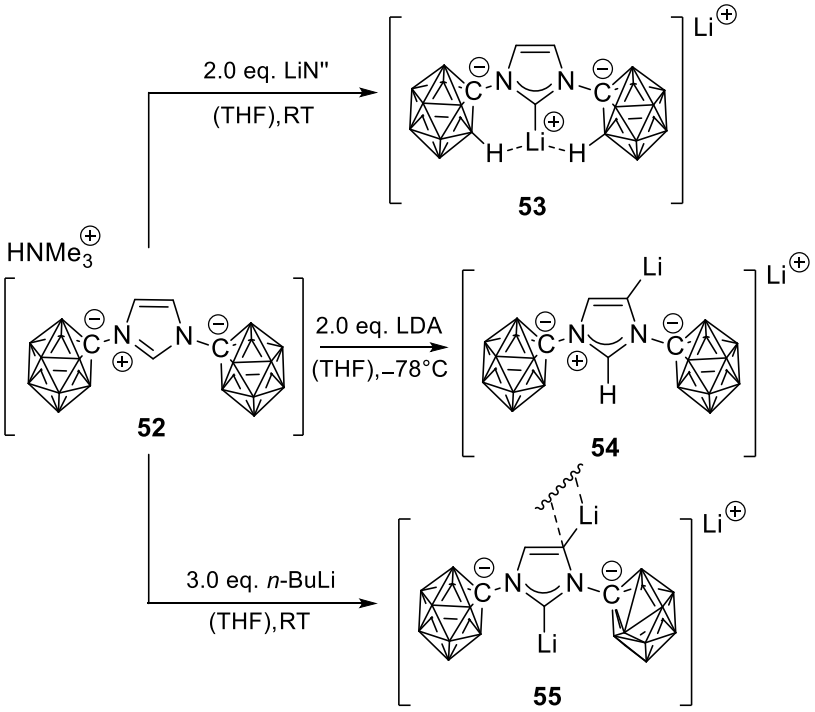

Scheme 1.2.7. Synthesis of lithium carboranylated anionic NHC adducts (unlabelled vertices in the icosahedra: BH).

Remarkably, in the studies with highly sterically demanding carborate ($CB_{11}H_{11}^-$) functionalised NHCs Lavallo was able to show the influence of the base on the outcome of the deprotonation reaction (Scheme 1.2.7).[77] For the deprotonation of the symmetrical precursor **52** the usage of 2.0 eq. of LiN" at RT or at –78 °C results in regioselective deprotonation on C2 position (**53**), while 2.0 eq. of LDA, a base with more sterically congested environment at the amide centre, deprotonates the precursor in abnormal fashion at –78 °C (**54**). However, at room temperature the excess of LDA yields a mixture of three compounds, specifically **53** and **54** mentioned above as well as anionic dicarbene **55**, which can be finally selectively isolated using of 3.0 eq. of *n*-BuLi (Scheme 1.2.7). In the solid state **55** shows dimeric structure with bridging lithium cations at C5 positions. Remarkably, having substituted carborate by similar sterically demanding, but neutral adamantyl substituents, the authors were not able to

deprotonate the C5 position even in the presence of the excess of LDA at RT. Consequently, the application of anionic carborane wingtips shows superior control over regioselectivity of deprotonation and facilitates the synthesis of unusual charged dicarbene lithium compounds.[77a] It is also worth to mention that the reactions of asymmetrical NHC with *N*-carborane and *N*-mesityl substituents shows a preference for C2 deprotonation in case LiN" and simultaneous deprotonations of C5 and C2 positions in case of *n*-BuLi as well. However in this case, all attempts to selectively deprotonate only the C5 position failed.[77b]

1.2.2 Stability and Properties

Generally, all alkali metal carbene interactions possess covalent interactions but are otherwise essentially ionic in nature. This can be seen from crystallographic data of numerous alkali metal complexes showing metal–ligand distances well above the sum of the corresponding covalent radii (Table 1.2.1). Due to decreasing Lewis acidity from Li^+ to K^+, stabilities of the metal carbene adducts are decreasing in the same direction. In solution this fact is also reflected by the shift of the value for C_C resonance to lower frequencies in ^{13}C NMR, as illustrated by a comparative study of alkali metal 1,3-dimethyl-3,4,5,6-tetrahydropyrimid-2-ylidene adduct **21** (^{13}C NMR shift for a corresponding free carbene was measured to be 242.7 ppm).[78]

In conclusion, by going through the literature on alkali metal NHC adducts it is evident, that anionic anchoring of NHCs brings great benefits to the stability of these compounds. Due to essentially ionic nature of M–NHC bonds, the complexes with neutral NHCs have only been reported with the most Lewis acidic alkali metal, lithium. Although Li NHC adducts are generally more stable with respect e.g. to 1,2-migrations, the heavier alkali metal NHCs adducts, especially that of potassium, seems to have less propensity for oligomerization and also the lability of these bonds makes them better transfer reagents.

Table 1.2.1. Comparison of M–C distances in alkali metal NHC adducts to sum of covalent radii of corresponding metals as well ^{13}C NMR chemical shifts for the C_C of 1,3-dimethyl-3,4,5,6-tetrahydropyrimid-2-ylidene adducts of alkali metals (**21)**.

M–NHC	Average M–C distance [Å][a]	Sum of corresponding covalent radii [Å][b]	^{13}C NMR shift for C_C for **21** (ppm)[c]
Li	2.134	2.03-2.08	219.4
Na	2.463	2.30-2.41	224.9
K	2.915	2.71-2.76	241.0

a). Carbene–metal distances compiled from the Cambridge Crystallographic Data Centre Base at the date of submission of a review by Bellemin-Laponnaz *et al*.[19e] **b).** see following references.[79] **c).** Comparative study published by Otto *et al*.[78]

1.3 Rare Earth Metal Complexes Bearing *N*-Heterocyclic Carbenes

For a long time, the researchers in organometallic chemistry were not interested in rare earth metals (REE), a set of 17 elements, which include scandium, yttrium and 15 lanthanoids. Apart from the historically misguided belief in their scarcity[80], these metals were deemed to generate uninteresting and unimportant chemistry.[81] The paucity of the accessible oxidation states as well as the seeming lack of orbital interactions and backbonding capability due to a limited radial extension of 4f orbitals were the reasons for this bad reputation.

However, in 2007, Evans appealed for an overturn of this assumption.[81] Based on some early observations for REE compounds, he postulated simple rules for the reactivity of lanthanoid complexes:

- The $4f^n$ configuration does not define the reactivity in most cases
- The optimized electrostatic interactions define the structure
- Sterics play a very important role for stability and reactivity

Keeping these rules in mind, the lanthanoids can actually accomplish unique chemistry with steric control over reactivity.[81] Nowhere in the periodic table there is such a large set of metals, which all have similar chemical properties but gradually change their size due to lanthanoid contraction. As matter of fact, there are numerous examples of a successful precise size optimization, which dramatically influences the reactivity of the respective compounds.[81] Therefore, combined with the high Lewis acidity of REEs, exciting reactivity can be achieved. Additionally, recent advances in accessing unusual oxidation states of lanthanoids open new ways for conducting redox chemistry with these metals.[81]

The most common ligands used for supporting rare earth metals are cyclopentadienyl derivatives, amides and alkoxides, which are preferred by hard Lewis acidic centres such as REEs. Hence, the soft neutral ligands, such as phosphines are not advantageous due mismatch of donor and acceptor orbitals.[82] However, despite often drawn analogy with phosphines[83], NHCs are more suitable for supporting REEs,[19c] since these two ligand classes are actually totally different, both sterically and electronically.[19e, 83] First of all, there are significant differences in the spatial orientation of their substituents.[20, 83] For phosphines the formal sp^3-hybridization of the phosphorus centre results in their typically cone-shaped form where the substituents are pointing away from the metal. In NHCs the cyclic azole core with *N*-substituents provides a structure in which the substituent groups are oriented more towards the cation. As a result, NHCs are generally considered to be sterically more demanding and thus more suitable for metal centres which require higher degree of steric protection. Moreover, NHC have generally stronger nucleophilic properties and do not require π-backbonding for

stabilization of their respective coordination compounds.[84] Therefore, they can be applied for the support of wider range of metal centres, including electropositive early transition metals as well main group elements.[4, 19e, 20] Especially in the past 15 years the investigations on the properties and reactivity of NHC complexes with electropositive metals gained on importance and lead to discovery of unusual and highly promising reactivity.[19c, 19e] Today many examples of NHC ligands tethered to early transition metals, lanthanoid and actinoid metals have been reported.[19c]

1.3.1 Structural Survey and Typical Synthetic Procedures

1.3.1.1 Complexes with Mono(dentate) NHC Ligands

Rare earth adducts with mono(dentate) NHCs can be either prepared by the substitution of weakly coordinating ligands by a free NHC (isolated or *in situ* generated) or simple ligand association, commonly used especially for metal complexes with low electron counts where stability benefits from additional electron density.

The first REE NHC complexes **Yb-85a-b** were prepared by a treatment of $[Yb(C_5Me_4Et)_2(THF)]$ with 1,3,4,5-tetramethyl-imidazol-2-ylidene (^{Me}IMe) or *N,N'*-diisopropyl-4,5-dimethylimidazol-2-ylidene (^{Me}I(*i*-Pr)) in THF (Scheme 1.3.1, **a**).[85] Subsequently, similar Yb(II), Sm(II), Sm(III) and Ce(III) complexes with different substitution patterns on the cyclopentadienyl ligands or NHC substituents have been accessed using ether a displacement of weakly coordinating donor molecule or simple association process of a free NHC with corresponding metallocene.[86]

Not only metallocenes are capable of associating with a free NHC. At the same time as reporting the first samarocenes NHC complexes, Arduengo also simultaneously described a coordination of ^{Me}IMe to a Eu(III) or Y(III) complex with a tris-(2,2,6,6-tetramethylheptane-3,5-dionato) ligand (THD) (Scheme 1.3.1, **b**).[86c]

Herrmann *et al*. also reported the formation of ^{H}IMe adducts with various lanthanide cations supported by tris(amido) ligands (R = $N(SiMe_3)_2$ or $N(SiHMe_2)_2$) as well as the first erbium tris(chloride) NHC adduct $[(^{H}IMe)_3ErCl_3]$.[87] Furthermore, NHC adducts of erbium and lutetium tris(alkyls) $[\{^{Me}I(i\text{-}Pr)\}M(CH_2SiMe_3)_3(THF)]$ and $[\{^{Me}I(i\text{-}Pr)\}_2M(CH_2SiMe_3)_3]$ (M = Er, Lu)[88] and Yb(II) ^{Me}IMe tris(pyrazoylborate) complex[89] were synthesized by solvent displacement reactions.

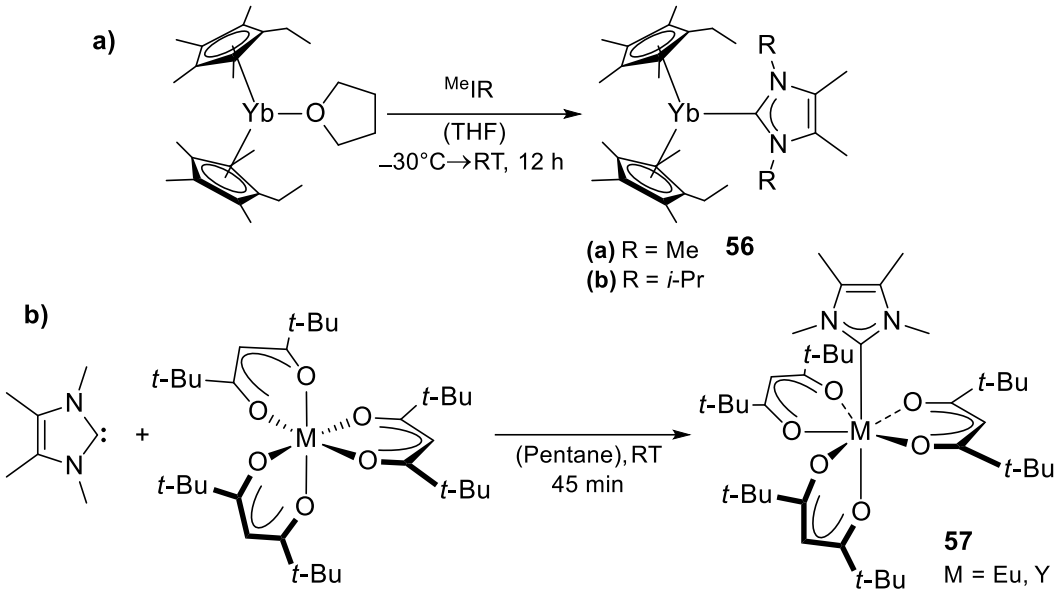

Scheme 1.3.1. Structure of exemplarily mono(NHC)adducts of rare earth metals obtained by a solvent displacement reaction (**a**) and an association with free NHC (**b**).

1.3.1.2 Complexes with Poly(dentate) NHC Ligands

The REE adducts with mono(dentate) neutral NHCs mentioned above are not particularly stable and their use is limited as they quickly degrade due to ligand dissociation. An elegant approach for stabilizing NHC complexes of rare earth metals is the application of poly(dentate) ligands, especially with additional anionic donors.

The synthesis of REE complexes supported by donor-functionalised NHC ligands can be achieved in two ways. The most widely applied protocol is a generation of alkali metal NHC adducts (in *situ* or isolated), which are then used as reagents for transferring the ligand to the REE centre. A second possibility include a direct deprotonation of the ligand precursor with a REE compound, of which mostly amides and alkyls are used as internal bases.

Complexes with Nitrogen-Anchors

One of the first teams to make use of anionic tethers was the group of Arnold. To achieve that, Arnold and co-workers designed an amido-functionalised imidazolium salt **36** (Section 1.2.1, Scheme 1.2.4), which can be conveniently deprotonated with *n*-BuLi or LiN".[62] A corresponding lithium amide-bromide adduct **38**, also already mentioned in Section 1.2.1, can transfer the NHC ligand to a series of rare-earth amides **58-59** (Scheme 1.3.2, **a**).[62, 90] Furthermore, Arnold *et al.* introduced a related amido-bis(NHC) ligand and reported the synthesis of corresponding yttrium complexes **62a-b** by a transamination reaction of YN"$_3$ and one equivalent of the lithium chloride adducts **61a** or **61b** (Scheme 1.3.2, **b**).[64]

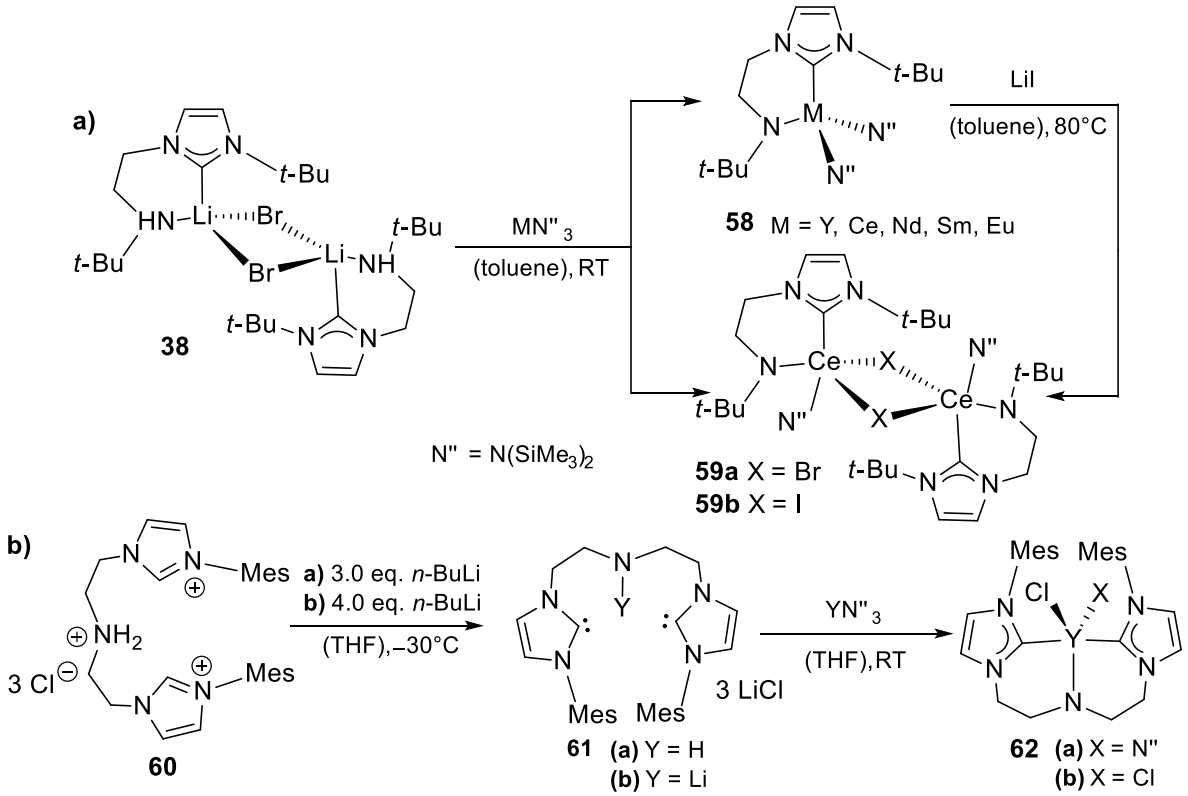

Scheme 1.3.2. Synthesis of a series of rare earth complexes with anionic *N*-anchored NHCs.

Gu *et al.* also examined the formation of rare earth complexes supported by CNC pincer diarylimido linked bis(NHC) ligands and noted a strong dependence of obtained products on the reaction conditions (Scheme 1.3.3).[91] For example, a reaction of pro-ligand **63b** with [MN"$_3$(μ-Cl)Li(THF)$_3$] at RT in THF yields the unwanted heterocyclic organic product **64b** formed by carbene C–C and C–N coupling. However, at lower temperatures, using the same metal precursor and additional equivalents of *n*-BuLi bis(amido) complexes **65b** are isolated. Also the treatment of the ligand precursor with 5.0 eq. of NaN" and MCl_3 at –78 °C yields this product. Interestingly, in contrast to the one pot reaction with NaN", a stepwise addition of NaN" to imidazolium precursor **63b** at –78 °C, followed by addition of $YbCl_3$ results in formation of cationic $[YbL_2]^+$ **66b** with an inverse crown pentagonal counter anion [{Na(μ-N"}$_5$(μ-Cl)]$^-$. Finally, a stepwise treatment of **63b** with *n*-BuLi at –30 °C leads after subsequent addition to [MN"$_3$(μ-Cl)Li(THF)] (M = Y, Er, Yb) precursors to isolation of zwitterionic complexes **67b**.[91] More recently the same group confirmed the utility of their synthetic approach for obtaining CNC-pincer alkyl rare earth compounds (**65a,c**) by applying differently substituted ligands.[92]

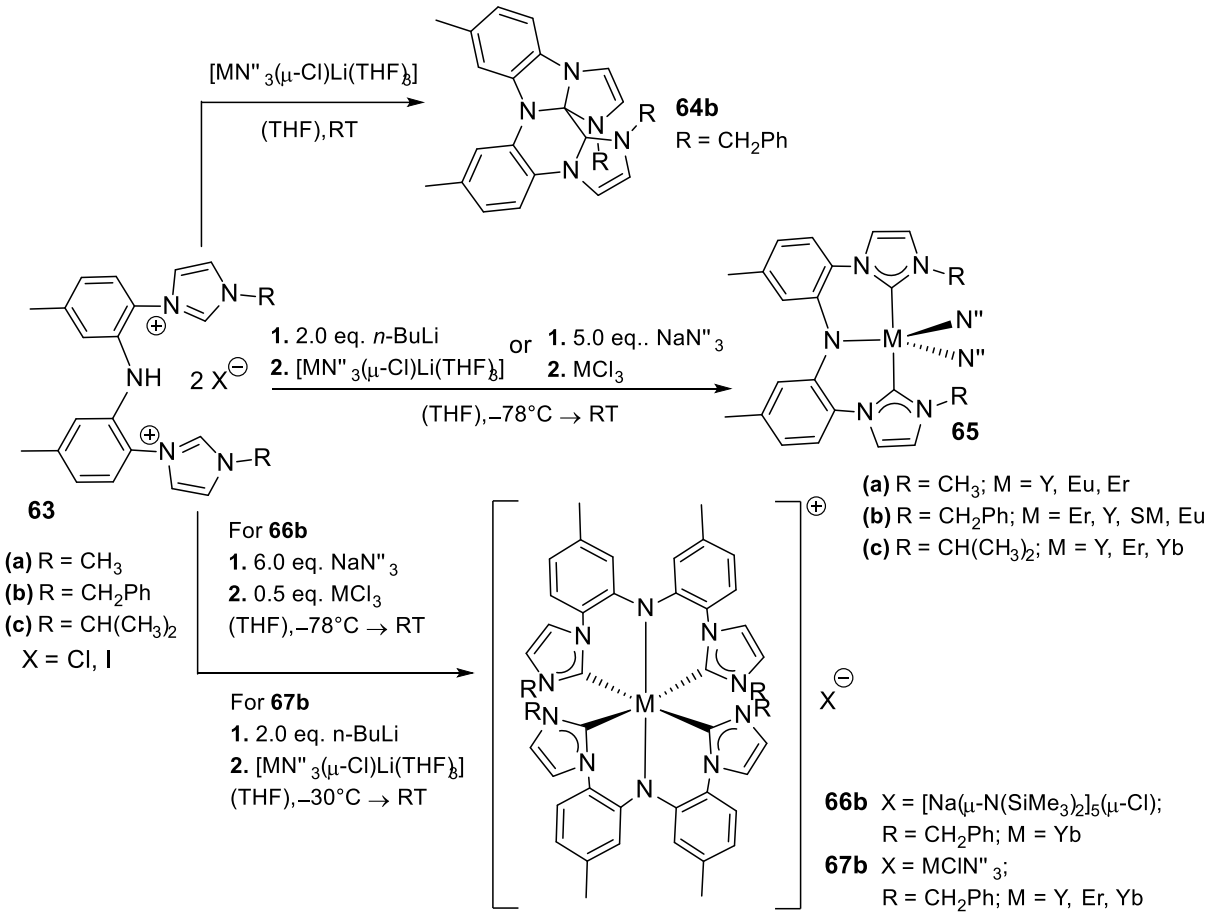

Scheme 1.3.3. Formation of rare earth complexes bearing CNC-pincer NHC ligands.

Complexes with Oxygen-Anchors

Concomitantly to the development of amido-functionalised NHC ligands Arnold introduced alkoxy-functionalised NHC precursors **41a-c** (Paragraph 1.2.1, Scheme 1.2.5).[4] Using the potassium based transmetallation reagent **42a** the group was able to access a number of REE NHC complexes such as pseudo octahedral complexes **68a** (M = Sc, Y, Ce, Scheme 1.3.4).[93] Furthermore, a treatment of REE metallocenes with **42a** yields mono- or bis(carbene) cyclopentadienyl complexes (**69a** and **70a**, Scheme 1.3.4).[5b]

Interestingly, in contrast to unsaturated alkoxy-functionalised NHCs a deprotonation of corresponding precursors of closely related saturated analogues with *n*-BuLi or KBn in hexanes/toluene yields bicyclic products **71a-c** instead of alkali metal NHC adducts (Scheme 1.3.5).[94] Using these compounds in a protonolysis reaction with rare earth amides and alkyls a series of structurally versatile complexes can be obtained.[5a, 94-95] The remaining proton of the ligand is hereby removed by alkyl- or amide-substituents on the metal precursor acting as internal base and thereby vacating a coordination site.

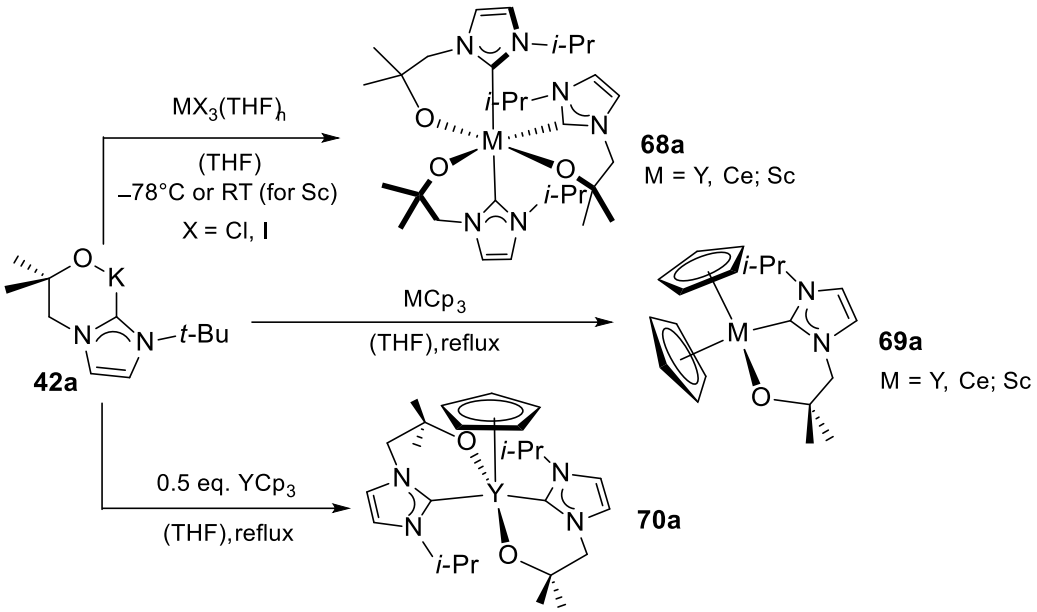

Scheme 1.3.4. Synthesis of rare earth complexes bearing alkoxy-functionalised imidazol-2-ylidenes.

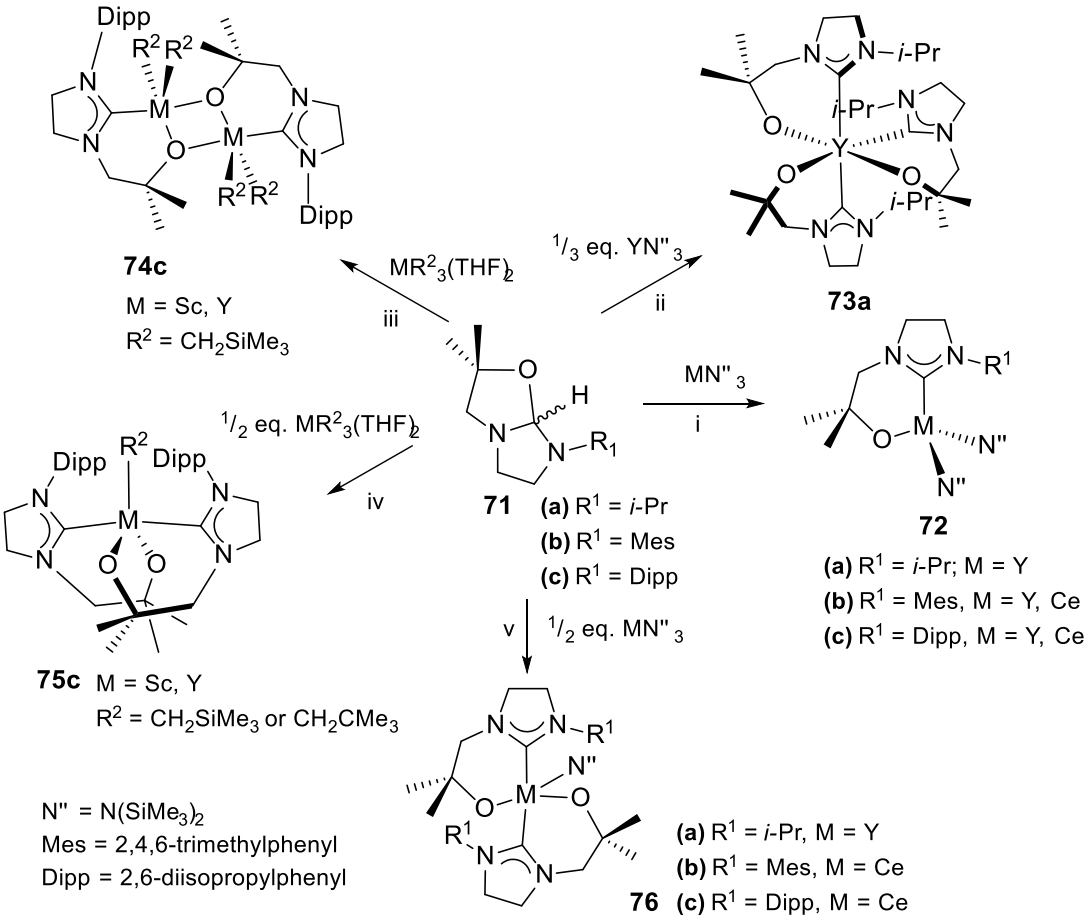

Scheme 1.3.5. Synthesis of REE complexes supported by alkoxy-functionalised imidazolin-2-ylidenes. *Reaction conditions*: i) **Y-72a-b**: (C_6D_6), RT; **Y-72c**: (THF), RT; **Ce-72b**: (hexanes), RT: **Ce-72c**: (toluene), RT ii) (C_6D_6), 85 °C iii) (hexanes), 0 °C iv) **Sc-75c**: (hexanes), 0 °C; **Y-75c**: (toluene), 0 °C v) **Y-76a**: (C_6D_6), 85 °C; **Ce-76b**: (toluene), RT; **Ce-76c**: (hexanes), RT.

Additionally, an interesting approach for using anionic oxygen-tethered NHCs was made by Shen. She introduced enol-functionalised NHC complexes **78** obtained by *in situ* reaction of NHC precursor **77** with NaN" and REE chlorides in THF at RT (Scheme 1.3.6).[96]

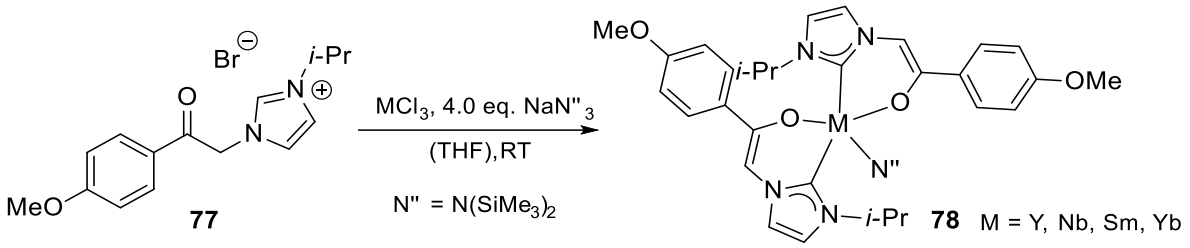

Scheme 1.3.6. Enol-functionalised NHC complexes of REE.

REE complexes supported by *N*-(3,5-di-*tert*-butyl-2-hydroxybenzyl)-functionalised NHC ligands can be also obtained in a one pot reaction with REE amides and alkali metal bases in order to fulfil stoichiometric requirements. In this manner the tris(NHC) complex **Y-80b** is obtained by a reaction of the *N*-(3,5-di-*tert*-butyl-2-hydroxybenzyl)-modified imidazolium pro-ligand **79b** with [LiY{N(*i*-Pr)$_2$}$_4$] and *n*-BuLi at –78 °C (Scheme 1.3.7).[97]

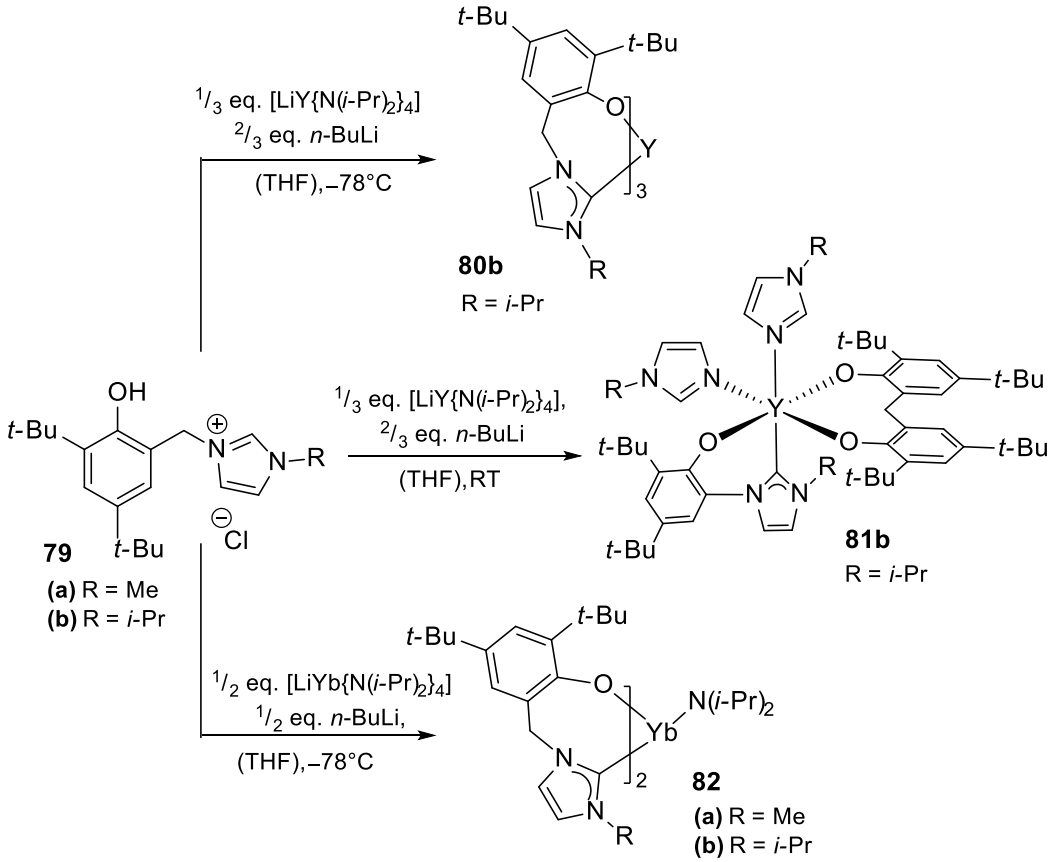

Scheme 1.3.7. Synthesis of Y and Yb *N*-(3,5-di-*tert*-butyl-2-hydroxybenzyl)-functionalised NHC complexes.

By conducting the same reaction at RT a mono(NHC) yttrium complex **81b** bearing a bis(phenolate) ligand and two *N*-bonded imidazoles is formed. The authors speculated that a cleavage of benzylic C–N bond by hydrogen transfer from phenol to the carbene centre followed by an attack of a N(*i*-Pr)$_2$-group on the unsaturated ligand fragment would result in the observed release of free amine and formation a methylene-bridged bis(phenolate).[97] Further experiments with [Li{Yb(N(*i*-Pr)$_2$}$_4$], *n*-BuLi and the pro-ligand in the stoichiometric ratio of 1:1:2 at –78 °C resulted in isolation of bis(NHC) ytterbium compounds **82a-b**. Interestingly, all attempts to prepare mono(NHC) ligated complexes were futile.[98]

Similar to *N*-(3,5-di-*tert*-butyl-2-hydroxybenzyl)-functionalised mono(NHC) ligands described above the same group also applied the 1,3-bis(3,5-di-*tert*-butyl-2-hydroxybenzyl)-functionalised analogue **83**. For the preparation of the respective complexes similar procedure, a one pot deprotonation reaction with [LiM{N(*i*-Pr)$_2$}$_4$(THF)] and *n*-BuLi in a 2:1:2 molar ratio in THF at –50 °C, is carried out (Scheme 1.3.8).[99]

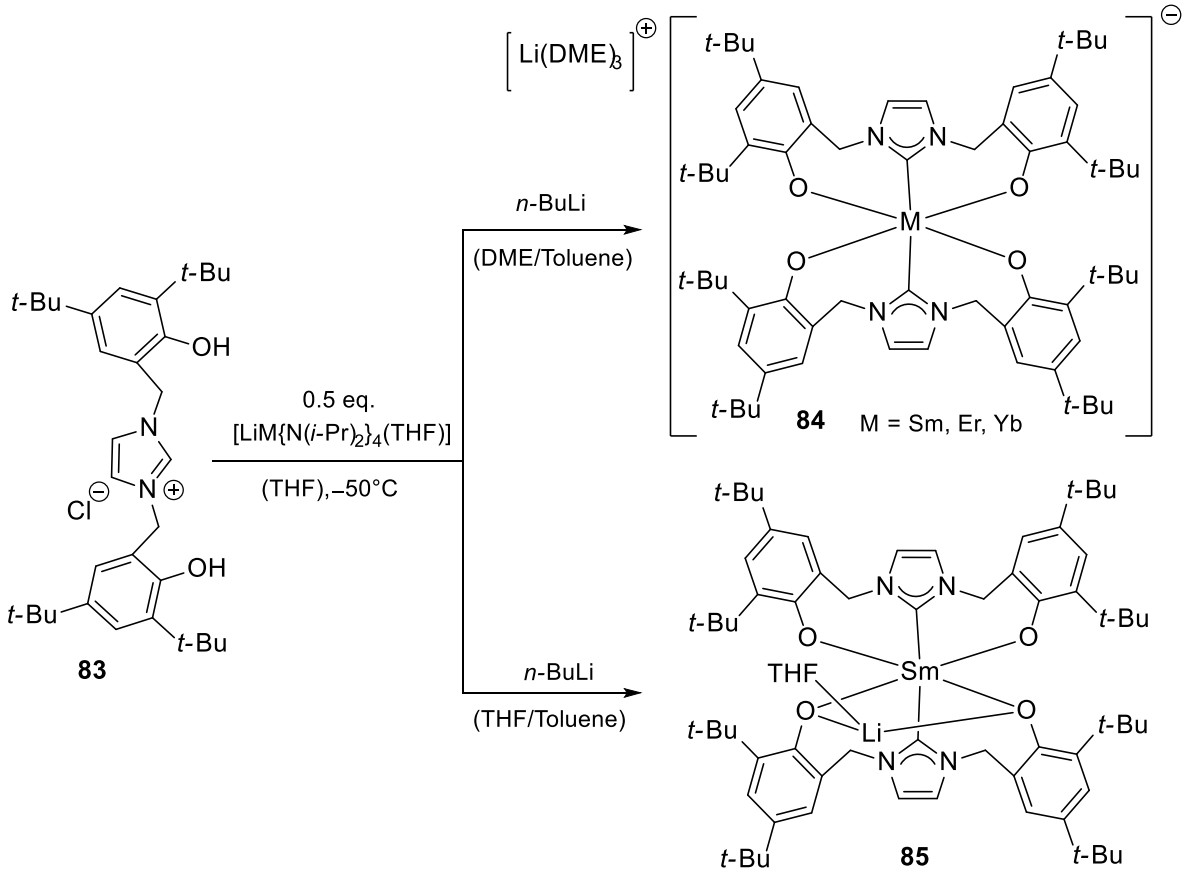

Scheme 1.3.8. Lanthanoid complexes bearing tridentate 1,3-bis(3,5-di-*tert*-butyl-2-hydroxybenzyl)-functionalised NHC ligands.

Remarkably, Shen noted that the solvents used for the crystallization had a significant effect on the solid state structure of the obtained complexes. Anionic [ML$_2$][Li(DME$_3$)] (M = Sm, Er, Y) compounds **84** are obtained upon crystallization from DME/toluene. However, in a

THF/toluene mixture the neutral species **Sm-85** incorporating alkali metal cation is favoured. Also the reaction of corresponding ligand precursor with $SmN"_3$ and NaN" in a 2:1.3 molar ratio affords the Et_2O-Na-analogue of **85**.[99] More recently, Ni and co-workers also introduced similar complexes bearing 1,3-bis(3,5-di-*tert*-butyl-2-hydroxybenzyl)-functionalised NHC ligands derived from 2,4-dihydro-imidazolium and pyrimidium analogues of tridentate NHC ligands **83**.[100]

Indenyl- and Fluorenyl-functionalised NHC complexes

Despite the evident dominance of cyclopentadienyl ligands in the coordination chemistry of lanthanides the obvious choice for additional stabilization of rare earth NHC complexes, indenyl and fluorenyl-substituted NHCs, were only introduced in 2006.[67] For the preparation of binuclear complex **86** Downing *et al.* used a twostep procedure (Figure 1.3.1). The group first generated corresponding potassium NHC adduct of their ligand and subsequently, reacted it with yttrium alkyl $[Y\{(CH_2SiMe_3)\}_3(THF)_2]$, which acts as internal base for the removal of the remaining acidic cyclopentadienyl proton.[101] Concomitantly, Cui and co-workers reported the closely related REE NHC complexes **87** supported by indenyl-substituted NHC ligand *via* double deprotonation with $[LiCH_2SiMe_3]$ and $[\{Ln(CH_2SiMe_3)_3\}(THF)_2]$ (Figure 1.3.1).[102] They later expanded this compound class by introducing more rare earth cations as well as fluorenyl-substituted NHC ligands.[103]

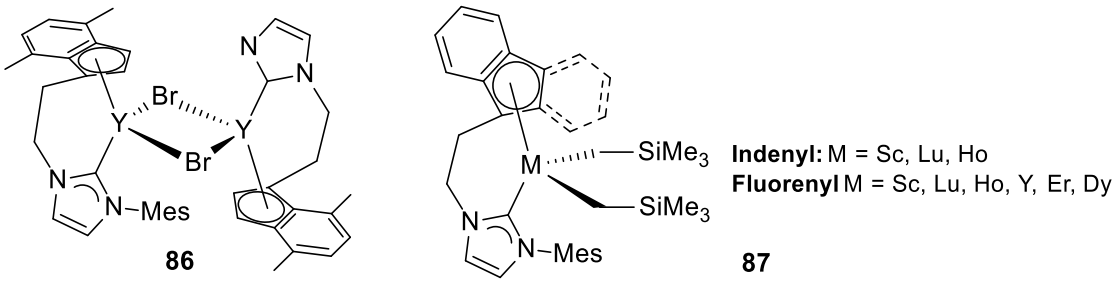

Figure 1.3.1. Reported indenyl- and fluorenyl functionalised NHC complexes of rare earth metals.

Cyclometallated NHCs

Several reports describe C–H activation of ligand side chains by metal-alkyl groups in rare earth NHC complexes.[89, 104] For example, Okuda presented cyclometallated rare earth compounds **88-89** formed by *ortho*-metalation of a methyl group of *N*-mesityl substituent by rare-earth alkyls $[MR_3(THF)_2]$ ($R = CH_2SiMe_3$) in THF at RT (Scheme 1.3.9, **a**).[104] Furthermore, an unusual synthesis of formally aryl-metallated rare earth CCC-pincer bis(NHC) complexes **91** was reported by Cui.[105] The corresponding ligand precursor **90** is hereby deprotonated with *n*-BuLi *in situ* in the presence of MCl_3 (Scheme 1.3.9, **b**). Unfortunately, the mechanism of the exchange of chlorides to bromides is unknown.

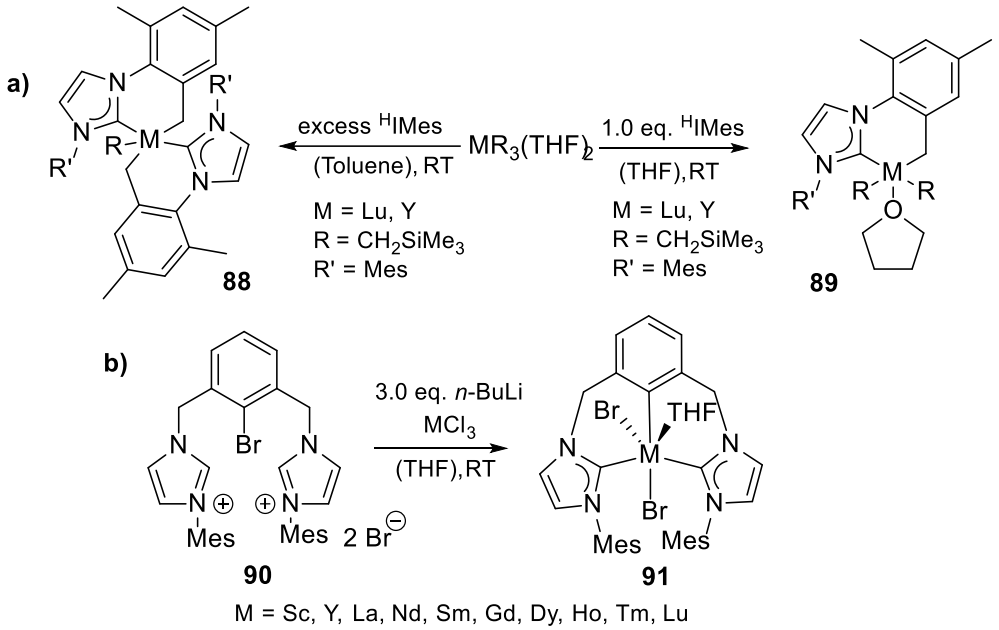

Scheme 1.3.9. a). C–H activation by rare earth alkyls, **b).** CCC pincer NHC complexes of REE.

1.3.2 Structure and Bonding

1.3.2.1 General Trends

A typical M–C_C bond length for yttrium and scandium NHC compounds lies between 2.1 Å and 2.4 Å. Extraordinary long metal–carbene bonds can be observed in the yttrium compounds **72a-c** (Scheme 1.3.5) and especially in **Y-68a** (2.588 Å, Scheme 1.3.4).[93c, 94] The ^{13}C NMR chemical shifts for C_C are observed in the range from 170 to 220 ppm with the highest resonance frequencies for saturated NHC compounds (e.g. **Y-75c**, Scheme 1.3.5, $\delta(C_C)$ = 216 ppm).

As expected, metal–NHC bonds in lanthanoid complexes are significantly longer due to greater ionic radii of cations. Typical bond lengths lie between 2.4 Å and 2.8 Å, and according to the lanthanoid contraction a general tendency of declining bond lengths from cerium to lutetium can be observed. The paramagnetism of lanthanoids often impedes an unambiguous characterization of their NHC compounds by NMR spectroscopy. Therefore, only few values for C_C resonances lying on the average around 200 ppm are reported. Interestingly, the paramagnetism of these compounds can also result in extreme shift of the chemical shift for C_C as seen for previously mentioned europium compound [(^{H}IMe)Eu(THD)$_3$] **Eu-57** ($\delta(C_C)$ = 46.5 ppm, Scheme 1.3.1, **b**). Moreover, particularly high chemical shifts have been detected for cerium(IV) compounds (e.g. 237.4 ppm for **Ce-72cCl**).[106]

1.3.2.2 Bonding

The exact bonding situation in metal NHC complexes is still under discussion[107], but detailed calculations suggest that for electron rich late transition metals the π-interaction between metal and NHC contributes up to 25-30 % of the total orbital interaction.[108] For the electron-deficient early transition and f-block metals, particularly those in high oxidation states, NHCs ligands are normally viewed as pure σ-donors. However, many compounds exhibit unusual close carbene–metal distances, which may be explained by π-interactions. Few computational studies have been conducted to clarify the nature of the carbene–metal bond in rare earth compounds.

By comparing titanium and yttrium tris(alkoxy-NHC) complexes **68a** (Scheme 1.3.4), Arnold and co-workers were the first to conduct such studies. In comparison to the titanium complex **Ti-68a** the yttrium compound **Y-68a** shows unusually long metal–carbene bonds. The comparison of the bond distances after the correction by ionic radii implied a backbonding contribution from the titanium(III)-d^1-metal.[93c] However, detailed investigations by DFT calculations suggested rather that the smaller size and therefore more polarizing nature of the titanium centre is the reason for this observation.[109]

Maron and Bourissou conducted a detailed computational investigation of the mono- and bis-adducts of $SmCl_3$ and the model carbene ligands **A-D** (Figure 1.3.2, **a**). The calculated orbitals showed that a carbene–Sm bond is formed by carbene-to-metal σ-donation with marginal chlorine-to-carbene back-donation interactions, whereas direct metal-to-carbene π-donation was not observed.[110]

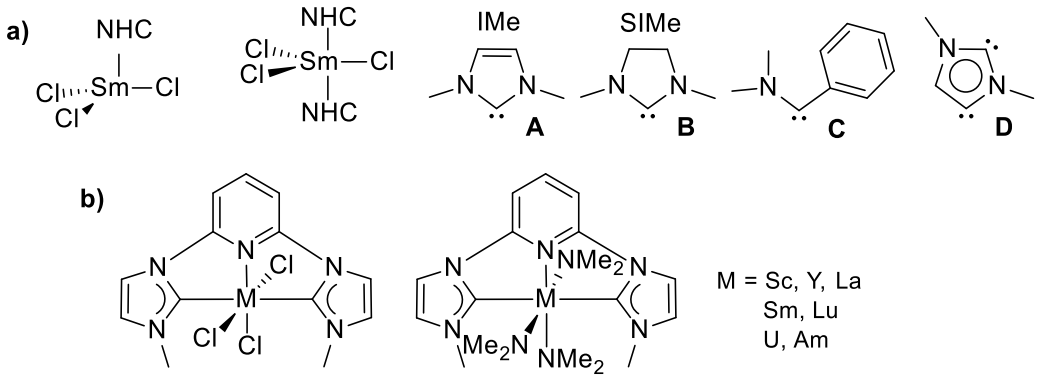

Figure 1.3.2. Model compounds for examination of the bonding mode by Maron and Bourissou.[110-111]

The same authors analysed the bonding properties of the complexes deriving from tridentate ligand 2,6-bis(methylimidazol-2-ylidyl)-pyridine and REE as well as actinoids trichlorides, triamides or the bare M(III) cations (Figure 1.3.2, **b**). The calculations showed stronger coordination energies in octahedral geometries for more electron-deficient metal fragments. As no $C_C \rightarrow M$ π-donation and no metal-to-NHC back-donation were observed, also this study

supports the assumption of only ionic bonding in these complexes.[111] Frequently observed distortion of in-plane and out-plane angles between metals and NHC also confirms that NHCs bind *via* polarized electrostatic interaction to this electropositive metals.[54, 63, 86c, 87]

Interestingly, in the same theoretical investigations Maron and Bourissou predicted an intrinsic preference of tridentate 2,6-bis(methylimidazol-2-ylidyl)-pyridine ligand for La over U and for Sm over Am (for bare ions).[111] In contrast to these theoretical expectations Mehdoui *et al.* were able to show experimentally the preference of ^{Me}IMe for U(III) instead of Ce(III) by addition of free NHC to an equimolar solution of [U(Cp*)$_2$I] and [Ce(Cp*)$_2$I] in toluene (Scheme 1.3.10).[86d] The formation of uranium(III) adduct **U-92** is more favourable both at room temperature (molar ration 80:20) and at –60 °C (molar ratio 90:10). The same behaviour was observed during the addition of ^{Me}IMe to [U(C$_5$H$_4$(*t*-Bu))$_3$] and [Ce(C$_5$H$_4$(*t*-Bu))$_3$] at -60 °C (U:Ce = 90:10) as well. Furthermore, crystallographic comparison of all four complexes shows that despite greater ionic radius of U(III), shorter U–C$_C$ bonds are observed (0.03 Å on average).[109b] Along with competition experiments these deviations suggest stronger, more covalent interactions between actinoids and NHC ligands than for lanthanoids. In a subsequent study Arnold *et al.* confirmed this by comparing the electronic structures at optimized geometries of analogues Ce(IV) and U(IV) NHCs using Mayer and natural analyses.[106]

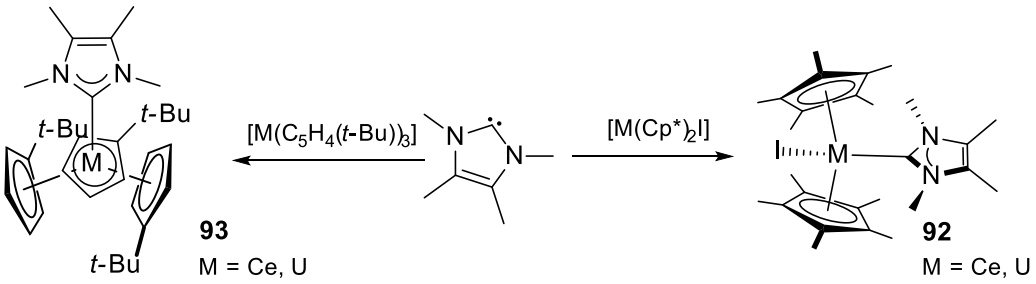

Scheme 1.3.10. NHCs in actinide(III)/lanthanide(III) differentiation.

1.3.3 Reactivity

Although rare earth metal complexes with NHC ligands are no longer laboratory curiosities, studies of their reactivity are still quite rare.

1.3.3.1 Stoichiometric Reactions

Already in their pioneering work in 2003 Arnold *et al.* started to probe the reactivity of the metal–NHC bonds in yttrium complexes by monitoring $^1J_{YC}$ coupling in ^{13}C NMR and observing that only strong donors such TMEDA and triphenylphosphane oxide leads to dissociation of the carbene.[62] Later the same group tested the liability of Y–NHC bond in bis(carbene)

complexes **Y-58** in a series of competition experiments with triphenyl- und trimethylphosphine oxides. Although the reaction of bis(trimethyl)silylamido analogue results only in intractable products, the dichloro ligated analogue of **Y-58** yields simple triphenyl- und trimethylphosphine oxide adducts with one remaining carbene attached.[64]

Arnold also reported the treatment of samarium analogue **Sm-58** with potassium-intercalated graphite (KC_8) in DME yielding dimeric compound **96** containing μ-OMe fragments as a product of DME cleavage. Moreover, interesting bimetallic dimers $[(NHC)M(N")(\mu\text{-}N")K(DME)]_2$ **94** with K-bound anionic dicarbene (NHDC) binding simultaneously to yttrium or samarium centres in "normal fashion" are observed by the reduction of compounds **Y-** or **Sm-58** through the addition of an equimolar amount of potassium naphtalenide (Scheme 1.3.11).[7] Quenching this yttrium dimer with electrophilic Me_3SiCl in THF affords a monomeric complex **95** obtained by backbone silylation and KCl elimination. The same kind of reactivity of alkali metal bonded anionic dicarbenes have been already described in Section 1.2.1.

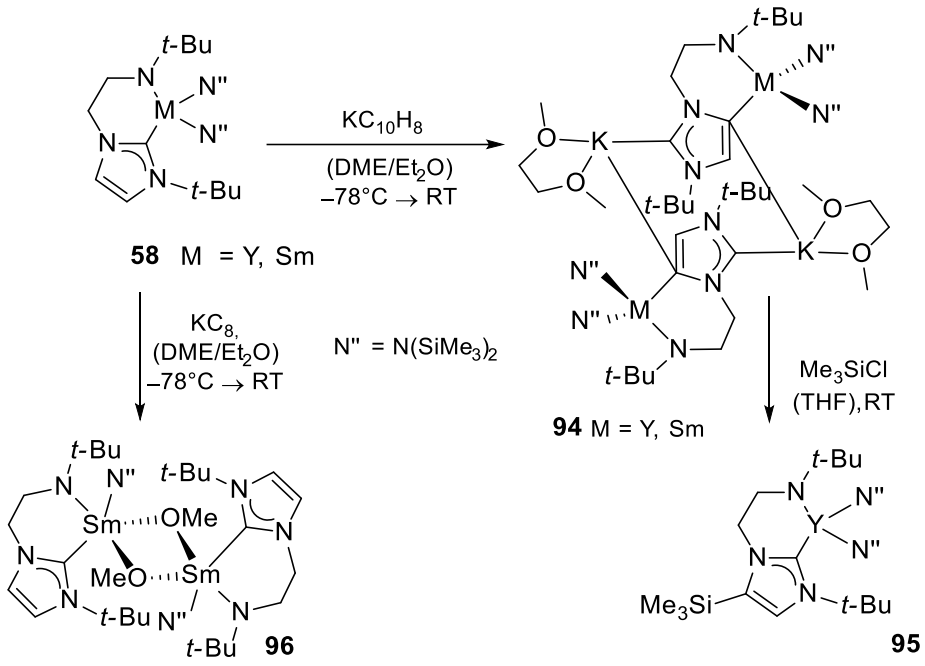

Scheme 1.3.11. Reactions of rare earth complexes bearing amido functionalised NHCs with KC_8.

Another example of regioselective C5 silylation was observed with **Nd-58**. Addition of Me_3SiI to this complex results in the formation of the backbone-silylated Nd NHC dimer **97** (Scheme 1.3.12).[90b] The authors speculated about the mechanism by proposing a nucleophilic substitution of a silyl amide ligand in the first step, followed by the deprotonation of the backbone by a liberated silyl amide. Subsequently, similar to other anionic abnormal carbenes (Section 1.2.1), these compounds would be immediately intercepted by electrophiles such as $[SiMe_3]^+$. Further reduction of **97** with KC_8 proved unsuccessful and yielded only niobium analogue **Nd-95** in low yield. Interestingly, by comparing the crystal structures of **Nd-58** to its

silylated analogue **Nd-95**, the influence of $SiMe_3$ is evident in elongation of Nd–C_C bond for silylated compound.[90b]

Furthermore, **Nd-97** reacted in a salt elimination reaction showing the exchange of iodine by azide as well as by an aryl amide.[90b, 112] Moreover, starting from **Nd-58** the synthesis of unique heterobimetallic rare earth complexes with direct metal–metal bonds have been achieved by applying [Ga(N(Ar)CH)$_2$][K(TMEDA)] (Ar = 2,6-diisopropylphenyl, Dipp) or K[CpFe(CO)$_2$] as reagents for displacement of iodine.[113]

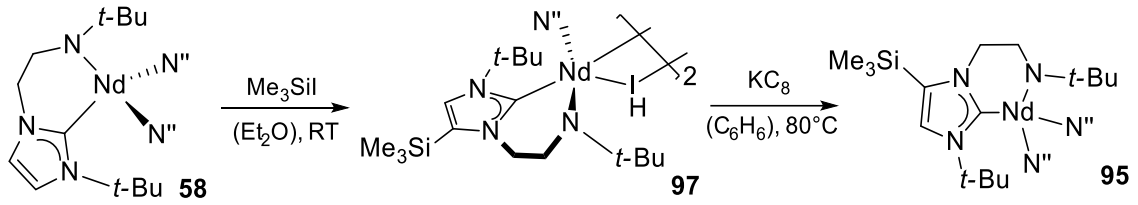

Scheme 1.3.12. Reactivity of neodymium amido-functionalised NHC complex.

Although the reductive chemistry of **Nd-97** was unsuccessful, later the same group was able to achieve an entry in redox chemistry of NHC complexes with lanthanoids by oxidizing the Ce(III) tris(alkoxy-NHC) complex **68a**.[93a, 106] Ce(IV) compound **98a** is obtained by a treatment of **68a** with benzoquinone followed by subsequent ligand redistribution (Scheme 1.3.13). Further improvement concerning the yield of the reaction can be achieved by the addition of another equivalent of corresponding potassium ligand adduct **42a**. Also the usage of XeF_2 and [Fe(Cp)$_2$][OTf] as oxidants is possible. The ^{1}H NMR spectrum of **98a** indicates fast fluxional behaviour of the pendant carbenes at RT. The decrease of the temperature results in decoalescence of ^{1}H NMR signals at –43.15 ºC and finally in the appearance of three sets of proton resonances at –75.15 ºC. Furthermore, the treatment of **98a** with two equivalents of 9-borabicyclo[3.3.1]nonane (9-BBN) confirms its bulk structure by producing the borane adduct **99a** *via* interception of pendant NHCs with borane.[93a] More recently, the oxidation of another previously mentioned cerium alkoxy-tethered NHC complex **Ce-72c** was also conveniently conducted at RT with Ph_3CCl yielding **Ce(IV)-72cCl**, which is also accessible by oxidation of CeN"$_3$ with Ph_3CCl and subsequent addition of **71c**.[106]

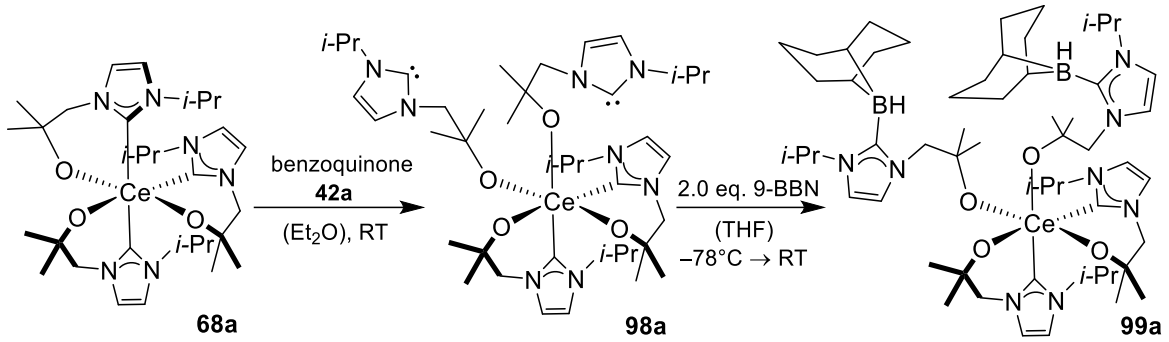

Scheme 1.3.13. Oxidation of **Ce-68a** followed by ligand redistribution.

Highly interesting C–Si and C–C bond formations resembling the reactivity of frustrated Lewis pairs by addition-elimination reactions across the M–C_C bond have been observed for Ce/Y amido (**72**) and Sc/Y alkyl complexes (**74c** and **75c**).[5a, 95a] The treatment of these compounds with polar organic E–X substrates (E = silyl, phosphinyl, stannyl, boranyl; X = halide, azide) produces compounds displaying E–NHC and M–X bonds (Scheme 1.3.14, **a**). The driving force of this reaction is a formation of more stable M–X bonds. The back-conversion to starting complexes can be pushed by thermolysis resulting in liberation of heteroatom-linked hydrocarbon, followed by conversion of remaining halide complex to the starting material *via* salt metathesis.[5a]

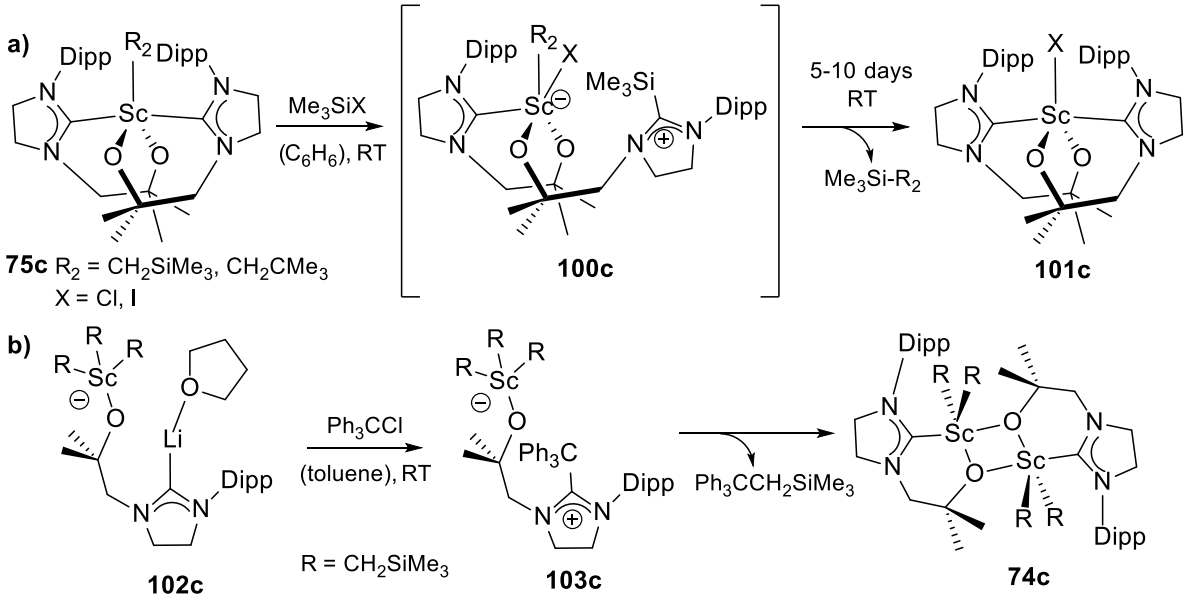

Scheme 1.3.14. a). C–Si bond formation by addition-elimination reactions on the example of **75c**. **b).** C–C bond formation by addition-elimination reaction at heterobimetallic Sc-Li compound **102c**.

Unfortunately, the complexes mentioned above cannot cleave even the weakest carbon–halogen bonds by addition across M–C_C bond. Only the deployment of lithium carbene “ate”

complex **102c** yields the desired C–C bond formation by using Ph_3CCl. Hereby, $Ph_3CCH_2SiMe_3$ and bimetallic Sc complexes **74c** are formed (Scheme 1.3.14, **b**).[5a]

Using the same frustrated Lewis base/acid type of reactivity the activation of acidic N–H and C–H bonds was also achieved.[5b] The cerium complex **69a** activates various alkynes RC≡CH (R = Me_3Si, Ph) at RT yielding a zwitterionic tris(cyclopentadienyl) cerium complexes with incorporated protonated imidazolium group (**106a**, Scheme 1.3.15, **a**). The authors proposed that **106a** is obtained due to ligand redistribution within an initially formed intermediate product **104a**, which is not preferable due its lesser degree of steric protection. This explanation would imply that the second redistribution product **105a** should be also formed but since it was not obtained, it probably oligomerises or polymerizes due to its steric unsaturation. Noteworthy, **106a** can also be also prepared by a direct reaction of **69a** with cyclopentadiene. Further investigations of the same reaction with Y or Sc analogues did not result in activation of alkynes or CpH, although it appears that a dynamic equilibrium of reversible C–H addition exists. These observations again confirmed the very often observed strong dependence of the reactivity of REE complexes on the size and Lewis acidity of the applied metal cation.

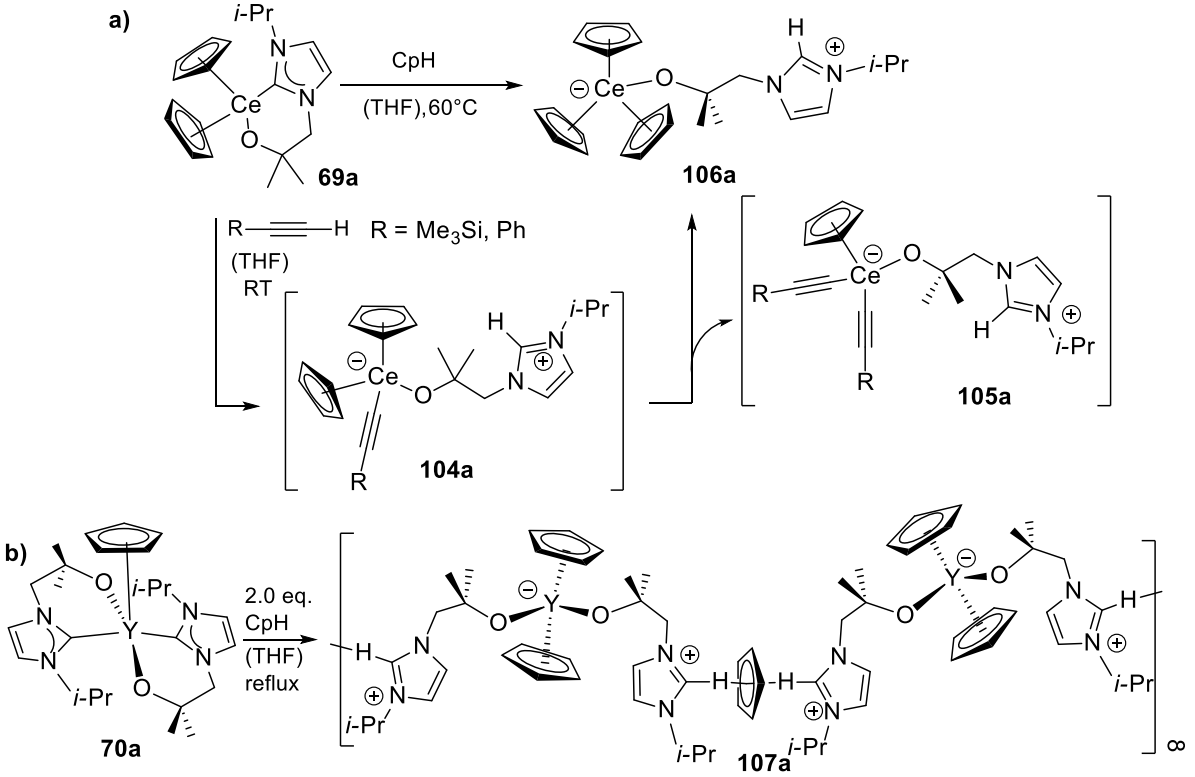

Scheme 1.3.15. Cleavage of acidic C–H bonds by rare earth NHC complexes.

Additionally, Y complex **70a** reacts with cyclopentadiene yielding polymer $[YCp_2(LH)_2(Cp)]_\infty$ **107a** (Scheme 1.3.15, **b**), which contains cyclopentadienyl moieties trapped between two imidazolium units though unusual C–H···(π-Cp) interactions. Interestingly, neither indene nor

fluorene react in this manner with **70a** despite their higher C–H acidity. Moreover, although pyrrole, indole and diphenylacetophenone form readily addition products with **Y-69a** and **Y-70a** due to formation of thermodynamically stable Y–O and Y–N bonds, the same reactions are not observed for cerium analogues. Since the experiments were conducted in THF, a high coordinating ability of this solvent to cerium or lesser Lewis acidity of the respective cation may be the cause for the inertness of the cerium complexes.

Another interesting entry in the reactivity of REE NHC complexes was made by Arnold by reporting an insertion of CO_2 into **M-72c** (M = Y, Ce) and **Ce-76b**. Unfortunately, the obtained insoluble products could not be properly characterised. An equally insoluble complex is formed by treating **Ce-76b** with COS. In contrast to **Ce-76b**, **Ce-72c** does not react with COS supporting the assumption that a labialization of carbene is necessary for binding such reagents.[114] However, the Sc NHC complex **68a** readily activates three equivalents of CO_2 in a "frustrated Lewis pair" reactivity type forming an insoluble polymeric product as well, which was characterised by elemental analysis, FT-IR spectroscopy and solid state NMR. The isolation of soluble insertion products is only possible in case of the reaction with CS_2 yielding **108a** and **109a** containing dithiocarboxylated imidazolium groups (Scheme 1.3.16).[93b]

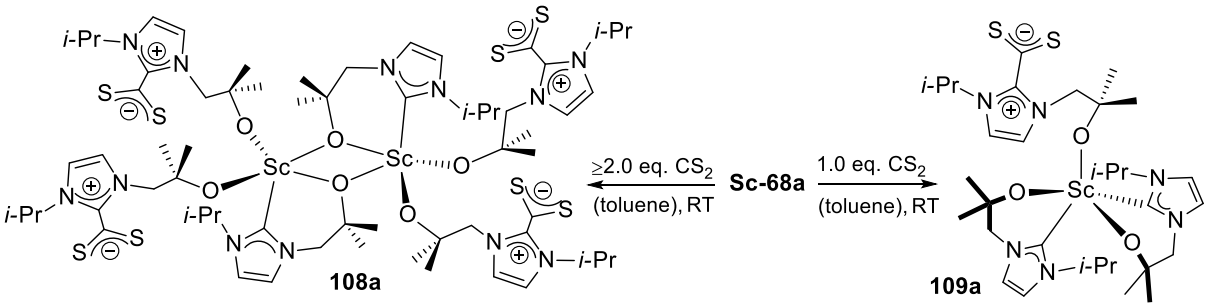

Scheme 1.3.16. Activation of carbon disulfide by scandium NHC complex **68a**.

1.3.3.2 Catalytic Applications

With the exception of polymerization reactions, the search for catalytic applications of REE NHC complexes is still in its infancy. However, some preliminary results show high potential for future exploration.

Polymerization reactions

For polymerization reactions with REE complexes ligated by (mono)carbenes the role of NHC was simply assigned to dissociation from the complex in order to vacate a coordination site.[86e] Therefore, further optimization of such systems through tuning of the NHC ligand is of limited use (e.g. using more bulky or less electron donating NHCs to enhance dissociation).

On the other hand, poly(dentate) NHCs are more promising candidates for these studies. In the past decades a number of rare earth NHC complexes have been tested revealing some

general trends. E. g., Wang *et al.* applied a series of complexes with fluorenyl and indenyl tethered NHCs **87** in various catalytic polymerization reactions.[102-103, 103c, 115] Presumably due to lower Lewis acidity the Dy and Er compounds were found to be inactive.[103c] For other systems the larger atomic radii corresponds to greater catalytic activity (Ho>Y>Lu>>Sc).

Also in the series of complexes **91** the catalytic activity in polymerization of isoprene strongly depends on the metal centre.[116] The largest (La) and the smallest metal centres (Sc, Tm, Lu) as well Sm (which is presumably reduced to its inactive divalent species by activator system AlR_3 (R = Et, Me, *i*-Bu)/[Ph_3C][$C(C_6F_5)$]) are inert. For the remaining compounds the highest activity corresponds to bigger cations as well (Nd>Gd≈Dy>Y≈Ho). Based on NMR data the authors suggested a novel yttrium hydrido aluminate cation [$LY(\mu\text{-}H)_2Al(i\text{-}Bu)_2$]+ (L = CCC-pincer NHC) cation as active species, hereby giving the NHCs a more important role than that of a space filling, easily replaceable ligand. All catalysts exhibit excellent *cis*-1,4-selectivity, maintaining it even up to 80 °C and therefore proving good stabilizing properties of NHCs.[116]

Cui and Chen also tested fluorenyl functionalised **M-91** (M = Y, Lu) for metal-mediated coordination-addition polymerization of biomass-derived renewable methylene butyrolatones.[103b] Both complexes exhibit exceptionally good activity for the polymerization of racemic γ-methyl-α-methylene-γ-butyrolactone ($_\gamma$MMBL) at RT in DMF. The authors proposed a mechanism starting with the initiation by rapid reaction of the pre-catalysts with DMF yielding compounds with dimethylamide and hydride groups as active species. As propagation mechanism they suggested a fast intramolecular Michael addition within the catalyst-monomer complex leading to eight-membered ester-enolate chelate complex. The subsequent ring opening though ligand exchange of the ester group by a new monomer is hereby the rate determining step (Scheme 1.3.17, **a**).

Yttrium complex **58** have been also employed for the ring opening polymerization of D- and L-lactide producing polymers with a low polydispersity and high heterotacticity. In **58** the yttrium cation was proposed to act as the Lewis acid and the free NHC as the Lewis base (Scheme 1.3.17, **b**).[117] Again, due to the limited role of NHC in the overall reaction further modification of the ligands in this system is expected to be of limited value. Similar systems, [(^{Me}I(*i*-Pr))Sm(Cp*)$_2$] and [(^{Me}I(*i*-Pr))Sm(C_5H_4(*t*-Bu))(C_3H_5)], have also been proposed to experience a catalytic initiation through a loss of an NHC ligand to start the polymerization of methylacrylate.[118]

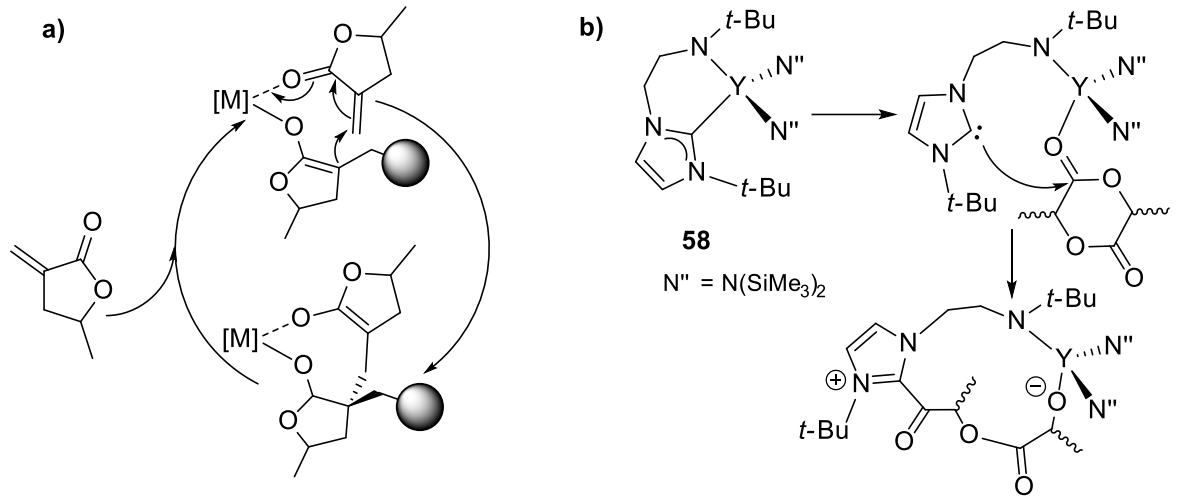

Scheme 1.3.17. Proposed propagation mechanisms for **a)** coordination-addition polymerization of γMMBL by *ansa*-half-sandwich complex **87**, **b)** ring opening polymerization of lactides by **Y-58**.

Ni also proposed that in ROP of L-lactide saturated analogues of bimetallic bis(phenolate) NHC complexes **85** are activated by breaking the metal–NHC bond hereby allowing monomer coordination-insertion mechanism to proceed as propagation reaction.[100a] Noteworthy, the potassium incorporated saturated analogue **Nd-85^{S}** is a more efficient pre-catalyst than the corresponding lithium compound, may be because of a possibly easier access to the metal centre due to the bending of the ligand framework by bigger K cation. Also here the polymerization activity depends on the size of rare earth cations (Y<Sm<La<Nd). More recently the same group also investigated similar rare earth complexes bearing potassium bridged bis(phenolate) pyrimidinium based NHC ligands in polymerization of *n*-hexyl isocyanate.[100b] As expected, the catalytic activity is severely affected by the radius of rare earth metal, solvent, polymerization temperature and the structure of the ligand. Interestingly, the pyrimidinium-bridged REE complexes are inactive, suggesting that NHC moiety plays an important role in initiation of the polymerization.

Other Catalytic Reactions

Some unusual catalytic reactions were also studied with rare earth NHC complexes. For example, the enol-functionalised NHC complexes **78** were employed for atom-economical synthesis of multisubstituted guanidines by an addition of primary and secondary amines to carbodiimide.[96] The Yb analogue was found to be the most active (probably due to steric reasons and its size) and tolerant towards functional groups.

Furthermore, the series of complexes **65b** was applied for the catalytic synthesis of propiolamidines by addition of C–H bonds of terminal alkynes to carbodiimides.[91] Most atypically, in this case the size of the metal cation did not have a significant influence on the catalytic activity.

Later, the same group also examined related complexes **65a,c** for catalytic activity toward the addition of the phosphine P–H bond to heterocumulenes (hydrophosphination).[92] Their results showed high activity in promoting the formation of phosphaguanidines, phosphaureas, and phosphathioureas with low catalyst loading at room temperature. More recently, hydrophosphination of alkenes and alkynes was also investigated in detail for structurally simple but easily recyclable bis(NHC) amido complexes $Yb(NHC)_2N"_2$ (NHC = ^{Me}IMe, ^{H}I(*i*-Pr)).[119] Also in this study the authors could successfully show the universality of this procedure by testing a wide range of substrates. Since the use of THF stabilized analogue of $[(THF)_2YbN"_2]$ showed inferior performance in this catalytic reaction, the important influence of stabilizing donating abilities of NHCs could be proven again.

Furthermore, divalent ytterbium silyl amide complexes $[(^{H}IMes)YbN"_2]$ and $[\{^{Me}I(i\text{-Pr})\}YbN"_2]$ were employed as catalysts for the catalytic cross-dehydrogenative coupling of amines with silanes.[120] Remarkably, before this work no efficient catalysts for coupling of $PhSiH_3$ with bulky amines such as HN", $HN(i\text{-Pr})_2$, $(Dipp)NH_2$ were known. Interestingly, the reaction in the presence of $[Yb\{N"_2(THF)_2]$ and bidentate donor $Me_2NCH_2CH_2NMe_2$ results only in sluggish catalysis thereby indicating the key role of NHC as a stabilizing σ-donor. Further work on this type of reactions was recently done by Sadow and co-workers who synthesized NHC adducts of divalent samarium and ytterbium alkyls $[\{^{H}I(t\text{-Bu})\}M\{C(SiHMe_2)_3\}]$ which are similarly active in catalytic dehydrocoupling of amines and organosilanes.[121] The investigations on deactivation of the catalyst indicate a key role of ^{H}I(*t*-Bu) dissociation suggesting that the usage of bidentate hemilabile carbene ligands could be advantageous in this case.

1.4 *N*-Heterocyclic Carbene Complexes of Silver(I) and Gold(I)

Coinage metal NHC complexes have been extensively studied due to their structural variety, high stability, easy preparation and numerous applications.[9a, 19d, 122] Among them, Ag(I) NHCs have become the most studied compounds as they are often used for transfer of NHC to other transition metals.[9a, 123] For many chemists the synthesis of NHC compounds of Ag(I) serves only the transmetallation purpose, but recently, silver NHCs gained on importance in their own right as photoluminescent materials[8] as well as antimicrobial and antitumor agents.[8b, 9] Au(I) NHCs can be easily prepared using the silver transfer route and over the years a plethora of structurally very versatile compounds have been reported.[122] Although Au(I) NHCs have been deemed uninteresting for a long time, since the first report of Au(I) NHC catalysed reaction in 2003[124] the number of described Au(I) complexes with good catalytic activities steadily increased resulting virtually in a Gold Rush in the past decade.[11] Furthermore, gold NHC compounds exhibit very interesting luminescent properties[10, 125] and show high potential for applications in material and medicinal chemistry[12].

1.4.1 Ag(I) NHC Complexes: General Synthetic Methods and Characterization

1.4.1.1 Synthesis

Generally, there are three main routes for the synthesis of silver NHCs.[9a, 123] The first one includes preparation of a free NHC which is then reacted with a silver salt (route **a**, Scheme 1.4.1). This method was firstly applied by Arduengo in 1993, who treated ^{H}IMes with $Ag(O_3SCF_3)$ to obtain the corresponding bis(NHC) complex.[126] While this method can be utilized for a plethora of compounds the conditions required for the generation of free carbenes can facilitate unwanted deprotonation of other acidic protons in the ligand framework, therefore causing its decomposition.

An alternative method for the preparation of Ag(I) NHC compounds is the deprotonation of the respective azolium salts in the presence of silver salt using an external base (route **b**, Scheme 1.4.1). Lin and Wang described this method by using basic phase transfer catalyst in the presence of AgBr and a benzimidazolium salt.[127] Unfortunately, this procedure did not lead to the successful synthesis in other cases.[128]

In the same study Lin and Wang also introduced the third possible way for generation of Ag(I) NHCs by reporting the reaction of a benzimidazolium salt of the mild internal base Ag_2O in

CH_2Cl_2 (route **c**, Scheme 1.4.1).[127] Hereby they paved the way for the synthesis of numerous compounds obtained by this facile and nowadays the most widely applied synthetic protocol.

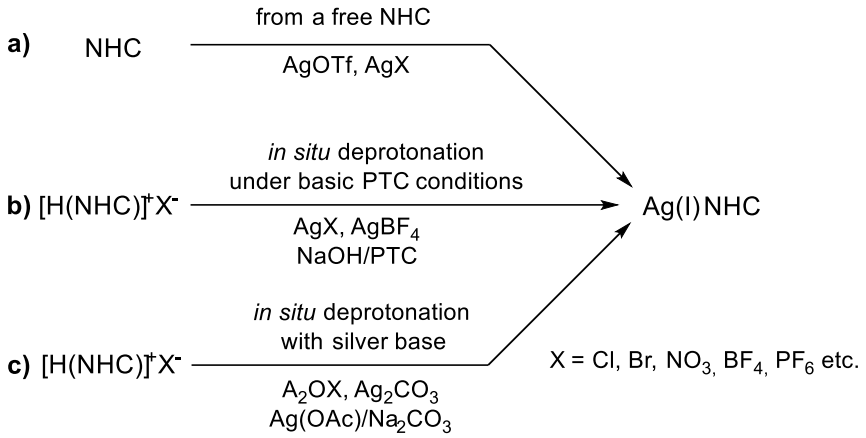

Scheme 1.4.1. Synthetic methods generally applied for the generation of Ag(I) NHC complexes.

The advantages of the Ag_2O technique are enormous and can be summarize as follows[123]:

- Reactions can be carried out under aerobic conditions
- No additional base is required
- No dried or degassed solvents are necessary
- Ag_2O is very mild base, which deprotonates almost exclusively the C2 position of the imidazolium salts and ignores other acidic positions

Also other silver bases such as Ag(OAc) or Ag_2CO_3 can employed, however, to some extent they require longer reaction times.[128-129] Generally, bis(imidazolium) salts react slower with Ag_2O than mono(imidazolium) salts.[9a, 128] Also the reactions with bulkier ligands proceed slower than with less sterically demanding substituents; in some cases with especially high steric hindrance of the ligand higher reaction temperatures are required instead of the “normal” procedure at RT[128]. Moreover, functional groups have been reported to affect the reactivity *via* this method as well.[33, 130]

The fact that silver NHC complexes can be synthesized in water using Ag_2O route suggests that the deprotonation and formation of carbene complexes proceed *via* a concerted mechanism.[9a] More detailed DFT calculations in order to understand the mechanism of the reaction of Ag_2O with *N,N'*-dimethyl imidazolium iodide in CH_2Cl_2 have been conducted by Peris, who has shown that the most favourable pathway for generation of Ag(I)-NHCs consists of the deprotonation and metalation of two imidazolium moieties in two steps (Scheme 1.4.2).[131] The first deprotonation of the C2 position of one of the imidazolium cations is driven by the difference in p*K*a value between $[NHC–H]^+$ and $[Ag_2–OH]^+$ acids. Additionally, the formation of a strong Ag–C bond contributes to overall stabilization of the first step. Notably, the second imidazolium salt assists the formation of the first silver NHC by C2–H···OAg

hydrogen bond. In the second step the driving force is almost entirely the formation of another Ag–C bond, since the p*K*a of $[AgOH_2]^+$ is very close to that of the imidazolium cation. Therefore, the deprotonation of the second $[NHC–H]^+$ by AgOH is an almost thermoneutral equilibrium that does not contribute to the overall thermodynamic stabilization of the system (>70 kcal·mol^{-1}). Notably, all of the steps in this mechanism have also very low Gibbs activation energies.

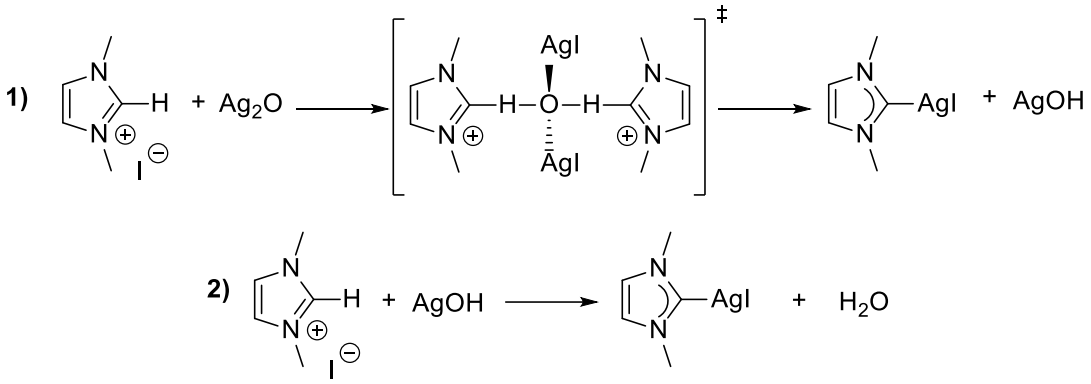

Scheme 1.4.2. The most favourable mechanism of the formation of Ag(I) NHC compounds in CH_2Cl_2 obtained by DFT calculations.

The Peris's results may explain some experimental observations described above, e. g. the slower kinetics of the deprotonation of poly(imidazolium) salts.[131] Because the formation of the first Ag NHC is assisted by a second imidazolium salt, topological restrictions on the poly(imidazolium) compounds may slow down the reaction.

1.4.1.2 Structural Trends and Properties

The structures of Ag(I) NHC complexes in the solid state are very diverse and quite complex, especially when halide anions are involved.[9a] The bonding motifs can be roughly characterised in seven categories, which are depicted in Figure 1.4.1.

Reliably predicting the solid state structure of silver NHCs containing halide anions is often very difficult, since the structure is affected by several parameters such as the nature of halide, sterics and flexibility of the ligand, solvent, silver–halide and silver–silver interactions.[9a] Noteworthy, argentophilic interactions often play an important role of many diverse architectures in the solid state. For the Ag(I) NHC complexes with non-coordinating anions the structural outcome is much easier to predict: in most cases a bis(NHC) complex with a non-coordinating anion for charge balance is obtained.

The silver–carbene bond distances in characterised solid state structures range from roughly 2.06 till 2.52 Å, for bis(carbene) complexes the range is even more narrow (2.06-2.12 Å).[9a] The C–Ag–C bond angles range from a significant deviation (≈160°) till almost perfectly linear compounds (≈170°).

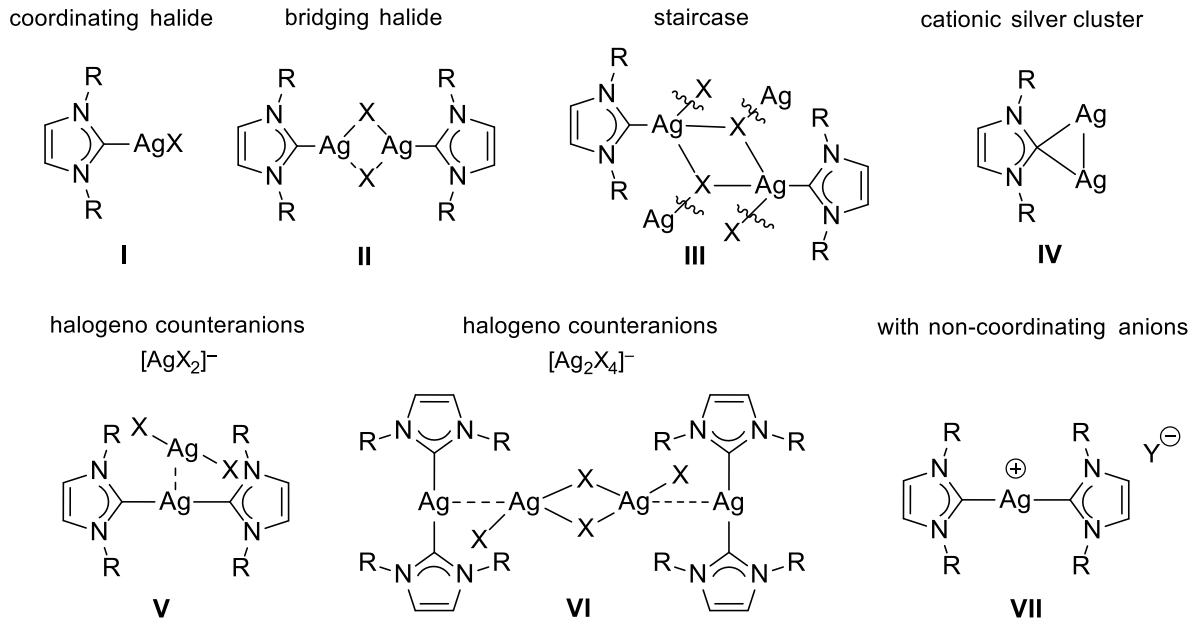

Figure 1.4.1. Bonding motifs of silver(I) NHC complexes (X = halide, Y = non-coordinating anion).

In the solution the most convenient way of monitoring the formation of silver NHC complexes is by recording NMR spectra, especially ^{13}C NMR. The resonance values for C_C in Ag(I) NHCs span quite a long range (213-163 ppm). For dinuclear bis(NHC) complexes the range for the chemical shift is much more narrow and the carbene resonance appears normally at around 180 ppm. The coupling constants for C_C to two naturally abundant silver isotopes, ^{107}Ag (51.839 %) and ^{109}Ag (48.161 %), both spin ½, amount to 180-234 Hz and 204-270 Hz respectively. However, the most compounds show no coupling pattern for the carbene resonance. There is also a significant number of Ag(I) NHC with no observable NCN resonance at all. In some cases, the appearance of C_C resonance was found to be dependent on the concentration of the sample; sharper singlets were observed in diluted samples.[128] Lin and others speculated that a fast fluxional behaviour on the NMR time scale is the reason for the variance in the appearance of carbene resonances.[127, 132] Therefore, according to this assumption, on NMR time scale static complexes show very pronounced coupling pattern to both silver isotopes which often extends to the backbone of the NHC ring. With increased fluxionally the signals broaden, eventually coalesce and finally become a sharp singlet. Moreover, such behaviour should be temperature dependent. Indeed, Bergbreiter studied the influence of the temperature on $^{13}C_C$ resonances by conducting VT NMR experiments with ^{13}C labelled silver NHC compounds.[132a] By analysing the data he postulated an equilibrium between neutral [(NHC)AgX] **110b** and cationic $[(NHC)_2Ag]AgX_2$ **110a** species (Scheme 1.4.3). Further evidence from DFT calculations and studies on ligand exchange rates with different halides supported the mechanism of the ligand exchange assisted by μ-halide and μ-NHC intermediates previously proposed by Lin (Scheme 1.4.3, **a**).[127] Interestingly, Bergbreiter and

co-workers were also able to obtain a sample of analogue cationic bis(NHC) complex with iodide as counter anion (**111**, Scheme 1.4.3, **b**). For this compound they observed no dynamic ligand exchange processes in the solution in the whole temperature range from –85 °C till +20 °C.[132a] Only the addition of **110b** promoted the dynamic behaviour, which also correlates to the concentration of mono(NHC) silver halide **110b**.

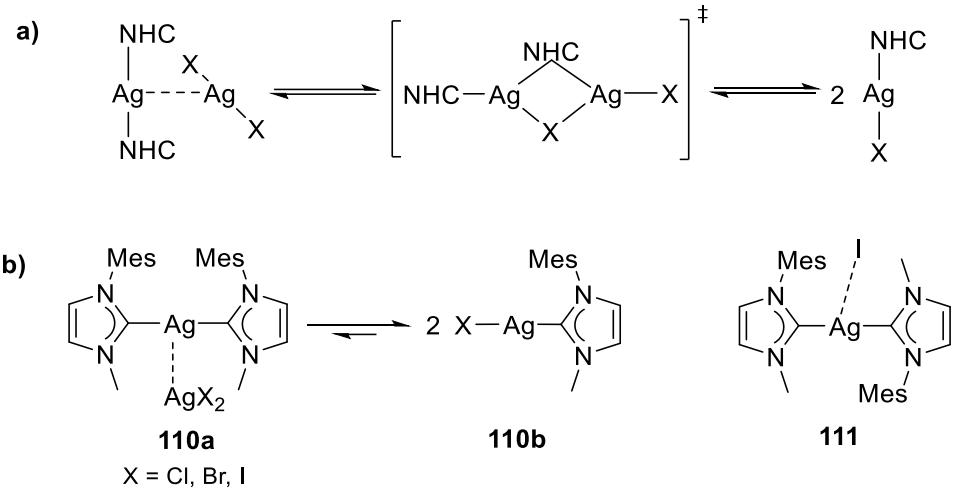

Scheme 1.4.3. Dynamic equilibrium on the ligand exchange for Ag NHC complexes containing halide anions.

The reason for the absence of carbene resonances for a significant number of compounds is however still unclear, but a fast dynamic behaviour combined with the poor relaxation of quaternary NCN carbon could account for this fact.[9a]

Theoretical calculations on Group 11 metal NHC complexes support experimental observations that the bond strength of M–C bond generally follows an order: Au>Cu>Ag.[133] Nevertheless, the bonds in Ag–NHCs are quite strong. Frenking and co-workers analysed the bonding orbitals in Ag(I) and postulated a hybridization of filled d_z^2 and s orbitals caused by Coulombic repulsion form the lone pair of the NHC.[133a] The same group also suggested that M–C bonds for coinage metals are mostly ionic in nature with non-negligible covalent interactions.[133b] Furthermore, by analysing both silver NHC halide and silver bis(NHC) complexes they followed that stabilization energy from the orbital interactions can comprise up to 30 % of π interactions suggesting quite a high degree of π-backbonding. Meyer and colleagues also confirmed these calculation by conducting theoretical studies on a series of complexes $[(TIME^{Me})_2M_3](PF_6)_3$ (M = Ag, Cu, Au; $TIME^{Me}$ = [1,1,1-tris(3-methylimidazolium-1-yl)methyl]ethane).[133c]

1.4.2 Au(I) NHC Complexes: Synthesis and Characterization

1.4.2.1 Synthetic Methods

Common methods for the synthesis of Au(I) NHC complexes include (Scheme 1.4.4)[19d, 122]: **a**) cleavage of electron rich olefins such as tetraazafulvalenes with Au(I) sources, **b**) direct reaction with a free NHC (isolated or generated in *situ*), **c**) protonation or alkylation of gold azoyl compounds previously formed from lithium azoyl and **d**) transmetallation using Ag(I) NHCs, which is recently became a very popular method.

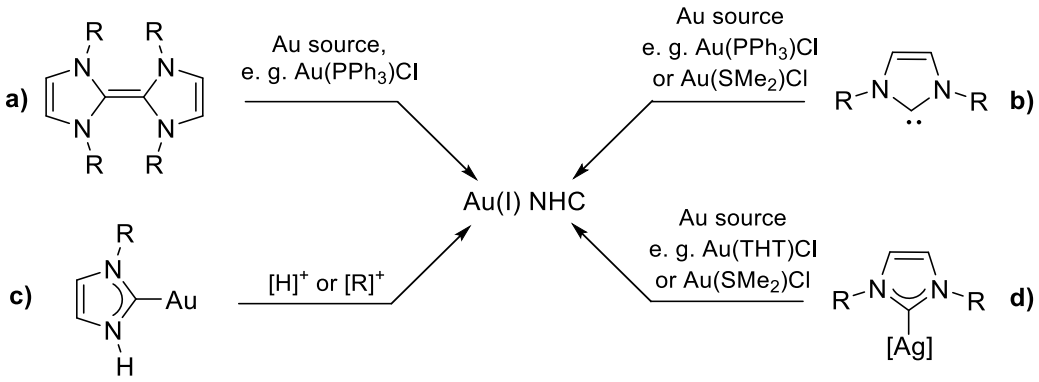

Scheme 1.4.4. General methods for the preparation of Au NHC complexes.

The transmetallation procedures can be carried out in various solvents using mostly [Au(SMe$_2$)Cl] or [Au(THT)Cl] (THT = tetrahydrothiophene) as metal sources. The driving force of the reaction is the precipitation of insoluble AgCl as well as a formation of a stronger Au–NHC bond.

1.4.2.2 Structural Trends and Properties

The ^{13}C NMR resonance values for C_C in Au NHC complexes span quite a big range and lie between approximately 156 and 252 ppm.[19d] Bis(imidazol-2-ylidene) complexes of gold(I) have generally higher values for $^{13}C_C$ chemical shifts than analogue neutral compounds of the type [(NHC)AuX] (X = halide, NHC = imidazol-2-ylidene) (ca. 180 ppm vs. ca. 168 ppm).

The geometries of the Au(I) NHC complexes can be also quite complex but generally, due to lesser propensity of gold for clustering, most of the compounds exhibit the geometries **I** and **VII** (see Figure 1.4.1, page 62)[19d, 122]. Due to a stronger Au–NHC bond the NHC complexes of gold are also generally less dynamic than their silver counterparts (for examples see Section 1.4.3). The Au–C_C distances for bis(NHC) complexes fall in the narrow range of 2.0-2.05 Å with the mean bond lengths of 2.02 Å. Furthermore, the C–Au–C bond angle does not deviate a lot from linearity staying normally in the range of approximately 170-179°.

A very interesting feature of gold complexes is their photophysical properties, which are often put into relation with intra- or intermolecular aurophilic interactions.[134] The term “aurophilicity” has been introduced by Schmidbaur in the early 1990s to describe the weak interaction between linearly coordinated monovalent $5d^{10}$ Au centres.[135] Due to relativistic effects, this leads to a mixing of gold 5d and 6s orbitals, herby resulting in the lowering the energy gap between the ground and excited states, which therefore facilitates electronic transitions.[136] By conducting DFT calculations Pyykkö predicted that NHC ligands would yield the strongest metal−metal interaction.[137] Therefore, it is not surprising that in the last decades several reports on the luminescence properties of mono- and especially polynuclear gold(I) complexes bearing NHC ligands have been published. The luminescence behaviour of Au(I) complexes supported by bis(NHC) ligands, which are mostly important for this thesis, will be discussed below.

1.4.3 Dinuclear Ag(I)-and Au(I) bis(NHC) Complexes

1.4.3.1 Structural Survey and Properties

Numerous dinuclear Ag(I) and Au(I) complexes bearing open-chain or macrocyclic bis(NHC) ligands with flexible or rigid linkers have been reported in the literature (for some examples see Figure 1.4.2). Also complexes with chiral dehydrohexitol[138] and calixarene[139] derivatives, but-2-yne-1,4-diyl[140], anionic triazone[141] or neutral diethylaminotriazinyl[142] as well ether[143] fragments as bridges have been reported. Most of the coinage metal bis(NHC) complexes show ether intramolecular or intermolecular metallophilic interactions in the solid state, which play along with the linker flexibility and steric demand of wingtip substituents a significant role for conformational behaviour in solution, structural diversity in solid state and photophysical properties.

Recently, Miguel investigated intermolecular argentophilic interactions as driving force for formation of molecular aggregates and dynamic guest-host systems in solution.[144] The cationic complexes **Ag-112c-d** display conformational flexibility around methylene bridge between two imidazol-2-ylidenes. Hereby two possible conformers can be isolated: *anti* and *syn* isomers, which correspond to the chair and boat conformation of hexane (see Figure 1.4.3). DFT calculations suggested that the *syn* isomer of **Ag-112d** is more stable by around 6.1 $kcal \cdot mol^{-1}$ and therefore, by decreasing the temperature of the solution, the equilibrium between two isomers can be completely shifted to the *syn* species. Nevertheless, both isomers can be isolated and for **Ag-112c** the corresponding *anti* conformer was crystallographically characterised after obtaining single crystals at elevated temperatures (40 °C). Further concentration dependent NMR and small-angle X-ray scattering (SAXS) studies revealed

higher propensity of these compounds for *syn*↔*anti* conversion and formation of molecular aggregates at higher concentrations. Moreover, the presence of additional silver ions increases the rate of the conversion and formation of complex structural architectures through dynamic host-guest systems as well.

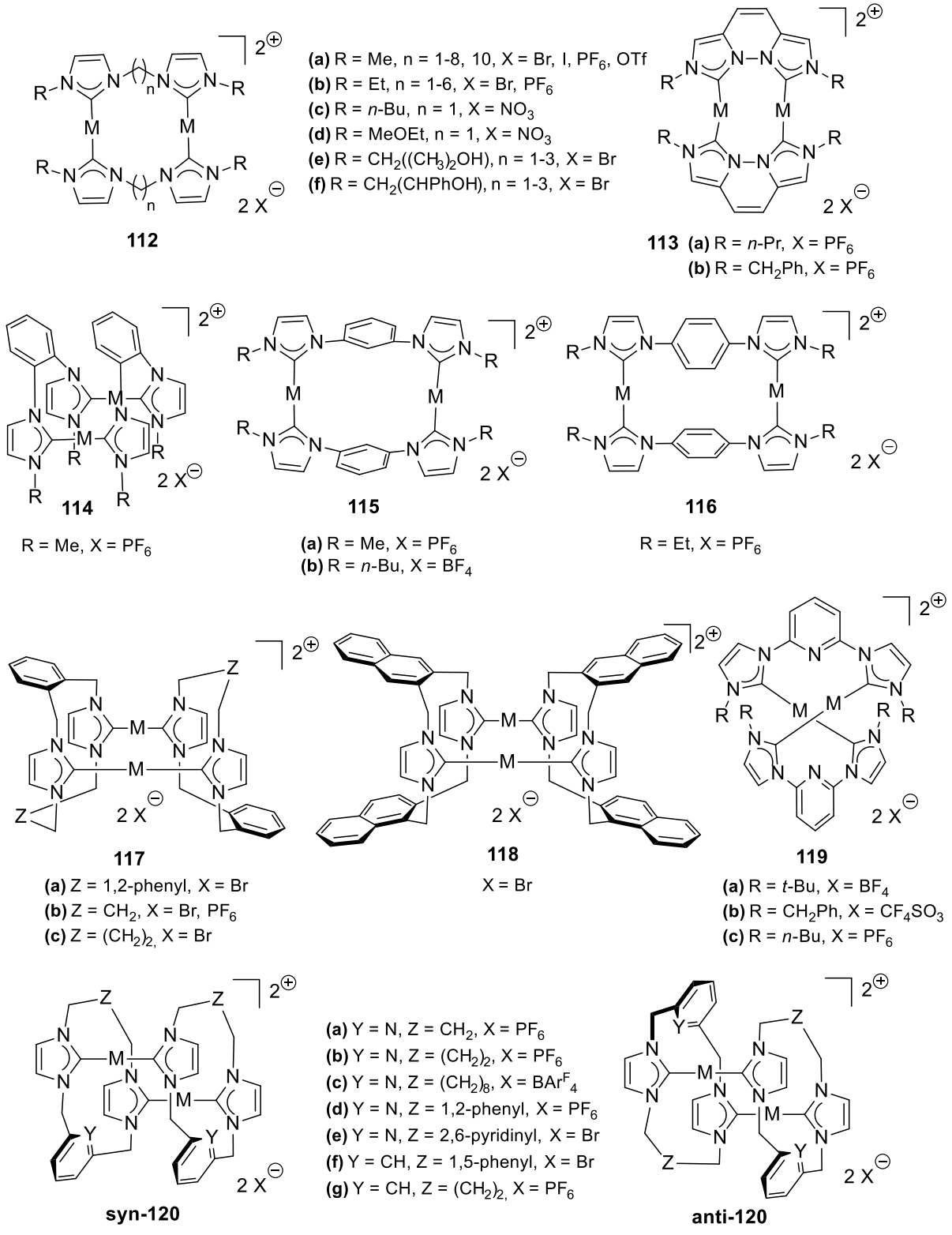

Figure 1.4.2. Molecular structures of exemplary dinuclear bis(NHC) complexes of coinage metals.

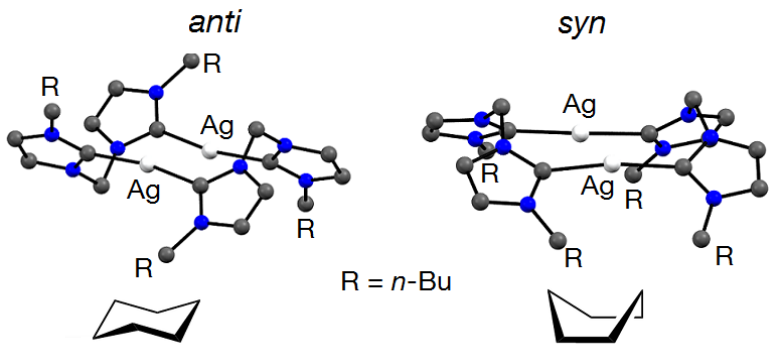

Figure 1.4.3. *Anti* and *syn* conformers of **Ag-112c.**

Also alkyl-bridged Au bis(NHC) complexes show conformational behaviour on NMR scale, although for smaller linkers this process is only evident at higher temperatures (>40 °C).[125, 145] In case of methylene, ethylene and propylene bridged Au complexes Engeser and co-workers found an evidence for aurophilic interactions being the defining force for the formation of the preferable *syn*-conformers (or rather an open-book conformation for n= 2-3) by conducting NMR and SC-XRD studies.[145a] On the contrary, longer alkyl chains favour the influence of π-π stacking on the structure in the solid state and formation of molecular aggregates in solution.

Au complexes bearing propylene linked bis(NHC)s have been also intensively studied by other groups. By comparing the data, it is evident that not only the linker itself is responsible for the geometrical arrangement but also the nature of *N*-substituents and anions. The propylene bridged complex **Au-112b**, crystallised by Engeser and co-workers, exhibits very long Au(I)–Au(I) distance which excludes intramolecular aurophilicity (Figure 1.4.4, **c** and **d**).[145a] However, crystal packing of **Au-112b** comprises of aggregates whose formation is defined by intermolecular Au(I)–Au(I) interactions (**c**) and π-π stacking (**c**, **d**). In contrast to the structure described above, Baron *et al.* reported a similar complex with *N*-methyl substituents (**Au-112a**) and PF_6 as counterion showing different U-shaped geometry with a short intramolecular Au(I)–Au(I) distance of 3.272 Å (Figure 1.4.4, **a**).[10b] The same cation with triflate ions showed another helical conformation with orthogonal NHC–Au–NHC bonds and even smaller Au(I)–Au(I) distance (3.032 Å) (Figure 1.4.4, **b**).[146] Both structures also exhibit intermolecular aurophilic interactions and π-π stacking in the solid state. However, it seems like bulkier wingtips such as in **Au-112e-f** favour an open conformation described above precluding additionally in contrast to the *N*-ethyl functionalised complex a formation of intermolecular aurophilic interactions.[147]

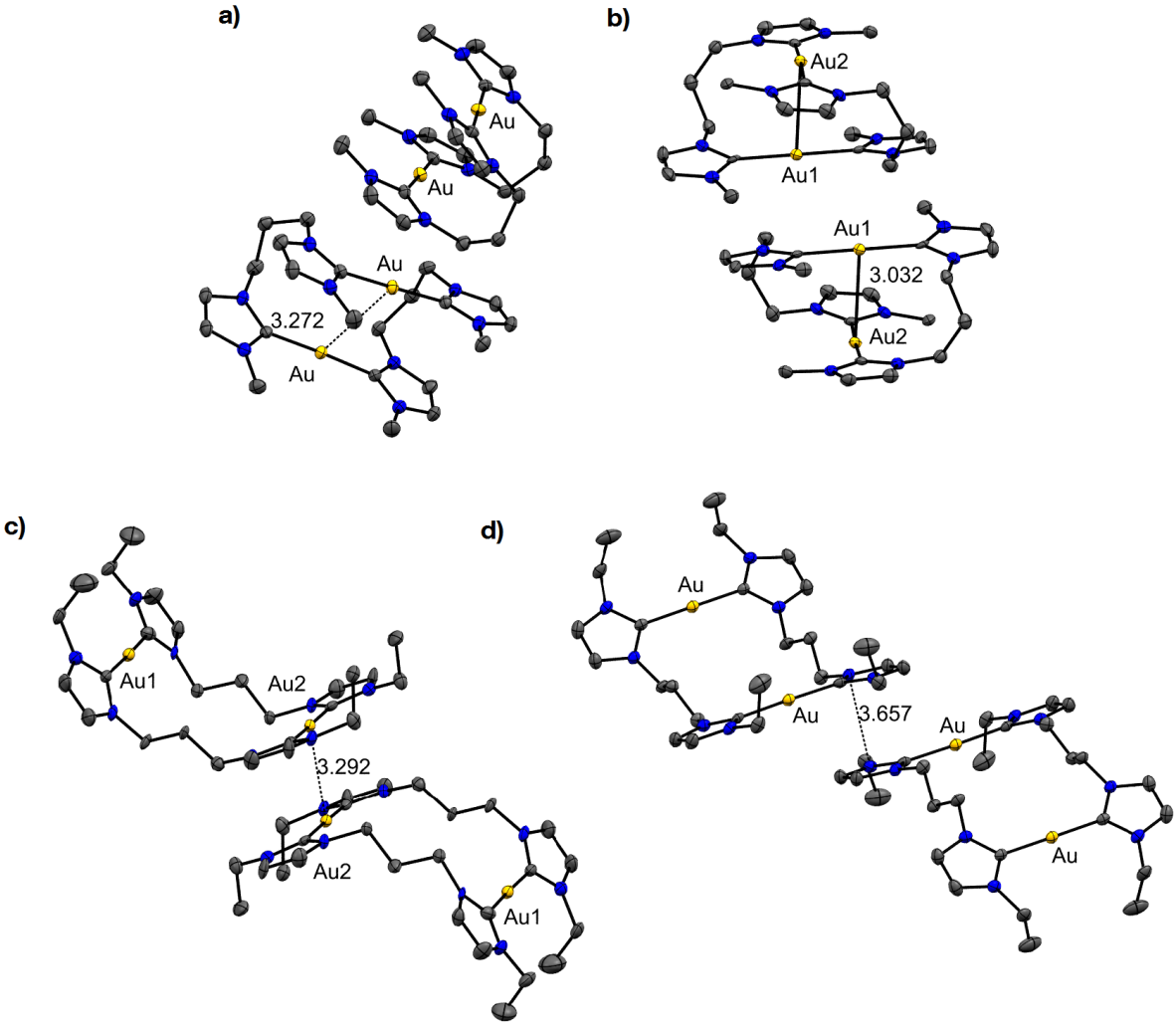

Figure 1.4.4. Structural diversity of the similar cations of 1,1'-(propan-1,3-diyl)-bridged bis(NHC) complexes of Au(I) depending on *N*-substituents and anions: **a) Au-112a-PF$_6$,**[10b] **b) Au-112a-OTf**,[146] **c) Au-112b-PF$_6$,**[145a] **d) Au-112b-Br**.[145a]

Alkyl bridged Au complexes show often weak luminescence in solution, but for many compounds significant emission intensities in solid state are observed. Especially propylene-linked bis(NHC) complex bearing *N*-methyl substituents (**Au-112a**, Figure 1.4.4, **a**) exhibits intensive blue emission in KBr discs at RT with exceptional quantum yield of 0.96.[10b] For this complex this property is related to a short intramolecular Au–Au distance in the solid state (3.272 Å). However, by extending their studies to other propylene bridged bis(carbene) complexes with different substitution patterns, the same group was able to show that the intramolecular aurophilicity is not the only defining feature for this behaviour, since complexes with even shorter Au–Au distance perform not necessary better in luminescence experiments.[145b, 148] For predicting the luminescence properties of complexes an interplay of various geometrical and electronic factors such as intermolecular aurophilic interactions, π-π

crystal stacking, the origin of the emitting state and *etc.* should be taken into account. Many authors also suggested that the nature of the anions and the presence of solvents are also very important features.[10a, 145b, 149] For example, Penney *et al.* investigated the influence of bromide anions on the emission spectra of alkyl-bridged (n = 1-3) Au complexes supported by NHCs derived from benzimidazol-2-ylides.[145b] Although in solution no difference between the complexes with bromide and PF_6 anions is observed, the substitution of bromide to hexafluorophosphate has pronounced effects of on the photophysical characteristics in the solid state. In all cases the quantum yield is substantially diminished upon replacing bromide with PF_6 and for ethylene as well as propylene linked complexes a red-shift of the emission maxima is observed. The authors also suggested that the high quantum yield observed by Baron *et al.* for Au-**112a**[10b] is actually due to the measurement method in a KBr pellet resulting in a possible anion exchange. Interestingly, Penney *et al.* also described in the same study mechanochromic properties of their compounds.[145b] The grinding of the crystalline samples of ethylene and propylene bridged complexes results in a red shift attributed to the loss of co-crystallised methanol. The subsequent subjection of the sample to methanol vapour returns the emission of the sample to its original state.

Also in case of coinage metal complexes bearing bis(NHC) ligands with more rigid bridging moieties, a formation of different conformers depending on the nature of the linker is observed. For example, both silver and gold compounds **114** with *ortho*-bridged phenylene crystallise as *syn* isomers.[148b] These compounds exhibit quite short metal–metal separations for a such rigid bridge (Ag: 3.289 Å; Au: 3.656 Å), but no evidence of π-π stacking in the crystal structure is observed. However, the *meta*-phenylene bridged complexes **M-115** (M = Ag, Au) exhibit the *anti* conformational isomerism in the solid state. Although long intramolecular metal–metal distances (Ag: 7.165 Å, Au: 7.140 Å) are characteristic for this structural motif, π-π interactions are present between phenyl rings of adjacent molecules as well as between a phenyl ring and an imidazol-2-ylidene ring of two faced molecules. In case of 1,3-phenylene bridged ligands Hahn published a report of an open ring stretched out conformation for **Au-122** characterised by long intramolecular M–M distances but intermolecular π-π interactions as well.[150]

Remarkably, the structures of M(I) bis(NHC) complexes differ significantly, if instead of 1,2-phenyl bridge a corresponding 2,5-pyridinyl or other *meta*-linked *N*-heterocyclic motif is used. Hereby in most cases, instead of an open-stretched out conformation described above, a twisted helical-like structure with short intramolecular M–M distances in the solid state is obtained in the solid state (**119**, Figure 1.4.2).[141-142, 151] Hereby short M–N contacts indicate that these interactions might be responsible for the observed helical geometry. The strengths of metal–nitrogen contacts also influence the metallophilic interactions, as seen in case of diethylaminotriazinyl and negatively charged triazinone bridging units, where the increased

nucleophilicity of the nitrogen results in shorter M–N distances and also consequently in shorter M–M contacts than in corresponding pyridinyl-linked congeners.[141-142] Curiously, although in all cases the structures of corresponding Ag and Au complexes are identical, Vaughan *et al.* also reported that in contrast to its silver analogue the Au complex supported by bis(benzimidazol-2-ylines) with *n*-butyl as wingtip substituents forms open ring stretched out structure in solid state.[142] But so far it is the only reported exception, which might indicate a stronger nature of Ag–N interactions than in comparable Au complexes. Some of the twisted complexes exhibit photoluminescent properties in the solid state.[141, 147, 151e] However, not all of them are also emissive in solution, suggesting that some degree of conformational fluxionality is existing, leading to the loss or the metallophilic interactions and/or efficient nonradiative deactivation of the excited state.[151e]

Coinage metal complexes bearing symmetrically or asymmetrically substituted macrocyclic bis(NHC) ligands moved into focus as well. Barnard *et al*. reported a series of rigid Au complexes with cyclophane ligand systems (**117a**, **118**, **120e-f**, Figure 1.4.2).[125] In complexes, where the bridging methylene groups are fused *ortho* into aromatic rings (**113a**, **115**), the phenyl group are *exo*(outwards)-positioned with respect to the molecular core. Such geometry allows close Au–Au contacts (3.0485 Å for **117a**) allowing the complex exhibit luminesce properties in solution. In comparison to **Au-117a**, **Au-120e-f** with *meta*-substituted phenyl or pyridinyl groups adopts a *meso* geometry for both aromatic rings, with one group inclining towards the metals and the other one away from them. This results in significant increase in Au–Au separation (3.7554 Å for **Au-120e** and 3.791 Å for **Au-120f**) and yields consequently non-emissive compounds. The asymmetric Au complex with *meta*-substituted pyridinyl and *ortho*-linked phenyl groups (**Au-120d**) also adopts the *anti*, *meso* geometry, where the pyridinyl moieties point towards the metal cations and the phenyl rings away from them.[152] In this case the intramolecular aurophilic interactions could be excluded as well.

Remarkably, the introduction of more flexibility into the macrocyclic systems by substituting one half of the ligand with alkyl chains instead of aryl-linkers allowed the same group to modify the intramolecular Au–Au distance of compounds **Au-117** and therefore their luminescence profile as well.[10a, 153] The relatively rigid *syn* and *anti* isomers of **Au-117b-c** co-crystallise, but can be further separated by fractional crystallization. Both conformers of the same compound show very similar Au–Au distance and therefore also exhibit similar electronic properties. In comparison to **117a** the luminescence profile of **117b** is significantly red shifted, which allowed the authors to use its natural luminesce for observing the distribution of this complex in cells by fluorescence microscopy without the interference with other cellular compounds.[10a] The butylene bridged **Au-117c** conformers, however, exhibit longer intramolecular Au–Au

distances which correlate to their poorer performance in luminescence experiments in comparison to **Au-117b**.[153]

Similar to the alkyl-linked open chained complexes mentioned above subsequent studies also revealed significant influence of counter anions on the emission profile of Au complexes bearing macrocyclic bis(NHC) ligands.[149] The step-wise addition of Br^- to **Au-117b** associated with PF_6^- in DMSO results in graduate decrease in emission maxima at around 400 nm and the appearance and gradual increase of a new emission band at 500 nm, which is attributed to **117b** associated with bromide. EXAFS data obtained in the presence of Br anions strongly suggested a formation of $(NHC)_2AuBr$ aggregates.

Asymmetric macrocyclic lutidinyl linked Ag and Au complexes have been investigated for their conformational behaviour as well.[152, 154] Also for the complexes **120a-d** *syn* and *anti*-isomerism was observed. Similar to **Au-117b-c** the alkyl-linked Au compounds **120a-b** are rigid on NMR scale and can be separated by crystallization.[152] However, a fast interconversion rate for the isomers of Ag complexes is observed. The mechanism of the isomerization is uncertain since the rigidity of the macrocycle should prevent the ligand from folding from one isomeric form to another. An alternative mechanism would involve the dissociation of Ag-bis(NHC) complex into two monomeric moieties which would re-associate forming another isomer. Since the measured activation barrier for this process is small in comparison to the Ag–NHC bond-dissociation energy in similar cationic bis(NHC) complexes, the authors suggested a possible involvement of the nitrogen on the lutidinyl linker in the process. However, a similar Ag complex with 1,5-phenyl and butyl bridged bis(NHC) macrocycle (**Ag-120g**) also isomerize on the NMR scale, although a little bit slower. More recently, Chaplin also observed high fluxionality of dodecanyl-bridged **Ag-120c**.[154b] Based on the evidence obtained by ESI-MS experiments he also proposed fragmentation of dinuclear molecules, which is however generally favoured for long alkyl linkers[146]. In the solid state the crystals of **Ag-120g** are comprised of dinuclear anti conformers. Notably, in contrast to these half aryl-half alkyl macrocyclic complexes, the Ag complexes with two aryl likers (**Ag-120d**) show no fluxional behaviour in solution.

Finally, the dinuclear complexes supported by π-conjugated *N,N*-connected bis(carbenes) **113** deserve special attention due to unusual ligand geometry, which forces extremely close M–M contacts (2.739 Å and 2.741 Å for **Ag-113b** and **Ag-113a** respectively, 2.779 Å for **Au-113b**).[155] As expected all these complexes show intense luminescence in solution.

1.4.3.2 Application of Au(I) NHC Compounds in Medicinal Chemistry

In the past decades Au(I) complexes have emerged as potential alternatives to common metal based drugs such as cisplatin, carboplatin, nedaplatin or lobaplatin, which are clinically applied

in cancer chemotherapy, but suffer from low resistance under physiological conditions and cause drastic side effects by unselective binding to other intracellular components.[156] The first Au(I) compound to be tested for its cytotoxic properties was Auronafin (Ridaura®), initially developed in 1982 to be used to treat rheumatoid arthritis. Nowadays, Auronafin has already successfully passed phase II of the clinical trials for the treatment of chromatic lymphocytic leukaemia, small lymphocytic lymphoma and prolymphocytic lymphoma.[157] Most of other Au(I) compounds showing antiproliferative activity against human cancer cell lines *in vitro are* linear coordinated complexes with soft ligands such as thiolates or phosphines.[157]

The mechanism by which the Au(I) complexes inhibit the growth in cancer cell line is believed to be attributed to mitochondria targeting and inhibition of the selenocysteine containing enzymes such as thioredoxin reductases (TrxR). By inhibiting TrxR these compounds induce severe oxidative stress inside the mitochondria, which ultimately cause apoptotic cell death.[12a, 158]

For development of Au(I) based drugs several factors should be considered. In the best case scenario the potential drugs should be soluble and stable in water and have labile ligands in order to undergo rapid solubilisation[158b, 159] and high reactivity with biomolecules.[157] Additionally, a low reduction potential is advantageous as it impedes deactivation due to reduction to colloidal gold, as seen e.g. for *Auronafin* in reactions with glutathione or other thiols. [157, 160] Thus, the goal in the design of Au(I) complexes is to insert the resistance against thiol-containing enzymes in the blood.[161] Furthermore, the complexes should exhibit certain degree of lipophilicity, which is necessary for efficient membrane permeability.[158b] Due to high stability of respective Au complexes and a variety of functionalization possibilities NHCs are convenient tools for fine-tuning of these properties.

A plethora of mono- and binuclear Au(I) NHC complexes have been reported to exhibit cytotoxic properties.[158b, 159, 161-162] For example, Berners-Price tested a series of Au(I) bis(NHC) complexes (**122**, Figure 1.4.5) for antiproliferative activity *in vitro* and reported the induction of mitochondrial damage with high selectivity for breast cancer cell lines.[158b] The remarkable activity of these compounds correlates to properties attributed to delocalized lipophilic cations (DLCs), which are known to accumulate selectively in the mitochondria of cancer cells due to overexpression of organic cation transporters (COTs) in the cell membrane and elevated mitochondrial membrane potential generated by the respiratory chain.[158b]

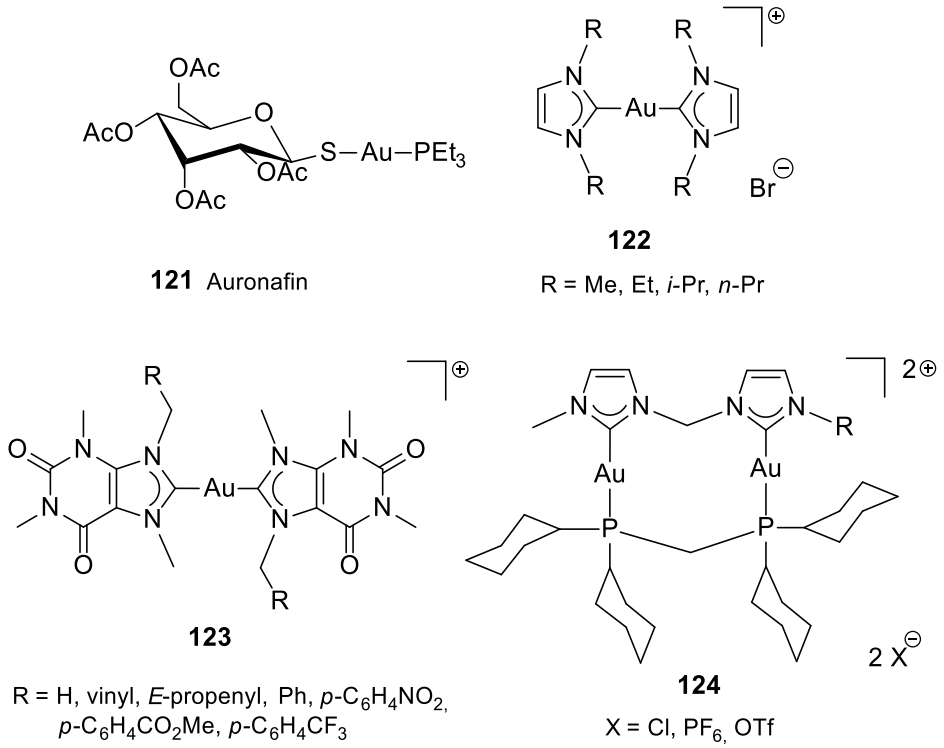

Figure 1.4.5. Auronafin and exemplary Au(I) bis(NHC) complexes showing antiproliferative activity in human cancer cell lines.

The same group also investigated dinuclear Au(I) bis(NHC) complexes described in previous section (**117a** and **120e**, Figure 1.4.4) and demonstrated their significant antimitochondrial activity as well.[163] Remarkably, they further developed homo-bimetallic complexes bearing modified macrocyclic ligands (**117b**) and hence were able to fine-tune their luminescence profile (see paragraph 1.4.3.1, Figure 1.4.4).[10a] Using its natural luminescence, the uptake and distribution of **117b** in mouse macrophage cancer cell line was monitored by fluorescence confocal microscopy. Interestingly, **117b** accumulates rather in lysosomes than in mitochondria.[10a, 153] If this is the reason for modest cytotoxicity values of **117b** in this cancer cell line, remains to be shown, but further preliminary experiments indicate greater potency of this complex in other cell lines.

Furthermore, Au(I) bis(NHC) compounds with substituted caffeine ligands (**123**, Figure 1.4.5) were reported to show activity against several cancer cell lines *in vitro* without affecting the non-tumorigenic ones.[162b, 162c, 164] Zou *et al*. also introduced the complex **124**, which shows inhibiting activity against thioredoxin reductase (TrxR). Remarkably, it also possesses high stability against the thiol groups of enzymes in comparison *Auronafin* and **112c**, which shows only modest IC_{50} values in HeLa cells (human cervix carcinoma).[159, 161]

All the Au(I) complexes mentioned above possess the disadvantage of to be not active *in vivo* against cancer cells.[161] Unfortunately, with some exception they are also not particularly

selective and show significant toxicity in healthy tissue. The accumulation of gold in the body may affect skin, blood, kidney, brain and other organs. However, these side effects strongly depends on the type of compound and on the dose.[165] Due to these impediments most of Au(I) NHC complexes are not commercialized so far as they did not pass the clinical trials.

1.5 Aims of this Thesis

Rare earth metal complexes bearing NHC ligands were first described in the rush that followed the discovery of the free stable NHC. Today, although they are still less common than late transition metals bearing NHC ligands[2b], the investigations on REE NHCs paved the way to a significant number of complexes, which equipped the scientists with a repertory of approaches to future compounds.[4, 19c] However, the knowledge concerning synthetic methods and especially reactivity is still somewhat limited in this field. The reports of catalytic activity are so far mostly limited to polymerization reactions; the systematic investigations on catalytic utility could provide further insight into this still under-explored complex class. Furthermore, REE NHC complexes show very promising reactivity for a range of very interesting reactions[19c, 19e], such as small molecule activation[93b, 114] or C–H bond activation[166] and their applicability should be further explored by gaining access to compounds containing polydentate ligands, which might show superior stability due to stabilization by anionic anchors or/and additional carbene moieties. Such sites promote a robust attachment of NHCs to hard Lewis acidic centre allowing the exposition of NHC coordination sites without complete dissociation of the whole ligand.[4] This generates an exciting possibility of a liberated NHC moiety participating in catalytic reactions as a non-innocent ligand.

The generation of NHC complexes with Lewis acidic metal centres, however, often requires a detour *via* alkali metal NHC intermediates, which are now widely recognised as efficient transmetallation agents.[19e] Therefore, the work described in second chapter of this thesis focuses on the synthesis and characterization of various donor-functionalised chelating NHC pro-ligands and the investigations towards their reactivity upon subjection to alkali metal bases. The deprotonation products should be fully characterised and, if possible, isolated, especially since fully characterised alkali metal adducts with poly(dentate) NHC ligands, particularly neutral ones, are rare. In order to maximize the chances for a successful transmetallation procedure investigations on the stability of the generated compounds should be conducted and optimal reaction conditions determined.

Subsequently, the respective REE compounds should be synthesized using various approaches, ether by transmetallation of alkali metal NHC adducts obtained in the second chapter or by a direct reaction of the ligand precursors with REE compounds acting as internal base. Optimal conditions for the synthesis of the respective complexes should be determined. Since the structural information on REE NHC compounds is limited, all complexes should be fully characterised und used for further studies towards their reactivity with small molecules or in redox chemistry. This work will be described in the third chapter of this thesis.

Linear coordinated Au(I) complexes show promising antiproliferative activity in cancer cells. Because of high complexity of biological medium, the fine-tuning of the steric and electronic properties of these compounds is crucial to cytotoxic properties and selectivity. Hereby, NHCs offer a possibility for efficient and fast optimization of respective complexes. Furthermore, the high stability of Au(I) NHC complexes makes them suitable candidates for rapid screening of potential metal-based drugs.[167] Although a variety of Au(I) NHC compounds have been reported to show high potential as anti-cancer drugs, they still suffer from several disadvantages (low stability again thiols, low selectivity and etc., see Section 1.4.3.2). Therefore, further investigations towards other ligand systems combining liphophilic and hydrophilic functional groups, which would allow simultaneously high membrane permeability as well as stability and solubility in biological medium, should be conducted. Additionally, ligand systems offering a possibility of post-synthetic modifications towards coupling with biological markers or anchoring of additional metals should be explored. Therefore, the fourth chapter of this thesis focuses on homo-dinuclear Ag(I) and Au(I) complexes supported by bridge-functionalised bis(NHC) ligands. Detailed investigations on conformational behaviour of these compounds are performed and correlated to possible antiproliferative activity in human cancer cell lines. Furthermore, first preliminary experiments towards post-synthetic modifications are conducted.

Chapter 2

Synthesis and Characterization of Donor-Functionalised *N*-Heterocyclic Carbenes and their Group I Adducts

2.1 Results and Discussion

This chapter describes the work towards modification of NHC ligand precursors with additional neutral or anionic donor sites. Reactivity studies towards generation of free NHCs or alkali metals NHC adducts are conducted in order to subsequently use these intermediates salt elimination reactions with rare earth metals. In favour of enhanced clarity and content structuring the reactions all bis(imidazolium) salts with internal rare earth metal bases as well as in multi-component systems will be discussed in Chapter 3. This section summarizes the reactions of these pro-ligands with alkali metal bases and, if applicable, the conversion of the obtained products with various organic substrates.

2.1.1 *N*-(3,5-Di-*tert*-butyl-2-hydroxyphenyl) and *N*-Bis(3,5-di-*tert*-butyl-2-hydroxybenzyl) Functionalised Mono(imidazolium) Salts $H_2(L1^R)Br$ and $H_3(L2)Br$

2.1.1.1 Synthesis and Characterization

The bidentate *N*-(3,5-di-*tert*-butyl-2-hydroxyphenyl)-functionalised pro-ligands **$H_2(L1^{Me})Br$** and **$H_2(L1^{Mes})Br$** are obtained according to published procedures (Scheme 2.1.1).[168]

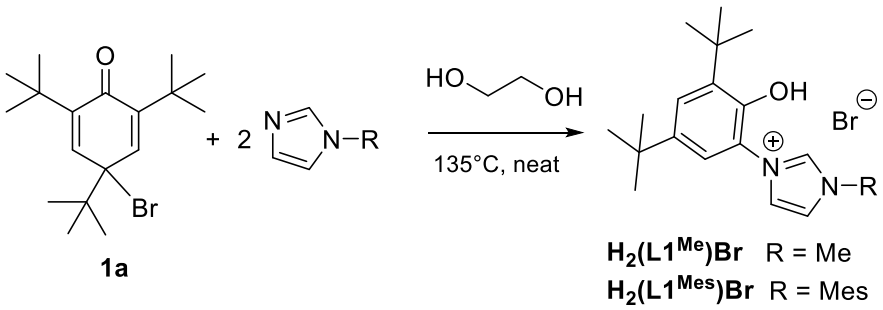

Scheme 2.1.1. Synthesis of bidentate *N*-(3,5-di-*tert*-butyl-2-hydroxyphenyl)-functionalised imidazolium bromides.

The exact mechanism of this reaction is unknown. Tashiro examined the conversion of 4-bromo-2,4,6-tri-*tert*-butyl-2,5-cyclohexadien-1-one **1a** with various substituted pyridines and made an observation that the presence of ethylene glycol (EG) is not necessary for the reaction to proceed.[169] Nevertheless, its presence increases the yields dramatically, but only by using a fixed molar ratio of **1a**:EG:pyridine (1:1:2). Based on the ESR experiments the authors proposed a radical mechanism for this conversion. Hereby the formation of isobutylene generated by debutylation at the C2 position was confirmed by trapping this gas in toluene and converting it with $AlCl_3$ to *tert*-butyltoluenes. The regioselectivity of the reaction was explained

with kinetic arguments. Furthermore, various side products such as 2,4,6-tri-*tert*-butylphenol, 2-bromo-4,6-di-*tert*-butylphenol, 2,4,6-tri-*tert*-butyl-4-hydroxycyclohexa-2,5-dien-1-one and 2,6-di-*tert*-butylcyclohexa-2,5-diene-1,4-dione are observed. It seems likely that the reaction of **1a** with substituted imidazoles could proceed *via* the same mechanism (Scheme 2.1.2), and the formation of the side-products mentioned earlier is probably the reason for low yields in this synthetic procedure (36 % for R = Me and 16 % for R = Mes).

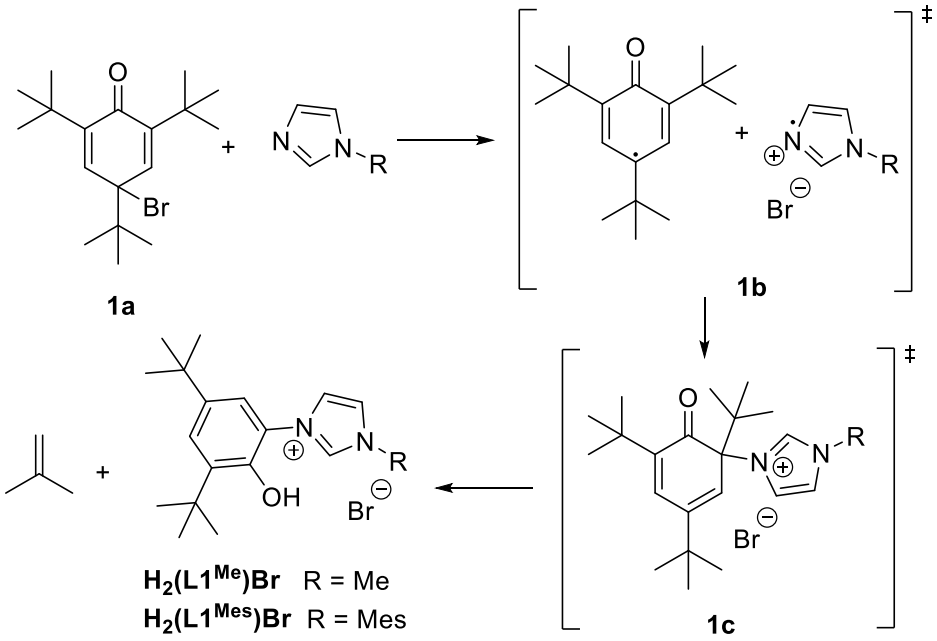

Scheme 2.1.2. Possible mechanism for the reaction of 4-bromo-2,4,6-tri-*tert*-butyl-2,5-cyclohexadien-1-one **1a** with substituted imidazoles based on the mechanism proposed by Tashiro for the similar reaction of **1a** with pyridines.[169]

The synthesis of the related tridentate *N*-bis(3,5-di-*tert*-butyl-2-hydroxybenzyl) functionalised mono(imidazolium) salt **H_3(L2)Br** has been already described and proceeds *via* double nucleophilic substitution (Scheme 2.1.3).[170]

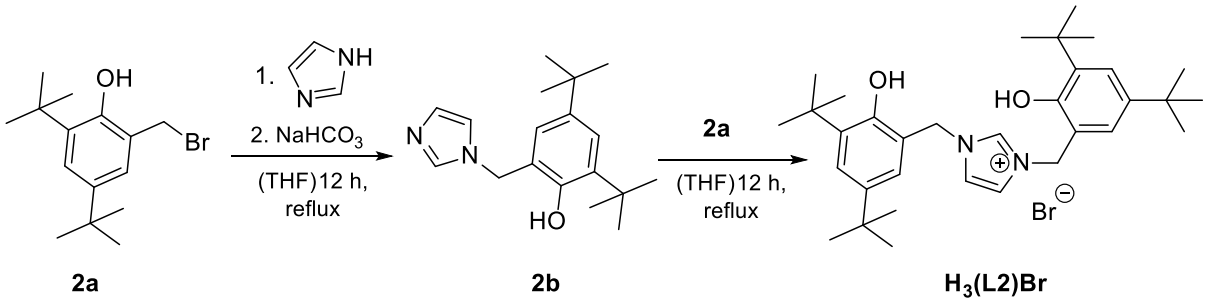

Scheme 2.1.3. Synthesis of tridentate *N*-functionalised imidazolium bromide **H_3(L2)Br**.

All compounds have been characterised by means of multinuclear NMR spectroscopy and ESI-MS. The purity of the material was confirmed by elemental analysis.

2.1.1.2 Deprotonation Studies

Bidentate ***H$_2$(L1^R)Br***

H$_2$(L1^{Me})Br can be successfully deprotonated on NMR scale with KN" or NaN" at RT in THF (Scheme 2.1.4). Hereby **Na(L1^{Me})** and **K(L1^{Me})** are obtained in quantitative yields. The ^{1}H NMR spectra of both compounds show the generation of symmetrical compounds with the formation of only one species for the potassium congener (Figure 2.1.1). In comparison to **K(L1^{Me})**, the Na NHC adduct is formed as a product mixture in ratio of 0.2:1.0 (**A**:**B**), which however could also indicate a formation of a single oligomeric product with different structural motifs. Such reactivity would be not surprising as a formation of complex alkali metal clusters was repeatedly observed (see Introduction, Section 1.2.1).[65]

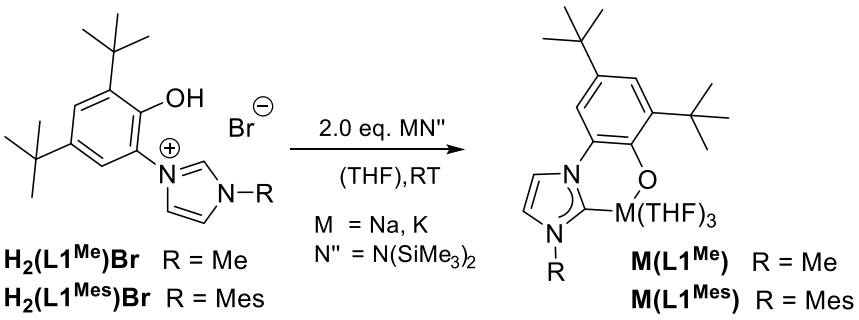

Scheme 2.1.4. Formation of alkali metal NHC adducts derived from **H$_2$(L1^R)Br**. The structures of **M(L1^R)** are simplified suggestions based on experimental data.

The value for K–C$_C$ resonance (212.67 ppm) in **K(L1^{Me})** lies within the range reported in the literature.[65b] Notably, a splitting of the carbon resonances attributed to methyl groups suggest that K NHC adduct could also exist as an oligomer in solution. In comparison to **K(L1^{Me})** the ^{13}C NMR spectrum of **Na(L1^{Me})** displays a second minor set of the singlets (see Experimental, SI, Figure 5.3.1-2). No resonance attributed to a carbene is detected in this case, probably due to longer relaxation time and lower sensibility of Na NHCs in comparison to K NHCs. Besides the missing carbene singlet and the resonance of one of the quaternary aryl-group-carbon (probably due to overlapping) for the main species (**B**), the resonance pattern of the product **B** is similar to **K(L1^{Me})**, indicating that also with Na an alkali metal NHC adduct could have been formed.

According to ^{29}Si INEPT NMR the conversion of **H$_2$(L1^{Me})Br** with KN" is quantitative as only a signal corresponding to HN" is visible. On the other hand, the spectrum of **Na(L1^{Me})** shows a number of different resonances ranging from –28.17 till 8.34 ppm. The most prominent are at –11.97 and 1.96 ppm, corresponding to NaN" and HN", which suggests that either NaN" is not completely consumed or it is incorporated into the compound. Such behaviour have been previously observed for the Na NHC adduct **21** (see Introduction, Scheme 1.2.1).[57] In any

case, these findings rather support the assumption that **Na(L1^{Me})** forms a complex polynuclear solvate in solution.

Both compounds, **Na(L1^{Me})** and **K(L1^{Me})**, are stable in solution at RT under inert atmosphere conditions for at least 4 days. Hereby, neither the ^{1}H NMR spectra of these alkali metal NHC adducts nor the appearance of the samples show any signs of decomposition. Unfortunately, to date no crystals suitable for SC-XRD could be obtained for both compounds.

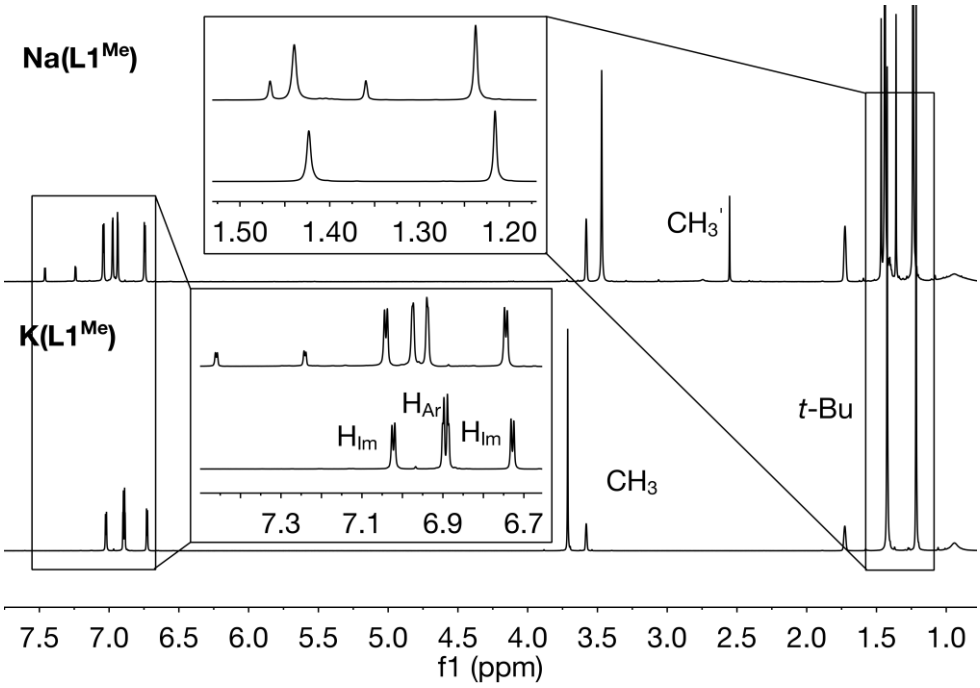

Figure 2.1.1. Comparison of ^{1}H NMR spectra of **Na(L1^{Me})** (top) and **K(L1^{Me})** (bottom) synthesized on NMR scale in THF-d_8 at RT.

Also by treating the mesityl-substituted analogue **H$_2$(L1^{Mes})Br** with 2.0 eq. of KN" a clean reaction is observed in THF at RT yielding the deprotonated K NHC adduct **K(L1^{Mes})** (Scheme 2.1.4).The ^{1}H NMR spectrum of the product suggests a symmetrical arrangement of the ligand in the obtained product (Figure 2.1.2). Also ^{13}C NMR proves high symmetry and besides the carbene resonance all expected singlets can be clearly assigned (Figure 5.3.3). Finally, ^{29}Si NMR confirms a complete consumption of KN" by displaying solely the singlet attributed to HN".

K(L1^{Mes}) is stable under inert conditions for at least 2 days. Unfortunately, this compound could not be characterised by SC-XRD due to decomposition during crystallization by slow diffusion of pentane into a solution of **K(L1^{Mes})** in THF at RT. Therefore, the exact structure of **K(L1^{Mes})** remains unknown.

In comparison to KN" the use of 2.0 eq. of NaN" for the deprotonation of 1.0 eq. of **H$_2$(L1^{Mes})Br** in THF at RT is not satisfactory. The NMR scale reaction contains still a lot of not-deprotonated

pro-ligand, and the multiplets attributed to deprotonated species are difficult to assign due to probable high degree of oligomerization (see SI, Figure 5.3.4). ^{13}C NMR spectrum further confirms the observations made in the proton NMR, also the carbonic carbon resonance is not detectable (SI, Figure 5.3.5). According to ^{29}Si NMR most of the NaN" was consumed and converted to HN", but a singlet at –11.93 ppm indicates a possible incorporation of NaN" into the cluster, since a free NaN" would react with the remaining pro-ligand. It is possible that due to complicated structure of the obtained Na NHC product the stoichiometry of the reaction was not exact. A formation of anionic dicarbenes cannot be excluded as well, as it has been previously observed for heavy alkali metals (see Introduction, Section 1.2.1).[65b] Therefore, further investigations on this reaction are necessary.

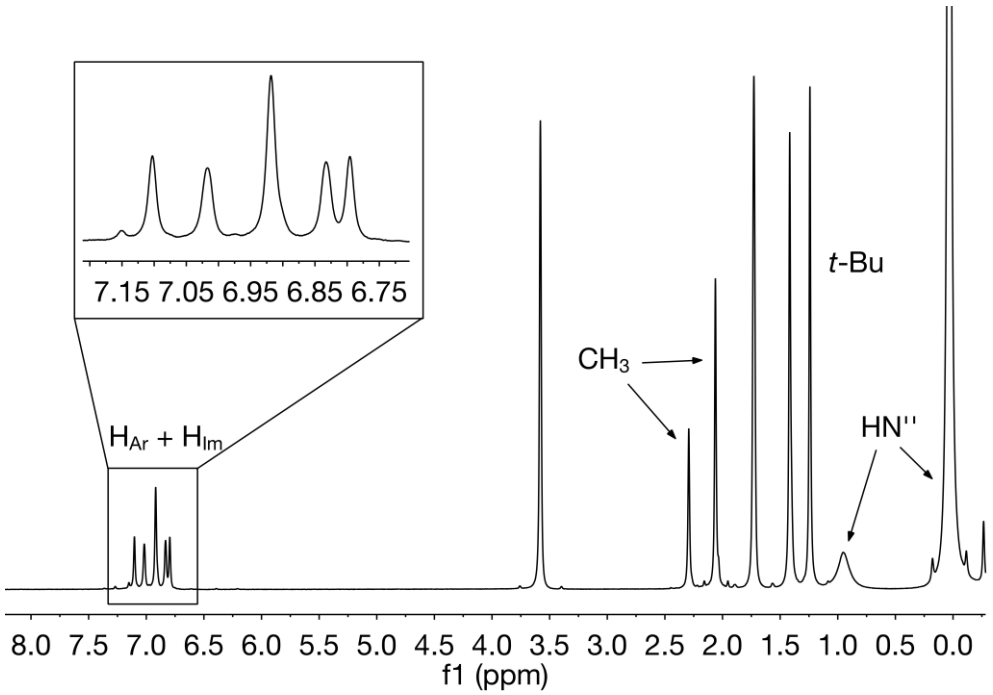

Figure 2.1.2. ^{1}H NMR spectrum of **K(L1^{Mes})** formed in a NMR scale reaction at RT in THF-d_8.

In summary, although structural information could not be obtained, the NMR experiments prove a clean formation of K NHC adducts with *N*-(3,5-di-*tert*-butyl-2-hydroxyphenyl)-functionalised imidazol-2-ylidenes on NMR scale. The sodium compounds have been also successfully synthesized but in contrast to K NHCs they exhibit higher degree of oligomerization or are possibly more prone to rearrangement.

*Tridentate **H$_2$(L2)Br***

The deprotonation of tridentate pro-ligand **H$_3$(L2)Br** can be conveniently performed in THF by addition of 3.0 eq. of KN" (Scheme 1.2.5). On NMR scale at RT the reaction proceeds cleanly and yields a highly symmetric product (Figure 2.1.3, bottom spectrum). ^{13}C NMR spectrum of **K(L2)** confirms the formation of desired K NHC as well, as the chemical shift value for carbenic

carbon (δ (K–C) = 212.76 ppm) lies within the range of other reported K NHC compounds.[57, 65b] Further spectroscopic characterization by ^{29}Si INEPT NMR confirms a clean conversion of **H_3(L2)Br** with KN" since besides the singlet attributable to HN" only a very minor impurity at 4.83 ppm is present.

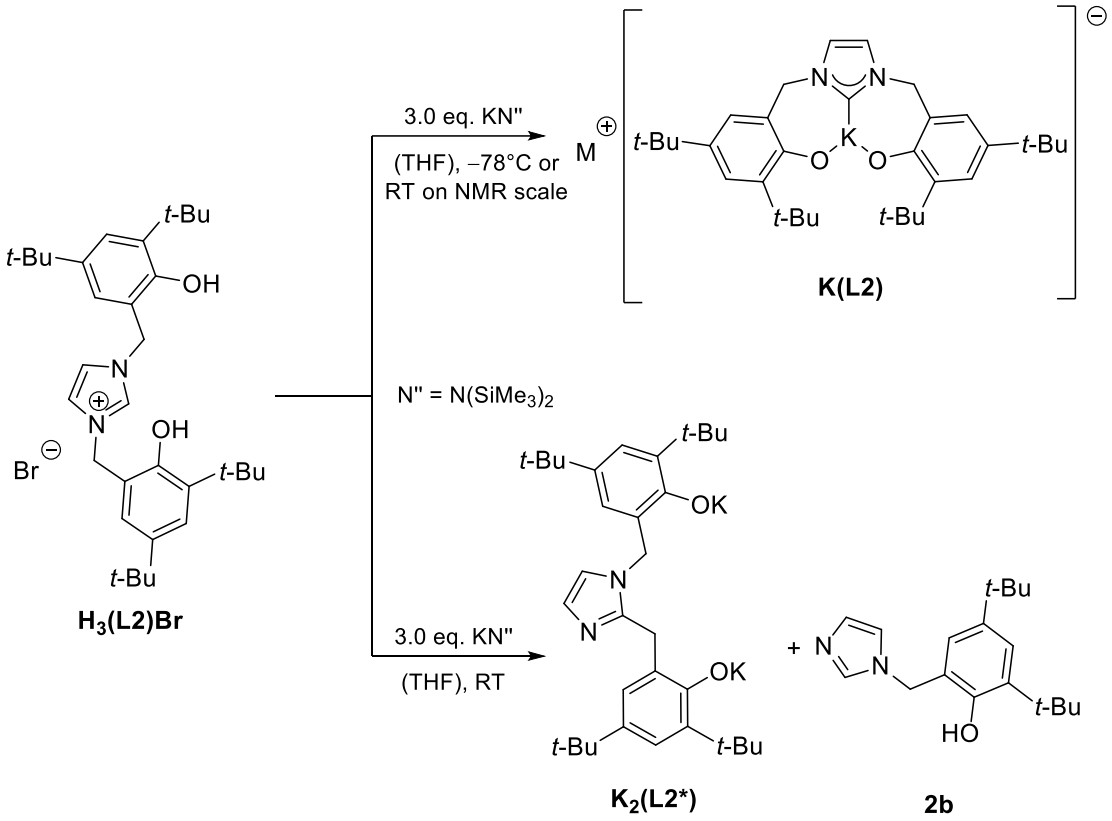

Scheme 2.1.5. Reaction of KN" with the pro-ligand **H_3(L2)Br**. The structure of **K(L2)** is a simplified suggestion.

On preparatory scale, the ^{1}H NMR spectrum of crude product obtained after the treatment of **H_2(L2)Br** with 3.0 eq. of KN" at RT for 18 h using standard Schlenk and glove box techniques reveals a formation of different products than in the NMR scale reaction described above (Figure 2.1.3). It is unlikely that **K(L2)** or other K NHC adducts are still present at this stage since no carbene resonance is visible in the ^{13}C NMR spectrum of the residue. Also the appearance of the brown filtrate stands in contrast to the bright orange suspension of the NMR scale reaction.

To obtain more information about the formed compound the ESI-MS analysis of the crude product formed after 2.5 h of the reaction time at RT was performed (see Figure 5.3.43, SI). The spectrum exhibits a main signal at 505.41 m/z, which belongs to ether the cation of the imidazolium salt **H_3(L2)Br** or its product by 1,2-shift of *N*-(3,5-di-*tert*-butyl-2-hydroxybenzyl) substituents plus H^+. The first case would indicate a presence of a K NHC adduct in the sample at the time of the injection and its re-protonation by formic acid. The second possibility,

however, would explain the asymmetrical set of resonances in ^{1}H NMR spectrum and the absence of the singlet attributed to carbenic carbon in ^{13}C NMR. The 1,2-rearragement is further strongly supported by the literature as Kawaguchi also observed the same reactivity of **Na(L2)** upon warming it up to RT.[171] Further signal at 723.50 m/z in the MS spectrum could not be assigned, but its isotope pattern suggests an organic molecule without bromide or potassium. Interestingly, a signal at 287.14 m/z indicates a cleavage between the imidazol-2-ylidene and one of *N*-substituents resulting in formation of [**2b**+H^{+}] (Scheme 2.1.3). Such decay has been already previously observed for similar asymmetrically substituted pro-ligand **79** by treating it with Li[YN(*i*-Pr$_2$)$_4$] and *n*-BuLi at RT (see Introduction, section 1.3.1.2).[97]

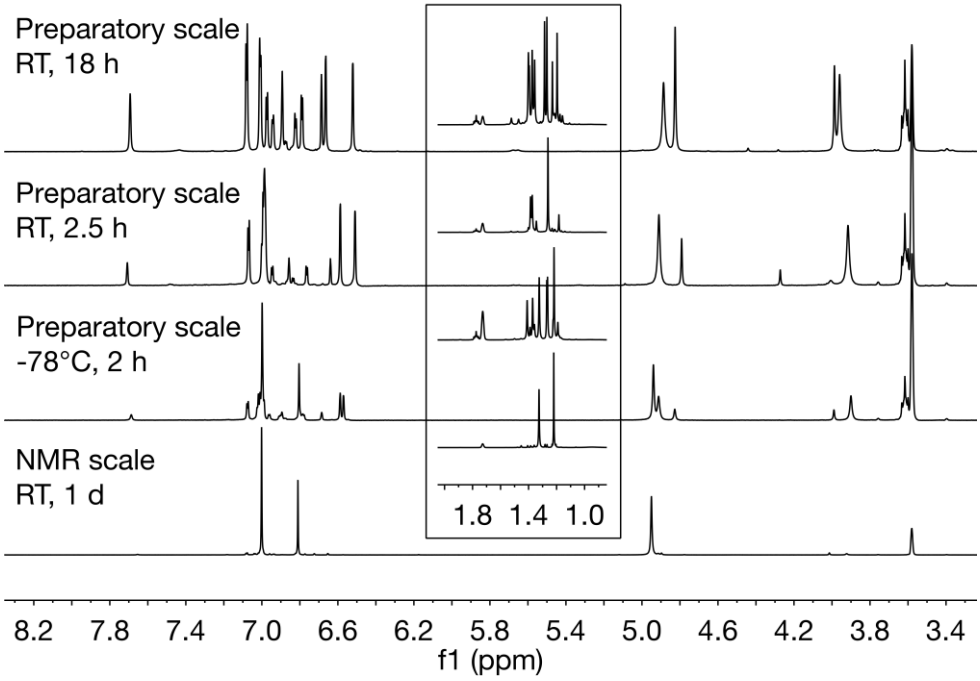

Figure 2.1.3. Comparison of the ^{1}H NMR spectra of the products of the reactions of **H$_3$(L2)Br** with KN" at various conditions. The spectra were recorded in THF-*d$_8$* at RT.

Further modification of the synthetic procedure by lowering the reaction temperature to –78 °C and shortening the reaction time to 2 h yields **K(L2)** as major but impure product. The impurities were the same as seen in the conversions at RT and their formation is probably indebted by warming up of the filtrate during the removal of the solvent.

Interestingly, the comparison of ^{29}Si NMR spectra of the reaction on preparatory scale at –78 °C with NMR scale reaction conducted at RT shows the increase in the intensity of the singlet at 4.6 ppm in comparison to HN" resonating at 1.9 ppm (Figure 2.1.4). Finally, by conducting the same experiment on preparatory scale at RT the singlet at 4.6 ppm is replaced by a number of new resonances in the positive region, suggesting a possible direct involvement of amide in the decomposition process.

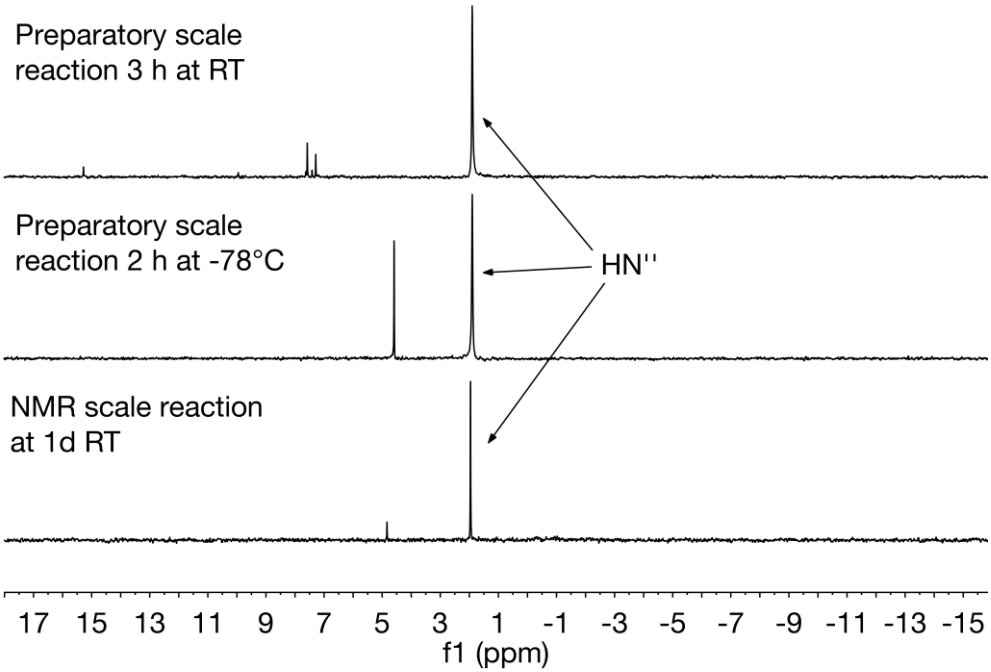

Figure 2.1.4. Comparison of ^{29}Si INEPT NMR spectra of the crude products obtained by the reaction of **H_3(L2)Br** with KN" at various conditions.

Unfortunately, the washing of the crude product with toluene results in further decomposition of **K(L2)**, similar to the **Na(L2)** adduct reported by Kawaguchi.[171] Due to thermal sensitivity of **K(L2)** no crystals suitable for SC-XRD could be obtained and therefore, the exact structure of this alkali metal NHC adduct remains unknown.

On exploratory NMR scale the deprotonation of **H_3(L2)Br** is also achieved in THF at RT by addition of NaN". Hereby, in contrast to a clean symmetric product **K(L2)** a formation of structurally diverse motifs is evident (Figure 2.1.5). In contrast to potassium analogue, the appearance of carbenic carbon is not detected in ^{13}C NMR spectrum of **Na(L2)**, but the resonance pattern of the remaining carbon nuclei suggests that at least 3 species of ligand framework are formed (SI, Figure 5.3.6). The comparison of the spectra to the spectra of the decomposition product of **K(L2)** excludes the formation of the same 1,2-rearragement products. Therefore, in this case either structurally different **Na(L2)** adducts have been formed or other decomposition pathways are present. Additionally, in comparison to **K(L2)**, the ^{29}Si NMR spectrum of **Na(L2)** displays singlets at –11.18 and 7.57 ppm. Therefore, similar to the reaction with **H_2(L1^R)Br** described above, NaN" could be incorporated into the oligomeric structure, as seen e.g. for compound **21** (see Introduction, Scheme 1.2.1).[57] Moreover, the resonances in the positive region of ^{29}Si NMR spectrum indicate possible presence of (poly)organosiloxane in the sample as well.[172]

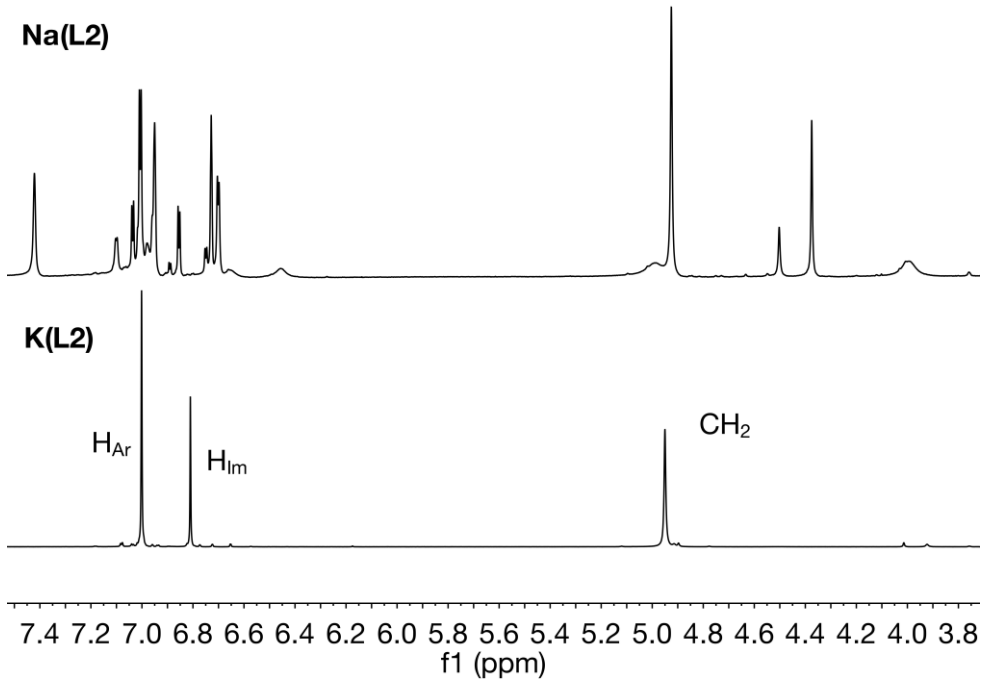

Figure 2.1.5. Comparison of the ^{1}H NMR spectra of the products obtained by the reactions of **H_3(L2)Br** with KN" and NaN" by at RT in THF-d_8 (NMR scale reactions).

In summary, *N*-(3,5-di-*tert*-butyl-2-hydroxyphenyl) and *N*-bis(3,5-di-*tert*-butyl-2-hydroxybenzyl) functionalised mono(NHC) ligands readily form alkali metal NHC adducts with potassium or sodium. However, although on smaller NMR scale these obtained compounds seem to be stable for at least 4 days at RT, on preparatory scale the isolation of respective complexes is impeded by their thermal instability. Therefore, the crystallographic characterization of **M(L1^{R})** and **M(L2)** (M = K, Na; R = Me, Mes) could not be performed so far due to decomposition processes during crystallization. It is possible that due to higher Lewis acidity of Li, an isolation of respective Li NHC compound could be more straightforward. Although the exact molecular structures remain unknown, especially the potassium compounds **K(L1^{R})** and **K(L2)** show great potential for application as transfer reagents *in situ* at –78 °C.

2.1.2 1,1'-(2-Hydroxyethane-1,1-diyl)-Bridge Functionalised Bis(imidazolium) Salts $H_3(L3^{R})X_2$

2.1.2.1 Synthesis and Characterization

The synthesis of 1,1'-(2-hydroxyethane-1,1-diyl)-bridged bis(NHC) pro-ligand **$H_3(L3^{Me})Cl_2$** has been previously reported by Zhong *et al*.[173] To investigate the implication of different wingtips on the solubility of potential complexes as well as the conformational changes, this class of ligands has been expanded for other *N*-substituents (*i*-Pr, Mes). Using 1-isopropylimidazole and 1-mesitylimidazole as precursors analogue synthetic method is applied (Scheme 2.1.6).

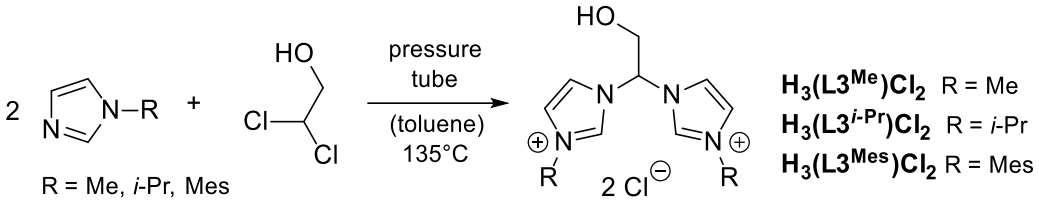

Scheme 2.1.6. Synthesis of 1,1'-(2-hydroxyethane-1,1-diyl)-functionalised bis(imidazolium) chlorides.

Unfortunately, the yields for **$H_3(L3^{i\text{-}Pr})Cl_2$** and **$H_3(L3^{Mes})Cl_2$** are quite low (48 % and 26 % respectively), especially for sterically demanding mesityl-substituents. Chloride-anion is a poor leaving group, but since the 2,2-dibromo or 2,2-diiodoethanol cannot be used due to their instability, high temperatures and long reactions times are required in this case. With the goal of increasing the yields and reducing the reaction times, the application of microwave irradiation was also investigated. For mesityl-substituted compounds the operation procedure at 110 °C and 100 W is found to yield small amounts of the desired compound after already 4 hours of the reaction time. Therefore, given the possibility of the usage of a microwave with sufficiently big enough reaction vessels and longer operation hours, this synthetic protocol could significantly improve the efficiency.

At first glance toluene seems like an unlikely solvent since the mono-substituted intermediates should have low solubility in such apolar solvent. Unfortunately, stirring 1-mesitylimidazole and 2,2-dichloroethanol in benzonitrile at 130 °C for 3 months does not yield bis(imidazolium) chlorides, also increasing the temperature to 140 °C and stirring the reaction mixture for another week under these conditions yields only an oily residue containing mono-substituted imidazolium salts. As a result, toluene proved itself as the best choice of the solvent. Apart from long reaction times, the procedure in the ACE pressure tubes is simple and all imidazolium salts can be obtained in high purity, as they precipitate out of toluene in contrast to the impurities.

If necessary, a salt metathesis reaction for the anion exchange to PF_6^- and BPh_4^- ions for all bis(imidazolium) chlorides can be performed in H_2O. For the small amounts of **$H_3(L3^{Me})Cl_2$** an anion exchange with stoichiometric amounts of $AgPF_6$ in acetonitrile shows better results due to good solubility of **$H_3(L3^{Me})(PF_6)_2$** in H_2O. All imidazolium salts were fully characterised by means of multinuclear NMR spectroscopy, ESI or FAB-MS and elemental analysis.

^{1}H NMR spectrum of **$H_3(L3^{i\text{-}Pr})Cl_2$** in DMSO-$d_6$ exhibits the expected shift of the imidazolium protons to high frequency (10.13 ppm), indicating the high tendency for easy deprotonation of NCHN-group with mild bases. In comparison to OH-proton corresponding to the triplet at 6.46 ppm the triplet attributed to the CH-group of the bridge is significantly shifted to higher frequency (7.25 ppm) as well. Therefore, the selective deprotonation of the OH group and the

C2 positions of the heterocyclic rings might pose some difficulties. The same tendencies in ^{1}H NMR spectra are observed for **H$_3$(L3^{Mes})Cl$_2$** and all bis(imidazolium) salts **H$_2$(L3^{R})X$_2$** balanced by non-coordinating anions.

Single crystals of **H$_3$(L3$^{i\text{-}Pr}$)(BPh$_4$)$_2$** could be obtained by crystallization from acetone/pentane mixture and characterised by X-Ray diffraction. The molecular structure of **H$_3$(L3$^{i\text{-}Pr}$)(BPh$_4$)$_2$**, which crystallise in triclinic $P\bar{1}$ space group, is shown in Figure 2.1.6. The observed bond distances and angles are similar to same cation with Cl$^-$ as counter ion, whose structure has been previously published by *Zhong et al*.[173a] **H$_3$(L3$^{i\text{-}Pr}$)(BPh$_4$)$_2$** shows a slightly smaller N2–C7–N3 bridge angle in comparison to **H$_3$(L3$^{i\text{-}Pr}$)Cl$_2$** (107.8(2) vs. 109.1(1)). Likely the packing effects with chloride forming a hydrogen bonds to imidazolium and OH protons are responsible for it.

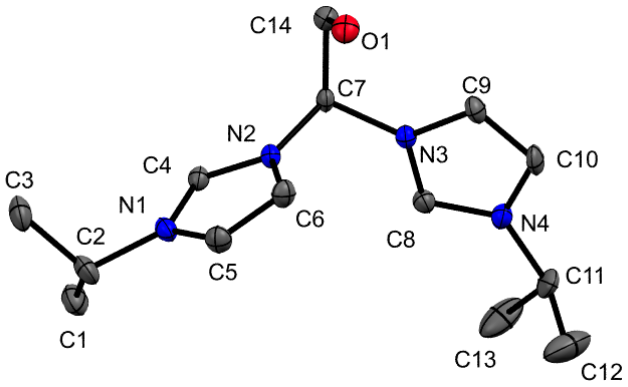

Figure 2.1.6. ORTEP style representation of the cation of the imidazolium salt **H$_3$(L3$^{i\text{-}Pr}$)(BPh$_4$)$_2$** showing the vibrational ellipsoids at 50 % probability level. BPh$_4^-$ anions, hydrogen atoms and co-crystallised acetone molecules are omitted for clarity. Selected bond lengths [Å] and bond angles [deg]: C4–N1 1.330(2), C4–N2 1.334(2), C7–N2 1.467(2), N3-C7 1.473(2); N1–C4–N2 108.3(1), N2–C7–N3 107.8(1).

In comparison to the **H$_3$(L3^{Me})X$_2$** (X = Cl, PF$_6$) the pro-ligands **H$_3$(L3$^{i\text{-}Pr}$)X$_2$** and **H$_3$(L3^{Mes})X$_2$** (X = Cl, PF$_6$, BPh$_4$) are not hygroscopic. As expected, **H$_3$(L3$^{i\text{-}Pr}$)Cl$_2$** and especially **H$_3$(L3^{Mes})Cl$_2$** are less soluble in water and more soluble in methanol. **H$_3$(L3^{Mes})X$_2$** and **H$_3$(L3$^{i\text{-}Pr}$)X$_2$** with non-coordinating anions show good solubility in acetonitrile, acetone, THF and DCM. Generally, in comparison to the methyl-substituted compounds, the pro-ligands with Mes- and *i*-Pr-substituents can be more easily obtained in higher purity and are more convenient to handle, although BPh$_4^-$-salts display high electrostatic properties.

2.1.2.2 Deprotonation Studies

The reactions of 1,1'-(2-hydroxyethane-1,1-diyl)-functionalised bis(imidazolium) salts with alkali metal bases have been conducted using mesityl substituted analogue **H$_3$(L3^{Mes})X$_2$** as a model compound due to its increased solubility in apolar solvents. Also additional steric

crowding of the mesityl wingtips is considered to be beneficial for the formation of more stable metal complexes.

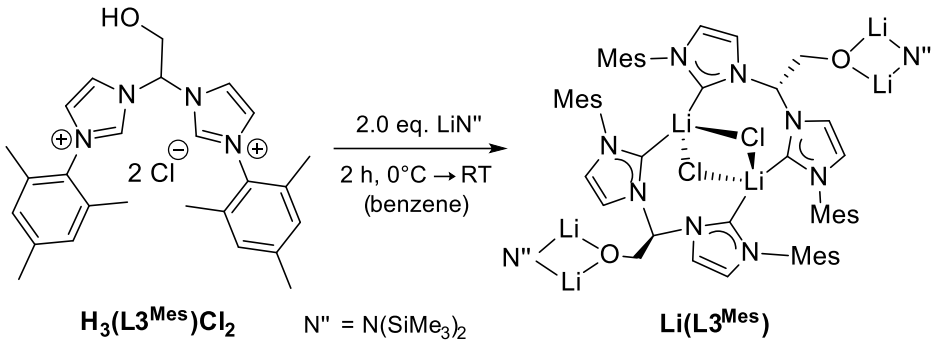

Scheme 2.1.7. The reaction of **$H_3(L3^{Mes})Cl_2$** with LiN" in C_6H_6 at RT. The proposed structure of **$Li(L3^{Mes})$** is based on the experimental data and analogies in the literature.

The deprotonation of **$H_3(L3^{Mes})Cl_2$** is conveniently achieved by a its treatment with LiN" in C_6H_6 yielding **$Li(L3^{Mes})$** (Scheme 2.1.7), which was characterised by ^{1}H, ^{13}C, ^{29}Si INEPT and ^{7}Li NMR spectroscopy. ^{1}H NMR spectrum of **$Li(L3^{Mes})$** is shown in Figure 2.1.7 and it indicates a highly symmetrical product lacking both imidazolium protons as well as the OH proton. Since the two imidazole-2-ylidene backbone protons couple to each other it is unlikely that an abnormal carbene is formed in solution. The coupling pattern and the chemical shift of the bridge also rather suggest the deprotonation of the OH proton and not of the bridge. Moreover, the mesityl substituents are rigid since CH protons and the CH_3 groups display distinct resonances.

Although the obtained material was extensively washed with hexane there is still silicon grease, HN" and possibly also LiN" present in the sample as seen in ^{29}Si NMR spectrum (silicon grease (−21.85 ppm), HN" (1.95 ppm) and LiN" (−10.91 ppm)). This persistence indicates a possible incorporation of bis(trimethylsilyl)amide into a Li NHC cluster, which was already observed in other cases (see Chapter 1. Section 1.2.1).[57]

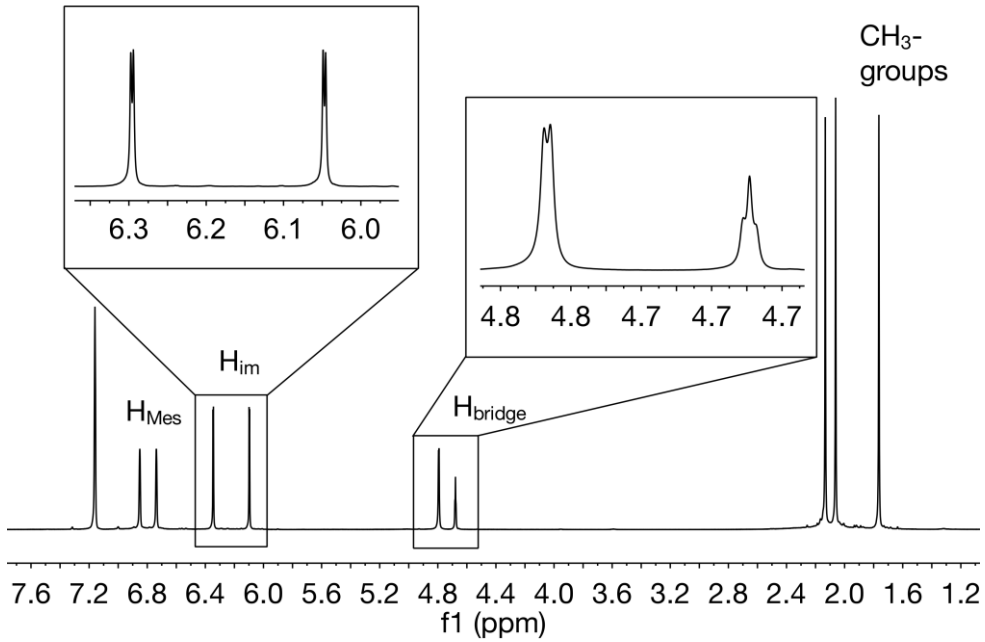

Figure 2.1.7. ^{1}H NMR spectrum of **Li(L3^{Mes})** in C_6D_6 at RT.

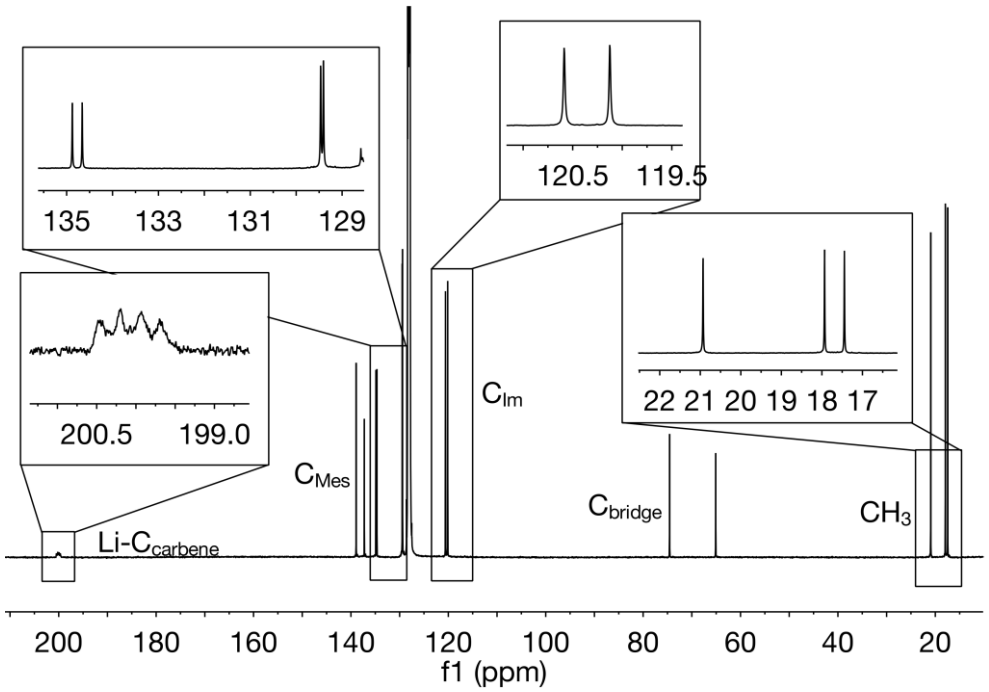

Figure 2.1.8. ^{13}C NMR spectrum of **Li(L3^{Mes})** in C_6D_6 at RT.

The ^{13}C NMR spectrum of **Li(L3^{Mes})** ultimately proves the formation of Li NHC adduct (Figure 2.1.8). The carbenic carbon resonates at relatively high frequency for these compounds (199 ppm) displaying a coupling pattern to Li nuclei (br q, $^{1}J_{Li\text{-}C}$ = 33 Hz). These values lie within the range reported for Li compounds associated with unsaturated NHCs and halogen

anions.[64-65] All other remaining singlets can be assigned to the ligand framework thereby confirming the high symmetry of **Li(L3^{Mes})** in solution. Finally, two signals are visible in the ^{7}Li NMR spectrum of **Li(L3^{Mes})** suggesting that the product contains two distinct Li centres.

Arnold *et al.* have previously described the isolation of LiBr NHC cluster with μ^2-bridging bromo ligands for amido-functionalised NHCs.[62] Therefore, since a preparation of **Li(L3^{Mes})** by deprotonation of **H$_3$(L3^{Mes})(PF$_6$)$_2$** with LiN" was unsuccessful, a possibility of incorporation of chloride ions was investigated by dissolving **Li(L3^{Mes})** adduct in aqueous HNO_3. As expected, the Li NHC decomposes hereby instantaneously. By subsequent addition of an aqueous $AgNO_3$ solution a formation of white AgCl precipitate strongly indicates the incorporation of chloride anions into **Li(L3^{Mes})**. The performed elemental analysis confirms these observations (6.86 wt.% of Cl, see Experimental Section).

In summary, all NMR data as well elemental analysis indicate a formation of a symmetrical $Li_xCl_yN"_z$-NHC cluster. Unfortunately, although **Li(L3^{Mes})** is stable in the solid state at RT, it gradually degrades within 1 day in solution. One of the main decomposition products is 1-mesitylimidazole (Figure 2.1.10), which can be doubtless identified by a comparison of the ^{1}H NMR spectrum of decomposed **Li(L3^{Mes})** to the spectrum of pure 1-mesitylimidazole. The other main decomposition product is more difficult to assign. However, a singlet at 8.23 ppm and the integral ratio of other corresponding multiplets in the aromatic region indicate a possible hydrolysis of the imidazolylidene ring to an open-chain species **B** or **C** whose aldehyde group resonates in the same region (for DIPP substituted imidazolylidene: 8.04 for **B** and 8.20 ppm **C**, see Figure 2.1.9)[174].

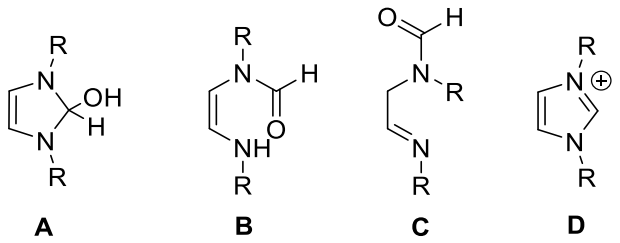

Figure 2.1.9. Chemical structures of the hydrolysis products of imidazole-derived carbenes.[174]

Hollóczki *et al*. examined the dependence of the ratio of hydrolysis products of free carbenes depending on the amount of water in the sample. With 0.5 eq. up to 4.0 eq. of H_2O the open chain products are observed, whether excess of H_2O leads to formation of imidazolium cations.[174] Therefore, it is possible, that small amount of water in the solvent used for the synthesis of **Li(L3^{Mes})** could cause such decomposition. But since the ^{1}H NMR spectrum of degraded **Li(L3^{Mes})** contains other impurities, which impede accurate integration, the definitive assignment of the resonances to these open chain products is difficult.

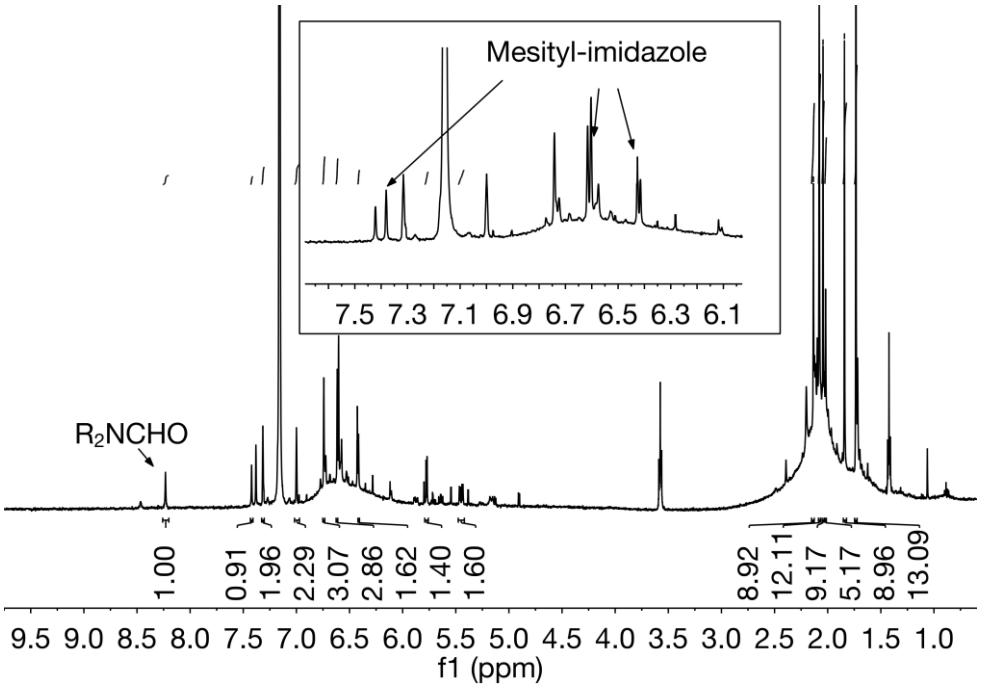

Figure 2.1.10. ^{1}H NMR spectrum of decomposed **Li(L3^{Mes})** in C_6D_6 at RT.

Due to its instability all attempts to crystallise **Li(L3^{Mes})** by various methods using different solvents failed so far. Hereby, a formation of fine white precipitate also indicated an elimination of LiCl.

Noteworthy, by performing the same reaction in toluene at RT overnight or in THF by slowly warming up the reaction mixture from 0 °C to RT for 3 h the decomposition occurs much faster as only 1-mesitylimidazole is detected as major product in both cases. The evident destruction of the bridge suggests a possible deprotonation of the 1,1'-(2-hydroxyethane-1,1-diyl) group due to high acidity of N*CH*(CH_2OH)N proton. Interestingly, Arnold *et al*. previously also reported an elimination of one of the *N*-alkyl-substituents of bis(adamantylethoxy)-functionalised imidazolium salt after it was treated with KH.[175] A similar mechanism could be also responsible for the elimination of 1-mesitylimidazole in this case.

The use of heavier alkali metal analogues of LiN" results in even faster decomposition of the ligand. For example, the treatment of **H$_3$(L3^{Mes})Cl$_2$** with KN" in THF yields almost instantaneously brown solution containing 1-mesitylimidazole as major product (Scheme 2.1.8). On NMR scale in C_6D_6 the reaction of **H$_3$(L3^{Mes})Cl$_2$** with NaN" proceeds slower, but nevertheless overnight the evidence of the same decomposition pathway is evident.

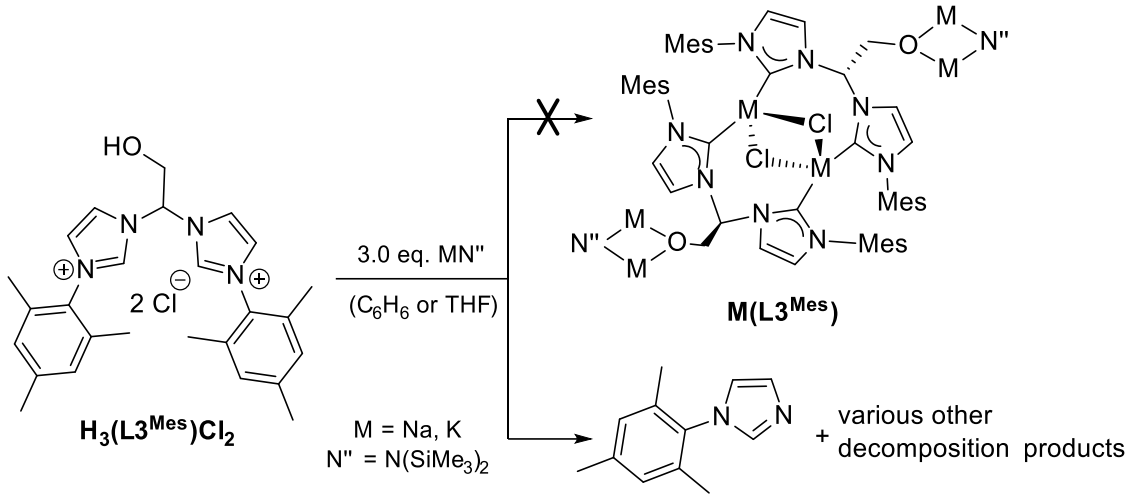

Scheme 2.1.8. Reaction of **$H_3(L3^{Mes})Cl_2$** with NaN" or KN" at RT in C_6H_6 or THF respectively.

By the way, the hydrolysis of **$Li(L3^{Mes})$** in presence of H_2O yields only 1-mesitylimidazole as major product as well (Scheme 2.1.9). The degradation by adding excess of H_2O to the material obtained by a reaction of **$H_3(L3^{Mes})Cl_2$** with NaN" in THF or C_6H_6 also results only in identification of this decomposition product. But these results should be treated with care as it is also possible that the decomposition already occurred before the addition of H_2O.

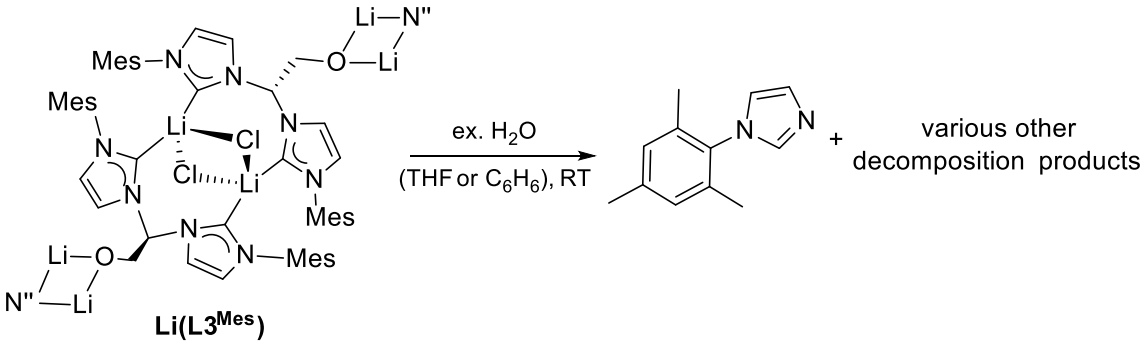

Scheme 2.1.9. Decomposition of **$Li(L3^{Mes})$** by addition of H_2O in excess.

Interestingly, a treatment of **$H_3(L3^{i\text{-}Pr})Cl_2$** with LiN" in THF (Scheme 2.1.10) yields a colourless residue, whose ^{1}H NMR spectrum indicates an asymmetrical, but deprotonated NHC (SI, Figure 5.3.7). However, the multiplets are too broad for definitive identification, suggesting a probable extreme oligomerization of the material. After dissolving the residue in THF and adding of 2M HCl solution in Et_2O, a formation of precipitate is observed. ^{1}H NMR of this solid in DMSO-*d*$_6$ confirms re-formation of **$H_2X(L3^{i\text{-}Pr})Cl_2$** with OH protons partially being substituted by X = D or K (Scheme 2.1.10, for ^{1}H NMR spectrum see SI, Figure 5.3.8). Hence, this observation strongly suggests that at least metastable Li NHC adduct is formed, that might be more favourable in contrast to **$H_3(L3^{Mes})Cl_2$** due to lesser steric hindrance of *i*-Pr.

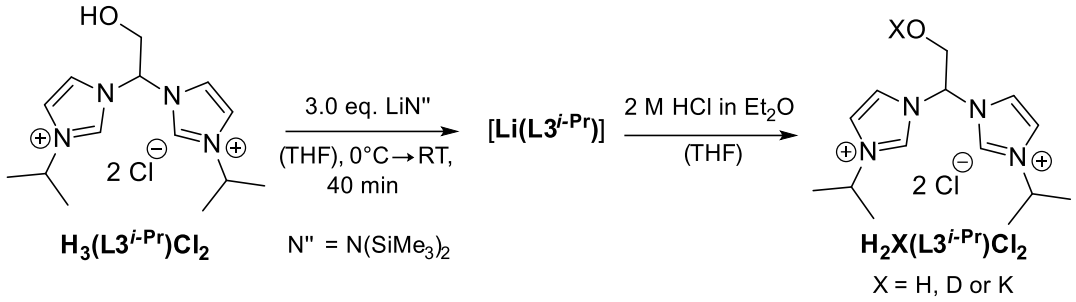

Scheme 2.1.10. Formation of **Li(L3$^{i\text{-Pr}}$)** and subsequent re-formation to **H$_2$X(L3$^{i\text{-Pr}}$)Cl$_2$** by hydrolysis.

In conclusion, only the usage of LiN'' as deprotonation agent for 1,1'-(2-hydroxyethane-1,1-diyl)-bridge functionalised bis(imidazolium) salts **H$_3$(L3^{R})Cl$_2$** shows the potential to be applied in transmetallation reaction with electropositive metals. However, similar to the alkali metal adducts of *N*-(3,5-di-*tert*-butyl-2-hydroxyphenyl) and *N*-bis(3,5-di-*tert*-butyl-2-hydroxybenzyl) functionalised mono(NHC) ligands described above, due to thermal sensitivity the generation of corresponding **Li(L3^{R})** compounds should be performed *in situ* below RT.

2.1.3 1,1'-(2-Hydroxypropan-1,3-diyl) Bridge Functionalised Bis(imidazolium) Bromide H$_3$(L4^{Mes})Br$_2$

2.1.3.1 Synthesis and Characterization

The pro-ligand **H$_3$(L4^{Mes})Br$_2$** can be prepared in high yield and high purity by a nucleophilic substitution reaction of 1,3-dibromo-propan-2-ol and 1-mesitylimidazole (Scheme 2.1.11). The use of benzonitrile as solvent is most favourable, due to its sufficient high polarity to solubilize the single substituted intermediate and possibility of applying high temperatures. **H$_3$(L4^{Mes})Br$_2$** was fully characterised by means of multinuclear NMR spectroscopy, FAB-MS and EA. The compound is well soluble in water, methanol, DCM and slightly in MeCN.

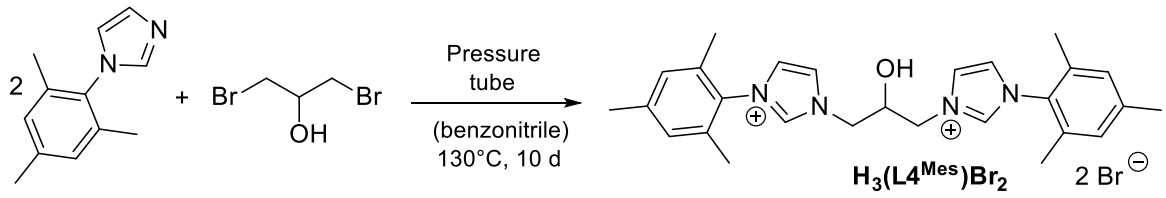

Scheme 2.1.11. Synthesis of **H$_3$(L4^{Mes})Br$_2$**.

The ^{1}H NMR spectrum of **H$_3$(L4^{Mes})Br$_2$** in DMSO-d_6 shows the expected symmetrical set of resonances. The doublet attributed to OH group is observed at 6.16 ppm suggesting the possibility of its deprotonation by sufficiently strong bases. Interestingly, the two CH_2-groups of the linker chain are not chemically equivalent. They correspond to two doublet of doublets

at 4.64 ppm and 2.26 ppm, respectively and display the germinal coupling constant of 13.7 Hz. However, the vicinal coupling constants to the proton in the middle of the bridge are quite different (2.3 Hz and 8.9 Hz). As a result, the CH resonance appears as multiplet at 4.55 – 4.45 ppm. Such interesting splitting pattern is caused by the different torsion angles between the CH-group and both CH_2-groups of the bridge (approximately 60º and 170º respectively). These angles are probably maintained in the solution due to hydrogen bonding of the OH group to imidazolium protons. In the solid state this effect has been also already previously observed and verified by SC-XRD.[176]

2.1.3.2 Deprotonation Studies

By attempting the deprotonation of **$H_3(L4^{Mes})Br_2$** *via* treating this compound with LiN" in benzene at RT analogue to the procedures described for **$Li(L3^{Mes})$**, no reaction is observed due to bad solubility of **$H_3(L4^{Mes})Br_2$** in this solvent. However, **$H_3(L4^{Mes})Br_2$** reacts with KN" at RT in THF (Scheme 2.1.12), yielding a highly symmetric product (Figure 2.1.11). Also the presence of carbene is confirmed by ^{13}C resonance at 214.31 ppm. Since other reported values for ^{13}C resonances of K NHC adducts with imidazol-2-ylidenes lie within the same range,[57, 65b] the obtained compound was tentatively assigned to be a K NHC adduct **$K(L4^{Mes})$**. Furthermore, ^{29}Si NMR shows the exclusive formation of HN", confirming a clean conversion. Unfortunately, after letting the sample to stand several days at RT slow decomposition of the product into various organic compounds including 1-mesitylimidazole is observed.

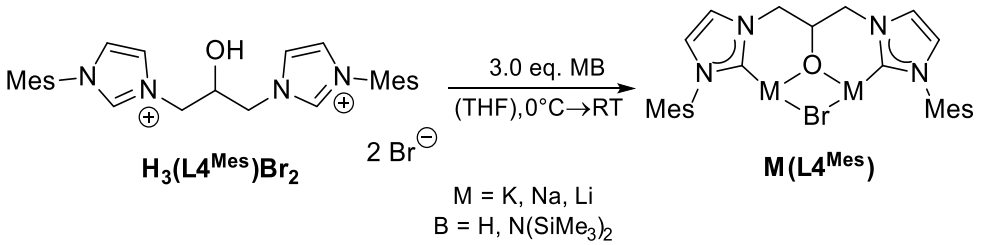

$H_3(L4^{Mes})Br_2$ **$M(L4^{Mes})$**

Scheme 2.1.12. Deprotonation of **$H_3(L4^{Mes})Br_2$** with alkali metal bases. The molecular structure of **$M(L4^{Mes})$** is a simplified suggestion based on NMR characterization and hydrolysis studies.

Due to promising results on NMR scale the possibility of the isolation of **$K(L4^{Mes})$** on preparatory scale was investigated subsequently. ^1H NMR spectrum of the brown residue obtained at 0 °C confirms the presence of **$K(L4^{Mes})$** but in comparison to the NMR scale reaction the sample is severely contaminated. Due to time-consuming removal of KBr the warming up of the solution cannot be excluded. Hereby, similar to the decomposition behaviour of pure **$M(L4^{Mes})$** on NMR scale at RT mentioned above the formation of 1-mesitylimidazole is observable among other impurities. All further purification attempts lead to even higher degree of contamination. Also crystallization with various methods in order to obtained crystals

suitable for SC-XRD failed. These difficulties stress out the high thermal sensitivity of **K(L4^{Mes})**. Notably, the product is also very air-sensitive and ignites upon exposure to the atmosphere, making further characterization by other methods challenging as well.

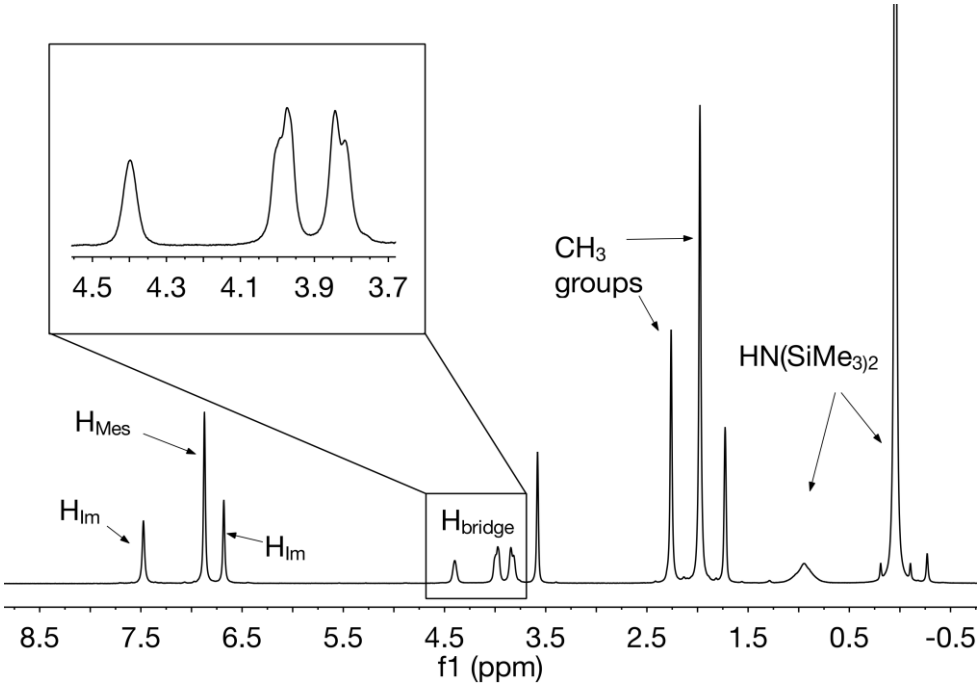

Figure 2.1.11. ^{1}H NMR spectrum von **K(L4^{Mes})** formed on NMR scale in THF-d_8 at RT.

The hydrolysis of **K(L4^{Mes})** with excess of H_2O performed in the same manner as with alkali metal adducts of 1,1'-(2-hydroxyethane-1,1-diyl)-bridged functionalised NHC described in previous section yields no re-formation of the imidazolium salt. However, this fact does not strongly imply that a K NHC is not formed as the decomposition could have occurred before the hydrolysis or due to reaction with H_2O. ^{1}H NMR spectrum of the obtained residue in DMSO-d_6 is very difficult to analyse due to numerous overlapping resonances (SI, Figure 5.3.9). However, the presence of a singlet at 8.58 ppm (attributed to NCHO) could indicate at least partial formation of open-chain products mentioned earlier (Section 2.1.2.2). The elimination of 1-mesitylimidazole is also likely. In conclusion, all data indicate a formation of a symmetrical K NHC adduct which is not stable at RT in solution. The hydrolysis of **K(L4^{Mes})** with aqueous HNO_3 solution and subsequent addition of aqueous $AgNO_3$ results in formation of white AgBr precipitate indicating the incorporation of bromide into **K(L4^{Mes})**. Based on these observations a suggestion for a possible molecular structure of **K(L4^{Mes})** is shown in Scheme 2.1.12.

To investigate the possibility of deprotonation of **H$_3$(L4^{Mes})Br$_2$** with KN" at lower temperatures for minimizing possible degradation, the formation of **K(L4^{Mes})** was monitored by ^{1}H NMR spectroscopy in 20 °C steps as J-Young NNR tube containing all reactants slowly warmed up. Hereby, the product formation was already observed at –78 °C (see SI, Figure 5.3.10-13). However, this result should be treated with care, since the reaction could have already started

in 30 seconds of exposure to RT during which the NMR tube was transported out of the glove box. Furthermore, the proton spectrum remains constant till the formation of the product visibly speeds up between 0 °C and 20 °C. Interestingly, a presence of smaller set of broad multiplets till –20 °C indicates that formation of **K(L4^{Mes})** could proceed *via* an intermediate. Notably, the same reaction conducted at preparatory scale (500mg of the pro-ligand) shows no signs of product formation by slowly warming up till –20 °C as well. Only at 0 °C the solution turned over blue to yellow and then at RT to expected dark brown further supporting the assumption of the existence of an intermediate. In summary, according to all these observations, the deprotonation of **H$_3$(L4^{Mes})Br$_2$** is most efficient at approximately 0 °C.

In order to exclude a possible destabilizing presence of HN" in the **K(L4^{Mes})** samples, a deprotonation of **H$_3$(L4^{Mes})Br$_2$** with KH was conducted under the same conditions. On exploratory NMR scale at RT a formation of symmetrical deprotonated species is evident but although the pattern of the resonances corresponds to **K(L4^{Mes})**, all multiplets are slightly shifted in comparison to ^{1}H NMR spectrum of **K(L4^{Mes})** (Figure 5.3.13). Unfortunately, after 2 hours at RT the product completely decomposes into various different molecules as indicated by the appearance of overlapping resonances in ^{1}H NMR spectrum. Hereby, the bridge resonances disappear and a presence of a distinct singlet at 8.04 ppm suggests similarly to hydrolysis experiments mentioned above the formation of open-chain products.

The thermal instability of **K(L4^{Mes})** could impede the successful transmetallation reactions to rare earth metals. Therefore, the deprotonation reactions with LiN" and NaN" were further investigated, since it has been previously reported that alkali metal NHC adducts are less thermally stable with heavier alkali metals and undergo rapid 1,2-shift of the imidazolylidene substituents.[4, 19e]

The reaction of **H$_3$(L4^{Mes})Br$_2$** with lighter homologues of KN" proceeds slower, e. g. on NMR scale the consumption of NaN" is not complete before 24 h at RT in THF, which is confirmed by monitoring the reaction by ^{29}Si NMR *via* the conversion of NaN" to HN". Interestingly, a silicon resonance at 7.61 ppm indicates a possible presence of terminal –O(SiMe$_3$) fragments previously observed in other reactions described above.[172, 177] Unfortunately, the ^{1}H NMR spectrum of the reaction shows broad hardly quantifiable resonances (SI, Figure 5.3.14). A formation of desirable Na NHC species cannot be excluded, however a resonance at 8.59 ppm indicates the generation of open chain products as well.[174] Moreover, the hydrolysis of the same reaction mixture by adding excess of H_2O indicates no re-formation of the bis(imidazolium) salt. Also here some resonances over 8 ppm could indicate the generation of open chain products.

LiN" reacts with **H$_3$(L4^{Mes})Br$_2$** much faster, approximately within 30 min in THF at RT. By monitoring the conversion by ^{1}H NMR spectroscopy broad singlets appear in the expected

region for deprotonated precursor (Figure 2.1.12). Although the integral ratio of resonances approximately matches the desired compound, the bad resolution precludes definitive identification.

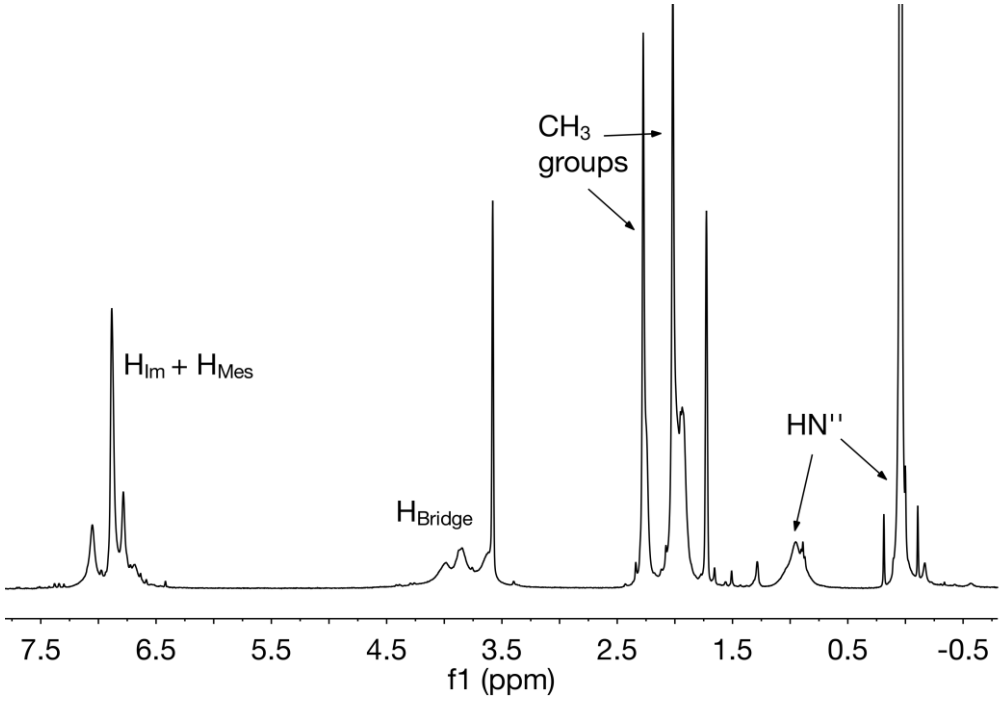

Figure 2.1.12. ^{1}H NMR spectrum of **Li(L4^{Mes})** in THF-d_8 at room temperature.

In ^{13}C NMR spectrum of **Li(L4^{Mes})** no Li–C_C resonance is visible, but other singlets appear in the expected region and can be clearly assigned. ^{29}Si NMR confirms the exclusive formation of HN". Moreover, no decomposition is observed by discoloration as seen for **K(L4^{Mes})** and also in ^{1}H NMR spectrum after 3 days at RT no impurities are detected. Furthermore, **Li(L4^{Mes})** could be also easily isolated on preparatory scale after the separation of eliminated LiBr by extracting the crude product with benzene. However, ^{1}H NMR of possible LiBr free **Li(L4^{Mes})** in C_6D_6 still shows broad, hardly quantifiable resonances, suggesting a probable high propensity for oligomerization as frequently observed for Li NHCs (Chapter 1, Section 1.2).

Up to date no crystals suitable for SC-XRD could be obtained by various crystallization methods and therefore the molecular structures of **M(L4^{Mes})** (M = K, Na, Li) in the solid state remain unknown. However, especially **K(L3^{Mes})** shows potential to be used as a NHC transfer reagent *in situ* at 0°C.

2.1.4 *N*-Furanyl Functionalised Bis(imidazolium) Salts $H_2(L5^R)X_2$ and $H_2(L6^R)X_2$

2.1.4.1 Synthesis and Characterization

The synthesis of a *N*-furanyl-functionalised methylene-bridged bis(NHC) pro-ligand **$H_2(L5^{Fu})Br_2$** has been previously published by Rieb *et al*.[178] Hereby, a nucleophilic substitution reaction of 1-furanylimidazole with CH_2Br_2 yields **$H_2(L5^{Fu})Br_2$**. Although CH_2Br_2 is used in excess, no mono-substituted products are observed due to higher reactivity of the mono-substituted intermediate resulting from further electrophilic activation by the *N*-substituent.[178] In the next step, if necessary, an anion exchange can be performed *via* salt metathesis reactions yielding **$H_2(L5^{Fu})(PF_6)_2$** or **$H_2(L5^{Fu})(BPh_4)_2$** (Scheme 2.1.13) in high yields.

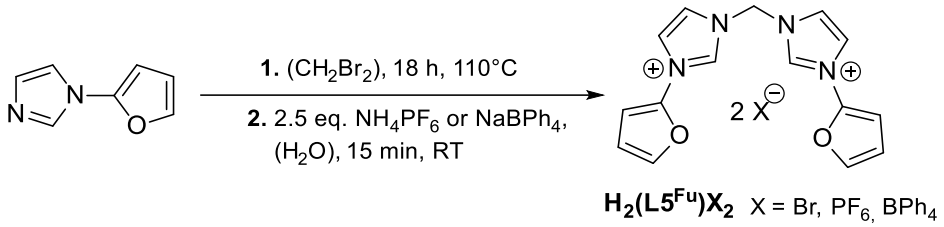

Scheme 2.1.13. Synthesis of the ligand class **$H_2(L5^{Fu})X_2$.**

To expand the ring size to accommodate the possibility of chelation of bigger cations a prolongation of the linker between two imidazolium moieties was conducted. Therefore, ethane-1,2-diyl-bridged **$H_2(L6^{Fu})Br_2$** is prepared in a nucleophilic substitution reaction with 1-furanylimidazole and 1,2-dibromoethane. In comparison to the synthetic procedure with an exess of CH_2Br_2, in this case, due to lower electrophilic activation of mono-substituted product a stoichiometric reaction in a pressure tube in THF yields better results (Scheme 2.1.14). Subsequently, if necessary, an anion exchange reaction is also conveniently performed in water analogue to methylene bridged compounds.

Both compound classes **$H_2(L5^{Fu})X_2$** and **$H_2(L6^{Fu})X_2$** are obtained in high yields and high purity. They have been fully characterised by multinuclear NMR spectroscopy, EA and FAB-MS or ESI-MS. Additional characterization by SC-XRD was conducted for **$H_2(L5^{Fu})(PF_6)_2$**, which crystalizes in orthorhombic space group *Pnma* (Figure 2.1.13).[178] All of the observed bond distances and bond angles lie within the range reported for similar compounds.[179]

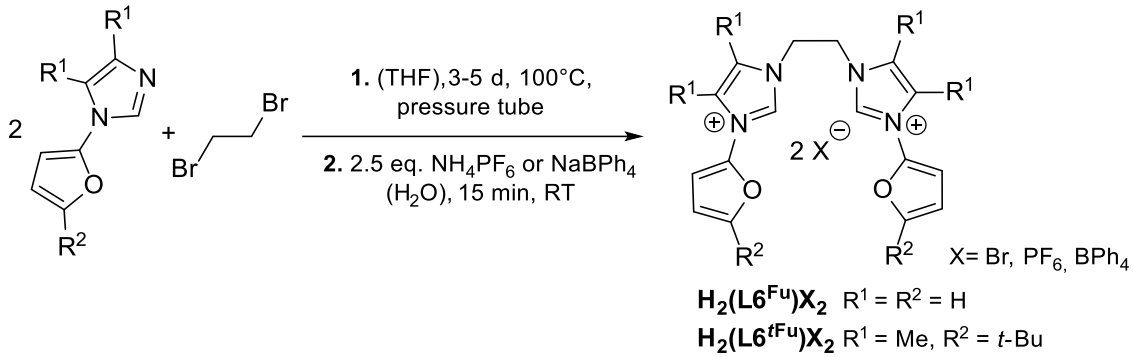

Scheme 2.1.14. Synthesis of the ethane-1,2-diyl-bridged *N*-furanyl-substituted bis(imidazolium) salts **$H_2(L6^R)X_2$** (R = Fu, *t*Fu).

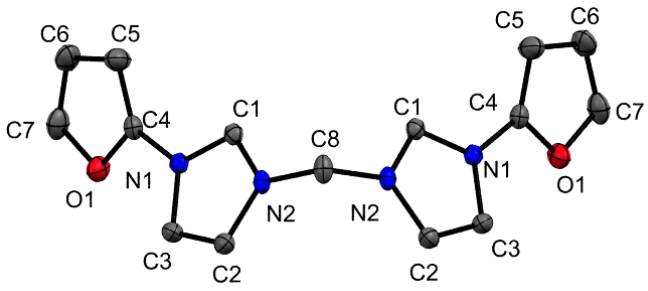

Figure 2.1.13. ORTEP style representation of the cation of **$H_2(L5^{Fu})(PF_6)_2$** showing the vibrational ellipsoids at 50 % probability level. Hydrogen atoms, PF_6^- and co-crystalized acetonitrile molecules are omitted for clarity. Selected bond lengths [Å] and bond angles [deg]: C1–N1 1.326(2), C1–N2 1.330(2), C8–N2 1.457(2); N2–C8–N2 110.0(4), N1–C1–N2 108.0(1). Symmetry transformations used to generate equivalent atoms: (c) x,–y+1/2, z.[178]

Since **$H_2(L5^{Fu})X_2$** and **$H_2(L6^{Fu})X_2$** (X = PF_6, BPh_4) have limited solubility in non-polar solvents, a modification of the ligand framework by introducing non-polar groups is expected to solve this problem. An alkylation can be also advantageous for possible complexes with respect to increased solubility and stability due to additional steric crowding. Therefore, a *tert*-butyl group on the furanyl-substituent and two methyl-groups on the imidazolium backbone were introduced into the ligand framework. To achieve that, 1-(5-(*tert*-butyl)furan-2-yl)-4,5-dimethyl-imidazole **5d** was prepared in a 4-step reaction (Scheme 2.1.15).

In the first step a preparation of 2-*tert*-butylfuran **5a** was conducted. A direct alkylation of furan is difficult due to resinification, therefore, 2-*tert*-butylfuran is isolated as a product of a Friedel-Crafts-Alkylation with subsequent decarboxylation of 2-furoic acid according to the method of Fitzpatrick *et al*.[180] Subsequently, due to stabilization effect of the alkyl-substituent in the 2-position, a bromination of 2-*tert*-butylfuran proceeds selectively and almost quantitatively with *N*-bromosuccinimide (NBS) at RT yielding 2-bromo-5-(*tert*-butyl)furan **5b**.

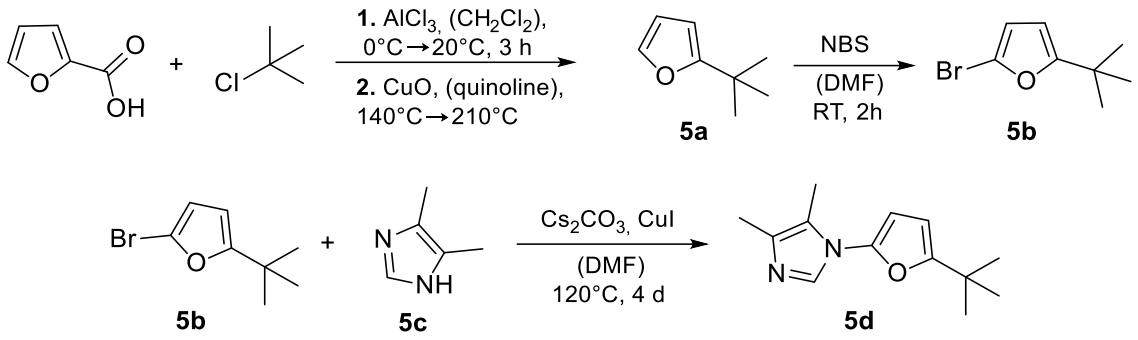

Scheme 2.1.15. Functionalization of 1-furanylimidazole.

In the next step 4,5-dimethylimidazole **5c** was prepared by the method published by Bredereck.[181] It is based on a combination of amination and formylation reactions of acetoin with subsequent closure to an aromatic ring system. The product of this synthesis is not a free base as Bredereck thought, but in fact a formic acid salt.[182] Fortunately, it does not disturb a subsequent Ullman type coupling reaction of **5c** with **5b** yielding 1-(5-(*tert*-butyl)furan-2-yl)-4,5-dimethyl-imidazole **5d** (Scheme 2.1.15).

The methylene bridged imidazolium salt **H_2(L5^{tFu})Br_2** is subsequently obtained in stoichiometric reaction with CH_2Br_2, but, probably due to significantly increased steric hindrance of **5d**, in quite low yields. The reaction in excess of dibromomethane similar to **H_2(L5^{Fu})Br_2** is significantly less clean making the isolation of pure **H_2(L5^{tFu})Br_2** according to this protocol very difficult. Only after *in situ* anion exchange to BPh_4^- pure **H_2(L5^{tFu})$(BPh_4)_2$** is obtained in low overall yield (Scheme 2.1.16).

In contrast to methylene bridged congener, the (ethane-1,2-diyl) bridged **H_2(L6^{tFu})Br_2** is easily obtained by applying the same synthetic method as for **H_2(L6^{Fu})Br_2** (Scheme 2.1.14). Notably, in contrast to the synthesis of **H_2(L6^{Fu})Br_2** the yield of the reaction increases, presumably due to increased basicity of the substrate **5d**. The steric hindrance seems to play here a less important role as for methylene bridged analogues.

H_2(L5^{tFu})X_2 and **H_2(L6^{tFu})X_2** (R = Me, Et; X = Br, PF_6, BPh_4) were also characterised by multinuclear NMR spectroscopy, FAB-MS or ESI-MS and EA. As expected, due to increased electron density in alkylated compounds the resonances in ^{1}H NMR spectra are shifted to lower frequencies in comparison to their unsubstituted analogues (e.g. δ (ppm) NCHN in DMSO-d_6: **H_2(L5^{Fu})Br_2** 10.20, **H_2(L5^{tFu})Br_2** 9.91; **H_2(L6^{Fu})Br_2** 9.95, **H_2(L6^{tFu})Br_2** 9.70).

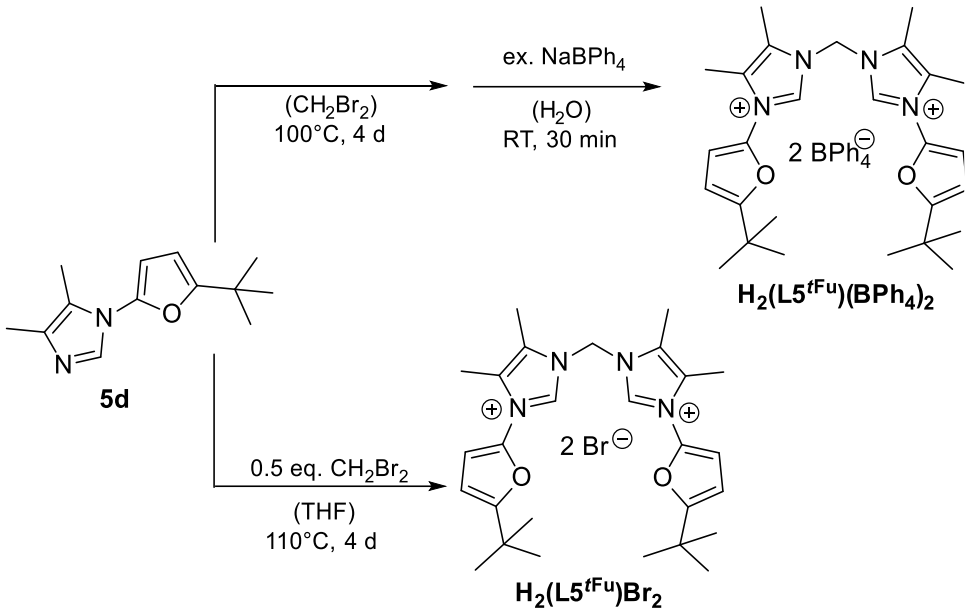

Scheme 2.1.16. Synthesis of the ligand class $\mathbf{H_2(L5^{tFu})X_2}$.

Single crystals of $\mathbf{H_2(L5^{tFu})(BPh_4)_2}$ and $\mathbf{H_2(L6^{tFu})Br_2}$ suitable for SC-XRD were grown by slow diffusion of diethyl ether into a solution of the respective compounds in acetonitrile. Furthermore, single crystals of $\mathbf{H_2(L6^{tFu})(PF_6)_2}$ could be obtained by slow diffusion of hexane into a solution of this bis(imidazolium) salt in THF. $\mathbf{H_2(L6^{tFu})Br_2}$ (Figure 2.1.15) crystallises in monoclinic space group *C*2/c. The molecular structures of $\mathbf{H_2(L5^{tFu})(BPh_4)_2}$ and $\mathbf{H_2(L6^{tFu})(PF_6)_2}$, which crystallise in triclinic system $P\bar{1}$, are shown in Figure 2.1.14 and Figure 2.1.16 respectively. All angles and distances in these molecules are comparable and also lie within the range of reported similar molecules.[179] A comparison between non-functionalised $\mathbf{H_2(L5^{Fu})(PF_6)_2}$ and its more apolar congener $\mathbf{H_2(L5^{tFu})(BPh_4)_2}$ shows almost no difference in bond distances and bond angles in the imidazolium moieties. However, slightly longer distances in the bridge and also bigger bridge angle N1–C4–N3 can be observed for alkylated imidazolium salt $\mathbf{H_2(L5^{tFu})(BPh_4)_2}$ (111.64° vs. 110.0° for $\mathbf{H_2(L5^{Fu})(PF_6)_2}$). This fact can be explained by the increased steric hindrance of the molecule. Furthermore, in comparison to the structure of $\mathbf{H_2(L5^{Fu})(PF_6)_2}$, where the carbon atoms between the two nitrogens of the imidazole rings are on the same side of the molecule, with increased steric hindrance a twist between the imidazolium moieties can be observed for all reported structures of alkylated compounds resulting in the NCHN fragments turning in different directions in solid state.

All pro-ligands described in this section are obtained as non-hygroscopic white powders. $\mathbf{H_2(L5^{Fu})Br_2}$ and $\mathbf{H_2(L6^{Fu})Br_2}$ are only soluble in water and methanol. Due to alkylation the bromide salts of modified more apolar ligands are also soluble in acetonitrile. As expected, the solubility of all pro-ligands in other polar organic solvents such as acetone, acetonitrile and THF increases dramatically through anion exchange to non-coordinating ions. The alkylated

bis(imidazolium) cations balanced by PF_6^- and BPh_4^- show therefore also excellent solubility in DCM. Unfortunately, all compounds with BPh_4^- as counter anion are extremely electrostatic, which makes the handling more difficult.

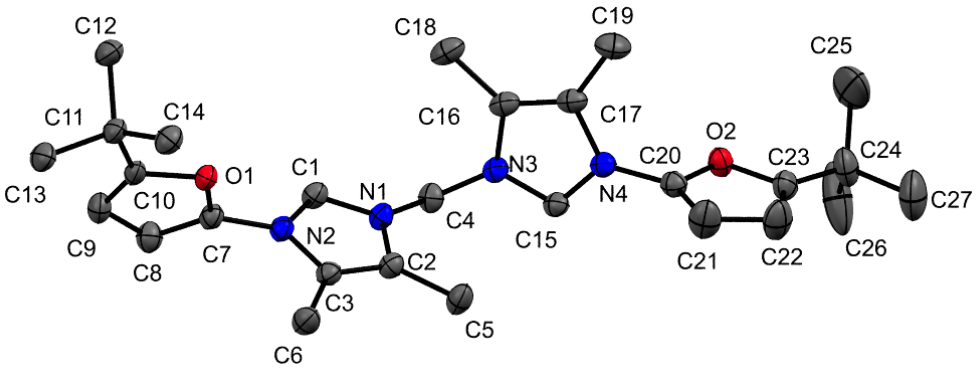

Figure 2.1.14. ORTEP style representation of the cation of **$H_2(L5^{tFu})(BPh_4)_2$** showing the vibrational ellipsoids at 50 % probability level. BPh_4^-, hydrogen atoms and co-crystalized diethyl ether molecules are omitted for clarity. Selected bond lengths [Å] and bond angles [deg]: C1–N1 1.330(2), C1–N2 1.330(2), C4–N1 1.471(2); N1–C4–N3 111.6(1), N1–C1–N2 108.1(1).

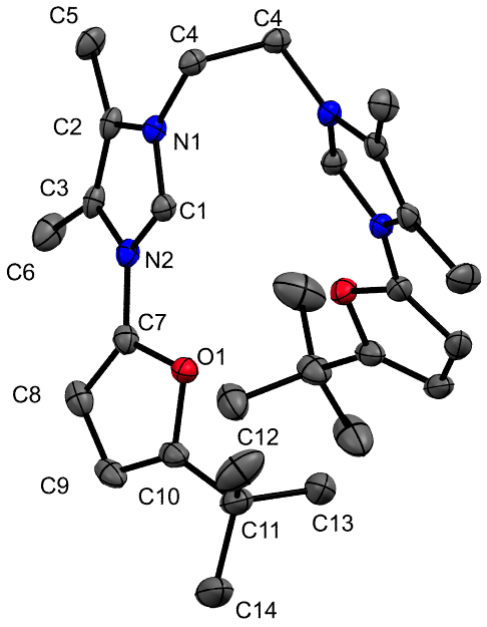

Figure 2.1.15. ORTEP style representation of the cation of **$H_2(L6^{tFu})Br_2$** showing the vibrational ellipsoids at 50 % probability level. Hydrogen atoms and bromide anions are omitted for clarity. Selected bond lengths [Å] and bond angles [deg]: C1–N1 1.327(3), C1–N2 1.338(2), C4–N1 1.467(3); N1–C4–C4 110.83(13), N1–C1–N2 107.88(16). Symmetry transformations used to generate equivalent atoms: (c) –x,y,1/2–z.

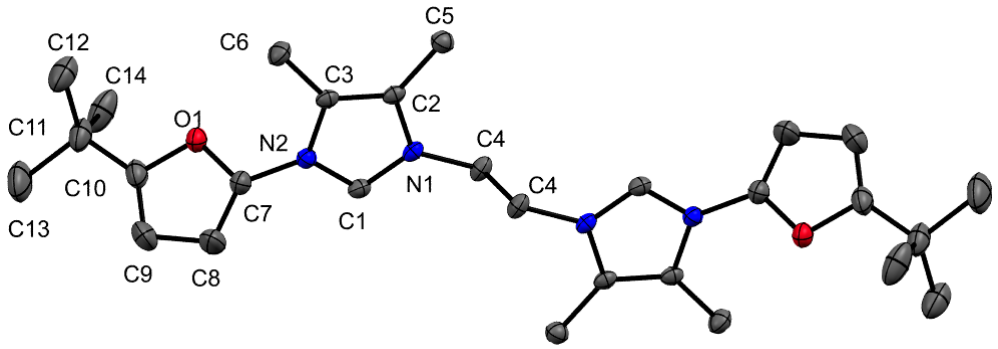

Figure 2.1.16. ORTEP style representation of the cation of $\mathbf{H_2(L6^{tFu})(PF_6)_2}$ showing the vibrational ellipsoids at 50 % probability level. PF_6^- anions and protons are omitted for clarity. Selected bond lengths [Å] and bond angles [deg]: C1–N1 1.322(2), C1–N2 1.334 (2), C4–N1 1.467(2); N1–C4–C4 110.4(1), N1–C1–N2 108.1(1). Symmetry transformations used to generate equivalent atoms: (c) –x, –y,–z.

2.1.4.2 Deprotonation Studies

The possibility of carbene generation by deprotonation of *N*-furanyl-substituted bis(NHC) pro-ligands with lithium or potassium bis(trimethyl)silylamides (KN" or LiN") was explored in a series of NMR scale reactions as well as on preparatory scale. Thereby, the impact of different reaction times, various solvents and counter anions has been investigated. Due to bad solubility of $\mathbf{H_2(L5^{Fu})X_2}$ and $\mathbf{H_2(L6^{Fu})X_2}$ (X = Br, PF_6, BPh_4) in organic solvents their deprotonation reactions were conducted in THF at room temperature.

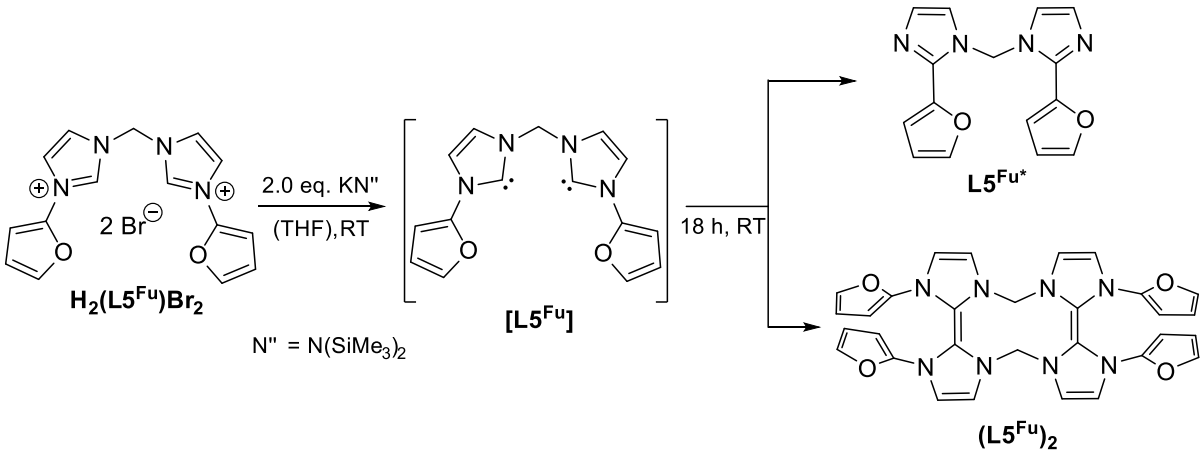

Scheme 2.1.17. Reaction of $\mathbf{H_2(L5^{Fu})Br_2}$ with KN" in THF at RT resulting in formation of two possible products.

$\mathbf{H_2(L5^{Fu})Br_2}$ reacts with KN" within seconds at RT in THF (Scheme 2.1.17). Hereby, the white suspension turns dark violet and high amount of precipitate is formed. After 10 minutes the ^{1}H NMR spectrum of the solution contains a set of new resonances, that can be tentatively

assigned to a symmetrical, carbene-containing product **[L5^{Fu}]**, and minor, unidentified resonances (Figure 2.1.17). No remaining starting material is observed at this point. The low resolution and significant broadening of the resonances is a result of high amount of eliminated KBr in the tube.

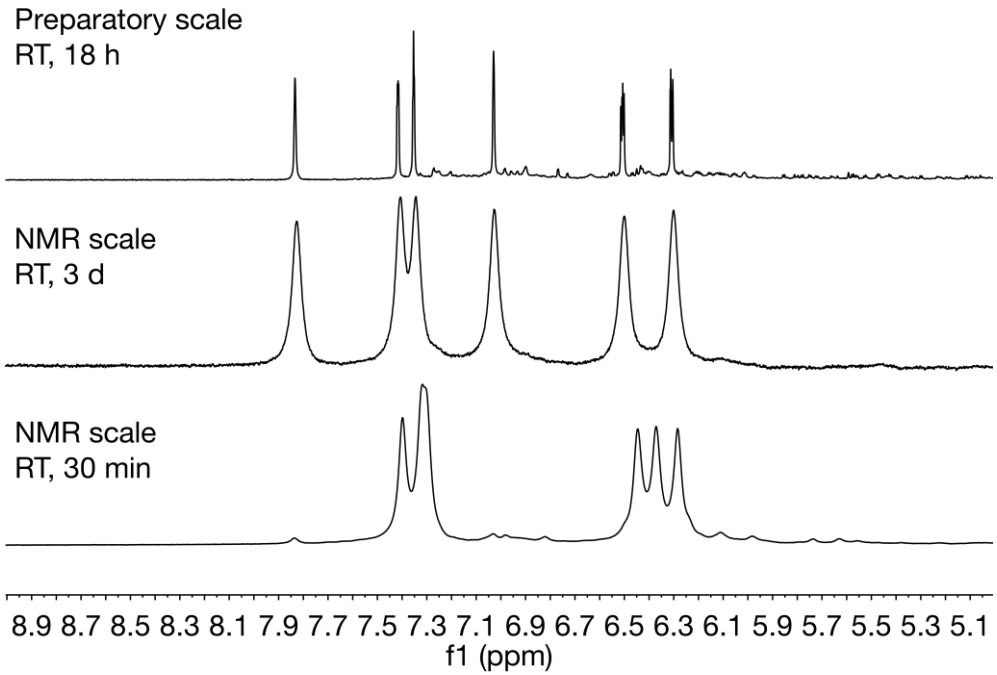

Figure 2.1.17. Comparison of the ^{1}H NMR spectra of the crude products obtained after treating **H$_2$(L5^{Fu})Br$_2$** with KN" in THF at various conditions. All spectra were recorded in THF-*d*$_8$ at RT.

Unfortunately, already after some minutes after the completion of the reaction these resonances are gradually replaced by a new set, which also can be assigned to a single symmetrical product. The quantification of the first set of resonances to solvent residue and subsequent comparison of the obtained integral ratio to the ratio of the second set of resonances to solvent residue reveals that **[K5^{Fu}]** has only been partially converted to new secondary product. Therefore, a high proportion of **[K5^{Fu}]** must have been converted to insoluble products. No further change is observed on NMR scale after allowing the reaction mixture to stand for 3 days at RT.

In the ^{13}C NMR spectrum, whose acquisition started 4 h after the start of the reaction and took approximately 8 h, the resonances of the new second product exhibit already almost the same intensity as the set for the desired NHC containing species **[L5^{Fu}]** (bottom spectrum in Figure 2.1.18). Nevertheless, the singlet at 218.30 ppm attributed to NCN of **[L5^{Fu}]** clearly indicates a presence of a free carbene or a potassium carbene adduct. NCN resonance in ^{13}C NMR spectrum for free unsaturated NHCs appears normally roughly around 211-220 ppm in C_6D_6.[19b] Generally, a coordination to alkali metal would cause a shift of the resonance to lower

frequencies.[19e] Since other ^{13}C NCN resonances, for example reported by *Arnold et al.* for potassium alkoxy-functionalised unsaturated NHC[65b], appear between 208 and 212 ppm (C_6D_6 and pyridine-d_5), it is more likely that in our case a free carbene is generated *in situ*, which then decomposes due to lack of electronic and steric stabilization. Comparisons with literature reports support this conclusion, since due to lower Lewis acidity among all alkali metals potassium bases favour the generation of non-anionically tethered free carbenes the most (see Chapter 1, section 1.2).[19e] All other 7 singlets in ^{13}C NMR spectrum, which do not correspond to the decomposition product, are attributed to the remaining carbon atoms of the ligand framework.

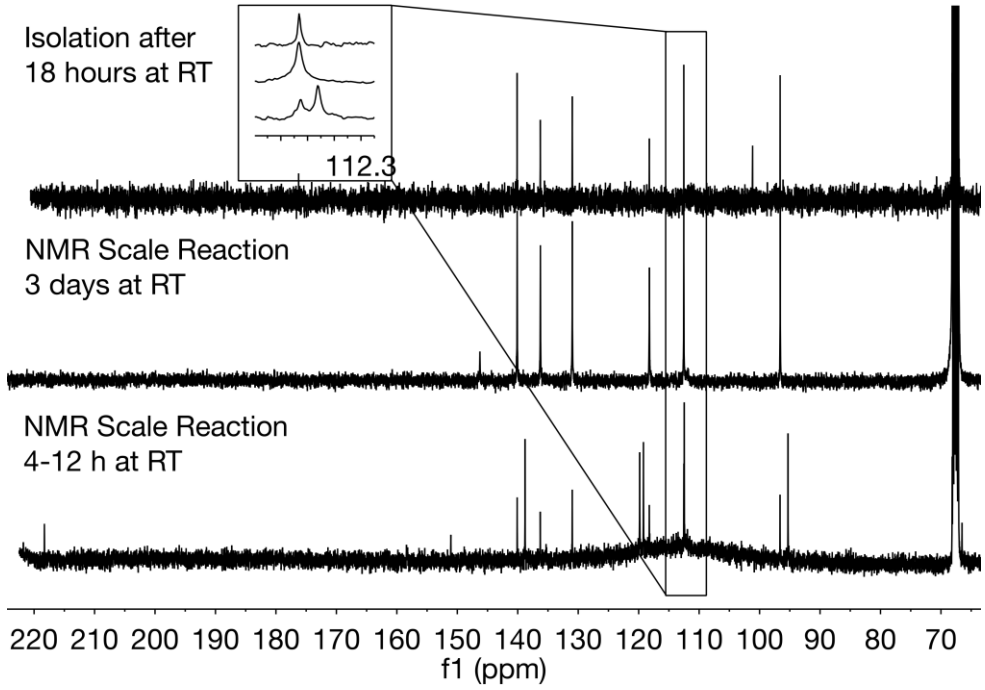

Figure 2.1.18. Comparison of the ^{13}C NMR spectra of the crude products obtained after treating **H_2(L5^{Fu})Br_2** with KN" in THF at various conditions. All spectra were recorded in THF-d_8 at RT.

On NMR scale HN" is generated causing the corresponding silicon nuclei resonating at approximately 1.9 ppm in the ^{29}Si INEPT NMR. No remaining KN" is observed here. However, there is a small silicon containing impurity resonating at 7.56 ppm. Normally, the terminal sites of silicon polymers –OSi$(CH_3)_3$ are attributed to this region,[172, 177] but, since the sample does not contain silicon grease, which would cause a singlet at approximately –22 ppm, it is hard to tell about the origin of this impurity.

After treating of **H_2(L5^{Fu})Br_2** with KN" on preparatory scale at RT the isolated residue contains the same decomposition product as major species as it has been seen in the NMR scale reaction after 3 days (Figure 2.1.17, top). ^{13}C NMR spectrum also shows high accordance with the NMR scale reaction (see Figure 2.1.18). Interestingly, the two upper spectra complement one another. All 6 concordant signals can be assigned to tertiary carbons of the ligand

framework according to the HSQC 2D NMR spectroscopy. Additionally, the middle spectrum shows the resonance at 146.24 ppm, which probably corresponds to quaternary carbon of the furanyl substituent, and the upper one a resonance at 101.15 ppm, attributed to the missing NCN. The repetition of the reaction on a bigger scale and the recording of ^{13}C NMR spectrum with greater number of scans confirmed this assumption. Unfortunately, due to substantial amount of impurities as a result of decomposition caused by H_2O in THF this spectrum is not shown in Figure 2.1.18.

In summary, all NMR data suggest that final product of deprotonation of **H_2(L5^{Fu})Br_2** is either bis(2-(furan-2-yl)-imidazol-1-yl)methane **L5^{Fu*}** formed by 1,2-shift of the *N*-substituents, e. g. furanyl, already previously reported for a range of different potassium NHC adducts[4, 66, 183], or tetraazafulvalene **(L5^{Fu})$_2$** formed by dimerization of two bis(carbene) molecules in a Wanzlick equilibrium[39a, 39c, 184]. A formation of intramolecular dimerized product is unlikely due to high ring strain of a hypothetical five-membered ring.[47, 185]

To elucidate the nature of the finally formed compound further, **H_2(L5^{Fu})Br_2** was treated with KN" at RT for 30 min, then filtered off. The filtrate was quickly injected into an ESI-MS spectrometer. The obtained spectrum is dominated by a cluster series ranging from 535.99 till 1575.98 mass units with mass difference of approximately 73.9 units (Figure 2.1.19). Such fragmentation pattern could result from either contamination with KCl clusters or from polymeric $(–OSiMe_2)_n$.[186] Since the isotopic pattern of each signal with the difference of 1 u indicate rather the presence of silicon isotopes and not potassium or chloride, which would result in the difference of 2 u, a formation of silicon polymers is more likely. Under harsh ionizing conditions in aqueous solution a hydrolysis of bis(trimethylsilyl)amide may be the cause for the formation of such fragmentation pattern.

Besides this signal pattern there is a signal at 281.19 mass units with the relative intensity of 23 %, which is tentatively assigned to [**L5^{Fu*}**+H^+] formed by 1,2-shift of the furanyl groups. The second possible decomposition pathway by means of intermolecular dimerization to tetraazafulvalene **(L5^{Fu})$_2$** is indicated by a signal at 561.19 m/z [**(L5^{Fu})$_2$**+H^+] (38 %). A formation of similar short-lived, intermolecular dimeric product formed by a deprotonation of 3,3'-methylenebis(1-(pyridin-2-yl)-imidazol-3-ium) hexafluorophosphate with KN" was previously suggested by Haslinger *et al*.[185] However, the appearance of the same signal could also be caused by a cluster of two molecules of **L5^{Fu*}** plus a proton as well. Therefore, an ESI-MS analysis could not definitely rule out one possibility from each other.

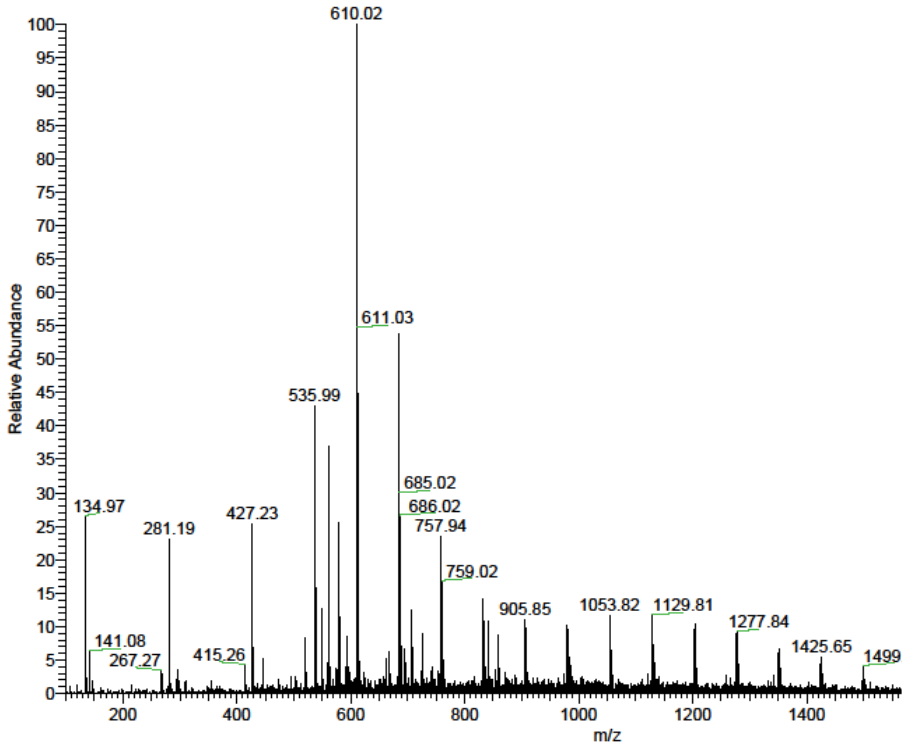

Figure 2.1.19. ESI-MS spectrum of the product of the reaction of $\mathbf{H_2(L5^{Fu})Br_2}$ with KN" at RT in THF. The spectrometer is operating with water/methanol solution containing 0.1 % formic acid.

Based on the obtained data and literature, however, it seems more likely that in case of methylene-bridged bis(imidazolium) salt $\mathbf{H_2(L5^{Fu})X_2}$ a deprotonation with potassium base KN" leads to 1,2-migration of furanyl group, since 1,2-migration would be entropically favoured and so far intermolecular tetraazafulvalenes were reported to be very unstable short-lived molecules, only isolable by Birch reduction of corresponding annulated disalt precursors and not *via* deprotonation of imidazolium halides (see Chapter 1, Section 1.1.3.1).[47]

By the way, the deprotonation products of $\mathbf{H_2(L5^{tFu})X_2}$ (X = Br, BPh_4) show more complicated resonance pattern in ^{1}H NMR spectra that their non-functionalised congeners. Even on NMR scale there is a lot of decomposition products and the major signals indicate an asymmetric nature of the obtained compounds implying that several reaction pathways, 1,2-migration, intermolecular dimerization and/or elimination could take place. Also not even an intermediate formation of potassium NHC adducts or some other carbene species is observed.

In contrast to methylene bridged bis(imidazolium) salts a reaction of ethane-1,2-diyl-bridged alkylated precursor $\mathbf{H_2(L6^{tFu})Br_2}$ with KN" generates tetraazafulvalene $\mathbf{L6^{tFu}}$ (Scheme 2.1.18), formed by rapid dimerization according to previously mentioned Wanzlick equilibrium.[39a, 39c, 43, 184] In comparison to its methylene bridged analogue, intermolecular dimerization is favourable due to entropic and kinetic reasons associated with the formation of the six-membered rings. These observations have been previously made by several groups, showing that

intramolecular dimerization of bis(imidazolium) salts is facilitated for longer alkyl tethers such as ethylene and propylene.[42a, 47, 185] On the other hand, more flexible chains such as butylene produce free carbenes (for more details see Chapter 1, Section 1.1.3.1).[42a]

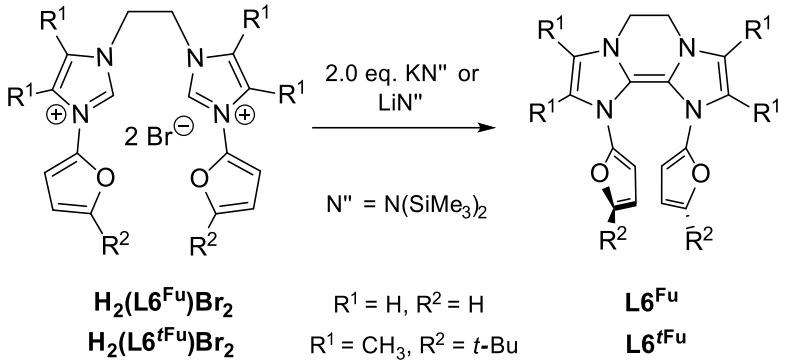

Scheme 2.1.18. Formation of tetraazafulvalenes. Reaction conditions: **L6^{Fu}**: (THF), RT; **L6^{tFu}**: (toluene or C_6H_6), RT.

The isolation of **L6^{tFu}** can be conveniently performed in high yields out of toluene or benzene. Also the treatment of non-modified **H$_2$(L6^{Fu})Br$_2$** with KN" on NMR scale in THF at RT yields in a clean reaction a deprotonated symmetrical product (see ^{1}H NMR spectrum, Figure 2.1.20), which is assigned to be analogue to its alkylated relative the tetraazafulvalene **L6^{Fu}** (Scheme 2.1.18). Both compounds are yellow in solution; **L6^{tFu}** also in the solid state. **L6^{tFu}** is stable in solution and as powder at RT under inert atmosphere conditions for many weeks. However, it is very air sensitive and rapidly decomposes when exposed to moisture and oxygen.

The ^{13}C NMR spectra of **L6^{Fu}** in THF-d_8 and **L6^{tFu}** in toluene-d_8 display singlets assigned to NCN at 113.63 and 121.32 ppm respectively. The chemical shift value for NCN resonance of **L6^{tFu}** is very similar to the reported δ-values of comparable tetraazafulvalenes, for **L6^{Fu}** this value is a little bit lower.[19b, 42a, 47, 185] Actually, this fact might indicate possibly another decomposition behaviour based on 1,2-shift of furanyl moieties rather than formal dimerization to **L6^{Fu}**. Such difference in reactivity of imidazolium salts for closely related compounds would be not very surprising, since Murphy also previously made an observation, that by substituting the backbone protons of bridged bis(imidazolium) salts by methyl groups the Wanzlick equilibrium could be exclusively shifted in the direction of corresponding dimer (Chapter 1, Section 1.1.3.1).[47] Since no structural characterization by SC-XRD for **L6^{Fu}** was conducted, a decomposition pathway by 1,2-shift cannot be definitely ruled out.

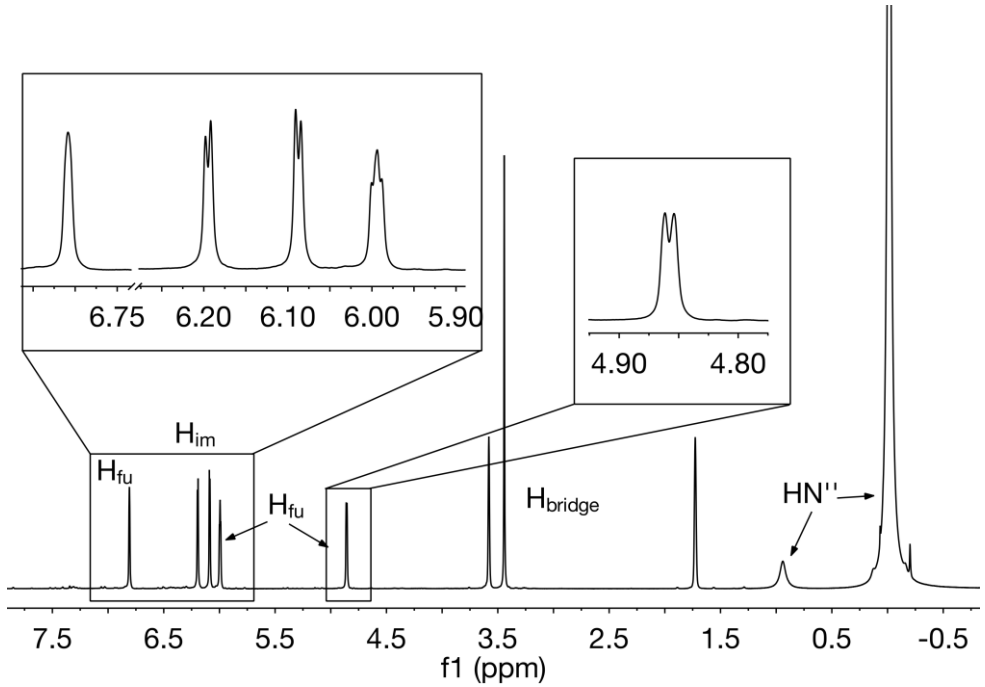

Figure 2.1.20. ^{1}H NMR spectrum of **L6^{Fu}** in THF-d_8 at RT.

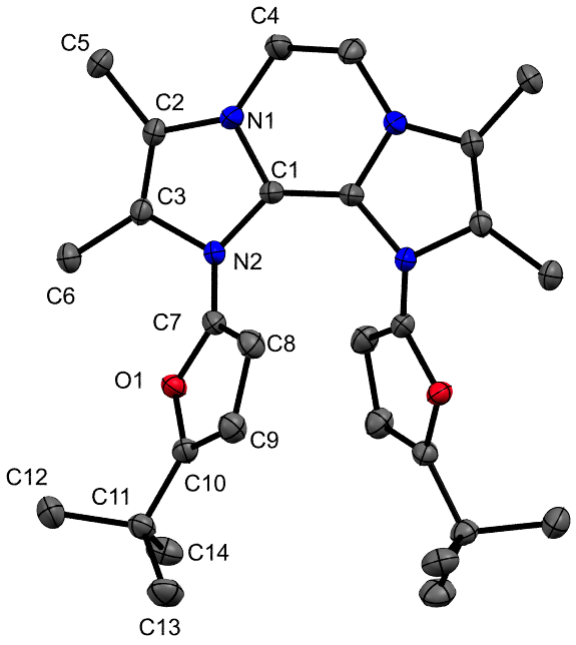

Figure 2.1.21. ORTEP style representation of **L6^{tFu}** showing the vibrational ellipsoids at 50 % probability level. Protons are omitted for clarity. Selected bond lengths [Å] and bond angles [deg]: C1–C1 1.345(2), C1–N1 1.416(2), C1–N2 1.417(1), N1–C4 1.419(4), C4–C4 1.537(6) ; N1–C1–N2 107.1(1), C1–C1–N1 120.2(1), N1–C4–C4 109.0(3). Symmetry transformations used to generate equivalent atoms: (c) –x,y,1/2–z.

Further structural characterization of **L6^{tFu}** was possible by obtaining single crystals by slow diffusion of pentane into a saturated solution of this tetraazafulvalene in toluene. The molecular

structure of **L6^{tFu}**, which crystalizes in monoclinic *C 2/c* space group, is shown in Figure 2.1.21. A formation of double bond is unmistakably proven by a bond distance of 1.345(2) Å between the two C1 carbons, lying hereby within the range of other dimerized unsaturated and saturated NHCs reported in literature.[19b, 42a] Moreover, the central olefinic framework is almost planar and both furanyl substituents are twisted parallel to each other in order to minimize the steric repulsion.

It is important to mention, that tetraazafulvalenes are very reactive compounds. Indeed, they have been reported to act as organic "super electron donors", since the oxidation of tetraazafulvalenes is strongly driven by formation of aromatic oxidized products.[187] For example, there are examples of such molecules acting as mediators for reducing iodoarenes to aryl radicals[188] or as initiators in polymerization reactions.[189]

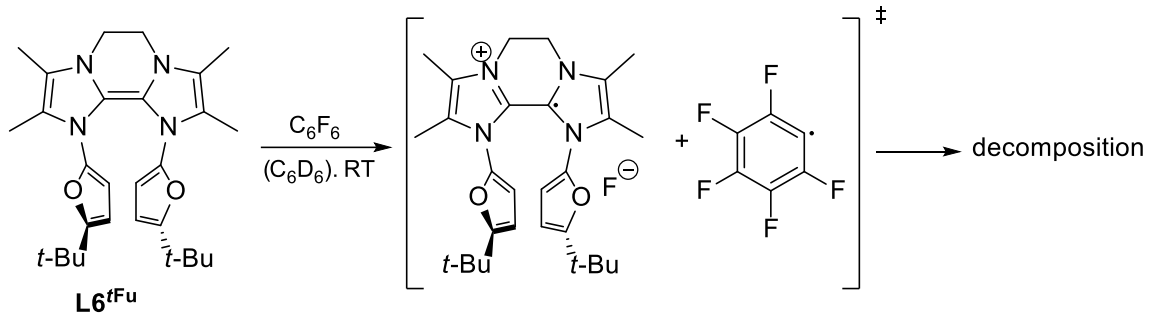

Scheme 2.1.19. Reaction of **L6^{tFu}** with C_6F_6 at RT in benzene.

L6^{tFu} is also no exception concerning its high reactivity. An instant reaction with C_6F_6 occurs at RT resulting in formation of a black precipitate (Scheme 2.1.19). Unfortunately, NMR spectra of the remaining solution are inconclusive due to appearance of numerous small resonances in ^{1}H and ^{13}C NMR spectra, also the ^{19}F resonance remains the same as for the educt. However, ^{1}H NMR spectrum of the black residue in THF-d_8 exhibits the presence of a set of broad resonances roughly in expected regions for the organic framework in question (SI, Figure 5.3.15). Interestingly, the chemical shift of a broad singlet at 14.16 ppm is too high to be assigned to an imidazolium proton and could actually indicate some radical as a product. This would be also in accordance with literature as it is known that tetraazafulvalenes can reduce iodoarenes to aryl-radicals (Scheme 2.1.19).[47, 188] Further characterization was not possible since no precipitate or crystalline material could be isolated by slow diffusion of hexane into a solution of the black residue in THF. Also no defined product and only various compounds resulting from radical decomposition could be postulated by analysing a NMR scale reaction of **L6^{tFu}** with benzoyl fluoride in C_6D_6 at room temperature.

Similar to the experiments described by Haslinger *et al.*[185]; an oxidation of **L6^{tFu}** with the radical thianthrenium hexafluorophosphate in benzene was attempted in order to obtain

corresponding dicationic annulated 2,2'-biimidazolium salt **(L6^{tFu})(PF$_6$)$_2$**. Unexpectedly, only bis(imidazolium) hexafluorophosphate **H$_2$(L6^{tFu})(PF$_6$)$_2$**, which was unambiguously characterised by SC-XRD, is isolated in this case (Scheme 2.1.20). This result suggests that an intermediate dicationic annulated 2,2'-biimidazolium salt **(L6^{tFu})(PF$_6$)$_2$** reacts further by hydrogen abstraction from the solvent or other molecules.

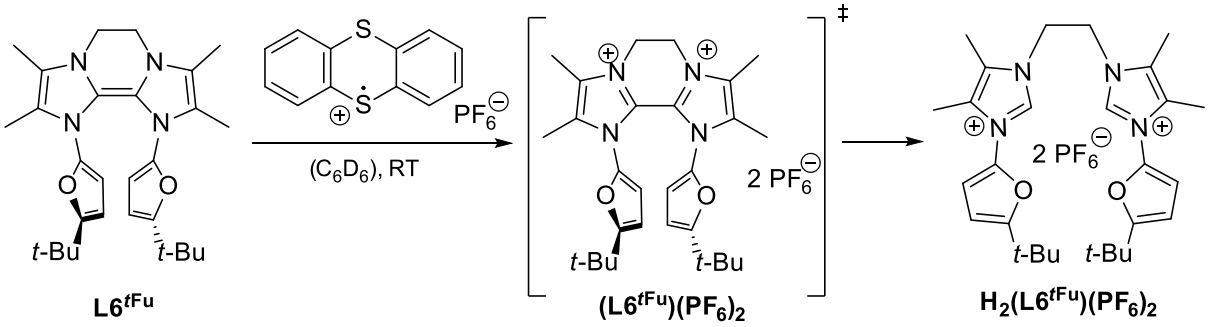

Scheme 2.1.20. Oxidation of tetraazafulvalene **L6^{tFu}** by cationic radical thianthrenium hexafluorophosphate ($Th^{\bullet+}PF_6^-$).

Also treating **L6^{tFu}** with I_2 at RT in C_6D_6 results in formation of brown precipitate soluble in THF. Although the oxidation of other known tetraazafulvalenes by iodine leads to the formation of corresponding dicationic annulated 2,2'-biimidazolium salts, ^{1}H NMR spectra of this product shows an asymmetrical (mono)imidazolium species with probably iodide as a counter anion (Figure 2.1.22). Since the reaction proceeds not absolutely cleanly and the benzene solution shows the presence of decomposition products, the proton for the (mono)imidazolium salt is probably abstracted from other tetraazafulvalene molecules. The other arm of the obtained (mono)imidazolium iodide could have undergone 1,2-shift of the furanyl moiety to C2 position of the imidazole-2-ylidene ring or formal addition of I^+ (Scheme 2.1.21). Also a possibility of annulated mono(imidazolium) salt cannot be excluded.

In summary, due to lack of anionic tethers, the deprotonation of *N*-furanyl functionalised bis(imidazolium) salts with potassium bases results in formation of 1,2-rearragement products for methylene-bridged compounds and tetraazafulvalenes for ethylene-bridged congeners. Therefore, only a deprotonation *in situ* with subsequent transfer of free carbenes to rare earth precursors at temperatures far below 0 °C could possibly lead to successful formation of desired REE NHC compounds. However, due to low solubility of **H$_2$(L5^{Fu})Br$_2$** and **H$_2$(L5^{Fu})Br$_2$** such procedure should be difficult to realize for these pro-ligands. Possibly the usage of modified more soluble pro-ligand **H$_2$(L5^{tFu})Br$_2$** could lead to success. The high propensity of **H$_2$(L6^{tFu})Br$_2$** for dimerization to tetraazafulvalene **L6^{tFu}** makes the successful application of the ethane-1,2-diyl-bridged analogue in two-step reactions rather unlikely.

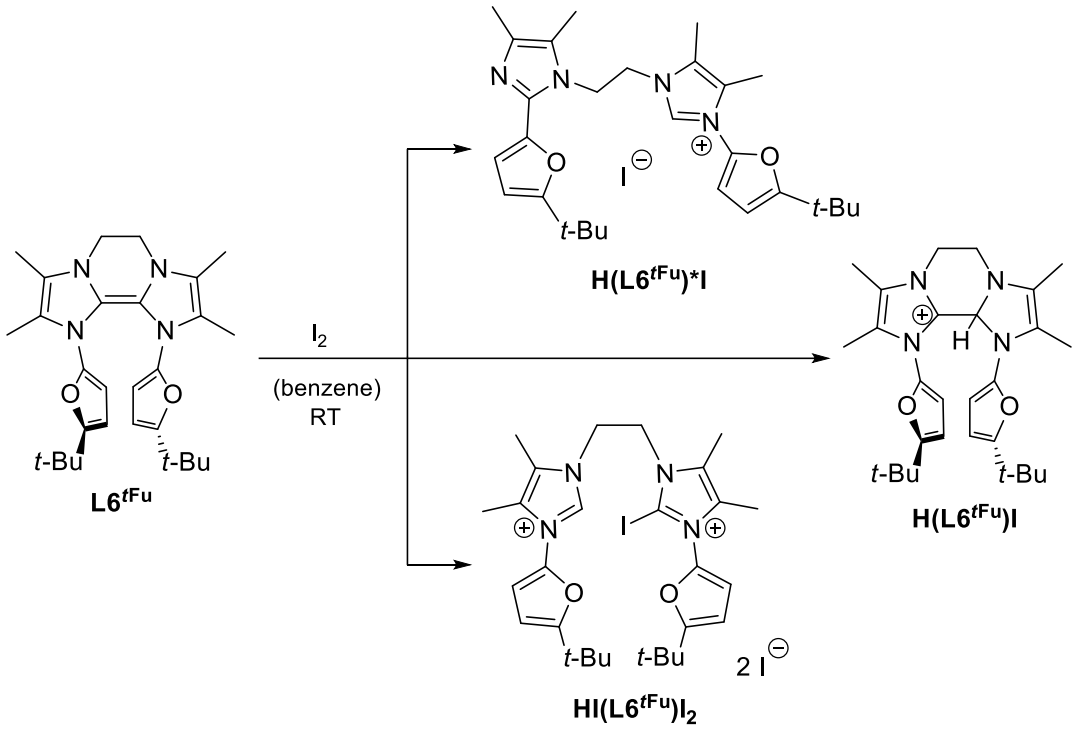

Scheme 2.1.21. Reaction of **L6^{tFu}** with the one equivalent of the oxidant I_2 in C_6D_6 at RT.

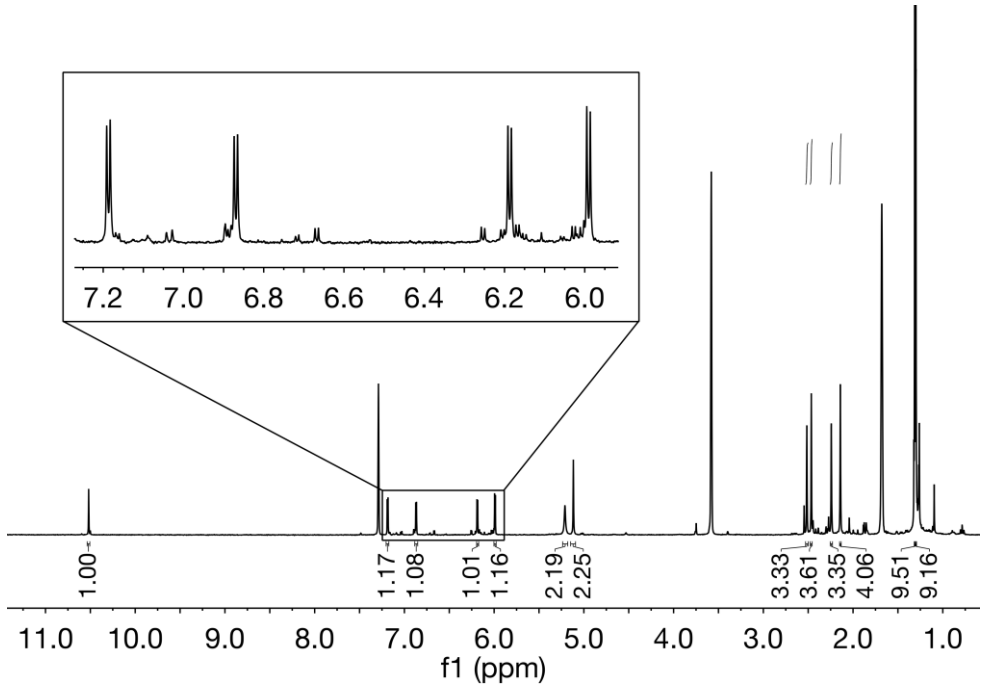

Figure 2.1.22. ^{1}H NMR spectrum of the product obtained by the oxidation of **L6^{tFu}** with I_2 in THF-d_8 at RT.

2.1.5 1,1'-(Prop-1-ene-1,3-diyl)-Bridge Functionalised Bis(imidazolium) Salts $H_2(L7^{Mes})X_2$

2.1.5.1 Synthesis and Characterization

Similarly to the synthesis of 2,3-bis(mesitylamino)propan-1-ol[190] a preparation of a bis(imidazolium) salt with a longer 1,1'-(2-hydroxyethane-1,2-diyl)-modified bridge through double nucleophilic substitution of 1-mesitylimidazole with 2,3-dibromopropan-1-ol was attempted. Unexpectedly, by conducting the reaction at similar conditions applied for the synthesis of $H_3(L3^R)Cl_2$ 1,1'-(prop-1-ene-1,3-diyl)bis(3-mesityl-imidazol-3-ium) dibromide $H_2(L7^{Mes})Br_2$ is obtained (Scheme 2.1.22.). In comparison to the synthesis of 2,3-bis(mesitylamino)propan-1-ol[190] mentioned above, after the first substitution step an elimination of HBr probably occurs, yielding a double bond and hydroxyl group containing mono-substituted intermediate. Such reactivity has been previously reported by *Eicher-Lorka et al*., who described an isolation of 1-[(*E*)-3-hydroxyprop-1-en-1-yl]pyridinium bromide by the reaction of pyridine with 2,3-dibromopropan-1-ol at 82 °C in MeCN.[191] It seems likely that a formation of a conjugated system facilitates such reactivity. Although a hydroxyl group is a poor leaving group, a second substitution step yielding $H_2(L7^{Mes})Br_2$ is possible as elimination reactions are generally favoured at high temperatures.[192] Therefore, it is not surprising, that the yield for this reaction is quite low (23 %). However, an increase in yield could be possible by the conversion of OH group into better leaving groups e. g. to *p*-toluenesulfonyl.[192]

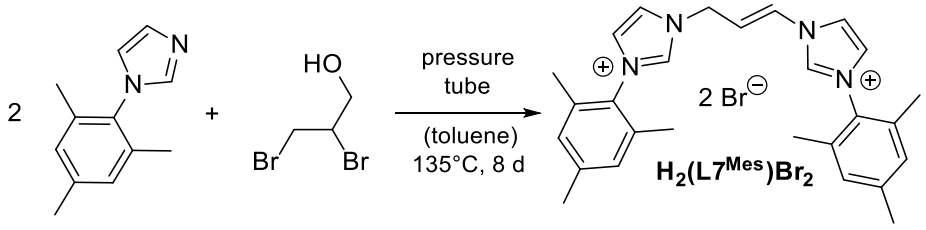

Scheme 2.1.22. Synthesis of bis(imidazolium) bromide $H_2(L7^{Mes})Br_2$.

N-allyl functionalised NHCs are desirable functionalised ligands, which offer a possibility of hemilabile behavior due to allyl double bond coordination. Several wingtip allyl functionalised mono(NHC) and bis(NHC) complexes have been characterised, some of them also applied in catalytic reactions.[193] So far *N,N*'-allyl bridge functional bis(NHC) ligands have not been previously reported.

$H_2(L7^{Mes})Br_2$ have been fully characterised by multinuclear NMR spectroscopy, MS and EA. Exclusive formation of the *E*-isomer is confirmed by ^{1}H NMR spectroscopy, which shows a vicinal coupling constant of 14.2 Hz between the two CH=CH protons.

Single crystals of **H_2(L7^{Mes})Br_2** suitable for SC-XRD were obtained by slow diffusion of diethyl ether into the saturated solution of **H_2(L7^{Mes})Br_2** in acetonitrile. The molecular structure of **H_2(L7^{Mes})Br_2**, which crystallises in monoclinic *P2₁/n* space group, is shown in Figure 2.1.23. The bond distance of 1.310 Å between C14 and C15 atoms can be clearly assigned to a double bond, also the formation of *E*-isomer is confirmed. The three carbons in the bridge form an angle of 122.7(3)°, which is characteristic of sp^2-hybridized carbons. All other bond distances and angles are comparable to the bis(imidazolium) salts mentioned above. The bond distances and angles in the heterocyclic ring systems are generally only marginally smaller than in the propyl-bridged relative of **H_2(L7^{Mes})Br_2** reported by *Song et al*.[194]

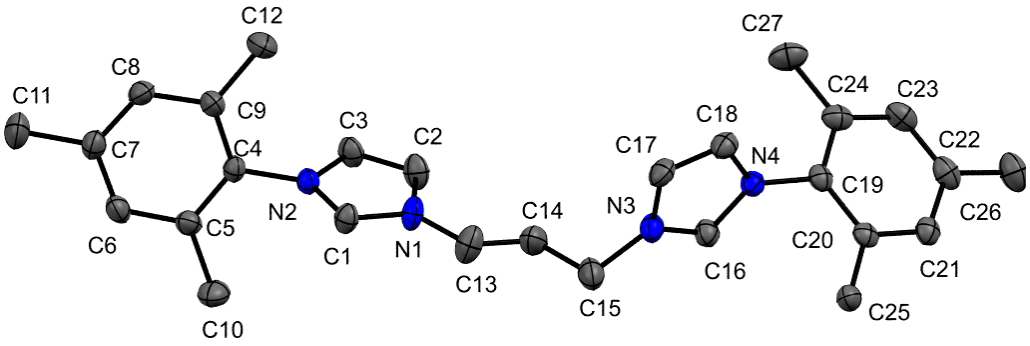

Figure 2.1.23. ORTEP style representation of the cation of **H_2(L7^{Mes})Br_2** showing the vibrational ellipsoids at 50 % probability level. Hydrogen atoms and bromide anions have been omitted for clarity. Selected bond lengths [Å] and bond angles [deg]: C1–N1 1.335(4), N2-C1 1.324(4), C16–N3 1.322(5), C16–N4 1.333(3), C13–N1 1.424(4), C13-C14 1.310(5), C14-C15 1.454(5), C15-N3 1.467(4); N1–C1–N2 108.1(3), N3–C16–N4 109.0(3), N1–C13–C14 122.7(3), C13-C14-C15 122.7(3), C14-C15-N3 111.8(3).

H_2(L7^{Mes})Br_2 shows good solubility in H_2O and MeOH. Therefore, if necessary, a salt metathesis reaction to BPh_4^- and PF_6^- can be conveniently performed in H_2O, yielding **H_2(L7^{Mes})$(BPh_4)_2$** and **H_2(L7^{Mes})$(PF_6)_2$** in high yields and purity. The obtained compounds with non-coordinating anions are well soluble in polar organic solvents such as methanol, acetonitrile, acetone, THF and DCM. As expected, **H_2(L7^{Mes})$(BPh_4)_2$** is extremely electrostatic.

No investigations towards the formation of alkali metal NHC adducts of this ligand system were conducted. The reaction of 1,1'-(prop-1-ene-1,3-diyl)-functionalised bis(NHC) pro-ligands with REE compounds and in multi-component systems will be discussed in Chapter 3. For the synthesis of silver and gold complexes see Chapter 4.

2.2 Conclusion and Outlook

Various literature known and novel donor-functionalised bis- and mono(NHC) precursors have been synthesized and fully characterised by multinuclear NMR spectroscopy, MS, EA and SC-XRD. All new compounds were obtained in good to acceptable yields and in high purity. Further improvements concerning the yields are expected to be achieved though modification of reaction conditions, e.g. through the use of microwave irradiation, or by modification of the substrates, such as increasing the propensity of leaving groups to react in nucleophilic substitution reactions.

The ligand precursors **$H_2(L1^R)Br$**, **$H_3(L2)Br$**, **$H_3(L3^R)X_2$**, **$H_3(L4^{Mes})Br_2$**, **$H_2(L5^R)X_2$** and **$H_2(L6^R)X_2$** have been investigated towards their reactivity with various alkali metal bases in order to probe the possibility of using the alkali metal NHC adducts as NHC transfer agents for rare earth metals.

The most promising results for the formation of sufficiently stable alkali metal NHC adducts show *N*-(3,5-di-*tert*-butyl-2-hydroxyphenyl)- and *N*-(3,5-di-*tert*-butyl-2-hydroxybenzyl)-functionalised mono(imidazolium) bromides **$H_2(L1^R)Br$** and **$H_3(L2)Br$**. On NMR scale the sodium and potassium NHC adducts of **$L1^R$** show no signs of degradation at RT in solution for many days. It is presumed that a rigid anchoring of generated oxy-group favours the stability of these compounds towards decomposition. Moreover, also the fact, that these compounds contain only one NHC moiety makes them resistant to some degradation pathways such as dimerization. However, no reactions on preparatory scale were conducted in case of **$M(L1^R)$** and further experiments towards isolation of all compounds (M = Li, Na, K) should to be performed. In case of **K(L2)** the conducted studies emphasize the temperature sensitivity of this compound. Although a successful isolation is possible at –78 °C, its thermal instability precludes further purification and crystallographic characterization.

The propensity of 1,1'-(2-hydroxyethane-1,1-diyl)-bridge functionalised bis(NHC) compounds **$H_3(L3^R)Cl_2$** to form alkali-metal NHC adducts was investigated on the example of deprotonation experiments with mesityl-substituted compound **$H_3(L3^{Mes})Cl_2$**. Hereby, only by using LiN" in benzene the alkali metal NHC compound **$Li(L3^{Mes})$** could be isolated. Unfortunately, although stable under inert atmosphere in solid state, **$Li(L3^{Mes})$** slowly decomposes in solution at RT yielding 1-mesitylimidazole due to destruction of the linking fragment. This thermal instability impedes further characterization of **$Li(L3^{Mes})$** by SC-XRD, but NMR data along with elemental analysis suggest a symmetrical lithium cluster incorporating chloride anions and bis(trimethylsilyl)amide. Regrettably, the deprotonation of the same precursor with heavier alkali metal bases resulted in even faster decomposition.

The deprotonation of 1,1'-(2-hydroxypropane-1,3-diyl) bridge functionalised mesityl-substituted bis(NHC) dibromide **$H_3(L4^{Mes})Br_2$** with potassium bases generates a symmetrical potassium NHC adduct **$K(L4^{Mes})$**, which degrades rapidly in solution at RT as well. Therefore, only NMR characterization of this product could be conducted. However, the experiments at lower temperatures show a potential for using this compound as *in situ* transfer reagent. Since lithium NHC compounds show generally higher stability than their heavier alkali metal analogues, it is possible that a Li NHC adduct of **$L4^{Mes}$** could be isolated, since NMR experiments indicated its higher resistance to degradation.

The reaction of *N*-furanyl-substituted bis(imidazolium) dibromide **$H_2(L5^{Fu})Br_2$** with KN" in THF at RT and at –78 °C results in generation of unstable free bis(carbene) as intermediate, which then decomposes *via a* 1,2-rearragement in corresponding bis(imidazole) with former *N*-substituents shifting to C2 position. However, due to longer ethane-1,2-diyl linker the deprotonation of **$H_2(L6^{R})Br_2$** (R = Fu, *t*Fu) yields corresponding tetraazafulvalenes as products of formal dimerization of NHCs according to Wanzlick equilibrium. The alkylated tetraazafulvalene **$L6^{tFu}$** was also isolated and characterised by SC-XRD and further applied in reactions showing its potential as organic electron donor.

Although it is clearly advantageous to have purified alkali metal derivatives in hand for salt elimination reactions, it is unsurprising their thermal instability often impedes further purification and crystallographic characterization. To circumvent this obstacle, the generation of alkali metal adducts of anionic tethered mono- and bis(NHC) adducts investigated in this thesis should be perform at lower temperatures (–78 °C) and only in *situ*. Also the use of internal bases, which already contain more Lewis acidic metals, is possible. As for *N*-furanyl-substituted NHCs, the lack of anionic anchor makes the generation of alkali metals NHC adducts with K or Na unlikely. In literature only lithium complexes with neutral bis(NHCs) are known.[59] Therefore, the most promising way for utilization of these ligands for supporting early transition metals is also the usage of internal bases, e. g. similarly to previously reported iron compounds.[178]

Chapter 3

Synthesis and Characterization of Rare Earth Metal Donor-Functionalised *N*-Heterocyclic Carbene Complexes

3.1 Results and Discussion

This Chapter describes the synthesis and characterization of *N*-(3,5-di-*tert*-butyl-2-hydroxyphenyl) functionalised NHC complexes of rare earth metals. The reactivity of *N*-furanyl, 1,1'-(2-hydroxyethane-1,1-diyl), 1,1'-(2-hydroxypropane-1,3-diyl) and 1,1'-(prop-1-ene-1,3-diyl) bridge functionalised bis(NHC) pro-ligands with rare earth metals acting as internal base as well in two-step transmetallation reactions with alkali metal bases and REE precursors is discussed as well.

3.1.1 *N*-(3,5-Di-*tert*-butyl-2-hydroxyphenyl) and *N*-(3,5-Di-*tert*-butyl-2-hydroxybenzyl) Functionalised Pro-Ligands $H_2(L1^R)Br$ and $H_3(L2)Br$

3.1.1.1 Reactions of $H_2(L1^R)Br$ (R = Me, Mes) with $Li[Ce\{N(i\text{-}Pr)_2\}_4](THF)$

REE tetrakis(diisopropylamides) are highly versatile and convenient REE precursors which are capable of acting as internal base in one-pot reactions with imidazolium pro-ligands. For example, Shen reported a series of REE complexes with *N*-(3,5-di-*tert*-butyl-2-hydroxybenzyl)-functionalised NHC ligands obtained by this convenient method (see Introduction, Section 1.3.1.2).[97-99] Generally, REE tetrakis(diisopropylamides) are more reactive than REE trimethylsilyl amides. Therefore, the reactivity of pro-ligands **$H_2(L1^R)Br$** (R = Me, Mes) with $Li[Ce\{N(i\text{-}Pr)_2\}_4](THF)$ has been firstly explored in a series of NMR scale reactions in benzene and THF.

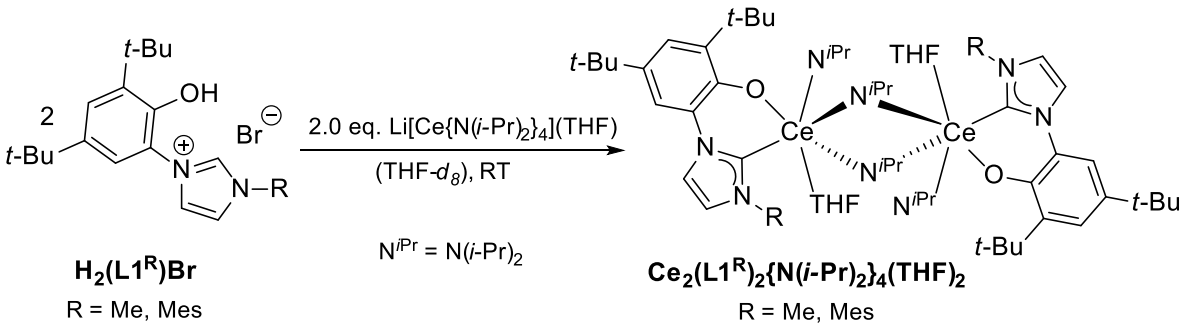

$H_2(L1^R)Br$
R = Me, Mes

$Ce_2(L1^R)_2\{N(i\text{-}Pr)_2\}_4(THF)_2$
R = Me, Mes

Scheme 3.1.1. Reaction of bidentate pro-ligands **$H_2(L1^R)Br$** with $Li[Ce\{N(i\text{-}Pr)_2\}_4](THF)$ at RT in THF.

Both *N*-methyl and *N*-mesityl-substituted imidazolium bromides react within minutes with $Li[Ce\{N(i\text{-}Pr)_2\}_4](THF)$ in THF at RT yielding yellow (R = Me) and orange (R = Mes) solutions respectively (Scheme 3.1.1). In both cases the ^1H NMR spectra of the obtained solutions display well-defined resonances indicating the formation of a major paramagnetic species as well as some minor ones. However, the major species produces quite a complicated

resonance pattern suggesting that the formed compounds are ether asymmetric and/or are forming oligomeric structures (see Figure 3.1.1 and Figure 3.1.2).

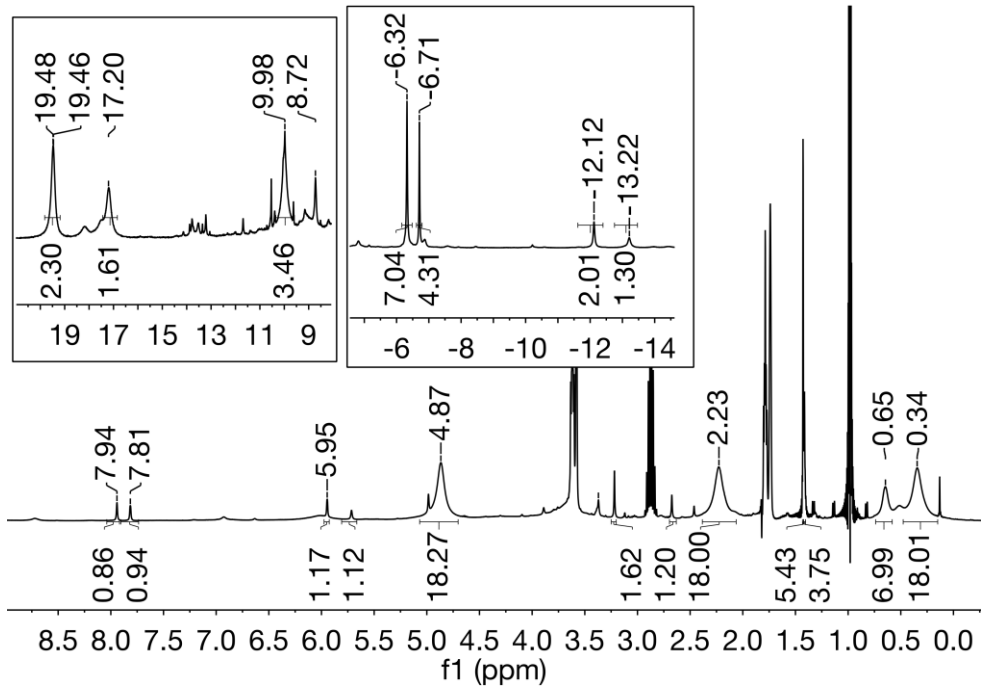

Figure 3.1.1. ^{1}H NMR spectrum of the reaction mixture obtained after the treatment of **$H_2(L1^{Me})Br$** with Li[Ce{N(*i*-Pr)$_2$}$_4$](THF) at RT in THF-d_8.

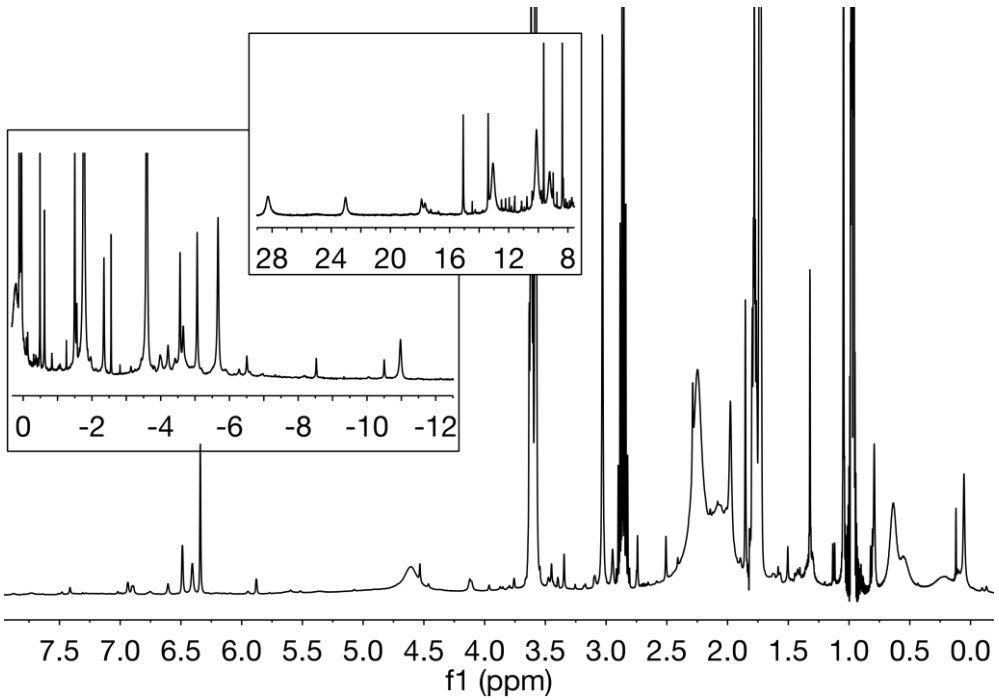

Figure 3.1.2. ^{1}H NMR spectrum of the reaction mixture obtained after the treatment of **$H_2(L1^{Mes})Br$** with Li[Ce{N(*i*-Pr)$_2$}$_4$](THF) at RT in THF-d_8.

^{1}H and also ^{7}Li NMR spectroscopy confirms the absence of eliminated LDA in both cases. Li incorporation intorespective Ce NHC clusters is rather unlikely, as only broad resonances at 0.3 ppm attributed to dissolved LiBr are observed. In comparison to the ^{1}H NMR spectrum of the reaction mixture with mesityl-substituted ligand, the resonances in the spectrum of the product with *N*-methyl-substituted NHC ligand can be reasonably integrated indicating bridging and terminal amide ligands. Unfortunately, in both cases no crystalline material suitable for further analysis could be obtained by slow diffusion of pentane into the solution of crude products in THF at RT. A suggestion for a possible structure is given in Scheme 3.1.1, however, since to date no crystals suitable for SC-XRD characterization were obtained, the exact molecular structures of both complexes remain unknown.

Due to insolubility of bromide salts in benzene the reactions described above are expected to proceed more smoothly in this apolar solvent. Therefore, the pro-ligands **$H_2(L1^R)Br$** were also treated with Li[Ce{N(*i*-Pr)$_2$}$_4$](THF) at RT in C_6D_6 (Scheme 3.1.2).

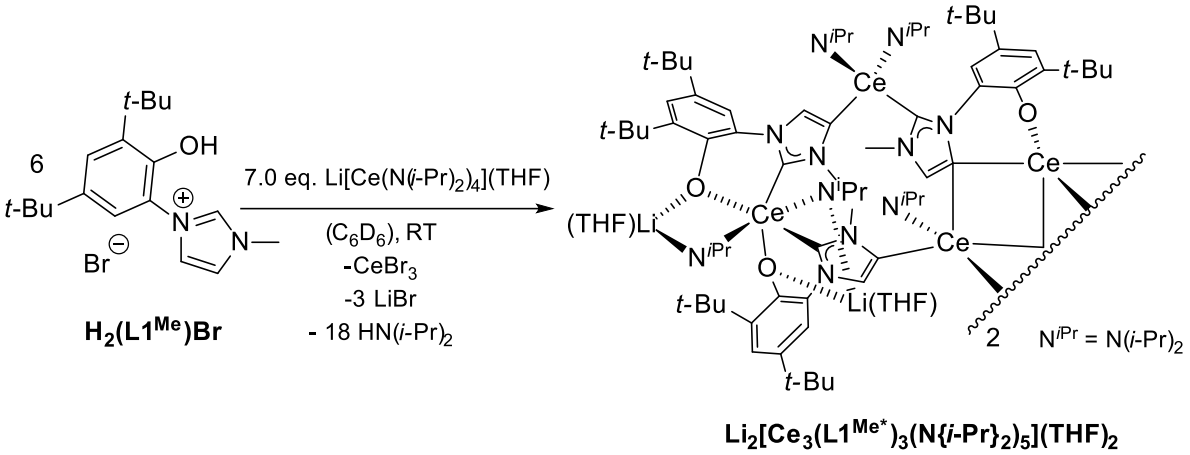

Scheme 3.1.2. Synthesis of the cerium-NHDC complex **$Li_2[Ce_3(L1^{Me*})_3(N\{i\text{-}Pr\}_2)_5](THF)_2$.**

$H_2(L1^{Me})Br$ is consumed within 10 min in benzene yielding a suspension comprising of yellow-green solution and fine colourless precipitate. The ^{1}H NMR spectrum shows a successful formation of cerium-organo compounds due to visible paramagnetic influence on the shift and the resolution of the resonances attributed to the ligands (Figure 3.1.3). However, the exact assignment of the resonances is difficult. In the ^{7}Li NMR spectrum a single broad resonance at 38.01 ppm suggests an incorporation of lithium into the obtained cerium-organo-compound, as LiBr precipitates out of benzene and the ^{7}Li chemical shift of lithium diisopropylamide is at around 3 ppm. Moreover, no LDA is observed in the ^{1}H NMR spectrum and only the formation of free amine can be confirmed.

After allowing the reaction mixture to stand for several days at RT bright orange crystalline fragments suitable for SC-XRD were obtained. The crystallographic analysis of these crystals also confirms the successful synthesis of a cerium complex, which crystallises in the triclinic

space group $P\bar{1}$ (Figure 3.1.4). For clarity a simplified solid state structure of **$Li_2[Ce_3(L1^{Me*})_3(N\{i\text{-}Pr\}_2)_5](THF)_2$** containing all relevant atom labels is shown again in Figure 3.1.5. Selected bond lengths and bond angles are collected in Table 3.1.1.

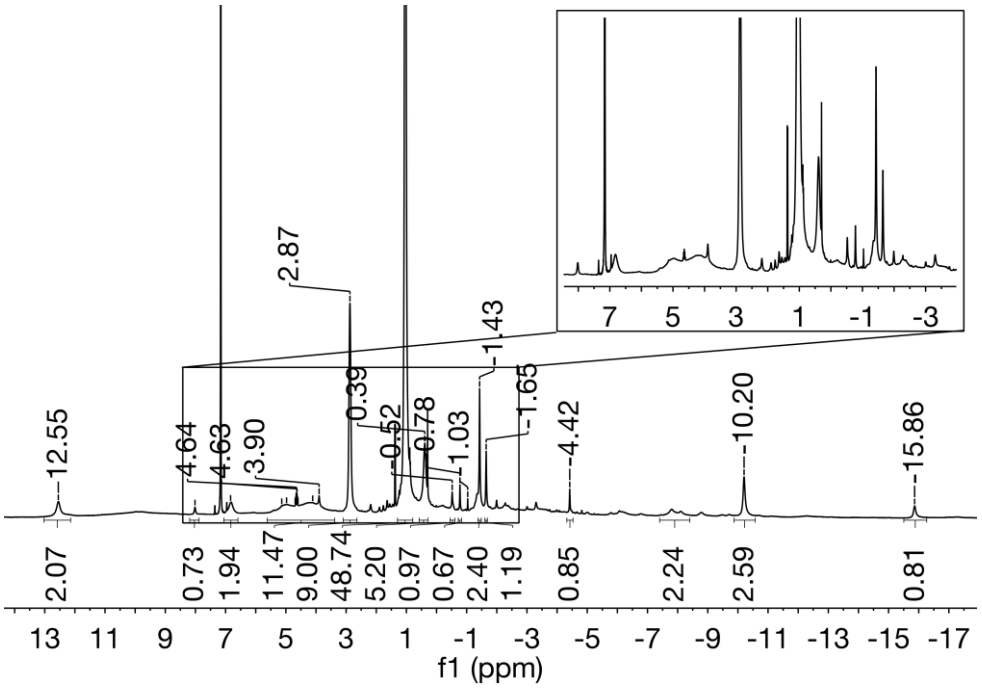

Figure 3.1.3. ^{1}H NMR spectrum of **$Li_2[Ce_3(L1^{Me*})_3(N\{i\text{-}Pr\}_2)_5](THF)_2$** in THF-$d_8$ at RT.

The molecular structure of **$Li_2[Ce_3(L1^{Me*})_3(N\{i\text{-}Pr\}_2)_5](THF)_2$** exhibits some unexpected features. Additionally to the desired deprotonation of the pro-ligand at the C2 position, also one of the backbone protons on the imidazolium moiety is absent. The whole cluster comprises of 6 cerium centres surrounded by 6 tridentate bridging ditopic carbanionic carbenes, also called anionic dicarbenes (NHDC), as well as 6 terminal and 4 bridging amido ligands. Four additional Li(THF) moieties counterbalance the charge, acting as a bridge between an amide and an anionic oxygen of four NHDC ligands. A remarkable feature of this cluster is that the anionic dicarbenes act as tridentate bridging ligands between cerium ions *via* normal C2 and abnormal C4 coordination modes. 2 of the ligands function also as bridging μ_2-NHDC ligands though the carbanionic position.

Metal complexes with NHDCs are very rare. They can be synthesized either by chemical reduction of corresponding metal NHC complexes, direct deprotonation of imidazolium precursors, by metal-mediated C–H activation of NHCs with unsaturated backbone or by C2-deprotonation of *a*NHC complexes. Arnold first reported the access to anionic dicarbenes by chemical reduction of samarium and yttrium complexes **58** with amido-functionalised NHCs a decade ago (**94**, see Introduction, Section 1.3.3.1).[7] In the transition metal chemistry Goicoechea reported K metal mediated C–H bond activation of M(^{H}IDipp)(Mes)$_2$ (M = Mn, Fe),

which were treated similar to the Y- and Sm-complexes of Arnold with KC_8 yielding respective M NHDC compounds.[195] Robinson's report on direct lithiation of a NHC lead to the increase of scientific interest in this field further.[73, 76a] Subsequently, zincations and magnesiations of NHCs at C2 and C4 positions were described.[76a, 196] Group 12 and 14 NHDC complexes were accessed by transmetallation of potassium NHDCs.[75, 197] Other transition metal NHDC complexes are almost exclusively homobimetallic and were synthesized using various stepwise metal-mediated C–H activation of NHC complexes with unsaturated backbone e.g. *via* oxidative addition to Pd(0).[198] Transition metal heterobimetallic systems were only recently accessed by deprotonation of the C2 position of a Ru *a*NHC complex with Ag_2O and subsequent transmetallation to other transition metals.[199]

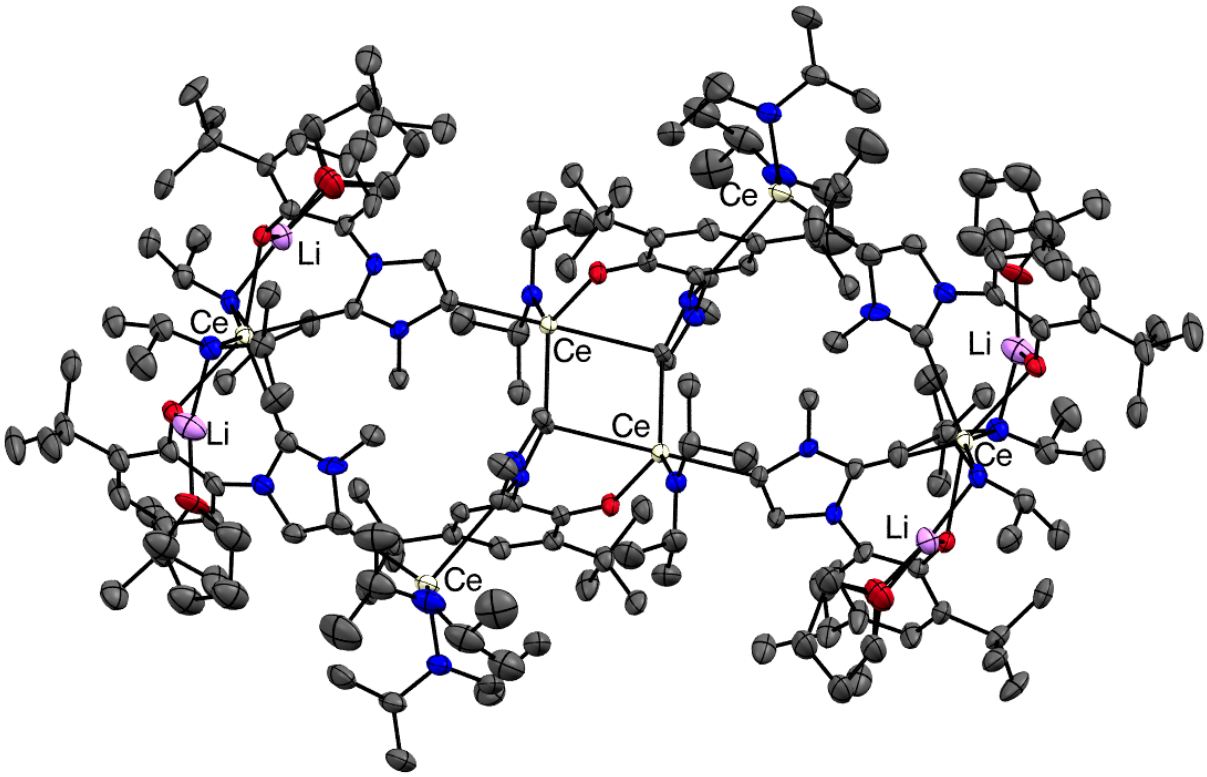

Figure 3.1.4. ORTEP style representation of **$Li_2[Ce_3(L1^{Me*})_3(N\{i\text{-}Pr\}_2)_5](THF)_2$** showing the vibrational ellipsoids at 50 % probability level. Hydrogen atoms and co-crystallised benzene molecules have been omitted for clarity. Symmetry transformations used to generate equivalent atoms: (i) –x, –y, –z.

To the best of our knowledge **$Li_2[Ce_3(L1^{Me*})_3(N\{i\text{-}Pr\}_2)_5](THF)_2$** is the first example of negatively charged carbon-bridged anionic dicarbene cerium complex. Though Arnold *et al*. reported similar coordination mode in heterobimetallic dinuclear Y-K and Sm-K NHDC complexes[7] **$Li_2[Ce_3(L1^{Me*})_3(N\{i\text{-}Pr\}_2)_5](THF)_2$** is also the first reported compound where HNDC are functioning as bridging ligands between two lanthanide centres.

In each symmetric unit of **$Li_2[Ce_3(L1^{Me*})_3(N\{i\text{-}Pr\}_2)_5](THF)_2$** there are three types of Ce centres exhibiting different coordination modes which are dictated by steric and electrostatic reasons. Ce1 is six-fold coordinated by two NHDC ligands (oxygen and C2 normally bonded) and two bridging amides resulting in a distorted trigonal antiprism as a coordination polyhedron. The second type of the cerium cations is tetrahedrally coordinated by two terminal amides and two NHDC ligands, which are bonded abnormally and normally respectively. Also this polyhedron is severely distorted as well, as negatively charged C4 site is bonding more strongly to cerium than the C2 position. Finally, the molecule centre is comprising of two Ce3 centres bridged by two carbanion bonded carbenes building together a planar rhomboid with C38–Ce3–C38 and Ce3–C38–Ce3 angles of 81.5(1)° and 98.5(1)° respectively. Each Ce(III) is five-coordinate by 3 abnormally bonded NHDCs, an aryloxide as well a terminal amide. Thereby, the coordination polyhedron resembles an extremely distorted trigonal bipyramid.

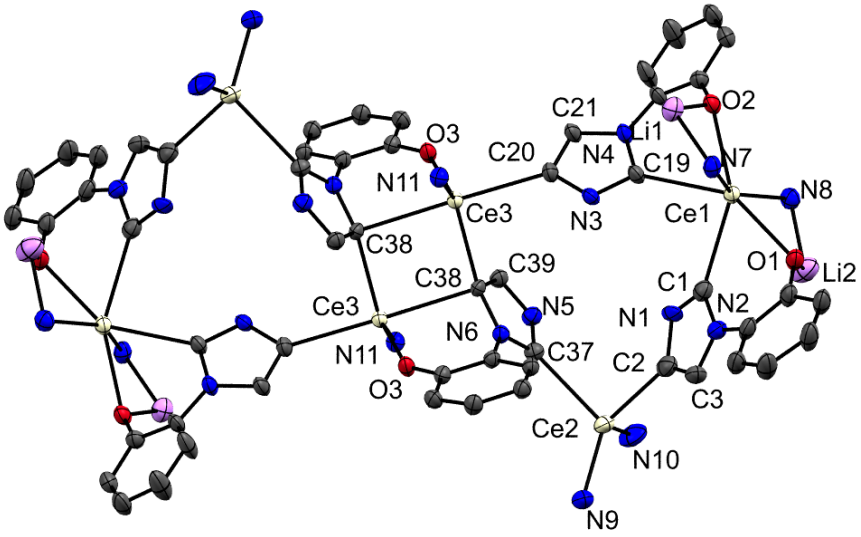

Figure 3.1.5. ORTEP style representation of the skeletal structure of **$Li_2[Ce_3(L1^{Me*})_3(N\{i\text{-}Pr\}_2)_5](THF)_2$** showing the vibrational ellipsoids at 50 % probability level. Hydrogen atoms, benzene and THF molecules, *N*-methyl and *t*-Bu substituents of **$L1^{Me}$** as well *i*-Pr substituents of the diisopropylamide ligands have been omitted for clarity. Symmetry transformations used to generate equivalent atoms: (i) –x, –y, –z.

Ce–C_C contacts to abnormally bonded anionic NHDC are shorter than to the same ligand with normal coordination mode (2.651(6)-2.685(6) Å for Ce–C4 vs. 2.710(5)-2.743(5) Å for Ce–C4). This is consistent with an increase in the ionic character of the metal–ligand interaction.

Table 3.1.1. Selected bond lengths and bond angles of **$Li_2[Ce_3(L1^{Me*})_3(N\{i\text{-}Pr\}_2)_5](THF)_2$**.

Bond	Length [Å]	Bond	Length [Å]	Bond	Length [Å]	Bonds	Angle [deg]	Bonds	Angle [deg]	Bonds	Angle [deg]
Ce1–C1	2.743(5)	C2–C3	1.352(9)	C39–C38	1.366(7)	O2–Ce1–N7	74.7(1)	C2–C3–N2	111.0(5)	O3–Ce3–N11	120.4(1)
Ce1–C19	2.728(5)	C3–N2	1.399(7)	C38–N6	1.413(6)	O2–Ce1–N8	97.3(1)	C2–Ce2–C37	94.4(2)	C20–Ce3–C38	90.6(2)
Ce1–N7	2.427(5)	Ce2–C2	2.667(7)	Ce3–C38	2.685(6)	N8–Ce1–O1	74.1(1)	N9–Ce2–N10	111.8(2)	N11–Ce3–C38	98.4(2)
Ce–O2	2.462(4)	Ce2–N9	2.303(5)	Ce3–N11	2.295(5)	O1–Ce1–C1	65.1(2)	C2–Ce2–N10	109.9(2)	O3–Ce3–C20	97.4(2)
Ce1–N8	2.439(5)	Ce2–N10	2.282(6)	Ce3–O3	2.232(3)	O1–Ce1–O2	147.3(1)	N9–Ce2–C37	120.0(2)	Ce3–C38–Ce3	98.5(1)
Ce1–O1	2.517(4)	Ce2–C37	2.710(5)	Ce3–C20	2.561(6)	N7–Ce1–N8	149.9(2)	N5–C37–N6	102.6(4)	C38–Ce3–C38	81.5(1)
C1–N1	2.371(7)	C37–N5	1.350(7)	Li1–O2	1.87(1)	C1–Ce1–C19	82.1(2)	N5–C39–C38	110.3(4)	O2–Li1–N7	97.3(5)
C1–N2	1.367(7)	C37–N6	1.373(7)	Li1–N7	2.07(1)	N1–C1–N2	102.1(5)	C39–C38–N6	101.4(4)	O1–Li2–N8	99.3(6)
N1–C2	1.418(9)	N5–C39	1.380(7)			N1–C2–C3	101.2(6)	Ce3–C38–Ce3	98.5(1)		

As expected, the Ce–C_{aNHC} bond distances in μ_2-C_{aNHC} bridging modes are also slightly longer than in Ce–C_{aNHC} terminal bond. The same is found for Ce–N and Ce–O bonds. The bond distances within the anionic dicarbene ring are comparable to the other anionic dicarbenes reported in literature.[7, 73, 195b] N–C_{NHC} bond distance is shorter than N–C_{aNHC}, also the deprotonation of backbone is visible by elongation of N–C_{aNHC} bond in comparison to N–CH distance. Furthermore, N1–C1–N2 bond angle is smaller than in comparable yttrium and samarium complexes reported by Arnold *et. al.* (approximately 102° vs. 108°).[7]

The deprotonation of the backbone of NHCs is unexpected but not unusual, as the outcome of the deprotonation is heavily dependent on the base, as previously observed for alkali metal NHC adducts (see Introduction, Section1.2.1). In comparison to the deprotonation using bis(trimethylsilylamides), especially the sterically congested stronger base LDA favours the formations of carbanions.[77] In conclusion, the synthetic route utilizing REE tetrakis(diisopropylamides) offers further possibility for the preparation of other lanthanide complexes with bridging anionic dicarbene moieties which were predicted to have unusual magnetic behaviour.[6]

To test the utility of thi approach further, **H_2(L1^{Mes})Br** was treated with Li[Ce{N(*i*-Pr)$_2$}$_4$](THF) under the same reaction condition as methyl-analogue in C_6D_6 yielding bright orange suspension (Scheme 3.1.3). ^{1}H NMR spectrum of the obtained mixture is shown in Figure 3.1.6. Unfortunately, it was not possible to reasonably integrate the broad resonances, which are visibly affected by the coordination of the ligand to Ce(III). Possibly, due to more sterically demanding mesityl-substituents a formation of Ce NHDC complex analogue to **Li_2[Ce_3(L1^{Me*})$_3$(N{*i*-Pr}$_2$)$_5$](THF)$_2$** is impeded, as the resonance pattern of the obtained compound does not resemble that of **Li_2[Ce_3(L1^{Me*})$_3$(N{*i*-Pr}$_2$)$_5$](THF)$_2$**.

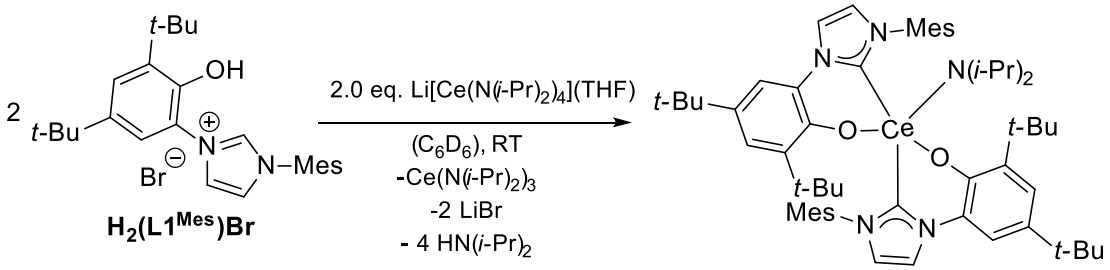

Scheme 3.1.3. Reaction of **H_2(L1^{Mes})Br** with Li[Ce{N(*i*-Pr)$_2$}$_4$](THF) at RT in C_6D_6. The structure of the formed complex is based on NMR data and literature.

Furthermore, in comparison to **Li_2[Ce_3(L1^{Me*})$_3$(N{*i*-Pr}$_2$)$_5$](THF)$_2$**, no ^{7}Li resonance could be detected for the reaction product of **H_2(L1^{Mes})Br** and Li[Ce{N(*i*-Pr)$_2$}$_4$](THF), suggesting that either all lithium ions have been removed as lithium bromide out of the solution or Li is paramagnetically affected due to close incorporation to the cerium centre. Both cases would

also imply that this compound has a different molecular structure than the Ce NHDC complex described above. Unfortunately, up to date no single crystals suitable for further analysis could be obtained by slow diffusion of pentane into the solution of the crude product in benzene. The formed **Ce(L1^{Mes})**-compound is stable for at least 15 days at RT in solution.

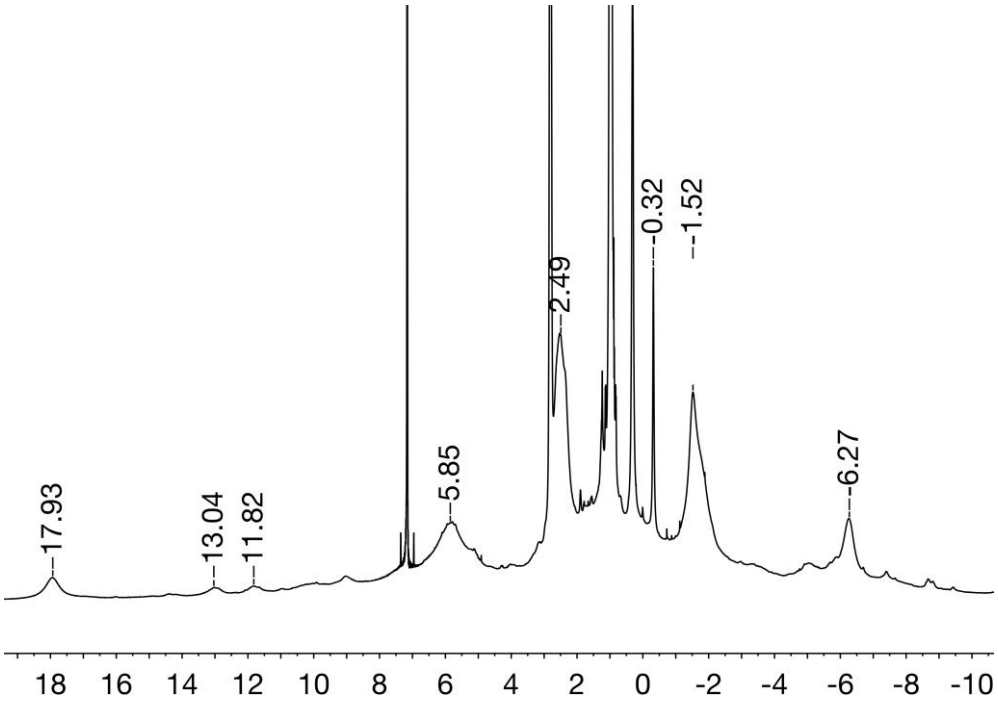

Figure 3.1.6. ^{1}H NMR spectrum of the reaction mixture obtained after the treatment of **H$_2$(L1^{Mes})Br** with Li[Ce{N(*i*-Pr)$_2$}$_4$](THF) at RT in C_6D_6.

The complicated structure of the **Li$_2$[Ce$_3$(L1^{Me*})$_3$(N{*i*-Pr}$_2$)$_5$](THF)$_2$** could be indebted to discrepancy in the stoichiometry between the ligand precursor and the cerium base. Shen previously successfully utilized REE diisopropylamides with related bidentate *N*-(3,5-di-*tert*-butyl-2-hydroxybenzyl)-modified imidazolium chlorides by adding extra amounts of alkali metal base to the reaction mixture.[97-98] By doing so she was able to isolate highly symmetric six-coordinate or five-coordinate REE-NHC complexes.

To elucidate this possibility in referring to our system 3.0 eq. of **H$_2$(L1^{Me})Br** were treated with 1.0 eq. of Li[Ce{N(*i*-Pr)$_2$}$_4$](THF) and 2.0 eq. of LDA in THF targeting a symmetric homoleptic complex **Ce(L1^{Me})$_3$** (Scheme 3.1.4). The reaction proceeds instantaneously and vigorous upon addition of cold THF at –26 °C. It is unclear if subsequent fast cooling down of the mixture to –78 °C and then slow warming up until RT overnight contributed much to overall reaction rate.

^{1}H NMR spectrum of the crude product, which could be separated from halides and other insoluble impurities by extraction with benzene, is shown in Figure 3.1.7 and it confirms a successful deprotonation of the ligand by showing the formation of HN(*i*-Pr)$_2$. The two broad singlets at 3.66 and 1.44 ppm suggest a presence of poorly resolved THF. The shift of all other

broad singlets indicates coordination to Ce(III), which would also imply a more symmetric compound as in cases described above due to significantly smaller number of the resonances. The formation of a completely symmetric complex **Ce(L1^{Me})** is however unlikely, as the analysis of the ^{1}H NMR spectrum presents the observation that the integral ratio of the resonances in the region between 7 and 11 ppm does not match the integral ratio attributed to the *tert*-butyl group at 2.37 ppm. Also the fact that only one resonance belonging to *tert*-butyl group(s) is visible indicates an elimination of *t*-Bu or a less constricted rotation of the *N*-(3,5-di-*tert*-butyl-2-oxyphenyl)-group around the Ce–O bond. Therefore, due to vigorous reaction a decomposition of the ligand resulting in *N*-bonded imidazoles is not completely unlikely. A formation of such decomposition product has been previously observed for similar systems comprising of bidentate *N*-(3,5-di-*tert*-butyl-2-hydroxybenzyl) NHC ligands, Li[Y{N(*i*-Pr)$_2$}$_4$] and *n*-BuLi in reactions at RT. Therefore, a suggestion for possible product is given in Scheme 3.1.4.

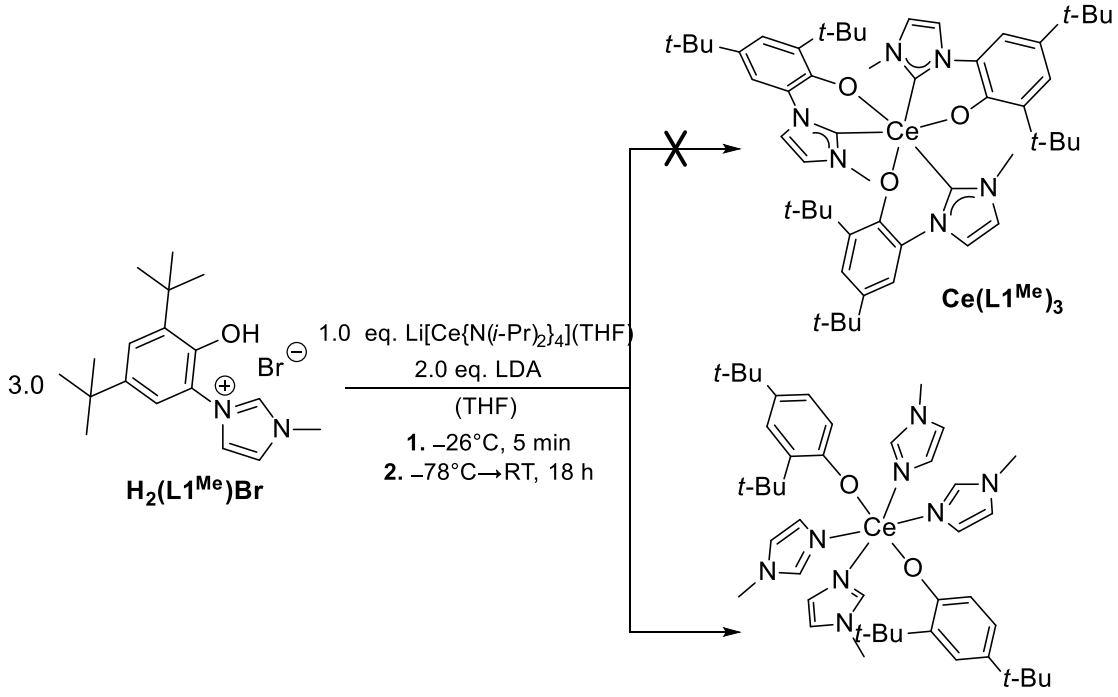

Scheme 3.1.4. One-pot reaction of **H$_2$(L1^{Me})Br** with Li[Ce{N(*i*-Pr)$_2$}$_4$](THF) and LDA.

To elucidate the nature of isolated product different crystallization methods have been applied in order to obtain crystals suitable for SC-XRD. Unfortunately, no crystalline material could be obtained by slow diffusion of pentane into the solution of crude product in toluene, benzene or benzene/DME mixture at RT. Also the crystallization from toluene/pentane mixture at –26 °C yields only fine colourless precipitate. By adding DME to the solution of the crude product in toluene solely big colourless crystals of Li(DME)Br could be identified by SC-XRD.

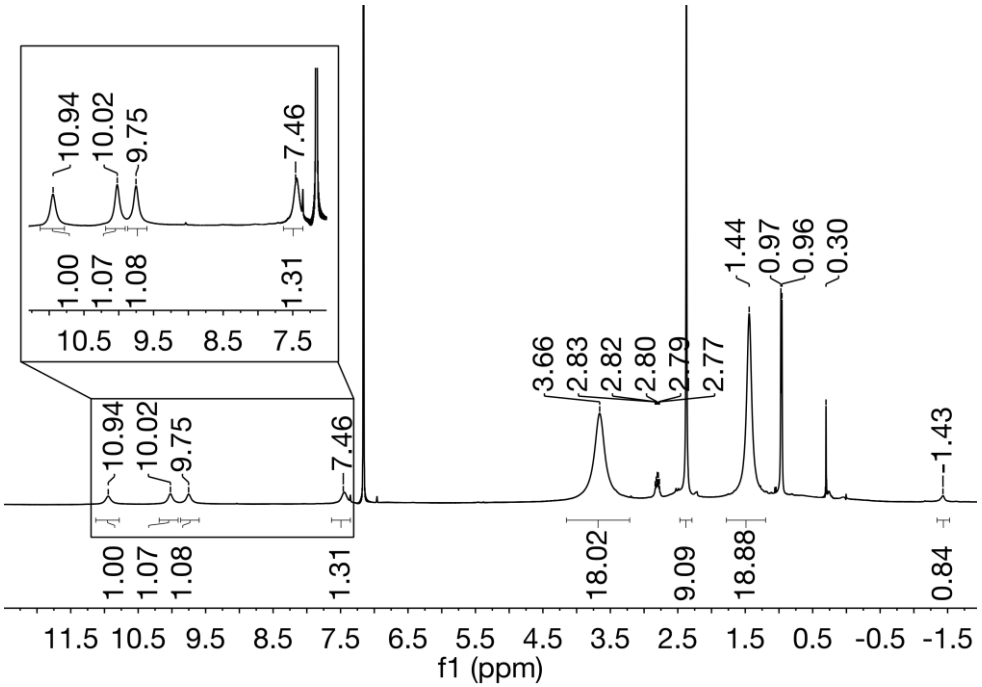

Figure 3.1.7. ^{1}H NMR spectrum of the crude product obtained in one port reaction of **$H_2(L1^{Me})Br$** with Li[Ce{N(*i*-Pr)$_2$}$_4$](THF) and LDA in THF. The spectrum was recorded in C_6D_6 at RT.

In summary, the usage of Li[Ce{N(*i*-Pr)$_2$}$_4$](THF) as internal base in reaction with *N*-(3,5-di-*tert*-butyl-2-hydroxyphenyl) functionalised imidazolium bromides proved to be a very productive approach for synthesis of unusual Ce NHC and Ce NHDC compounds. Although the formation of alkali metal NHC adducts with this ligand have been successfully proved (see Chapter 2, Section 2.1.1.2), so far the reactivity of these intermediates has not been explored. Due to a possibility of robust attachment of NHCs to REE centres as well as sufficiently high stability of **$K(L1^R)$** the two step reactions present also a highly promising synthetic approach, which should be further explored.

3.1.1.2 Reactions of H_3(L2)Br with REE Precursors

In Situ Transmetallation Reactions

Due to positive results obtained in deprotonation studies with **H_3(L2)Br** and alkali metal bis(trimethylsilyl)amides (see Chapter 2, Section 2.1.1.2), a series of experiments probing the propensity of generated **M(L2)** (M = Na, K) for transferring NHC to various REE precursors were performed. Hereby **M(L2)** was formed *in situ* at various reactions conditions and subsequently transferred to a solution or suspension of respective REE precursor.

In the first tentative experiments the transmetallation reactions were conducted at RT in THF using NaN" or KN" as bases and $CeCl_3(THF)_2$. Unfortunately, at RT these reactions yield merely organic decomposition products and/or decomposition products bonded to alkali metals. Therefore, analogue to the 1,2-shift of *N*-(3,5-di-*tert*-butyl-2-hydroxybenzyl) substituent

observed in **Na(L2)** by Kawaguchi[171], it is likely, that a rearrangement of the ligand framework occurs also in these cases bevor even the ligand can react with $CeCl_3(THF)_2$. Notably, also Shen observed the same type of reactivity of her bidentate *N*-(3,5-di-*tert*-butyl-2-hydroxybenzyl) functionalised NHC ligand in two step transmetallation reaction *in situ* with *n*-BuLi and $YbCl_3$.[98]. Therefore, further transmetallation reactions with **H_3(L2)Br** were conducted at –78 °C.

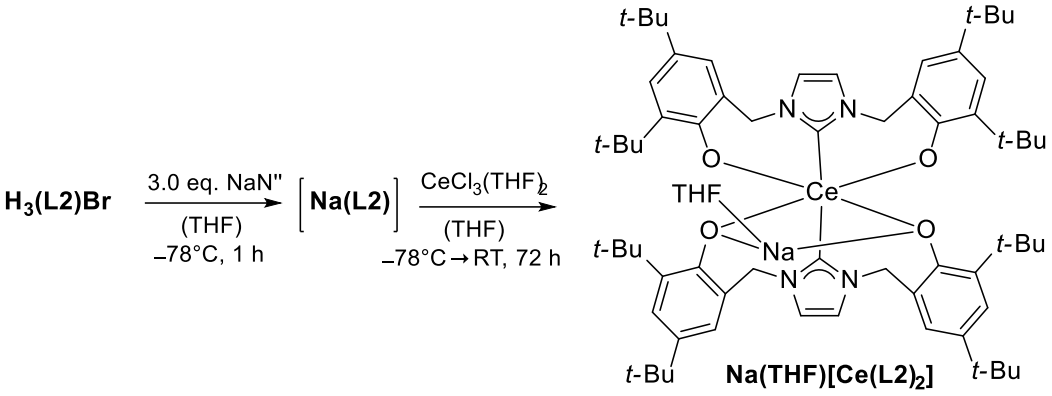

Scheme 3.1.5. *In situ* transmetallation reaction of **H_3(L2)Br** with NaN" and $CeCl_3(THF)_2$. The structure of the possible Ce NHC complex is a suggestion based on NMR data.

The reaction of *in situ* formed **Na(L2)** with $CeCl_3(THF)_2$ at –78 °C (Scheme 3.1.5) yields a dark brown residue whose ^{1}H NMR spectrum shows the presence of well-defined resonances indicating the formation of one major species as well as some minor ones (Figure 3.1.8). The appearance of partly very broad resonances in the region unusual for diamagnetic organic molecules clearly suggests a coordination of organic ligands to Ce(III) centre. The limited number of resonances also indicates a formation of a compound with high intrinsic symmetry. The singlets at 1.24 and –5.01 ppm can be tentatively assigned to *t*-Bu groups. Further resonances 11.06, 9.10, 8.94 and 6.14 ppm are probably attributed to the aryloxo-moieties and both chemically inequivalent methylene linkers. Imidazol-2-ylidene backbone protons resonate as broad small singlets at 18.35 and 14.35 ppm. The integral ratios of the resonances attributed to imidazole-backbone and the *t*-Bu group at –5.01 ppm does not exactly match the rest of the ligand framework, probably due to high paramagnetic influence on these group, which might lead to overestimating or underestimating the integral values. Additional analysis of the crude product by ^{29}Si NMR spectroscopy lead to expected detection of grease, HN" as well as NaN". Further smaller singlets in the positive region at 7.41, 7.58, 15.97 and 17.73 ppm indicate a formation of terminal $–OSiMe_3$ sites[172, 177], which might be caused by at least partial silylation of aryloxo-substituents.

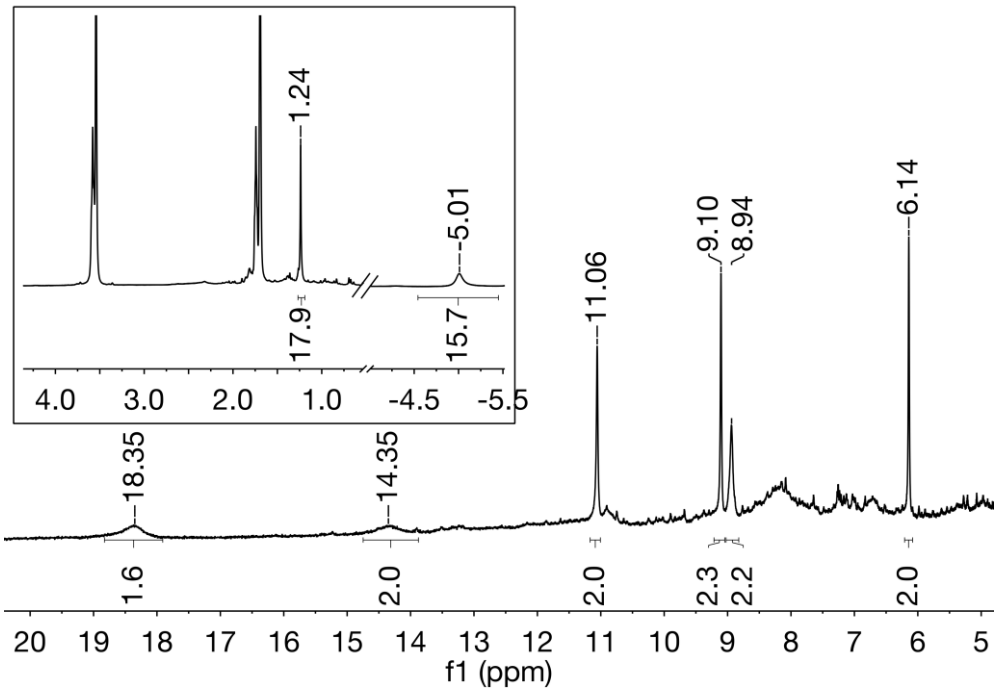

Figure 3.1.8. ^{1}H NMR spectrum of the crude product obtained in an *in situ* transmetallation reaction of **Na(L2)** and $CeCl_3(THF)_2$ at –78 °C in THF. The spectrum was recorded in THF-d_8 at RT.

Unfortunately, to date it was not possible to obtained crystalline material for further analysis neither by slow diffusion of pentane into saturated solution of the crude product in THF at RT nor by crystallization in a THF/toluene mixture at –26 °C. Due to lack of crystallographic characterization the exact molecular structure of the obtained complex remains unknown. Since the reaction did not proceed cleanly, the formation of **Na[Ce(L2)$_2$]** is still possible (Scheme 3.1.5). The complexes of the type M(THF)[REE(L2)$_2$] (M = alkali metal) have been already observed for other rare earth metals from other synthetic methods.[99]

The alternative precursor $Ce(BH_4)_3(THF)_4$ was treated with **K(L2)** at –78 °C, as it is expected to react *via* elimination of KBH_4 in a transmetallation reaction (Scheme 3.1.6). ^{1}H NMR spectrum of the obtained brown residue indicates a relatively clean conversion displaying only a limited number of the resonances that could be attributed to desired Ce NHC species as well (Figure 3.1.9). The broad singlets at 20.42, 6.04 and 6.48 ppm could be tentatively assigned to $Ce(BH_4)_nX$-fragments. The other resonances could be attributed to the rest of the ligand framework with some left-over resonances indicating a formation of a side-product. Further characterization by ^{29}Si NMR spectroscopy confirms a clean reaction as only the presence of HN'' and silicon grease is detected.

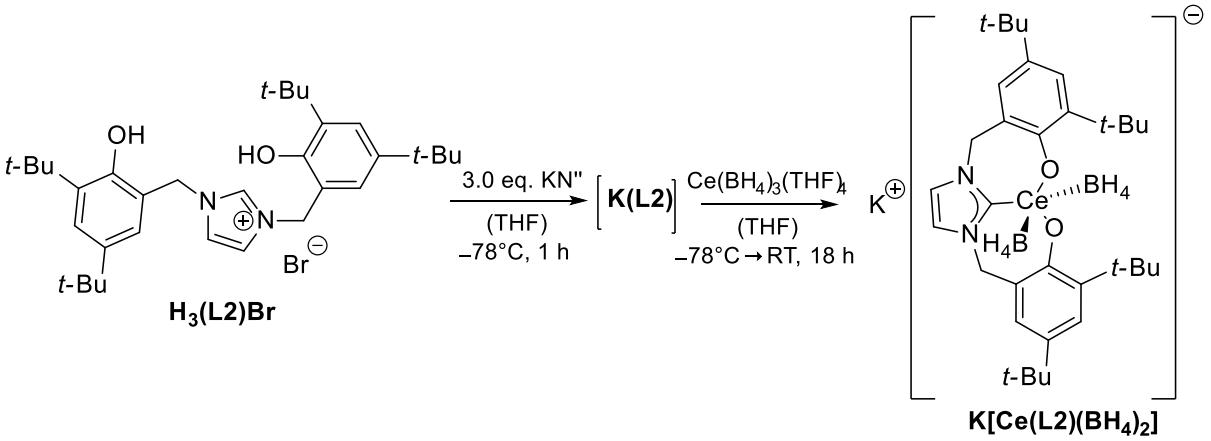

Scheme 3.1.6. *In situ* transmetallation reaction of **H_3(L2)Br** with KN" and $Ce(BH_4)_3(THF)_4$. The structure of the possible Ce NHC complex is a suggestion based on NMR data.

Further purification was conducted by the addition of toluene to the solution of crude product in THF at –26 °C. The formation of a fine, colourless precipitate is observed, which is no longer soluble in THF. Therefore, an elimination of KBH_4 is likely. ^{1}H NMR spectrum of the remaining solution still displays resonances attributed to the crude product, however, it also shows the formation of additional cerium NHC compounds with less symmetry and also some possible decomposition products. Further attempts to obtain crystalline material by slow diffusion of pentane into the solution of crude product in THF at RT failed unfortunately.

Besides the previously observed decomposition behaviour by 1,2-rearragement and elimination of one of the *N*-substituents in the alkali metal NHC adducts (see Chapter 2), another possible decomposition pathway is a migration of other nucleophilic ligands on the metal to carbene. Such rearrangement was observed for similar backbone saturated *N*-(3,5-di-*tert*-butyl-2-hydroxyphenyl) mono(NHC) Group IV chloro benzyl (Bn) complexes.[200] Interestingly, a migration of Bn-group to carbene was especially favoured for Ti, as the rearrangement product was already obtained in a reaction at –35 °C. For heavier analogues, Zr and Hf, the targeted carbene complexes obtained under the same reaction conditions were stable at RT. However, in contrast to very stable Hf complex the corresponding Zr compound could be converted to the rearrangement product by heating it to 60 °C. Therefore, similar to this rearrangement behaviour the same process could occur in **$K[Ce(L2)(BH_4)_2]$**, which could produce eliminated KBH_4 as a result of migration of BH_3 to carbene and subsequently the dimerization or oligomerization due to vacations of the coordination sites.

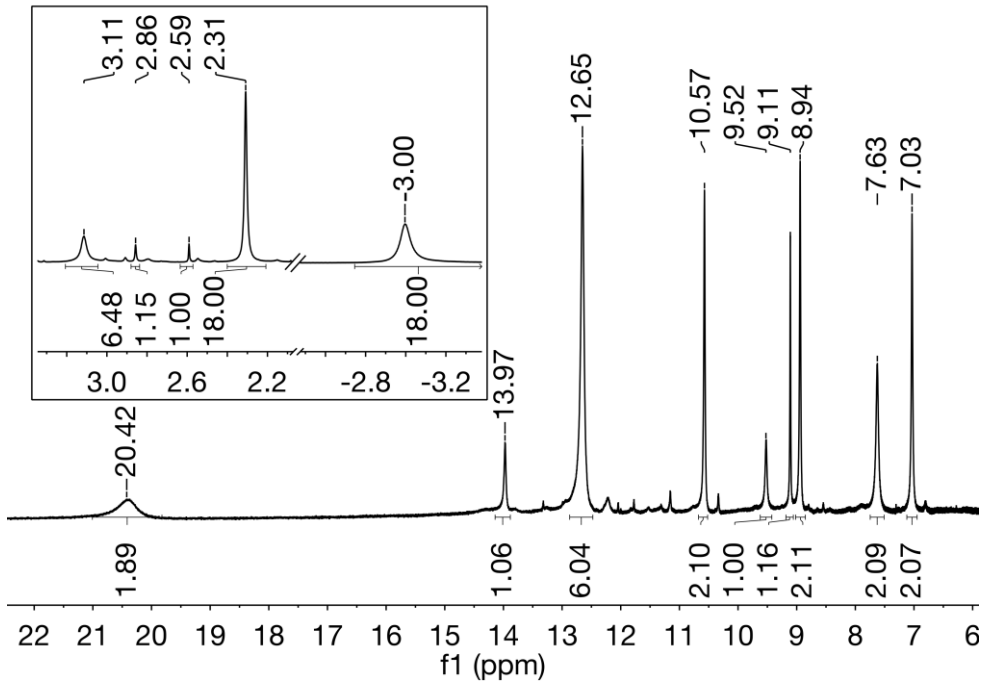

Figure 3.1.9. ^{1}H NMR spectrum of the crude product isolated after treating $Ce(BH_4)_3(THF)_4$ suspension in THF with *in situ* formed **K(L2)** at –78 °C in THF. The spectrum was recorded in THF-d_8 at RT.

In summary, similar to the reactions with $CeCl_3(THF)_2$ a formation of a **K[Ce(L2)(BH$_4$)$_2$]** is conceivable (Scheme 3.1.6), albeit a more symmetric but impure compound **K(THF)[Ce(L2)$_2$],** analogue to the compounds isolated by Shen[99] (see Introduction, Scheme 1.3.8), could exist. Furthermore, a formation of more complicated oligomeric structures is possible as well. Unfortunately, due to internal rearrangement processes leading to elimination of KBH_4 further characterization of the complexes was so far unsuccessful.

*Reactions of **H$_3$(L2)Br** with Li[Ce{N(i-Pr)$_2$}$_4$](THF)*

REE amides have been previously used for the synthesis of REE bearing bis(*N*-(3,5-di-*tert*-butyl-2-hydroxybenzyl) NHC ligands by Shen.[98] Based on this study the reactivity of Li[Ce{N(*i*-Pr)$_2$}$_4$](THF) with **H$_3$(L2)Br** was tentatively explored. Hereby a reaction of **H$_3$(L2)Br** with Li[Ce{N(*i*-Pr)$_2$}$_4$](THF) is visible within minutes at RT in THF (Scheme 3.1.7), as a dark solution containing large amounts of HN(*i*-Pr)$_2$ is formed (Figure 3.1.10). Furthermore, ^{1}H NMR spectrum shows the presence of LDA as well as a set of paramagnetically affected resonances. The broad singlets at 19.12, 2.23, 0.63, 0.17 ppm and a multiplet –7.70 –7.0 ppm can be tentatively assigned to terminal or bridging amides coordinated to Ce(III). The remaining resonances cleanly match the expected integral ratio for C2-deprotonated ligand. Further characterization by ^{13}C, HSQC or COSY 2D NMR was inconclusive. According to ^{1}H NMR spectroscopy the compound is stable at RT for at least 5 d. A crystallization by slow diffusion of pentane into a solution of the crude product in THF at RT yields no crystalline

material. Also a crystallization attempt in THF/toluene mixture at –26 °C is unsuccessful as a formation of crystalline material could not be induced. Therefore, it is unclear if in this case a Ce NHC complex or other Ce(III) complex with *N*-bonded imidazoles resulting form 1,2-rearragement of the ligand have been formed.[97]

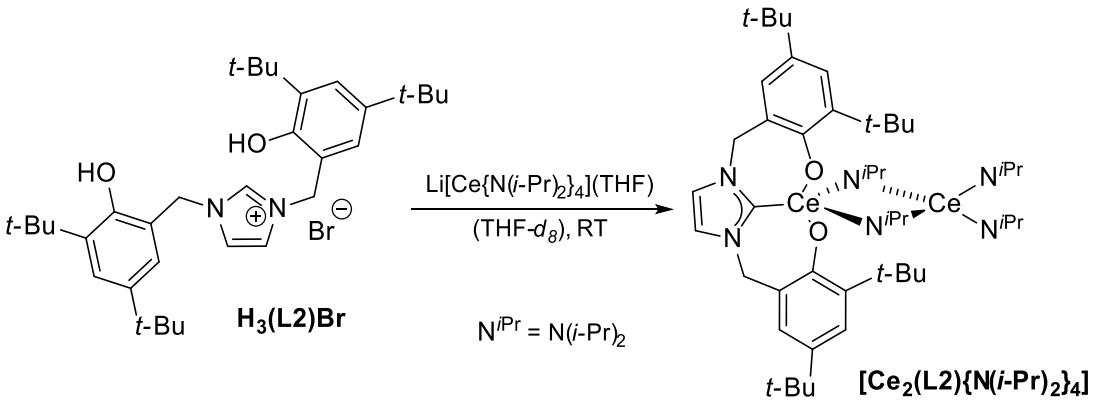

Scheme 3.1.7. Reaction of **H_3(L2)Br** with Li[Ce{N(*i*-Pr)$_2$}$_4$](THF) in THF-d_8 at RT. The Ce NHC product is suggested based on NMR data.

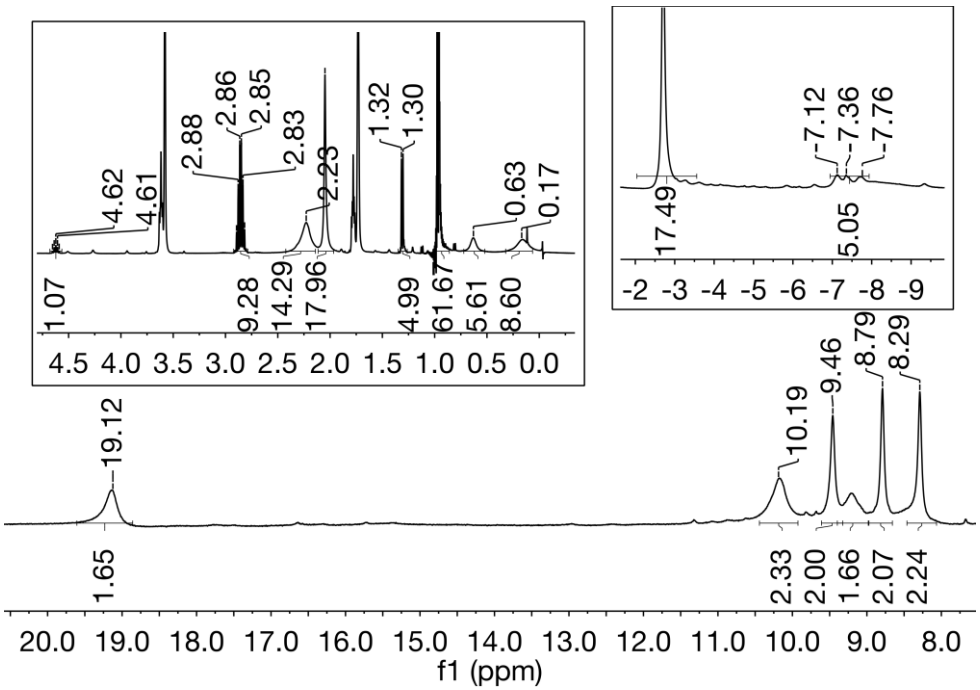

Figure 3.1.10. ^{1}H NMR spectrum of the reaction mixture obtained after the treatment of **H_3(L2)Br** with Li[Ce{N(*i*-Pr)$_2$}$_4$](THF) in THF-d_8 at RT.

To facilitate salt elimination Li[Ce{N(*i*-Pr)$_2$}$_4$](THF) was treated with **H_3(L2)Br** in benzene at RT as well. However the obtained ^{1}H NMR spectrum displays even more complicated resonance pattern as corresponding reaction in THF (Figure 3.1.11). The unmistakable influence of paramagnetic cerium centre is evident and therefore it can be concluded that also in this case

a Ce NHC compound has been synthesized. Similarly to the reaction of Li[Ce{N(*i*-Pr)$_2$}$_4$](THF) with **H$_2$(L1^{Me})Br** mentioned above, a formation of a complicated oligomeric structures is highly likely. Interestingly, a ^{7}Li resonance at 16.11 ppm suggest an incorporation of Li into molecular structure further supporting the assumption that complicated oligomeric structure has been formed. Unfortunately, to date, no single crystals suitable for SC-XRD could be obtained by slow diffusion of pentane into the solution of the crude product in benzene. Further crystallization, especially at low temperatures, should be therefore conducted.

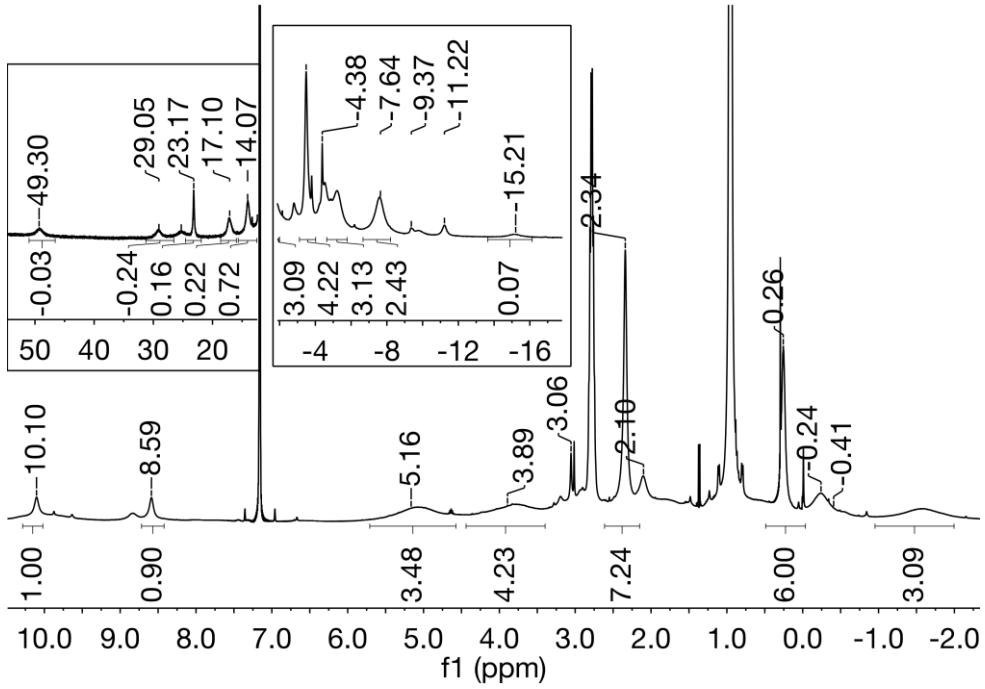

Figure 3.1.11. ^{1}H NMR spectrum of the reaction mixture obtained after the treatment of **H$_3$(L2)Br** with Li[Ce{N(*i*-Pr)$_2$}$_4$](THF) at RT in C_6D_6.

Since all the reactions described above were carried out using incorrect stoichiometry the addition of an additional equivalents of LDA was carried out in an attempt to yield higher yields and possibly more easily identifiable compounds due to higher intrinsic symmetry. Such a procedure has been previously successfully applied by Shen for other rare earth metals.[99] Therefore a mixture of 2.0 eq. of **H$_3$(L2)Br**, 1.0 eq. of Li[Ce{N(*i*-Pr)$_2$}$_4$](THF) and 2.0 eq. of LDA was used in a one-pot reaction in THF (Scheme 3.1.8.). Unfortunately, even at –26 °C the reaction proceeds instantaneously and vigorously upon addition of cold THF. A fast cooling down of the reaction to –78 °C and subsequent slow warming up until RT was undertaken, but ideally, this reaction should be repeated at –78 °C.

Correspondingly, the recorded ^{1}H NMR spectrum of the crude product showed a formation of structurally complicated hardly quantifiable cerium-organo species on the one hand as well as a formation of decomposition products on the other hand (SI, Figure 5.3.16). Analogue to the

previously reported reactivity of *N*-(3,5-di-*tert*-butyl-2-hydroxybenzyl) mono(NHC) pro-ligand **79** with other lithium tetrakis(diisopropylamide) rare earth metallates,[97] due to a very exothermic reaction the decomposition and rearrangement of the ligand to *N*-bonded imidazoles and to bis(aryloxo)-ligands are conceivable (Scheme 3.1.8). Any further attempts to purify the mixture by different crystallization methods (slow diffusion of pentane into a solution of the crude product in toluene or benzene at RT, crystallization out of toluene/pentane or toluene/DME/pentane solvent mixture at –26 °C) were unsuccessful. Therefore, due to high reactivity of LDA this synthetic protocol needs further modification including the lowering of the reaction temperatures as well as a step-wise addition of LDA.

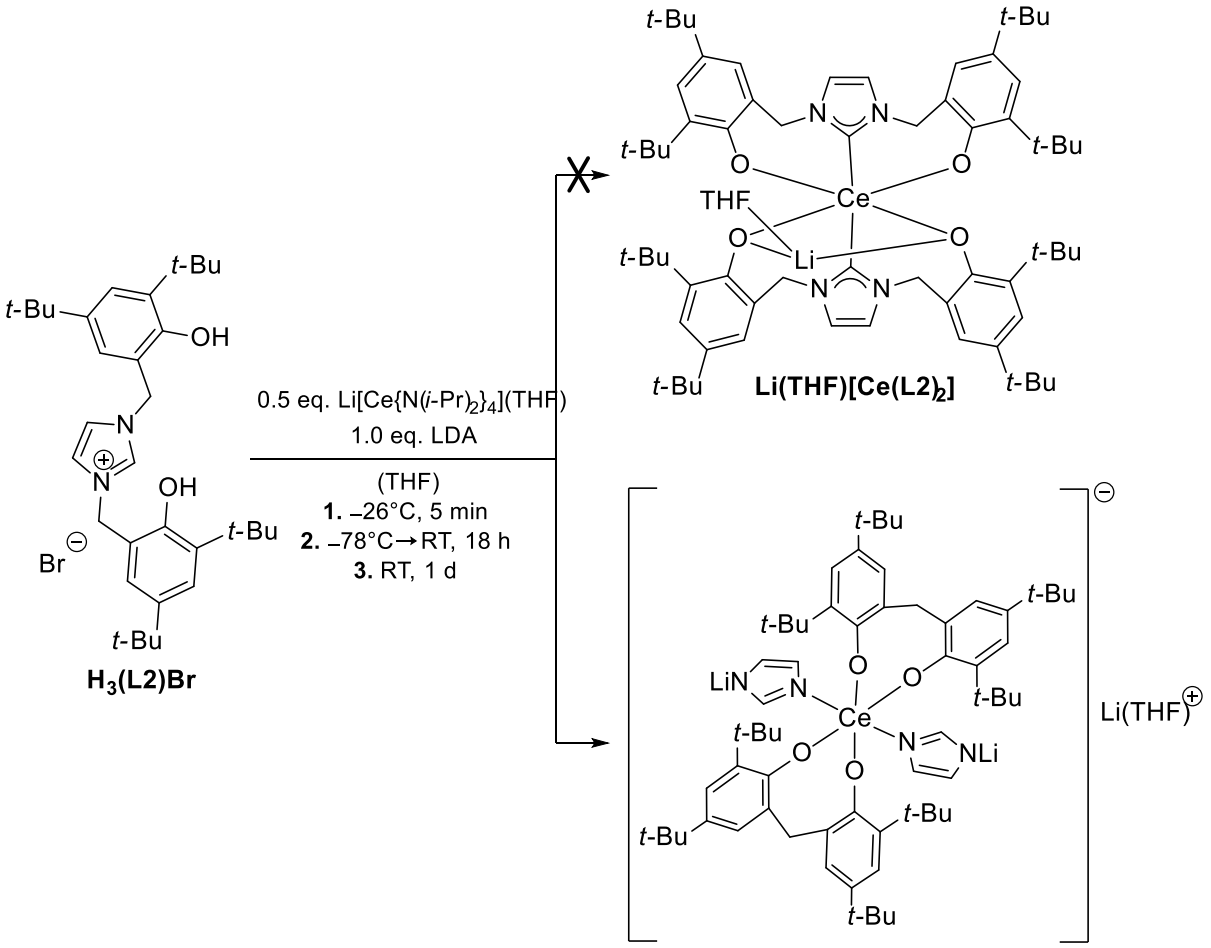

Scheme 3.1.8. Reaction of **H_3(L2)Br** with Li[Ce{N(*i*-Pr)$_2$}$_4$](THF) and LDA.

In summary, all of the experiments described in this section indicate a highly promising approach for targeting the corresponding REE NHC compounds. Further experiments towards isolation and crystallization should be therefore performed. Moreover, all synthetic protocols should be further modified to minimize competing rearrangement reactions e. g. by lowering the reaction temperature.

3.1.2 1,1'-(2-Hydroxyethane-1,1-diyl)-Bridge Functionalised Pro-Ligands $H_3(L4^R)X_2$

3.1.2.1 Transmetallation Reactions *in Situ*

Although **Li(L3^{Mes})** can be readily isolated, due to its unknown exact molecular structure, it was generated and used *in situ* to ensure stoichiometric control. Therefore, to test the propensity of **Li(L3^{Mes})** for transferring bis(NHC) ligand to REE, the chosen REE precursors were treated with a solution of **Li(L3^{Mes})** formed *in situ* at 0 °C or at RT (e.g. as seen in Scheme 3.1.9).

No reaction of *in situ* formed **Li(L3^{Mes})** with CeN''_3 is observed at RT in benzene (Scheme 3.1.9). Also ^{1}H NMR spectrum of the residue obtained after the stirring of the same reaction mixture for 18 h at 60 °C shows no sign of any transfer of NHC ligand to the cerium centre. No reaction was observed in benzene with $CeCp_3$ either (Scheme 3.1.10).

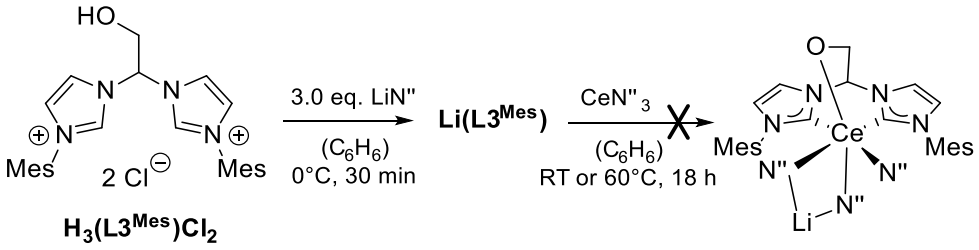

$H_3(L3^{Mes})Cl_2$

Scheme 3.1.9. Reaction conditions used for the treatment of CeN''_3 with **Li(L3^{Mes}).**

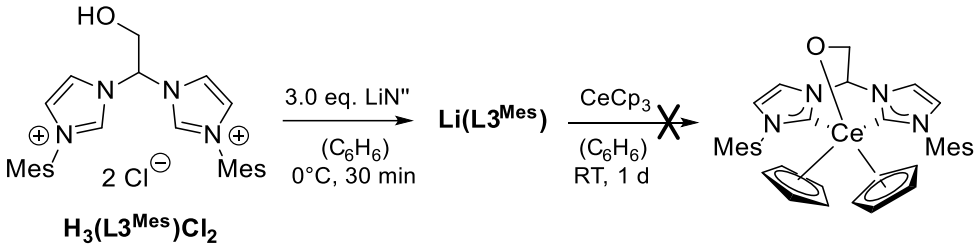

$H_3(L3^{Mes})Cl_2$

Scheme 3.1.10. Reaction conditions used for the treatment of $CeCp_3$ with **Li(L3^{Mes}).**

However, the use of the metal precursor $Ce(BH_4)_3(THF)_4$ results in the formation of various diamagnetic products (Scheme 3.1.11). The ^{1}H NMR spectrum of the crude product shows no remaining resonances attributable to the Li NHC adduct but instead numerous smaller resonances, especially in the aliphatic region (see Figure 5.3.17, SI). A set of resonances attributable to a single major product is assignable to a product similar to 1-mesitylimidazole, but with different chemical shift values. Therefore, since no resonances in the region expected for 1,1'-(2-hydroxyethane-1,1-diyl) bridge are detected, a possible main product could be 2-mesitylimidazole formed by 1,2-shift of the *N*-mesityl-substituent and degradation of the bridge. Both processes have been already observed for alkali metal NHC adducts described in

Chapter 2. Moreover, a coordination of imidazoles *via* nitrogen atoms to cerium or lithium cation would be likely in the presence of these metals. Such reactivity would be not surprising, as Shen observed on several occasions a coordination of imidazole moieties to REE and lithium as a result of the degradation of a NHC ligand due to thermally induced decomposition.[97-98] In the case of the reaction described here the observed chemical shifts rather suggest a coordination to Li.

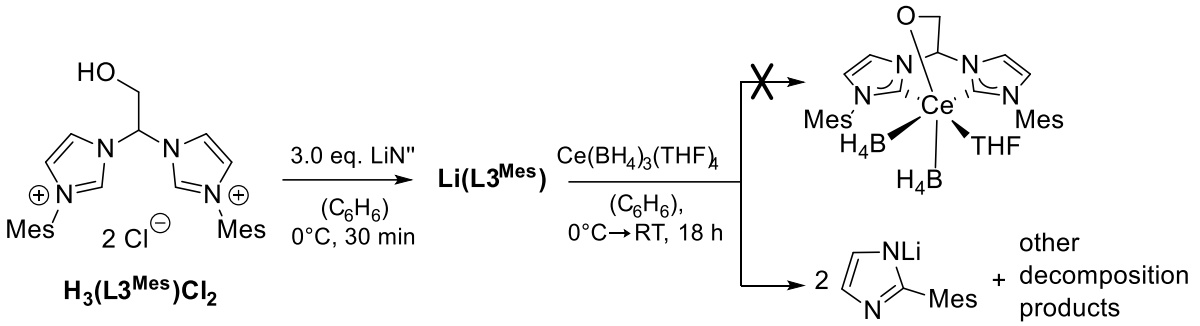

$H_3(L3^{Mes})Cl_2$

Scheme 3.1.11. Reaction of $Ce(BH_4)_3(THF)_4$ with **Li(L3^{Mes})** formed *in situ*.

Since **Li(L3^{Mes})** is not a useful reagent in reactions with respect to the tested cerium precursors, different rare earth metals have been considered. Due to its higher Lewis acidity yttrium is expected to form stronger M–C_C bonds. Moreover, the diamagnetic nature of Y nucleus facilitates the characterization of the products. Therefore, a solution of **Li(L3^{Mes})** was treated with a suspension of YCp_3 in benzene (Scheme 3.1.12). The reaction of **Li(L3^{Mes})** with YCp_3 is clearly visible by slow consumption of REE precursor and change of the colour of the solution from yellow-orange to intense pink. Unfortunately, the ^{1}H NMR spectrum of the crude product displays extremely high number of overlapping resonances in aromatic and aliphatic region (SI, Figure 5.3.18). Although two resonances attributed to a possibly intact linker between two imidazole-2-ylidenes are visible, they do not correlate with the number and intensity of other resonances suggesting that in most cases the decomposition of the ligand framework must have been occurred. Furthermore, no doublet expected for a Y–C bond is found in the ^{13}C NMR spectrum. However, ^{7}Li NMR spectrum indicates a possible formation of LiCp due to the presence of a broad singlet at 6.96 ppm. This would suggest a transfer of the ligand to Y ion in a salt elimination reaction. Finally, ^{29}Si NMR sheds no more light on the possible products as only the formation of HN" is evident. Further characterization of the residue obtained after the filtration of the pink solution by ^{1}H and ^{7}Li NMR spectroscopy in pyridine-d_5 only confirms the formation of LiCp.

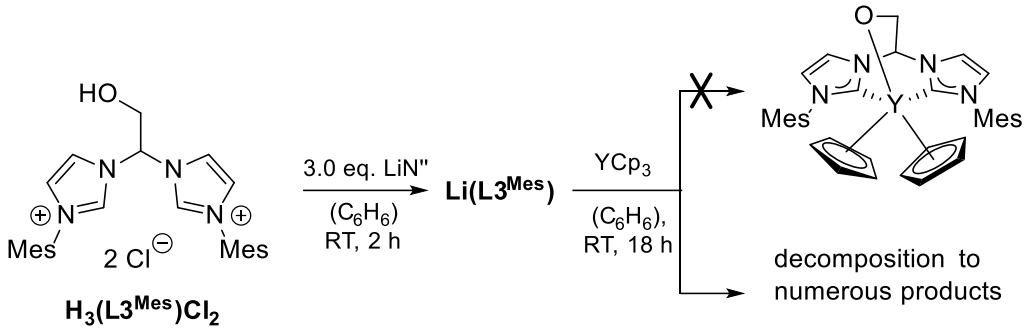

Scheme 3.1.12. Reaction of YCp_3 with **Li(L3^{Mes})** formed *in situ*.

Although it was not possible to isolate the corresponding potassium bis(NHC) adduct due to its higher instability in comparison to **Li(L3^{Mes}),** a possibility of generation of [**K(L3^{Mes})**] *in situ* for subsequent use as NHC transfer reagent to a cerium centre was considered as an alternative due to apparent inertness of **Li(L3^{Mes})** towards some cerium precursors.

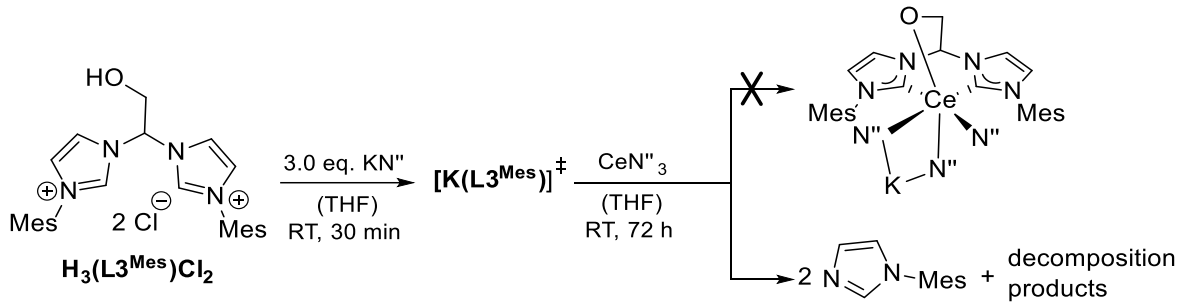

Scheme 3.1.13. Generation of **[K(L3^{Mes})]** *in situ* and subsequent reaction with $CeN"_3$.

Because of the previously mentioned thermal instability of K bis(NHC)s (see Chapter 2, Section 2.1.2.2), **H_3(L3^{Mes})Cl_2** was allowed to react for only 30 min with KN" in THF at RT (Scheme 3.1.13). A subsequent rapid transfer of [**K(L3^{Mes})**] solution to a solution of $CeN"_3$ in THF resulted in isolation of a crude product, whose ^{1}H NMR spectrum is hardly quantifiable (SI, Figure 5.3.19). However, some broad resonances and well as resonances in the negative region including a broad singlet attributed to bis(trimethylsilyl)amide groups coordinated to Ce at –1.72 ppm indicate a possible formation of desired compounds. Unfortunately, after attempting to wash the crude product with hexane only various diamagnetic decomposition products as well as 1-methylimidazole are detected in the washing solution as well as in the remaining residue. This behaviour is similar to the degradation pathway of alkali metal adducts of 1,1'-(2-hydroxyethane-1,1-diyl)-bridged functionalised bis(NHC) described in Chapter 2, Section 2.1.2.2, suggesting that a potential REE ligand complex is either highly air-sensitive and/or thermally unstable. Similar results were obtained by treating **H_3(L3^{Mes})$(BPh_4)_2$** with KN" and subsequent transfer of the resulting solution to $CeCp_3$.

Since neither potassium nor lithium adducts of 1,1'-(2-hydroxyethane-1,1-diyl) bridge modified *N*-mesityl functionalised bis(NHC)s show particularly promising behaviour towards transmetallation to REEs, the use of an analogous isopropyl-functionalised pro-ligand was considered. In the reaction of **$H_3(L3^{i\text{-}Pr})Cl_2$** with LiN" in THF it was possible to recover the bis(imidazolium) chloride out of **$Li(L3^{i\text{-}Pr})$** by hydrolysis with HCl (see Chapter 2. Section 2.1.2.2), therefore proving that **$Li(L3^{i\text{-}Pr})$** is quite stable with respect to ligand rearrangement. Therefore, to test the reactivity of isopropyl wingtip modified precursors in two step reactions with LiN" and cerium borohydride, a synthetic protocol similar to the reactions with **$H_3(L3^{Mes})X_2$** has been chosen (Scheme 3.1.14). Unfortunately, similar to the cases described above the formation of 1-isopropylimidazole as main species is observed in ^{1}H NMR spectrum of the crude product, although the appearance of a broad singlet at –0.15 ppm attributed to $LiBH_4$[201] supports a successful salt elimination reaction (SI, Figure 5.3.20).

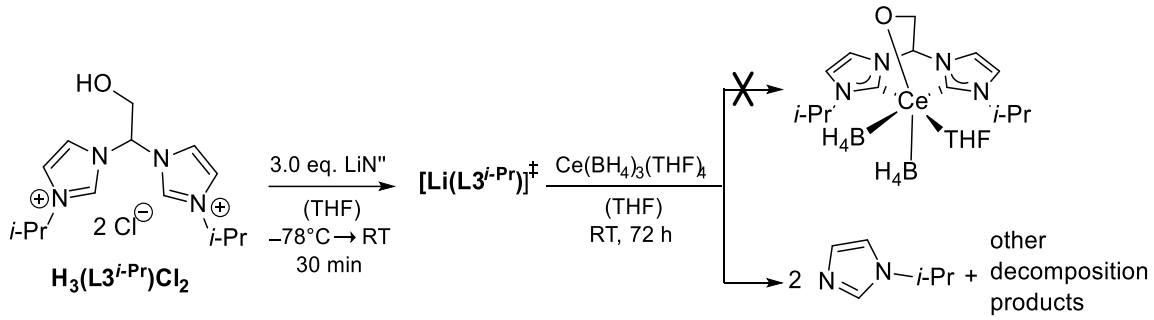

Scheme 3.1.14. Generation of **$[Li(L3^{i\text{-}Pr})]$** *in situ* and subsequent reaction of this intermediate with $Ce(BH_4)_3(THF)_4$.

In conclusion, although the pro-ligands **$H_3(L3^R)X_2$** tend to form at least meta-stable alkali metal NHC adducts the synthetic approach to corresponding REE NHC complexes *via* two-step transmetallation reaction proved to be unsuccessful. The reason for it is either the inertness of **$Li(L3^{Mes})$** towards many precursors and the decomposition of the ligand yielding substituted imidazoles if the reaction occurs.

3.1.2.2 Direct Conversion of Bis(imidazolium) Precursors with Rare Earth Amides and Alkyls

The reactivity of 1,1'-(2-hydroxyethane-1,1-diyl)-bridge functionalised bis(imidazolium) salts with $Li[Ce(N\{i\text{-}Pr\}_2)_4](THF)$ has been investigated as well. On a NMR scale, $Li[Ce(N\{i\text{-}Pr\}_2)_4](THF)$ reacts with **$H_3(L3^{Mes})Cl_2$** at RT in THF forming an orange slurry (Scheme 3.1.15). After separation of the precipitate by centrifugation the ^{1}H NMR spectrum of the supernatant shows new resonances in the aromatic region (SI, Figure 5.3.21). Unfortunately, most of them can be attributed to 1-mesitylimidazole. However, a broad singlet at 0.62 ppm suggest at least a partial retention of cerium diisopropyl amide-moieties. Therefore, it is

possible that the chloride anions block coordination sites on cerium leading to decomposition of the NHC ligands due to lack of the possibility for ligation. Shen previously also noted the difficulty of the synthesis of Ce NHC halide complexes by various methods due to competition of halide and NHC.[98] Therefore, the use of the same ligand precursor balanced by a non-coordinating anion was further investigated.

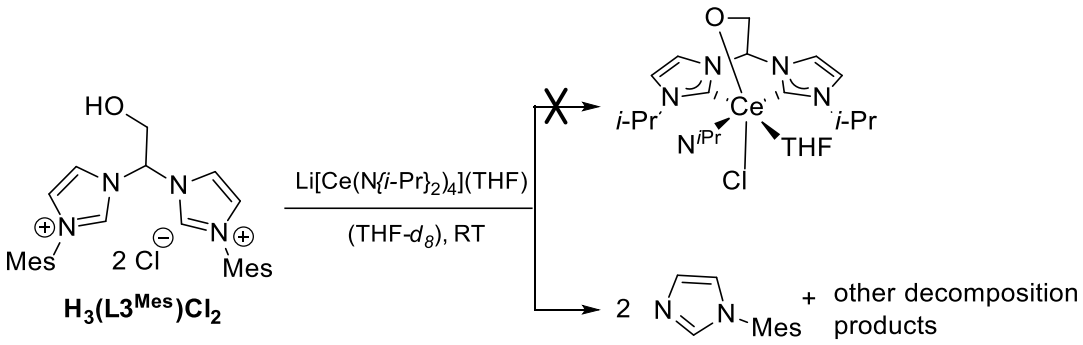

Scheme 3.1.15. Reaction of $\mathbf{H_3(L3^{Mes})Cl_2}$ with lithium tetrakis(diisopropylamide)cerate.

On NMR scale the treatment of $\mathbf{H_3(L3^{Mes})(BPh_4)_2}$ with Li[Ce(N{*i*-Pr}$_2$)$_4$](THF) in THF at RT (Scheme 3.1.16.) results in colour change of the suspension from orange to dark red and subsequently to orange again. Centrifugation and recording of ^{1}H NMR spectrum of the supernatant reveals the predominant presence of HN(*i*-Pr)$_2$ and BPh_4^- (Figure 3.1.12). Further smaller set of resonances attributed to diisopropyl amide shifted to higher frequencies strongly suggest the formation of LDA. More useful information can be obtained from inspection of the broad resonances attributed to a minor product. The singlets at 10.91 and 2.36 ppm are coincident with two of the resonances caused by the cerium precursor. However, they are not matched by the other resonances at 0.96 ppm and –0.6 ppm expected for Li[Ce(N{*i*-Pr}$_2$)$_4$](THF), instead a new resonance at 0.63 ppm is observed. Together with the

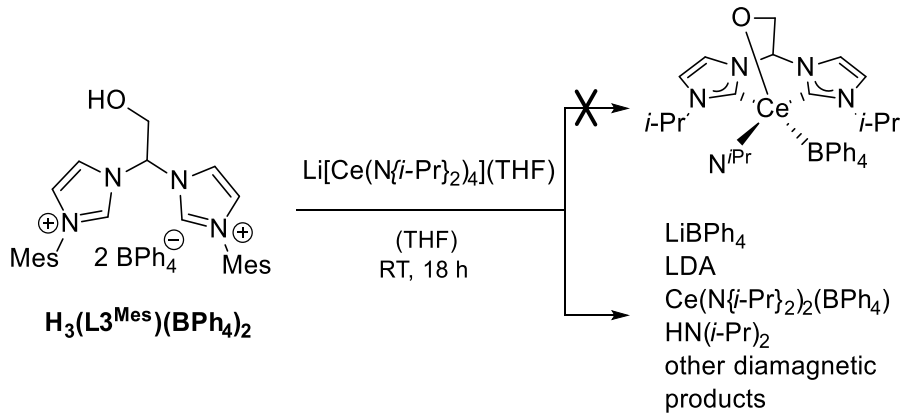

Scheme 3.1.16. Reaction of $\mathbf{H_3(L3^{Mes})(BPh_4)_2}$ with lithium tetrakis(diisopropylamide)cerate.

formation of HN(*i*-Pr)$_2$ this fact suggest at least partial consumption of amide coordinated to cerium precursor. Finally, some other small broad resonances (e.g. 7.79 and 5.10 ppm) present in this spectrum indicate a formation of cerium complexes. Unfortunately, further crystallization of out THF/hexane solvent mixture yielded only colourless crystals which were identified as LiBPh$_4$(THF) by SC-XRD.

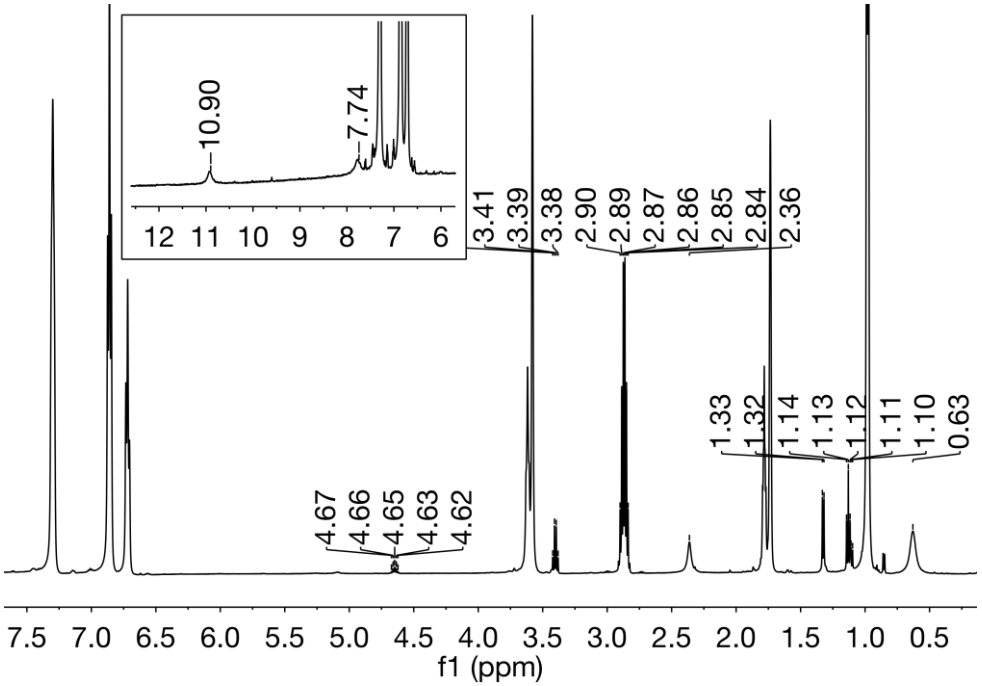

Figure 3.1.12. ^{1}H NMR spectrum of the reaction mixture obtained after the treatment of **H$_3$(L3^{Mes})(BPh$_4$)$_2$** with Li[Ce(N{*i*-Pr}$_2$)$_4$](THF) in THF-*d*$_8$ at RT.

Due to promising results on exploratory NMR scale an isolation of possible product on preparative scale was conducted (Scheme 3.1.16.). Hereby similar to NMR scale reaction the formation of LiBPh$_4$, LDA and free amine is observed. Furthermore, ^{1}H NMR spectrum of the crude product displays a number of additional resonances influenced by a paramagnetic centre since they are appearing in the region unusual for diamagnetic molecules. However, after attempts to purify the crude product by extraction with benzene these disappear after evaporation of the washing solution. Also the benzene-insoluble residue comprises of LiBPh$_4$ or Ce(BPh$_4$)$_3$ suggesting once again a decomposition of possible obtained Ce NHC complex.

To exclude the possibility of unsuccessful ligation due to the size of the REE cation, the usage of Sc(III) alkyls was further investigated (Scheme 3.1.17.). Unfortunately, the reaction of *in situ* formed ScBn$_3$ with **H$_3$(L3^{Mes})Cl$_2$** yields only 1-mesitylimidazole (for ^{1}H NMR spectrum see SI, Figure 5.3.22) as a main product, once again confirming the fact that bis(imidazolium) chlorides react in elimination of *N*-substituted imidazoles with REE internal bases due to blocking of the coordination sites by halogen anions.

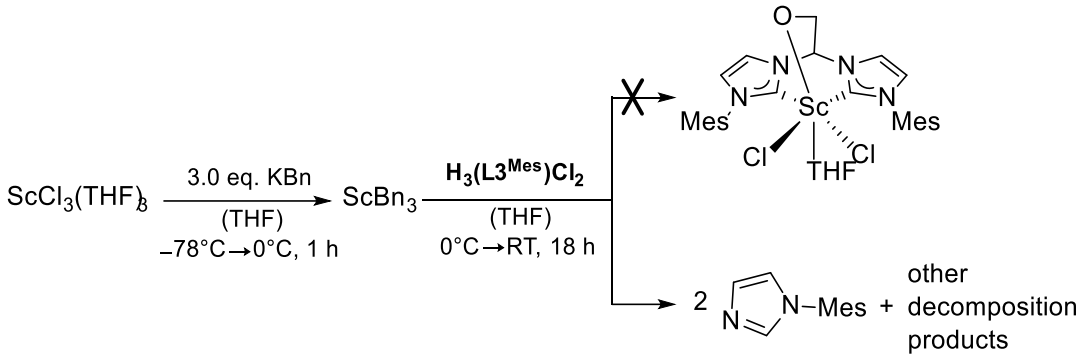

Scheme 3.1.17. Generation of $ScBn_3$ *in situ* and subsequent reaction of **$H_3(L3^{Mes})X_2$** (X = Cl, PF_6) with this internal base.

Although no 1-mesitylimidazole is formed in the reaction of $ScBn_3$ with **$H_3(L3^{Mes})(PF_6)_2$**, the ^1H NMR spectrum of the crude product shows numerous, small resonances in the aromatic region, once again suggesting that no thermodynamically stable product is formed in this case either (SI, Figure 5.3.23). Moreover, after 2 days at RT many resonances are replaced by even a higher number of new resonances suggesting that even if some Sc NHC species have been formed they might not be stable at RT. These results correlate with the observation in experiments with Ce(III) amides. A possible pathway by which a meta-stable NHC complexes with electropositive metals could degrade is indicated by the reports of Romain *et al.* and Ayoub *et al*.[200, 202] These studies describe Group IV complexes showing rearrangement of metal-bonded benzyl group to carbenic carbon. Such reactivity is especially favourable for small titanium centres. Therefore, in our case, similar processes could be responsible for unsuccessful synthesis of corresponding Sc NHC benzyl complexes.

In summary, although 1,1'-(2-hydroxyethane-1,1-diyl) bridged bis(imidazolium) salts readily react with internal bases of rare earth metals, in most cases decomposition of the ligand under formation of substituted imidazoles have been observed. Therefore, the usage of this ligand type in the reaction with electropositive metals seems like a highly unpromising approach with respect to the goal of obtaining REE NHC compounds.

3.1.3 1,1'-(2-Hydroxypropane-1,3-diyl)-Bridge Functionalised Pro-Ligand $H_3(L4^{Mes})Br_2$

3.1.3.1 Transmetallation Reactions *in Situ*

A clean formation of **$K(L4^{Mes})$** by deprotonation of **$H_3(L4^{Mes})Br_2$** with KN" could be unmistakably proven by NMR analysis. Therefore, this intermediate was subsequently used in

transmetallation reactions *in situ* using REE halides due to expected clean elimination of potassium halides.

The REE precursor $ScCl_3(THF)_3$ was chosen to begin with due to diamagnetic nature of the respective nucleus. The reaction conditions for the first step of the reaction leading to the formation of **K(L4^{Mes})** were previously optimized in Chapter 2. The pro-ligand is firstly treated with KN" solution in THF at 0 °C. In order to ensure a complete conversion of the ligand precursor to potassium NHC adduct the reaction mixture is subsequently stirred for a short period of time at RT as well and then quickly transferred to a suspension of $(REE)Cl_3(THF)_x$ in THF (Scheme 3.1.18.). After the work up a brown residue is obtained as crude product which is further analysed by NMR spectroscopy.

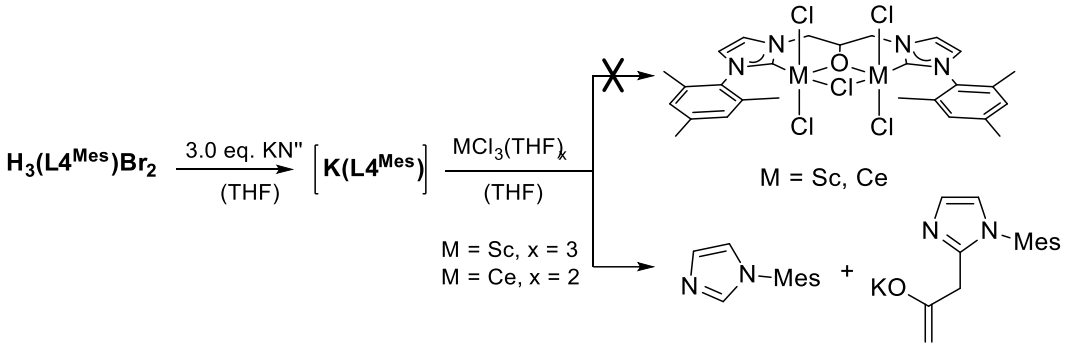

Scheme 3.1.18. *In situ* transmetallation reaction of **H$_3$(L4^{Mes})Br$_2$** with KN" and REE chlorides (REE = Sc, Ce). For exact reaction conditions see Experimental Section, Table 5.2.17.

The ^{1}H NMR spectrum of the obtained product obtained after the treatment of $ScCl_3(THF)_3$ with **[K(L4^{Mes})]** is shown in Figure 3.1.13 (lower spectrum). It displays two sets of low-intensity, broad resonances between 6.56 – 7.5 ppm and 1.5 –2.5 ppm. Furthermore, no resonances in the spectral region expected for the linker between two imidazol-2-ylidenes moieties are visible, indicating the decomposition of the ligand framework. Furthermore, low-intensity resonances in the aromatic and aliphatic region suggest a formation of 1-mesitylimidazole, whose proportion in the sample strongly increases with time if a solution is allowed to stand at RT (Figure 3.1.13, second from the top). Further purification attempts by crystallization from a THF/toluene solution at –26 °C yielded a brown amorphous residue, which contained 1-mesitylimidazole as a minor product. Other observed sharp resonances in the aromatic region indicate either a formation of other organic by-products or possibly Sc- or K-bonded rearrangement products (e. g. imidazoles). Unfortunately, further crystallization by slow diffusion of Et_2O into a solution of crude product in THF at RT yielded no crystalline material.

Additionally, a slight variation in reaction conditions in two subsequent experiments (see Experimental Section, Table 5.2.17) does not result in significant changes in the ^{1}H NMR spectrum of the obtained crude product mixture. It was not further possible to obtain better

resolution of the spectra from variable temperature NMR studies (–60 °C – 60 °C) or by an addition of KO(*t*-Bu), which was added to attempt to break down a putative Sc-NHC-Cl cluster. Further characterization by ^{29}Si NMR was not informative as only the presence of HN'' and silicon grease are determined.

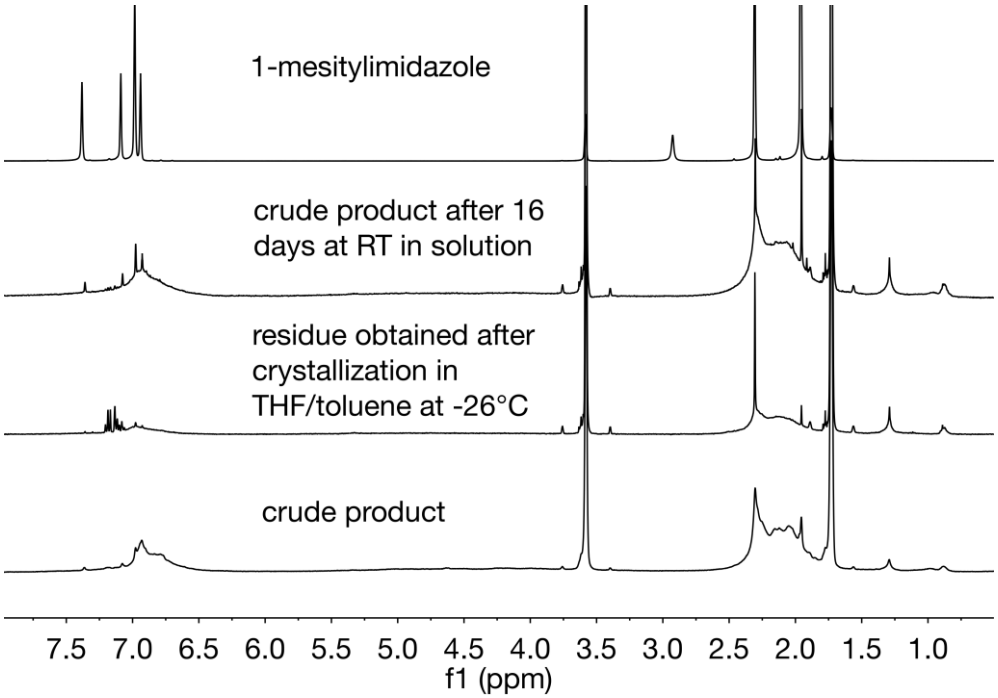

Figure 3.1.13. Comparison of the ^{1}H NMR spectra of the crude product obtained after a reaction of **K(L4^{Mes})** with $ScCl_3(THF)_3$ (bottom) to the spectra of the same sample after a purification procedure (second from the bottom), after storing the solution for approximately 2 weeks at RT (second from the top) and pure 1-mesitylimidazole (top). All spectra were recorded in THF-d_8 at RT.

Similar to the Group IV NHC complexes reported by Dagorne which show migration of ligands to carbene for smaller metal centre[200], to exclude the possibility of the decomposition of possibly formed REE-**L4^{Mes}** compounds due to a smaller size of Sc ion, a transmetallation reaction with $CeCl_3(THF)_2$ was conducted using the same reaction conditions (Scheme 3.1.18.). ^{1}H NMR spectrum of the obtained crude product resembles that of the residue in the $ScCl_3(THF)_3$ reaction. Interestingly, recrystallization at low-temperature of the crude product from THF/toluene yielded an amorphous residue whose analysis revealed the formation of the same species as in the low-temperature crystallization with scandium analogue (Figure 3.1.14). This observation strongly suggests a decomposition of the pro-ligand into various organic compounds and/or K-bonded decomposition products.

Due to likely incorporation of KCl in to the products obtained in THF the driving force of the transmetallation reaction of **K(L4^{Mes})** with REE chlorides is expected to be lower than using REE iodides, as KI will precipitate out of THF completely. Therefore, to investigate this possibility an *in situ* transmetallation reaction using $CeI_3(THF)_{2.5}$ was conducted as well

(Scheme 3.1.19.). ^{1}H NMR spectrum of the obtained crude product showing a number of broad small resonances is depicted in Figure 3.1.15. Most the resonances are observed in the diamagnetic region of the spectrum, however, their poor resolution could indicate an influence of a paramagnetic centre. Also a group of resonances between 4.5 ppm – 5.5 ppm indicate an intact alkyl linker in the ligand. Otherwise the spectrum is not very informative. Further purification of the material was performed by cooling down the mixture to –26 °C in THF/toluene, which produced a fine solid as precipitate.

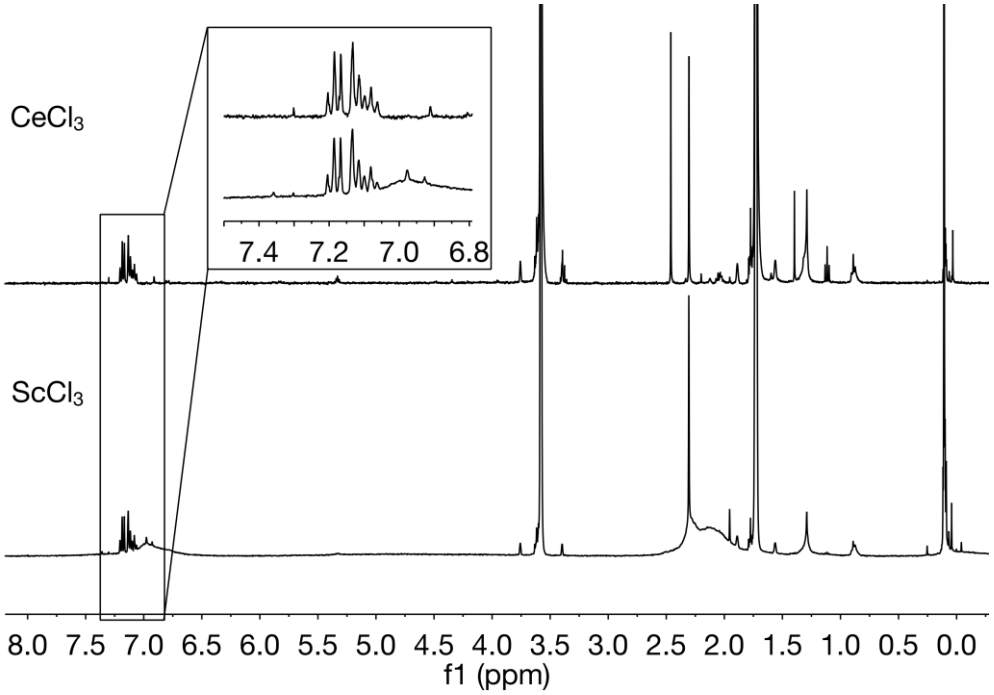

Figure 3.1.14. Comparison of the ^{1}H NMR spectra of the amorphous residues obtained in low-temperature crystallization experiments with the solutions of the respective crude products of the reactions of **K(L4^{Mes})** with $MCl_3(THF)_x$ (M = Sc, Ce) in THF/toluene solvent mixtures. All spectra were recorded in THF-d_8 at RT.

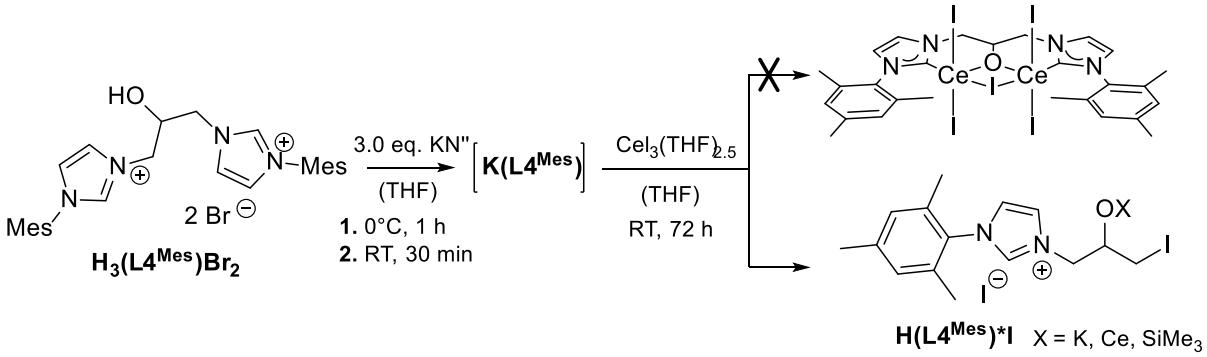

Scheme 3.1.19. Two-step reaction of **H$_3$(L4^{Mes})Br$_2$** with KN" and $CeI_3(THF)_{2.5}$.

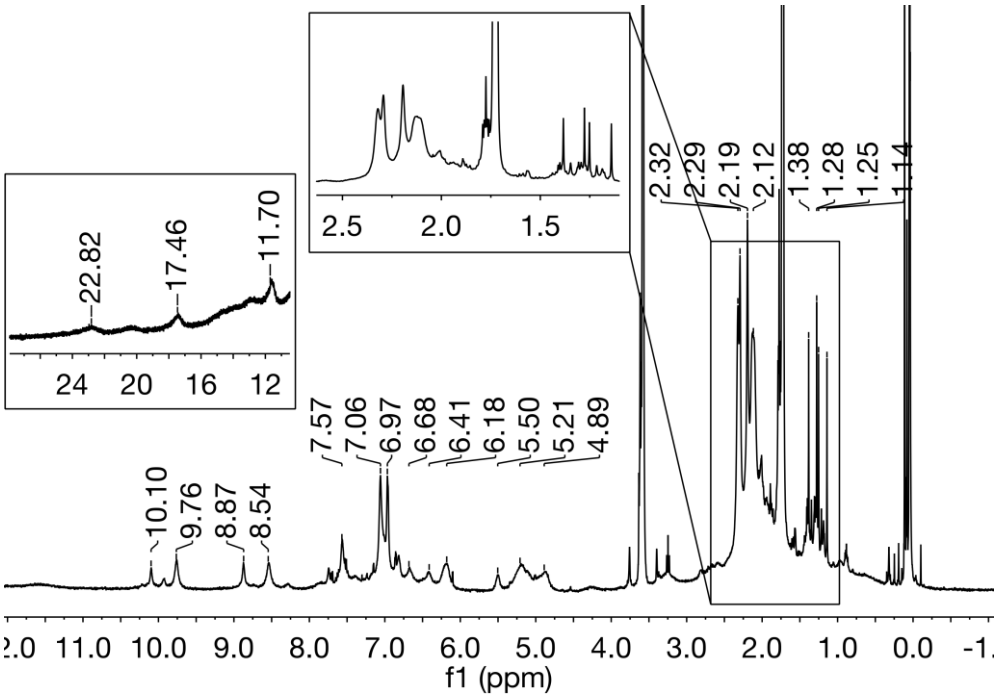

Figure 3.1.15. ^{1}H NMR spectrum of the crude product obtained in a reaction of *in situ* formed **K(L4^{Mes})** with $CeI_3(THF)_{2.5}$. The spectrum was recorded in THF-d_8 at RT.

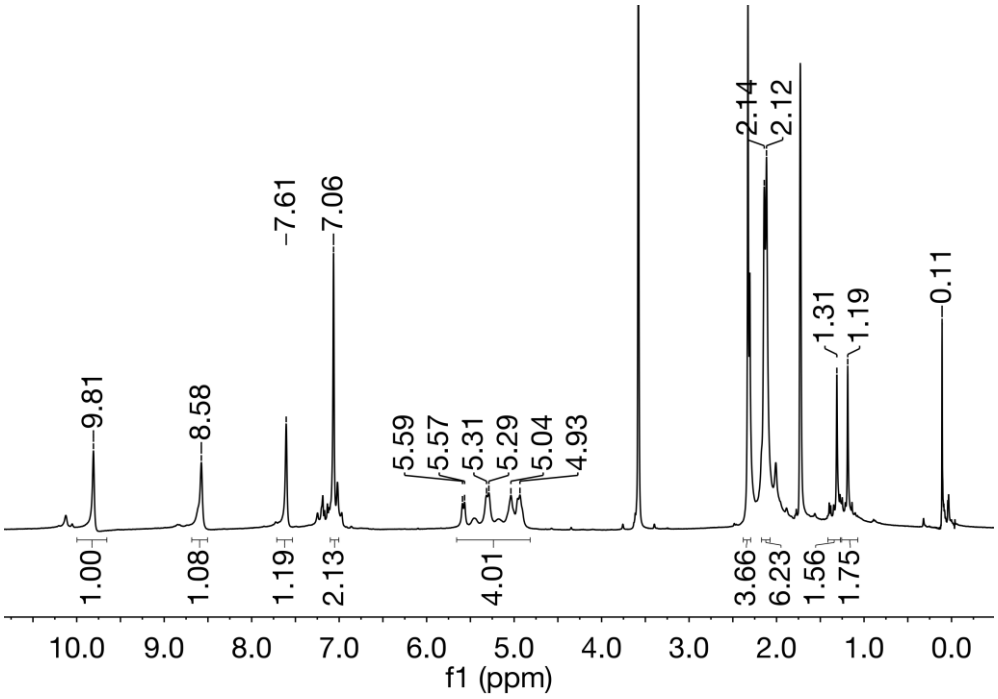

Figure 3.1.16. ^{1}H NMR spectrum of **H(L4^{Mes})*I**, which precipitated after cooling down the solution of the product mixture obtained in a transmetallation reaction of **K(L4^{Mes})** with $CeI_3(THF)_{2.5}$. The spectrum was recorded in THF-d_8 at RT.

The spectroscopic characterization of the amorphous material obtained by this crystallization method revealed the presence of well-defined resonances indicating the formation of one

major species as well as some negligibly minor ones (for ^{1}H NMR spectrum see Figure 3.1.16). The resonances attributed to the major product are tentatively assigned to mono(imidazolium) species with *N*-mesityl and *N*-alkyl substituent. By comparing the spectra in Figure 3.1.15 and Figure 3.1.16 it is evident that this imidazolium compound is already present in the crude product mixture. Furthermore, the OX group in the *N*-alkyl substituent must be still present due to complicated nature of the resonance pattern attributed to this fragment (m, 4.93 ppm – 5.59 ppm). A proposed structure for the obtained mono(imidazolium) species is given in Scheme 3.1.24. Notably, ^{29}Si NMR spectrum of the crude product contains additionally to resonances of the silicon grease and HN", three smaller resonances at 21.79, 17.39 and 16.51 ppm suggesting a formation of terminal –OSiMe$_3$ groups.[172, 177] Therefore, a silylation of the OH group in **H(L4^{Mes})*I** would be not surprising, as it has been previously observed in the reactions of Fe(II) bis(trimethylsilylamide) with ligands moieties containing OH groups (see Chapter 4, Section 4.1.1.4).[203]

Since the treatment of REE halides with **K(L4^{Mes})** was unsuccessful an application of more soluble REE precursors with less coordinating ligands was considered to be more promising. The treatment of CeCp$_3$ with the K NHC adduct yields a brown, very air sensitive residue. ^{1}H NMR spectrum displays numerous sharp resonances in aromatic and aliphatic region (SI, Figure 5.3.24). Some smaller broad singlets at 17.08, –3.34 and –3.86 ppm indicate a possible presence of a paramagnetic compound. Otherwise the spectrum is difficult to assign to any tractable species. Further characterization by ^{29}Si NMR spectroscopy is not informative as only the presence of silicon grease could be confirmed. Unfortunately, no solid material could be obtained by cooling down the solution to –26 °C or by slow diffusion of pentane into solutions of the crude product in THF at RT.

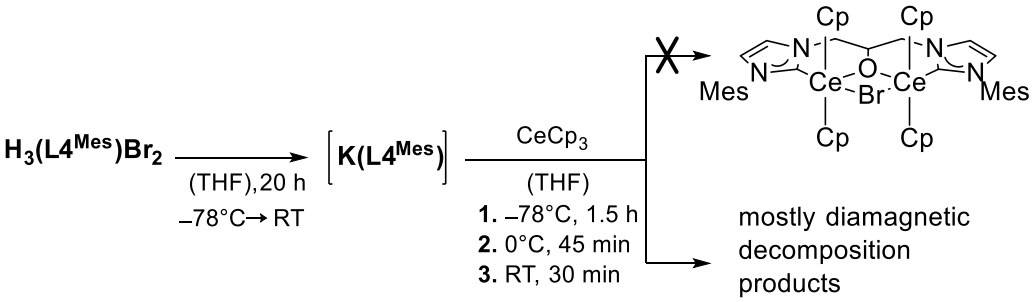

Scheme 3.1.20. The reaction of **H$_3$(L4^{Mes})Br$_2$** with KN" and CeCp$_3$ in a two-step transmetallation procedure *in situ.*

A more promising approach indicated ^{1}H NMR spectrum of the crude product obtained after the treatment of CeN"$_3$ with **K(L4^{Mes})** (Figure 3.1.17), although KN" is not expected to eliminate easily. A broad resonance at –2.06 ppm proves the retention of at least some of the CeN"-groups. Various broad resonances outside of the usual diamagnetic region indicate the

presence of other paramagnetically affected ligand motifs as well. Interestingly, the mesityl groups appear to be static on the NMR timescale as both CH protons as well *ortho*-CH_3-groups are not chemically equivalent. Especially, a CH_3-group resonance at 0.48 ppm is noticeable. Moreover, all resonances are shifted to lower frequencies in comparison to imidazolium compounds or even 1-mesitylimidazole. Furthermore, there is another sharp singlet in the aromatic region with an integral ratio matching two imidazole backbone protons. As the other two protons attributed to imidazole are not observable, a deprotonation of the C4 positions is possible (see Scheme 3.1.21). At this point it is difficult to tell if the bridge between two heterocycles moieties is still intact, however additional small bad resoluble resonances over 10 ppm could indicate a retention of the linker. Intense broad resonances at 0.05 and –0.21 ppm in the ^{1}H NMR spectrum indicate the presence of HN" or other N"$^-$ anions.

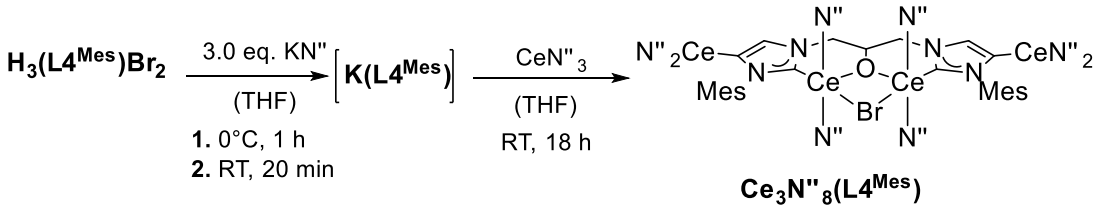

Scheme 3.1.21. Two-step transmetallation reaction using **H_3(L4^{Mes})Br_2**, KN" and CeN"$_3$.

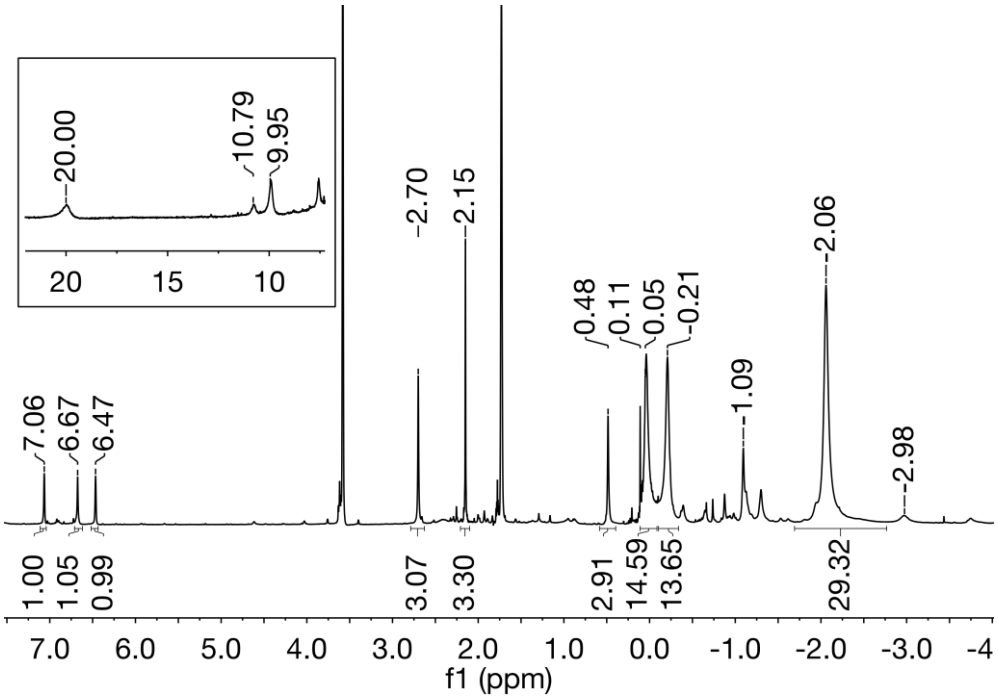

Figure 3.1.17. ^{1}H NMR spectrum of **CeN"$_2$(L4^{Mes})** in THF-d_8 at RT.

^{29}Si NMR of the crude product proves the formation of HN", however as expected in rather small quantities. Further small resonance at 25.58 ppm suggests possibly analogue to the experiments mentioned above at least partial silylation of the OH-group.[172, 177]

Unfortunately, it was not possible to obtain crystalline material by cooling down the crude product in THF/toluene solvent mixture for further characterization of possibly formed complex. A suggestion for the molecular structure of **$Ce_3N"_8(L4^{Mes})$** is depicted in Scheme 3.1.21, albeit a rearrangement and the decomposition of the ligand to *N*-bonded imidazoles is also conceivable.

Another promising REE precursor which can be used in the reactions with **$K(L4^{Mes})$** is $Ce(BH_4)_3(THF)_4$, since the eliminated KBH_4 would precipitate out THF as well. Interestingly, in comparison to all previously mentioned transmetallation experiments yielding dark brown solutions, the treatment of $Ce(BH_4)_3(THF)_4$ with **$K(L4^{Mes})$** produces a violet suspension. ^{1}H NMR spectrum of the residue displays various broad resonances, many of them apparently paramagnetically shifted (Figure 3.1.18). Although sharp resonances in the aliphatic region of the spectrum indicate the formation of some decomposition products, the successful synthesis of cerium complexes is likely. Furthermore, a broad multiplet at 1.0 ppm could be tentatively assigned to a possible carbene-borane adduct, which resonate approximately in this region.[204] A formation of such compound is possible by a reaction of BH_4^- with imidazolium moieties.[204]

Unfortunately, similar to other experiments with $Ce(BH_4)_3(THF)_4$, further crystallization at low-temperatures or crystallization by slow diffusion of more apolar solvent into the solution of crude product in THF at RT results in precipitation of fine colourless solid, whose reactivity under exposure to moisture indicates the presence of borohydride species. Further NMR spectroscopic analysis of the material show the presence of broad resonance at –0.91 ppm suggesting that indeed probably KBH_4 or $Ce(BH_4)_nX_m$ is eliminated in this case.[201]

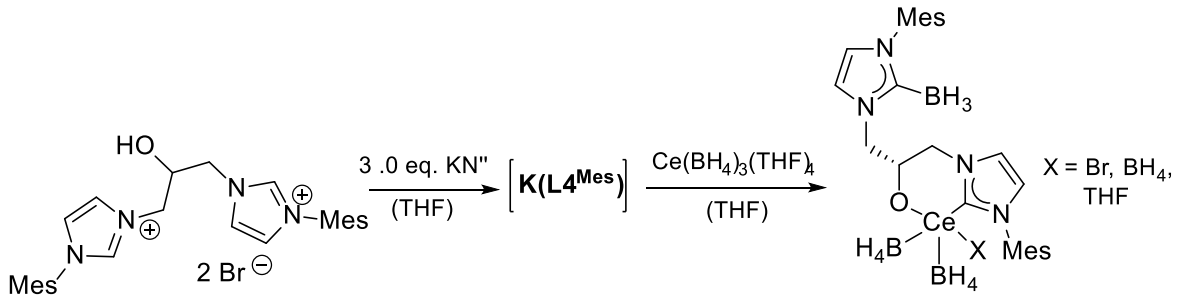

$H_3(L4^{Mes})Br_2$ **$Ce(BH_4)_2[(L4^{Mes})BH_3]$**

Scheme 3.1.22. The reaction of **$H_3(L4^{Mes})Br_2$** with KN" and $Ce(BH_4)_3(THF)_4$ in a two-step transmetallation reaction. For exact reaction conditions see Experimental Section, Table 5.2.17.

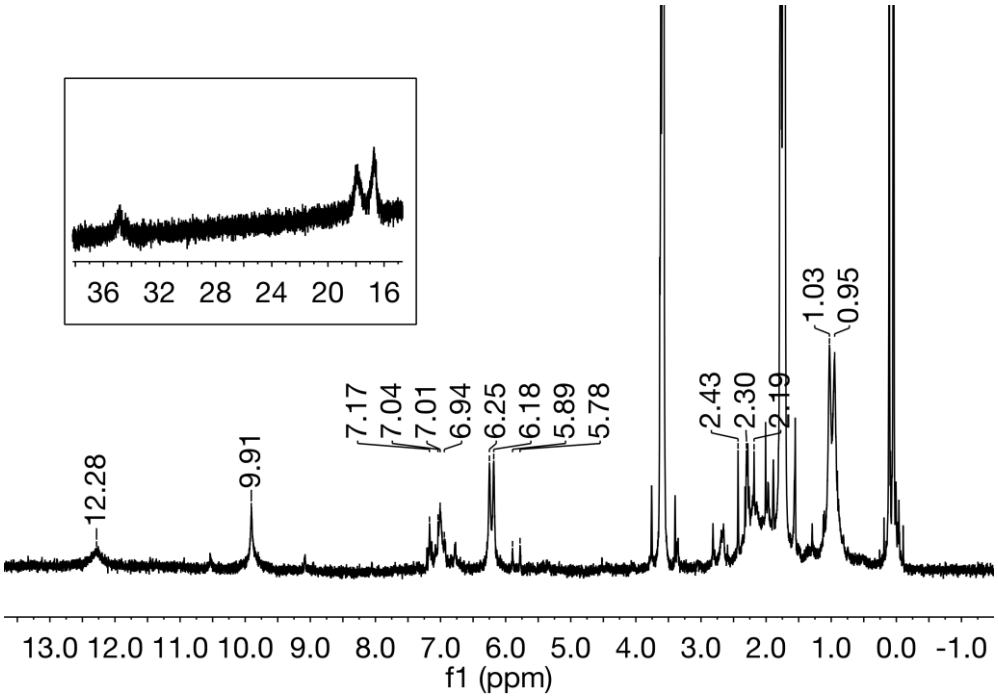

Figure 3.1.18. ^{1}H NMR spectrum of the crude product obtained in a reaction of **K(L4^{Mes})** with $Ce(BH_4)_3(THF)_4$. The spectrum was recorded in THF-d_8 at RT.

Increasing the amount of the reactants in order to decrease the influence of the decomposition pathways did not show any improvements concerning the composition of the sample. Interestingly, the repetition of the experiments never resulted in the same ^{1}H NMR spectrum although the reaction conditions were varied only slightly (see Table 5.2.17, Experimental Section). This further supports the assumption that decomposition pathways are dominant in this case.

In summary, due to higher reactivity of **K(L4^{Mes})** the usage of **H$_3$(L4^{Mes})Br$_2$** in two-step transmetallation procedures is more promising than that of **Li(L3^{Mes})**. However, although some interesting results were obtained the formation of impure and probably very unstable compounds stresses out the difficult controllability of the reactions with alkali metal bis(NHC) adducts and REE precursors. As a consequence, the possibility of application of REE compounds acting as internal base was considered worth of investigation.

3.1.3.2 Direct Conversion of H$_3$(L4^{Mes})Br$_2$ with Li[Ce{N(*i*-Pr)$_2$}$_4$](THF)

The possibility of the usage of Li[Ce{N(*i*-Pr)$_2$}$_4$](THF) as internal base for the deprotonation of **H$_3$(L4^{Mes})Br$_2$** was tentatively explored in THF and benzene, although more promising results were obtained in benzene. ^{1}H NMR spectrum of the crude product shows the presence of a number of broad singlets appearing at unusually high or low frequency, therefore indicating a formation of possibly targeted compounds (Figure 3.1.19). Unfortunately, no crystalline

material could be obtained so far by low-temperature crystallization from fluorobenzene/pentane mixtures.

In conclusion, this synthetic protocol is a very promising approach which needs further investigation.

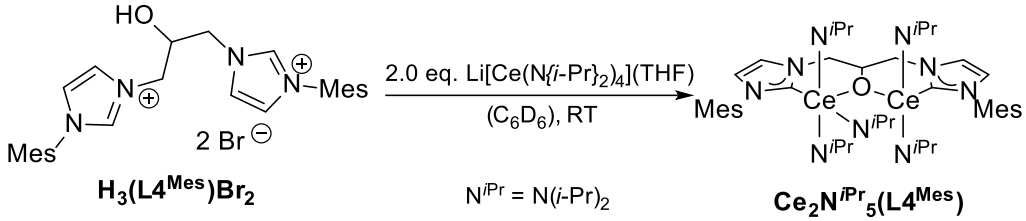

$H_3(L4^{Mes})Br_2$ **$Ce_2N^{iPr}_5(L4^{Mes})$**

Scheme 3.1.23. Reaction conditions used for the treatment of **$H_3(L4^{Mes})Br_2$** with Li[Ce{N(*i*-Pr)$_2$}$_4$](THF).

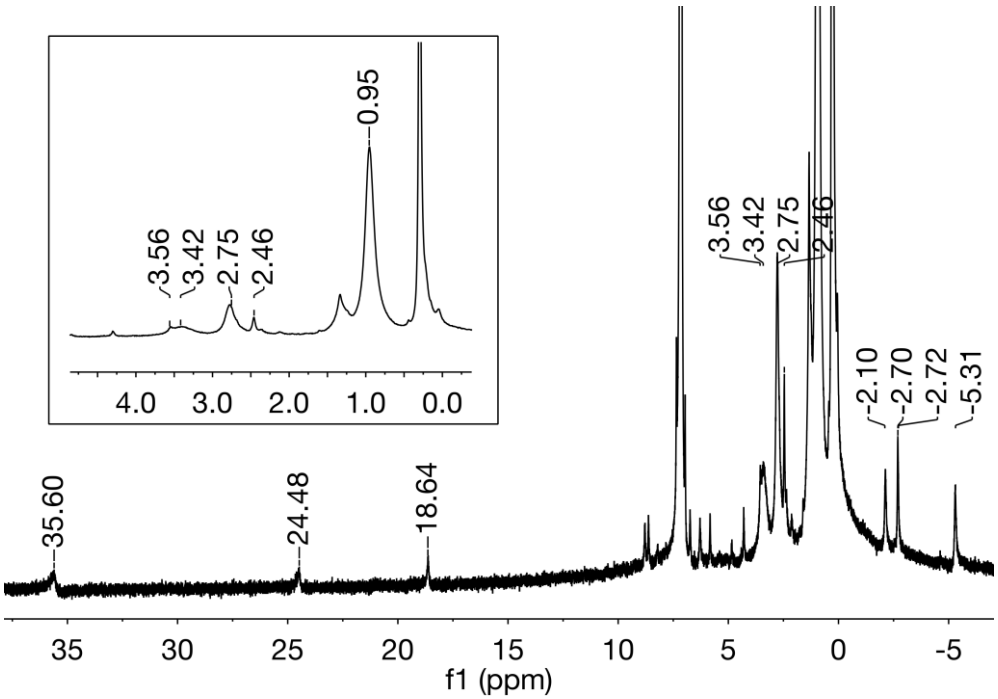

Figure 3.1.19. ^{1}H NMR spectrum the crude product obtained after the treatment of **$H_3(L4^{Mes})Br_2$** with Li[Ce{N(*i*-Pr)$_2$}$_4$](THF) at RT in C_6H_6.

3.1.4 *N*-Furanyl Functionalised Pro-Ligands $H_2(L5^R)X_2$ and $H_2(L6^R)X_2$

3.1.4.1 Transfer Reactions *in Situ*

Since the isolation of alkali metal adducts of neutral *N*-furanyl functionalised bis(NHC)s was unsuccessful (see Chapter 2, Section 2.1.1.2), the generation of this type of bis(NHC)s *in situ* followed by a reaction with a REE precursor was considered as a promising approach.

Therefore, **$H_2(L5^{Fu})Br_2$** was treated with KN" in THF at RT for 30 min. Subsequently, the resulting solution was added to a solution of $CeN"_3$ or a suspension of $CeCl_3(THF)_2$ in THF (Scheme 3.1.24). Unfortunately, ^{1}H NMR spectra of the crude products obtained after the workup of both reactions is not very informative as it exhibits numerous very small broad resonances in the region expected for diamagnetic molecules (SI, Figure 5.3.25). Both spectra are similar, the only significant difference is a broad singlet at –1.69 ppm in the reaction with $CeN"_3$, which indicates the presence of soluble by-product comprising of $CeN"_n$–fragment(s) formed by incomplete consumption of the REE precursor. Furthermore, the analysis of the residue, which remained in the second step of the reaction with $CeCl_3$ revealed the formation of **$L5^{Fu*}$** (Scheme 3.1.24). Such reactivity of **$H_2(L5^{Fu})Br_2$** with KN " has been already described in Chapter 2, Section 2.1.4.2, which leads to the conclusion that controlling the *in situ* deprotonation of **$H_2(L5^{Fu})Br_2$** with KN" is very difficult.

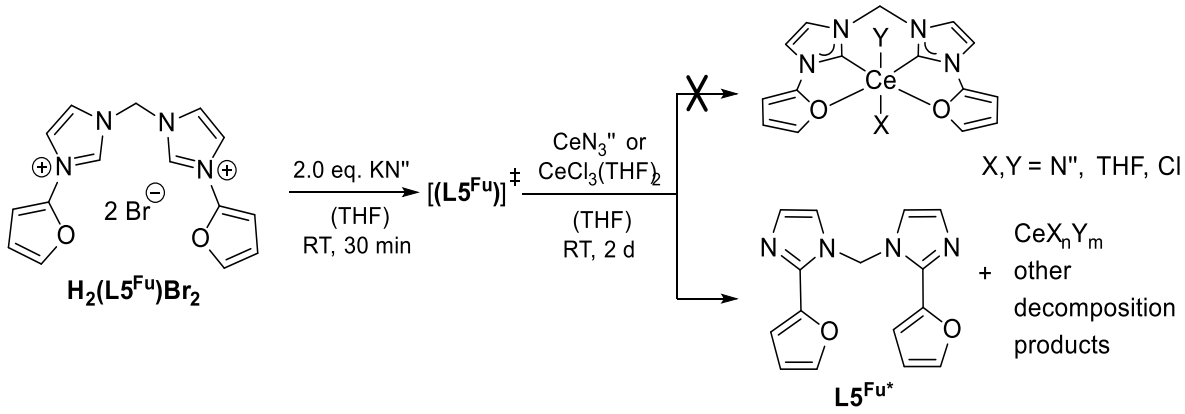

Scheme 3.1.24. Reaction of **$H_2(L5^{Fu})Br_2$** with KN" and $CeN"_3$ in a two-step reaction *in situ*.

A more soluble pro-ligand **$H_2(L5^{tFu})Br_2$** reacts with KN" in toluene at RT. Although the deprotonation studies of this bis(imidazolium) bromide were not satisfactory (see Section 2.1.1.2), a possibility of fast generation of bis(NHC) ligand **$L5^{tFu}$** with subsequent transfer to $Ce(BH_4)_3(THF)_4$ precursor was nevertheless investigated (Scheme 3.1.25). Interestingly, after the work up a very intense blue residue is obtained which shows extremely high sensitivity to air and moisture. This fact is very curious as such intense coloration is frequently observed for Ce(IV) organyls rather than for Ce(III) species.[205] The ^{1}H NMR spectrum of the crude product in toluene-d_8 displays besides the intense resonance attributed to HN" numerous small singlets including some in the negative region from –4 ppm till 0 ppm as well as single resonance at 14.38 ppm (Figure 5.3.26). These observations might indicate a coordination of organic ligands to paramagnetic cerium(III) centre. Unfortunately, to date it was not possible to obtain any crystalline or at least a purified solid material for further characterization as any purification or crystallization attempt lead to formation of fine colourless precipitate. This decomposition product probably contains KBH_4 or $Ce(BH_4)_x$.

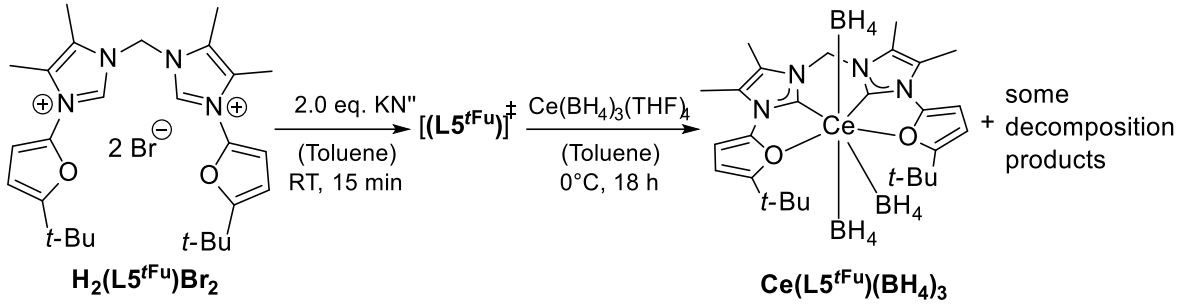

$H_2(L5^{tFu})Br_2$ **$Ce(L5^{tFu})(BH_4)_3$**

Scheme 3.1.25. Reaction of **$H_2(L5^{tFu})Br_2$** with KN" and $Ce(BH_4)_3(THF)_4$ in a two-step procedure *in situ.*

In summary, it has been shown that due to difficult controllability of NHC generation with methylene bridged *N*-furanyl functionalised bis(imidazolium) salts using KN", the targeted Ce bis(NHC) compounds are not accessible by this preparation method. The conduction of the reactions at lower temperatures might be more promising. Moreover, the instability of possibly obtained intermediates and products presents a problematic issue which poses further restrictions to possible success of this synthetic approach.

Due to these considerations the decision of using *N*-furanyl modified precursors **$H_2(L5^{tFu})X_2$** and **$H_2(L6^{tFu})X_2$** (R = Me, Et; R' = H, *t*-Bu; X = Br, BPh_4) in a series of explorative NMR scale reactions with CeN"$_3$, which might act as internal base, was further made as it might be a more promising way to obtained the desired REE bis(NHC) compounds.

3.1.4.2 Direct Conversion of Bis(imidazolium) Precursors with Rare-Earth Amides

The non-alkylated pro-ligands **$H_2(L5^{Fu})Br_2$** and **$H_2(L6^{Fu})Br_2$** react sluggishly with CeN"$_3$ in THF at RT (Scheme 3.1.26). ^{1}H NMR spectra of the brown (methylene-bridged) or black-green (ethylene-bridged) suspensions are not particularly informative as it exhibits plenty of tiny broad resonances in the region expected for diamagnetic molecules (see SI, Figures 5.3.27-28). In addition, a singlet resonance attributable to HN" and two very broad singlets in the negative region are observed. The smaller resonance at –3.9 ppm is assigned to unreacted CeN"$_3$, the bigger ones with a shoulder at –0.8 ppm (methylene-bridged) and –1.16 ppm (ethylene-bridged) indicate other CeN"-containing moieties, possibly additionally coordinated by Br or THF. ^{29}Si NMR spectra of both reaction solutions do not shed more light on possible products as only the singlets attributed to silicon grease (–21.5 ppm), HN" (1.9 ppm) and unidentified decomposition products previously observed in reactions with KN" are detected. Generally, similar observations were made when reactions were repeated in pyridine-d_5 rather than THF.

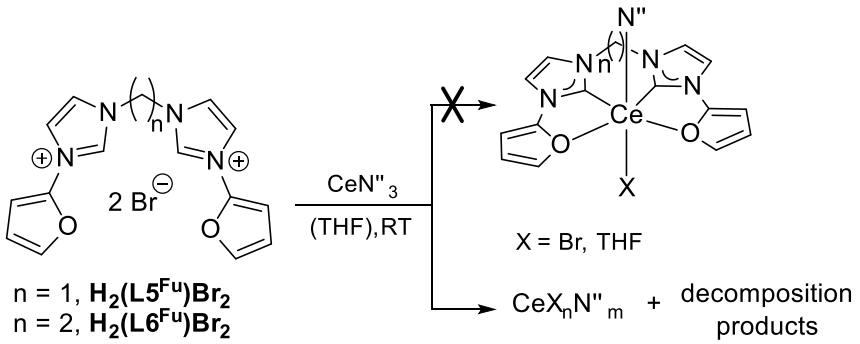

Scheme 3.1.26. Reactions of $\mathbf{H_2(L5^{Fu})Br_2}$ and $\mathbf{H_2(L6^{Fu})Br_2}$ with CeN"$_3$ at RT in THF-d_8.

The results mentioned above could indicate that the success of the synthetic approach *via* CeN"$_3$ might be impeded by bromide anions which could block coordination sites on cerium. Additionally, the low solubility of non-alkylated imidazolium cations balanced by bromide is probably slowing down the reaction, allowing decomposition to occur at a competitive rate. To circumvent these obstacles the corresponding bis(imidazolium) tetraphenylborates $\mathbf{H_2(L5^{Fu})(BPh_4)_2}$ and $\mathbf{H_2(L6^{Fu})(BPh_4)_2}$ were treated with CeN"$_3$ under analogous reaction conditions (Schemes 3.1.27-29).

The treatment of $\mathbf{H_2(L5^{Fu})(BPh_4)_2}$ with CeN"$_3$ in THF at RT yields a brown solution. ^{1}H NMR spectrum displays besides the resonances attributed to BPh_4^- a set of 7 resonances in the region expected for diamagnetic organic molecules (Figure 3.1.20). However, if the deprotonated pro-ligand should form a symmetric molecule a set of 6 resonances would be expected. Although the small triplet appearing at lower frequency (6.64 ppm) than the resonance attributed to *para*-CH of BPh_4^- have the integral ratio of 1.0 compared to other signals, a matching integral ratio could be just a coincidence. In this case this resonance can be tentatively assigned to a BPh_4^- interacting with a cerium centre.

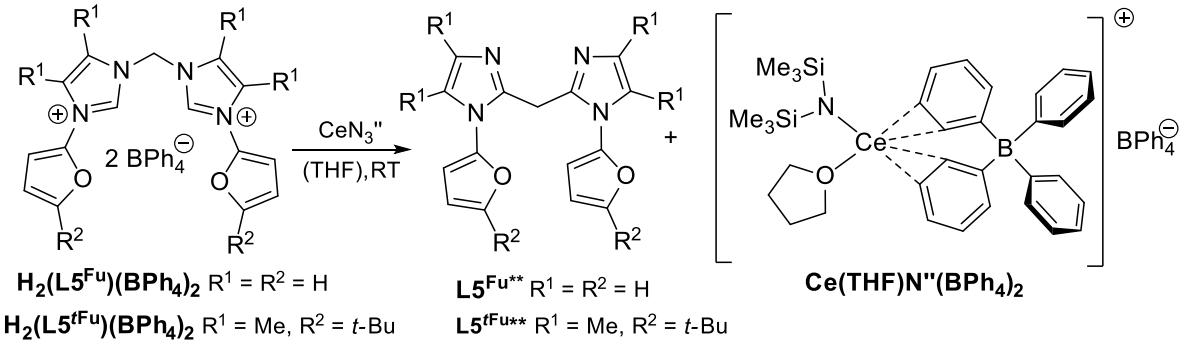

Scheme 3.1.27. Reactivity of $\mathbf{H_2(L5^{R})(BPh_4)_2}$ with CeN"$_3$ at RT in THF-d_8.

The pattern of the remaining resonances is similar to the spectrum of $\mathbf{L5^{Fu*}}$ but the chemical shift values are quite different. Especially a very significant shift of singlet attributed to the methylene linker at 4.89 ppm is notable. Such a large shift to lower frequency could indicate

that the CH_2-group is attached to carbon atoms instead of electronegative nitrogens. Therefore, a possible shift of methylene group to C2 position yielding e.g. **L5^{Fu**}** could be the reason for this observation (Scheme 3.1.27). The overall deprotonation of the pro-ligand is confirmed by the formation of HN" and after 1 day at RT the amount of formed **L5^{Fu**}** matches nicely the required 2.0 equiv. of generated HN". Additionally, a broad singlet at 1.96 ppm proves the consumption of CeN"$_3$ through the shift to higher frequency.

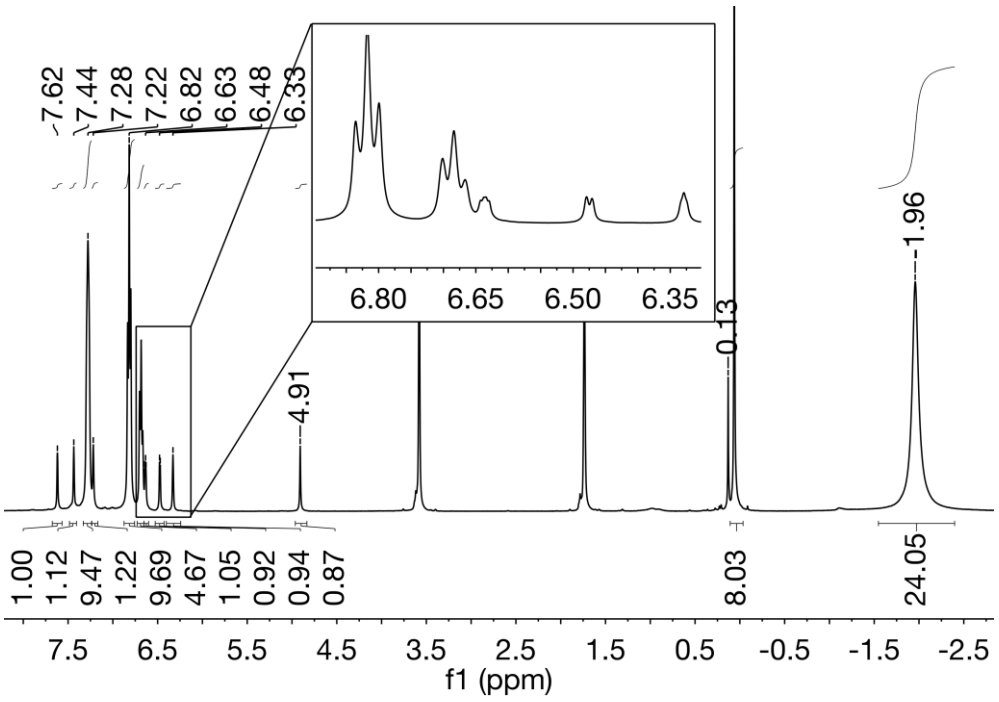

Figure 3.1.20. ^{1}H NMR spectrum of the reaction mixture obtained after the treatment of **H_2(L5^{Fu})(BPh_4)$_2$** with CeN"$_3$ in THF-d_8 after 1 h at RT.

Interestingly, by comparing the ^{1}H NMR spectra of the same reaction solution at different points of time an unexpected trend for the shift of the BPh_4^- resonances to lower frequencies is observed (Figure 3.1.21). Such differences could indicate a possible agnostic interaction of BPh_4^- which cerium centre (see Scheme 3.1.27), which was already previously observed for other rare earth cations and different ligand motifs.[206] Additionally, slow disappearance of the resonances attributed to **L5^{Fu**}** indicates its instability at RT or further reactions leading to insoluble products. Further characterization by ^{29}Si and ^{13}C NMR spectroscopy is not particularly informative. Besides the resonances attributed to HN" and silicon grease only smaller singlets caused by impurities are present in the positive region (7.57 and 15.73 ppm).

The ^{1}H NMR spectrum acquired after the treatment of the related alkylated precursor **H_2(L5^{tFu})(BPh_4)$_2$** with CeN"$_3$ under the same reaction conditions shows similar features including the significant shift of the resonance attributed to the methylene-bridge (4.62 ppm) and a broad singlet at –1.95 ppm assigned to Ce-coordinated N" group(s) (see SI, Figure

5.3.29). Therefore, it is quite likely that the parent **$H_2(L5^{Fu})(BPh_4)_2$** and alkylated **$H_2(L5^{tFu})(BPh_4)_2$** pro-ligands react in the same manner (Scheme 3.1.27).

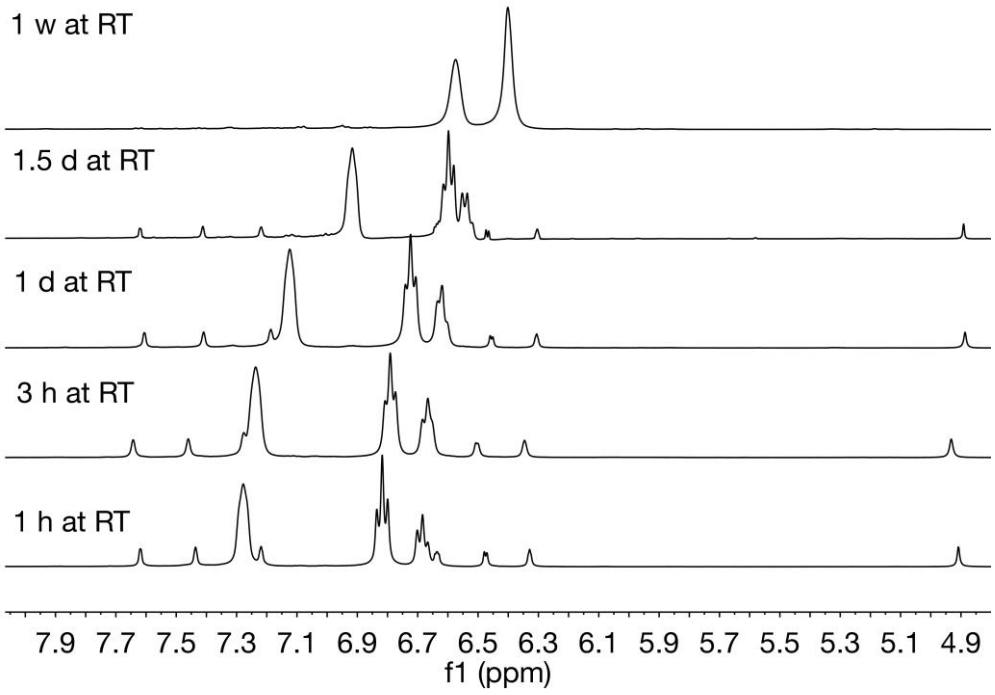

Figure 3.1.21. Comparison of the ^{1}H NMR spectra of the reaction mixture obtained after the treatment of **$H_2(L5^{Fu})(BPh_4)_2$** with CeN"$_3$, allowed to stand for several days at RT.

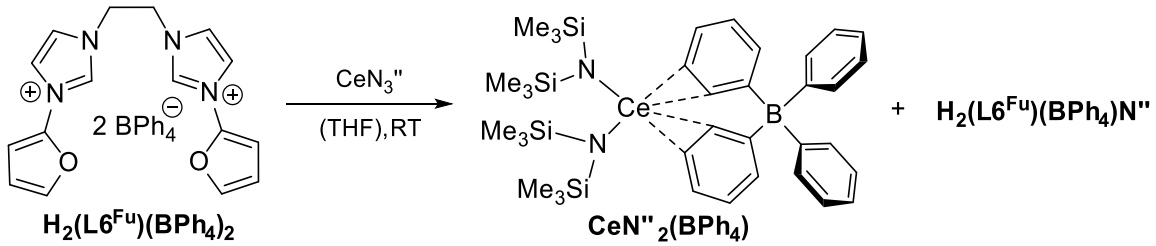

Scheme 3.1.28. Reaction of **$H_2(L6^{Fu})(BPh_4)_2$** with CeN"$_3$ at RT in THF-d_8.

Interestingly, due to lower solubility of ethane-1,2-diyl-bridged non-alkylated congener **$H_2(L6^{Fu})(BPh_4)_2$** in THF it does not react with CeN"$_3$ although an intense change in colour of the solution form yellow over violet to red-brown suggest a possible electrostatic interaction of BPh_4^- with Ce(III) coordinated by N"-groups (Scheme 3.1.28). Also the shift of the BPh_4 anions to lower frequency by simultaneously losing the resolution further supports this assumption (Figure 3.1.22). ^{29}Si NMR spectrum show similar to the reactions above only the presence of grease, HN" and an impurity at 7.57 ppm. **$H_2(L6^{Fu})(BPh_4)_2$** also shows the same behaviour towards CeN"$_3$ in pyridine-d_5.

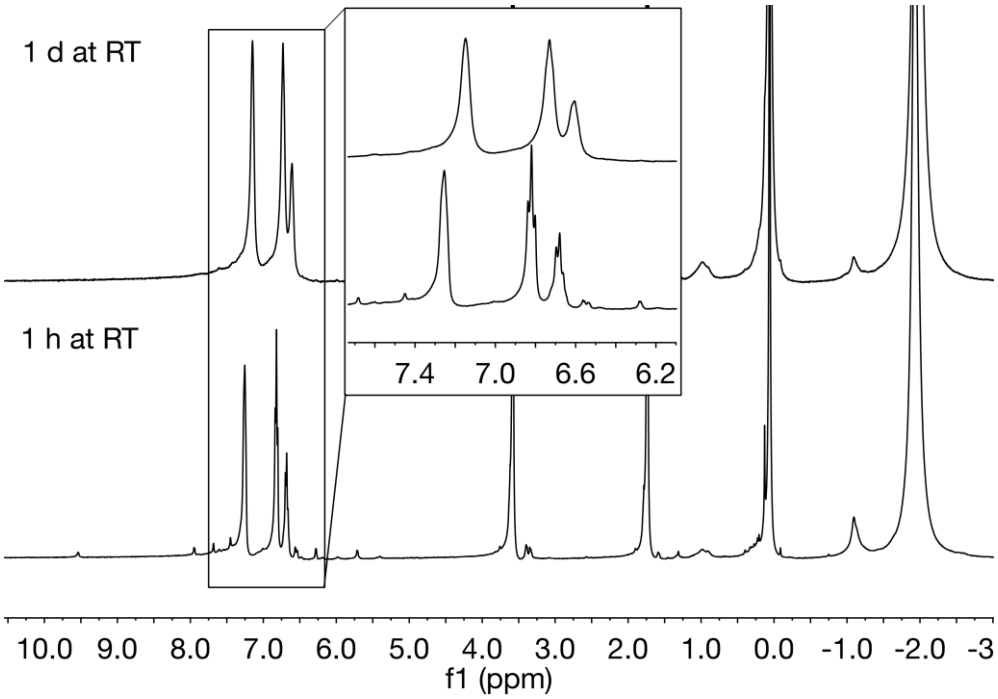

Figure 3.1.22. Comparison of the ^{1}H NMR spectra of the reaction mixture at different time intervals obtained after the treatment of **H_2(L6^{Fu})(BPh_4)$_2$** with CeN"$_3$ at RT in THF-*d_8*.

As expected, in contrast to **H_2(L6^{Fu})Br_2**, **H_2(L6^{tFu})Br_2** slowly reacts with CeN"$_3$ at RT in pyridine due to increased solubility (Scheme 3.1.29). ^{1}H NMR spectrum of the obtained orange-brown solution displays a set of resonances indicating an asymmetric product derived from deprotonated pro-ligand. Also the treatment of **H_2(L6^{tFu})(BPh_4)$_2$** with CeN"$_3$ in pyridine-*d_5* yields the same organic product but in a much cleaner and quicker reaction (for ^{1}H NMR spectrum see Figure 3.1.23). The presence of some CeN"-fragments is evident through the appearance of two broad singlets in the negative chemical shift spectral window. The most striking feature is a complex multiplet at 3.5 – 4.0 ppm assigned to the ethane-1,2-diyl-bridge, which implies diastereotopic environments and thus significant steric congestion. The amount of generated HN" is a little larger than required for a full deprotonation of one equivalent of the pro-ligand. Nevertheless, considering the certain degree of decomposition always present in such reactions, it can be considered as a clean reaction, especially since also the amount of BPh_4^- matches the stoichiometry of generated asymmetric **L6^{tFu}**-derivative as well. Further characterization by ^{13}C NMR spectroscopy did not shed more light on the molecular structure of the compound due to onset of the decomposition of the obtained material.

Therefore, all data indicate either a formation of asymmetric organic product or asymmetrical coordination of the ligand to the cerium centre. It is difficult to definitely exclude one option from another, but due to appearance of the resonances in the region expected for diamagnetic molecules as well as the good resolution of these signals a formation of an undesired

asymmetric organic product **(L6^{tFu})*** e. g. as suggested in Scheme 3.1.29, is more likely. The resonances attributed to **(L6^{tFu})*** disappear within 5 d storage of the solution at RT.

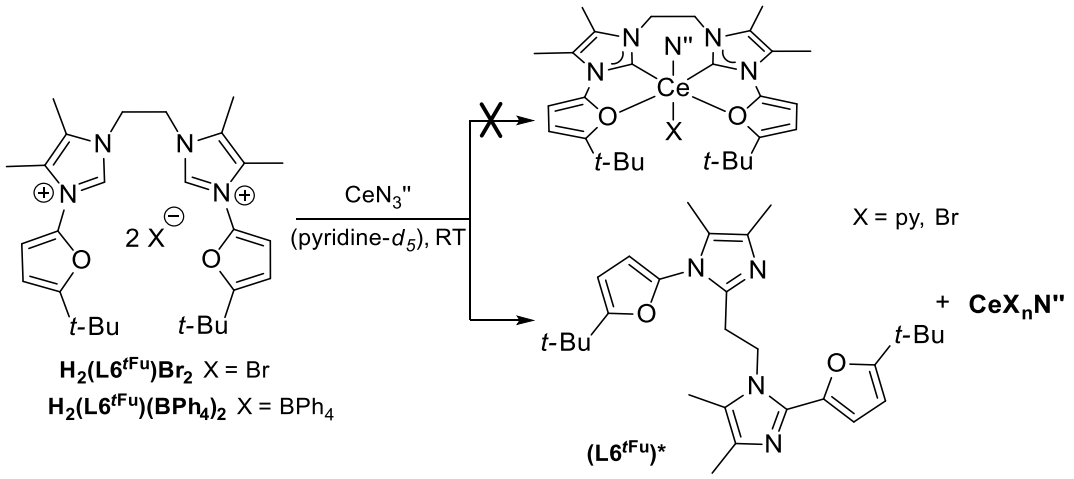

Scheme 3.1.29. Schematic representation of the reaction of **H$_2$(L6^{tFu})X$_2$** with CeN"$_3$ in pyridine at RT.

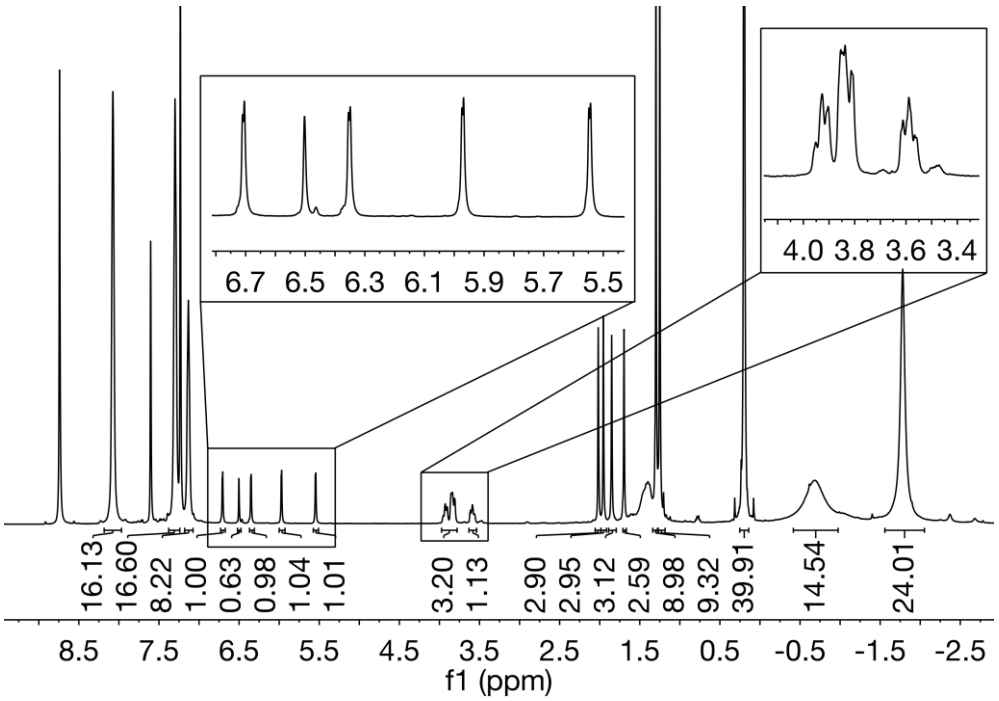

Figure 3.1.23. ^{1}H NMR spectrum of the reaction mixture obtained after the treatment of **H$_2$(L6^{tFu})(BPh$_4$)$_2$** with one equivalent of CeN"$_3$ in pyridine-d_5 at RT.

In summary, it has been shown that in many cases the pK_B value of CeN"$_3$ is not sufficient enough to be used as internal base for non-alkylated precursors, especially if the bis(imidazolium) cations are balanced by bromide. In other cases, where a definitive reaction is observed, the experimental data rather suggest a formation of various diamagnetic organic compounds or alkali metal bonded decomposition products, usually arising from rearrangement of the NHC alkyl groups, rather than novel cerium NHC compounds. Possibly,

both synthesis and work-up at lower temperatures, the use of other cerium precursors with more sterically congested ancillary ligands and lower pK_B values such as Li[Ce{N(*i*-Pr)$_2$}$_4$(THF)] could allow the isolation of Ce complexes.

3.1.4.3 Reactivity of Tetraazafulvalene L6^{tFu} with Rare Earth Precursors

As expected, **L6^{tFu}** does not react with CeN"$_3$ in benzene at RT. Increasing the reaction temperature to 80 °C results in only decomposition of **L6^{tFu}** to *N*-furanyl substituted imidazole **5d**. However, the treatment of **L6^{tFu}** with Ce(BH$_4$)$_3$(THF)$_4$ in benzene at RT results in noticeable change of colour from yellow suspension to bright orange (Scheme 3.1.30).

The ^{1}H NMR spectrum of this reaction conducted on NMR scale in C_6D_6 is shown in Figure 3.1.24. A broad singlet at approximately 27 ppm (attributed to BH_4^- bonded to Ce(III)) as well the two broad singlets at 3.87 ppm and 1.64 ppm (coordinated THF) indicate still the presence of unreacted cerium precursor. Furthermore, there are two smaller broad singlets in the negative region at –10.87 and –2.18 ppm suggesting a formation of a possibly new cerium coordination compound. Since **L6^{tFu}** does not contain any HN" or KN", the undesired formation of CeN"$_n$-species can be excluded and these resonances can be attributed to some other borohydride-containing complex. Interestingly, the resonances attributed to **L6^{tFu}** are significantly shifted to lower frequencies in comparison to the proton spectrum of pure tetraazafulvalene. Also the resolution of the signals significantly worsens. Further characterization by ^{10}B NMR spectroscopy does not shed more light in to the nature of possible product as only the BH_4^- resonating at 30.48 ppm is detectable. Also the ^{13}C NMR spectrum is not informative due to paramagnetic influence.

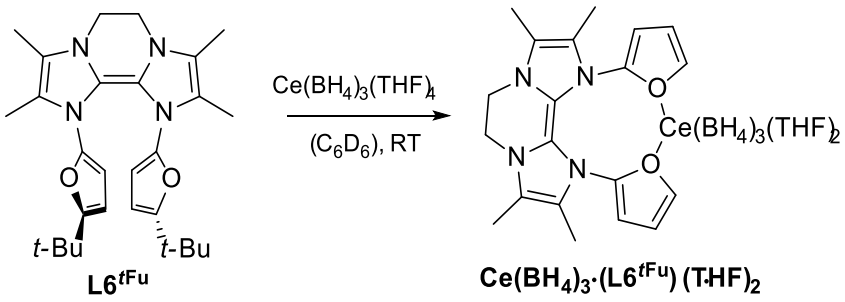

Scheme 3.1.30. Treatment of **L6^{tFu}** with Ce(BH$_4$)$_3$(THF)$_4$ in C_6D_6 at RT.

The isolation of the crude product of the reaction of **L6^{tFu}** with Ce(BH$_4$)$_3$(THF)$_4$ can be also easily performed out of benzene at RT or out of toluene at –15 °C. Unfortunately, no crystalline material suitable for further characterization could be obtained either by precipitation with hexane or by crystallization at –18 °C out of toluene.

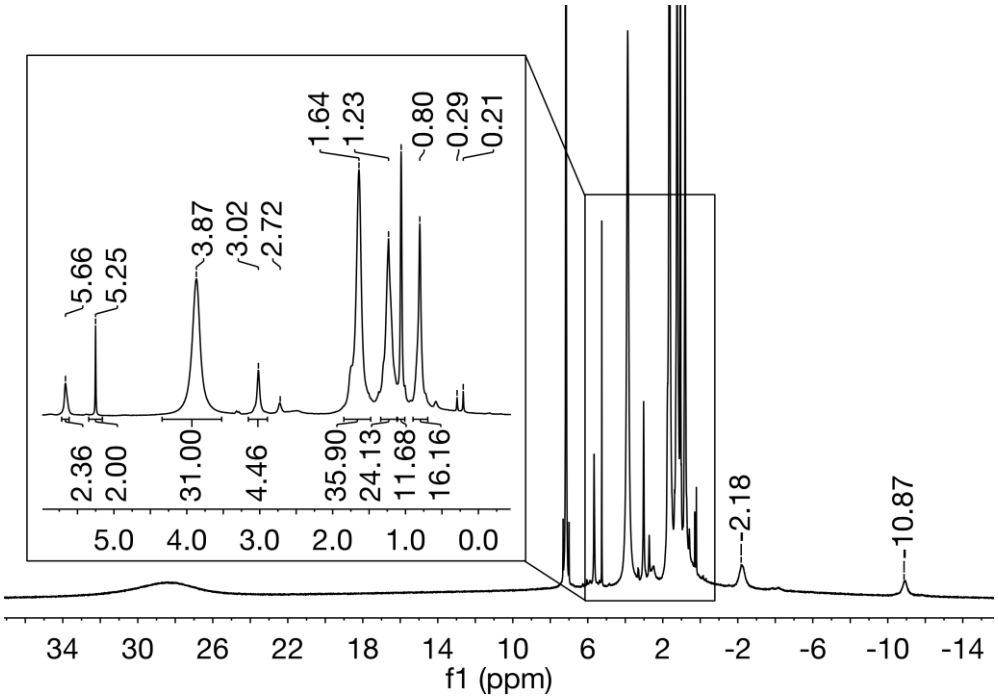

Figure 3.1.24. ^{1}H NMR spectrum of the reaction mixture obtained after the treatment of **L6^{tFu}** with $Ce(BH_4)_3(THF)_4$ in C_6D_6 at RT.

In conclusion, due to limited redox ability of rare earth cations the tetraazafulvalene **L6^{tFu}** is not expected to react with REE precursors. However, some interaction of **L6^{tFu}** is observed with $Ce(BH_4)_3(THF)_4$, which could possibly involve some electron transfer. The other possibility is a coordination of **L6^{tFu}** to Ce via the two O donation as a bidentate chelating neutral ligand. Although being rather a weak donor the coordination of furanyl-moieties to lanthanide canters have been investigated theoretically and experimentally by other authors in different ligand systems.[207]

3.1.5 1,1'-(Prop-1-ene-1,3-diyl)-Bridge Functionalised Pro-Ligands $H_2(L7^{Mes})X_2$

Due to lack of easily accessible possibility of generating anionic anchor in this ligand system the application of two step procedures *via* alkali metal NHC adduct is considered to have little promise to succeed. Therefore, only the reactivity with REE precursors acting as internal base has been tentatively investigated.

Li[Ce{N(*i*-Pr)$_2$}$_4$](THF) reacts both with bromide and tetraphenylborate salts of **$H_2(L7^{Mes})X_2$** at RT in THF yielding yellow-brown solutions (Scheme 3.1.31). ^{1}H NMR spectra of both samples confirms, as expected, the formation of free amine (see SI, Figures 5.3.30-31). Otherwise the data is unfortunately not particularly informative, especially in case of **$H_2(L7^{Mes})Br_2$**. Although the ^{1}H NMR spectrum displays smaller broader resonances outside of the usual diamagnetic

spectral region, numerous sharp resonances between 0 ppm and 10 ppm make quantitative analysis of the data impossible.

A reaction of **$H_2(L7^{Mes})(BPh_4)_2$** with lithium tetrakis(diisopropylamide)cerate looks more promising as the reaction generally proceeds more cleanly. Besides decomposition products evident by a number of sharp small singlets in the aliphatic and aromatic region, higher-intensity resonances outside of the 0 – 10 ppm spectral window indicate a formation of cerium organo compounds. Unfortunately, no crystalline material suitable for further characterization could be obtained by crystallization out THF/hexane mixtures at –30 °C.

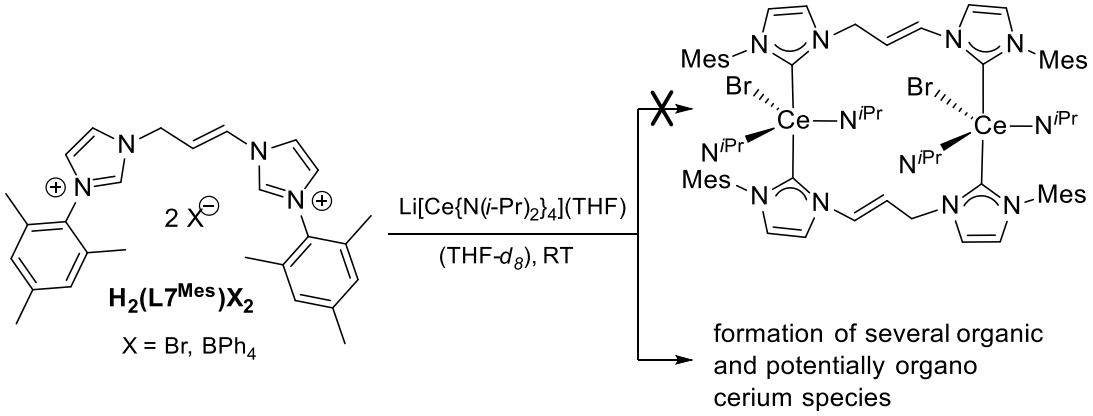

Scheme 3.1.31. Reaction of **$H_2(L7^{Mes})Br_2$** with Li[Ce{N(*i*-Pr)$_2$}$_4$](THF).

In conclusion, since in both cases incomplete consumption of the ligand precursor was observed (either visibly for bromide species or by the presence of corresponding resonances in the ^{1}H NMR spectrum for the BPh_4 salt), the stoichiometry of the reaction is probably completely off. Therefore, further experiments, especially with **$H_2(L7^{Mes})(BPh_4)_2$**, need to be conducted with different stoichiometric ratios. Additionally, a less coordinating solvent such as C_6H_6 could be beneficial for these type of reactions as it facilitates the elimination of LiBr.

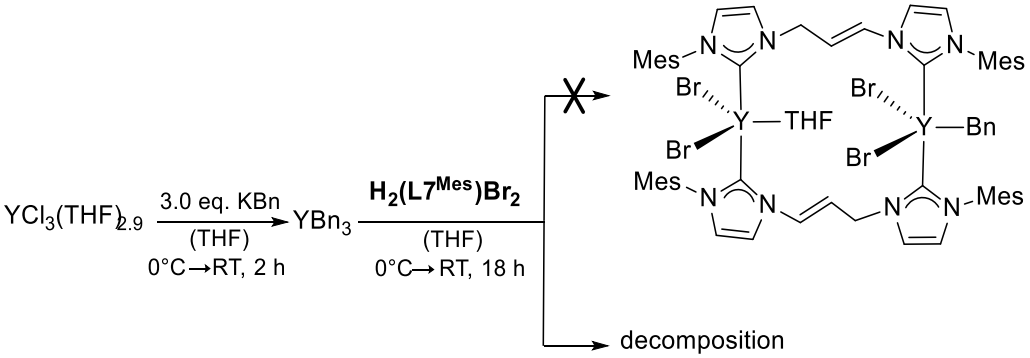

Scheme 3.1.32. Treatment of **$H_2(L7^{Mes})Br_2$** with *in situ* formed YBn_3.

To shed more light into the process involving the deprotonation of **$H_2(L7^{Mes})Br_2$** by REE internal bases a precursor with diamagnetic nucleus was used. YBn_3 was generated *in situ* and then

used for treating the **$H_2(L7^{Mes})Br_2$** in THF (Scheme 3.1.32.). Hereby a complete consumption of the pro-ligand is observed as insoluble ligand precursor is consumed during the reaction. However, the ^{1}H NMR spectrum of the crude product is unfortunately not quantifiable (SI, Figure 5.3.32). In the aromatic and aliphatic spectral region broad resonance clusters are visible. In the region expected for a 1,1'-(prop-1-ene-1,3-diyl) linker only unrelated tiny resonances are observed. Also here a possibility of Bn-migration to carbenic carbon analogue to Group IV NHC complexes cannot be excluded.[200]

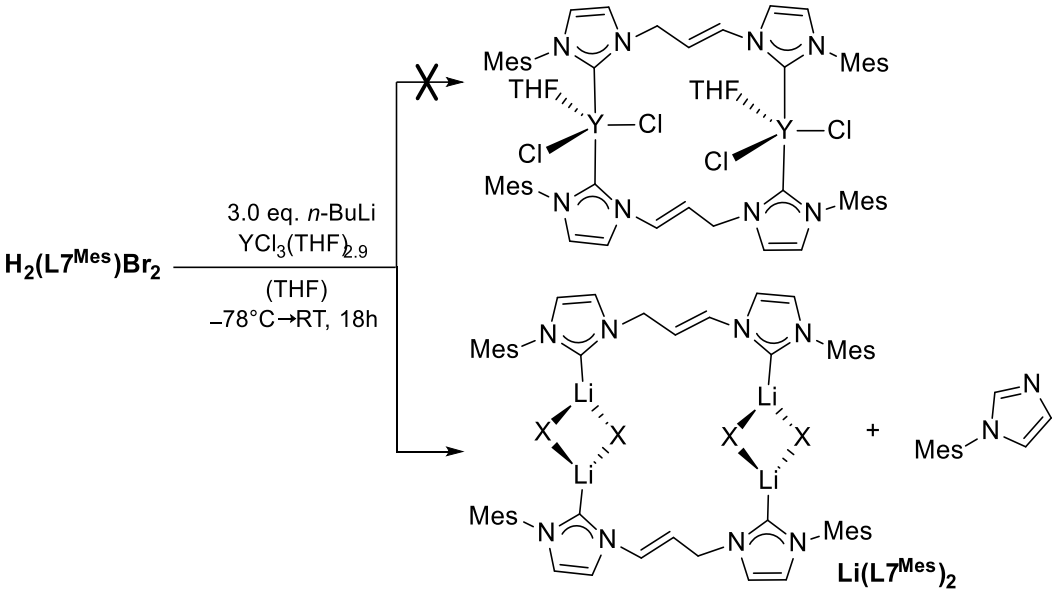

Scheme 3.1.33. One-pot reaction of **$H_2(L7^{Mes})Br_2$** and $YCl_3(THF)_{2.9}$ with *n*-BuLi in THF. Instead of **$Li(L7^{Mes})_2$** a formation of intermolecular tetraazafulvalene or an Y NHC compound is possible.

Since the usage of REE precursors as internal bases in the reaction with **$H_2(L7^{Mes})X_2$** apparently impose some difficulties a possibility of a one-pot reaction with a REE precursor and *n*-BuLi as a base was studied as well. The treatment of the suspension of $YCl_3(THF)_{2.9}$ and **$H_2(L7^{Mes})Br_2$** in THF with *n*-BuLi yields a brown residue (Scheme 3.1.33). In the ^{1}H NMR spectrum of the crude product well-defined resonances indicate the formation of two major species as well as some minor ones (Figure 3.1.25). The broader singlets at 7.38, 7.08, 6.98, 6.94, 2.30 and 1.95 ppm correspond to 1-mesitylimidazole confirming hereby the decomposition of the bridge. The other major species still contains an intact propylene-linker (*E*-configuration, $^3J_{CH=CH}$ = 14 Hz), also three clear corresponding duplets attributed to imidazole backbone confirm the retention of the ligand framework. The missing resonances for the imidazole backbone and N*CH*CH$_2$N of the bridge are probably overlapped by the resonances belonging to the mesityl protons. Additionally, the remaining resonances attributed to CH_3-groups indicate a sterically hindered environment for the mesityl moieties due to appearance of three distinct singlets. Since a formation of intramolecular tetraazafulvalene is

impeded by an *E*-configuration of the linker and 1,2-shift of *N*-substituents in organic by-products without the coordination to metal centres would not impose such restrictions, a formation of intermolecular dimer is possible, although quite unlikely (see Introduction, Section 1.1.3.1). Lithium or yttrium 1,2-rearragement compounds could also lead to such resonance pattern. Since in the ^{13}C NMR spectrum no carbene resonance was observed the formation of such products is possible as well. Shen also observed such decomposition pattern by deprotonation of **79** with *n*-BuLi by subsequently trying to transfer the generated NHC ligand to $YbCl_3$.[98]

To obtain more data on the formed compounds the crude product was washed with toluene in order to remove easily soluble organic impurities. Unexpectedly, ^1H NMR spectrum of the residue shows besides the presence of 1-mesitylimidazole as major species also the formation of unusually high frequency shifted imidazolium compounds (for ^1H NMR spectrum see Figure 3.1.26). This observation might indicate an unusual counter anion as halide salts of $\mathbf{H_2(L7^{Mes})X_2}$ are insoluble in THF. It is possible that solubilisation in toluene enables an oligomerization of the compound which leads to decomposition due to further rearrangement. However, the introduction of traces of water might be responsible for it as well.

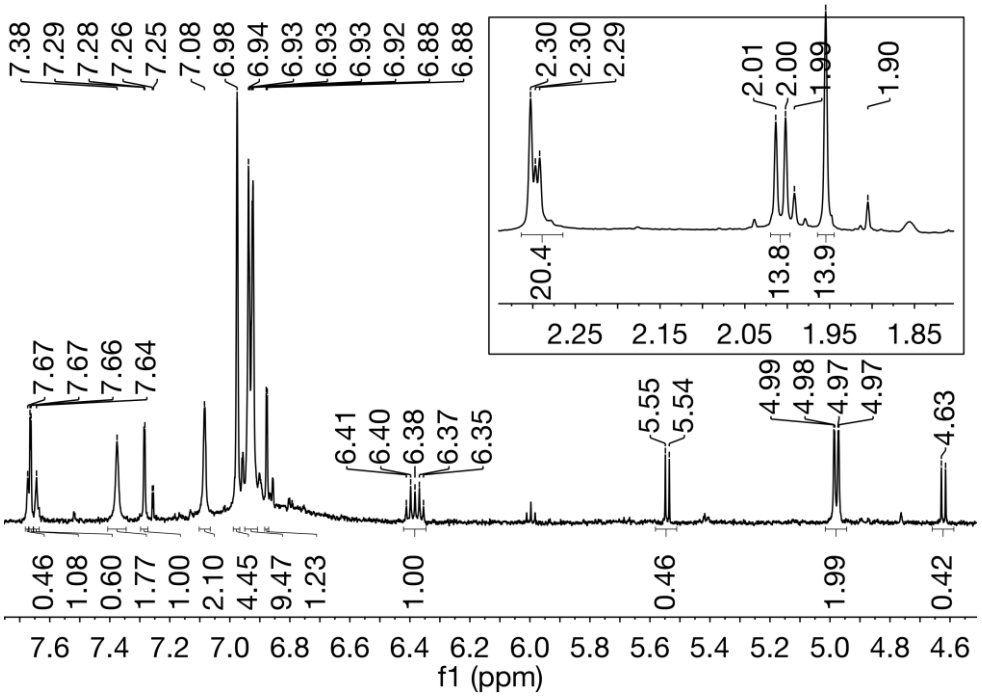

Figure 3.1.25. ^1H NMR spectrum of the crude product obtained in a one-pot reaction of $\mathbf{H_2(L7^{Mes})Br_2}$ with *n*-BuLi and $YCl_3(THF)_{2.9}$. The spectrum was recorded in THF-d_8 at RT.

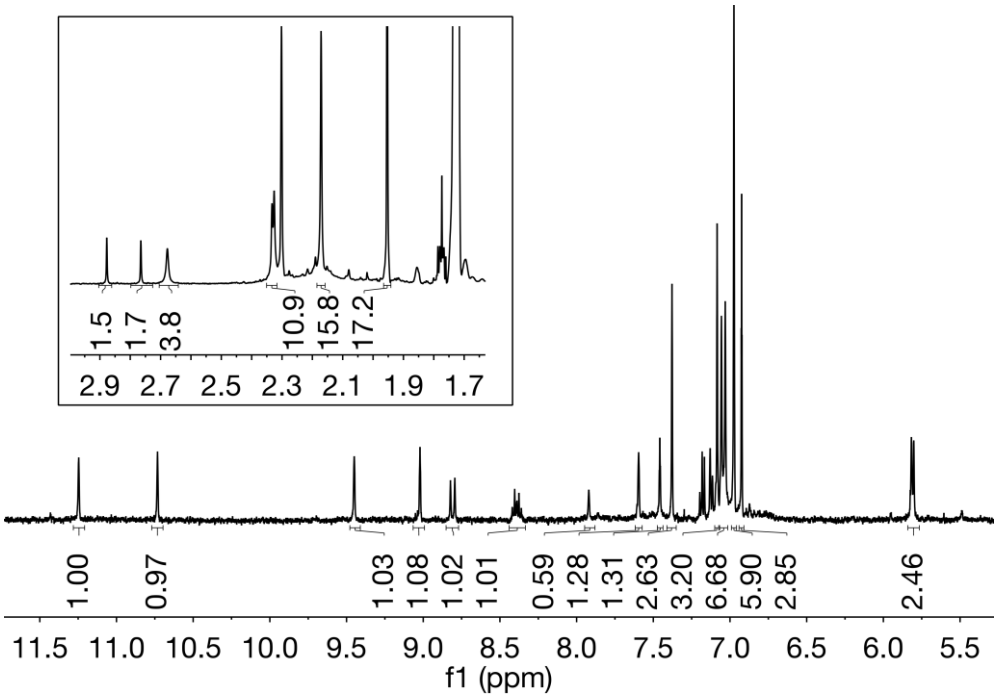

Figure 3.1.26. ^{1}H NMR spectrum of the residue obtained after washing the product of the reaction of **$H_2(L7^{Mes})Br_2$** with *n*-BuLi and $YCl_3(THF)_{2.9}$ with toluene. The spectrum was recorded in THF-d_8 at RT.

3.2 Conclusion and Outlook

The work described in this chapter focuses on various synthetic approaches for the preparation of *N*-heterocyclic carbene complexes of rare earth metals. The first route utilizes the alkali metal NHC adducts studied in Chapter 2 and explores the possibility of follow-up transmetallation reactions *in situ* using various rare earth metal precursors. Hereby, the reactions performed at lower temperatures show more promising results than at RT. The second approach investigates the propensity of corresponding imidazolium pro-ligands to react directly with REE amides or alkyls acting as internal base. In these experiments lithium tetrakis(diisopropylamide)cerate Li[Ce{N(*i*-Pr)$_2$}$_4$](THF) performs generally better than Ce(N{SiMe$_3$}$_2$)$_3$ or Sc(CH$_2$Ph)$_3$, due to the high pK_B value and the possibility of removal of halide anions by eliminating LiBr.

Using the second approach a novel hexanuclear Ce(III) NHDC complex has been synthesized *via* a direct conversion of *N*-(3,5-di-*tert*-butyl-2-hydroxyphenyl) and *N*-methyl functionalised imidazolium bromide with Li[Ce{N(*i*-Pr)$_2$}$_4$](THF). **Li$_2$[Ce$_3$(L1^{Me*})$_3$(N{*i*-Pr}$_2$)$_5$](THF)$_2$** has been characterised by multinuclear NMR spectroscopy and SC-XRD. To the best of our knowledge this is the first example of negatively charged carbon-bridged anionic dicarbene cerium complex, with HNDCs functioning as bridging ligands between two lanthanide centres. Generally, rare earth NHDC compounds are extremely rare. There are only two further examples of similar REE complexes, dinuclear Sm-K and Y-K complexes supported by anionic amido-functionalised NHDCs.[7] This novel synthetic route offers further possibility for the preparation of other lanthanide complexes with bridging anionic dicarbene moieties which were predicted to have unusual magnetic behaviour.[6] Further experiments towards the reactivity of **Li$_2$[Ce$_3$(L1^{Me*})$_3$(N{*i*-Pr}$_2$)$_5$](THF)$_2$** with electrophiles and small molecules are of high interest.

Generally, due to possibility of relatively inflexible robust attachment all *N*-(3,5-di-*tert*-butyl-2-hydroxyphenyl) and *N*-(3,5-di-*tert*-butyl-2-hydroxybenzyl) functionalised NHCs to REE cations the pro-ligands **H$_2$(L1^R)Br** (R = Me, Mes) and **H$_3$(L2)Br** show good preliminary results concerning their propensity to form targeted cerium(III) NHC compounds using both reaction procedures described above. Hereby strong evidence for the formation of desired cerium organo compounds has been observed by NMR spectroscopy. However, the paramagnetic nature of these molecules often impedes definitely assignment of the resonances in the spectra. Therefore, the exact molecular structure of the obtained compounds remains unknown. Further experiments towards isolation, crystallization and characterization of all obtained crude products should be conducted in order to improve the stoichiometry of the reactions and therefore the purity of the obtained compounds. Conducting the experiments at low temperatures (–78 °C) is advisable.

Unfortunately, the treatment of *N*-furanyl (**$H_2(L5^R)X_2$** and **$H_2(L6^R)X_2$**), 1,1'-(2-hydroxyethane-1,1-diyl) bridge (**$H_3(L3^R)X_2$**), and 1,1'-(prop-1-ene-1,3-diyl) bridge (**$H_2(L7^{Mes})X_2$**) functionalised bis(imidazolium) salts with alkali metal bases and subsequent transfer to a REE precursor yields only diamagnetic decomposition products. The main products in reactions with *N*-furanyl-substituted pro-ligands are various compounds formed by 1,2-shift of the *N*-substituents. The reason for this reactivity is probably the lack of anionic anchoring which could promote robust attachment to alkali metals and REE centres. The bridge functionalised pro-ligands (**$H_3(L3^R)X_2$** and **$H_2(L7^{Mes})X_2$)** frequently react under destruction of the linker resulting in elimination of substituted imidazoles. Generally, the same type of reactivity was observed directly with REE amides or alkyls acting as internal base.

Also the NMR analysis of the reactions with 1,1'-(2-hydroxypropane-1,3-diyl) bridge functionalised NHC precursor **$H_3(L4^{Mes})Br_2$** showed mostly strong evidence for the elimination of 1-mesitylimidazole. Preliminary good results were merely obtained in two-step transmetallation reactions using $KN(SiMe_3)_2$/$Ce(N\{SiMe_3\}_2)_3$ or $KN(SiMe_3)_2$/$Ce(BH_4)_3(THF)_4$ systems. Also the treatment of **$H_3(L4^{Mes})Br_2$** with $Li[Ce\{N(i\text{-}Pr)_2\}_4](THF)$ on exploratory scale was successful according to ^1H NMR analysis. Further experiments should be conducted on preparatory scale and more efforts directed towards the crystallization of these complexes. Also in this case the application of low temperatures is highly recommended.

Generally, in comparison to the NHC complexes derived from mono(imidazolium) salts such as **$H_2(L1^R)Br$** or **$H_3(L2)Br$** described above the REE complexes supported by bis(NHC) ligands pose additional synthetic challenges due to proximity of two NHC moieties in one molecule. Additionally, the alkyl linker between two imidazole-2-ylidenes is probably a weak point as it can be destroyed due to unwanted deprotonation of the CH-groups. So far only one example of a REE complex supported by amido-bridge functionalised bis(NHC) ligand was reported in the literature.[64] A development of bis(NHC) ligands with rigid linkers containing protons which are less susceptible to deprotonation might be a more promising approach to the preparation of REE bis(NHC) complexes.

Chapter 4

Synthesis and Characterization of dinuclear Ag(I) and Au(I) bis(NHC) complexes

Influence of *N*-Substituents and Reaction Conditions on Structure and Cytotoxic Properties

4.1 Results and Discussion

This Chapter focuses on the synthesis and characterization of dinuclear silver(I) and gold(I) complexes supported by 1,1'-(2-hydroxyethane-1,1-diyl) and 1,1'-(prop-1-ene-1,3-diyl) bridged functionalised bis(NHC) ligands. Hereby, the conformational behaviour of Ag(I) and Au(I) 1,1-(2-hydroxyethane-1,1-diyl) bridge-functionalised bis(NHC) complexes is studied as a function of *N*-substituents and reaction conditions and is further correlated to their cytotoxic properties. Furthermore, with the intention to synthesize heterometallic complexes first tentative experiments towards deprotonation of the bridge are described for 1,1'-(2-hydroxyethane-1,1-diyl) and 1,1'-(prop-1-ene-1,3-diyl) bridged functionalised bis(NHC) complexes of Au(I).

Parts of this chapter were incorporated into a manuscript "Influence of Wingtip Substituents and Reaction Conditions on Structure, Properties and Cytotoxicity of Ag(I)- and Au(I)-bis(NHC) Complexes", which was accepted for publication in *Dalton Transactions*, 2017, DOI: 10.1039/C6DT04559F.

4.1.1 1,1'-(2-Hydroxyethane-1,1-diyl)-Bridge Functionalised bis(NHC) Complexes of Ag(I) and Au(I) $M_2(HL3^R)_2X_2$

4.1.1.1 Synthesis and Characterization of Ag(I) bis(NHC) Complexes

Zhong *et al.* previously reported the synthesis and characterization of 1,1'-(2-hydroxyethane-1,1-diyl) functionalised bis(NHC) coinage metal complexes showing interesting conformational behaviour and offering a wide range of possibilities for further modification of the bridge between two NHC moieties.[173b] The work in this chapter follows up the report mentioned above as a further reaching comparative study. It explores the conformational behaviour of the complexes depending on counter anions, solvents, *N*-substituents and reaction temperature.

Ag complexes supported by 1,1'-(2-hydroxyethane-1-diyl) functionalised bis(NHC) ligands can be obtained under mild conditions *via* silver base route, the most widely applied protocol (Scheme 4.1.1).[9a, 19d, 123] The deprotonation and metalation of $\mathbf{H_3(L3^R)Cl_2}$ (R = Me, *i*-Pr) using 2.5 eq. of Ag_2O is performed in H_2O. A subsequent addition of a saturated solution of either NH_4PF_6 or $NaBPh_4$ to the crude product yields the desired complexes $\mathbf{Ag_2(HL3^R)_2(X)_2}$ (R = Me, *i*-Pr; X = PF_6, BPh_4). For the mesityl-modified ligand-precursor a direct reaction of $\mathbf{H_3(L3^{Mes})(X)_2}$ (X = PF_6, BPh_4) with 2.5 eq. of Ag_2O in acetonitrile was found to produce better results due to decreased solubility of the precursor and the complexes in water. The yields for all complexes with the exception of $\mathbf{Ag_2(HL3^{Me})_2(BPh_4)_2}$ and $\mathbf{Ag_2(HL3^{Mes})_2(BPh_4)_2}$ are reasonable (42%-65%), particularly since priority of this work was set on high purity. The low

yields for **$Ag_2(HL3^{Me})_2(BPh_4)_2$** (6 %) and **$Ag_2(HL3^{Mes})_2(BPh_4)_2$** (15 %) result from very tenuous purification procedures.

Generally, better yields and more straightforward purification procedures are observed for the PF_6^- salts rather than in their BPh_4^- analogues. In contrast to the PF_6, which precipitate as crystalline solids, tetraphenylborate salts often produce heavily contaminated oil or tend to form colloidal suspensions. Moreover, depending on the purification procedure a contamination with acetone is observed for BPh_4^- salts. However, this solvent cannot be removed due to co-crystallization in the solid state.

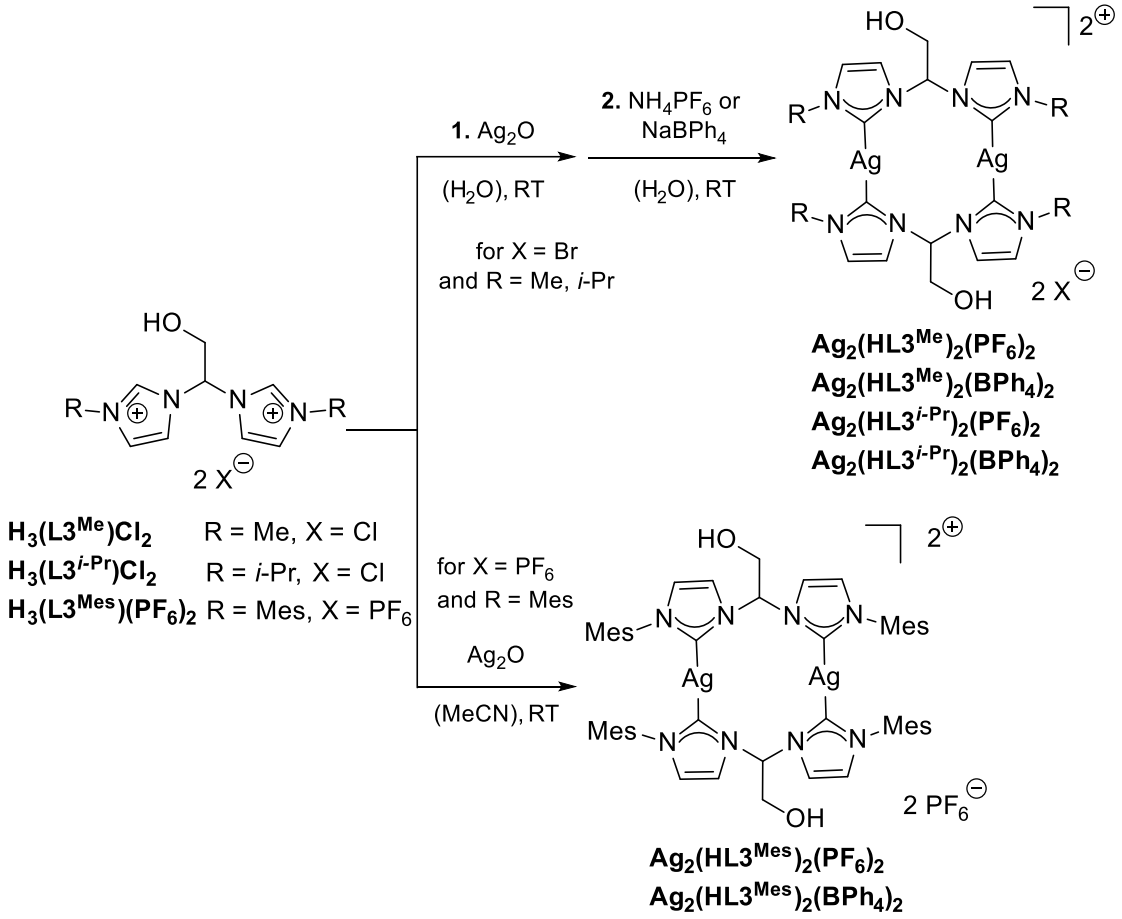

Scheme 4.1.1. Synthesis of 1,1'-(2-hydroxyethane-1,1-diyl) bridge-functionalised Ag bis(NHC) complexes.

Interestingly, all synthetic procedures performed in MeCN show significant amount of acetamide as a by-product formed by hydrolysis of the solvent. This side-reaction is probably catalysed by Ag containing intermediates, as stirring the purified complexes in wet acetonitrile under the same conditions does not produce acetamide. Hydrolysis of nitriles by silver nanoparticles[208] or by Ag complexes containing coordinated acetonitrile molecules[209] has precedent. Due to good solubility of acetamide in H_2O, it can be conveniently separated from the obtained complexes by washing the crude products with H_2O.

Multinuclear NMR spectroscopy, SC-XRD, EA and MS confirm the successful synthesis of dinuclear Ag bis(NHC) complexes. All compounds are isolated as white solids and are stable for many weeks under aerobic conditions and exposure to light. **$Ag_2(HL3^{Me})_2(BPh_4)_2$** shows very limited solubility in acetone and is insoluble in acetonitrile. However, it is reasonably soluble in MeOH, EtOH, DMSO and DMF. All other compounds show good solubility in DMSO, acetonitrile and acetone. **$Ag_2(HL3^{Mes})_2(X)_2$** (X = PF_6, BPh_4) complexes are also soluble in DCM.

Table 4.1.1. ^{13}C NMR resonances of carbenic carbons for reported 1,1'-(2-hydroxyethane-1,1-diyl) bridge-functionalised silver bis(NHC) complexes.

Complex	MeCN-d_3 (δ [ppm], m, J [Hz])	DMSO-d_6 (δ [ppm], m, J [Hz]),
$Ag_2(HL3^{Me})_2(PF_6)_2$	n.d.[a]	181.44 dd, $^1J^{107}_{AgC}$ = 182.5, $^1J^{109}_{AgC}$ = 211.7
$Ag_2(HL3^{Me})_2(BPh_4)_2$	n.d.[b]	n.d.[a]
$Ag_2(HL3^{i\text{-}Pr})_2(PF_6)_2$	181.35, br d, $^1J_{AgC}$ = 182.60	179.71, dd, $^1J^{107}_{AgC}$ = 182.4, $^1J^{109}_{AgC}$ = 209.9
$Ag_2(HL3^{i\text{-}Pr})_2(BPh_4)_2$	181.34, br d, $^1J_{AgC}$ = 205.80	179.65, dd, $^1J^{107}_{AgC}$ = 179.7, $^1J^{109}_{AgC}$ = 209.7
$Ag_2(HL3^{Mes})_2(PF_6)_2$	183.23, dd, $^1J^{107}_{AgC}$ = 181.9, $^1J^{109}_{AgC}$ = 211.1	181.48, dd, $^1J^{107}_{AgC}$ = 182.2, $^1J^{109}_{AgC}$ = 210.4
$Ag_2(HL3^{Mes})_2(BPh_4)_2$	182.17, s	n.d.[a]

[a]not detectable[173b]; [b]insoluble in MeCN.

As expected, ^1H NMR spectra of Ag(I) complexes indicates a symmetrical coordination of the ligand to Ag(I) centres. Ultimately, ^{13}C NMR resonances for Ag–C_C clearly prove the successful synthesis of the target compounds (Table 4.1.1). The obtained values lie within the range reported in the literature.[9a, 19d] No NCN resonance is observable for **$Ag_2(HL3^{Me})_2(PF_6)_2$** in acetonitrile-d_3 and **$Ag_2(HL3^{Me})_2(BPh_4)_2$** in DMSO-$d_6$, which is not unusual.[9a] Most compounds described in the literature show no coupling of carbene carbon atoms to Ag(I) centres (see Introduction, Section 1.4.1.2). The reason for the complete absence of carbene signals is,

however, still unclear, but a fast dynamic behaviour combined with the poor relaxation of quaternary NCN carbon could account for it.[9a] In summary, for the complexes counterbalanced by PF_6^-, the fluxionality in acetonitrile apparently correlates with the steric demand of wingtip substituents (Me>>*i*-Pr>Mes). For the complexes with BPh_4 anions the same trend is not evident.

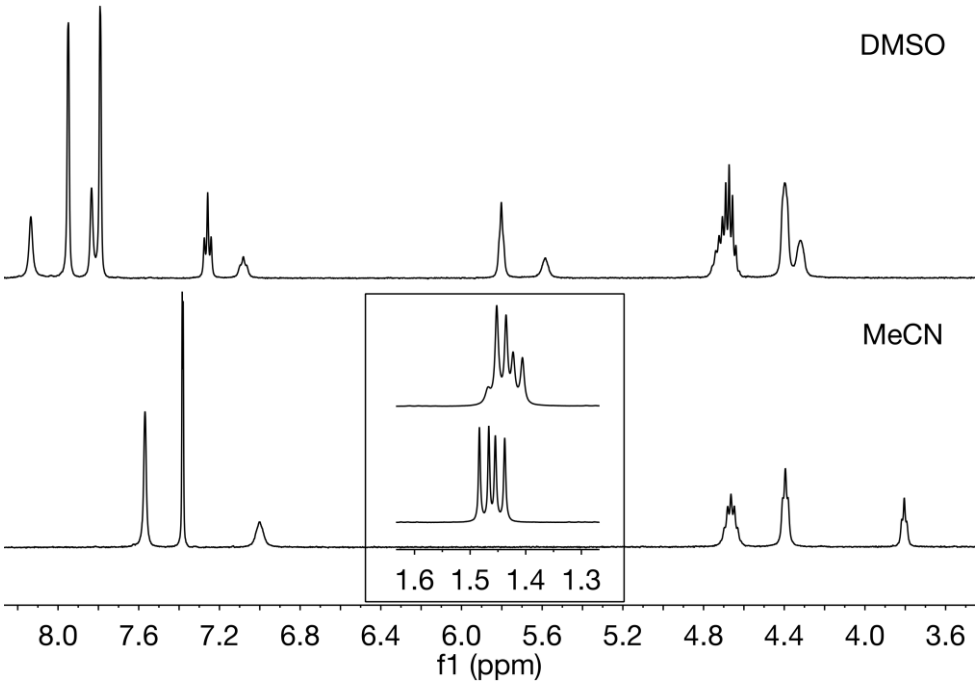

Figure 4.1.1. ^{1}H NMR spectra of **$Ag_2(HL3^{i\text{-}Pr})_2(PF_6)_2$** in CD_3CN (bottom) and DMSO-*d_6* (top) at RT.

The ^{1}H NMR spectra of **$Ag_2(HL3^{Me})_2(PF_6)_2$**, **$Ag_2(HL3^{i\text{-}Pr})_2(PF_6)_2$** and **$Ag_2(HL3^{i\text{-}Pr})_2(BPh_4)_2$** change if recorded in acetone-*d_6* or DMSO-*d_6*. In this case additional sets of signals with lower intensity appear (e.g. for **$Ag_2(HL3^{i\text{-}Pr})_2(PF_6)_2$** see Figure 4.1.1, for stoichiometric ratios see Table 4.1.2; for comparison of ^{1}H NMR spectra for other compounds, see SI). Also in the ^{13}C NMR spectra in DMSO the presence of minor products is now clearly visible. Moreover, the carbene resonances of the main species exhibit now a coupling to both silver isotopes and appear as doublet of doublets, hereby suggesting lesser dynamic behaviour at RT (Table 4.1.1). The mesityl-substituted congener, however, shows no splitting of the signals neither in ^{1}H NMR nor in ^{13}C NMR spectra recorded in DMSO.

Table 4.1.2. The ratio of minor and major species of $\mathbf{Ag_2(HL3^R)_2(X)_2}$ observed by ^{1}H NMR spectroscopy.

Complex	MeCN-d_3	DMSO-d_6
$\mathbf{Ag_2(HL3^{Me})_2(PF_6)_2}$	n.o.	0.2:1.0
$\mathbf{Ag_2(HL3^{Me})_2(BPh_4)_2}$	n.d.[b]	0.2:1.0
$\mathbf{Ag_2(HL3^{i\text{-}Pr})_2(PF_6)_2}$	n.o.	0.4:1.0
$\mathbf{Ag_2(HL3^{i\text{-}Pr})_2(BPh_4)_2}$	n.o.	0.4:1.0
$\mathbf{Ag_2(HL3^{Mes})_2(PF_6)_2}$	n.o.	n.o.
$\mathbf{Ag_2(HL3^{Mes})_2(BPh_4)_2}$	n.o.	n.o.

[b]insoluble in MeCN, **n.d.** not determined, **n.o.** the splitting of the resonances have not been observed

In order to elucidate thermal behaviour and possible interconversion between the two species, a variable temperature NMR study on $\mathbf{Ag_2(HL3^{i\text{-}Pr})_2(BPh_4)_2}$ was carried out in MeCN and DMSO (SI, Figures 5.3.36-37). Neither in MeCN, nor in DMSO a significant influence of the temperature on the ^{1}H NMR spectra is observed. Furthermore, ^{1}H diffusion ordered (DOSY) NMR experiments for $\mathbf{Ag_2(HL3^{i\text{-}Pr})_2(X)_2}$ (X = PF_6, BPh_4) in DMSO show that there is no difference in diffusion coefficients for the major and the minor set of the ligand signals, indicating that the two species have the same or a very similar hydrodynamic radius. These observations suggest that the new set of the signals in DMSO could be another isomer, whose existence is not observed in MeCN due to dynamic processes.

Coinage metal bis(NHC) complexes have been previously reported to exhibit either *syn* or *anti* isomerism, which has analogies to boat or chair-like conformation of cyclohexane (see Introduction, Figure 1.4.3).[10b, 125, 173b, 210] For methylene bridged Ag bis(NHC) cations a fast interconversion, depending on temperature and concentration, which in turn increases intermolecular argentophilic interactions, was recently investigated by NMR studies and small angle X-ray scattering.[144] The implication of a 1,1'-(2-hydroxyethane-1,1-diyl) functionalised bridge, which breaks the C_{2v} symmetry to C_s, was previously addressed by Zhong *et al*. for $\mathbf{M_2(HL3^{Me})_2(PF_6)_2}$ (M = Ag, Au, Cu) as well.[173b] In this case, additionally to syn- and anti-conformation, the hydroxymethyl substituents can point away from the metal centres (exo), towards them (endo) or in opposite directions (meso) (Figure 4.1.2). By comparing gas phase free energies, the theoretical calculations predicted the syn, exo conformation to be most favourable for $\mathbf{M_2(HL3^{Me})_2(PF_6)_2}$. (M = Ag, Au)[173b] These results are also consistent with the solid state structure of $\mathbf{Au_2(HL3^{Me})_2(PF_6)_2}$, which co-crystallises with a water molecule hydrogen-bonded to both OH groups of the ligand, therefore further reducing the energy gap

to the anti isomer. Further calculations, considering the presence of H_2O and MeCN show that the anti, exo species is more favourable for the analogue silver complex. This fact was experimentally confirmed by X-ray diffraction as well.[173b] However, in the previous study the influence of different solvents and wingtip substituents on conformation has not been addressed. Thus, to gain better insight into the correlation between different conformers and solvents as well as wingtip substituents, DFT calculations on the isopropyl functionalised Ag(I) and Au(I) bis(NHC) complexes both in MeCN and DMSO have been carried out by David Mayer under the supervision of Dr. Markus Drees.

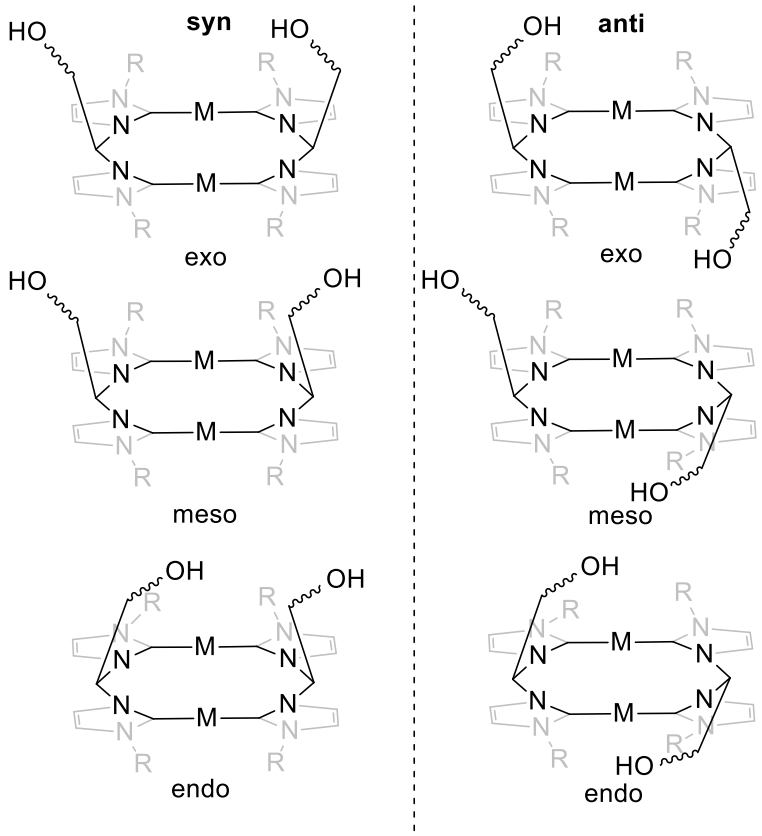

Figure 4.1.2. Possible stereoisomers of dinuclear coinage metal of 1,1'-(2-hydroxyethane-1,1-diyl) bridge-functionalised bis(NHC) complexes of Ag(I) and Au(I).

Since the ωB97X-D functional has been already successfully applied for **$M_2(HL3^{Me})_2(PF_6)_2$** (M = Ag, Au, Cu), this functional was used again to ensure the comparability to former calculations.[173b] In terms of C–C, C–N and C–M bond lengths the results show an excellent accordance with the obtained crystal structures (Table 4.1.3). The free energies were calculated for all optimized structures both in gas phase and with an implicit solvent model. The gas phase calculations predict the syn, exo conformation to be the lowest energy species and, as expected, the meso and endo conformations are calculated to be significantly higher in energy. However, by changing to a more precise description in favour of real experimental conditions using a SMD solvent model, the order of the free energies of the isomers changes

entirely. This time the anti, exo isomer is calculated to be the lowest energy species. However, an endergonic gap to the syn, meso isomer is just ΔG = 0.97 kJ/mol, which implies two thermoneutral species (Figure 4.1.3).

Table 4.1.3. Mean bonding lengths of **$[Ag_2(HL3^{i\text{-}Pr})_2]^{2+}$** determined by SC-XRD experiments compared to calculations (ωB97x-D, 6-31+g(d), LANL3DZ).

	mean $d_{C\text{-}C}$ [Å]	**mean $d_{C\text{-}N}$ [Å]**	**mean $d_{C\text{-}O}$ [Å]**	**mean $d_{C\text{-}Ag}$ [Å]**
SC-XRD	1.468	1.401	1.406	2.088
Calculations	1.488	1.401	1.408	2.138
Δ = (Calc.-Exp.)	0.020 (1.3%)	---	0.002 (0.14%)	0.050 (2.3%)

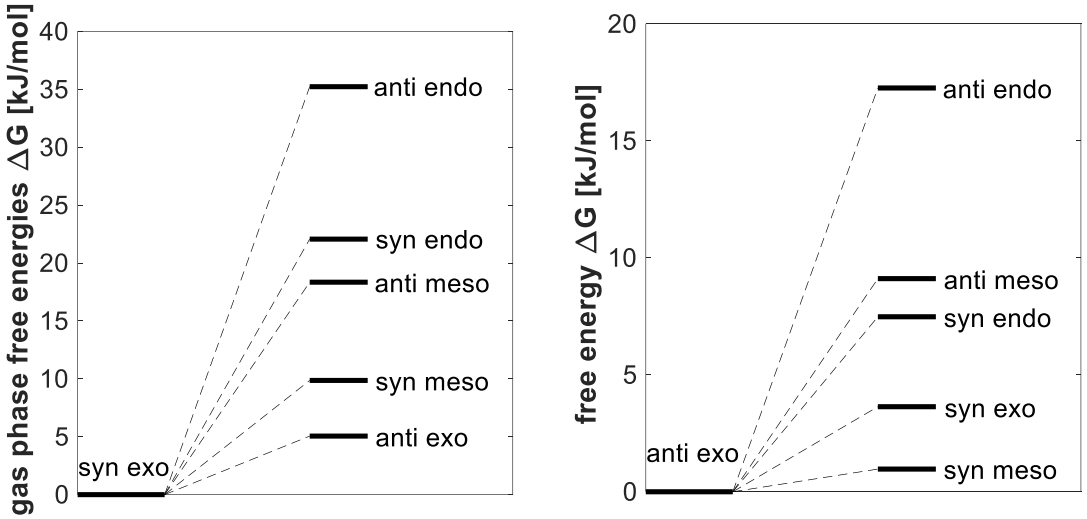

Figure 4.1.3. Calculated gas phase free energies ΔG and free energies ΔG in acetonitrile of **$[Ag_2(HL3^{i\text{-}Pr})_2]^{2+}$** for the different isomers referred to the particular lowest energy species.

Based on these results, the free energies for the anti, exo as well as the syn, meso conformations have been calculated for the silver and gold complexes in acetonitrile as well as dimethylsulfoxide (Table 4.1.4). Therefore, within the accuracy of the calculations, the anti, exo/syn, meso isomer pair can be regarded as thermoneutral isomers. The most important feature in comparison to the calculation results of the *N*-methyl-substituted isomers is the distortion of the assumed geometry in the case of more sterically demanding substituents. As expected, by changing to a more sterically demanding wingtip, the influence of the CH_2OH

group decreases. For every isomer form the calculations predict a stronger deviation from the anti or syn isomerism towards a torsion of the NHC planes out of the metal carbene plane, a behaviour that was not found for the *N*-methyl-substituted complexes. This might give an answer to the differences in energies, as the syn configuration was found to be higher in energy for **$Ag_2(HL3^{Me})_2(PF_6)_2$** than for the isopropyl-substituted congener.

Table 4.1.4. Free energy values (kJ/mol) of the calculated syn, meso complexes of **$[M_2(HL3^{i\text{-}Pr})_2]^{2+}$** in acetonitrile and dimethylsulfoxide referenced to the corresponding anti, exo species.

$[M_2(NHC)_2]^{2+}$	MeCN (syn, meso) [kJ/mol]	DMSO (syn, meso) [kJ/mol]
$[Ag_2(HL3^{i\text{-}Pr})_2]^{2+}$	+0.97	+0.13
$[Au_2(HL3^{i\text{-}Pr})_2]^{2+}$	+1.1	+0.11

In conclusion, according to these calculations two products observed in the ^{1}H NMR spectrum of **$Ag_2(HL3^{i\text{-}Pr})_2(PF_6)_2$** in DMSO are the syn/anti isomer pair.

To confirm DFT calculations an H,H-NOESY NMR spectrum of **$Ag_2(HL3^{i\text{-}Pr})_2(PF_6)_2$** was recorded in MeCN-$d_3$ and DMSO-d_6 (see SI, Figures 5.3.38-39). As expected, an interaction of the OH protons with the residual water in the solvent is observed. According to these data a spatial proximity of the NCHN-bridge proton to the backbone protons of imidazol-2-ylidenes is suggested for the major species in DMSO (Figure 4.1.4). As such correlation is only possible for the meso or endo isomers, these observations confirm DFT calculations by supporting the assumption of the existence of the syn, meso species of **$Ag_2(HL3^{i\text{-}Pr})_2(PF_6)_2$** in the unrefined product mixture. For the minor species visible in DMSO such spatial proximity was not observed. However, spatial proximity of CH_2-group of the bridge to the backbone protons of imidazol-2-ylidenes is evident instead. Therefore, the resonances of the minor species can be attributed to the anti, exo isomer, as due to distortion of the ligand these protons are forced to proximity (see XRD studies presented below). Furthermore, in the spectrum recorded in MeCN a spatial proximity of NCHN-protons as well as CH_2-protons in the bridge to imidazole-2-ylidene backbone is suggested. These facts indicate either the presence of a meso isomer or a mixture of different species as well. Interestingly, in contrast to H,H-NOESY NMR spectrum of **$Ag_2(HL3^{i\text{-}Pr})_2(PF_6)_2$** in MeCN-$d_3$ the spectrum recorded in DMSO-d_6 also suggests the presence of syn-anti aggregates. A formation of molecular dimers as a result of intermolecular argentophilic interactions was previously suggested for similar methylene bridged Ag bis(NHC) complexes.[12] In the case described here the existence of dynamic dimer systems is conceivable as the hydrodynamic radius of **$[Ag_2(HL3^{i\text{-}Pr})_2]^{2+}$** calculated on the basis of ^{1}H-

DOSY NMR experiments ($r_H = k \cdot T/[6\pi \cdot \eta \cdot D]$)[211]) increases in DMSO (7.7 Å in MeCN vs. 8.6 Å DMSO for **$Ag_2(HL3^{i\text{-}Pr})_2(PF_6)_2$**).

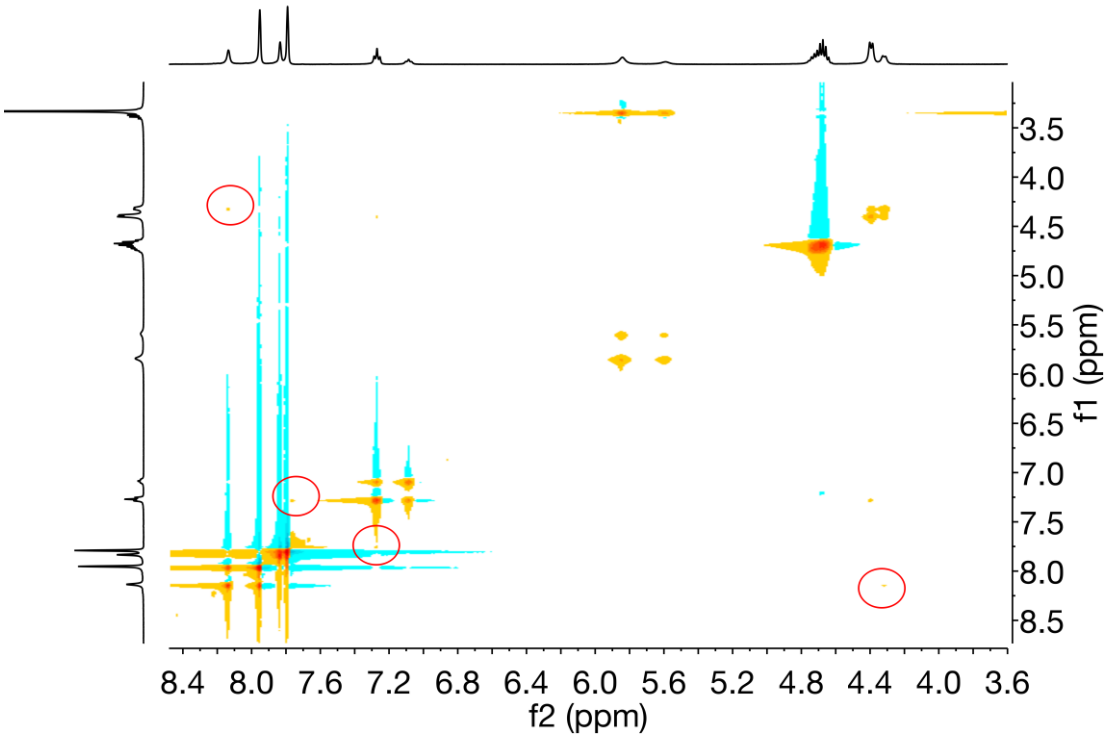

Figure 4.1.4. H,H-NOESY NMR spectrum of **$Ag_2(HL3^{i\text{-}Pr})_2(PF_6)_2$** in DMSO-$d_6$ at RT (enlargement in the aromatic region).

For further characterization and confirmation of DFT and NMR results single crystals suitable for SC-XRD have been grown through slow diffusion of Et_2O into a saturated solution of the respective Ag(I) complexes in MeCN. The obtained data unambiguously prove the successful synthesis of dinuclear bis(NHC) complexes and confirm the computational results. For comparison of all obtained Ag(I) bis(NHC) complexes the relevant bond distances and angles are given in Table 4.1.5.

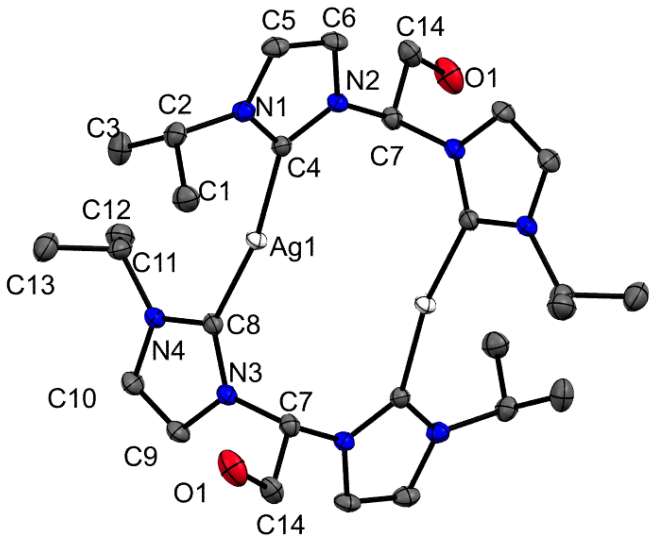

Figure 4.1.5. ORTEP style representation of the cation of **$Ag_2(HL3^{i\text{-}Pr})_2(PF_6)_2$** with ellipsoids at 50 % probability. Hydrogen atoms, PF_6^- and co-crystallised diethyl ether molecules are omitted for clarity.

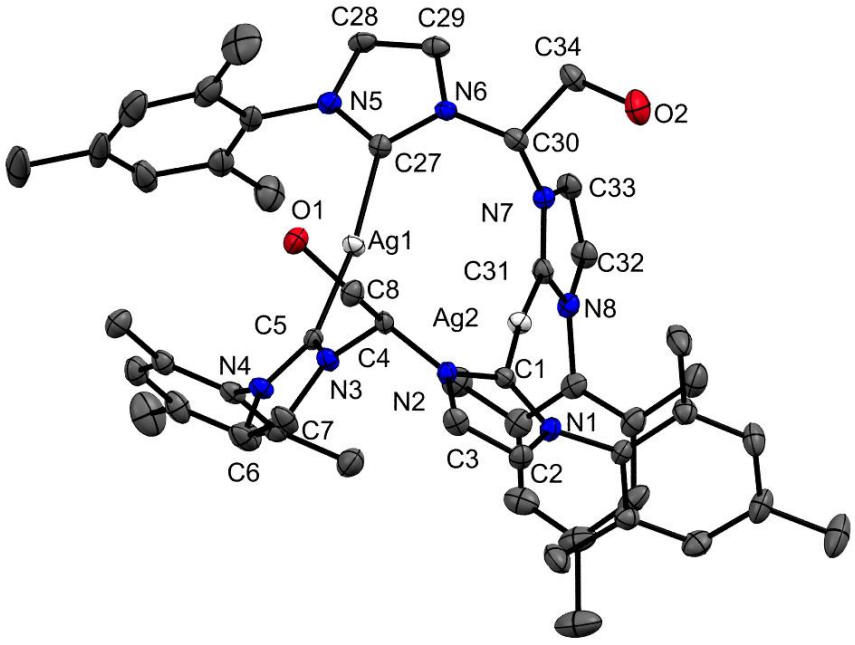

Figure 4.1.6. ORTEP style representation of the cation of **$Ag_2(HL3^{Mes})_2(PF_6)_2$** with ellipsoids at 50 % probability. Hydrogen atoms, PF_6^- and co-crystallised acetonitrile molecules are omitted for clarity.

The molecular structure of **$Ag_2(HL3^{i\text{-}Pr})_2(PF_6)_2$**, crystallizing in the monoclinic space group *P* $2_1/c$, is shown in Figure 4.1.5. It exhibits a similar spatial arrangement to **$Ag_2(HL3^{Me})_2(BPh_4)_2$** (SI, Figure 5.3.50), **$Ag_2(HL3^{i\text{-}Pr})_2(BPh_4)_2$** (SI, Figure 5.3.51) and to previously reported **$Ag_2(HL3^{Me})_2(PF_6)_2$**[173b]. **$Ag_2(HL3^{Mes})_2(PF_6)_2$**, however, shows significant structural differences to its less sterically hindered congeners (Figure 4.1.6). It crystallises in the monoclinic space group *P* $2_1/c$ as the syn, exo isomer, whereas for methyl and isopropyl

wingtips the anti, exo isomers were obtained. Since the Ag···Ag distances for **$Ag_2(HL3^{Me})_2(PF_6)_2$** and **$Ag_2(HL3^{i\text{-}Pr})_2X_2$** are longer than the sum of the van der Waals radii of two Ag(0) atoms (3.44 Å)[212], intramolecular argentophilic interactions can be excluded for these compounds in the solid state. On the other hand, as a consequence of the different conformation and bulky substituents**,** the silver cations in **$Ag_2(HL3^{Mes})_2(PF_6)_2$** come much closer to each other. This results in an Ag···Ag distance of 3.3314(5) Å, hereby suggesting weak argentophilic interactions in the solid state. Regardless of the conformation, the Ag–C_c bonds for all complexes lie within the same range, with **$Ag_2(HL3^{Mes})_2(PF_6)_2$** showing on the average slightly shorter distances, probably due to packing effects. The C_c–Ag–C_c angles slightly deviate from linearity as a consequence of the linker and wingtip substituents. All values for bond distances and bond angles are comparable to the literature values.[9a, 173b]

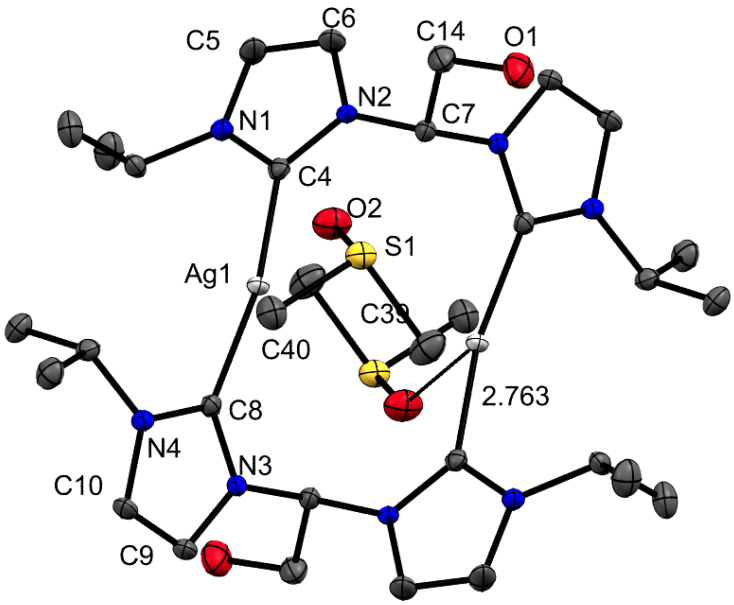

Figure 4.1.7. ORTEP style representation of the cation of **$Ag_2(HL3^{i\text{-}Pr})_2(BPh_4)_2$·DMSO** with ellipsoids at 50 % probability. Hydrogen atoms, BPh_4^- and co-crystallised DMSO molecules are omitted for clarity.

Interestingly, X-ray characterization of single crystals obtained by slow diffusion of diethyl ether into a solution of **$Ag_2(HL3^{i\text{-}Pr})_2(BPh_4)_2$** in a mixture of DMSO and methanol reveals the crystallization of the anti, exo isomer with DMSO molecules coordinated to the Ag(I) cations (Ag–O = 2.763(2) Å) (Figure 4.1.7). Additionally, two other DMSO molecules are interacting with the metals centres at the longer distance of 3.372(2) Å (Ag–O) on the respective opposite side. The steric repulsion of the nearby located hydroxymethyl group of the ligand could account for the elongation of the Ag–O distances in this case. This observation suggests that the coordinating ability of DMSO could in fact be responsible for the separation of the resonances attributed to different isomers the ^{1}H NMR spectrum in DMSO. However, it should

Table 4.1.5. Selected bond lengths (Å) and angles (deg) for the reported Ag(I) bis(NHC) complexes.

	$Ag_2(HL3^{Me})_2(PF_6)_2$[a,*]	$Ag_2(HL3^{Me})_2(BPh_4)_2$	$Ag_2(HL3^{i\text{-}Pr})_2(PF_6)_2$[c]	$Ag_2(HL3^{i\text{-}Pr})_2(BPh_4)_2$[c]	$Ag_2(HL3^{i\text{-}Pr})_2(BPh_4)_2\cdot DMSO$[c]	$Ag_2(HL3^{Mes})_2(PF_6)_2$
M···M	3.4556(9)-3.8964(8)	3.4181(4)	3.4600(6)	3.6474(4)	3.6029(8)	3.3314(5)
M–C_c	2.065(5)-2.100(5)	2.087(2)-2.090(2)	2.087(2)-2.090(2)	2.086(2)-2.094(2)	2.099(2)-2.102(2)	2.071(2)-2.088(3)
N–C_c	1.334(6)-1.370(6)	1.349(2)-1.359(3)	1.344(2)-1.360(2)	1.347(3)-1.357(3)	1.345(3)-1.358(3)	1.348(3)-1.361(3)
N–C_b	1.446(6)-1.466(6)	1.456(3)-1.467(2)	1.452(2)-1.464(2)	1.457(3)-1.461(3)	1.458(3)-1.459(2)	1.456(3)-1.461(3)
N–C_c–N	102.8(4)-105.0(4)	103.9(2)-104.2(2)	104.2(1)-104.5(2)	104.4(2)-104.6(2)	104.1(2)-104.3(2)	103.8(2)-104.1(2)
N–C_b–N	110.1(4)-111.5(4)	108.2(2)	110.3(1)	110.6(2)	110.3(2)	109.482)-109.8(2)
C_c–Ag–C_c	168.5(2)-175.8(2)	170.61(8)	169.3(7)	171.74(8)	165.65(8)	172.3(1)-175.4(1)

*reported previously[173b], **a** contains two molecules in the asymmetric unit, **b** contains an intramolecular mirror plane, **c** contains an intramolecular inversion centre; C_c = carbene, C_b = bridge CH

be noted that the DMSO coordination and loss are probably dynamic on the NMR scale, since no additional signal for DMSO was observed. Also the H,H-NOESY NMR experiment with **$Ag_2(HL3^{i\text{-}Pr})_2(BPh_4)_2$** shows no signs of interaction of DMSO with the ligand.

It should be noted that an interconversion between the syn- and anti-isomers is conceivable either by folding of the 12-membered metallacycle or via M–C bond cleavage, which leads to a contemporary ligand dissociation and re-association forming the other isomer species. Both mechanisms have been previously suggested for Ag(I) bis(NHC) complexes.[144, 146, 152] However, in our case a conformational change by folding would break symmetry and therefore should have a substantial activation barrier. Since the VT-^{1}H-NMR study mentioned above show no dependence of the isomer ratios on the temperature, there is also a possibility that interconversion between two species doesn't happen at all or at least not in DMSO.

4.1.1.2 Transmetallation to Gold(I)

Treating **$Ag_2(HL3^R)(PF_6)_2$** (R = Me, *i*-Pr, Mes) and **$Ag_2(HL3^R)(BPh_4)$** (R = Me, *i*-Pr) with AuCl(SMe_2) or AuCl(THT) (THT = tetrahydrothiophene) produces the corresponding Au(I) bis(NHC) complexes in good yields (31 %-81 %) and high purity (Scheme 4.1.2). Due to insolubility of **$Ag_2(HL3^{Me})_2(BPh_4)_2$** in MeCN, the transmetallation is carried out in dry acetone, for all other complexes in dry acetonitrile. For **$Ag_2(HL3^{Mes})_2(BPh_4)_2$** a clean transfer of NHC ligand to Au(I) was unsuccessful neither at RT nor at 50 °C due to formation of numerous species, which cannot be separated by various precipitation or crystallization procedures or column chromatography. Generally, similar to Ag(I) analogues the use of PF_6^- as a counter anion results in better yields and an easier synthetic procedure than for BPh_4^- analogues. All bulk material has been characterised by multinuclear NMR spectroscopy, ESI-MS and elemental analysis, confirming the successful isolation. The Au(I) bis(NHC) complexes show the same solubility behaviour as their silver counterparts.

^{1}H NMR spectra of all Au bis(NHC) compounds show higher resolutions than the spectra of Ag congeners. Moreover, no differences in signal pattern are visible in the ^{1}H NMR spectra in DMSO in comparison to MeCN. These observations suggest a less fluxional nature of the corresponding Au compounds, which is in accordance with the general agreement that an Au–C_c bond is stronger than the corresponding Ag–C_c bond.[19d, 133c] Generally, in comparison to Ag(I) analogues a slight shift of the ^{1}H resonances to higher frequencies indicates a stronger deshielding effect of Au nuclei. There is also a slight shift of the carbene signals to higher frequency, which is in the range of those in previously published reports.[19d, 173b]

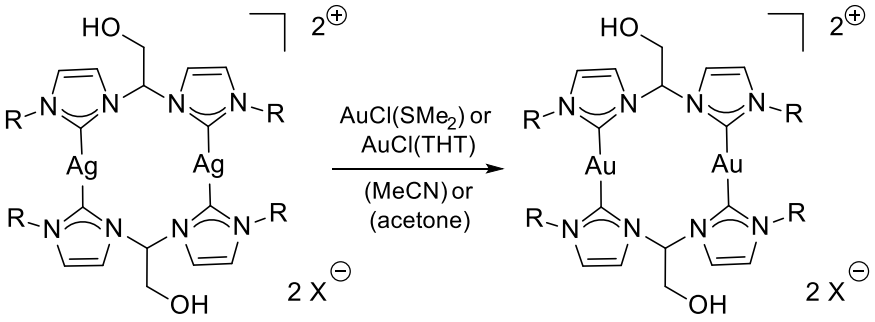

$Ag_2(HL3^{Me})_2(PF_6)_2$ R = Me, X = PF_6	**$Au_2(HL3^{Me})_2(PF_6)_2$** R = Me, X = PF_6
$Ag_2(HL3^{Me})_2(BPh_4)_2$ R =Me, X = BPh_4	**$Au_2(HL3^{Me})_2(BPh_4)_2$** R =Me, X = BPh_4
$Ag_2(HL3^{i\text{-}Pr})_2(PF_6)_2$ R = *i*-Pr, X = PF_6	**$Au_2(HL3^{i\text{-}Pr})_2(PF_6)_2$** R = *i*-Pr, X = PF_6
$Ag_2(HL3^{i\text{-}Pr})_2(BPh_4)_2$ R = *i*-Pr, X = BPh_4	**$Au_2(HL3^{i\text{-}Pr})_2(BPh_4)_2$** R = *i*-Pr, X = BPh_4
$Ag_2(HL3^{Mes})_2(PF_6)_2$ R = Mes, X = PF_6	**$Au_2(HL3^{Mes})_2(PF_6)_2$** R = Mes, X = PF_6

Scheme 4.1.2. Transmetallation reaction to the respective Au(I) compounds using Ag(I) bis(NHC) complexes as transfer reagents.

The solid state structure of **$Au_2(HL3^{Me})_2(PF_6)_2$** has been previously reported by Zhong *et al*.[173b] This compound was isolated after the transmetallation at 45 °C as isomeric pure material, which crystallised as syn, exo conformer.[173b] By repeating the reaction at room temperature but otherwise under the same conditions, a mixture of two **$Au_2(HL3^{Me})_2(PF_6)_2$** isomers is obtained as the crude product. Also, the transmetallation of **$Ag_2(HL3^{i\text{-}Pr})_2(PF_6)_2$** to **$Au_2(HL3^{i\text{-}Pr})_2(PF_6)_2$** at RT yields two isomers in even higher ratios in contrast to the close relative **$Au_2(HL3^{i\text{-}Pr})_2(BPh_4)_2$**, which is isolated as almost isomeric pure material after the transmetallation at 50 °C. These unexpected observations lead to the suspicion that the reaction temperature has a significant impact on the formation of different isomers.

To address this question, a series of NMR scale transmetallation reactions at different temperatures was carried out for PF_6^- counterbalanced complexes.[203] The isomer ratios obtained before the purification procedures are collected in Table 4.1.6. Assuming that during crystallization there is no interconversion between the two species, based on the crystallographic data previously published[173b] and presented below, the downfield shifted minor species can be assigned to an anti isomer and the species appearing at lower frequencies as the corresponding syn species.

As already observed for the respective Ag complexes, the conformation strongly depends on the wingtip substituents. For Me and Mes-substituted complexes a strong preference for syn, exo species exists. For isopropyl analogues this preference is less pronounced. These observations are in accord with published[173b] and previously mentioned DFT calculations on methyl- and isopropyl substituted bis(NHC) complexes of Au(I). By comparing the values, it is also evident that they also strongly support the hypothesis of the isomer formation for a particular ligand as a temperature dependent process. For all tested material the obtained

minor to major product ratios show a steady progress from lower to higher energy. With increased reaction temperature a definitive preference for a syn conformation is evident for methyl- and isopropyl-substituted Au bis(NHC) complexes. In contrast to these observations, the proportion of an anti isomer is increased for the mesityl-substituted analogue at higher reaction temperature, but nevertheless a syn isomer remains the preferable product.

Importantly, the subsequent work-up of the crude products severely affects the isomer ratios. For example, the anti isomer of **$Au_2(HL3^{Me})_2(PF_6)_2$** is found after repeated fractional precipitation only in traces. On the other hand, for **$Au_2(HL3^{i\text{-}Pr})_2(X)_2$** (X = PF_6, BPh_4) the same procedure leads to an enrichment of the anti, exo species. In some cases, due to more elaborate repeated precipitation it was even possible to completely reverse the end-product ratio, as seen e.g. for **$Au_2(HL3^{i\text{-}Pr})_2(BPh_4)_2$**, where the syn isomer cannot be detected by ^{1}H NMR spectroscopy afterwards. However, a purification by column chromatography results in a reversed effect, namely in extreme enrichment of syn **$Au_2(HL3^{i\text{-}Pr})_2(PF_6)_2$** rendering the proportion attributed to anti compound almost negligible. Also the purification of **$Au_2(HL3^{Mes})_2(PF_6)_2$** by column chromatography or recrystallization yields the pure syn, exo isomer. Unfortunately, so far the crystallization of the syn isomer of the isopropyl-species remained elusive. Therefore, it cannot be said with certainty if the species in question is a syn, meso species, as implied by DFT calculations and H,H-NOESY NMR experiment on **$Ag_2(HL3^{i\text{-}Pr})_2(PF_6)_2$**, or analogue to **$Au_2(HL3^{Me})_2(PF_6)_2$** and **$Au_2(HL3^{Mes})_2(PF_6)_2$** a syn, exo isomer. Unfortunately, the H,H-NOESY NMR spectrum of **$Au_2(HL3^{i\text{-}Pr})_2(PF_6)_2$** was inconclusive (Figure 5.3.40, SI).

Table 4.1.6. The ratios of anti/syn isomers for not purified Au complexes prepared at different T.

Complex	RT	45-50 °C	90 °C
$Au_2(HL3^{Me})_2(PF_6)_2$	0.2:1.0	0.0:1.0*	n.d.
$Au_2(HL3^{i\text{-}Pr})_2(PF_6)_2$	0.7:1.0	0.2:1.0-0.3:1.0	0.1:1.0
$Au_2(HL3^{Mes})_2(PF_6)_2$	0.3:1.0	0.5:1.0	0.5:1.0

***Reported by Zhong *et al.*[173b]; **n.d**. not determined

The solid state structures of Au bis(NHC) complexes have been further elucidated by SC-XRD, resulting in a confirmation of NMR experiments. Single crystals of **$Au_2(HL3^{i\text{-}Pr})_2(PF_6)_2$** and **$Au_2(HL3^{i\text{-}Pr})_2(BPh_4)_2$** have been grown by slow diffusion of Et_2O into a saturated solution of respective purified bulk material in MeCN at RT. **$Au_2(HL3^{i\text{-}Pr})_2(PF_6)_2$** crystallises in the monoclinic space group *P* $2_1/c$ as the anti, exo isomer (Figure 4.1.8). Although the proportion of syn species in the bulk material is high, so far, single crystals of a syn isomer could not be

obtained. As expected, since no syn isomer was present in the purified **$Au_2(HL3^{i\text{-}Pr})_2(BPh_4)_2$** sample, the XRD structure shows the anti, exo isomer in analogy to **$Au_2(HL3^{i\text{-}Pr})_2(PF_6)_2$**. The isomeric pure sample of **$Au_2(HL3^{Mes})_2(PF_6)_2$** obtained by recrystallization was crystallised out of mixture of DCM and THF at –4 °C. Its structure is shown in Figure 4.1.9, revealing it to be, a syn, exo isomer, crystallizing in the monoclinic space group *P* 2_1. For comparison all relevant bond distances and angles are collected in Table 4.1.7.

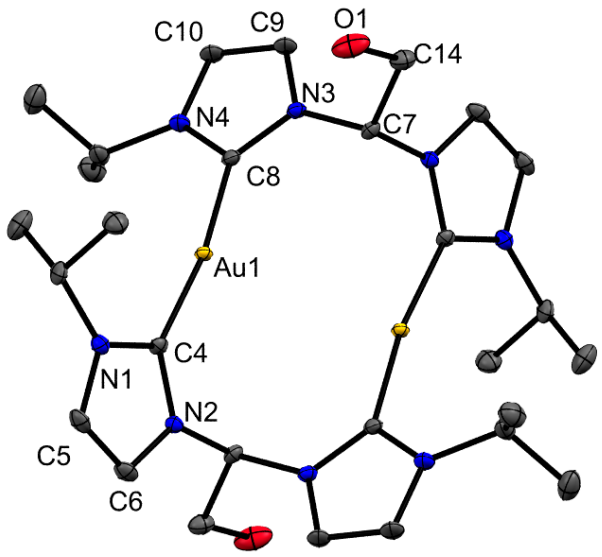

Figure 4.1.8. ORTEP style representation of the cation of **$Au_2(HL3^{i\text{-}Pr})_2(PF_6)_2$** with ellipsoids at 50 % probability. Hydrogen atoms, PF_6^- and co-crystallised diethyl ether molecules are omitted for clarity.

The Au–C_c bond lengths are generally shorter than the distances in the respective Ag complexes. This also reflects the general assumption that bond strengths in coinage metal NHC complexes correlate in the order: Au>Cu>Ag.[133a] The Au–C_c bond lengths as well the bond distances in the ligand framework for all Au complexes in this study are comparable and lie within the ranges reported in the literature.[10b, 125, 148] Similar to silver complexes the C_c–Au–C_c bond angles (171.0°-175.2°) slightly deviate from linearity. The Au···Au separation for the anti, exo isomers of the methyl and isopropyl analogues is too long for any significant interaction. However, the Au···Au distance in **$Au_2(HL3^{Mes})_2(PF_6)_2$** amounts to 3.2999(4) Å, which is smaller than the sum of van der Waals radii of two Au atoms (3.32 Å).[212] This might indicate at least weak intramolecular aurophilic interactions.[134-135]

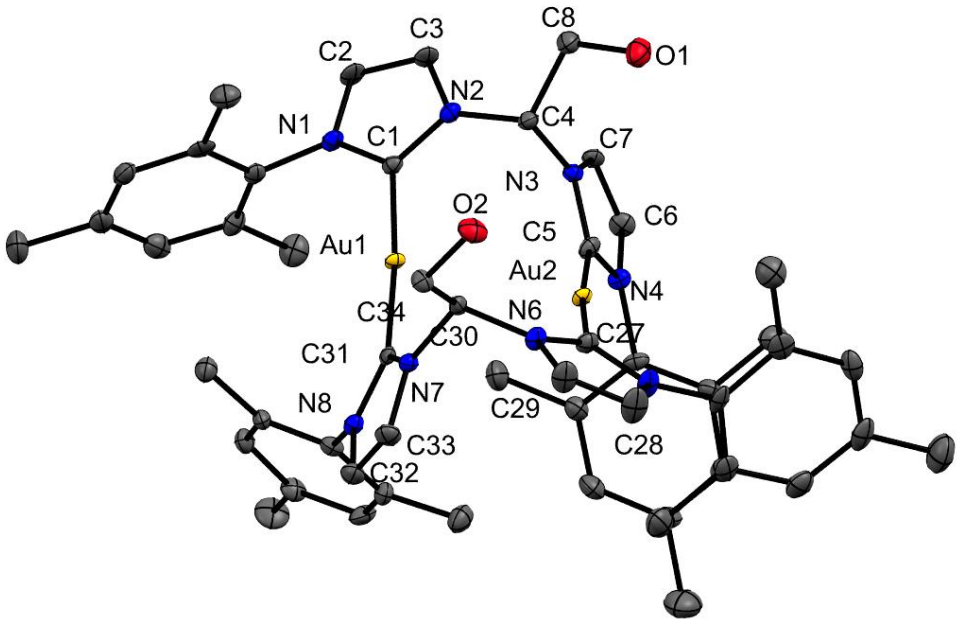

Figure 4.1.9. ORTEP style representation of the cation of **$Au_2(HL3^{Mes})_2(PF_6)_2$** with ellipsoids at 50 % probability. Hydrogen atoms, PF_6^- and co-crystallised tetrahydrofuran molecules are omitted for clarity.

Table 4.1.7. Selected bond lengths (Å) and angles (deg) for the reported Au(I) bis(NHC) complexes.

	$Au_2(HL3^{Me})_2(PF_6)_2$[b,*]	**$Au_2(HL3^{i\text{-}Pr})_2(PF_6)_2$[c]**	**$Au_2(HL3^{i\text{-}Pr})_2(BPh_4)_2$[c]**	**$Au_2(HL3^{Mes})_2(PF_6)_2$**
M···M	3.6401(5)	3.5728(5)	3.6242(3)	3.2999(4)
M–C_c	2.013(9)-2.022(8)	2.020(2)	2.018(3)	2.016(4)-2.021(3)
N–C_c	1.32(1)-1.39(1)	1.345(3)-1.357(3)	1.349(4)-1.356(4)	1.342(5)-1.355(5)
N–C_b	1.46(1)	1.454(3)-1.464(3)	1.460(4)-1.466(4)	1.456(7)-1.471(6)
N–C_c–N	103.8(8)-105.0(7)	104.6(2)-105.0(2)	104.5(3)-105.1(2)	104.9(4)-105.5(4)
N–C_b–N	110.0(6)	110.2(2)	109.5(2)	108.3(4)-108.4(4)
C_c–Ag–C_c	171.0-175.5	171.16(9)	173.0(1)	173.5(2)-175.2(2)

*reported by Kühn[173b], **a** contains 2 molecules in the asymmetric unit, **b** contains an intramolecular mirror plane, **c** contains an intramolecular inversion centre; C_c = carbene, C_b = bridge CH.

Since Au···Au or Ag···Ag interactions are considered responsible for luminescent properties of respective coinage metal complexes[136], the photophysical properties of all synthesized compounds were investigated at room temperature in solid state and in acetonitrile solution (see SI). The excitation wavelengths for all in this study reported gold complexes lie within the

UV range (below 400 nm) and can be attributed to π–π* ligand-centred (LC) transitions although they are significantly red-shifted and more intense in comparison to those of corresponding ligand precursors due to the influence of coordinated Au(I).[147] Unfortunately, no emission was observed upon excitation of the solution of Au bis(NHC) complexes in acetonitrile. Also in the solid state no luminescence was observed even for **$Au_2(HL3^{Mes})_2(PF_6)_2$** and **$Ag_2(HL3^{Mes})_2(PF_6)_2$**, which show weak metallophilic interactions. Tubaro *et al*. previously published a study of a series of Au bis(NHC) complexes with different metal centre separations, reporting that the compounds with shorter Au···Au distance not necessarily perform better in photoluminescence experiments.[148a] Apparently, cation/anion interactions, π–π stacking of the ligand and the nature of wingtip substituents play also an important role.[8b, 147-149] Furthermore, no evidence of π–π stacking was observed in solid-state packing for all compounds in this study.

4.1.1.3 Antiproliferative Activity

In the past decades gold(I) compounds emerged as alternative to conventional metal-based anti-cancer drugs (see Introduction, Section 1.4.3.2). Charged cationic Au NHC species have been reported to show remarkable selectivity for cancer cells[158b, 213], which makes them attractive study objects. Hereby, the steric and electronic properties of NHC ligands in corresponding complexes are crucial to selective cytotoxic properties.[12a, 12b]

Table 4.1.8. Cell viability IC_{50} values of screened Au(I) bis(NHC) complexes against human lung (A549) and liver (HepG2) tumour cells incubated for 48 h.

Complex	IC_{50} [μM]	
	A549	HepG2
$Au_2(HL3^{Me})_2(PF_6)_2$[a]	>100	69.4±6.2
$Au_2(HL3^{i\text{-}Pr})_2(PF_6)_2$[b]	>100	>100
$Au_2(HL3^{i\text{-}Pr})_2(BPh_4)_2$[c]	>100	>100
$Au_2(HL3^{Mes})_2(PF_6)_2$[a]	42.2±2.2	14.9±0.9

[a] syn, exo conformation; [b] a mixture of anti/syn isomers; [c] almost exclusively in anti, exo conformation

$Au_2(HL3^{R})(PF_6)_2$ (R = Me, *i*-Pr, Mes) and **$Au_2(HL3^{i\text{-}Pr})(BPh_4)_2$** have been evaluated for their cytotoxicity against human lung A549 and human liver HepG2 cancer cell lines. The obtained IC_{50} values are summarized in Table 4.1.8. **$Au_2(HL3^{Me})_2(PF_6)_2$** shows only moderate cytotoxic effects against HepG2, while being non-toxic in cancer cells A549. In addition, for

$Au_2(HL3^{i\text{-}Pr})_2(PF_6)_2$ and **$Au_2(HL3^{i\text{-}Pr})_2(BPh_4)_2$** no anti-proliferative effects have been observed (IC_{50} > 100 µM). However, a dose-dependent inhibition of cell growth is evident in both cell lines for **$Au_2(HL3^{Mes})_2(PF_6)_2$** with a significant increase in cytotoxicity for HepG2. Such differences between the complexes can be related to an effect commonly known for delocalized lipophilic cations.[12a, 214] An elevated mitochondrial membrane potential in carcinoma cells increases the level of accumulation of large liphophilic cations in mitochondria. Also a possibly easier transportation process though ion channels into a cell of a complex in a syn, exo conformation in comparison to anti, exo could play a certain role in increasing the cytotoxic properties, since also **$Au_2(HL3^{Me})_2(PF_6)_2$**, as a syn, exo isomer mainly, shows unexpectedly increased activity in HepG2. Notably, the corresponding ligand precursors, imidazolium hexafluorophosphates, show no cytotoxicity suggesting that the growth inhibition of cancer cells is likely the consequence of incorporation of metal cations.

Unfortunately, **$Au_2(HL3^{Mes})_2(PF_6)_2$** shows lower antiproliferative activity in A549 and HepG2 than literature-known, monometallic Au(I) bis(NHC) complexes (A549, IC_{50} = 3.2-55.6 µM) and HepG2, IC_{50} = 3.6-10.52 µM) as well as Auranofin and Cisplatin.[215] The moderate IC_{50} values of **$Au_2(HL3^{Mes})_2(PF_6)_2$** could be possibly linked to the low solubility of **$Au_2(HL3^{Mes})_2(PF_6)_2$** in aqueous medium. However, the IC_{50} values of homo-bimetallic Au(I) bis(NHC) complexes have been previously reported to vary extremely within different cancer cell lines.[10a] Therefore, it is conceivable that this complex could show greater potency in other cell types. In addition, the modification of hydrophilicity could be beneficial.

4.1.1.4 Reactivity of Au(I) 1,1'-(2-Hydroxyethane-1,1-diyl)-Bridge Functionalised Bis(NHC) Complexes with Bases

1,1'-(2-Hydroxyethane-1,1-diyl)-bridge functionalised bis(NHC) complexes of Au(I) offer an intriguing possibility of anchoring other biologically active molecules or metals to the hydroxyl-moieties in the ligand framework.

To explore this reactivity a series of NMR experiments have been performed using **$Au_2(HL3^{Me})_2(PF_6)_2$** and various bis(trimethylsilyl)amide bases.[203] LiN" reacted readily with **$Au_2(HL3^{Me})_2(PF_6)_2$** at 50 °C in THF yielding a precipitate, whose ^{1}H NMR spectrum indicated a formation of a symmetric compound. Further analysis by ^{29}Si NMR suggested a possible silylation of the hydroxyl-group instead of desired coordination to Li.[172, 177] Interestingly, by attempting to crystallise the deprotonation product an anti, exo isomer of **$Au_2(HL3^{Me})_2(PF_6)_2$** was obtained. Since this conformer was already present in small amounts in the initial sample, it is possible that only a major species, the syn, exo isomer, reacts with LiN".

Further studies with $FeN"_2(THF)$ confirmed the assumption that the bis(trimethylsilyl)amide bases silylate the hydroxyl-group of **$Au_2(HL3^{Me})_2(PF_6)_2$** complexes.[203] By treating

$Au_2(HL3^{Me})_2(PF_6)_2$ with one equivalent of $FeN"_2(THF)$ in THF at 50 °C a corresponding syn, exo isomer of silylated dinuclear Au(I) bis(NHC) complex have been isolated and characterised by SC-XRD. ^{29}Si NMR confirms the formation of this new compound as similar to the reaction of **$Au_2(HL3^{Me})_2(PF_6)_2$** with LiN" various resonances in positive region of the spectrum appear (7.65 ppm, 11.86 ppm, 32.33 ppm and 35.08 ppm).[172, 177] Such reactivity is not new, other authors also observed a silylation of different oxygen containing substrates by using LiN" as base in Pd-catalysed synthesis of aryl amines.[216] Also in these cases the reaction mixtures were heated to 65 °C, which probably facilitates the transfer of the TMS-group from N to O.

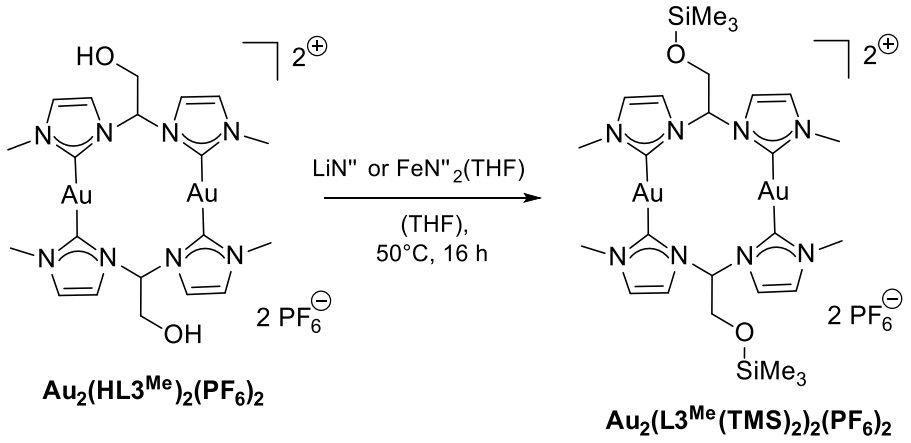

$Au_2(HL3^{Me})_2(PF_6)_2$ **$Au_2(L3^{Me}(TMS)_2)_2(PF_6)_2$**

Scheme 4.1.3. Reaction of **$Au_2(HL3^{Me})_2(PF_6)_2$** with bis(trimethylsilyl)amides bases.[203]

Based on these results and the literature it is obvious that deprotonation of the 1,1'-(2-hydroxyethane-1,1-diyl)-bridge functionalised bis(NHC) complexes of Au(I) with bis(trimethylsilyl)amide bases at elevated temperatures is unsuccessful regarding the goal of isolation of heterometallic compounds. Therefore, further experiments with congeners supported by mesityl and isopropyl *N*-substituted ligands would be more promising due to increased solubility in apolar solvents which would make the use of higher temperatures unnecessary. First exploratory experiments with **$Au_2(HL3^{i\text{-}Pr})_2(BPh_4)_2$** showed that although this complex does not react with $Li[Ce\{N(i\text{-}Pr)_2\}_4](THF)$ at RT in C_6H_6, a slow reaction was observed with KBn at RT in C_6H_6. However, the analysis of the products of the reaction indicate rather decomposition than the formation of desired compounds. Further experiments in this direction are necessary.

4.1.2 1,1'-(Prop-1-ene-1,3-diyl)-Bridge Functionalised Bis(NHC) Complexes of Ag(I) and Au(I) $M_2(L7^{Mes})_2(X)_2$

4.1.2.1 Synthesis of Ag(I) and Au(I) bis(NHC) Complexes

The ligand precursor $\mathbf{H_2(L7^{Mes})X_2}$ is an interesting precursor which offers an exciting possibility of formation of large delocalized system by deprotonation of the propenyl bridge. Since Pd is known to form very stable NHC and allyl complexes, this metal was chosen to explore this possibility. Various Pd(II) bis(NHC) complexes with longer alkyl bridges have been previously synthesized by Strassner *via* direct conversion of the corresponding imidazolium precursors with $Pd(OAc)_2$ or *via* transmetallation of the ligand from corresponding silver complexes.[217] Therefore, the same synthetic procedures were chosen for our system (Scheme 4.1.4).

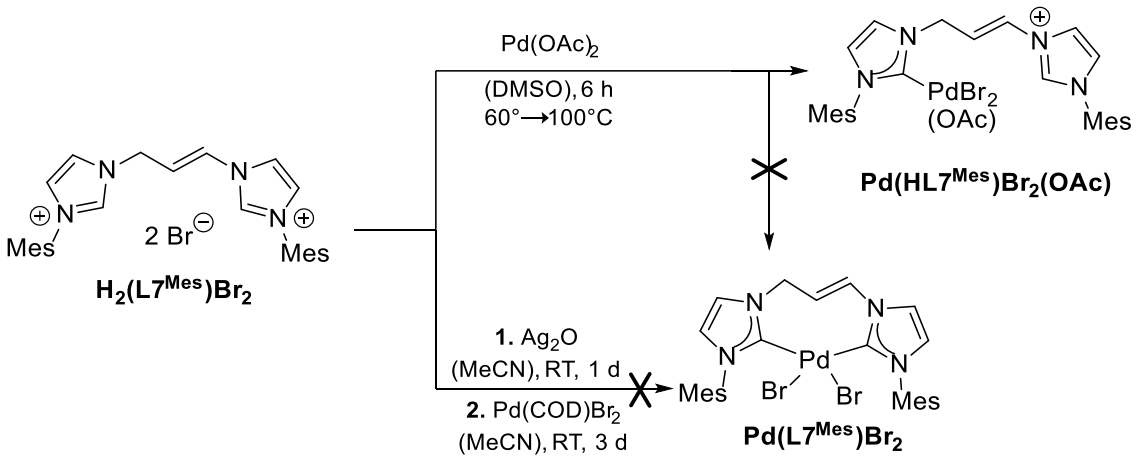

Scheme 4.1.4. Attempted synthesis of Pd(II) complexes supported by 1,1'-(prop-1-ene-1,3-diyl)-bridge functionalised bis(NHC) ligands.

Unfortunately, stirring the reactants in DMSO at 60-100 °C yields only singly deprotonated imidazolium species which cannot not be further separated from the crude product mixture. Further approach *via* transmetallation of NHC ligand from corresponding Ag(I) bis(NHC) complexes formed *in situ* is unsuccessful as well, as only various undistinguishable decomposition and maybe some Pd species are detected by ^{1}H NMR spectroscopy. Also here, the crude product cannot be further purified by any crystallization of precipitation procedures. In summary, it is quite likely that a formation of square planar complexes with Pd(II) is impeded by the rigidity of the propenyl-linker. Based on these first experiments a postsynthetic modification of dinuclear bis(NHC) complexes of Au(I) was considered as a more promising approach on the way to heterometallic allyl complexes.

Analogue to the silver complexes described above the dinuclear Ag(I) complexes supported by 1,1'-(prop-1-ene-1,3-diyl)-bridge functionalised bis(NHC) ligand have been synthesized applying silver base route (Scheme 4.1.5). All bulk material has been characterised by

multinuclear NMR spectroscopy, elemental analysis and ESI-MS. ^{1}H NMR spectra of the obtained products indicates though unusual splitting pattern of the resonances the presence of two conformers formed by different modes of linking of two ligands to silver centres. However, due to dynamic nature of the complexes the chemical shift between two species is not as clearly distinguishable as in case of corresponding Au complexes (see below).

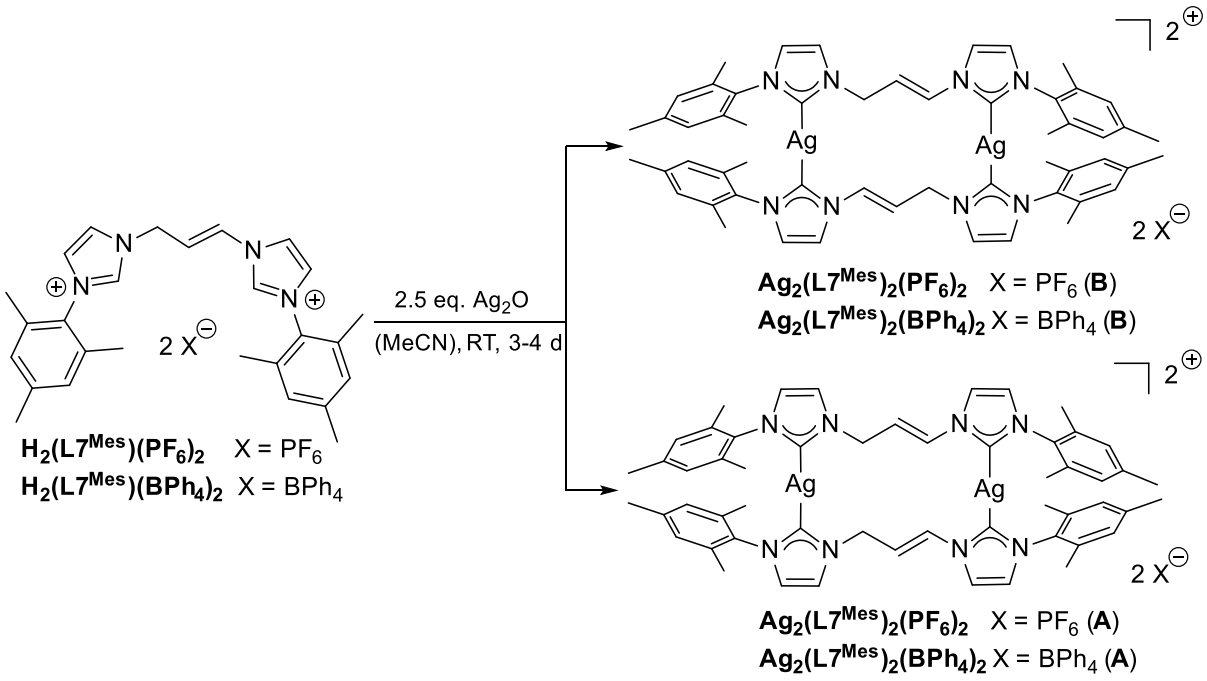

Scheme 4.1.5. Synthesis of Ag(I) 1,1'-(prop-1-ene-1,3-diyl)-bridge functionalised bis(NHC) complexes.

To confirm the results and gain better insight into the molecular structure of the complexes SC-XRD experiment was performed on the crystals obtained by slow diffusion of E_2O into a solution of **Ag$_2$(L7^{Mes})$_2$(PF$_6$)$_2$** in acetonitrile at RT. The ORTEP style representation of the cation of **Ag$_2$(L7^{Mes})$_2$(PF$_6$)$_2$**, which crystallises in orthorhombic space group *Pbcn*, is shown in Figure 4.1.10. In this case the conformer **B** is obtained. Due to rigidity of the bridge the compound is strongly folded along the axis between two imidazol-2-ylidenes lying criss-cross from each other. Nevertheless, all bond angles and distances in the ligand framework are comparable to other Ag(I) bis(NHC) complexes reported in this thesis and in the literature.[9a, 173b] Also C_C–Ag–C_C bond angle does not deviate too much from linearity. Furthermore, as expected, the Ag···Ag separation is too big for any interaction (5.277(1) Å).

A transmetallation to analogue Au(I) bis(NHC) compounds have been performed in acetonitrile at RT temperature as well (Scheme 4.1.6). In this case according to NMR spectroscopy a formation of two conformers is unambiguous due to more static nature of the complexes. All bulk material has been further characterised by ESI-MS and elemental analysis.

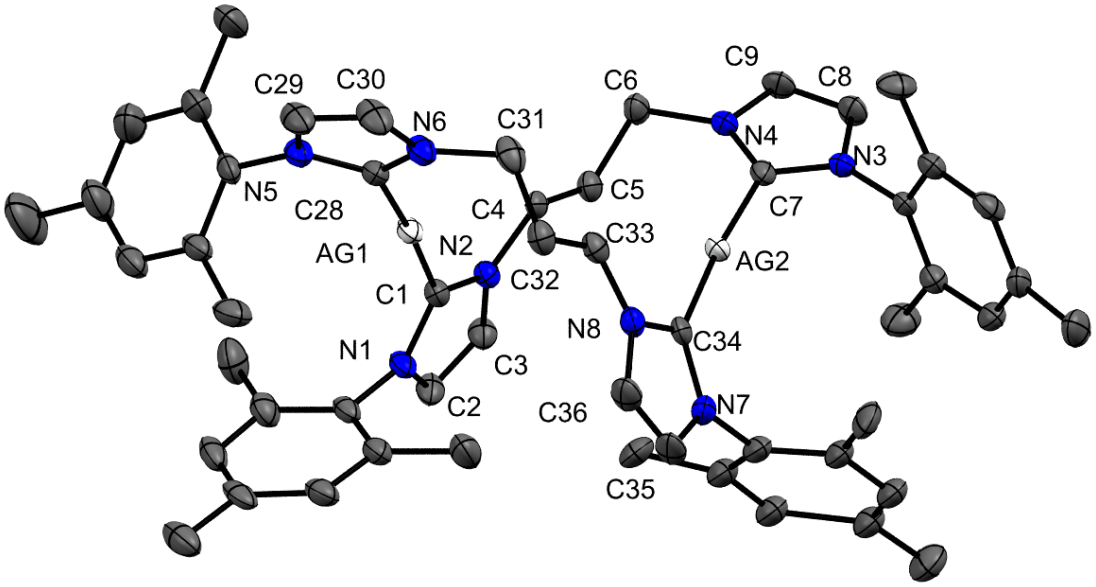

Figure 4.1.10. ORTEP style representation of the cation of **$Ag_2(L7^{Mes})_2(PF_6)_2$** with ellipsoids at 50 % probability. Hydrogen atoms, PF_6^- and co-crystallised acetonitrile molecules are omitted for clarity. Selected bond lengths [Å] and bond angles [deg]: Ag–C_C 2.067(5)-2.076(5), N–C_C 1.346(6)-1.363(6), N–C6/C31 1.471(6)-1.478(6); C5/C31–C6/C32 1.495(6)-1.496(7), C4/C32–C5/C33 1.323(7)-1.326(7), N–C4/C33 1.406(6)-1.441(5), N–C_C–N 104.2(4)-105.0(4), C_C–Ag–C_C 175.0(2)-176.0(2).

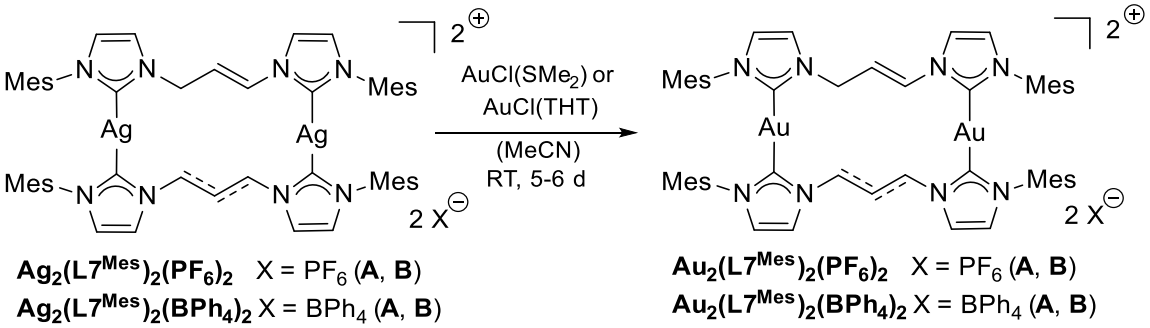

Scheme 4.1.6. Synthesis of **$Au_2(L7^{Mes})_2(X)_2$** complexes.

Single crystals of **$Au_2(L7^{Mes})_2(PF_6)_2$** have been grown by slow diffusion of Et_2O into the solution of conformer mixture in acetonitrile at RT. **$Au_2(L7^{Mes})_2(PF_6)_2$** crystallises as symmetric **B** conformer in orthorhombic space group *P bcn* as well. It is also folded analogue to respective silver compound along the axis between two criss-cross imidazol-2-ylidenes (Figure 4.1.11). Despite this the C_C–Au–C_C angles are nearly linear. Furthermore, all bond distances and bond angles are also comparable to other Au(I) bis(NHC) compound reported in this thesis and in the literature.[10b, 125, 148] Similar to **$Ag_2(L7^{Mes})_2(PF_6)_2$** the Au···Au distance (5.410(1) Å) is too great for an aurophilic interaction.

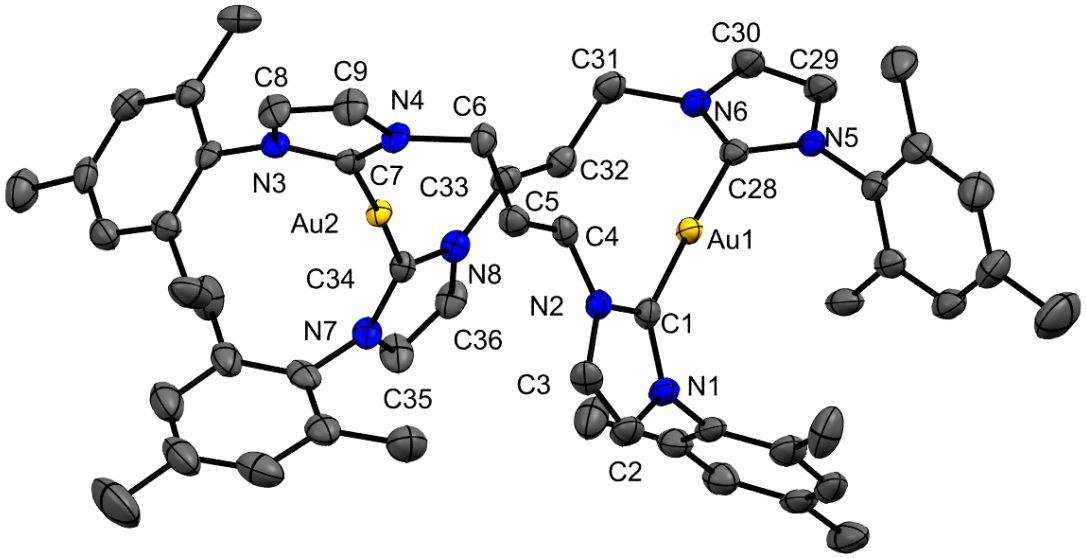

Figure 4.1.11. ORTEP style representation of the cation of **$Au_2(L7^{Mes})_2(PF_6)_2$** with ellipsoids at 50 % probability. Hydrogen atoms, PF_6^- and co-crystallised acetonitrile molecules are omitted for clarity. Selected bond lengths [Å] and bond angles [deg]: Au–C_C 2.019(5)-2.026(5), N–C_C 1343(6)-1.370(6), N–C6/C311.489(6)-1.490(6); C5/C31–C6/C32 1.500(7), C4/C33–C5/C32 1.315(7)-1.320(7), N–C4/C33 1.413(6)-1.423(6), N–C_C–N 104.7(4)-105.3(4), C_C–Au–C_C 177.1(2).

4.1.2.2 Reactivity of 1,1'-(Prop-1-ene-1,3-diyl)-Bridge Functionalised bis(NHC) Complexes with Bases

A series of reaction on explorative NMR scale towards deprotonation of the allyl bridge of **$Au_2(L7^{Mes})_2(PF_6)_2$** using Pd(II) bases ($Pd(OAc)_2$ or $Pd(acac)_2$) and well external base/$PdCl_2$ systems in acetonitrile have been conducted.[203] The mild Pd bases were not strong enough to induce the deprotonation even at 90 °C. A Cs_2CO_3/$PdCl_2$ system suggested a transmetallation of the NHC ligand to Pd under formation of mono(imidazolium) compounds at 45 °C-90 °C; at RT no reaction was observed. The use of a system with stronger basicity, KN"/$PdCl_2$, indicated a reaction already at 45 °C. However, the characterization of the obtained product was impeded by the insolubility of the obtained crude product in acetonitrile or THF. Therefore, further experiments with other transition metal systems are necessary.

4.2 Conclusion and Outlook

Formation of different conformers of dinuclear silver(I) and gold(I) 1,1'-(2-hydroxyethane-1,1-diyl)-bridge-functionalised bis(NHC) complexes with various wingtip substituents (R = methyl, isopropyl and mesityl) has been investigated by using multinuclear NMR spectroscopy, SC-XRD and DFT calculations. The ratio of anti/syn isomers strongly depends both on wingtip substituents and the metal centre. Moreover, the reaction temperature plays a significant role during the transmetallation process for the ratio of gold(I) conformers, which are further affected by purification procedures. The 1,1'-(2-hydroxyethane-1,1-diyl)-bridge-functionalised bis(NHC) complexes of Au(I) counterbalanced by PF_6 anions have been applied in a standard MTT assay performed for screening the antiproliferative activity against human lung and liver cancer cells. An application of sterically hindered mesityl wingtip substituents shows hereby the best results. Likely, the fine-tuning of lipophilicity and conformational isomerism are crucial for designing gold bis(NHC) based anti-cancer drugs. Since isomer formation could be further significantly influenced by purification procedures, an investigation towards the selective application of the different isomers should be conducted.

The experiments towards further functionalization of the OH group in the bridge are an interesting approach. It might be possible to couple a biological marker and other metals, which are known to inhibit the tumour cell growth to that functionality. Also the possibility of inducing stronger aurophilic interactions by further modifying the bridge and wingtip substituents is worth of the investigation. Such modification could enhance the natural luminescent properties of Au(I)-NHC complexes for visualizing its intracellular distribution.[10a]

First preliminary results in the experiments with $\mathbf{Au_2(HL3^{Me})_2(PF_6)_2}$ and bis(trimethylsilylamide)bases of alkali metals and iron(II) aimed on modification of the bridge show a high preference for the transfer of the TMS group to the hydroxyl-group of the ligand. Since higher reaction temperatures were necessary in these cases due to low solubility of $\mathbf{Au_2(HL3^{Me})_2(PF_6)_2}$ in THF, further experiments with more soluble analogues $\mathbf{Au_2(HL3^{R})_2(X)_2}$ (R = *i*-Pr, Mes) are considered to be more promising. Also the application of other bases is conceivable.

Although it was not possible to obtain Pd(II) complexes supported by 1,1'-(prop-1-ene-1,3-diyl)-bridge functionalised bis(NHC) ligands, novel dinuclear bis(NHC) complexes of Ag(I) and Au(II) were readily isolated and fully characterised by multinuclear NMR spectroscopy, ESI-MA, EA and SC-XRD. Due to rigidity of the bridge these compounds exhibit interesting folded structure in the solid state. A post-synthetic modification of the bridge towards deprotonation and the formation of large delocalized NHC-allyl-NHC system supporting heterometallic Au(I)/Pd(II) complexes was attempted using various Pd(II) internal bases and systems

comprising of Pd(II) salts and various external bases. It is clear that mild bases such as $Pd(OA)_2$, $Pd(acac)_2$ and Cs_2CO_3 are not sufficiently strong enough to induce the deprotonation. Further experiments with stronger bases are therefore necessary.

Chapter 5

Experimental Section

5.1 General Procedures

5.1.1 Schlenk Technique

Unless otherwise stated, all syntheses were carried out under argon atmosphere using standard Schlenk and glove box techniques. Anhydrous benzene was obtained from commercial suppliers. All other solvents were dried via a MBraun MB SPS purification system; where necessary degassed by three freeze-pump-thaw cycles and stored over 4 Å molecular sieves and argon atmosphere. Deuterated solvents were purchased from *Eurisotop* and if necessary dried over elemental potassium and distilled prior to use.

5.1.2 NMR Spectroscopy

1H NMR spectra were recorded on a Bruker AV400US with broad band probe and a gradient coil (^{1}H NMR, 400.13 MHz), a Bruker DRX-400 spectrometer with broad band probe (^{1}H NMR, 400.13 MHz) and a Bruker Avance III 500 with DHC dual cryoprobe (^{1}H NMR, 500.12 MHz) and Bruker Avance III 500 with prodigy cryoprobe (^{1}H NMR, 500.12 MHz). ^{13}C NMR spectra were run on a Bruker AV400US (^{13}C NMR, 100.53 MHz), a Bruker DRX-400 spectrometer (^{13}C NMR, 100.61 MHz), a Bruker Avance III 500 with DCH dual cryoprobe (^{13}C NMR, 125.77 MHz). ^{7}Li NMR were recorded on a Bruker DRX-400 spectrometer with broad band probe (^{7}Li NMR, 155.52 MHz) and on a Bruker Avance III 500 with prodigy cryoprobe (^{7}Li NMR, 194.40 MHz) ^{29}Si INEPT NMR spectra were run on Bruker AV500C QNP Cryo probe (^{29}Si INEPT-NMR, 99.41 MHz), on a Bruker AV400US (^{29}Si INEPT-NMR, 79.49 MHz) and Bruker Avance III 500 with prodigy cryoprobe (^{29}Si INEPT-NMR, 99.37 MHz). DOSY spectra were recorded on Bruker AVHD400 (^{1}H NMR, 400.13 MHz). If necessary, 2D-experimetns were used for a correct assignment of the signals. HH-COSY NMR, HSQC NMR, NOESY and DOSY were run either on Bruker AV400US or on Bruker DRX-400 spectrometers (^{1}H NMR, 400.13 MHz; ^{13}C NMR, 100.62 MHz). Chemical shifts (δ) are reported relative to the residual signal of the deuterated solvent. The following abbreviation were used for the characterization of NMR spectra: s – singlet, d –doublet, t – triplet, q – quartet, p – pentet, hept – heptet, br – broad, virt – virtual, dd – doublet of doublets, dt – doublet of triplets, m – multiplet. NMR spectra were analysed by using MestReNova© (Version 8.0.0.-10524, Mestrelab Research S.L.).

5.1.3 Elemental Analysis

Elemental analyses were carried out by the microanalytical laboratory at the Technical University of Munich. All values are given in per cent.

5.1.4 Mass Spectrometry

FAB+ mass spectra were collected at Finnigan MAT 90. ESI mass spectrometry was performed at Thermo Scientific LCQ Fleet Spectrometer. A time-of-flight analyser was used for mass detection. As eluent a mixture of acetonitrile and formic acid (0.1 Vol.%) was used.

5.1.5 UV/VIS Spectroscopy

UV-VIS spectra were recorded at Agilent Cary 60 Spectrometer. The molar extinction coefficient is given $L \cdot mol^{-1} \cdot cm^{-1}$.

5.1.6 Fluorescence Spectroscopy

For luminescence experiments, the samples in solution were placed in fluorimetric 1 cm path quartz cuvettes and the solid state samples (powder) were placed in a covered quartz laboratory dish. Uncorrected emission spectra were obtained with a Hamamatsu C11347 Absolute PL Quantum Yield Spectrometer.

5.1.7 DFT-Calculations

DFT calculations were performed by B.Sc. David Mayer and Dr. Marcus Drees from the group of Prof. Roland A. Fisher at Technische Universität München.

All calculations were carried out using the Gaussian 09 package.[218] To ensure the comparability to the already published results[173b], the density functional ωB97x-D[219] and the method PM6[220] as well as the basis sets 6-31+g(d), 6-311++g(d,p)[221] and LANL3DZ[221a, 222] (incl. ECP for metals) were employed as implemented.

Suitable input geometries were based on molecular structures obtained by SC-XRD, as available. To achieve atomic coordinates for the remaining isomers of silver and gold bis(NHC) complexes, the crystallographic data was slightly modified using GaussView 5. The coordinates were pre-optimized on the PM6 theory of level and then refined employing a double zeta basis set (6-31+g(d) for non-metals and LANL3DZ for metals). All optimized geometries were checked by frequency determination for negative eigenfrequencies, corresponding to the local minima on potential energy hypersurface. The optimized parameters using DFT approach have been compared with the mean experimental bonding lengths and are in excellent agreement with them (see Table 4.1.3, Chapter 4, Section 4.1.1.1).

NMR chemical shifts were calculated at the ωB97x-D/6-311++g(d,p) level using a GIAO (gauge independent atomic orbital) approach.[223] Absolute isotropic magnetic shielding constants were transformed into chemical shifts by referring to TMS (tetramethylsilane, 30.59 ppm for CH_3CN and 30.52 ppm for DMSO).

To display the solvent behaviour, the optimization, frequency and NMR-shielding calculations were all performed using an SCRF ansatz with an implicit solvent model (SMD, as recommended by Truhlar and Cramer, c.p.).[224]

5.1.8 SC-XRD Crystallography

X-ray structural analyses were carried out by Dr. Alexander Pöthig and M.Sc. Christian Jandl at the Sc-XRD laboratory of TUM Catalysis Research Centre.

Data were collected on single crystal X-ray diffractometers equipped with one of the following setups using the APEXII or APEXIII software package: A CCD detector (APEX II, *κ*-CCD), a fine-focus sealed tube and a graphite monochromator (**A**, **B**, **C**); a CCD detector (APEX II, *κ*-CCD), a fine-focus sealed tube and a Triumph monochromator (**A**, **B**, **C**); a CCD detector (APEX II, *κ*-CCD), a FR591 rotating anode and a Montel mirror optic (**A**, **B**, **C**); a CMOS detector (APEX III, *κ*-CMOS), an IMS microsource and a Helios optic (**A**, **B**, **C**); a CMOS detector (APEX III, *κ*-CMOS), a TXS rotating anode and a Helios optic (**A**, **B**, **C**).[225] For all measurements MoK_α radiation (λ = 0.71073 Å) was used. The crystals were fixed on the top of a glass fibre or kapton micro sampler with perfluorinated ether, transferred to the diffractometer and frozen under a stream of cold nitrogen. A matrix scan was used to determine the initial lattice parameters. Reflections were merged and corrected for Lorentz and polarization effects, scan speed, and background using SAINT.[226] Absorption corrections, including odd and even ordered spherical harmonics were performed using SADABS.[226] Space group assignments were based upon systematic absences, *E* statistics, and successful refinement of the structures. Structures were solved using direct methods (SHELXL-97) or intrinsic phasing (SHELXT) with the aid of successive difference Fourier maps, and were refined against all data using the APEXII or APEX III software package in conjunction SHELXL-2014 and SHELXLE. [225, 227] Hydrogen atoms were calculated in ideal positions as follows: Methyl hydrogen atoms were refined as part of rigid rotating groups, with a C–H distance of 0.98 Å and $U_{iso(H)} = 1.5 \cdot U_{eq(C)}$. Other H atoms were placed in calculated positions and refined using a riding model, with methylene and aromatic C–H distances of 0.99 Å and 0.95 Å, respectively, other C–H distances of 1.00 Å and $U_{iso(H)} = 1.2 \cdot U_{eq(C)}$. Non-hydrogen atoms were refined with anisotropic displacement parameters. Full-matrix least-squares refinements were carried out by minimizing $\Sigma w(F_o^2-F_c^2)^2$ with the SHELXL-97 weighting scheme.[227a] Neutral

atom scattering factors for all atoms and anomalous dispersion corrections for the non-hydrogen atoms were taken from *International Tables for Crystallography*.[228] A split layer refinement was used to treat with disordered anion/solvent molecules and additional SIMU, DELU and SAME restraints were employed to stabilize the refinement of the layers. In case of unrefinably disordered solvent molecules (e.g. on special positions) these were treated as a diffuse contribution to the overall scattering without specific atom positions using the PLATON/SQUEEZE procedure.[229] Images were created with Mercury 3.8.[230]

5.1.9 MTT-Assay

The cell toxicity studies were performed by M.Sc. Wolfgang Heydenreuter and M.Sc. Jonas Drechsel from the group of Prof. Dr. Stephan A. Sieber at Technical University of Munich.

The assay was performed in 96 well plates. A549/HepG2 cells were grown to 30-40 % confluence. The medium was removed and 100 µL medium/well containing 1 µL DMSO compound stock were added to the cells and incubated for 48 h. All concentrations as well as a DMSO control were done in triplicates. 20 µL Thiazolyl Blue Tetrazolium bromide (5 mg/mL in PBS, Sigma Aldrich) were added to the cells and incubated for 2-4 h until complete consumption was observed. After removal of the medium, the resulting formazan was dissolved in 200 µL of DMSO. Optical density was measured at 570 nm (562 nm) and background subtracted at 630 nm (620 nm) by a TECAN Infinite® M200 Pro.

For calculation of IC_{50} values, residual viabilities for the respective compound concentration were fitted to

$$V = \frac{100}{1 + 10^{(\log(IC_{50}) - \log(c)) \cdot N}}$$

V: viability [%]; c: Inhibitor concentration [M]; N: Hill slope

using Graphpad Prism 6.0.

5.2 Synthetic Procedures

5.2.1 General

All chemicals and solvents were purchased from common commercial suppliers or the stock room of Technische Universität München and used without further purification. $LiN(SiMe_3)_2$ was obtained as solid material from commercial suppliers and recrystallised before use from hexanes at –26 °C. 2-(*tert*-butyl)furan[180], 4,5-dimethylimidazole[181], 1-(furan-2-yl)imidazole[178], 1-mesitylimidazole[32b], 1-isopropylimidazole[231], 2,2-dichloroethanol[232], 4-bromo-2,4,6-tri-*tert*-butylcyclohexa-2,5-dien-1-one[233], 2-bromomethyl-4,6-di-*tert*-butylphenol[234], 1,1'-methylenebis(3-(furan-2-yl)imidazolium bromide **$H_2(L5^{Fu})Br_2$**[178], 1,1'-methylenebis(3-(furan-2-yl)imidazolium hexafluorophosphate **$H_2(L5^{Fu})(PF_6)_2$**[178], 1,1'-(2-hydroxyethane-1,1-diyl)bis(3-methylimidazolium) chloride **$H_3(L3^{Me})Cl_2$**[173a], *N*-(3,5-di-*tert*-butyl-2-salicyl)-imidazole[183b], 3-(3,5-di-*tert*-butyl-2-hydroxyphenyl)-1-methylimidazolium bromide **$H_2(L1^{Me})Br_2$**[168a], 3-(3,5-di-*tert*-butyl-2-hydroxyphenyl)-1-mesitylimidazol-3-ium bromide **$H_2(L1^{Mes})Br_2$**[168b], 1,3-bis(3,5-di-*tert*-butyl-2-hydroxybenzyl)imidazolium bromide **$H_3(L2)Br_2$**[183b], NaCp[235], $K(CH_2Ph)$[236], $[Ce\{N(SiMe_3)_2\}_3]$[237], $Ce(BH_4)_3(THF)_2$[238], $CeCp_3$[239], $Li[Ce\{N(i\text{-}Pr)_2\}_4](THF)$[205], $Sc(CH_2Ph)(THF)_3$[240], $[Fe\{N(SiMe_3)_2\}_2\cdot(THF)]$[241] were synthesized according to the respective literature procedures. YCp_3 was provided by the group of Polly L. Arnold. $CeCl_3(THF)_2$, $CeI_3(THF)_{2.5}$ and $ScCl_3(THF)_3$ were obtained by stirring the corresponding rare earth halide hydrate with an excess of Me_3SiCl or Me_3SiI respectively in THF overnight and isolated by filtration, washing with THF and drying under dynamic vacuum.

$KN(SiMe_3)_2$

6.0 g (149.6 mmol, 1.0 eq.) of potassium hydride is suspended in 150 mL of toluene. 20.0 g (124.0 mmol, 0.8 eq.) of hexamethyldisilazane is added to the mixture at room temperature. The white suspension is stirred for 2 hours. The solution is filtered off and the amount of toluene is reduced *in vacuo*. After the storage of the solution at −26 °C for 2 days a formation of white precipitate is observed. The product is filtered off and dried under dynamic vacuum. Yield: 10.88 mg (44 %).

^{1}H NMR (400 MHz, Benzene-d_6) δ 0.14 (s, 18H, $SiMe_3$).

^{13}C{^{1}H} NMR (126 MHz, C_6D_6) δ 7.22 ($SiMe_3$).

^{29}Si INEPT NMR (99 MHz, C_6D_6) δ −20.60 ($SiMe_3$).

Lithium diisopropylamide

To a solution of 9.25 mL (93.3 mmol, 1.0 eq.) of diisopropylamine in 10 mL of hexane 26.13 mL of a solution of *n*-BuLi 2.5 M in hexanes is slowly added at −78 °C. The suspension is slowly warmed up to room temperature and stirred for 2 days. Subsequently the amount of solvent is reduced to 5 mL *in vacuo*. The white precipitate is separated by filtration, washed with hexane and dried under dynamic vacuum. The compound is obtained as white solid. Yield: 6.48 g (92.5 %). ^{1}H NMR spectrum shows two sets of resonances in a ratio of 1:2 resulting from a coexistence of two different species: tetramer **1** and trimer **2**.[242]

^{1}H NMR (400 MHz, C_6D_6) δ 3.13 (virt p, $^{3}J_{HH}$ = 6.3 Hz, 2H, NCH (**1**)), 3.03 (virt p, $^{3}J_{HH}$ = 6.5 Hz, 2H, NCH (**2**)), 1.16 (d, $^{3}J_{HH}$ = 6.0 Hz, 12H, CH_3 (**1**)), 1.12 (d, $^{3}J_{HH}$ = 6.1 Hz, 12H, CH_3 (**2**)).

5.2.2 Synthetic Procedures Described in Chapter 2

5.2.2.1 Reactivity Studies with *N*-(3,5-Di-*tert*-butyl-2-hydroxyphenyl) and *N*-(3,5-Di-*tert*-butyl-2-hydroxybenzyl) Functionalised Imidazolium Salts $H_2(L1^R)Br$ and $H_3(L2)Br$

Route **A**

Unless otherwise stated 1.0 eq. of imidazolium salt and 2.0 eq. (for **$H_2(L1^R)Br$**) or 3.0 eq. (for **$H_3(L2)Br$**) of the base (NaN" or KN") are placed into a J-Young NMR tube and 0.6 mL of THF-d_8 is added at RT. An overview of the conducted experiments is given in Table 5.2.1.

$Na(L1^{Me})$

Experiment No. 1 (Table 5.2.1). The reaction is complete after 1 hour at RT yielding a rose solution. Yield: quant. After 2 days two species are visible in a ratio of 0.2:1.0 (**A**:**B**).

^{1}H NMR (400 MHz, THF-d_8) δ 7.46 (d, $^{3}J_{HH}$ = 1.9 Hz, 1H, N*CH*CHN, **A**), 7.04 (d, $^{3}J_{HH}$ = 2.8 Hz, 1H, NCH*CH*N, **A**), 6.97 (d, $^{3}J_{HH}$ = 1.6 Hz, 1H, N*CH*CHN, **B**), 6.94 (virt d, $^{4}J_{HH}$ = 1.5 Hz, 2H, Ar-H, **A** and **B**), 6.74 (virt d, $^{4}J_{HH}$ = 2.7 Hz, 2H, Ar-H, **A** and **B**), 3.47 (s, 3H, CH_3, **B**), 2.55 (s, 3H, CH_3, **A**), 1.47 (s, 9H, *t*-Bu, **A**), 1.44 (s, 9H, *t*-Bu, **B**), 1.36 (s, 9H, *t*-Bu, **A**), 1.24 (s, 9H, *t*-Bu, **B**).

^{13}C{^{1}H} NMR (101 MHz, THF) δ 163.65 (NC*C*O, **A**), 162.57 (NC*C*O, **B**), 148.25 (N*C*CO, **A**), 147.61 (CH(*t*-Bu)*C*CH, **A**), 143.53 (CH(*t*-Bu)*C*CO, **A**), 139.13 (N*C*CO, **B**), 133.83 ((*t*-Bu)C*CH*C(*t*-Bu), **A**), 131.11 (NC*CH*C(*t*-Bu), **A**), 129.03 (CH(*t*-Bu)*C*CH and CH(*t*-Bu)*C*CO, **B**), 122.39 ((*t*-Bu)C*CH*C(*t*-Bu), **B**), 121.91 (N*CH*CHN, **B**), 120.71 (NCH*CH*N, **B**), 119.10 (NCH*CH*N, **A**), 118.89 (NC*CH*C(*t*-Bu), **B**), 114.76 (N*CH*CHN, **A**), 37.77 (CH_3, **B**), 36.31

(*C*(CH_3)$_3$, **B**), 35.66 (*C*(CH_3)$_3$, **A**), 35,10 (*C*(CH_3)$_3$, **A**), 34.33 (*C*(CH_3)$_3$, **B**), 32.57 (C(*C*H_3)$_3$, **A**), 32.28 (C(*C*H_3)$_3$, **B**), 30.61 (C(*C*H_3)$_3$, **A**), 30.34 (C(*C*H_3)$_3$, **B**), 14.28 (CH_3, **A**).

^{29}Si INEPT NMR (99 MHz, THF) δ 1.96 (HN(Si(CH_3)$_3$)$_2$), −11.97 (Na N(Si(CH_3)$_3$)$_2$).

K(L1^{Me})

Experiment No. 2 (Table 5.2.1). The reaction is complete after 1 hour at RT yielding a yellow solution. Yield: quant.

^{1}H NMR (400 MHz, THF-d_8) δ 7.02 (d, $^{3}J_{HH}$ = 2.8 Hz, 1H, N*CH*CHN), 6.91 – 6.88 (m, 2H, Ar-H), 6.73 (d, $^{3}J_{HH}$ = 2.8 Hz, 1H; NCH*CH*N), 3.71 (s, 3H, CH_3), 1.42 (s, 9H, *t*-Bu), 1.22 (s, 9H, *t*-Bu).

^{13}C{^{1}H} NMR (101 MHz, THF) δ 212.67 (N*C*N), 163.54 (NC*C*O), 138.80 (N*C*CO), 132.09 (CH(*t*-Bu)*C*CH), 128.06 (CH(*t*-Bu)*C*CO), 123.61 (N*CH*CHN), 122.42 ((*t*-Bu)C*CH*C(*t*-Bu)), 122.40 (NCH*CH*N), 118.85 (NC*CH*C(*t*-Bu)), 38.27 (CH_3), 38.25 (CH_3), 36.30 (*C*(CH_3)$_3$), 34.38 (*C*(CH_3)$_3$), 32.75 (C(*CH*$_3$)$_3$), 30.62 (C(*CH*$_3$)$_3$).

^{29}Si INEPT NMR (99 MHz, THF) δ 1.90 (HN(Si(CH_3)$_3$)$_2$).

K(L1^{Mes})

Experiment No. 4 (Table 5.2.1). The reaction is complete after 1 h at RT. Yield: quant.

^{1}H NMR (400 MHz, THF-d_8) δ 7.10 (s, 1H, Ar-H), 7.02 (s, 1H, N*CH*CHN), 6.92 (s, 2H, H_{Mes}), 6.83 (s, 1H, NCH*CH*N), 6.80 (s, 1H, Ar-H), 2.29 (s, 3H, *para*-CH_3), 2.06 (s, 6H, *ortho*-CH_3), 1.42 (s, 9H, *t*-Bu), 1.24 (s, 9H, *t*-Bu).

^{13}C{^{1}H} NMR (101 MHz, THF-d_8) δ 163.79 (NC*C*O), 140.32 (N*C*CO), 138.80 (*ortho*-CH_3C*C*N), 137.41 (*para*-*C*CH_3), 136.38 (*ortho*-CH_3*C*CN), 131.67 (CH(*t*-Bu)*C*CH), 129.26 (CH(*t*-Bu)*C*CO), 126.88 (CH_{Mes}), 123.52 ((*t*-Bu)C*CH*C(*t*-Bu)), 122.14 (NCH*CH*N and N*CH*CHN), 119.02 (NC*CH*C(*t*-Bu)), 36.22 (*C*(CH_3)$_3$), 34.25 (*C*(CH_3)$_3$), 32.70 (C(*C*H_3)$_3$), 30.39 (C(*C*H_3)$_3$), 21.09 (*para*-CH_3), 18.40 (*ortho*-CH_3).

^{29}Si INEPT NMR (99 MHz, THF-d_8) δ 1.90 (HN(Si(CH_3)$_3$)$_2$).

K(L2)

Experiment No. 6 (Table 5.2.1). The reaction is complete after 30 min at RT. Yield: quant.

^{1}H NMR (400 MHz, THF-d_8) δ 7.00 (br s, 4H, Ar-*CH*), 6.81 (s, 2H, N*CHCH*N), 4.95 (s, 4H, CH_2), 1.33 (s, 18H, *t*-Bu), 1.22 (s, 18H, *t*-Bu).

$^{13}C\{^{1}H\}$ NMR (101 MHz, THF-d_8) δ 212.76 (NCN), 168.69 (NCCO), 137.31 (NCCO), 128.95 (CH(*t*-Bu)CCH), 126.43 ((*t*-Bu)C*CH*C(*t*-Bu)), 126.11 (CH(*t*-Bu)CCO), 123.96 (NC*CH*C(*t*-Bu)), 118.78 (N*CHCH*N), 55.58 (CH_2), 36.08 ($C(CH_3)_3$), 34.39 ($C(CH_3)_3$), 32.80 ($C(CH_3)_3$), 30.35 ($C(CH_3)_3$).

^{29}Si INEPT NMR (99 MHz, THF-d_8) δ 4.77, 1.90 ($HN(Si(CH_3)_3)_2$), –20.73 ($KN(Si(CH_3)_3)_2$).

Table 5.2.1. Overview of the NMR scale reactions aimed on the investigation of reactivity of *N*-(3,5-di-*tert*-butyl-2-hydroxyphenyl) and *N*-(3,5-di-*tert*-butyl-2-hydroxybenzyl) functionalised imidazolium bromides with alkali metal bis(trimethylsilyl)amides.

Ex. No.	Compound	Amount of the pro-ligand	Amount of the base		Solvent
			NaN"	KN"	
1	**$H_2(L1^{Me})Br$**	20.0 mg (6.96×10^{-5}mol)	25.5 mg (1.39×10^{-4}mol)		THF-d_8
2		20.0 mg (6.96×10^{-5}mol)		27.7 mg (1.39×10^{-4}mol	THF-d_8
3	**$H_2(L1^{Mes})Br$**	20.0 mg (4.24×10^{-5}mol)	15.6 mg (8.48×10^{-5}mol)		THF-d_8
4		20.0 mg (4.24×10^{-5}mol)		16.9 mg (8.48×10^{-5}mol)	THF-d_8
5	**$H_3(L2)Br$**	14.7 mg (2.51×10^{-5}mol)	13.8 mg (7.53×10^{-5}mol)		THF-d_8
6		15.0 mg (2.56×10^{-5}mol)		15.3 mg (7.68×10^{-5}mol)	THF-d_8

Route **B**: Preparatory Scale

In a Schlenk tube 1.0 eq. of **$H_3(L2)Br$** is treated with 3.0 eq. of KN" at various reaction conditions. Subsequently, the precipitate is separated by filtration and the crude product is obtained by evaporation of the solvent. An overview of the conducted experiments is given in Table 5.2.2. The purification of the crude product obtained in Ex. No. 3 is attempted by washing with toluene.

Table 5.2.2. Overview of the experiments aimed on the isolation of potassium NHC adduct derived from **H_3(L2)Br**.

Ex. No.	Amount of **H_3(L2)Br**	Amount of KN"	Reaction conditions
1	500.0 mg (0.85 mmol)	510.9 mg (2.56 mmol)	RT, 18 h
2	500.0 mg (0.85 mmol)	510.9 mg (2.56 mmol	RT, 2.5 h
3	500.0 mg (0.85 mmol)	519.5 mg (2.60 mmol	–78 °C, 2.5 h

5.2.2.2 Synthesis and Reactivity Studies of 1,1'-(2-hydroxyethane-1,1-diyl)-Bridge Functionalised Bis(imidazolium) Salts $H_3(L3^R)X_2$

General Procedure for the Synthesis of 1,1'-(2-Hydroxyethane-1,1-diyl)-Bridged Bis(imidazolium) Salts **$H_3(L3^R)X_2$**

The synthesis of this ligand class is based on the preparation of **$H_3(L3^{Me})Cl_2$**.[173a]

*General Procedure for the Synthesis of **$H_3(L3^R)Cl_2$***

1.0 eq. of 2,2-dichloroethanol and 3.0 eq. of respective substituted imidazole are placed in an ACE pressure tube and non-dried toluene is added to the mixture. The tube is sealed under air and the reaction mixture is stirred at 135 °C for a specified amount of time. Subsequently the hot brown suspension is filtered off and the precipitate is washed with MeCN and Et_2O. The product is dried under dynamic vacuum.

*Salt metathesis for **$H_3(L3^R)Cl_2$** (R = i-Pr, Mes)*

1.0 eq. of bis(imidazolium) chloride is completely dissolved in water by slightly heating the mixture. A saturated aqueous solution of 2.5 eq. of NH_4PF_6 or $NaBPh_4$ respectively is added to this solution. The obtained precipitate is filtered off, washed with water and diethyl ether twice and dried under dynamic vacuum.

1,1'-(2-hydroxyethane-1,1-diyl)bis(3-methylimidazolium) chloride $H_3(L3^{Me})(PF_6)_2$

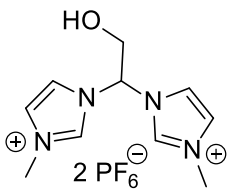

$H_3(L3^{Me})(PF_6)_2$

Sum formula: $C_{10}H_{16}F_{12}N_4OP_2$

Molar mass: 498.19 g·mol^{-1}

To a suspension of 203.0 mg (0.72 mmol, 1.0 eq.) of **$H_3(L3^{Me})Cl_2$** in 5 mL of dry acetonitrile a solution of 360.0 g (1.43 mmol, 2.0 eq.) of $AgPF_6$ in 5 mL of dry acetonitrile is added. The suspension is stirred at RT for 30 min. The precipitate is subsequently separated by centrifugation and washed twice with 2 mL of MeCN. The combined organic solutions are filtered through celite and the solvent is removed under reduced pressure. The crude viscous product is purified by repeated fractional precipitation from acetone/pentane mixture. The compound is obtained as brown solid. Yield: 30.5 mg (9 %).

^{1}H NMR (400 MHz, DMSO-d_6) δ 9.39 (s, 2H, NC*H*N), 7.95 (virt t, $^3J_{HH} \approx {}^4J_{HH}$ = 1.9 Hz, 2H, NC*H*CHN), 7.82 (virt t, $^3J_{HH} \approx {}^4J_{HH}$ = 1.8 Hz, 2H), 6.96 (t, $^3J_{HH}$ = 5.1 Hz, 1H, NC*H*(CH_2OH)N), 6.16 (br s, 1H, OH), 4.31 (br s, 2H, NCH(*CH_2*OH)N), 3.90 (s, 6H, CH_3).

^{13}C{^{1}H} NMR (101 MHz, DMSO) δ 137.56 (NCHN), 124.33 (NCH*CH*N), 121.07 (N*CH*CHN), 70.15 (N*CH*(CH_2OH)N), 60.08 (NCH(*CH_2*OH)N), 36.23 (CH_3).

Anal. Calcd.: C, 24.11; H, 3.24; N, 11.25. **Found:** C, 24.06; H, 3.17; N, 11.07.

ESI-MS ($[M]^+$): m/z 1348.51 (15 %) [3×**$H_3(L3^{Me})(PF_6)_2$**−1×PF_6^-]$^+$, 850.83 (82 %) [2×**$H_3(L3^{Me})(PF_6)_2$**−1×PF_6^-]$^+$, 352.86 (100 %) [**$H_3(L3^{Me})(PF_6)_2$**−1×PF_6^-]$^+$, 103.97 (43 %) [**$H_3(L3^{Me})(PF_6)_2$**−2×PF_6^-]$^{2+}$.

1,1'-(2-hydroxyethane-1,1-diyl)bis(3-iso-propylimidazolium) chloride $H_3(L3^{i\text{-}Pr})Cl_2$

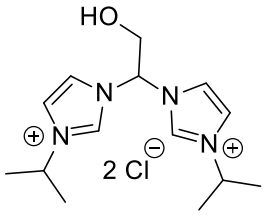

$H_3(L3^{i\text{-}Pr})Cl_2$

Sum formula: $C_{14}H_{24}Cl_2N_4O$

Molar mass: 335.27 g·mol^{-1}

9.00 g (82.0 mmol, 3.0 eq.) of 1-isopropylimidazole and 3.13 g (27.0 mmol, 1.0 eq.) of 2,2-dichloroethanol are stirred in 15 mL of toluene for 38 days. The compound is obtained as beige solid. Yield: 4.34 g (48 %).

^{1}H NMR (400 MHz, DMSO-d_6) δ 10.13 (virt t, $^4J_{HH}$ = 1.6 Hz, 2H, NC*H*N), 8.36 (virt t, $^3J_{HH} \approx {}^4J_{HH}$ = 1.9 Hz, 2H, NC*H*CHN), 8.08 (virt t, $^3J_{HH} \approx {}^4J_{HH}$ = 1.7 Hz, 2H, NCH*CH*N), 7.25 (t, $^3J_{HH}$ = 5.9 Hz, 1H, NC*H*(CH_2OH)N), 6.46 (t, $^3J_{HH}$ = 5.8 Hz, 1H, OH), 4.68 (hept, $^3J_{HH}$ = 6.7 Hz, 2H, *CH(*$CH_3)_2$), 4.43 (virt t, $^3J_{HH}$ = 5.9 Hz, 2H, CH*CH_2*OH), 1.51 (d, $^3J_{HH}$ = 6.6 Hz, 12H, (*CH_3*)$_2$CH).

^{13}C{^{1}H} NMR (101 MHz, DMSO) δ 136.12 (N*CH*N), 121.64 (N*CH*CHN), 121.13 (NCH*CH*N), 69.99 (N*CH*(CH_2OH)N), 59.87 (CH*CH_2*OH), 52.93 (*CH*($CH_3)_2$), 22.14 (CH_3), 22.10 (CH_3).

Anal. Calcd.: C, 50.15; H, 7.22; N, 16.71. **Found**: C, 49.91; H, 7.24; N, 16.43.

FAB-MS ([M]$^+$): m/z 299.1 [**H$_3$(L3$^{i\text{-Pr}}$)Cl$_2$**−1×Cl$^-$]$^+$.

1,1'-(2-hydroxyethane-1,1-diyl)bis(3-isopropylimidazolium) hexafluorophosphate

H$_3$(L3$^{i\text{-Pr}}$)(PF$_6$)$_2$

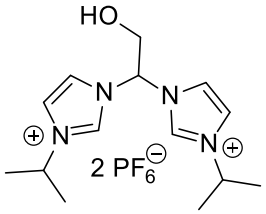

H$_3$(L3$^{i\text{-Pr}}$)(PF$_6$)$_2$

Sum formula: $C_{14}H_{24}F_{12}N_4OP_2$

Molar mass: 554.30 g·mol^{-1}

To a solution of 1.00 g (2.89 mmol, 1.0 eq.) of **H$_3$(L3$^{i\text{-Pr}}$)Cl$_2$** in 20 mL of water a solution of 1.12 g (6.86 mmol, 2.3 eq.) of NH_4PF_6 in 10 mL of water is added. The compound is obtained as white solid. Yield: 1.15 g (70 %).

^{1}H NMR (400 MHz, DMSO-d_6) δ 9.45 (virt t, $^4J_{HH}$ = 2.0 Hz, 2H, NCHN), 8.07 (virt t, $^3J_{HH} \approx {}^4J_{HH}$ = 1.7 Hz, 2H, N*CH*CHN), 8.03 (virt t, $^3J_{HH} \approx {}^4J_{HH}$ = 1.7 Hz, 2H, NCH*CH*N), 6.88 (t, $^3J_{HH}$ = 5.3 Hz, 1H, *CH*CH$_2$OH), 6.14 (s, 1H, OH), 4.70 (hept, $^3J_{HH}$ = 6.7 Hz, 2H, *CH*(CH$_3$)$_2$), 4.32 (d, $^3J_{HH}$ = 5.2 Hz, 2H, CH*CH$_2$*OH), 1.50 (d, $^3J_{HH}$ = 6.5 Hz, 12H, (*CH$_3$*)$_2$CH).

^{13}C{^{1}H} NMR (101 MHz, DMSO) δ 135.83 (N*CH*N), 121.47 (N*CH*CHN), 121.26 (NCH*CH*N), 70.41 (N*CH*(CH$_2$OH)N), 60.11 (CH*CH$_2$*OH), 52.97 (*CH*(CH$_3$)$_2$), 22.14 (CH$_3$), 22.06 (CH$_3$).

Anal. Calcd.: C, 30.34; H, 4.36; N, 10.11. **Found**: C, 30.41; H, 4.57; N, 9.92.

FAB-MS ([M]$^+$): m/z 408.9 [**H$_3$(L3$^{i\text{-Pr}}$)(PF$_6$)$_2$**−1×PF$_6^-$]$^+$.

1,1'-(2-hydroxyethane-1,1-diyl)bis(3-isopropylimidazol-3-ium) tetraphenylborate

H$_3$(L3$^{i\text{-Pr}}$)(BPh$_4$)$_2$

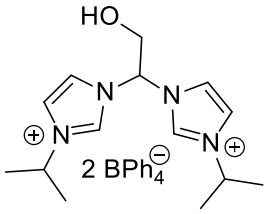

H$_3$(L3$^{i\text{-Pr}}$)(BPh$_4$)$_2$

Sum formula: $C_{62}H_{64}B_2N_4O$

Molar mass: 902.84 g·mol^{-1}

To a solution of 1.00 g (2.98 mmol, 1.0 eq.) of **H$_3$(L3$^{i\text{-Pr}}$)Cl$_2$** in 30 mL of water a solution of 2.35 g (6.86 mmol, 2.3 eq.) of $NaBPh_4$ in 40 mL of water is added. The compound is obtained as white solid. Yield: 88 %.

^{1}H NMR (400 MHz, DMSO-d_6) δ 9.47 (virt t, $^4J_{HH}$ = 1.6 Hz, 2H, N*CH*N), 8.08 (virt t, $^3J_{HH} \approx {}^4J_{HH} \approx$ 1.9 Hz, 2H, N*CH*CHN), 8.03 (virt t, $^3J_{HH} \approx {}^4J_{HH} \approx$ 1.9 Hz, 2H, NCH*CH*N),

7.25 – 7.12 (m, 16H, *ortho*-CH, BPh_4), 6.95 – 6.87 (m, 17H, N*CH*(CH_2OH)N and *meta*-CH, BPh_4,), 6.83 – 6.72 (m, 8H, *para*-CH, BPh_4), 6.16 (s, 1H, OH), 4.70 (virt p, $^3J_{HH}$ = 6.6 Hz, 2H, *CH*(CH_3)$_2$), 4.32 (d, $^3J_{HH}$ = 5.3 Hz, 2H, CH*CH*$_2$OH), 1.51 (d, $^3J_{HH}$ = 6.7 Hz, 6H, CH(*CH*$_3$)$_2$), 1.49 (d, $^3J_{HH}$ = 6.7 Hz, 6H, CH(*CH*$_3$)$_2$).

^{13}C{^{1}H} NMR (101 MHz, DMSO) δ 163.37 (q, $^1J_{CB}$ = 49.33 Hz, CB, BPh_4), 135.84 (N*CH*N), 135.6 – 135.5 (m, *ortho*-CH, BPh_4), 125.32 (q, $^3J_{CB}$ = 2.69 Hz, *meta*-CH, BPh_4), 121.54 (s, *para*-CH, BPh_4), 121.49 (N*CH*CHN), 121.24 (NCH*CH*N), 70.37 (N*CH*(CH_2OH)N), 60.09 (CH(*CH*$_2$OH)), 52.97 (*CH*(CH_3)$_2$), 22.14 (CH(*CH*$_3$)$_2$), 22.07 (CH(*CH*$_3$)$_2$).

Anal. Calcd. (+ 1×acetone): C, 81.25; H, 7.34; N, 5.83. **Found**: C, 80.94; H, 7.35; N, 5.83.

ESI-MS ([M]$^+$): m/z 1485.92 (10 %) [2×**H$_3$(L3$^{i\text{-Pr}}$)(BPh$_4$)$_2$**−3×BPh_4^-]$^+$, 1256.52 (20 %) [2×**H$_3$(L3$^{i\text{-Pr}}$)(BPh$_4$)$_2$**−2×BPh_4^-+2×$CHOO^-$]$^+$, 919.57 (25 %) [2×**H$_3$(L3$^{i\text{-Pr}}$)(BPh$_4$)$_2$**−4×BPh_4^-+CH_3CN+$CHOO^-$−CH_3]$^+$, 696.77 (75 %) [2×**H$_3$(L3$^{i\text{-Pr}}$)(BPh$_4$)$_2$**−3×BPh_4^-+*i*-Pr-Im−H$^+$]$^{2+}$.

1,1'-(2-hydroxyethane-1,1-diyl)bis(3-mesitylimidazolium) chloride H$_3$(L3^{Mes})Cl$_2$

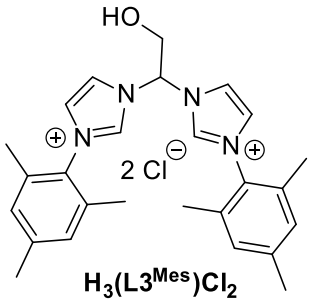

H$_3$(L3^{Mes})Cl$_2$

Sum formula: $C_{26}H_{32}Cl_2N_4O$

Molar mass: 487.47 g·mol^{-1}

11.02 g (60.0 mmol, 3.0 eq.) of 1-mesitylimidazole and 2.27 g (20.0 mmol, 1.0 eq.) of 2,2-dichloroethanol are stirred in 15 mL of toluene for 42 days. The compound is obtained as white solid. Yield: 2.47 g (26 %).

^{1}H NMR (400 MHz, DMSO-*d$_6$*) δ 10.31 (virt t, $^4J_{HH}$ = 1.5 Hz, 2H, N*CH*N), 8.63 (virt t, $^3J_{HH} \approx {}^4J_{HH} \approx$ 1.7 Hz, 2H, N*CH*CHN), 8.13 (virt t, $^3J_{HH} \approx {}^4J_{HH}$ = 1.8 Hz, 2H, NCH*CH*N), 7.38 (t, $^3J_{HH}$ = 5.7 Hz, 1H, N*CH*(CH_2OH)N), 7.16 (s, 4H, H_{Mes}), 6.55 (t, $^3J_{HH}$ = 5.5 Hz, 1H, OH), 4.61 (t, $^3J_{HH}$ = 5.6 Hz, 2H, CH*CH*$_2$OH), 2.33 (s, 6H, *para*-CH_3), 2.06 (s, 12H, *ortho*-CH_3).

^{13}C{^{1}H} NMR (101 MHz, DMSO) δ 140.60 (*C*(*para*-CH_3)), 138.83 (N*CH*N), 134.27 (N*CC*(*ortho*-CH_3)), 130.90 (*C*(*ortho*-CH_3)), 129.39 (CH_{Mes}), 124.72 (NCH*CH*N), 122.14 (N*CH*CHN), 70.86 (N*CH*(CH_2OH)N), 59.70 (NCH(*CH*$_2$OH)N), 20.65 (*para*-CH_3), 17.05 (*ortho*-CH_3).

Anal. Calcd.: C, 64.06; H, 6.62; N, 11.49. Found: C, 63.60; H, 6.62; N, 11.47.

ESI-MS ([M]$^+$): m/z 938.89 (12 %) [2×**H$_3$(L3^{Mes})Cl$_2$**−1×Cl^-]$^+$, 450.55 (10 %) [**H$_3$(L3^{Mes})Cl$_2$**−1×Cl^-]$^+$, 208.26 (100 %) [**H$_3$(L3^{Mes})Cl$_2$**−2×Cl^-]$^{2+}$.

1,1'-(2-hydroxyethane-1,1-diyl)bis(3-mesitylimidazolium) hexafluorophosphate
$H_3(L3^{Mes})(PF_6)_2$

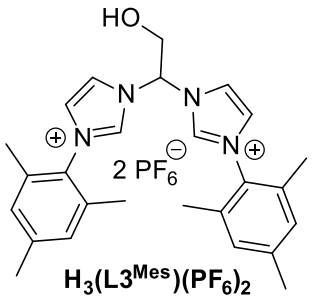

$H_3(L3^{Mes})(PF_6)_2$

Sum formula: $C_{26}H_{32}F_{12}N_4OP_2$
Molar mass: 706.50 g·mol^{-1}

To a solution of 1.00 g (2.05 mmol, 1.0 eq.) of **$H_3(L3^{Mes})Cl_2$** in 100 mL of hot water a solution of 836.0 mg (5.13 mmol, 2.5 eq.) of NH_4PF_6 in 5 mL of water is added. The compound is obtained as white solid. Yield: 1.30 g (89 %).

^{1}H NMR (400 MHz, DMSO-d_6) δ 9.82 (virt t, $^4J_{HH}$ = 1.5 Hz, 2H, NC*H*N), 8.36 (virt t, $^3J_{HH} \approx {}^4J_{HH}$ = 1.8 Hz, 2H, NC*H*CHN), 8.16 (virt t, $^3J_{HH} \approx {}^4J_{HH} \approx$ 1.7 Hz, 2H, NCHC*H*N), 7.18 (s, 4H, H_{Mes}), 7.08 (t, $^3J_{HH}$ = 5.1 Hz, 1H, NC*H*(CH_2OH)N), 6.32 (s, 1H, OH), 4.48 (br s, 2H, CHC*H*$_2$OH), 2.34 (s, 6H, *para*-CH_3), 2.05 (s, 12H, *ortho*-CH_3).

^{13}C{^{1}H} NMR (101 MHz, DMSO) δ 140.65 (*C*(*para*-CH_3)), 138.51 (NC*H*N), 134.22 (NC*C*(*ortho*-CH_3)), 130.85 (*C*(*ortho*-CH_3)), 129.33 (CH_{Mes}), 124.97 (NCH*CH*N), 122.06 (N*CH*CHN), 71.31 (N*CH*(CH_2OH)N), 59.90 (NCH(*CH*$_2$OH)N), 20.60 (*para*-CH_3), 16.95 (*ortho*-CH_3).

Anal. Calcd.: C, 44.2; H, 4.57; N, 7.93. **Found**: C, 44.39; H, 4.94; N, 7.91.

FAB-MS ([M]$^+$): m/z 560.7 [**$H_3(L3^{Mes})(PF_6)_2$**−1×PF_6^-]$^+$.

1,1'-(2-hydroxyethane-1,1-diyl)bis(3-mesitylimidazolium) tetraphenylborate
$H_3(L3^{Mes})(BPh_4)_2$

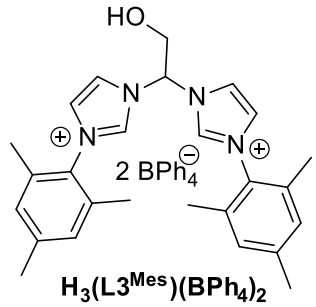

$H_3(L3^{Mes})(BPh_4)_2$

Sum formula: $C_{74}H_{72}B_2N_4O$
Molar mass: 1055.04 g·mol^{-1}

To a solution of 500 mg (1.03 mmol, 1.0 eq.) of **$H_3(L3^{Mes})Cl_2$** in 75 mL of hot water a solution of 877.5 g (2.56 mmol, 2.5 eq.) of $NaBPh_4$ in 130 mL of water is added. The compound is obtained as white solid. Yield: 910.5 mg (84 %)

^{1}H NMR (400 MHz, DMSO-d_6) δ 9.80 (virt t, $^{4}J_{HH}$ = 1.5 Hz, 2H, NC*H*N), 8.35 (virt t, $^{3}J_{HH} \approx {}^{4}J_{HH} \approx$ 1.75 Hz, 2H, NC*H*CHN), 8.14 (virt t, $^{3}J_{HH} \approx {}^{4}J_{HH} \approx$ 1.75 Hz, 2H, NCH*CH*N), 7.17 (br s, 20H, 4H_{Mes} and 16 *meta*-CH, BPh_4), 7.08 (t, $^{3}J_{HH}$ = 5.1 Hz, 1H, N*CH*(CH_2OH)N), 6.92 (virt t, $^{3}J_{HH}$ = 7.3 Hz, 16H, *ortho*-CH, BPh_4), 6.79 (t, $^{3}J_{HH}$ = 7.1 Hz, 8H, *para*-CH, BPh_4), 4.48 (t, $^{3}J_{HH}$ = 5.3 Hz, 2H, CH*CH_2*OH), 2.34 (s, 6H, *para*-CH_3), 2.04 (s, 12H, *ortho*-CH_3).

^{13}C{^{1}H} NMR (101 MHz, DMSO) δ 163.35 (q, $^{1}J_{CB}$ = 49.3 Hz, CB, BPh_4), 140.65 (*C*(*para*-CH_3)), 138.49 (N*CH*N), 135.50-135.60 (m, *ortho*-CH, BPh_4), 134.21 (NCC(*ortho*-CH_3)), 130.84 (*C*(*ortho*-CH_3), 129.33 (CH_{Mes}), 125.3 (q, $^{3}J_{CB}$ = 2.73 Hz, *meta*-CH, BPh_4), 124.96 (N*CH*CHN), 122.04 (NCH*CH*N), 121.51 (s, *para*-CH, BPh_4), 71.32 (N*CH*(CH_2OH)N), 59.91 (NCH(*CH_2*OH)N), 20.61 (*para*-CH_3), 16.95 (*ortho*-CH_3).

Anal. Calcd.: C, 84.24; H, 6.88; N, 5.31. **Found**: C, 83.64; H, 7.01; N, 5.29.

FAB-MS ([M]$^{+}$): m/z 734.7 [$\mathbf{H_3(L3^{Mes})(BPh_4)_2}$−1×$BPh_4^{-}$]$^{+}$.

General Procedures for Deprotonation Experiments with Bis(imidazolium) Salts ***$H_3(L3^R)X_2$***

*Route **A**: Exploratory NMR Scale Reactions*

Unless otherwise stated 1.0 eq. of a bis(imidazolium) salt and 3.0 eq. of MN" (M = Li, Na, K, N" = $N(SiMe_3)_2$) are placed into a J-Young NMR tube and 0.6 mL of respective deuterated solvent is added at RT. The reaction is monitored by NMR spectroscopy. An overview of the conducted experiments is given in Table 5.2.3.

*Route **B**: Experiments on Preparatory Scale*

Unless otherwise stated, 1.0 eq. of a bis(imidazolium) salt and 3.0 eq. of MN" (M = Li, K) are suspended in the solvent of the choice in a Schlenk tube. Subsequently, the reaction mixture is stirred at various conditions. The precipitate is separated by filtration and crude product is obtained by evaporation of the solvent. Depending on pro-ligand different purification procedures by a combination of crystallization, precipitation or extraction in different solvents can be applied. An overview of the conducted experiments is given in Table 5.2.4.

Lithium NHC adduct Li($L3^{Mes}$)

Experiment No. 6 (Table 5.2.4). The obtained crude product was washed with hexanes twice to yield a slightly beige powder. Yield: 100.0 mg.

^{1}H NMR (500 MHz, Benzene-d_6) δ 6.85 (s, 2H, H_{Mes}), 6.74 (s, 2H, H_{Mes}), 6.35 (d, $^{3}J_{HH}$ = 1.7 Hz, 2H, N*CH*CHN), 6.10 (d, $^{3}J_{HH}$ = 1.7 Hz, 2H, NCH*CH*N), 4.79 (d, $^{3}J_{HH}$ = 1.9 Hz, 2H,

NCH(*CH*$_2$O)N), 4.69 (t, $^3J_{HH}$ = 1.9 Hz, 1H, N*CH*(CH$_2$O)N), 2.13 (s, 6H, CH$_3$), 2.06 (s, 6H, CH$_3$), 1.76 (s, 6H, CH$_3$), 0.10 (s, 54H, SiMe$_3$).

^{13}C{^{1}H} NMR (126 MHz, C_6D_6) δ 200.07 (q, $^1J_{Li\text{-}C}$ = 33.4 Hz, NCN), 138.93 (*ortho*-CH$_3$C*C*N), 137.25 (*para*-CH$_3$*C*), 134.88 (*ortho*-CH$_3$*C*CN), 134.66 (*ortho*-CH$_3$*C*CN), 129.47 (CH$_{Mes}$), 129.41 (CH$_{Mes}$), 120.59 (N*CH*CHN), 120.13 (NCH*CH*N), 74.56 (*CH*CH$_2$OH), 65.09 (CH*CH$_2$*O), 20.93 (*para*-CH$_3$), 17.93 (*ortho*-CH$_3$), 17.45 (*ortho*-CH$_3$), 2.66 (SiMe$_3$).

^{29}Si INEPT NMR (99 MHz, C_6D_6) δ 1.94 (N(SiMe$_3$)$_2$).

^{7}Li NMR (194 MHz, C_6D_6) δ 1.98, 1.15.

Anal. Found: C, 54.28; H, 7.32; N, 9.70, Cl, 6.86.

Table 5.2.3. Overview of exploratory NMR scale reactions with 1,1'-(2-hydroxyethane-1,1-diyl)-bridge functionalised bis(imidazolium) salts and alkali metal bis(trimethylsilyl)amides.

Ex. No.	Compound	Amount of the pro-ligand	Amount of the base		Solvent
			LiN"	NaN"	
1	**H$_2$(L3^{Mes})Cl$_2$**	15.0 mg (3.08×10^{-5} mol)		16.9 mg (9.21×10^{-5} mol)	THF-d_8
2		15.0 mg (3.08×10^{-5} mol)		16.9 mg (9.21×10^{-5} mol)	C_6D_6
3	**H$_2$(L3^{Mes})(PF$_6$)$_2$**	7.1 mg (1.00×10^{-5} mol)	5.0 mg (2.99×10^{-5} mol)		C_6D_6

Table 5.2.4. Overview of the conducted experiments towards the isolation of alkali metal adducts of 1,1'-(2-hydroxyethane-1,1-diyl)-bridge functionalised NHC.

Ex. No.	Compound	Amount of the pro-ligand	Amount of the base		Solvent	Reaction conditions
			LiN"	KN"		
1	**$H_2(L3^{Mes})Cl_2$**	400.0 mg (0.82 mmol)	398.2 mg (2.38 mmol, 2.9 eq.)		10 mL of benzene	15-20 °C, 2 h
2		121.4 mg (0.25 mmol)	125.0 mg (0.75 mmol)		5 mL of benzene	RT, 18 h
3		295.7 mg (0.61 mmol)	284.2 mg (1.70 mmol, 2.8 eq.)		5 mL of benzene	from 0 °C to RT in 3 h
4		111.0 mg (0.23 mmol)	114.3 mg (0.68 mmol, 2.97 eq.)		5 mL of toluene	RT, 18 h
5		100.0 mg (0.21 mmol)	58.0 mg (0.35 mmol, 1.65 eq.)		5 mL of THF	**1.** 0 °C, 90 min **2.** RT, 90 min
6		500 mg (1.03mmol)	499.8 mg (2.99 mmol, 2.9 eq.)		6 mL of benzene	**1.** 8-10 °C, 45 min **2.** RT, 30 min
7		500 mg (1.03mmol)	499.8 mg (2.99 mmol, 2.9 eq.)		6 mL of benzene	**1.** 8-10 °C, 40 min **2.** RT, 30 min
8		63.2 mg (0.13 mmol)		76.3 mg (0.38 mmol, 2.95 eq.)	6 mL of THF	RT, 15 min
9	**$H_3(L3^{i\text{-}Pr})Cl_2$**	50.0 mg (0.15 mmol)	74.9 mg (0.45 mmol)		5 mL of THF	**1.** 0 °C, 20 min **2.** RT, 20 min

Hydrolysis Experiments with Alkali Metal NHC Adducts of **(L3^{R})**

Li(L3^{Mes}) + ex. H_2O

30 mg of **Li(L3^{Mes})** is dissolved in 3.0 mL of benzene in a Schlenk tube. Subsequently, 1.0 mL of H_2O is added and the reaction mixture is stirred for 2.5 h at RT. The solvent mixture is removed *in vacuo* and the residue is analysed by ^{1}H NMR spectroscopy in DMSO-d_6.

H$_3$(L3^{Mes})Cl$_2$ + NaN"+ ex. H_2O

30 mg (6.15×10^{-4} mol, 1.0 eq.) of **H$_3$(L3^{Mes})Cl$_2$** and 33.8 mg (1.85×10^{-4} mol, 3.0 eq.) of NaN" are suspended in 3.0 mL of C_6H_6 or THF and stirred for 2.5 hours at RT. Subsequently, the suspension is filtered off and 1.0 mL of H_2O is added to the filtrate and stirred for 30 min at RT. The solvent is removed in *vacuo* and the residue analysed by ^{1}H NMR spectroscopy in DMSO-d_6.

H$_3$(L3$^{i\text{-}Pr}$)Cl$_2$ + LiN"+ 2 M HCl in Et_2O

The crude product is obtained according to the description in the experiment No. 9 (Table 5.2.4). In the next step the yellow residue is dissolved in 3.0 mL of THF and 1.0 mL of 2 M HCl solution in diethyl ether was added. The reaction mixture was stirred for 5 min at RT, at which a formation of white precipitate is observed. The precipitate is isolated by filtration and dried under dynamic vacuum.

5.2.2.3 Synthesis and Reactivity Studies of 1,1'-(2-Hydroxypropane-1,3-diyl)-Bridge Functionalised Bis(imidazolium) Salt H$_3$(L4^{Mes})Br$_2$

1-(2-hydroxy-3-(1-mesitylimidazolium-3-yl)propyl)-3-mesitylimidazolium dibromide H$_3$(L4^{Mes})Br$_2$

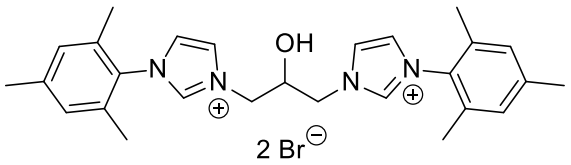

H$_3$(L4^{Mes})Br$_2$

Sum formula: $C_{27}H_{34}Br_2N_4O$
Molar mass: 590.40 g·mol^{-1}

3.91 g (21.0 mmol, 2.5 eq.) of 1-mesitylimidazole and 1.83 g (8.4 mmol, 1.0 eq.) of 1,3-dibromo-2-propanol are placed in an ACE pressure tube and non-dried benzonitrile is added to the mixture. The tube is sealed under air and the reaction mixture is stirred at 110 °C for 2 days and then at 130 °C for 8 days. Subsequently the suspension is cooled down and filtered

off. The precipitate is washed with benzonitrile and diethyl ether and the crude product is dried under dynamic vacuum. **$H_3(L4^{Mes})Br_2$** is obtained as white solid. Yield: 4.32 g (87 %)

^{1}H NMR (400 MHz, DMSO-d_6) δ 9.52 (s, 2H, NC*H*N), 8.14 (virt t, $^3J_{HH} \approx {}^4J_{HH}$ = 1.7 Hz, 2H, N*CH*CHN), 7.99 (virt t, $^3J_{HH} \approx {}^4J_{HH}$ = 1.6 Hz, 2H, NCH*CH*N), 7.15 (s, 4H, H_{Mes}), 6.16 (d, $^3J_{HH}$ = 6.1 Hz, 1H, OH), 4.64 (dd, $^3J_{HH}$ = 13.7 Hz, $^4J_{HH}$ = 2.3 Hz, 2H, CH_2(CHOH)CH_2), 4.55 – 4.45 (m, 1H, CH_2(*CH*OH)CH_2), 4.26 (dd, $^3J_{HH}$ = 13.7 Hz, $^4J_{HH}$ = 8.9 Hz, 2H, CH_2(CHOH)CH_2), 2.33 (s, 6H, *para*-CH_3), 2.05 (br s, 12H, *ortho*-CH_3).

^{13}C{^{1}H} NMR (101 MHz, DMSO) δ 140.24 (*C*(*para*-CH_3)), 138.04 (NCHN), 134.33 (N*C*C(*ortho*-CH_3)), 131.11 (*C*(*ortho*-CH_3), 129.25 (CH_{Mes}), 123.90 (N*CH*CHN), 123.65 (NCH*CH*N), 67.46 CH_2(*CH*OH)CH_2, 52.47 (CH_2(CHOH)CH_2), 20.59 (*para*-CH_3), 17.05 (*ortho*-CH_3).

Anal. Calcd.: C, 54.93; H, 5.80; N, 9.49. **Found**: C, 54.41; H, 5.83; N, 9.30.

FAB-MS ($[M]^+$): m/z 511 [**$H_3(L4^{Mes})Br_2$**−1×Br^-]$^+$.

Route **A**: Deprotonation Experiments with **$H_3(L4^{Mes})Br_2$** on NMR Scale

Unless otherwise stated 1.0 eq. of **$H_3(L4^{Mes})Br_2$** and 3.0 eq. of the base (LiN", NaN", KN", KBn, KH) are placed into a J-Young NMR tube and 0.6 mL of respective deuterated solvent is added at RT. An overview of the conducted experiments is given in Table 5.2.5.

Lithium NHC Adduct Li(L4^{Mes})

Experiment No. 1 (Table 5.2.5). The reaction is complete after 1 hour at RT. Yield: quant.

^{1}H NMR (400 MHz, THF-d_8) δ 7.05 (br s, 2H, N*CH*CHN), 6.88 (br s, 4H, H_{Mes}), 6.78 (br s, 2H, NCH*CH*N), 4.15 – 3.55 (m, 5H, NCH_2CHCH_2N), 2.27 (s, 6H, *para*-CH_3), 2.02 and 1.94 (br s, 12H, *ortho*-CH_3), 0.04 ($SiMe_3$)

^{13}C{^{1}H} NMR (101 MHz, THF-d_8) δ 139.26 (*ortho*-CH_3C*C*N), 137.80 (*para*-CH_3*C*), 136.34 (*ortho*-CH_3*C*CN), 129.42 (CH_{Mes}), 129.25 (CH_{Mes}), 122.51(N*CH*CHN), 119.77 (NCH*CH*N), 74.86 (NCH_2*CH*CH_2N), 59.69 (NCH_2CHCH_2N), 21.17 (*para*-CH_3), 18.57 (*ortho*-CH_3), 18.26 (*ortho*-CH_3), 2.74 ($SiMe_3$)

^{29}Si INEPT NMR (79 MHz, THF-d_8) δ −0.25 (N($SiMe_3$)$_2$).

Table 5.2.5. Overview of the NMR scale reaction aimed on the investigation of the reactivity of **$H_3(L4^{Mes})Br_2$** with various alkali metal bases.

Ex. No.	Amount of **$H_3(L4^{Mes})Br_2$**	Amount of the base					Solvent
		LiN"	NaN"	KN"	KBn	KH	
1	11.5 mg (1.94×10^{-5}mol)	9.6 mg (5.74×10^{-5}mol, 2.96 eq.)					THF-d_8
2	15.0 mg (2.54×10^{-5}mol)		13.9 mg (7.58×10^{-5}mol)				THF-d_8
3	11.6 mg (1.96×10^{-5}mol)			11.6 mg (5.80×10^{-5} mol, 2.96 eq.)			THF-d_8
4	10.4 mg (1.76×10^{-5} mol)				6.9 mg (5.28×10^{-5} mol)		C_6D_6
5	20.5 mg (3.74×10^{-5} mol)					4.2 mg (1.04×10^{-4} mol)	THF-d_8

Potassium NHC Adduct K(L4^{Mes})

Experiment No. 3 (Table 5.2.5). The reaction is complete after 1 hour at RT. Yield: quant.

^{1}H NMR (400 MHz, THF-d_8) δ 7.47 (s, 2H, N*CH*CHN), 6.87 (s, 4H, H_{Mes}), 6.68 (s, 2H, NCH*CH*N), 4.40 (s, 1H, CH_2(*CH*O)CH_2), 4.14 – 3.68 (m, 4H, *CH_2*(CHO)*CH_2*), 2.26 (s, 6H, *para*-CH_3), 1.98 (s, 12H, *ortho*-CH_3), 0.95 (s, 3H, NH), 0.04 (s, 54H, $SiMe_3$).

^{13}C{^{1}H} NMR (101 MHz, THF-d_8) δ 214.31 (NCN), 140.40 (*ortho*-CH_3C*C*N), 137.41 (*para*-CH_3*C*), 136.24 (*ortho*-CH_3*C*CN), 129.38(CH_{Mes}), 122.29 (N*CH*CHN), 119.86 (NCH*CH*N), 79.19 (CH_2(*CH*O)CH_2), 59.83 (*CH_2*(CHO)*CH_2*), 21.26 (*para*-CH_3), 18.47 (*ortho*-CH_3), 2.87 ($SiMe_3$).

^{29}Si INEPT NMR (79 MHz, THF-d_8) δ 1.62 ($N(SiMe_3)_2$).

Monitoring of the Formation of **K(L4^{Mes})** by ^{1}H NMR at Different Temperatures

15.0 mg (2.54×10^{-5} mol, 1.0 eq.) of **H_3(L4^{Mes})Br_2** and 15.2 mg (7.62×10^{-5} mol, 3.0 eq.) of KN**"** are placed into a J-Young NMR tube in a glove box and 0.6 mL of deuterated THF is added at RT. Without stirring, the sealed tube is transported out of box within 15-30 sec and the J-Young NMR tube is placed into an isopropanol/dried ice bath (–78 °C). Subsequently, the formation of K NHC adduct is monitored by ^{1}H NMR in steps of 20 °C. After 30 min at 20 °C the NMR tube contains yellow solution which turns brown at RT within 2 hours.

Route **B**: Experiments on Preparatory Scale

General Procedure

Unless otherwise stated, 1.0 eq. of **H_3(L4^{Mes})Br_2** and 3.0 eq. of the base are suspended in THF in a Schlenk tube at specified temperatures. The reaction mixture is stirred by concomitantly allowing it to warm up to RT. Subsequently, the precipitate is separated by filtration and the crude product is obtained by evaporation of the solvent. An overview of conducted experiments is given in Table 5.2.6.

H_3(L4^{Mes})Br_2 + KN"

Experiment No. 2 (Table 5.2.6) yields brown residue as crude product. Further purification was attempted by precipitation or partial precipitation with hexane out of THF or crystallization out toluene/pentane mixture at −26 °C.

$H_3(L4^{Mes})Br_2$ + LiN"

Experiment No. 1 (Table 5.2.6) yields colourless residue as crude product. Further purification is conducted by overlaying the solution of crude product in 3 mL of THF with 7 mL of pentane and storing the mixture at −26 °C. Hereby a formation of white non-crystalline precipitate is observed.

$H_3(L4^{Mes})Br_2$ + KH

Experiment No. 3 (Table 5.2.6). **$H_3(L4^{Mes})Br_2$** and KH are suspended in 3 mL of THF respectively in two separate Schlenk tubes. After cooling of both vessels to –78 °C, the KH suspension is cannulated to the pro-ligand. Additional 3 mL of THF are used for washing of the Schlenk tube with KH in order to ensure a complete transfer. The reaction mixture is allowed to warm up slowly to the RT overnight. Subsequently, the obtained brown suspension is filtered off. 10 mL of hexane is added to the filtrate resulting in formation of precipitate, which is separated by filtration as well and further analysed.

Table 5.2.6. Experiments aimed on the isolation of alkali metal NHC adducts derived from **$H_3(L4^{Mes})Br_2$**.

Ex. No.	Amount of **$H_3(L4^{Mes})Br_2$**	Amount of the base			Amount of THF	Reaction conditions
		LiN"	KN"	KH		
1	237.0 mg (0.40 mmol)	198.2 mg (1.18 mmol, 2.95 eq.)			6 mL	Slowly warming up from 0 °C until RT within 3.5 h
2	500 mg (0.85 mmol)		498.4 mg (2.50 mmol, 2.95 eq.)		6 mL	Slowly warming up from 0 °C until RT within 3 h
3	500.0 mg (0.85 mmol)			498.4 mg (2.50 mmol)	9 mL	Slowly warming up from –78 °C until RT within 18 h

Hydrolysis Experiments with Alkali Metal NHC Adducts of **$(L4^{Mes})$**

30 mg (5.08×10^{-5} mol, 1.0 eq.) of **$H_3(L4^{Mes})Br_2$** and 30.4 mg of KN" or 27.8 mg of NaN" (1.52×10^{-4} mol, 3.0 eq.) are suspended in 3.0 mL of THF and stirred for 2.5 hours at RT. Subsequently, the suspension is filtered off and 1.0 mL of H_2O is added to the filtrate and

stirred for another 30 min at RT. The solvent is removed in *vacuo* and the residue is analysed by ^{1}H NMR spectroscopy in DMSO-d_6.

5.2.2.4 Synthesis and Reactivity Studies of *N*-Furanyl Functionalised Bis(imidazolium) Salts $H_2(L5^R)X_2$ and $H_2(L6^R)X_2$

2-Bromo-5-(*tert*-butyl)furan 5b

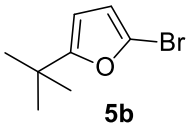

5b

Sum formula: $C_8H_{11}BrO$

Molar mass: 203.08 g·mol^{-1}

This synthesis is based on the preparation of tetrakis(5-bromo-furan-2-yl)methane.[243] In a round flask 10.67 g (85.95 mmol, 1.0 eq.) of 2-(*tert*-butyl)furan is dissolved in 100 mL of DMF at room temperature. 16.83 g (94.50 mmol, 1.1 eq.) of *N*-bromosuccinimide (NBS) is added in small portions. The yellow solution is stirred for 2 h at RT. Subsequently 50 mL of water and 50 mL of diethyl ether are poured into the reaction vessel. The organic layer is separated and the aqueous phase is extracted three times with 40 mL of diethyl ether. The combined organic solutions are washed with 20 mL of 0.1 M aqueous NaOH solution twice, then with 20 mL of water once and dried over $NaSO_4$. The solvent is removed by rotatory evaporation to yield yellow liquid as crude product. It is purified by distillation at reduced pressure. **5b** is obtained as colourless liquid (b.p. 61 °C at 5 mbar). Yield: 13.59 g (78 %).

^{1}H NMR (400 MHz, Chloroform-*d*) δ 6.15 (d, $^{3}J_{HH}$ = 3.2 Hz, 1H, H_{fu}), 5.92 (d, $^{3}J_{HH}$ = 3.2 Hz, 1H, H_{fu}), 1.26 (s, 9H, *t*-Bu).

1-(5-(tert-butyl)furan-2-yl)-4,5-dimethylimidazole ***5d***

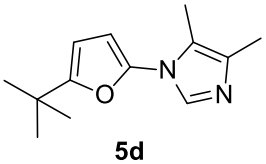

5d

Sum formula: $C_{13}H_{18}N_2O$

Molar mass: 218.30 g·mol^{-1}

This synthesis is based on the preparation of 1-(thiophen-2-yl)imidazole.[244] In a 500 mL Schlenk round flask equipped with a reflux condenser and overpressure valve 4.95 g (34.00 mmol, 1.4 eq.) of 4,5-dimethylimidazole, 5.06 g (25.00 mmol, 1.0 eq.) of 2-bromo-5-(*tert*-butyl)furan and 24.43 g (75.00 mmol, 3.0 eq.) of Cs_2CO_3 are placed. The equipment is evacuated and placed under argon atmosphere. Subsequently 150 mL of dry DMF and 2.38 g (12.30 mmol, 0.5 eq.) of CuI are added under the counter flow of argon. The reaction mixture is stirred at room temperature for 1 hour and then at 120 °C for 4 days. After the dark

suspension is cooled to the RT 100 mL of water and then 200 mL of hexane are poured into the reaction flask. The inhomogeneous mixture is filtered off and the organic layer is separated. After the aqueous phase is extracted three times with 30 mL hexane, the combined organic solutions are washed three times with 30 mL of saturated aqueous $NaHCO_3$ solution and dried over $MgSO_4$. The removal of the solvent under reduced pressure is followed by a purification of the crude product by a vacuum distillation. The compound is obtained as slightly yellow liquid (b.p. 73 °C at 1.7×10^{-2} mbar). Yield: 2.79 g (51 %).

^{1}H NMR (400 MHz, Chloroform-*d*) δ 7.51 (s, 1H, H_{im}), 6.05 (d, $^3J_{HH}$ = 3.2 Hz, 1H, H_{fu}), 6.00 (d, $^3J_{HH}$ = 3.1 Hz, 1H, H_{fu}), 2.18 (s, 3H, CH_3), 2.11 (s, 3H, CH_3), 1.28 (s, 9H, *t*-Bu).

General Procedure for the synthesis of (methylene and ethylene-bridged) bis(imidazolium) salts **$H_2(L5^{Fu})(BPh_4)_2$**, **$H_2(L5^{tFu})X_2$** and **$H_2(L6^{R})X_2$** (R = Fu, *t*Fu, X = Br, PF_6, BPh_4))

2.1 or 2.7 eq. of respective substituted imidazole and 1.0 eq. of CH_2Br_2 or 1,2-dibromoethane are placed into ACE pressure tube and non-dried THF is added. The reaction mixture in the sealed pressure tube is stirred at 100 °C-110 °C for several days. After cooling to the RT the formed precipitate is filtered off, washed with THF and Et_2O and dried *in vacuo*.

Salt metathesis

1.0 eq. of bis(imidazolium) bromide is dissolved in minimal amount of water. An aqueous solution of 2.2 or 2.5 eq. of NH_4PF_6 or $NaBPh_4$ is added. The reaction mixture is vigorously stirred at room temperature for approximately 30 min. The obtained precipitate is filtered off and washed with plenty of water and dried under dynamic vacuum.

1,1'-methylenebis(3-(furan-2-yl)imidazolium) ditetraphenylborate ***$H_2(L5^{Fu})(BPh_4)_2$***

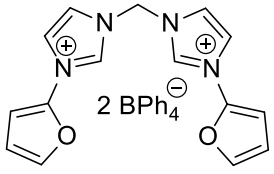

$H_2(L5^{Fu})(BPh_4)_2$

Sum formula: $C_{63}H_{54}N_4B_2O_2$

Molar mass: 920.77 g·mol^{-1}

To a solution of 300.0 mg (0.68 mmol, 1.0 eq.) of **$H_2(L5^{Fu})Br_2$** in 3.0 mL of water a solution of 580.5 mg (1.70 mmol, 2.5 eq.) of $NaBPh_4$ in 5.0 mL of water is added. The compound is obtained as white solid. Yield: 262.6 mg (42 %).

^{1}H NMR (400 MHz, DMSO-d_6) δ 10.01 (s, 2H, NCHN), 8.38 (s, 2H, N*CH*CHN), 8.20 (s, 2H, NCH*CH*N), 7.90 (s, 2H, CHCH*CH*O), 7.18 (br s, 16H, *ortho*-CH, BPh_4), 6.99 (d, $^3J_{HH}$ = 3.3 Hz,

2H, *CH*CHCHO), 6.92 (virt t, $^{3}J_{HH}$ = 7.3 Hz, 16H, *meta*-CH, BPh_4), 6.84 – 6.74 (m, 12H, 2 CH*CH*CHO, NCH_2N, 8 *para*-CH, BPh_4).

$^{13}C\{^{1}H\}$ NMR (101 MHz, DMSO) δ 163.4 (q, $^{1}J_{CB}$ = 49.3 Hz, CB, BPh_4), 142.27 (CHCH*CH*O), 140.49 (NCO), 136.49 (NCHN), 135.54 (br s, *ortho*-CH, BPh_4), 125.31 (q, $^{3}J_{CB}$ = 2.1 Hz, *meta*-CH, BPh_4), 123.27 (N*CH*CHN), 121.53 (s, *para*-CH, BPh_4), 120.56 (NCH*CH*N), 112.75 (CH*CH*CHO), 100.65 (*CH*CHCHO), 58.95 (NCH_2N).

Anal. Calcd.: C, 82.18; H, 5.91; N, 6.08. **Found**: C, 80.66; H, 5.88; N, 6.13.

ESI-MS ($[M]^+$): m/z 601.05 (84 %) $[\mathbf{H_2(L5^{Fu})(BPh_4)_2}-1\times BPh_4^-]^+$, 141.05 (100 %) $\mathbf{H_2(L5^{Fu})(BPh_4)_2}-2\times BPh_4^-]^{2+}$.

1,1‘-(ethane-1,2-diyl)-bis(3-(furan-2-yl)imidazolium) dibromide $H_2(L6^{Fu})Br_2$

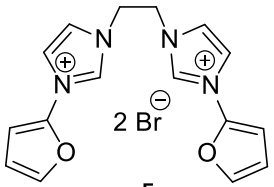

$\mathbf{H_2(L5^{Fu})Br_2}$

Sum formula: $C_{16}H_{16}Br_2N_4O_2$
Molar mass: 456.14 g·mol^{-1}

1.41 g (10.47 mmol, 2.7 eq.) of 1-(furan-2-yl)-*1H*-imidazole is treated with 710.0 mg (3.78 mmol, 1.0 eq.) of 1,2-dibromoethane in 8 mL of THF for 3 days at 100 °C. The compound is obtained as off-white solid. Yield: 829.4 mg (48 %).

^{1}H NMR (400 MHz, DMSO-d_6) δ 9.95 (virt t, $^{3}J_{HH} \approx {}^{4}J_{HH}$ = 1.6 Hz, 2H, NCHN), 8.33 (virt t, $^{3}J_{HH} \approx {}^{4}J_{HH}$ = 1.8 Hz, 2H, N*CH*CHN), 7.99 (virt t, $^{3}J_{HH} \approx {}^{4}J_{HH}$ = 1.8 Hz, 2H, NCH*CH*N), 7.90 – 7.81 (m, 2H, CHCH*CH*O), 6.96 (d, $^{3}J_{HH}$ = 3.5 Hz, 2H, *CH*CHCHO), 6.78 (dd, $^{3}J_{HH}$ = 3.5 Hz, $^{3}J_{HH}$ = 2.0 Hz, 2H, CH*CH*CHO), 4.90 (s, 4H, $N(CH_2)_2N$).

$^{13}C\{^{1}H\}$ NMR (101 MHz, DMSO) δ 141.79 (CH*CH*O), 140.92 (N*C*O), 135.52 (N*CH*N), 123.65 (N*CH*CHN), 120.17 (NCH*CH*N), 112.59 (CH*CH*CHO), 100.07 (*CH*CHCHO), 48.83 (N(*CH_2*)$_2$N).

Anal. Calcd.: C, 42.13; H, 3.54; N, 12.28. **Found**: C, 41.61; H, 3.52; N, 12.48.

ESI-MS ($[M]^+$): m/z 374.74 (14 %) $[\mathbf{H_2(L6^{Fu})Br_2}-1\times Br^-]^+$, 295.02 (8 %) $[\mathbf{H_2(L6^{Fu})Br_2}-H^+-2\times Br^-]^+$, 148.1 (100 %) $[\mathbf{H_2(L6^{Fu})Br_2}-2\times Br^-]^{2+}$.

1,1'-(ethane-1,2-diyl)-bis(3-(furan-2-yl)imidazolium) dihexafluorophosphate
$H_2(L6^{Fu})(PF_6)_2$

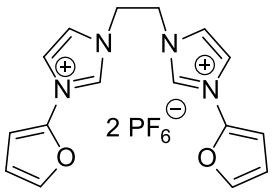

$H_2(L6^{Fu})(PF_6)_2$

Sum formula: $C_{16}H_{16}F_{12}N_4O_2P_2$
Molar mass: 586.26 g·mol^{-1}

To a solution of 400.0 mg (0.88 mmol, 1.0 eq.) of **$H_2(L6^{Fu})Br_2$** in 10 mL of H_2O a solution of 357.3 mg (2.19 mmol, 2.5 eq.) of NH_4PF_6 in 1 mL of H_2O is added. To increase the yield, the amount of H_2O is reduced *in vacuo*. **$H_2(L6^{Fu})(PF_6)_2$** is obtained as white solid. Yield: 406.3 mg (79 %).

^{1}H NMR (400 MHz, DMSO-d_6) δ 9.77 (virt t, $^3J_{HH} \approx {}^4J_{HH} \approx$ 1.6 Hz, 2H, N*CH*N), 8.30 (virt t, $^3J_{HH} \approx {}^4J_{HH} \approx$ 1.9 Hz, 2H, N*CH*CHN), 7.88 (virt t, $^3J_{HH} \approx {}^4J_{HH}$ = 1.8 Hz, 2H, NCH*CH*N), 7.87 (dd, $^3J_{HH}$ = 2.0 Hz, $^3J_{HH}$ = 1.0 Hz, 2H, CHCH*CHO*), 6.91 (dd, $^3J_{HH}$ = 3.6 Hz, $^3J_{HH}$ = 1.0 Hz, 2H, *CH*CHCHO), 6.79 (dd, $^3J_{HH}$ = 3.5 Hz, $^3J_{HH}$ = 2.0 Hz, 2H, CH*CH*CHO), 4.80 (s, 4H, N(CH_2)$_2$N).

^{13}C{^{1}H} NMR (101 MHz, DMSO) δ 141.81 (CHO), 140.87 (N*C*CH), 135.47 (NCHN), 123.61 (N*CH*CHN), 120.30 (NCH*CH*N), 112.61 (C*CH*CH), 99.99 (CH*CH*CHO), 48.96 (N(CH_2)$_2$N).

Anal. Calcd.: C, 32.78; H, 2.75; N, 9.56. **Found**: C, 32.42; H, 2.74; N, 9.84.

ESI-MS ([M]$^+$): m/z 1026.44 (11 %) [2×**$H_2(L6^{Fu})(PF_6)_2$**−3×PF_6^-]$^+$, 440.82 (63 %) [**$H_2(L6^{Fu})(PF_6)_2$**−1×PF_6^-]$^+$, 148.04 (100 %) [**$H_2(L6^{Fu})(PF_6)_2$**−2×PF_6^-]$^{2+}$.

1,1'-(ethane-1,2-diyl)-bis(3-(furan-2-yl)imidazolium) ditetraphenylborate $H_2(L6^{Fu})(BPh_4)_2$

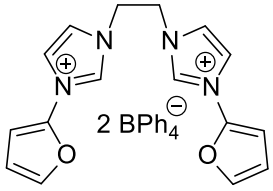

$H_3(L6^{Fu})(BPh_4)_2$

Sum formula: $C_{64}H_{56}B_2N_4O_2$
Molar mass: 934.80 g·mol^{-1}

To a solution of 200.0 mg (0.44 mmol, 1.0 eq.) of **$H_2(L6^{Fu})Br_2$** in 10 mL of water a solution of 355.4 mg (1.09 mmol, 2.5 eq.) of $NaBPh_4$ in 7 mL of water is added. The compound is obtained as white solid. Yield: 299.2 mg (73 %).

^{1}H NMR (400 MHz, Acetonitrile-d_3) δ 8.61 (s, 2H, NCHN), 7.66 (s, 2H, N*CH*CHN), 7.55 (s, 2H, CHCH*CH*O), 7.35 (s, 2H, NCH*CH*N), 7.30 (br s, 16H, *ortho*-CH, BPh_4), 7.00 (virt t, $^3J_{HH}$ = 7.3 Hz, 16H, *meta*-CH, BPh_4), 6.85 (virt t, $^3J_{HH}$ = 7.3 Hz, 8H, *para*-CH, BPh_4), 6.65 (br s, 4H, 2 *CH*CHCHO and 2 CH*CH*CHO), 4.48 (s, 4H, N(CH_2)$_2$N).

$^{13}C\{^{1}H\}$ NMR (101 MHz, Acetonitrile-d_3) δ 164.77 (q, $^{1}J_{CB}$ = 49.4 Hz, CB, BPh_4), 143.04 (CHCH*CH*O), 141.30 (NCO), 137.52 – 136.27 (m, *ortho*-CH, BPh4), 135.39 (NCHN), 126.63 (q, $^{3}J_{CB}$ = 2.8 Hz, *meta*-CH, BPh_4), 124.30 (N*CH*CHN), 122.80 (*para*-CH, BPh_4), 122.37 (NCH*CH*N), 113.56 (CH*CH*CHO), 102.17(*CH*CHCHO), 49.66 ($N(CH_2)_2N$).

Anal. Calcd.: C, 82.23; H, 6.04; N, 5.99. **Found**: C, 81.99; H, 6.03; N, 6.30.

ESI-MS ($[M]^+$): m/z 615.21 (58 %) [**$H_2(L6^{Fu})(BPh_4)_2$**−1×BPh_4^-]$^+$, 148.08 (100 %) [**$H_2(L6^{Fu})(BPh_4)_2$**−2×BPh_4^-]$^{2+}$.

1,1'-methylenebis(3-(5-(tert-butyl)furan-2-yl)-4,5-dimethylimidazolium) dibromide

$H_2(L5^{tFu})Br_2$

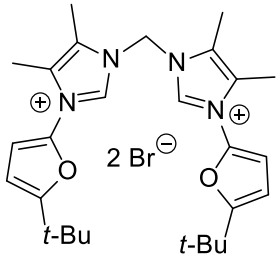

$H_2(L5^{tFu})Br_2$

Sum formula: $C_{27}H_{38}Br_2N_4O_2$

Molar mass: 610.44 g·mol^{-1}

2.00 g (9.16 mmol, 2.1 eq.) of **5d** is treated with 758.4 mg (4.36 mmol, 1.0 eq.) of CH_2Br_2 in 10 mL of THF for 4 d at 110 °C. **$H_2(L5^{tFu})Br_2$** is obtained as white solid. Yield: 407.0 mg (15 %).

^{1}H NMR (400 MHz, DMSO-d_6) δ 9.91 (s, 2H, NC*H*N), 6.82 (d, $^{3}J_{HH}$ = 3.4 Hz, $2H_{fu}$), 6.75 (s, 2H, NCH_2N), 6.43 (d, $^{3}J_{HH}$ = 3.4 Hz, $2H_{Fu}$), 2.44 (s, 3H, CH_3), 2.27 (s, 3H, CH_3), 1.29 (s, 9H, *t*-Bu).

$^{13}C\{^{1}H\}$ NMR (101 MHz, DMSO) δ 163.38 (*C*CHCH), 137.43 (N*CH*N), 136.54 (CHCH*C*), 127.67 (N*C*CH_3), 127.47 (N*C*CH_3), 106.01 (C*CH*CH), 104.90 (CH*CH*C), 55.91 (NCH_2N), 32.52 (*C*$(CH_3)_3$), 28.50 (C(*CH*$_3)_3$), 8.60 (NC*C*H_3), 8.27 (NC*C*H_3).

Anal. Calcd.: C, 53.13; H, 6.27; N, 9.18. **Found**: C, 52.84; H, 6.23; N, 8.99.

ESI-MS ($[M]^+$): m/z 1140.84 (14 %) [2×**$H_2(L5^{tFu})Br_2$**−1×Br^-]$^+$, 528.77 (60 %) [**$H_2(L5^{tFu})Br_2$**−1×Br^-]$^+$, 449.34 (34 %) [**$H_2(L5^{tFu})Br_2$**−H^+−2×Br^-]$^+$, 225.30 (100 %) [**$H_2(L5^{tFu})Br_2$**−2×Br^-]$^{2+}$.

1,1'-methylenebis(3-(5-(tert-butyl)furan-2-yl)-4,5-dimethylimidazolium) ditetraphenylborate $H_2(L5^{tFu})(BPh_4)_2$

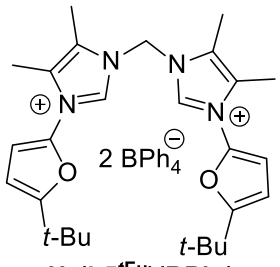

$H_2(L5^{tFu})(BPh_4)_2$

Sum formula: $C_{75}H_{78}B_2N_4O_2$
Molar mass: 1089.10 g·mol^{-1}

To a solution of 838.0 mg (1.37 mmol, 1.0 eq.) of **$H_2(L5^{tFu})Br_2$** in 10 mL of water a solution of 1.57 g (3.43 mmol, 2.5 eq.) of $NaBPh_4$ in 10 mL of water is added. The compound is obtained as off-white solid. Yield: 1.91 g (75 %).

^{1}H NMR (400 MHz, DMSO-d_6) δ 9.78 (s, 2H, NC*H*N), 7.18 (br s, 16H, *ortho*-CH, BPh_4), 6.92 (virt t, $^3J_{HH}$ = 7.4 Hz, 16H, *meta*-CH, BPh_4), 6.78 (m, 10H, $2H_{fu}$ and 8 *para*-CH, BPh_4), 6.66 (s, 2H, N*C*H_2N), 6.42 (d, $^3J_{HH}$ = 3.4 Hz, $2H_{fu}$) 2.42 (s, 3H, CH_3), 2.26 (s, 3H, CH_3), 1.29 (s, 9H, *t*-Bu).

^{13}C{^{1}H} NMR (101 MHz, DMSO) δ 163.80 (q, $^1J_{CB}$ = 49.39 Hz, CB, BPh_4,), 163.97 (s, *C*CHCH), 137.88 (s, N*CH*N), 136.85 (s, CHCH*C*), 136.0 (m, *ortho*-CH, BPh_4), 128.11 (s, N*C*CH_3), 125.79 (q, $^3J_{CB}$ = 2.65 Hz, *meta*-CH, BPh_4), 121.97 (s, *para*-CH, BPh_4) 106.55 (C*CH*CH), 105.39 (CH*CH*C), 56.30 (N*C*H_2N), 32.98 (*C*$(CH_3)_3$), 28.95 (C(*CH*$_3)_3$), 8.98 (NC*C*H_3), 8.57 (NC*C*H_3).

Anal. Calcd.: C, 82.71; H, 7.22; N, 5.14. **Found**: C, 81.64; H, 7.12; N, 5.25.

FAB-MS ([M]$^+$): m/z 768.6 [**$H_2(L5^{tFu})(BPh_4)_2$**−1×BPh_4^-]$^+$.

1,1'-(ethane-1,2-diyl)-bis(3-(5-(tert-butyl)furan-2-yl)-4,5-dimethylimidazolium) dibromide $H_2(L6^{tFu})Br_2$

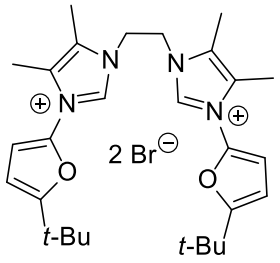

$H_2(L6^{tFu})Br_2$

Sum formula: $C_{28}H_{40}Br_2N_4O_2$
Molar mass: 624.46 g·mol^{-1}

4.15 g (18.9 mmol, 2.1 eq.) of 1-(5-(*tert*-butyl)furan-2-yl)-4,5-dimethylimidazole **5d** is treated with 1.70 g (9.1 mmol, 1.0 eq.) of 1,2-dibromoethane in 10 mL of THF for 3 days at 100 °C. The compound is obtained as white solid. Yield: 3.07 g (52 %).

^{1}H NMR (400 MHz, DMSO-d_6) δ 9.70 (s, 2H, NC*H*N), 6.74 (d, $^{3}J_{HH}$ = 3.4 Hz, 2H$_{fu}$), 6.40 (d, $^{3}J_{HH}$ = 3.4 Hz, 2H$_{Fu}$), 4.74 (s, 4H, NCH_2CH_2N), 2.34 (s, 3H, CH_3), 2.27 (s, 3H, CH_3), 1.28 (s, 9H, *t*-Bu).

^{13}C{^{1}H} NMR (101 MHz, DMSO) δ 163.1 (*C*CHCH), 136.77 (N*C*HN), 136.26 (CHCH*C*), 127.56 (N*C*CH$_3$), 127.04 (N*C*CH$_3$), 105.32 (CH*CH*CH), 104.83 (CH*CH*C), 45.4 (NCH$_2$*C*H$_2$N), 32.47 (*C*(CH$_3$)$_3$), 28.46 (C(*CH*$_3$)$_3$), 8.66 (NC*C*H$_3$), 7.77 (NC*C*H$_3$)

Anal. Calcd.: C, 53.86; H, 6.46; N, 8.97. **Found**: C, 53.90; H, 6.49; N, 9.06.

FAB-MS ([M]$^+$): m/z 544.9.1 [**H$_2$(L6^{tFu})Br$_2$**−1×Br$^-$]$^+$.

1,1'-(ethane-1,2-diyl)-bis(3-(5-(tert-butyl)furan-2-yl)-4,5-dimethylimidazolium) dihexafluorophosphate H$_2$(L6^{tFu})(PF$_6$)$_2$

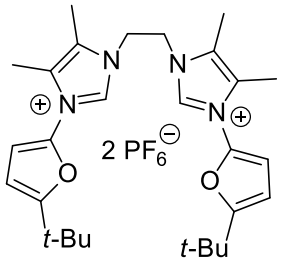

H$_2$(L6^{tFu})(PF$_6$)$_2$

Sum formula: $C_{28}H_{40}F_{12}N_4O_2P_2$
Molar mass: 754.58 g·mol^{-1}

To a solution of 500.0 mg (0.80 mmol, 1.0 eq.) of **H$_2$(L6^{tFu})(PF$_6$)$_2$** in 40 mL of water a solution of 327.0 mg (2.00 mmol, 2.5 eq.) of NH_4PF_6 in 5 mL of water is added. The compound is obtained as white solid. Yield: 553.0 mg (92 %).

^{1}H NMR (400 MHz, DMSO-d_6, 300 K) δ 9.52 (s, 2H, NC*H*N), 6.71 (d, $^{3}J_{HH}$ = 3.4 Hz, 2H$_{fu}$), 6.40 (d, $^{3}J_{HH}$ = 3.4 Hz, 2H$_{Fu}$), 4.67 (s, 4H, NCH_2CH_2N), 2.32 (s, 3H, CH_3), 2.27 (s, 3H, CH_3), 1.28 (s, 9H, *t*-Bu).

^{13}C{^{1}H} NMR (101 MHz, DMSO, 300 K) δ 163.16 (*C*CHCH), 136.71 (CHCH*C*), 136.21 (N*C*HN), 127.53 (N*C*CH$_3$), 127.17 (N*C*CH$_3$), 105.34 (CH*CH*CH), 104.86 (CH*CH*C), 45.44 (NCH$_2$*C*H$_2$N), 32.48 (*C*(CH$_3$)$_3$), 28.45 (C(*CH*$_3$)$_3$), 8.62 (NC*C*H$_3$), 7.65 (NC*C*H$_3$).

Anal. Calcd.: C, 44.57; H, 5.34; N, 7.43. **Found**: C, 44.81; H, 5.54; N, 7.52.

FAB-MS ([M]$^+$): m/z 608.6 [**H$_2$(L6^{tFu})(PF$_6$)$_2$**−1×PF$_6^-$]$^+$.

1,1'-(ethane-1,2-diyl)bis(3-(5-(tert-butyl)furan-2-yl)-4,5-dimethyl-imidazolium) ditetraphenylborate $H_2(L6^{tFu})(BPh_4)_2$

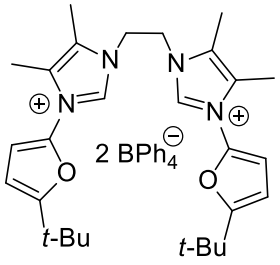

$H_2(L6^{tFu})(BPh_4)_2$

Sum formula: $C_{76}H_{80}B_2N_4O_2$

Molar mass: 1103.12 g·mol^{-1}

To a solution of 500.0 mg (0.80 mmol, 1.0 eq.) of **$H_2(L6^{tFu})Br_2$** in 5 mL of hot water a solution of 602.8 mg (1.76 mmol, 2.5 eq.) of $NaBPh_4$ in 25 mL of hot water is added. The compound is obtained as white solid. Yield: 619.0 mg (70 %).

^{1}H NMR (400 MHz, DMSO-d_6, 300 K) δ 9.52 (s, 2H, NC*H*N), 7.17 (br s, 16H, *ortho*-CH, BPh_4), 6.92 (virt t, $^3J_{HH}$ = 7.4 Hz, 16H, *meta*-CH, BPh_4), 6.78 (virt t, $^3J_{HH}$ = 7.2 Hz, 8H, *para*-CH, BPh_4), 6.71 (d, $^3J_{HH}$ = 3.4 Hz, $2H_{fu}$), 6.40 (d, $^3J_{HH}$ = 3.4 Hz, $2H_{fu}$), 4.67 (s, 2H, NCH_2CH_2N), 2.31 (s, 3H, CH_3), 2.26 (s, 3H, CH_3), 1.28 (s, 9H, *t*-Bu).

^{13}C{^{1}H} NMR (101 MHz, DMSO, 300 K) δ 163.30 (q, $^1J_{CB}$ = 49.35 Hz, CB, BPh_4), 163.15 (s, *C*CHCH), 136.69 (s, CHCH*C*), 136.21 (s, N*CH*N), 135.53 (virt t, $^2J_{CB}$ = 1.1 Hz, *ortho*-CH, BPh_4), 127.52 (s, N*C*CH_3), 127.16 (s, N*C*CH_3), 125.28 (q, $^3J_{CB}$ = 2.7 Hz, *meta*-CH, BPh_4), 121.50 (s, *para*-CH, BPh_4) 105.34 (C*CH*CH), 105.86 (CH*CH*C), 45.43 (NCH_2N), 32.47 (*C*$(CH_3)_3$), 28.45 (C(*CH*$_3)_3$), 8.63 (NC*C*H_3), 7.66 (NC*C*H_3)

Anal. Calcd.: C, 82.75; H, 7.31; N, 5.08. **Found**: C, 81.32; H, 7.12; N, 5.19.

ESI-MS ($[M]^+$): m/z 783.47 (98 %) [**$H_2(L6^{tFu})(BPh_4)_2$**−1×BPh_4^-]$^+$, 463.13 (12 %) [**$H_2(L6^{tFu})(BPh_4)_2$**−H^+−2×BPh_4^-]$^+$, 232.34 (100 %) [**$H_2(L6^{tFu})(BPh_4)_2$**−2×BPh_4^-]$^{2+}$.

General Procedures for Deprotonation Experiments with Bis(imidazolium) Salts **$H_2(L5^R)X_2$** and **$H_2(L6^R)X_2$**

Route **A**: NMR Scale

Unless otherwise stated 1.0 eq. of a bis(imidazolium) salt and 2.0 eq. of MN" (M = Li, K; N" = $N(SiMe_3)_2$) are placed into a J-Young NMR tube and 0.6 mL of respective deuterated solvent is added at RT. An overview of the conducted experiments is given in Table 5.2.7.

Table 5.2.7. Investigation of the reactivity of *N*-furanyl modified bis(imidazolium) salts with alkali metal bis(trimethylsilyl)amides.

Exp. No.	Compound	Amount of the pro-ligand	Amount of the base		Solvent
			LiN"	KN"	
1	**$H_2(L5^{Fu})Br_2$**	20.0 mg (4.56×10^{-5} mol)		18.2 mg (9.11×10^{-5} mol)	THF-d_8
2	**$H_2(L6^{Fu})Br_2$**	20.0 mg (4.38×10^{-5} mol)		17.5 mg (8.77×10^{-5} mol)	THF-d_8
3	**$H_2(L5^{tFu})Br_2$**	29.4 mg (4.63×10^{-5} mol)	16.1 mg (9.26×10^{-5} mol, 1.92 eq.)		C_6D_6
4		28.3 mg (4.82×10^{-5} mol)	15.5 mg (9.62×10^{-5} mol)		THF-d_8
5	**$H_2(L6^{tFu})Br_2$**	20.1 mg (3.22×10^{-5} mol)	10.5 mg (6.28×10^{-5} mol, 1.95 eq.)		Toluene-d_8

Tetraazafulvalene $L6^{Fu}$

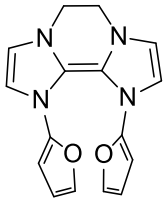

$L6^{Fu}$

Sum formula: $C_{16}H_{14}N_4O_2$
Molar mass: 294.31 g·mol^{-1}

Experiment No. 2 (Table 5.2.7). Yield: quant.

^{1}H NMR (400 MHz, THF-d_8) δ 6.81 (br s, 2H, O*CH*CHCHC), 6.19 (d, $^3J_{HH}$ = 2.6 Hz, 2H. N*CH*CHN), 6.09 (d, $^3J_{HH}$ = 2.6 Hz, 2H, NCH*CH*N), 5.99 (virt t, $^3J_{HH}$ = 2.7 Hz, 2H, OCH*CH*CHC), 4.86 (d, $^3J_{HH}$ = 3.2 Hz, 2H, OCHCH*CH*C), 3.44 (s, 4H, $N(CH_2)_2N$).

^{13}C{^{1}H} NMR (101 MHz, THF) δ 150.35 (N*C*O), 135.27 (O*CH*CHCHC), 120.97 (NCH*CH*N), 113.63 (NCN), 113.33 (N*CH*CHN), 111.64 (OCH*CH*CHC), 89.28 (OCHCH*CH*C), 45.71 ($N(CH_2)_2N$).

Route **B**: Experiments on Preparatory Scale

Unless otherwise stated, in a Schlenk tube 1.0 eq. of a bis(imidazolium) salt and 2.0 eq. of KN" are suspended in the solvent of the choice. The reaction mixture is stirred at RT. Subsequently, the precipitate is separated by filtration and crude product is obtained by evaporation of the solvent. Depending on pro-ligand different purification procedures by a combination of crystallization, precipitation or extraction in different solvents can be applied.

Table 5.2.8. Deprotonation experiments with *N*-furanyl modified pro-ligands on preparatory scale.

Ex. No.	Compound	Amount of the pro-ligand	Amount of KN"	Solvent	Reaction Conditions
1	**$H_2(L5^{Fu})Br_2$**	500.0 mg (1.13 mmol)	496.3 mg (2.49 mmol, 2.2 eq.)	25 mL of THF	RT, 18 h
2		200.5 mg (0.46 mmol)	186.3 mg (0.93 mmol, 2.05 eq.)	5 mL of THF	RT, 18
3	**$H_2(L5^{tFu})Br_2$**	200.0 mg (0.33 mmol)	127.5 mg (6.39 mmol, 1.95 eq.)	6 mL of toluene	RT, 18 h
4	**$H_2(L5^{tFu})(BPh_4)_2$**	207.0 mg (0.19 mmol)	74.0 mg (0.37 mmol, 1.95 eq.)	10 mL of toluene	RT, 72 h
5	**$H_2(L6^{tFu})Br_2$**	500.0 mg (0.80 mmol)	311.5 mg (1.56 mmol, 1.95 eq.)	10 mL of toluene	RT, 18-72 h
6		500.0 mg (0.80 mmol)	311.5 mg (1.56 mmol, 1.95 eq.)	10 mL of benzene	RT, 18 h
7		506.0 mg (0.81 mmol)	315.2 mg (1.58 mmol, 1.95 eq.)	6 mL of benzene	RT, 7 d

Bis(2(furan-2-yl)-imidazol-1-yl)methane $L5^{Fu*}$

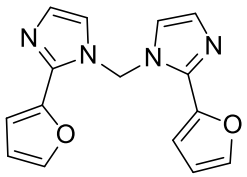

$L5^{Fu*}$

Sum formula: $C_{15}H_{12}N_4O_2$

Molar mass: 280.29 g·mol^{-1}

Experiment No. 1 (Table 5.2.8). The progressing reaction is visible by rapid colour change from colourless suspension to dark violet, almost black solution with a lot of precipitate. After stirring overnight at RT, the precipitate is filtered off and washed with 10 mL of THF. The filtrate is evaporated into dryness yielding oily and sticky dark residue.

^{1}H NMR (400 MHz, THF-d_8) δ 7.83 (br s, 2H. NC*H*CHN), 7.42 (dd, $^{3}J_{HH}$ = 2.0 Hz, $^{4}J_{HH}$ = 1.0 Hz, 1H: OC*H*CHCHC), 7.35 (virt t, $^{3}J_{HH} \approx {}^{4}J_{HH} \approx$ 1.4 Hz, 1H. NCH*CH*N), 7.03 (br s, 1H. NCH_2N), 6.51 (dd, $^{3}J_{HH}$ = 3.4 Hz, 2.0 Hz, 1H, OCH*CH*CHC), 6.31 (dd, $^{3}J_{HH}$ = 3.4 Hz, $^{4}J_{HH}$ = 1.0 Hz, 1H, OCHCH*CH*C).

^{13}C{^{1}H} NMR (101 MHz, THF) δ 146.24 (N*C*O), 140.11 (O*CH*CHCHC), 136.27 (OCH*CH*CHC), 130.98 (OCHCH*CH*C), 118.24 (NCH*CH*N), 112.53 (N*CH*CHN), 101.15 (NCN), 96.60 (NCH_2N).

Tetraazafulvalene L6^{tFu}

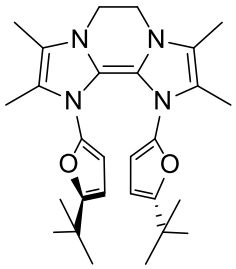

L6^{tFu}

Sum formula: $C_{28}H_{38}N_4O_2$

Molar mass: 462.64 g·mol^{-1}

Experiment No. 7 (Table 5.2.8). The amount of the reaction solution is reduced until yellow precipitate is formed. The precipitate is separated by filtration and crude product is purified by recrystallization from toluene at −26 °C. **L6^{tFu}** is obtained as yellow solid. Yield: 117.0 mg (31 %).

^{1}H NMR (400 MHz, Toluene-d_8) δ 5.69 (s, 2H, H_{fu}), 5.38 (s, 2H, H_{fu}), 3.03 (s, 4H, CH_2), 1.84 (s, 6H, CH_3), 1.51 (s, 6H, CH_3), 1.23 (s, 18H, *t*-Bu).

^{13}C{^{1}H} NMR (101 MHz, Toluene) δ 157.06 (O*C*(*t*-Bu)), 147.73 (OCN), 121.32 (NCN), 119.31 (Im-*C*CH_3), 114.66 (Im-*C*CH_3), 103.22 (CH_{fu}), 97.00 (CH_{fu}), 43.85 (CH_2), 32.91 (*C*$(CH_3)_3$), 29.54 (C(*C*$H_3)_3$), 11.20 (Im-CH_3), 9.38 (Im-CH_3).

Anal. Calcd.: C, 72.69; H, 8.28; N, 11.66. **Found**: C, 71.68; H, 8.34; N, 11.66.

Reactivity Studies with **L6^{tFu}**

Unless otherwise stated, 1.0 eq. of **L6^{tFu}** and 1.0 eq. of the substrate are placed into a J-Young NMR tube and 0.6 mL of C_6D_6 are added at RT. If necessary, the obtained precipitate is

separated by filtration and dissolved in THF-d_8 for further NMR analysis. An overview of conducted experiments is given in Table 5.2.9.

Table 5.2.9. Reactivity studies of **L6^{tFu}** with various substrates on NMR scale.

Ex. No.	Substrate	Amount of substrate	Amount of **L6^{tFu}**
1	C_6F_6	8.0 mg (4.30×10^{-5}mol)	19.9 mg (4.30×10^{-5}mol)
2	PhCOF	4.7 mg (3.78×10^{-5}mol)	17.5 mg (3.78×10^{-5}mol)
3	I_2	7.8 mg (1.69×10^{-5}mol)	4.3 mg (1.69×10^{-5}mol)
4	$Th^{\cdot+}PF_6^-$	15.6 mg (4.32×10^{-5}mol, 2.0 eq.)	10.0 mg (2.16×10^{-5}mol)

5.2.2.5 Synthesis of 1,1'-(Prop-1-ene-1,3-diyl)-Bridge Functionalised Bis(imidazolium) Salts $H_2(L7^{Mes})Br_2$

1,1'-(prop-1-ene-1,3-diyl)bis(3-mesitylimidazolium) dibromide $H_2(L7^{Mes})Br_2$

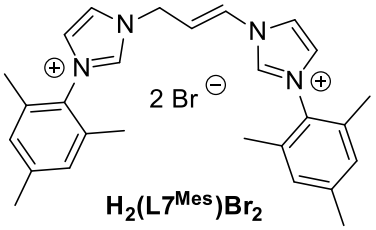

$H_2(L7^{Mes})Br_2$

Sum formula: $C_{27}H_{32}Br_2N_4$

Molar mass: 572.39 g·mol^{-1}

6.00 g (32.0 mmol, 2.5 eq.) of 1-mesitylimidazole and 2.82 g (13.0 mmol, 1.0 eq.) of 2,3-dibromo-1-propanol are placed in an ACE pressure tube and non-dried toluene is added to the mixture. The tube is sealed under air and the reaction mixture is stirred at 110 °C for 8 days. Subsequently the reaction mixture is cooled down and 20 mL of acetonitrile is added. The suspension is filtered off and the precipitate is washed with acetonitrile and diethyl ether. The sample is dried under dynamic vacuum. **$H_2(L7^{Mes})Br_2$** is obtained as off-white solid. Yield: 1.70 g (23 %).

^{1}H NMR (400 MHz, DMSO-d_6) δ 9.86 (s, 1H, NC*H*N), 9.58 (s, 1H, NC*H*N), 8.53 (virt t, $^3J_{HH} \approx {}^4J_{HH}$ = 1.7 Hz, 1H, N*CH*CHN), 8.16 (virt t, $^3J_{HH} \approx {}^4J_{HH}$ = 1.7 Hz, 1H, N*CH*CHN), 8.13 (virt t, $^3J_{HH} \approx {}^4J_{HH} \approx$ 1.7 Hz, 1H, N*CH*CHN), 8.03 (virt t, $^3J_{HH} \approx {}^4J_{HH} \approx$ 1.7 Hz, 1H, N*CH*CHN), 7.59 (d, $^3J_{HH}$ = 14.2 Hz, 1H, CH_2CH*CH*), 7.18 (s, 2H, H_{Mes}), 7.16 (s, 2H, H_{Mes}), 6.93 (dt, $^3J_{HH}$ = 14.2 Hz,

$^{3}J_{HH}$ = 7.1 Hz, 1H, CH_2*CH*CH), 5.26 (d, $^{3}J_{HH}$ = 7.0 Hz, 2H, *CH*$_2$CHCH), 2.34 (br s, 6H, *para*-CH_3), 2.07 (s, 6H, *ortho*-CH_3), 2.07 (s, 6H, *ortho*-CH_3).

^{13}C{^{1}H} NMR (101 MHz, DMSO) δ 140.44 (*C*(*para*-CH_3)), 140.24 (*C*(*para*-CH_3)), 137.54 (N*CH*N), 137.20 (N*CH*N), 134.35 (N*C*(C(*ortho*-CH_3))$_2$), 134.26 (N*C*(C(*ortho*-CH_3))$_2$), 131.13 (C(*ortho*-CH_3)), 130.85 (C(*ortho*-CH_3)), 129.30 (CH_{Mes}), 129.24 (CH_{Mes}), 127.96 (CH*CH*N), 124.67 (N*CH*CHN), 124.04 (N*CH*CHN), 123.26 (NCH*CH*N), 120.57 (NCH*CH*N), 118.28 (CH_2*CH*CH), 47.69 (*CH*$_2$CHCH), 20.60 (*para*-CH_3), 17.18 (*ortho*-CH_3), 17.10 (*ortho*-CH_3).

Anal. Calcd.: C, 56.66; H, 5.64; N, 9.79. **Found**: C, 56.32; H, 5.67; N, 9.92.

FAB-MS ([M]$^{+}$): m/z 492.7 [**H$_2$(L7^{Mes})Br$_2$**−1×Br^{-}]$^{+}$.

1,1'-(prop-1-ene-1,3-diyl)bis(3-mesitylimidazolium) dihexafluorophosphate

H$_2$(L7^{Mes})(PF$_6$)$_2$

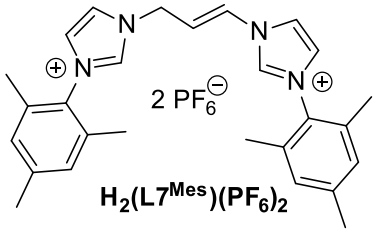

Sum formula: $C_{27}H_{32}F_{12}N_4P_2$
Molar mass: 702.51 g·mol^{-1}

To a solution of 500.0 mg (0.87 mmol, 1.0 eq.) of **H$_2$(L7^{Mes})Br$_2$** in 12 mL of hot water a solution of 356.0 mg (2.18 mmol, 2.5 eq.) of NH_4PF_6 in 3 mL of water is added. The obtained suspension is vigorously stirred for 30 min. Subsequently, the crude product is filtered off, washed with water and dried under dynamic vacuum. **H$_2$(L7^{Mes})(PF$_6$)$_2$** is obtained as colourless electrostatic solid. Yield: 545.9 mg (89 %)

^{1}H NMR (400 MHz, DMSO-d_6) δ 9.77 (br s, 1H, N*CH*N), 9.48 (br s, 1H, N*CH'*N), 8.46 (t, $^{3}J_{HH}$ = 1.8 Hz, 1H, N*CH*CHN), 8.12 – 8.09 (m, 2H, N*CH'*CH'N, NCH*CH*N), 8.02 (t, $^{3}J_{HH}$ = 1.8 Hz, 1H, NCH'*CH'*N), 7.54 (d, $^{3}J_{HH}$ = 14.1 Hz, 1H, NCH$_2$CH*CH*N), 7.18 (s, 2H, H_{Mes}), 7.17 (s, 2H, H'$_{Mes}$), 6.83 (dt, $^{3}J_{HH}$ = 14.1 Hz, $^{3}J_{HH}$ = 7.1 Hz, 1H, NCH$_2$*CH*CHN), 5.23 (d, $^{3}J_{HH}$ = 7.0 Hz, 2H, N*CH*$_2$CHCHN), 2.34 (br s, 6H, *para*-CH_3), 2.06 (s, 6H, *ortho*-CH_3), 2.04 (s, 6H, *ortho*-CH_3).

^{13}C{^{1}H} NMR (101 MHz, DMSO) δ 140.65 (*C*(*para*-CH_3)), 140.47 (*C*(*para*-CH_3)), 137.55 (NC'HN), 137.38 (NC'HN), 137.22 (NCHN), 137.14 (NCHN), 134.36 (NC*C*(*ortho*-CH_3)), 134.29 (NC*C*(*ortho*-CH_3)), 131.16 (N*C*C(*ortho*-CH_3)), 130.89 (N*C*C(*ortho*-CH_3)), 129.49 (CH, Mes), 129.44 (CH, Mes), 129.24 (C'H, Mes), 129.19 (C'H, Mes), 128.30 (NCH$_2$CH*CH*N), 128.11 (NCH$_2$CH*CH*N), 124.88 (NCH*CH*N), 124.32 (NCH'*CH'*N), 124.30 (NCH'*CH'*N), 123.22 (N*C'H*C'HN), 120.55 (N*CH*CHN), 120.39 (N*CH*CHN), 118.21 (NCH$_2$*CH*CHN), 117.98

(NCH$_2$*C*HCHN), 47.82 (NCHCH*C*H$_2$N), 20.70 (*para*-CH$_3$), 20.52 (*para*-CH$_3$), 17.04 (*ortho*-CH$_3$), 16.90 (*ortho*-CH$_3$).

Anal. Calcd.: C, 46.16; H, 4.59; N, 7.98. **Found**: C, 45.79; H, 4.54; N, 7.99.

ESI-MS ([M]$^+$): m/z 1258.82 (17 %) [2×**H$_2$(L7^{Mes})(PF$_6$)$_2$**−1×PF$_6^-$]$^+$, 557.17 (100 %) [**H$_2$(L7^{Mes})(PF$_6$)$_2$**−1×PF$_6^-$]$^+$, 206.30 (77 %) [**H$_2$(L7^{Mes})(PF$_6$)$_2$**−2×PF$_6^-$]$^{2+}$.

1,1'-(prop-1-ene-1,3-diyl)bis(3-mesitylimidazolium) ditetraphenylborate H$_2$(L7^{Mes})(BPh$_4$)$_2$

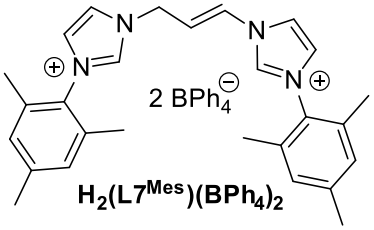

Sum formula: $C_{75}H_{72}B_2N_4$

Molar mass: 1051.05 g·mol^{-1}

To a solution of 299.0 mg (0.52 mmol, 1.0 eq.) of **H$_2$(L7^{Mes})Br$_2$** in 25 mL of hot H$_2$O a solution of 448.0 mg (1.30 mmol, 2.5 eq.) of NaBPh$_4$ in 25 mL of H$_2$O is added. The obtained suspension is vigorously stirred overnight at RT. The crude product is filtered off, washed with water and dried under dynamic vacuum. **H$_2$(L7^{Mes})(BPh$_4$)$_2$** is obtained as white highly electrostatic solid. Yield: 346.3 mg (63 %).

^{1}H NMR (400 MHz, DMSO-*d$_6$*) *δ* 9.75 (s, 1H, NC*H*N), 9.45 (s, 1H, NC*H*N), 8.43 (virt t, $^3J_{HH} \approx {}^4J_{HH}$ = 1.8 Hz, 1H, NC*H*CHN), 8.13 – 8.03 (m, 2H, NCH*CH*N), 7.97 (virt t, $^3J_{HH} \approx {}^4J_{HH}$ = 1.8 Hz, 1H, NC*H*CHN), 7.52 (d, $^3J_{HH}$ = 14.1 Hz, 1H, CH$_2$CH*CH*), 7.25 – 7.11 (m, 20H, 4H$_{Mes}$ and 16 *ortho*-CH, BPh$_4$), 6.94 (virt t, $^3J_{HH}$ = 7.4 Hz, 16H, meta-CH, BPh$_4$), 6.82 – 6.79 (m, 9H, CH$_2$*CH*CH and 8 *para*-CH, BPh$_4$), 5.19 (d, $^3J_{HH}$ = 7.2 Hz, 2H, *CH$_2$*CHCH), 2.34 (s, 6H, *para*-CH$_3$), 2.06 (s, 6H, *ortho*-CH$_3$), 2.04 (s, 6H, *ortho*-CH$_3$).

^{13}C{^{1}H} NMR (101 MHz, DMSO) *δ* 163.37 (q, $^1J_{CB}$ = 49.3 Hz, CB, BPh$_4$), 140.61 (*C*(*para*-CH$_3$)), 140.42 (*C*(*para*-CH$_3$)), 137.39 (N*CH*N), 137.11 (N*CH*N), 135.54 (m, *ortho*-CH, BPh$_4$), 134.28 (N*C*C(*ortho*-CH$_3$)), 134.22 (N*C*C(*ortho*-CH$_3$)), 131.11 (*C*(*ortho*-CH$_3$), 130.84 (*C*(*ortho*-CH$_3$), 129.32 (CH$_{Mes}$), 129.28 (CH$_{Mes}$), 128.15 (CH$_2$CH*CH*), 125.31 (q, $^3J_{CB}$ = 2.7 Hz, *meta*-CH, BPh$_4$), 124.85 (N*CH*CHN), 124.26 (N*CH*CHN), 123.17 (NCH*CH*N), 121.53 (s, *para*-CH, BPh$_4$), 120.40 (NCH*CH*N), 118.02 (CH$_2$*CH*CH), 47.75 (*CH$_2$*CHCH), 20.61 (*para*-CH$_3$), 16.96 (*ortho*-CH$_3$).

Anal. Calcd.: C, 85.71; H, 6.91; N, 5.33. **Found**: C, 85.10; H, 6.89; N, 5.31.

FAB-MS ([M]$^+$): m/z 730.5 [**H$_2$(L7^{Mes})(BPh$_4$)$_2$**−1×BPh$_4^-$]$^+$.

5.2.3 Synthetic Procedures Described in Chapter 3

5.2.3.1 *N*-(3,5-Di-*tert*-butyl-2-hydroxyphenyl) and *N*-(3,5-Di-*tert*-butyl-2-hydroxybenzyl) Functionalised Pro-ligands $H_2(L1^R)Br$ and $H_3(L2)Br$

General Procedures for Salt Elimination Reactions of Corresponding Alkali Metal NHC Adducts with REM Precursors

Route **A**

Unless otherwise stated, 3.0 eq. of **$H_2(L1^R)Br$** are suspended in THF and subsequently treated with the solution of KN" (6.0 eq.) in THF at specified temperature. The reaction mixture is then stirred for a specified amount of time. In the next step the solution of corresponding alkali metal NHC adduct is transferred to a suspension of 1.0 eq. of chosen REM precursor in THF through a cannula equipped with a glass fibre filter. The resulting mixture is stirred again for a specified amount of time at various temperatures. After the completion of the reaction the solution is separated by filtration. Crude product is obtained after the evaporation of the solvent into dryness.

Route **B**

Unless otherwise stated, 1.0 eq. of **$H_3(L2)Br$** and 3.0 eq. of MN" (M = Na, K) are placed into a Schenk tube and the respective solvent is added at specified temperature. The reaction mixture is subsequently stirred for a specified amount of time. In the next step the solution of corresponding alkali metal NHC adduct is transferred to a suspension/solution of 1.0 eq. of a chosen REM precursor in THF through a cannula equipped with a glass fibre filter. The resulting mixture is stirred again for a specified amount of time at various temperatures. After the completion of the reaction the resulting solution is separated by filtration. Crude product is obtained after the evaporation of the solvent into dryness.

All experiments described in this section are depicted in Table 5.2.10. The purification of the obtained compounds was attempted by slow diffusion of pentane into a solution of respective sample in THF at RT as well as out THF/toluene mixtures by cooling down to –26 °C.

General Procedure for the Reaction of **$H_2(L1^R)Br$** and **$H_3(L2)Br$** with Li[Ce{N(*i*-Pr)$_2$}$_4$](THF)

Route **A**: NMR Scale

Unless otherwise stated 1.0 eq. of respective imidazolium salt and 1.0 eq. of Li[Ce{N(*i*-Pr)$_2$}$_4$](THF) were placed into a J-Young NMR tube and 0.6 mL of respective deuterated solvent are added at RT. An overview of conducted experiments is given in Table 5.2.11.

Table 5.2.10. Overview of conducted two-steps reactions of **$H_2(L1^{Me})Br$** and **$H_3(L2)Br$** with various alkali metal bases and REM precursors.

Ex. No.	Route	Pro-ligand	Amount of pro-ligand	Amount of the base		Reaction conditions for the 1st step	REM precursor	Amount of the REM precursor	Reaction conditions for the 2nd step
				NaN"	KN"				
1	A	**$H_2(L1^{Me})Br$**	300.0 mg (1.05 mmol)		416.4 mg (2.09 mmol)	10 mL of THF –78 °C, 2 h	$Ce(BH_4)_3(THF)_4$	164.6 mg (3.48×10^{-4} mol)	15 mL of THF slowly warming up from –78 °C until RT over 18 h
2	B	**$H_3(L2)Br$**	500.0 mg (0.85 mmol)	477.5 mg (2.60 mmol)		3 mL of THF RT, 2 h	$CeCl_3(THF)_2$	333.5 mg (0.85 mmol)	5 mL of THF RT, 72 h
3	B		416.2 mg (0.71 mmol)	397.5 mg (2.17 mmol)		2.5 mL of THF –78 °C, 1 h	$CeCl_3(THF)_2$	277.6 mg (0.71 mmol)	5 mL of THF slowly warming up from –78 °C until RT, stirring at RT for 72 h
4	B		500.0 mg (0.85 mmol)		519.5 mg (2.60 mmol)	3 mL of THF RT, 2 h	$CeCl_3(THF)_2$	333.5 mg (0.85 mmol)	6 mL of THF RT, 24 h
5	B		500.0 mg (0.85 mmol, 1.0 eq.)		528.0 mg (2.64 mmol, 3.1 eq.)	2.5 mL of THF –78 °C, 1 h	$Ce(BH_4)_3(THF)_4$	404.0 mg (0.85 mmol. 1.0 eq.)	5 mL of THF slowly warming up from –78 °C until RT over 18 h

Table 5.2.11. Overview of the NMR scale reactions investigating the reactivity of **$H_2(L1^R)Br$** and **$H_3(L2)Br$** with Li[Ce{N(i-Pr)$_2$}$_4$](THF).

Ex. No.	Compound	Amount of the pro-ligand	Amount of Li[Ce{N(*i*-Pr)$_2$}$_4$](THF)	Solvent
1	**$H_2(L1^{Me})Br$**	10.0 mg (3.48×10^{-5} mol)	21.6 mg (3.48×10^{-5} mol)	THF-d_8
2		15.0 mg (5.21×10^{-5} mol)	32.0 mg (5.21×10^{-5} mol)	C_6D_6
3		15.0 mg (5.22×10^{-5} mol)	37.7 mg (6.09×10^{-5} mol, 1.17 eq.)	C_6D_6
4	**$H_2(L1^{Mes})Br$**	10.0 mg (2.12×10^{-5} mol)	13.1 mg (2.12×10^{-5} mol)	THF-d_8
5		20.0 mg (4.24×10^{-5} mol)	30.7 mg (4.96×10^{-5} mol, 1.17 eq.)	C_6D_6
6	**$H_3(L2)Br$**	10.0 mg (1.70×10^{-5} mol)	10.6 mg (1.70×10^{-5} mol)	THF-d_8
7		15.0 mg (2.56×10^{-5} mol)	15.9 mg (2.56×10^{-5} mol)	C_6D_6

Cerium NHDC Complex $Li_2[Ce_3(L1^{Me*})_3(N\{i\text{-}Pr\}_2)_5](THF)_2$

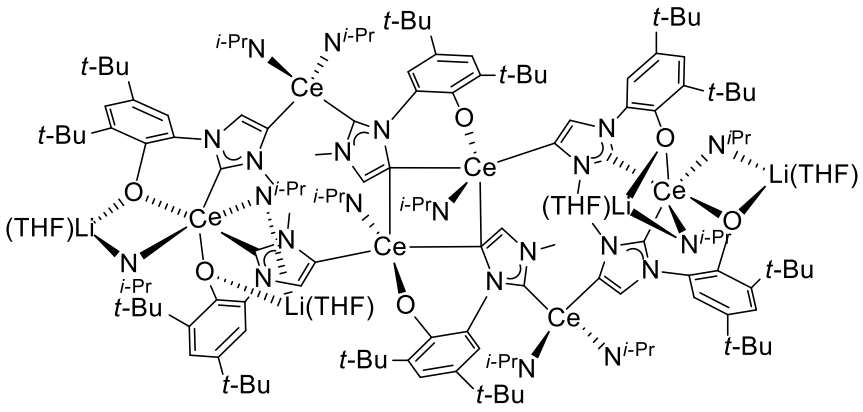

$Li_2[Ce_3(L1^{Me*})_3(N\{i\text{-}Pr\}_2)_5](THF)_2$

Sum formula:
$Ce_6Li_4C_{184}H_{316}N_{22}O_{10}$
Molar mass:
3865.22 g·mol^{-1}

Experiment No. 3 (Table 5.2.11). After approximately 1 week bright orange crystals are formed. Yield: quant.

^{7}Li NMR (156 MHz, C_6D_6) δ 38.01.

Route **B**: Preparatory Scale

1.0 eq. of respective imidazolium bromide and 1.0 eq. of Li[Ce{N(*i*-Pr)$_2$}$_4$](THF) are dissolved in THF, in which the reaction is instantaneously observed by visible rapid change of colour and consumption of the ligand precursor. The reaction mixture is further stirred for a specified amount of time at RT. Subsequently, toluene is added to the solution and the Schlenk tube is placed into the fridge (–26 °C) for crystallization. If applicable, the obtained solid is filtered off and further analysed by NMR spectroscopy. If no precipitation is observed, the solvent is removed *in vacuo* yielding the analysable crude product.

An overview of all conducted experiments in this section is given in Table 5.2.12.

Route **B**: Preparatory Scale

2.0 eq. of **H$_3$(L2)Br** or 3.0 eq. of **H$_2$(L1^{Me})Br**, 1.0 eq. of Li[Ce{N(*i*-Pr)$_2$}$_4$](THF) and 2.0 eq. of LDA are dissolved in 3 mL of THF at –26 °C in a glove box. A reaction is observed instantaneously in all cases and is more vigorous as by using route **A**. The Schlenk tube is quickly transported out of the box and placed into cryogenic bath (–78 °C). The reaction mixture is allowed to slowly warm up from –78 °C until RT over 18 h. Subsequently it is stirred for another 24 h at RT. Crude product is obtained after the evaporation of the solvent into dryness. Further purification was attempted by slow diffusion of pentane into a solution of the respective crude product in benzene or toluene. Also a crystallization out of toluene/DME solvent mixture is conducted yielding Li(DME)Br as colourless crystals.

An overview of all conducted experiments in this section is given in Table 5.2.12.

Table 5.2.12. Experiments investigating the reactivity of **$H_2(L1^R)Br$** and **$H_3(L2)Br$** with Li[Ce{N(*i*-Pr)$_2$}$_4$](THF) on preparatory scale.

Ex. No.	Route	Pro-ligand	Amount of pro-ligand	Amount of cerate	Amount of LDA	Reaction conditions
1	B	**$H_2(L1^{Me})Br$**	50.0 mg (0.17 mmol)	107.8 mg (0.17 mmol)		1.5 mL of THF RT, 1 h
2	C		500.0 mg (1.74 mmol)	362.3 mg (0.58 mmol)	130.8 mg (1.16 mmol)	3 mL of THF **1.** Addition of THF at –26 °C **2.** Slowly warming up from –78 °C until RT over 18 h
3	B	**$H_2(L2)Br$**	100.0 mg (0.17 mmol)	105.9 mg (0.17 mmol)		1.5 mL of THF RT, 1 h
4	C		500.5 mg (0.85 mmol)	268.0 mg (0.43 mmol)	94.6 mg (0.85 mmol)	3 mL of THF **1.** Addition of THF at –26 °C **2.** Slowly warming up from –78 °C until RT over 18 h **3.** RT, 1 d

5.2.3.2 1,1'-(2-Hydroxyethane-1,1-diyl)-Bridge Functionalised Pro-Ligands $H_3(L3^R)X_2$

General Procedure for Salt Elimination Reactions of Corresponding Alkali Metal NHC Adducts with REM Precursors

Unless otherwise stated, 1.0 eq. of **$H_3(L3^R)X_2$** and 3.0 eq. of the base are placed into a Schenk tube and the respective solvent is added at specified T. The reaction mixture is then stirred for a specified amount of time. Subsequently, the solution of corresponding alkali metal NHC adduct is transferred to a suspension/solution of 1.0 eq. of REM precursor in the same solvent through a cannula equipped with a glass fibre filter. The resulting mixture is stirred again for a specified amount of time at various temperatures. After the completion of the reaction the solution is separated by filtration. Crude product is obtained after the evaporation of the solvent into dryness. All experiments described in this section are depicted in Table 5.2.15.

General Procedure for the Reaction of Bis(imidazolium) Salts **$H_3(L3^{Mes})X_2$** with REM Precursors Acting as Internal Base

Route **A**

Unless otherwise stated 1.0 eq. of a bis(imidazolium) salt and 1.0 eq. of Li[Ce{N(*i*-Pr)$_2$}$_4$](THF) are placed into a J-Young NMR tube and 0.6 mL of respective deuterated solvent is added at RT. An overview of conducted experiments is given in Table 5.2.13.

Table 5.2.13. NMR scale reactions investigating the reactivity of **$H_3(L3^{Mes})X_2$** with Li[Ce{N(*i*-Pr)$_2$}$_4$](THF).

Ex. No.	Compound	Amount of the pro-ligand	Amount of Li[Ce{N(*i*-Pr)$_2$}$_4$](THF)	Solvent
1	**$H_3(L3^{Mes})Cl_2$**	9.2 mg (1.89×10^{-5} mol)	11.7 mg (1.89×10^{-5} mol)	THF-d_8
2	**$H_3(L3^{Mes})(BPh_4)_2$**	18.4 mg (1.74×10^{-5} mol)	10.8 mg (1.74×10^{-5} mol)	THF-d_8

Route B

Unless otherwise stated, 1.0 eq. of **$H_3(L3^{Mes})(BPh_4)_2$** and 1.0 eq. of Li[Ce{N(*i*-Pr)$_2$}$_4$](THF) are dissolved in THF. The reaction mixture is stirred for the specified amount of time at RT. Subsequently, the suspension is filtered off and the filtrate evaporated into dryness yielding crude product. An overview of conducted experiments is given in Table 5.2.14.

Table 5.2.14. Reaction conditions used for treating **$H_3(L3^{Mes})(BPh_4)_2$** with Li[Ce{N(*i*-Pr)$_2$}$_4$](THF).

Ex. No.	Amount of **$H_3(L3^{Mes})(BPh_4)_2$**	Amount of Li[Ce{N(*i*-Pr)$_2$}$_4$](THF)	Reaction conditions
1	109.5 mg (1.04×10^{-4} mol, 1.2 eq.)	54.2 mg (8.74×10^{-5} mol, 1.0 eq.)	5 mL of THF, RT, 72 h
2	150.0 mg (1.42×10^{-4} mol)	88.1 mg (1.42×10^{-4} mol)	10 mL of THF, RT, 18 h

Table 5.2.15. Overview of the conducted two-step reactions of 1,1'-(2-hydroxyethane-1,1-diyl)-bridge functionalised bis(imidazolium) salts with alkali metal bases and REM precursors.

Ex. No.	Pro-ligand	Amount of pro-ligand	Amount of the base		Reaction conditions for the 1st step	REM precursor	Amount of the REM precursor	Reaction conditions for the 2nd step
			LiN"	KN"				
1	**$H_3(L3^{Mes})Cl_2$**	102.7 mg (2.11×10^{-4} mol, 1.0 eq.)	97.5 mg (5.83×10^{-4} mol, 2.8 eq.)		5 mL of C_6H_6 RT, 2 h	CeN"$_3$	101.9 mg (1.64×10^{-4} mol, 0.8 eq.)	10 mL of C_6H_6 RT, 18 h
2		100.0 mg (2.05×10^{-4} mol, 1.0 eq.)		81.8 mg (4.10×10^{-4} mol, 2.0 eq.)	6 mL of THF RT, 30 min	CeN"$_3$	127.5 mg (2.05×10^{-4} mol, 1.0 eq.)	10 mL of THF RT, 72 h
3		100.0 mg (2.05×10^{-4} mol)		122.8 mg (6.15×10^{-4} mol)	6 mL of THF RT, 15 min	CeN"$_3$	127.5 mg (2.05×10^{-4} mol)	10 mL of THF RT, 72 h
4		72.7 mg (1.49×10^{-4} mol)	74.85 mg (4.47×10^{-4} mol)		10 mL of THF 0 °C, 30 min	$Ce(BH_4)_3(THF)_4$	70.6 mg (1.49×10^{-4} mol)	15 mL of THF **1.** 0 °C-RT, 2 h **2.** RT, 18 h
5		100.2 mg (2.05×10^{-4} mol, 1.0 eq.)	96.1 mg (5.74×10^{-4} mol, 2.8 eq.)		5 mL of C_6H_6 RT, 2 h	YCp_3	47.5 mg (1.67×10^{-4} mol, 0.8 eq.)	10 mL of C_6H_6 RT, 18 h

Ex. No.	Pro-ligand	Amount of pro-ligand	Amount of the base		Reaction conditions for the 1st step	REM precursor	Amount of the REM precursor	Reaction conditions for the 2nd step
			LiN"	KN"				
6		80.0 mg (0.16 mmol, 1.0 eq.)		83.0 mg (0.42 mmol, 2.6 eq.)	5 mL of THF RT, 30 min	YCp_3	39.4 mg (0.17 mmol, 1.1 eq.)	7 mL of THF **1.** RT, 18 h **2.** 80 °C, 1 h
7	**$H_3(L3^{Mes})(BPh_4)_2$**	134.0 mg (1.31×10^{-4} mol, 1.0 eq.)		78.2 mg (3.92×10^{-4} mol, 3.0 eq.)	8 mL of THF RT, 30 min	$CeCp_3$	49.0 mg (1.46×10^{-4} mol, 1.1 eq.)	10 mL of THF **1.** RT, 72 h **2.** 80 °C, 30 min
8		100 mg (9.76×10^{-5} mol, 1.0 eq.)		58.4 mg (2.90×10^{-4} mol, 2.9 eq.)	8 mL of THF RT, 30 min	YCp_3	27.7 mg (9.76×10^{-5} mol, 1.0 eq.)	10 mL of THF RT, 18 h
9	**$H_3(L3^{i\text{-}Pr})Cl_2$**	50.0 mg (2.98×10^{-4} mol)	74.9 mg (8.95×10^{-4} mol)		8 mL of THF **1.** –78 °C, 30 min **2.** 80 °C, 30 min	$Ce(BH_4)_3(THF)_4$	70.6 mg (2.98×10^{-4} mol)	10 mL of THF RT, 72 h

Route **C**

Unless otherwise stated, 1.0 eq. of $ScCl_3(THF)_3$ and 3.0 eq. of potassium benzyl (KBn) are placed into a Schlenk tube and 5 ml of THF are added at –78 °C. The reaction mixture is stirred of a specified amount of time at different temperatures. The solution of formed $ScBn_3$ is then subsequently transferred to the suspension of 1.0 eq. of respective bis(imidazolium) salt in THF. The resulting reaction mixture is stirred again for a specified amount of time at the specified temperature. In the next step the reaction solution is separated from the precipitate and the crude product is obtained by removing the solvent *in vacuo*. An overview of conducted experiments is given in Table 5.2.16.

Table 5.2.16. Overview of the reaction conditions used for treating $\mathbf{H_3(L3^{Mes})X_2}$ with $ScBn_3$.

Ex. No.	Amount of $ScCl_3(THF)_3$	Amount of KBn	Reaction conditions for the 1st step	Pro-ligand	Amount of the pro-ligand	Reaction conditions for the 2nd step
1	75.4 mg (0.21 mmol)	80.0 mg (0.62 mmol)	5 mL of THF **1.** –78 °C, 30 min **2.** 0 °C, 30 min	$\mathbf{H_3(L3^{Mes})Cl_2}$	100 mg (0.21 mmol)	10 mL of THF slowly warming up from 0 °C until RT within 18 h
2	52.0 mg (0.14 mmol)	55.3 mg (0.43 mmol)	5 mL of THF **1.** –78 °C, 30 min **2.** 0 °C, 30 min	$\mathbf{H_3(L3^{Mes})(PF_6)_2}$	100 mg (0.14 mmol)	10 mL of THF slowly warming up from –78 °C until RT within 18 h

5.2.3.3 1,1'-(2-Hydroxypropane-1,3-diyl)-Bridge Functionalised Pro-Ligand $\mathbf{H_3(L4^{Mes})Br_2}$

General Procedure for Salt Elimination Reactions of Corresponding Potassium NHC Adduct with REM Precursors

Route **A**

Unless otherwise stated, 1.0 eq. of $\mathbf{H_3(L4^{Mes})Br_2}$ are suspended in THF and subsequently treated with the solution of KN" (3.0 eq.) at specified temperature. The reaction mixture is then stirred for a specified amount of time. Subsequently, the solution of potassium NHC adduct is

transferred to a suspension/solution of 1.0 eq. of chosen REM precursor in THF through a cannula equipped with a glass fibre filter. The resulting mixture is stirred again for a specified amount of time at various temperatures. After the completion of the reaction the solution is separated by filtration. Crude product is obtained after the evaporation of the solvent into dryness.

Route **B**

Unless otherwise stated, 1.0 eq. of **$H_3(L4^{Mes})Br_2$** and 3.0 eq. of KN" are placed into a Schenk tube and THF is added at specified temperature. The reaction mixture is subsequently stirred for a specified amount of time. In the next step the solution of corresponding alkali metal NHC adduct is transferred to a suspension/solution of 1.0 eq. of chosen REM precursor in THF through a cannula equipped with a glass fibre filter. The resulting mixture is stirred again for a specified amount of time at various temperatures. After the completion of the reaction the solution is separated by filtration. Crude product is obtained after the evaporation of the solvent into dryness.

All experiments described in this section are depicted in Table 5.2.17. The purification of the obtained compounds was attempted by slow diffusion of pentane or Et_2O into a solution of crude product in THF at RT as well as out THF/toluene mixtures by cooling down to –26 °C.

The Reactions of Bis(imidazolium) Salt **$H_3(L4^{Mes})Br_2$** with Li[Ce{N(*i*-Pr)$_2$}$_4$](THF)

Route **A**

10 mg (1.7×10^{-5} mol, 1.0 eq.) of **$H_3(L4^{Mes})Br_2$** and 10.5 mg (1.7×10^{-5} mol, 1.0 eq.) of Li[Ce{N(*i*-Pr)$_2$}$_4$](THF) are placed into a J-Young NMR tube and 0.6 mL of THF-d_8 are added at RT.

Route **B**

150.0 mg (0.25 mmol. 1.0 eq.) of **$H_3(L4^{Mes})Br_2$** and 157.5 mg (0.25 mmol, 1.0 eq.) of Li[Ce{N(*i*-Pr)$_2$}$_4$](THF) are placed into a Schenk tube and 1.5 mL of benzene are added. The reaction mixture is stirred at RT for 4 h. Subsequently, the solution is filtered off and the solvent removed *in vacuo*. The purification of the obtained product mixture by crystallization *via* slow diffusion of pentane into a solution of the crude product in C_6F_6 at RT as well as *via* crystallization of out C_6F_6 at –26 °C was further attempted.

Table 5.2.17. Overview of the conducted two-step reactions of **$H_3(L4^{Mes})Br_2$** with alkali metal bases and REM precursors.

Ex. No.	Route	Amount of **$H_3(L4^{Mes})Br_2$**	Amount of KN"	Reaction conditions for the 1st step	REM precursor	Amount of the REM precursor	Reaction conditions for the 2nd step
1	A	200 mg (0.34 mmol)	230 mg (1.01 mmol)	5 mL of THF **1.** 0 °C, 1.5 h **2.** RT, 1.5 h	$CeCl_3(THF)_2$	132 mg (0.34 mmol)	7 mL of THF slowly warming up from 0 °C until RT within 20 h
2	B	1.000 g (1.69 mmol)	1.014 g (5.08 mmol)	5 mL of THF **1.** 0 °C, 1 h **2.** RT, 30 min	$CeI_3(THF)_{2.5}$	1.187 g (1.69 mmol)	10 mL of THF RT, 72 h
3	A	200 mg (0.34 mmol)	230 mg (1.01 mmol)	5 mL of THF **1.** 0 °C, 1 h **2.** RT, 20 min	$CeN"_3$	209.9 gm (0.34 mmol)	8 mL of THF RT, 18 h
4	A	150 mg (0.25 mmol)	152.0 mg (0.75 mmol)	5 mL of THF slowly warming up from –78 °C until RT over 20 h	$CeCp_3$	85.2 mg (0.25 mmol)	8 mL of THF **1.** –78 °C, 1.5 h **2.** 0 °C, 45 min **3.** RT, 30 min
5	A	300.0 mg (0.51 mmol)	304.0 mg (1.52 mmol)	5 mL of THF slowly warming up from –30 °C until 0 °C over 2 h	$Ce(BH_4)_3(THF)_4$	240.3 mg (0.51 mmol)	10 mL of THF slowly warming up from 0 °C until RT over 18 h

Ex. No.	Route	Amount of **$H_3(L4^{Mes})Br_2$**	Amount of KN"	Reaction conditions for the 1st step	REM precursor	Amount of the REM precursor	Reaction conditions for the 2nd step
6	A	1.00 g (1.69 mmol)	1.014 g (5.08 mmol)	14 mL of THF slowly warming up from –78 °C until –30 °C over 24 h	$Ce(BH_4)_3(THF)_4$	801.4 mg (1.69 mmol)	21 mL of THF slowly warming up from –30 °C until RT, stirring at RT for 6 d
7	A	1.00 g (1.69 mmol)	1.014 g (5.08 mmol)	14 mL of THF RT, 1.5 h	$Ce(BH_4)_3(THF)_4$	801.4 mg (1.69 mmol)	22 mL of THF RT, 18 h
8	A	200.0 mg (0.34 mmol)	230.0 mg (1.01 mmol)	5 mL of THF **1.** 0 °C, 1 h **2.** RT, 15 min	$ScCl_3(THF)_3$	124.2 mg (0.34 mmol)	8 mL of THF slowly warming up from 0 °C until RT over 15 h
9	A	200.0 mg (0.34 mmol, 1.2 eq.)	230.0 mg (1.01 mmol, 3.6 eq.)	5 mL of THF **1.** 0 °C, 1.5 h **2.** RT, 2 h	$ScCl_3(THF)_3$	103.7 mg (0.28 mmol, 1.0 eq.)	8 mL of THF slowly warming up from 0 °C until RT over 15 h
10	A	300.0 mg (0.51 mmol)	304.0 mg (1.53 mmol)	5 mL of THF **1.** 0 °C, 1.5 h **2.** RT, 2 h	$ScCl_3(THF)_3$	186.7 mg (0.51 mmol)	8 mL of THF slowly warming up from 0 °C until RT, stirring at RT for 72 h

Table 5.2.18. Overview of the conducted two-step reactions using *N*-furanyl-substituted bis(imidazolium)salts.

Ex. No.	Pro-ligand	Amount of the pro-ligand	Amount of KN"	Reaction conditions for the 1st step	REM precursor	Amount of the REM precursor	Reaction conditions for the 2nd step
1	**$H_2(L5^{Fu})Br_2$**	69.8 mg (1.58×10^{-4} mol, 1.1 eq.)	34.0 mg (1.7×10^{-4} mol, 1.08 eq.)	6 mL of THF RT, 30 min	$CeN"_3$	89.2 mg (1.44×10^{-4} mol, 1.0 eq.)	12 ml of THF RT, 48 h
2		42.8 mg (9.67×10^{-5} mol, 1.0 eq.)	37.2 mg (1.84×10^{-4} mol, 1.9 eq.)	6 mL of THF RT, 30 min	$CeN"_3$	60.1 mg (9.67×10^{-5} mol, 1.0 eq.)	11 mL of THF slowly warming up from 0 °C until RT
3		137.4 mg (3.12×10^{-4} mol, 1.1 eq.)	62.2 mg (3.25×10^{-4} mol, 1.15 eq.)	6 mL of THF RT, 30 min	$CeCl_3(THF)_2$	110.4 mg (2.82×10^{-4} mol, 1.0 eq.)	12 ml of THF RT, 48 h
4	**$H_2(L5^{tFu})Br_2$**	200.0 mg (1.64×10^{-4} mol, 1.0 eq.)	96.5 mg (4.84×10^{-4} mol, 2.9 eq.)	5 mL of toluene RT, 30 min	$Ce(BH_4)_3(THF)_4$	160.8 mg (1.70×10^{-4} mol, 1.04 eq.)	10 mL of toluene RT, 72 h
5		59.5 mg (9.67×10^{-5} mol, 1.0 eq.)	37.6 mg (1.89×10^{-4} mol, 1.95 eq.)	6 mL of toluene RT. 15 min	$Ce(BH_4)_3(THF)_4$	31.4 mg (9.26×10^{-5} mol, 0.95 eq.)	12 mL of toluene 0 °C–4 °C, 4 d

5.2.3.4 *N*-Furanyl-Functionalised Pro-Ligands $H_2(L5^R)X_2$ and $H_2(L6^R)X_2$

General Procedure for Salt Elimination Reactions with KN" and REM Precursors

Unless otherwise stated, 1.0 eq. of the corresponding bis(imidazolium) salt are suspended in a solvent of the choice and treated with the solution of 2.0 eq. of KN" in the same solvent. The reaction mixture is stirred for specified amount of time at RT. Subsequently, the solution of formed alkali metal NHC adduct is transferred to a solution/suspension of corresponding REM precursor *via* filtration though a cannula equipped with a glass fibre filter. The reaction mixture is stirred again for the specified amount of time at RT. After the completion of the reaction the precipitate is separated by filtration and crude product is obtained by evaporation of the filtrate. An overview of the conducted reactions is given in Table 5.2.18.

General Procedures for the Reaction of Bis(imidazolium) Salts **$H_2(L5^R)X_2$** with $CeN"_3$

Route **A**

Unless otherwise stated 1.0 eq. of a bis(imidazolium) salt and 1.0 eq. of $Ce\{N(SiMe_3)_2\}_3$ are placed into a J-Young NMR tube and 0.6 mL of respective deuterated solvent are added at RT. An overview of the conducted reactions is given in Table 5.2.19.

Route **B**

34.6 mg (7.83×10^{-5} mol,1.0 eq.) of **$H_2(L5^{Fu})Br_2$** suspended in 5 mL of THF are treated with the solution of 51.0 mg (8.21×10^{-5} mol, 1.05 eq.) of $CeN"_3$ in 5 mL of THF at –30 °C. The reaction mixture is stirred for 18 h and concomitantly allowed to slowly warm up to RT. After the completion of the reaction the precipitate is separated by filtration and the crude product is obtained by evaporation of the filtrate.

Reactivity of Tetraazafulvalene **$L6^{tFu}$** with REM Precursors

Unless otherwise stated, 1.0 eq. of **$H_2(L6^{tFu})X_2$** and 2.0 eq. of KN" are placed into a Schenk tube and the respective solvent is added at RT. The reaction mixture is stirred for a specified amount of time at RT. Subsequently, the solution of **$L6^{tFu}$** is transferred to a suspension/solution of 1.0 eq. of REM precursor in the same solvent and stirred again for a specified amount of time at various temperatures. After the completion of the reaction the solution is separated by filtration and the crude product is obtained after the evaporation of the solvent into dryness. All conducted experiments in this section are depicted in Table 5.2.20.

Table 5.2.19. Overview of the NMR scale reactions investigating the reactivity of *N*-furanyl modified bis(imidazolium)salts with cerium tris(bis(trimethylsilyl)amides).

Ex. No.	Compound	Amount of the pro-ligand	Amount of CeN"$_3$	Solvent
1	**$H_2(L5^{Fu})Br_2$**	10.0 mg (2.27×10^{-5} mol)	14.1 mg (2.27×10^{-5} mol)	THF-d_8
2	**$H_2(L5^{Fu})(BPh_4)_2$**	14.7 mg (1.60×10^{-5} mol)	9.9 mg (1.60×10^{-5} mol)	THF-d_8
3		20.0 mg (2.17×10^{-5} mol)	13.5 mg (2.17×10^{-5} mol)	THF-d_8
4	**$H_2(L6^{Fu})Br_2$**	10.0 mg (2.19×10^{-5} mol)	13.6 mg (2.19×10^{-5} mol)	THF-d_8
5		14.7 mg (3.22×10^{-5} mol)	20.0 mg (3.22×10^{-5} mol)	Pyridine-d_5
6	**$H_2(L6^{Fu})(BPh_4)_2$**	20.2 mg (2.16×10^{-5} mol)	13.4 mg (2.16×10^{-5} mol)	THF-d_8
7		20.0 mg (2.14×10^{-5} mol)	13.3 mg (2.14×10^{-5} mol)	THF-d_8
8		30.1 mg (3.22×10^{-5} mol)	20.0 mg (3.22×10^{-5} mol)	Pyridine-d_5
9	**$H_2(L5^{tFu})Br_2$**	21.3 mg (3.49×10^{-5} mol)	13.9 mg (6.98×10^{-5} mol)	THF-d_8
10	**$H_2(L5^{tFu})(BPh_4)_2$**	22.6 mg (2.07×10^{-5} mol)	12.9 mg (2.07×10^{-5} mol)	THF-d_8
11		25.0 mg (2.99×10^{-5} mol)	9.2 mg (4.59×10^{-5} mol)	THF-d_8
12		14.7 mg (1.35×10^{-5} mol)	15.0 mg (2.41×10^{-5} mol, 1.79 eq.)	Pyridine-d_5
13	**$H_2(L6^{tFu})Br_2$**	20.1 mg (3.22×10^{-5} mol)	20.0 mg (3.22×10^{-5} mol)	Pyridine-d_5
14	**$H_2(L6^{tFu})(BPh_4)_2$**	17.8 mg (1.61×10^{-5} mol)	10.0 mg (1.61×10^{-5} mol)	Pyridine-d_5

Table 5.2.20. Overview of the experiments investigating the reactivity of **L6^{tFu}** with REM precursors.

Ex. No.	Compound	Amount of **H_2(L6^{tFu})X_2**	Amount of KN"	Reaction conditions for the 1st step	REM precursor	Amount of the REM precursor	Reaction conditions for the 2nd step
1	**H_2(L6^{tFu})Br_2**	148.3 mg (0.24 mmol)	99.5 mg (0.50 mmol)	5 mL of C_6H_6 RT, 30 min	CeN"$_3$	147.6 mg (0.24 mmol)	10 ml of C_6H_6 **1.** RT, 18 h **2.** 80 °C, 18 h
2	**H_2(L6^{tFu})$(BPh_4)_2$**	71.0 mg (6.44×10^{-5} mol, 1.0 eq.)	27.0 mg (1.35×10^{-4} mol, 2.1 eq.)	5 mL of C_6H_6 RT, 1 h	CeN"$_3$	40.0 mg (6.44×10^{-5} mol, 1.0 eq.)	10 mL of C_6H_6 RT, 18 h
	H_2(L6^{tFu})Br_2	200.0 mg (0.32 mmol, 1.0 eq.)	124.6 mg (0.62 mmol, 1.95 eq.)	6 mL of toluene RT, 20 min	$Ce(BH_4)_3(THF)_4$	124.5 mg (0.32 mmol, 1.0 eq.)	12 mL of toluene RT, 72 h
3		200.0 mg (0.32 mmol, 1.0 eq.)	124.6 mg (0.62 mmol, 1.95 eq.)	6 mL of C_6H_6 6 °C, 2 h	$Ce(BH_4)_3(THF)_4$	124.5 mg (0.32 mmol, 1.0 eq.)	12 mL of C_6H_6 6 °C, 18 h
4		200.0 mg (0.32 mmol, 1.0 eq.)	124.6 mg (0.62 mmol, 1.95 eq.)	5 mL of toluene RT, 1.5 h	$Ce(BH_4)_3(THF)_4$	124.5 mg (0.32 mmol, 1.0 eq.)	11 mL of toluene –15 °C, 3 d

5.2.3.5 1,1'-(Prop-1-ene-1,3-diyl)-Bridge Functionalised Bis(imidazolium) Salts $H_2(L7^{Mes})Br_2$

General Procedures for the Reaction of **$H_2(L7^{Mes})Br_2$** with Li[Ce{N(*i*-Pr)$_2$}$_4$](THF)

Route **A**

Unless otherwise stated 1.0 eq. of respective bis(imidazolium) salt and 1.0 eq. of Li[Ce{N(*i*-Pr)$_2$}$_4$](THF) are placed into a J-Young NMR tube and 0.6 mL of THF-d_8 are added at RT. An overview of conducted experiments is given in Table 5.2.21.

Table 5.2.21. Overview of the NMR scale reactions investigating the reactivity of 1,1'-(prop-1-ene-1,3-diyl)-bridged functionalised imidazolium salts **$H_2(L7^{Mes})X_2$** with Li[Ce{N(*i*-Pr)$_2$}$_4$](THF).

Ex. No.	Pro-ligand	Amount of the pro-ligand	Amount of Li[Ce{N(*i*-Pr)$_2$}$_4$](THF)	Solvent
1	**$H_2(L7^{Mes})Br_2$**	8.8 mg (1.54×10^{-5} mol)	9.5 mg (1.53×10^{-5} mol)	THF-d_8
2	**$H_2(L7^{Mes})(BPh_4)_2$**	10.6 mg (1.01×10^{-5} mol)	6.3 mg (1.01×10^{-5} mol)	THF-d_8

Route **B**

42.7 mg (1.04×10^{-4} mol, 1.2 eq.) of $ScCl_3(THF)_{2.9}$ and 34.1 mg (2.62×10^{-4} mol, 3.0 eq.) of potassium benzyl (KBn) are placed into a Schlenk tube and 5 ml of THF are added at 0 °C. The reaction mixture is slowly warmed up until RT. Subsequently, the solution of formed $ScBn_3$ is transferred to the suspension of 50.0 mg (8.73×10^{-5} mol, 1.0 eq.) of **$H_2(L7^{Mes})Br_2$** in 5 mL of THF. The resulting reaction mixture is stirred again for 30 min at 0 °C, then for 18 h at RT. After the completion of the reaction the brown solution is separated from the precipitate by filtration and crude product is obtained by removing the solvent *in vacuo*.

Route **C**

68.2 mg (0.12 mmol, 1.0 eq.) of **$H_2(L7^{Mes})Br_2$** and 48.5 mg (0.12 mmol, 1.0 eq.) of $YCl_3(THF)_{3.5}$ are suspended in 5 mL of THF and cooled down to –78 °C. 0.22 mL of *n*-BuLi (1.6 M solution in THF, 0.36 mmol, 3.0 eq.) are slowly added to the mixture. The reaction mixture is subsequently allowed to warm up until RT over 18 h. After the completion of the reaction the

resulting brown solution is separated from formed precipitate by filtration and the crude product is obtained after the evaporation of the solvent into dryness.

5.2.4 Synthetic Procedures Described in Chapter 4

5.2.4.1 Synthesis of Ag(I) bis(NHC) Complexes $Ag_2(HL3^R)_2X_2$ and $Ag_2(L7^{Mes})_2X_2$

General Procedure

Route **A**

This preparation method is based on the synthesis of similar Ag(I) complexes published by Kühn.[173b] In a Schlenk tube 1.0 eq. of bis(imidazolium) chloride and 3.0 eq. of Ag_2O are suspended in 3-6 mL of water. The mixture is stirred 18 h at RT under exposure to light. Subsequently, the suspension is centrifuged and the precipitate is washed with water (3×5 mL). The combined aqueous solutions are filtered over celite and a saturated aqueous solution of either NH_4PF_6 or $NaBPh_4$ is added to the solution. The obtained suspension is stirred and precipitate is again separated by centrifugation. The brown precipitate is washed with water (3×5 mL) and dried under dynamic vacuum. Purification is carried out by repeated fractional precipitation from specified solvent mixtures, as brown, oily, silver containing impurities precipitate before the desired compounds.

Route **B**

In a Schlenk tube 1.0 eq. of bis(imidazolium) tetraphenylborate or bis(imidazolium) hexafluorophosphate and 3.0 eq. of Ag_2O are suspended in a mixture of 5 mL of acetonitrile and 0.5 mL of water. The mixture is then stirred 18 h at RT under exposure to light. Subsequently, the suspension is centrifuged and the precipitate is washed with acetonitrile (3×5 mL). The combined supernatants are filtered over celite and the solvent is removed under vacuum. The crude product is washed with water (3×5 mL) and dried again under dynamic vacuum. It is then subsequently dissolved in specified solvent mixtures and purified repeatedly by fractional precipitation with pentane or diethyl ether.

$Ag_2(HL3^{Me})_2(BPh_4)_2$

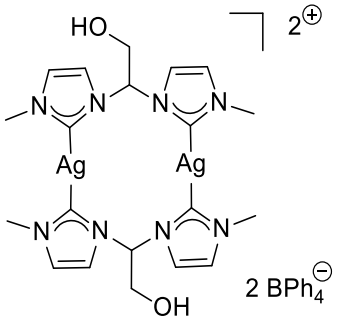

$Ag_2(HL3^{Me})_2(BPh_4)_2$

Sum formula: $C_{68}H_{68}Ag_2B_2N_8O_2$

Molar mass: 1266.70 g·mol^{-1}

$Ag_2(HL3^{Me})_2(BPh_4)_2$ is synthesized according to the route **A**. 500.0 mg (1.80 mmol, 1.0 eq.) of **$H_3(L3^{Me})Cl_2$** and 1.04 g (4.50 mmol, 2.5 eq.) of silver oxide are stirred in 5 mL of water for 18 hours. The crude product is precipitated by adding a saturated solution of $NaBPh_4$ in water. **$Ag_2(HL3^{Me})_2(BPh_4)_2$** is purified by repeated fractional precipitation from wet acetone with pentane yielding white solid containing 1.5 equivalents of acetone. Yield: 71.6 mg (6 %).

^{1}H NMR (400 MHz, DMSO-d_6) δ 8.07 and 7.96 (2 br s, 4H, N*CH*CHN), 7.57 (br s, 4H, NCH*CH*N), 7.36 (t, $^3J_{HH}$ = 6.9 Hz, 2H, N*CH*(CH_2OH)N), 7.20 – 7.14 (m, 16H, *ortho*-CH, BPh_4), 6.92 (virt t, $^3J_{HH}$ = 7.4 Hz, 16H, *meta*-CH, BPh_4), 6.86 – 6.64 (m, 8H, *para*-CH, BPh_4), 5.84 (s, 2H, OH), 4.40 and 4.34 (d, $^3J_{HH}$ = 7.1 Hz and br s, 4H, CH(*CH_2*OH)), 3.85 (s, 12H, CH_3).

^{13}C{^{1}H} NMR (101 MHz, DMSO) δ 163.36 (q, $^1J_{CB}$ = 49.35 Hz, CB, BPh_4), 135.54 (br s, *ortho*-CH, BPh_4), 125.31 (q, $^3J_{CB}$ = 2.70 Hz, *meta*-CH, BPh_4), 124.67 (N*CH*CHN), 121.52 (s, *para*-CH. BPh_4), 118.50 (NCH*CH*N), 74.26 (N*CH*(CH_2OH)N), 60.09 (NCH(*CH_2*OH)N), 38.49 (CH_3).

Anal. Calcd. for **$Ag_2(HL3^{Me})_2(BPh_4)_2$** + 1.5 eq. acetone: C, 64.32; H, 5.73; N, 8.28. Found: C, 63.82; H, 5.49; N, 8.26.

ESI-MS ([M]$^+$): m/z 946.45 (14 %) [**$Ag_2(HL3^{Me})_2(BPh_4)_2$**−1×$BPh_4^-$]$^+$, 672.25 (40 %) [**$Ag_2(HL3^{Me})_2(BPh_4)_2$**−2×$BPh_4^-$ +$CHOO^-$]$^+$, 314.21 (100 %) [**$Ag_2(HL3^{Me})_2(BPh_4)_2$**−2×$BPh_4^-$]$^{2+}$.

$Ag_2(HL3^{i\text{-}Pr})_2(PF_6)_2$

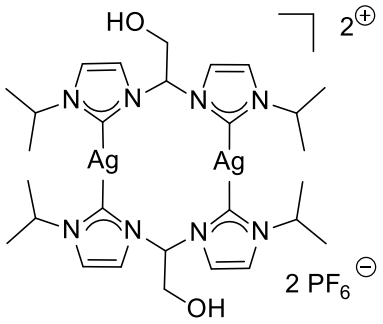

Sum formula: $C_{28}H_{44}Ag_2F_{12}N_8O_2P_2$

Molar mass: 1030.38 g·mol^{-1}

$Ag_2(HL3^{i\text{-}Pr})_2(PF_6)_2$

$Ag_2(HL3^{i\text{-}Pr})_2(PF_6)_2$ is synthesized according to the route **A**. 200.0 mg (0.60 mmol, 1.0 eq.) of **$H_3(L3^{i\text{-}Pr})Cl_2$** and 346.0 mg (1.49 mmol, 2.5 eq.) of silver oxide are stirred in 3 mL of water for 66 hours. The crude product is precipitated by adding a saturated solution of NH_4PF_6 in water. **$Ag_2(HL3^{i\text{-}Pr})_2(PF_6)_2$** is purified by repeated fractional precipitation from wet acetonitrile with diethyl ether. The compound is obtained as white solid. Yield: 198.6 mg (65 %).

^{1}H NMR (400 MHz, MeCN-d_3) δ 7.57 (br s, 4H, N*CH*CHN), 7.38 (d, $^3J_{HH}$ = 1.8 Hz, 4H, NCH*CH*N), 7.03 (br s, 2H, N*CH*(CH_2OH)N), 4.67 (virt p, $^3J_{HH}$ = 6.8 Hz, 4H, CH_3*CH*CH_3), 4.39 (d, $^3J_{HH}$ = 5.4 Hz, 4H, *CH_2*OH), 3.90 (s, 2H, OH), 1.48 (d, $^3J_{HH}$ = 6.7 Hz, 12H, CH_3), 1.45 (d, $^3J_{HH}$ = 6.7 Hz, 12H, CH_3H).

DOSY NMR (400 MHz, CD_3CN) D [m^{2}s^{-1}] = 8.45×10^{-10}.

DOSY NMR (400 MHz, DMSO-d_3) D [m^{2}s^{-1}] = 1.28×10^{-10}.

^{13}C{^{1}H} NMR (101 MHz, CD_3CN) δ 181.32 (br d, $^1J_{AgC}$ = 182.60 Hz, NCN), 120.63 (N*CH*CHN), 119.61 (NCH*CH*N), 76.73 (N*CH*(CH_2OH)N), 61.92 (NCH(*CH_2*OH)N), 55.77 (CH_3*CH*CH_3), 23.88 (*CH_3*$CHCH_3$), 23.50 (CH_3CH*CH_3*).

Anal. Calcd.: C, 32.64; H, 4.30; N, 10.88. **Found**: C, 32.45; H, 4.27; N, 10.68.

ESI-MS ([M]$^+$): m/z 884.92 (100 %) [**$Ag_2(HL3^{i\text{-}Pr})_2(PF_6)_2$**−1×$PF_6^-$]$^+$, 370.31 (98 %) [**$Ag_2(HL3^{i\text{-}Pr})_2(PF_6)_2$**−2×$PF_6^-$]$^{2+}$.

$Ag_2(HL3^{i\text{-}Pr})_2(BPh_4)_2$

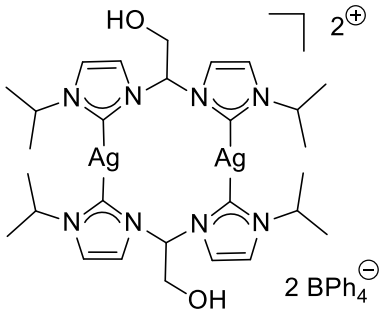

$Ag_2(HL3^{i\text{-}Pr})_2(BPh_4)_2$

Sum formula: $C_{76}H_{84}Ag_2B_2N_8O_2$

Molar mass: 1378.92 g·mol^{-1}

$Ag_2(HL3^{i\text{-}Pr})_2(BPh_4)_2$ is synthesized according to the route **A**. 1.00 g (2.98 mmol, 1.0 eq.) of **$H_3(L3^{i\text{-}Pr})Cl_2$** and 1.73 g (7.46 mmol, 2.5 eq.) of Ag_2O are stirred in 10 mL of H_2O for 13 days. The crude product is precipitated by adding a saturated solution of $NaBPh_4$ in H_2O. **$Ag_2(HL3^{i\text{-}Pr})_2(BPh_4)_2$** is purified by fractional precipitation from acetone with pentane. The compound is obtained as white solid containing 0.5 eq. of acetone. Yield: 881.0 mg (43 %).

^{1}H NMR (400 MHz, Acetonitrile-d_3) δ 7.54 (br s, 4H, N*CH*CHN), 7.35 (br s, 4H, NCH*CH*N), 7.27 (m, 16H, *ortho*-CH, BPh_4), 6.99 (t, $^3J_{HH}$ = 7.4 Hz, 18H, N*CH*N and *meta*-CH, BPh_4), 6.88 – 6.79 (m, 8H, *para*-CH, BPh_4), 4.72 – 4.57 (m, 4H, *CH*$(CH_3)_2$), 4.38 (t, $^3J_{HH}$ = 5.1 Hz, 4H, *CH*$_2$OH), 3.80 (s, 2H, OH), 1.47 (d, $^3J_{HH}$ = 6.7 Hz, 12H, CH_3), 1.43 (d, $^3J_{HH}$ = 6.8 Hz, 12H, CH_3).

DOSY NMR (400 MHz, CD_3CN) D [m^{2}s^{-1}] = 1.12×10^{-9} ($Ag_2(NHC)_2^{2+}$), 1.42×10^{-9} (BPh_4^-).

DOSY NMR (400 MHz, DMSO-d_3) D [m^{2}s^{-1}] = 1.31×10^{-10} ($Ag_2(NHC)_2^{2+}$), 2.21×10^{-10} (BPh_4^-).

^{13}C{^{1}H} NMR (101 MHz, CD_3CN) δ 181.34 (br d, $^1J_{AgC}$ = 205.80 Hz, NCN), 164.78 (q, $^1J_{CB}$ = 49.4 Hz, CB, BPh_4), 136.73 (q, $^2J_{AgC}$ = 1.4 Hz, *ortho*-CH, BPh_4), 126.58 (q, $^3J_{CB}$ = 2.8 Hz, *meta*-CH, BPh_4), 122.76 (*para*-CH, BPh_4), 120.72 (N*CH*CHN), 119.74 (NCH*CH*N), 76.73 (N*CH*N), 62.00 (*CH*$_2$OH), 55.83 (*CH*$(CH_3)_2$), 24.00 (CH_3), 23.62 (CH_3).

Anal. Calcd for **$Ag_2(HL3^{i\text{-}Pr})_2(BPh_4)_2$** + 0.5 eq. of acetone: C, 66.11; H, 6.23; N, 7.96. **Found**: C, 65.97; H, 6.18; N, 8.22.

ESI-MS ([M]$^+$): m/z 1058.72 (54 %) [**$Ag_2(HL3^{i\text{-}Pr})_2(BPh_4)_2$**−1×$BPh_4^-$]$^+$, 370.32 (100 %) [**$Ag_2(HL3^{i\text{-}Pr})_2(BPh_4)_2$**−2×$BPh_4^-$]$^{2+}$.

$Ag_2(HL3^{Mes})_2(PF_6)_2$

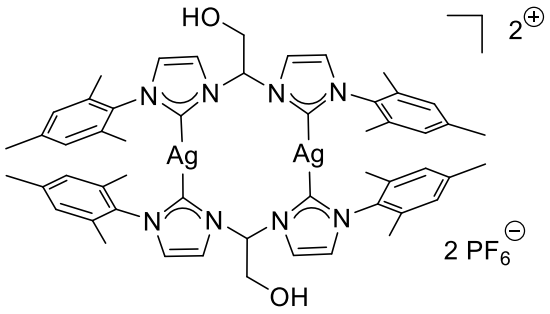

$Ag_2(HL3^{Mes})_2(PF_6)_2$

Sum formula: $C_{52}H_{60}Ag_2F_{12}N_8O_2P_2$

Molar mass: 1334.77 g·mol^{-1}

$Ag_2(HL3^{Mes})_2(PF_6)_2$ is synthesized according to the route **B**. 500.0 mg (0.71 mmol, 1.0 eq.) of **$H_3(L3^{Mes})(PF_6)_2$** and 410.0 mg (1.80 mmol, 2.5 eq.) of silver oxide are stirred in 6 mL of acetonitrile for 5 days. The crude product is purified by repeated fractional precipitation from DCM with pentane. The compound is obtained as white solid. Yield: 195.4 mg (42 %).

^{1}H NMR (400 MHz, MeCN-d_3) δ 7.75 (s, 4H, N*CH*CHN), 7.21 (t, $^3J_{HH}$ = 5.9 Hz, 2H, N*CH*(CH_2OH)N), 7.12 (s, 4H. NCH*CH*N), 7.01 (s, 4H, H_{Mes}), 6.95 (s, 4H, H_{Mes}), 4.57 (virt t, $^3J_{HH}$ = 5.4 Hz, 4H, CH*CH_2*OH), 3.98 (t, $^3J_{HH}$ = 4.8 Hz, 2H, OH), 2.45 (s, 12H, CH_3), 1.66 (s, 12H, CH_3), 1.34 (s, 12H, CH_3).

^{13}C{^{1}H} NMR (126 MHz, MeCN-d_3) δ 183.23 (dd, $^1J^{107}_{AgC}$ = 181.9 Hz, $^1J^{109}_{AgC}$ = 211.1 Hz, NCN), 140.50 (*ortho*-CH_3C*C*N), 135.83 (*para*-CH_3*C*), 135.35 (*ortho*-CH_3*C*CN), 135.25 (*ortho*-CH_3*C*CN), 130.28 (s, CH_{Mes}), 125.67 (d, $^3J_{AgC}$ = 6.0 Hz, N*CH*CHN), 120.09 (d, $^3J_{AgC}$ = 5.2 Hz, NCH*CH*N), 76.01 (*CH*CH_2OH), 61.38 (s, CH*CH_2*OH), 21.25 (s, *para*-CH_3), 17.38 (s, *ortho*-CH_3), 17.28 (s, *ortho*-CH_3).

Anal. Calcd.: C, 46.79; H, 4.53; N, 8.40. **Found**: C, 46.73; H, 4.45; N, 8.21.

ESI-MS ([M]$^+$): m/z 1189.07 (40 %) [**$Ag_2(HL3^{Mes})_2(PF_6)_2$**−1×$PF_6^-$]$^+$, 522.45 (100 %) [**$Ag_2(HL3^{Mes})_2(PF_6)_2$**−2×$PF_6^-$]$^{2+}$.

$Ag_2(HL3^{Mes})_2(BPh_4)_2$

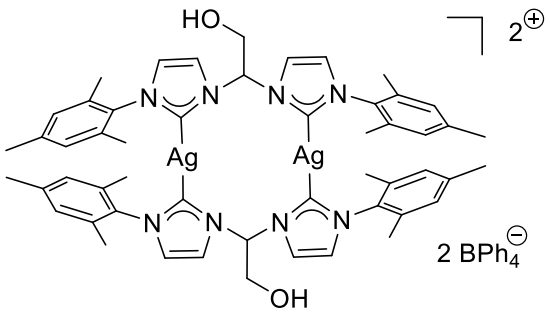

$Ag_2(HL3^{Mes})_2(BPh_4)_2$

Sum formula: $C_{100}H_{100}Ag_2B_2N_8O_2$

Molar mass: 1686.31 g·mol^{-1}

$Ag_2(HL3^{Mes})_2(BPh_4)_2$ is synthesized according to the route **B**. 400.0 mg (0.38 mmol, 1.0 eq.) of **$H_3(L3^{Mes})(BPh_4)_2$** and 219.6 mg (0.95 mmol, 2.5 eq.) of Ag_2O are stirred in 4 mL of MeCN for 66 hours. The crude product is purified by repeated fractional precipitation from MeCN with Et_2O. The compound is obtained as off-white solid. Yield: 49.0 mg (15 %).

^{1}H NMR (400 MHz, Acetonitrile-d_3) δ 7.73 (virt t, 4H, N*CH*CHN), 7.29 – 7.24 (m, 16H, *ortho*-CH, BPh_4), 7.20 (t, $^3J_{HH}$ = 5.9 Hz, 2H, N*CH*(CH_2OH)N), 7.09 (virt t, 4H, NCH*CH*N), 7.02 – 6.93 (m, 24H, 8 CH, Mes and 16 *meta*-CH, BPh_4), 6.83 (t, $^3J_{HH}$ = 7.2 Hz, 8H, *para*-CH, BPh_4), 4.55 (virt t, $^3J_{HH}$ = 5.5 Hz, 4H, NCH(*CH_2*OH)N), 3.97 (t, $^3J_{HH}$ = 5.3 Hz, 2H, OH), 2.45 (s, 12H, *para*-CH_3), 1.65 (s, 12H, *ortho*-CH_3), 1.33 (s, 12H, *ortho*-CH_3).

^{13}C{^{1}H} NMR (101 MHz, Acetonitrile-d_3) δ 182.22 (NCN), 164.52 (q, $^1J_{CB}$ = 49.4 Hz), 140.53 (*ortho*-CH_3*C*CN), 137.24 – 136.28 (m, *ortho*-CH, BPh_4), 135.84 (*para*-CH_3*C*), 135.36 (*ortho*-CH_3*C*CN), 135.26 (*ortho*-CH_3*C*CN), 130.30 (CH, Mes), 126.57 (q, $^3J_{CB}$ = 2.8 Hz, *meta*-CH, BPh_4), 125.70 (d, $^3J_{AgC}$ = 6.0 Hz, N*CH*CHN), 122.74, 120.11 (d, $^3J_{AgC}$ = 5.3 Hz, NCH*CH*N), 76.02 (N*CH*(CH_2OH)N), 61.43 (NCH(*CH_2*OH)N), 21.28 (*para*-CH_3), 17.41 (*ortho*-CH_3), 17.31 (*ortho*-CH_3).

Anal. Calcd.: C, 71.35; H, 5.99; N, 6.66. **Found**: C, 71.28; H, 6.07; N, 6.41.

ESI-MS ($[M]^+$): m/z 1362.91 (52 %) [**$Ag_2(HL3^{Mes})_2(BPh_4)_2$**−1×$BPh_4^-$]$^+$, 522.45 (100 %) [**$Ag_2(HL3^{Mes})_2(BPh_4)_2$**−2×$BPh_4^-$]$^{2+}$.

$Ag_2(L7^{Mes})_2(PF_6)_2$

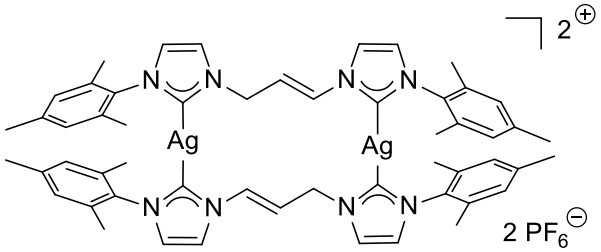

$Ag_2(L7^{Mes})_2(PF_6)_2$

Sum formula: $C_{54}H_{60}Ag_2F_{12}N_8P_2$
Molar mass: 1326.79 g·mol^{-1}

$Ag_2(L7^{Mes})_2(PF_6)_2$ is synthesized according to the route **B**. 450.0 mg (0.64 mmol, 1.0 eq.) of **$H_2(L7^{Mes})(PF_6)_2$** and 371.0 mg (1.60 mmol, 2.5 eq.) of Ag_2O are stirred in 5 mL of wet MeCN for 4 days. The crude product is purified by repeated fractional precipitation from DCM with pentane. The compound is obtained as white solid. Yield: 326.0 mg (77 %).

^{1}H NMR spectrum shows two isomers, but the signals of the second species are very small and therefore difficult to integrate.

^{1}H NMR (400 MHz, Acetonitrile-d_3) δ 7.70 (s, 2H, N*CH*CHN), 7.64 (d, $^3J_{HH}$ = 14.3 Hz, 1H, N*CH*CHCH_2N), 7.43 (br s, 2H, N*CH'*CHN), 7.10 (br s, 2H, NCH*CH*N), 7.07 (br s, 2H,

NCH*CH'*N), 6.92 (br s, 8H, H_{Mes}), 6.31 (dt, $^3J_{HH}$ = 14.4, 7.3 Hz, 2H, NCH*CH*CH_2N), 4.98 (d, $^3J_{HH}$ = 7.3 Hz, 4H, NCHCH*CH*$_2$N), 2.42 (s, 6H, *para*-CH_3), 2.40 (s, 6H, *para*-CH_3), 1.68 (s, 12H, *ortho*-CH_3), 1.53 – 1.47 (m, 12H, *ortho*-CH_3).

^{13}C{^{1}H} NMR (101 MHz, CD_3CN) δ 185.05 (dd, $^1J^{107}_{AgC}$ = 180.1 Hz, $^1J^{109}_{AgC}$ = 208.8 Hz, NCN), 182.06 (dd, $^1J^{107}_{AgC}$ = 185.1 Hz, $^1J^{109}_{AgC}$ = 214.1 Hz, NC'N), 140.41 (*ortho*-CH_3C*C*N), 139.99 (*ortho*-CH_3C*C'*N), 137.07 (*para*-CH_3*C*), 135.83 (*para*-CH_3*C'*), 135.56 (*ortho*-CH_3*C*CN), 135.33 (*ortho*-CH_3*C'*CN), 132.83 (d, $^3J_{AgC}$ = 2.4 Hz, N*CH*CHCH$_2$N), 130.10 (CH, Mes), 129.89 (C'H, Mes), 125.48 (d, $^3J_{AgC}$ = 5.75 Hz, N*CH*CHN), 124.22 (d, $^3J_{AgC}$ = 5.85 Hz, N*CH'*CHN), 123.03 (d, $^3J_{AgC}$ = 5.89 Hz, NCH*CH*N), 118.79 (d, $^3J_{AgC}$ = 4.96 Hz, NCH*CH'*N), 117.11 (NCH*CH*CH$_2$N), 50.93 (NCHCH*CH*$_2$N), 21.27 (para-CH_3), 21.20 (para-CH_3'), 17.66 (ortho-CH_3), 17.37 (ortho-CH_3').

Anal. Calcd.: C, 48.88; H, 4.56; N, 8.45. **Found**: C, 48.52; H, 4.52; N, 8.32.

ESI-MS ([M]$^+$): m/z 1181.28 (15 %) [**Ag$_2$(L7^{Mes})$_2$(PF$_6$)$_2$**−1×PF_6^-]$^+$, 518.74 (100 %) [**Ag$_2$(L7^{Mes})$_2$(PF$_6$)$_2$**−2×PF_6^-]$^{2+}$.

Ag$_2$(L7^{Mes})$_2$(BPh$_4$)$_2$

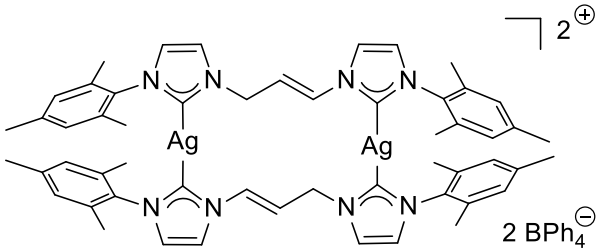

Ag$_2$(L7^{Mes})$_2$(BPh$_4$)$_2$

Sum formula: $C_{102}H_{100}Ag_2B_2N_8$

Molar mass: 1675.33 g·mol^{-1}

Ag$_2$(L7^{Mes})$_2$(BPh$_4$)$_2$ is synthesized according to the route **B**. 242.3 mg (0.23 mmol, 1.0 eq.) of **H$_2$(L7^{Mes})(BPh$_4$)$_2$** and 134.2 mg (0.58 mmol, 2.5 eq.) of Ag_2O are stirred in 5 mL of wet MeCN for 3 days. The crude product is purified by repeated fractional precipitation from DCM with pentane. The compound is obtained as white solid. Yield: 91.7 mg (24 %).

^{1}H NMR (400 MHz, Acetonitrile-d_3) δ 7.64 – 7.57 (m, 4H, N*CH*CHN and N*CH*CHCH$_2$N), 7.37 (virt t, $^3J_{HH} \approx {}^4J_{HH}$ = 1.7 Hz, 2H, N*CH'*CHN), 7.30 – 7.24 (m, 16H, *ortho*-CH, BPh_4), 7.08 (virt t, $^3J_{HH} \approx {}^4J_{HH}$ = 1.6 Hz, 2H, NCH*CH*N), 7.02 (br s, 2H, NCH*CH'*N), 6.98 (virt t, $^3J_{HH}$ = 7.4 Hz, 16H, *meta*-CH, BPh_4), 6.92 (s, 4H, H_{Mes}), 6.91 (s, 4H, H_{Mes}), 6.83 (t, $^3J_{HH}$ = 7.2 Hz, 8H, *para*-CH, BPh_4), 6.22 (dt, $^3J_{HH}$ = 14.5 Hz, 7.3 Hz, 2H, NCH*CH*CH$_2$N), 4.91 (d, $^3J_{HH}$ = 7.2 Hz, 4H, NCHCH*CH*$_2$N), 2.40 (s, 6H, *para*-CH_3), 2.42 (s, 6H, *para*-CH_3), 1.68 (s, 12H, *ortho*-CH_3), 1.49 (s, 12H, *ortho*-CH_3).

$^{13}C\{^{1}H\}$ NMR (101 MHz, CD_3CN) δ 184.96 (dd, $^{1}J^{107}_{AgC}$ = 180.5 Hz, $^{1}J^{109}_{AgC}$ = 209.0 Hz, NCN), 181.94 (dd, $^{1}J^{107}_{AgC}$ = 181.0 Hz, $^{1}J^{109}_{AgC}$ = 213.7 Hz, NC'N), 164.68 (q, $^{1}J_{CB}$ = 2.7 Hz, CB, BPh_4), 140.35 (*ortho*-CH_3CCN), 139.93 (*ortho*-$CH_3CC'N$), 136.99 (*para*-CH_3C), 136.73 – 136.51 (m, *ortho*-CH, BPh_4), 135.75 (*para*-CH_3C'), 135.48 (*ortho*-CH_3CCN), 135.25 (*ortho*-$CH_3C'CN$), 132.73 (d, $^{3}J_{AgC}$ = 2.5 Hz, N*C*H$CHCH_2N$), 130.03 (CH, Mes), 129.83 (CH', Mes), 126.52 (q, $^{3}J_{CB}$ = 49.3 Hz, *meta*-CH, BPh_4), 125.38 (d, $^{3}J_{AgC}$ = 5.8 Hz, N*C*HCHN), 124.17 (d, $^{3}J_{AgC}$ = 5.9 Hz N*C*H'CHN), 122.97 (d, $^{3}J_{AgC}$ = 5.9 Hz, $NCHCHN$), 122.69 (s, *para*-CH, BPh_4), 118.72 (d, $^{3}J_{AgC}$ = 5.2 Hz NCH*C*H'N), 116.98 (NCH_2CHCHN), 50.87 (NCH_2CHCHN), 21.21 (*para*-CH_3), 21.15 (*para*-CH_3), 17.62 (*ortho*-CH_3), 17.34 (*ortho*-CH_3).

Anal. Calcd.: C, 73.13; H, 6.02; N, 6.69. **Found**: C, 73.44; H, 6.10; N, 6.52.

ESI-MS ($[M]^+$): m/z 1354.89 (54 %) [**$Ag_2(L7^{Mes})_2(BPh_4)_2$**$-1\times BPh_4^-]^+$, 1080.85 (8 %) [**$Ag_2(L7^{Mes})_2(BPh_4)_2$**$-2\times BPh_4^- + CHOO^-]^+$, 518.66 (100 %) [**$Ag_2(L7^{Mes})_2(BPh_4)_2$**$-2\times BPh_4^-]^{2+}$.

5.2.4.2 Synthesis of Au(I) bis(NHC) Complexes $Au_2(HL3)_2X_2$ and $Au_2(L7)_2X_2$

General Procedure

The synthesis of Au(I) complexes is based on the transmetallation reaction via respective Ag(I) complexes published by Kühn.[173b] In a Schlenk tube the 1.0 eq. of respective Ag(I) complex and 2.1 eq. of $AuCl(SMe_2)$ are placed. The reaction vessel is evacuated and placed under argon atmosphere. 3-5 mL of dry acetonitrile is added and the suspension is stirred at specified temperature for a specified amount of time. Subsequently the precipitate is separated by centrifugation and the solid is washed with 1 mL of acetonitrile twice. The combined organic solutions are filtered over celite and the solvent is removed under reduced pressure to yield the crude product. The complexes are purified by ether recrystallization from suitable solvent mixtures, fractional precipitation or chromatography.

$Au_2(HL3^{Me})_2(BPh_4)_2$

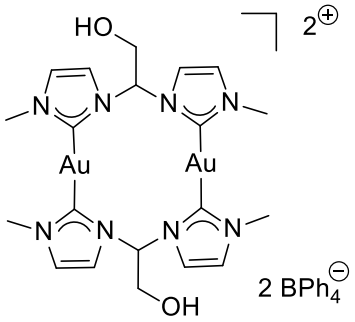

$Au_2(HL3^{Me})_2(BPh_4)_2$

Sum formula: $C_{68}H_{68}Au_2B_2N_8O_2$

Molar mass: 1444.90 g·mol^{-1}

50.0 mg (3.95×10^{-5} mol, 1.0 eq.) of **$Ag_2(HL3^{Me})_2(BPh_4)_2$** and 24.4 mg ($8.29\times10^{-5}$ mol, 2.1 eq.) of $AuCl(SMe_2)$ are stirred at RT in 5 mL of dry acetone for 17 hours. The crude product is purified by repeated fractional precipitation from acetone by Et_2O or pentane. The compound is obtained as off-white solid. Yield: 29.5 mg (52 %).

^{1}H NMR (400 MHz, DMSO-d_6) δ 8.02 (s, 4H, N*CH*CHN), 7.64 (s, 4H, NCH*CH*N), 7.17 (br s, 16H, *ortho*-CH, BPh_4), 6.92 (virt t, $^3J_{HH}$ = 7.3 Hz, 16H, *meta*-CH, BPh_4), 6.78 (t, $^3J_{HH}$ = 7.1 Hz, 10H, 8 *para*-CH, BPh_4 and 2 N*CH*(CH_2OH)N), 4.36 (d, $^3J_{HH}$ = 7.3 Hz, 4H, NCH(*CH_2*OH)N), 3.90 (s, 12H, CH_3).

ESI-MS ($[M]^+$): m/z 1125.04 (7 %) [**$Au_2(HL3^{Me})_2(BPh_4)_2$**−1×$BPh_4^-$]$^+$, 850.72 (28 %) [**$Au_2(HL3^{Me})_2(BPh_4)_2$**−2×$BPh_4^-$ +$CHOO^-$]$^+$, 403.4 (100 %) [**$Au_2(HL3^{Me})_2(BPh_4)_2$**−2×$BPh_4^-$]$^{2+}$.

$Au_2(HL3^{i\text{-}Pr})_2(PF_6)_2$

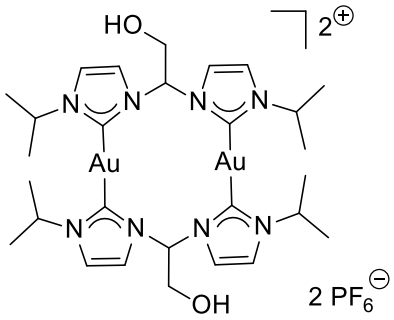

Sum formula: $C_{28}H_{44}Au_2F_{12}N_8O_2P_2$

Molar mass: 1208.58 g·mol^{-1}

$Au_2(HL3^{i\text{-}Pr})_2(PF_6)_2$

100.0 mg (0.10 mmol, 1.0 eq.) of **$Ag_2(HL3^{i\text{-}Pr})_2(PF_6)_2$** and 57.2 mg (0.19 mmol, 2.0 eq.) of $AuCl(SMe_2)$ are stirred at RT in 3 mL of MeCN for 10 days. The crude product is purified by repeated fractional precipitation from acetone by pentane. The compound is obtained as white solid containing two conformation isomers in a 4/5 (syn/anti) ratio. Yield: 94.7 mg (81 %).

^{1}H NMR (400 MHz, Acetonitrile-d_3) δ 7.69 (d, $^3J_{HH}$ = 2.1 Hz, 4H, N*CH*CHN, syn-isomer), 7.57 (d, $^3J_{HH}$ = 2.2 Hz, 4H, N*CH*CHN, anti-isomer), 7.45 (d, $^3J_{HH}$ = 2.2 Hz, 4H, NCH*CH*N, syn-isomer), 7.44 – 7.38 (m, 6H, NCH*CH*N and N*CH*(CH_2OH)N, anti-isomer), 7.35 (t, $^3J_{HH}$ = 6.5 Hz, 2H, N*CH*(CH_2OH)N), 5.02 (hept, $^3J_{HH}$ = 6.85 Hz, 4H, *CH*(CH_3)$_2$, syn-isomer), 4.89 (hept, $^3J_{HH}$ = 6.7 Hz, 4H, *CH*(CH_3)$_2$, anti-isomer), 4.38 (virt t, $^3J_{HH}$ = 5.7 Hz, 4H, NCH(*CH_2*OH)N, anti-isomer), 4.32 (virt t, $^3J_{HH}$ = 6.1 Hz, 4H, NCH(*CH_2*OH)N, syn-isomer), 3.87 (t, $^3J_{HH}$ = 5.4 Hz, 2H, OH, anti-isomer), 3.80 (t, $^3J_{HH}$ = 5.7 Hz, 2H, OH, syn-isomer), 1.57 – 1.42 (m, 48H, CH_3, anti- and syn-isomers).

^{13}C{^{1}H} NMR (101 MHz, CD_3CN) δ 184.19 (NCN), 121.19 (NCH*CH*N, syn), 120.67 (NCH*CH*N, anti), 119.99 (N*CH*CHN, anti), 119.63 (N*CH*CHN, syn), 75.76 (N*CH*(CH_2OH)N, syn), 74.89 (N*CH*(CH_2OH)N, anti), 62.20 (CH*CH_2*OH, syn), 61.96 (CH*CH_2*OH, anti), 55.39 (*CH*(CH_3)$_2$,

anti), 55.35 (*CH*$(CH_3)_2$, syn), 23.78 (CH_3, syn), 23.50 (CH_3, anti), 23.28 (CH_3, anti), 22.91 (CH_3, syn).

Anal. Calcd.: C, 27.83; H, 3.67; N, 9.27. **Found**: C, 27.92; H, 3.73; N, 9.22.

ESI-MS ($[M]^+$): m/z 1058.72 (32 %) [**$Au_2(HL3^{i\text{-}Pr})_2(PF_6)_2$**$-1\times PF_6^-]^+$, 459.45 (100 %) [**$Au_2(HL3^{i\text{-}Pr})_2(PF_6)_2$**$-2\times PF_6^-]^{2+}$.

$Au_2(HL3^{i\text{-}Pr})_2(BPh_4)_2$

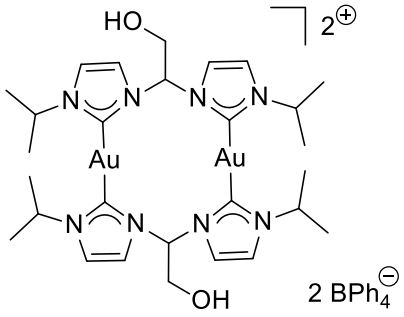

$Au_2(HL3^{i\text{-}Pr})_2(BPh_4)_2$

Sum formula: $C_{76}H_{84}Au_2B_2N_8O_2$
Molar mass: 1557.11 g·mol^{-1}

200.0 mg (0.15 mmol, 1.0 eq.) of **$Ag_2(HL3^{i\text{-}Pr})_2(BPh_4)_2$** and 89.7 mg (0.30 mmol, 2.1 eq.) of $AuCl(SMe_2)$ are stirred at RT in 6 mL of MeCN for 4 days. The crude product is purified by repeated recrystallization from acetone/toluene mixture at –26 °C. The compound is obtained as white solid with an approximate isomer ratio anti/syn of 2:1. Yield: 69.5 mg (31 %).

^{1}H NMR (400 MHz, Acetonitrile-d_3) δ 7.68 (d, $^3J_{HH}$ = 2.2 Hz, 4H, *anti*-N*CH*CHN), 7.56 (d, $^3J_{HH}$ = 2.2 Hz, 4H, *syn*-N*CH*CHN), 7.43 (d, $^3J_{HH}$ = 2.2 Hz, 4H, *anti*-NCH*CH*N), 7.39 (d, $^3J_{HH}$ = 2.2 Hz, 4H, *syn*-NCH*CH*N), 7.35 (t, $^3J_{HH}$ = 6.6 Hz, 4H, *syn&anti*-N*CH*(CH_2OH)N), 7.30 – 7.22 (m, 32H, *ortho*-CH, BPh_4), 6.99 (virt t, $^3J_{HH}$ = 7.4 Hz, 32H, *meta*-CH, BPh_4), 6.88 – 6.79 (m, 16H, *para*-CH, BPh_4), 5.01 (virt p, $^3J_{HH}$ = 6.8 Hz, 4H, *anti-CH*$(CH_3)_2$), 4.90 (virt p, $^3J_{HH}$ = 6.7 Hz, 4H, *syn-CH*$(CH_3)_2$), 4.35 (d, $^3J_{HH}$ = 6.0 Hz, 4H, *anti-*CH_2OH), 4.29 (br s, 4H, *syn-*CH_2OH), 3.79 (br s, 2H, *anti*-OH), 1.54 – 1.41 (m, 48H, *syn&anti* CH(CH_3)$_2$).

^{13}C{^{1}H} NMR (101 MHz, CD_3CN) δ 183.99 (NCN), 164.68 (q, $^1J_{CB}$ = 49.2 Hz, CB, BPh_4), 136.67 – 136.57 (m, *ortho*-CH, BPh_4), 126.51 (q, $^3J_{CB}$ = 2.7 Hz, *meta*-CH, BPh_4), 122.67 (*para*-CH, BPh_4), 121.17 (*anti*-N*CH*CHN), 120.66 (*syn*-N*CH*CHN), 119.91 (*anti*-NCH*CH*N), 119.63 (*syn*-NCH*CH*N), 75.69 (anti-N*CH*(CH_2OH)N), 74.92 (*syn*-N*CH*(CH_2OH)N), 62.17 (*anti*-NCH(CH_2OH)N), 61.95 (*syn*-NCH(CH_2OH)N), 55.35 (*anti-CH*$(CH_3)_2$), 55.32 (*syn-CH*$(CH_3)_2$), 23.78 (*anti*-CH_3), 23.50 (*syn*-CH_3), 23.25 (*syn*-CH_3'), 22.89 (*anti*-CH_3').

Anal. Calcd.: C, 58.62; H, 5.44; N, 7.2. **Found**: C, 58.13; H, 5.33; N, 7.26.

ESI-MS ($[M]^+$): m/z 1237.20 (48 %) [**$Au_2(HL3^{i\text{-}Pr})_2(BPh_4)_2$**$-1\times BPh_4^-]^+$, 962.83 (6 %) [**$Au_2(HL3^{i\text{-}Pr})_2(BPh_4)_2$**$-2\times BPh_4^- + CHOO^-]^+$, 459.51 (100 %) [**$Au_2(HL3^{i\text{-}Pr})_2(BPh_4)_2$**$-2\times BPh_4^-]^{2+}$.

$Au_2(HL3^{Mes})_2(PF_6)_2$

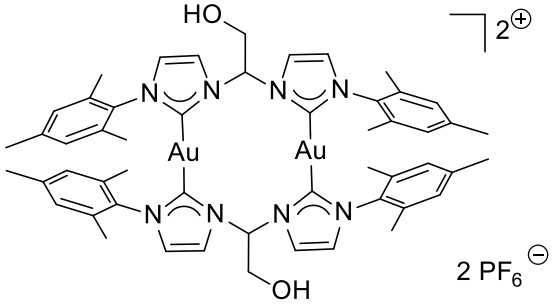

Sum formula: $C_{52}H_{60}Au_2F_{12}N_8O_2P_2$

Molar mass: 1512.97 g·mol^{-1}

$Au_2(HL3^{Mes})_2(PF_6)_2$

200.0 mg (0.5 mmol, 1.0 eq.) of **$Ag_2(HL3^{Mes})_2(PF_6)_2$** and 98.3 mg (0.3 mmol, 2.2 eq.) of AuCl(SMe_2) are stirred in 5 mL MeCN at 50 °C for 3 days. The crude product is purified by a double recrystallization from DCM/THF mixture at –26 °C. The compound is obtained as white crystalline solid. Yield: 167.3 mg (74 %).

^{1}H NMR (400 MHz, Acetonitrile-d_3) δ 7.78 (d, $^3J_{HH}$ = 2.0 Hz, 4H, NC*H*CHN), 7.63 (t, $^3J_{HH}$ = 5.6 Hz, 2H, NC*H*(CH_2OH)N), 7.11 (d, $^3J_{HH}$ = 2.0 Hz, 4H, NCH*CH*N), 6.99 (br s, 4H, H_{Mes}), 6.93 (br s, 4H, H_{Mes}), 4.55 (virt t, $^3J_{HH}$ = 5.6 Hz, 4H, NCH(*CH_2*OH)N), 3.99 (t, $^3J_{HH}$ = 5.4 Hz, 2H, OH), 2.45 (s, 12H, *para*-CH_3), 1.66 (s, 12H, *ortho*-*CH_3*), 1.37 (s, 12H, *ortho*-*CH_3*).

^{13}C{^{1}H} NMR (101 MHz, CD_3CN) δ 185.49 (NCN), 140.61 (*ortho*-CH_3C*C*N), 135.30 (*para*-CH_3*C*), 135.23 (*ortho*-CH_3*C*CN), 135.07 (*ortho*-CH_3*C*CN), 130.22 (CH_{Mes}), 125.73 (NC*H*CHN), 120.31 (NCH*CH*N), 74.03 (*CH*CH_2OH), 61.46 (CH*CH_2*OH), 21.25 (*para*-CH_3), 17.41 (*ortho*-CH_3), 17.30 (*ortho*-CH_3).

Anal. Calcd.: C, 41.28; H, 4.00; N, 7.41. **Found**: C, 41.24; H, 3.28; N, 7.40.

ESI-MS ([M]$^+$): m/z 1367.00 (20 %) [**$Au_2(HL3^{Mes})_2(PF_6)_2$**−1×$PF_6^-$]$^+$, 611.75 (100 %) [**$Au_2(HL3^{Mes})_2(PF_6)_2$**−2×$PF_6^-$]$^{2+}$.

$Au_2(L7^{Mes})_2(PF_6)_2$

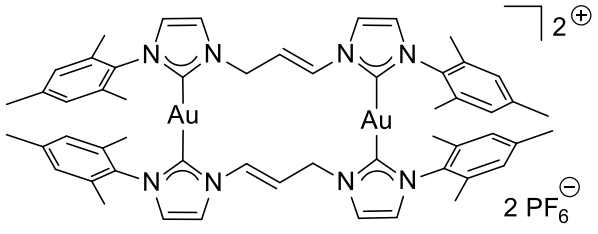

Sum formula: $C_{54}H_{60}Au_2F_{12}N_8P_2$

Molar mass: 1504.99 g·mol^{-1}

$Au_2(L7^{Mes})_2(PF_6)_2$

250.0 mg (1.88×10^{-4} mol, 1.0 eq.) of **$Ag_2(L7^{Mes})_2(PF_6)_2$** and 126.9 mg (3.96×10^{-4} mol, 2.1 eq.) of AuCl(THT) are stirred at RT in 6 mL of dry MeCN for 6 days. The crude product is purified

by fractional precipitation from DCM with pentane. The compound is obtained as white solid with an approximate isomer ratio A:B of 46:54. Yield: 282.0 mg (99 %).

^{1}H NMR (400 MHz, Acetonitrile-d_3) δ 7.81 (d, $^{3}J_{HH}$ = 14.3 Hz, 2H, NCH$_2$CH*CH*N, A), 7.74 (d, $^{3}J_{HH}$ = 2.1 Hz, 2H, N*CH*CHN, A), 7.72 (d, $^{3}J_{HH}$ = 2.1 Hz, 2H, N*CH*CHN, B), 7.47 (d, $^{3}J_{HH}$ = 1.9 Hz, 2H, N*CH*'CH'N, A), 7.40 (d, $^{3}J_{HH}$ = 1.9 Hz, 2H, N*CH*'CH'N, B), 7.19 (d, $^{3}J_{HH}$ = 2.0 Hz, 2H, NCH*CH*N, A), 7.16 (d, $^{3}J_{HH}$ =1.9 Hz, 2H, NCH'*CH*'N, B), 7.09 (d, $^{3}J_{HH}$ = 1.9 Hz, 2H, NCH'*CH*'N, A), 7.07 – 7.01 (m, 4H, NCH*CH*N and N*CH*CHCH$_2$N, B), 6.98 (s, 4H, H$_{Mes}$, A), 6.92 (s, 4H, H'$_{Mes}$, A), 6.91 (s, 4H, H$_{Mes}$, B), 6.90 (s, 4H, H'$_{Mes}$, B), 6.45 – 6.28 (m, 4H, NCH*CH*CH$_2$N, A and B), 5.02 (d, $^{3}J_{HH}$ = 6.7 Hz, 4H, NCHCH*CH$_2$*N, A), 4.66 (dd, $^{3}J_{HH}$ = 4.9 Hz, $^{4}J_{HH}$ = 1.9 Hz, 4H, NCHCH*CH$_2$*N, B), 2.43 (s, 12H, *para*-CH$_3$, A), 2.41 (s, 6H, *para*-CH$_3$, B), 2.40 (s, 6H, *para*-CH$_3$, B), 1.74 (s, 12H, *ortho*-CH$_3$, A), 1.67 (s, 12H, *ortho*-C'H$_3$, A), 1.65 (s, 12H, *ortho*-CH$_3$, B), 1.52 (s, 12H, *ortho*-C'H$_3$, B).

^{13}C{^{1}H} NMR (101 MHz, CD$_3$CN) δ 186.62 (NCN, A), 185.94 (NCN, B), 185.10 (NC'N, A), 185.07 (NC'N, B), 140.86 (*ortho*-CH$_3$C*C*N; A), 140.59 (*ortho*-CH$_3$C*C*N; B), 140.54 (*ortho*-C'H$_3$C'*C'*N; A), 140.21 (*ortho*-C'H$_3$C'*C'*N; B), 136.32 (*para*-CH$_3$*C*, A), 135.91 (*ortho*-CH$_3$*C*CN, A), 135.71 (*para*-CH$_3$*C*, B), 135.52 (*ortho*-CH$_3$*C*CN, B), 135.41 (*ortho*-C'H$_3$*C'*C'N, A), 135.36 (*ortho*-C'H$_3$*C'*C'N, B), 135.19 (*para*-C'H$_3$*C'*, A), 135.12 (*para*-C'H$_3$*C'*, B), 131.68 (N*CH*CHCH$_2$N, A), 130.15 (CH, Mes, A), 130.06 (C'H, Mes, A), 129.94 (CH, Mes, B), 129.89 (C'H, Mes, B), 128.47 (N*CH*CHCH$_2$N, B), 125.56 (NCH*CH*N, B), 125.49 (NCH*CH*N, A), 124.42 (N*CH*'CH'N, A), 124.07 (NCH'*CH*'N, B), 123.86 (N*CH*'CH'N, B), 123.18 (NCH'*CH*'N, A), 120.32 (N*CH*CHN, A), 120.17 (NCH*CH*CH$_2$N, A), 118.68 (N*CH*CHN, B), 117.63 (NCH*CH*CH$_2$N, B), 50.90 (NCHCH*CH$_2$*N, B), 49.58 (NCHCH*CH$_2$*N, B), 21.29 (br s, *para*-CH$_3$, A), 21.25 (*para*-CH$_3$, B), 21.18 (*para*-C'H$_3$, B), 18.05 (*ortho*-CH$_3$, A), 17.66 (*ortho*-C'H$_3$, A), 17.62 (*ortho*-CH$_3$, B), 17.39 (*ortho*-C'H$_3$, B).

Anal. Calcd.: C, 43.10; H, 4.02; N, 7.45. **Found**: C, 42.46; H, 3.99; N, 7.34.

ESI-MS ([M]$^+$): m/z 1359.47 (20 %) [**Au$_2$(L7^{Mes})$_2$(PF$_6$)$_2$**−1×PF$_6^-$]$^+$, 607.92 (100 %) [**Au$_2$(L7^{Mes})$_2$(PF$_6$)$_2$**−2×PF$_6^-$]$^{2+}$.

Au$_2$(L7^{Mes})$_2$(BPh$_4$)$_2$

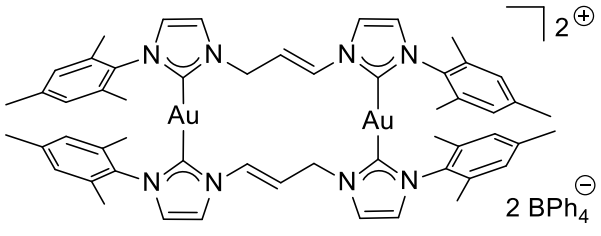

Au$_2$(L7^{Mes})$_2$(BPh$_4$)$_2$

Sum formula: $C_{102}H_{100}Au_2B_2N_8$

Molar mass: 1853.53 g·mol^{-1}

52.7 mg (0.03 mmol, 1.0 eq.) of **$Ag_2(L7^{Mes})_2(BPh_4)_2$** and 19.5 mg (0.07 mmol, 2.1 eq.) of $AuCl(SMe_2)$ are stirred at RT in 3 mL of MeCN for 5 days. The crude product is purified by fractional precipitation from THF with pentane. The compound is obtained as white electrostatic solid with an approximate isomer ratio A:B of 50:50. Yield: 40.0 mg (67 %).

^{1}H NMR (400 MHz, Acetonitrile-d_3) δ 7.82 (d, $^3J_{HH}$ = 14.4 Hz, 2H, NCH_2CHCHN, A), 7.70 (d, $^3J_{HH}$ = 2.0 Hz, 2H, $NCHCHN$, A), 7.65 (d, $^3J_{HH}$ = 2.1 Hz, 2H, $NCHCHN$, B), 7.42 (d, $^3J_{HH}$ = 1.8 Hz, 2H, $NCHCHN$, A), 7.34 (d, $^3J_{HH}$ = 1.9 Hz, 2H, $NCHCHN$, B), 7.30 – 7.24 (m, 16H, *ortho*-CH, BPh_4), 7.15 (d, $^3J_{HH}$ = 2.0 Hz, 2H, $NCH'CH'N$, A), 7.11 (d, $^3J_{HH}$ = 1.9 Hz, 2H, $NCH'CH'N$, B), 7.09 – 7.02 (m, 4H, 2 NCH_2CHCHN, B and 2 $NCH'CH'N$, A), 7.01 – 6.95 (m, 22H, 16 *meta*-CH, BPh_4, $4H_{Mes}$, A and 2 $NCHCH'N$, B), 6.93 – 6.88 (m, 14H, $H_{Mes,}$ 4H A and 8H B), 6.86 – 6.79 (m, 8H, *para*-CH, BPh_4), 6.37 (dt, $^3J_{HH}$ = 14.4 Hz, $^3J_{HH}$ = 5.0 Hz, 2H, B), 6.27 (dt, $^3J_{HH}$ = 14.4 Hz, $^3J_{HH}$ = 7.3 Hz, 2H, A), 4.96 (d, $^3J_{HH}$ = 7.0 Hz, 4H, A), 4.60 (dd, $^3J_{HH}$ = 5.1 Hz, $^3J_{HH}$ = 1.9 Hz, 4H, B), 2.43 (s, 12H, *para*-CH_3), 2.41 (s, 6H, *para*-CH_3), 2.40 (s, 6H, *para*-CH'_3), 1.73 (s, 12H, *ortho*-CH_3), 1.67 (s, 12H, *ortho*-CH_3), 1.65 (s, 12H, *ortho*-CH_3), 1.51 (s, 12H, *ortho*-CH_3).

$^{13}C\{^1H\}$ NMR (101 MHz, CD_3CN) δ 186.54 (NCN, A), 185.84 (NCN, B), 185.04 (NC'N, A), 184.99 (NC'N, B), 164.73 (q, $^1J_{CB}$ = 49.2 Hz, CB, BPh_4), 140.81 (*ortho*-CH_3CCN; A), 140.55 (*ortho*-CH_3CCN, B), 140.51 (*ortho*-$C'H_3C'C'N$, A), 140.17 (*ortho*-$C'H_3C'C'N$, B), 136.80 – 136.60 (m, *ortho*-CH, BPh_4), 135.88 (*ortho*-CH_3CCN, A), 135.69 (*para*-CH_3C, A), 135.51 (*ortho*-CH_3CCN, B), 135.39 (*ortho*-$CH_3C'CN$, A), 135.35 (*ortho*-$CH_3C'CN$, B), 135.17 (*para*-CH_3C, B), 135.12 (*para*-CH_3C', A), 132.46 (*para*-CH_3C', B), 131.72 ($NCHCHCH_2N$, A), 130.14 (CH, Mes, A), 130.03 (CH, Mes, B), 129.92 (C'H, Mes; A), 129.87 (C'H, Mes, B), 128.43 ($NCHCHCH_2N$, B), 126.57 (q, $^3J_{CB}$ = 2.7 Hz, *meta*-CH, BPh_4), 125.46 ($NC'HC'HN$, A), 125.45 ($NC'HC'HN$, B), 124.41 ($NCHCHN$, A), 124.02 ($NC'HC'HN$, B), 123.84 ($NCHCHN$, B), 123.11 ($NC'HC'HN$, A), 122.74 (*para*-CH, BPh_4), 120.32 ($NCHCHN$, A), 120.12 ($NCHCHCH_2N$, A), 118.64 ($NCHCHN$, B) 117.56 ($NCHCHCH_2N$, B), 50.84 ($NCHCHCH_2N$, A), 49.54 ($NCHCHCH_2N$, B), 21.29 (*para*-CH_3), 21.29 (*para*-CH_3), 21.25 (*para*-CH_3), 21.20 (*para*-CH_3), 18.06 (*ortho*-CH_3), 17.67 (*ortho*-CH_3), 17.63 (*ortho*-CH_3), 17.43 (*ortho*-CH_3).

Anal. Calcd.: C, 66.10; H, 5.44; N, 6.05. **Found**: C, 62.47; H, 5.04; N, 6.28.

ESI-MS ($[M]^+$): m/z 1533.38 (8 %) $[\mathbf{Au_2(L7^{Mes})_2(BPh_4)_2}-1\times BPh_4^-]^+$, 1258.70 (6 %) $[\mathbf{Au_2(L7^{Mes})_2(BPh_4)_2}-2\times BPh_4^-+CHOO^--H^+]^+$, 607.87 (100 %) $[\mathbf{Au_2(L7^{Mes})_2(BPh_4)_2}-2\times BPh_4^-]^{2+}$.

5.3 Supporting Information

5.3.1 NMR Spectra

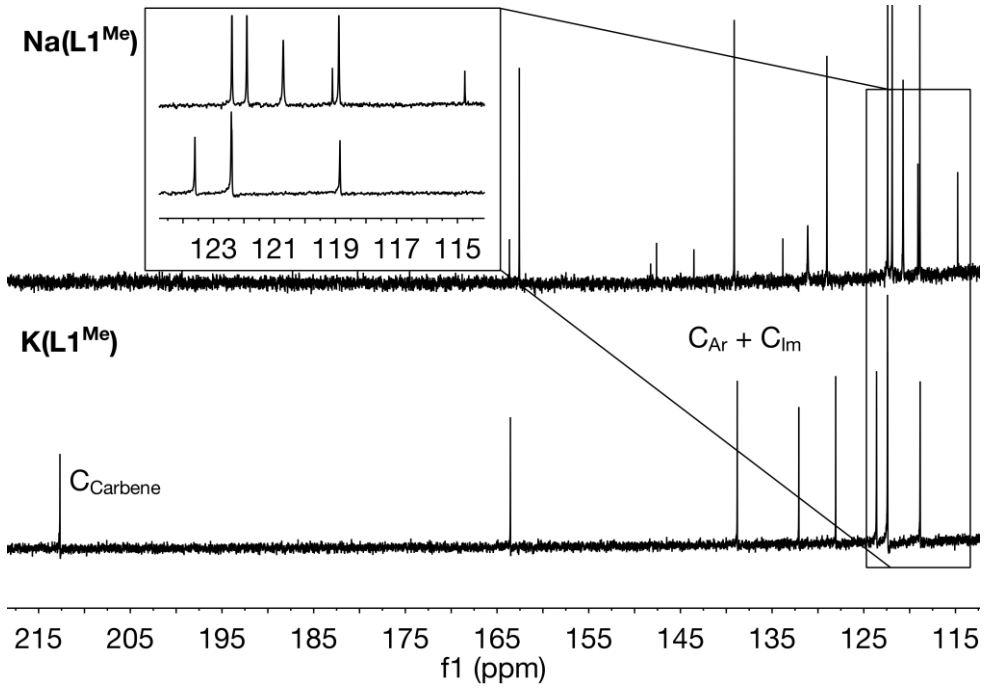

Figure 5.3.1. Comparison of the ^{13}C NMR spectra of **K(L1^{Me})** to **Na(L1^{Me})** in the aromatic region. The spectra were recorded in THF-d_8 at RT.

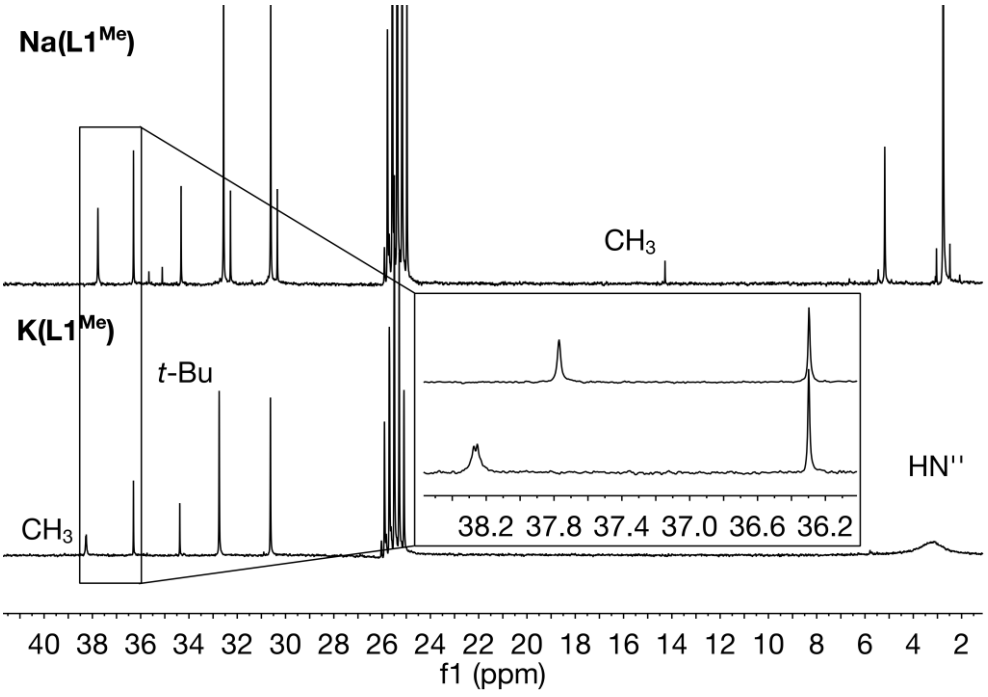

Figure 5.3.2. Comparison of the ^{13}C NMR spectra of **K(L1^{Me})** to **Na(L1^{Me})** in the aliphatic region. The spectra were recorded in THF-d_8 at RT.

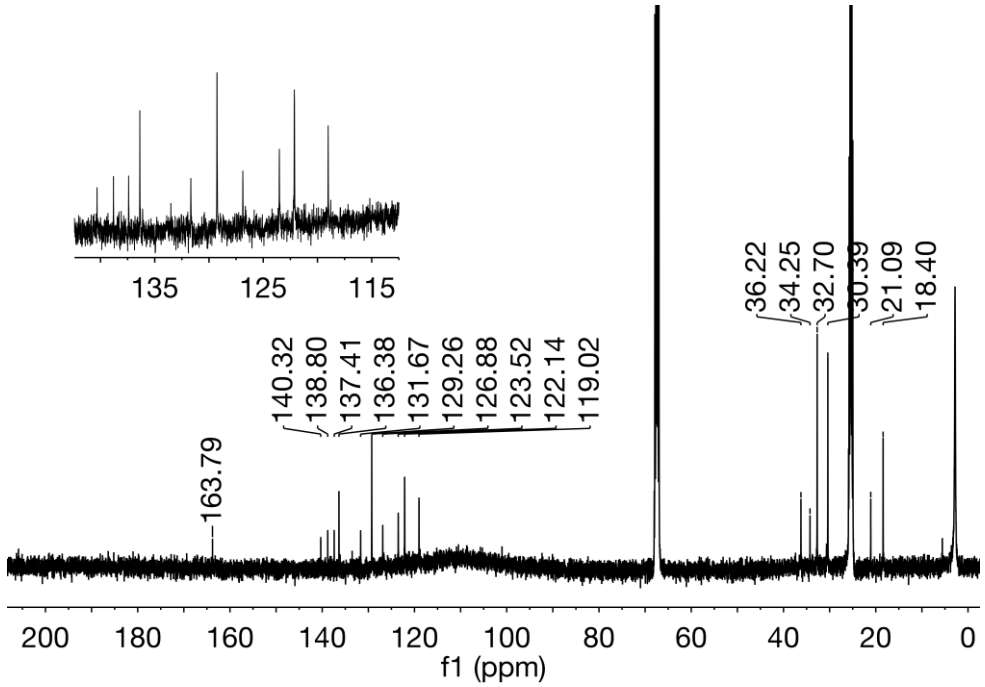

Figure 5.3.3. ^{13}C NMR spectrum of **K(L1^{Mes})** formed in a NMR scale reaction of **H$_2$(L1^{Mes})Br** with KN'' in THF-d_8 at RT.

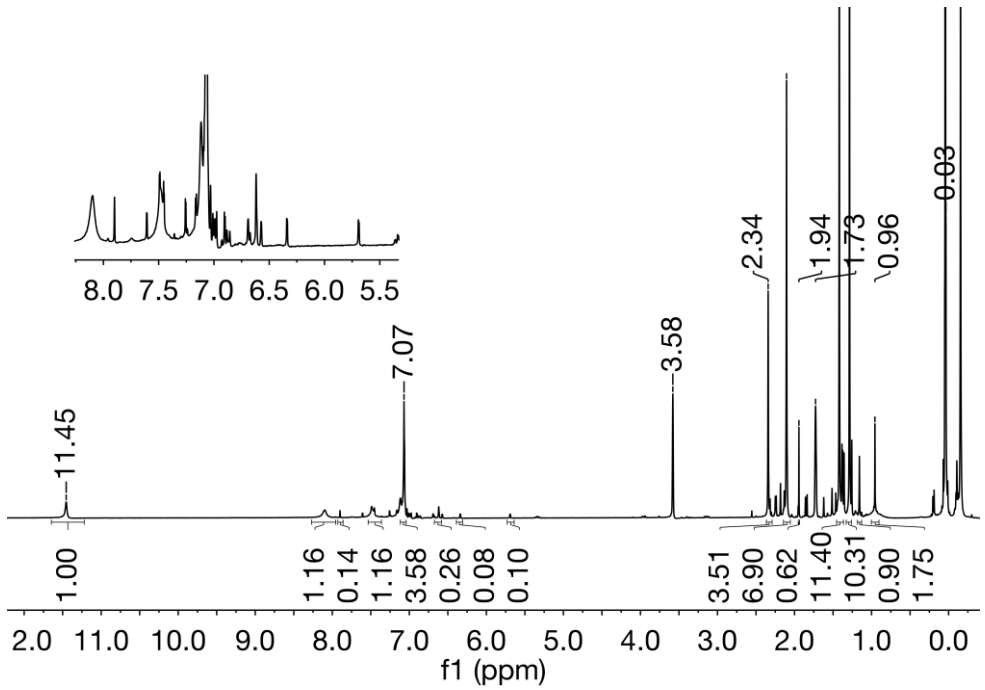

Figure 5.3.4. ^{1}H NMR spectrum of **Na(L1^{Mes})** formed in a NMR scale reaction of **H$_2$(L1^{Mes})Br** with NaN'' in THF-d_8 at RT.

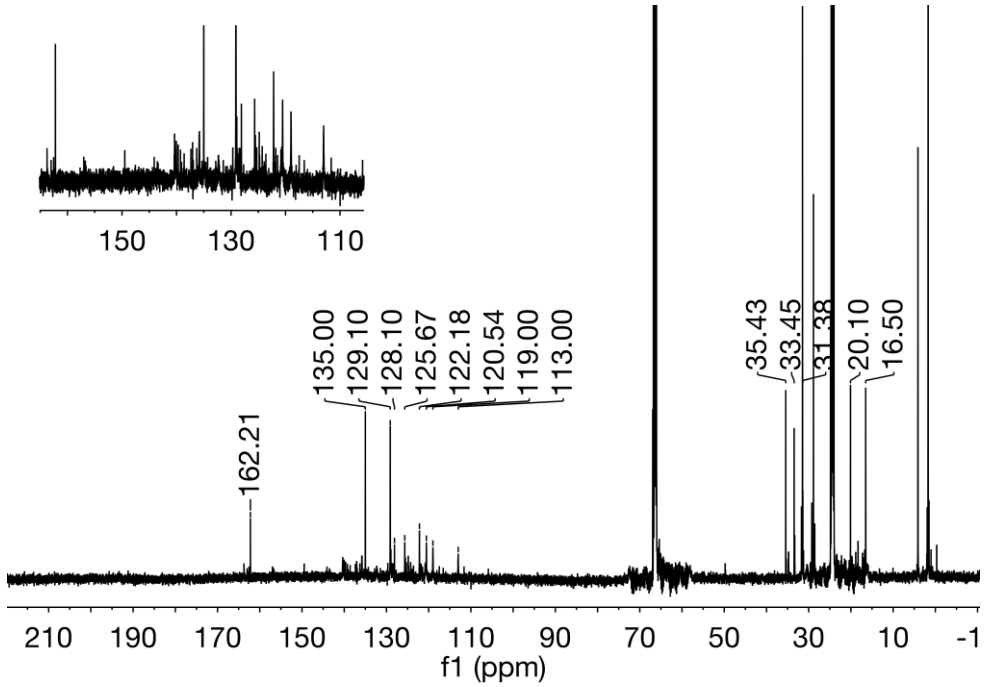

Figure 5.3.5. ^{13}C NMR spectrum of **Na(L1^{Mes})** formed in a NMR scale reaction of **H$_2$(L1^{Mes})Br** with NaN" in THF-d_8 at RT.

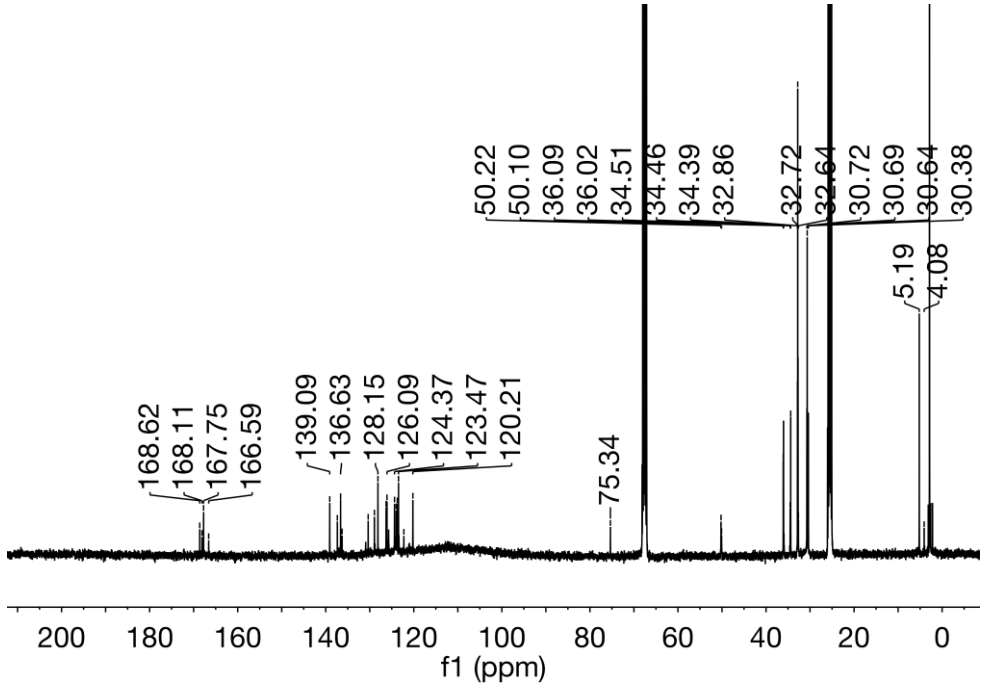

Figure 5.3.6. ^{13}C NMR spectrum of **Na(L2)** formed in a NMR scale reaction of **H$_3$(L2)Br** with NaN" in THF-d_8 at RT.

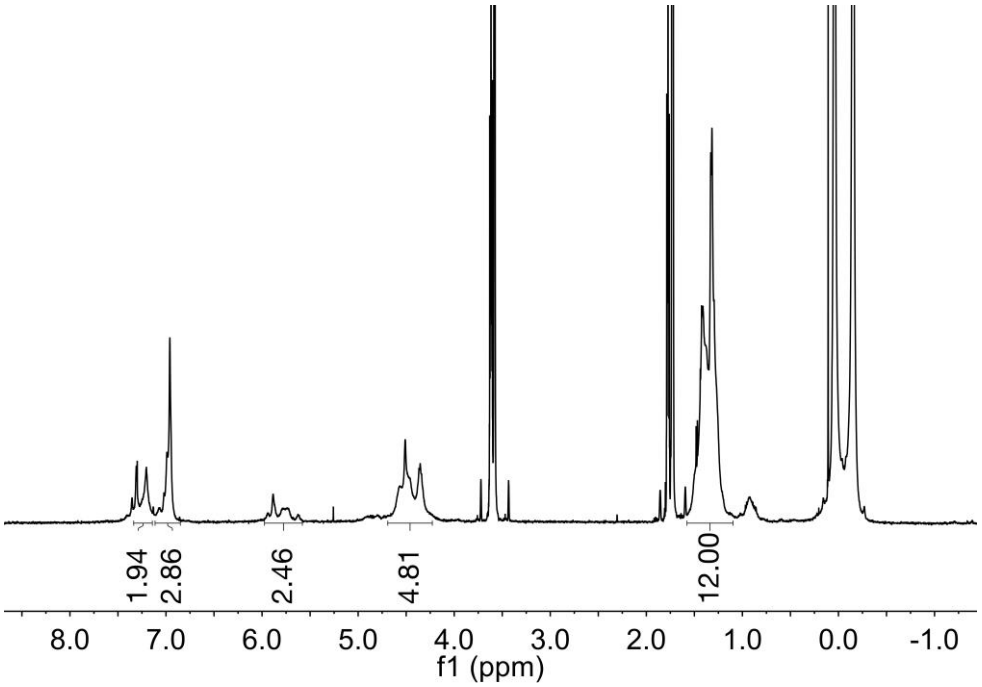

Figure 5.3.7. ^{1}H NMR spectrum of **Li(L3$^{i\text{-Pr}}$)** obtained in a deprotonation reaction of **H_3(L3$^{i\text{-Pr}}$)Cl_2** with LiN" in THF at RT.

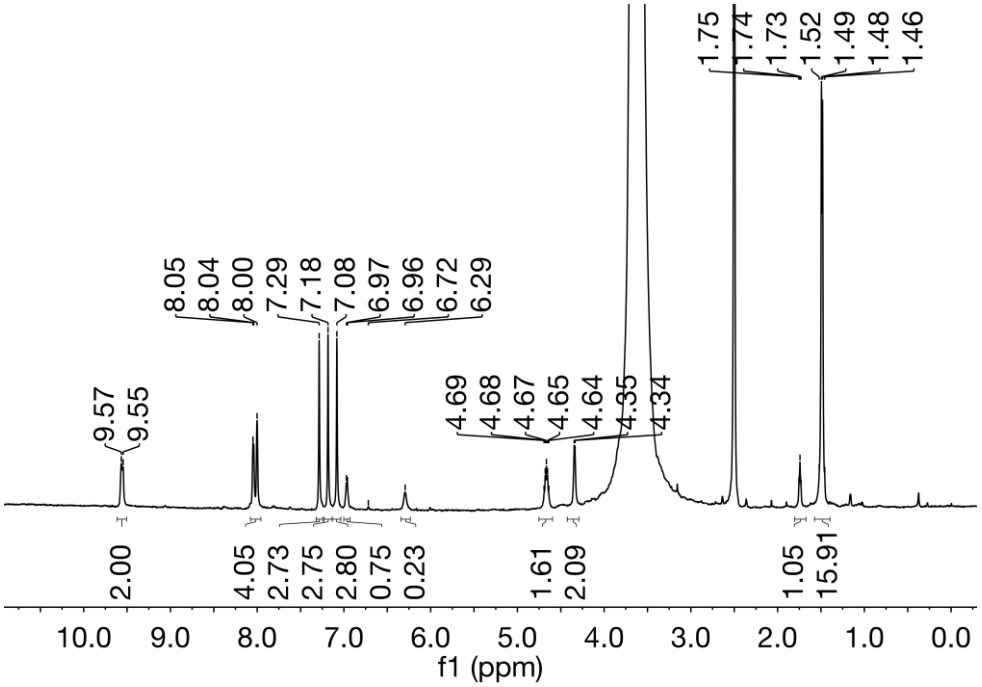

Figure 5.3.8. ^{1}H NMR spectrum of the product obtained after the hydrolysis of **Li(L3$^{i\text{-Pr}}$)** with 2M HCl solution in Et_2O. The spectrum is recorded in DMSO-d_6 at RT.

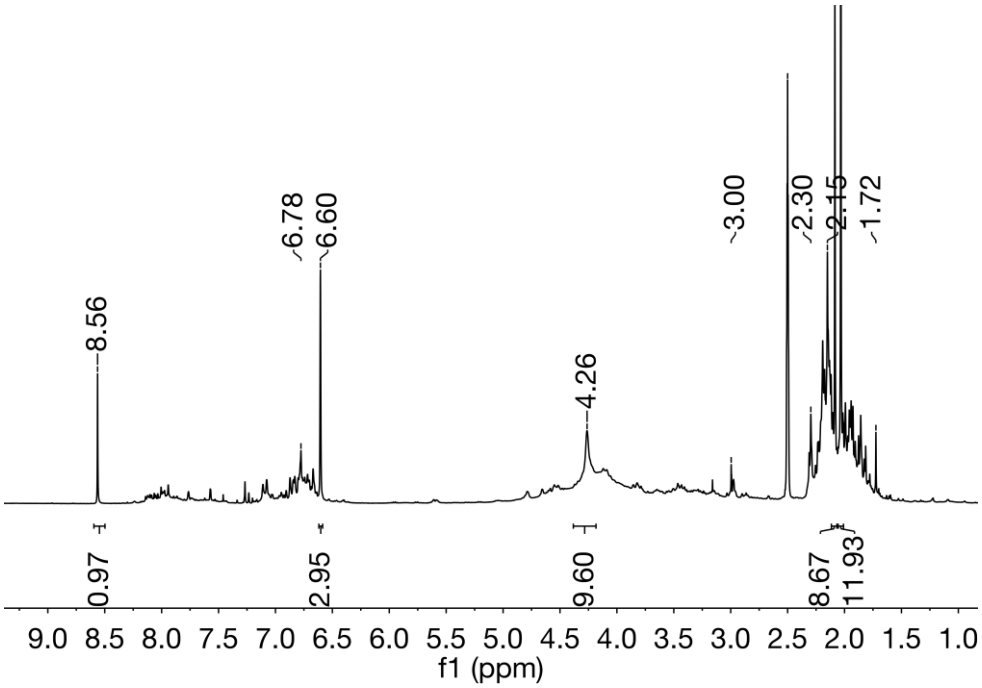

Figure 5.3.9. ^{1}H NMR spectrum of the hydrolysis product obtained in decomposition reaction of **K(L4^{Mes})** with excess of H_2O at RT in THF. The spectrum is recorded in DMSO-d_6 at RT.

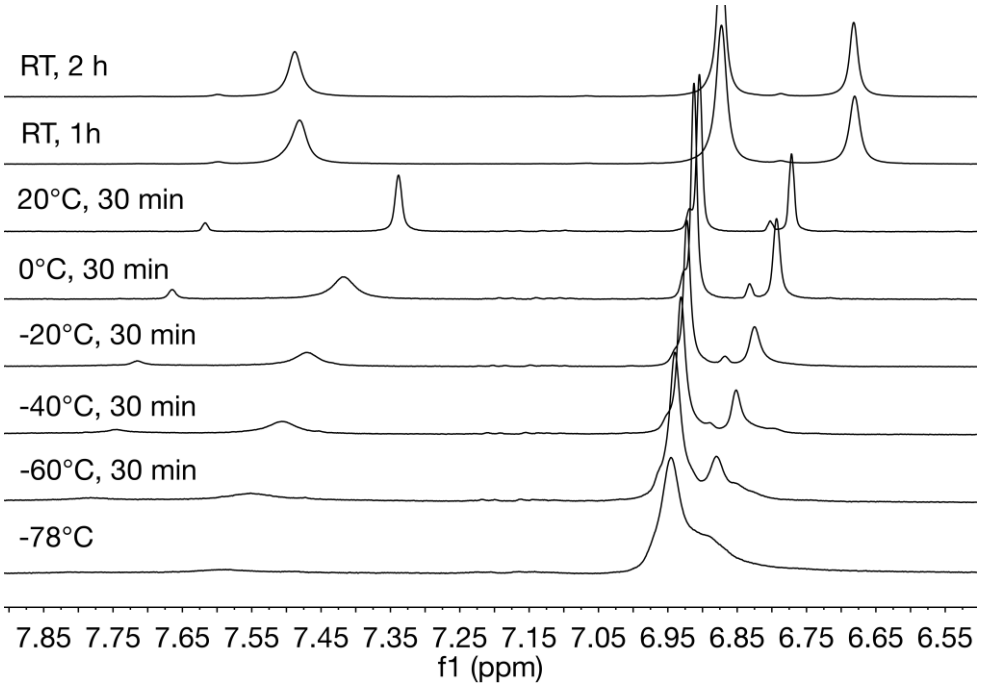

Figure 5.3.10. Monitoring of the formation of **K(L4^{Mes})** by ^{1}H NMR spectroscopy as the reaction tube containing the educts was slowly allowed to warm up after the start of the reaction at –78 °C. The figure shows a section (6.55 – 7.85 ppm) of the spectra which were recorded in THF-d_8.

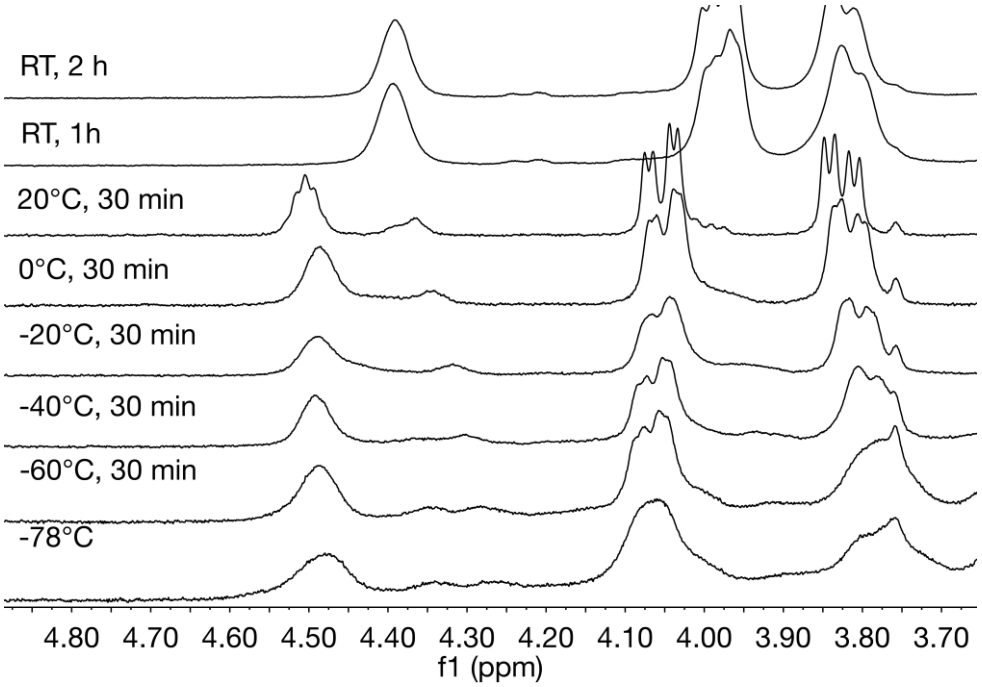

Figure 5.3.11. Monitoring of the formation of **K(L4^{Mes})** by ^{1}H NMR spectroscopy as the reaction tube containing the educts was slowly allowed to warm up after the start of the reaction at –78 °C. The figure shows a section (3.70 – 4.80 ppm) of the spectra which were recorded in THF-d_8.

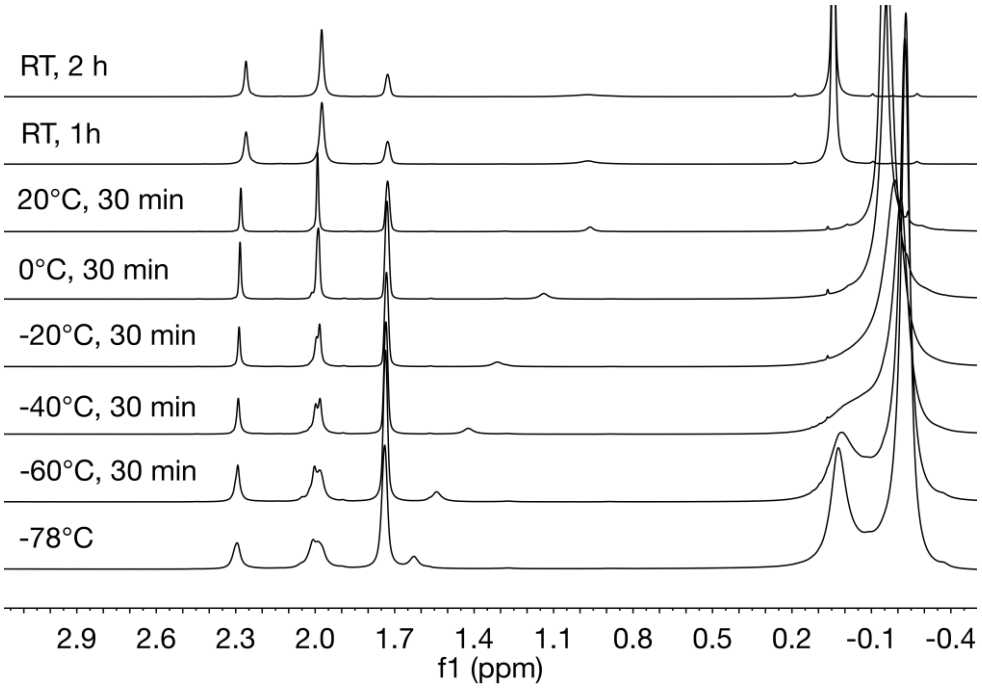

Figure 5.3.12. Monitoring of the formation of **K(L4^{Mes})** by ^{1}H NMR spectroscopy as the reaction tube containing the educts was slowly allowed to warm up after the start of the reaction at –78 °C. The figure shows a section (–0.40 – 3.00 ppm) of the spectra which were recorded in THF-d_8.

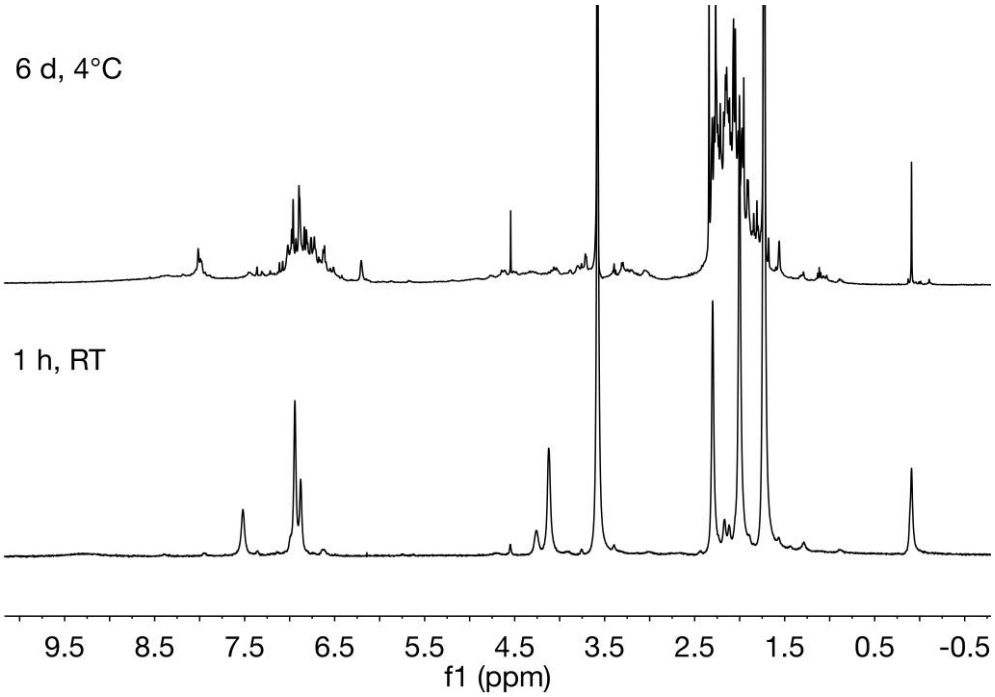

Figure 5.3.13. ^{1}H NMR spectra of the product(s) obtained in the reaction of **$H_3(L4^{Mes})Br_2$** with KH in THF after 1 h (bottom) at RT and 6 d at 4 °C (top) after the start of the reaction.

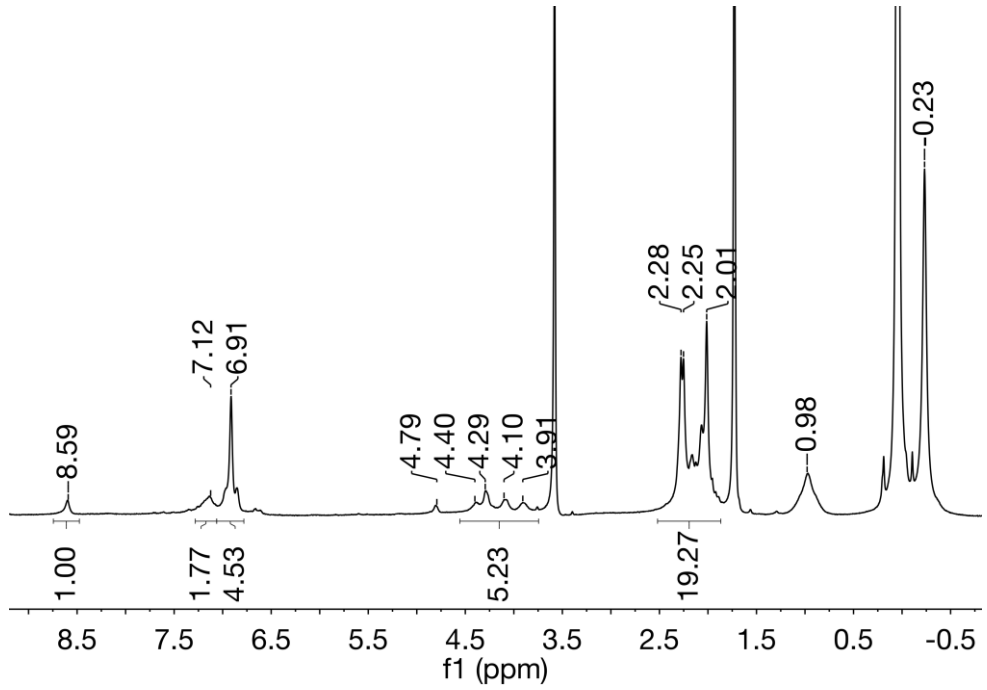

Figure 5.3.14. ^{1}H NMR spectra of the product(s) obtained after the treatment of **$H_3(L4^{Mes})Br_2$** with NaN" in THF-d_8 at RT

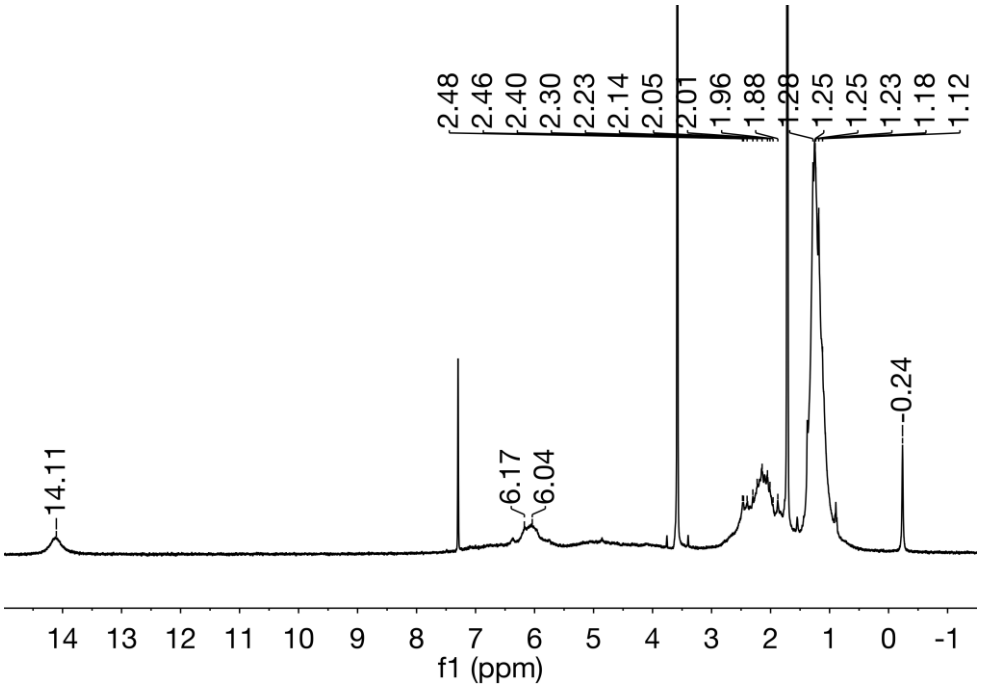

Figure 5.3.15. ^{1}H NMR spectrum of the residue formed in the reaction of **L6^{tFu}** with C_6F_6 in THF-d_8 at RT.

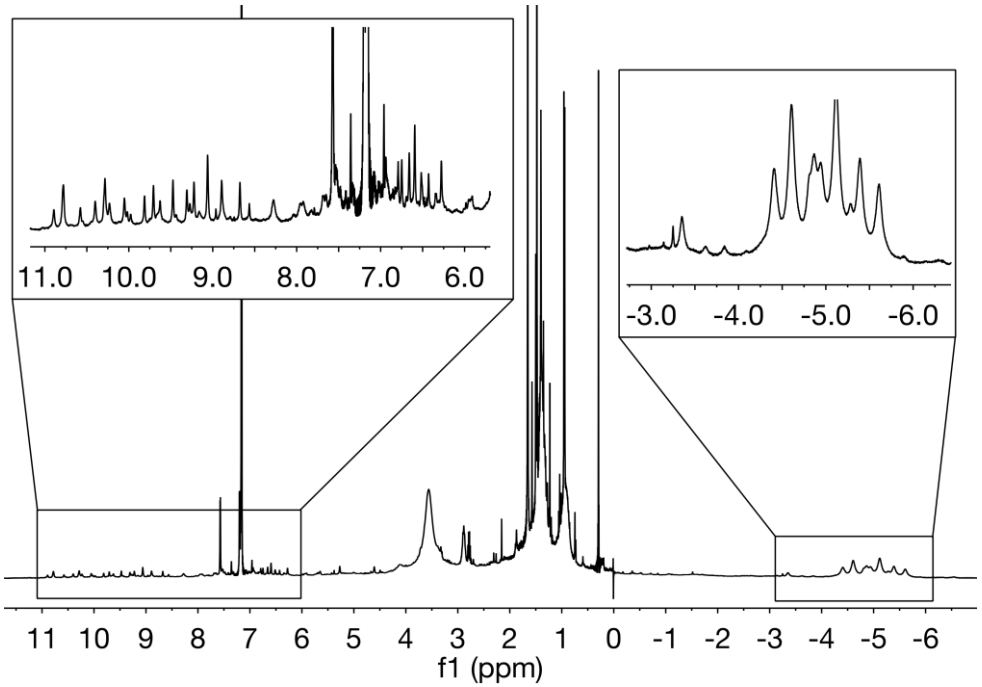

Figure 5.3.16. ^{1}H NMR spectrum of the crude product formed in the reaction of **H_3(L2)Br** with Li[Ce{N(*i*-Pr)$_2$}$_4$](THF) and LDA in C_6D_6 at RT.

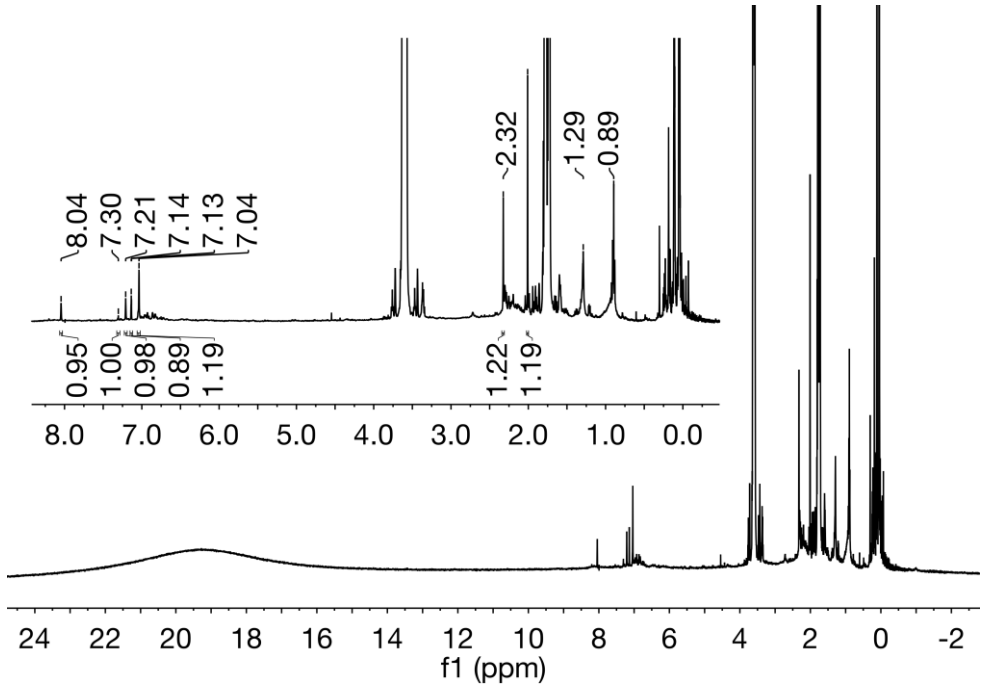

Figure 5.3.17. ^{1}H NMR spectrum of the crude product obtained in the reaction of $Ce(BH_4)_3(THF)_4$ with *in situ* formed **Li(L3^{Mes})** in THF-d_8 at RT.

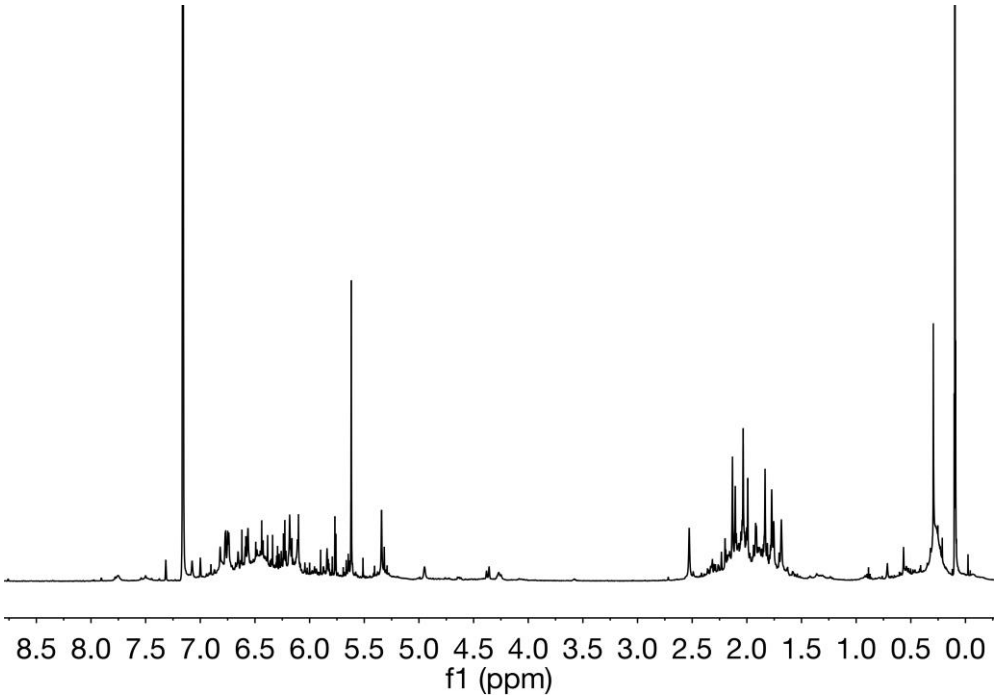

Figure 5.3.18. ^{1}H NMR spectrum of crude product obtained in the reaction of YCp_3 with *in situ* formed **Li(L3^{Mes})** in C_6D_6 at RT.

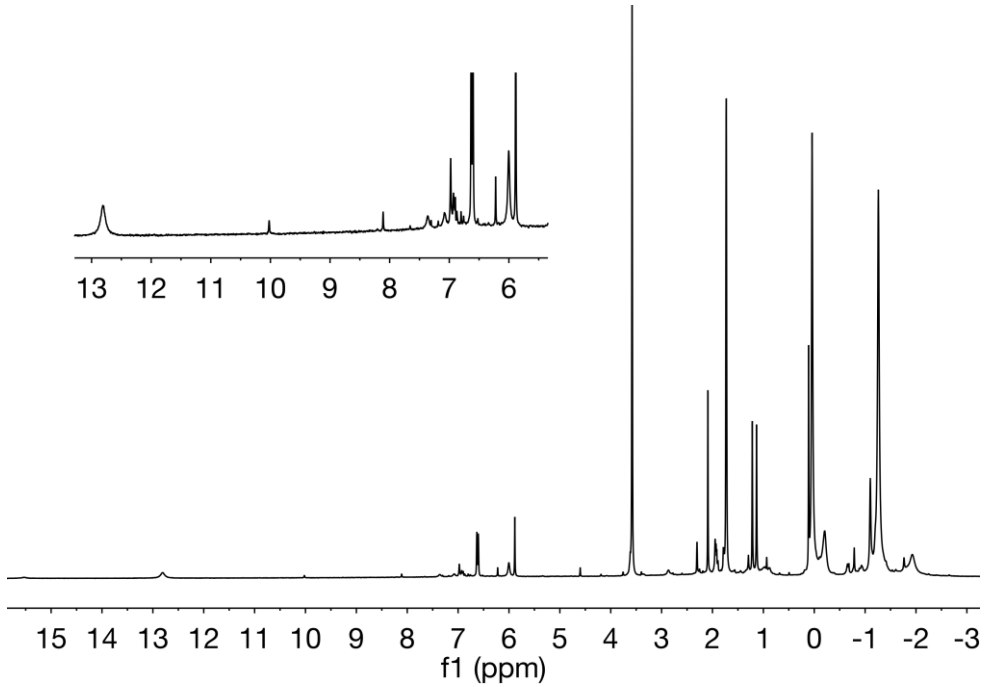

Figure 5.3.19. ^{1}H NMR spectrum of the crude product obtained in two-step reaction of **H_3(L3^{Mes})Cl_2** with KN" and $CeN"_3$ in THF-d_8 at RT.

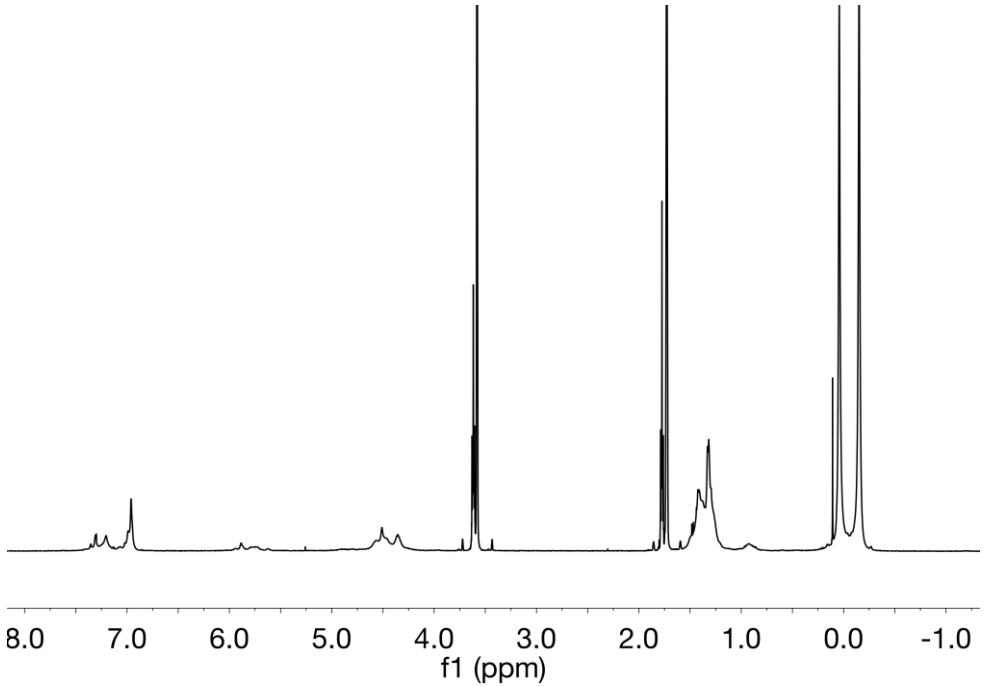

Figure 5.3.20. ^{1}H NMR spectrum of the crude product obtained in two step reaction of **H_3(L3$^{i\text{-}Pr}$)Cl_2** with KN" and $Ce(BH_4)_3(THF)_4$ in THF-d_8 at RT.

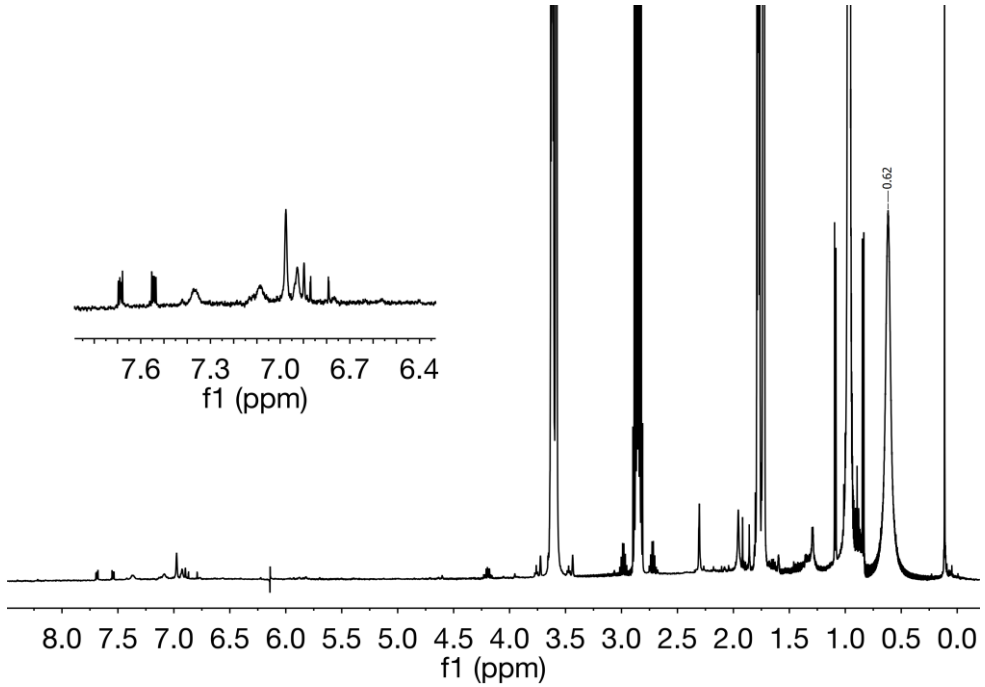

Figure 5.3.21. ^{1}H NMR spectrum of the crude product obtained in the reaction of **$H_3(L3^{Mes})Cl_2$** with Li[Ce{N(*i*-Pr)$_2$}$_4$](THF) in THF-d_8 at RT.

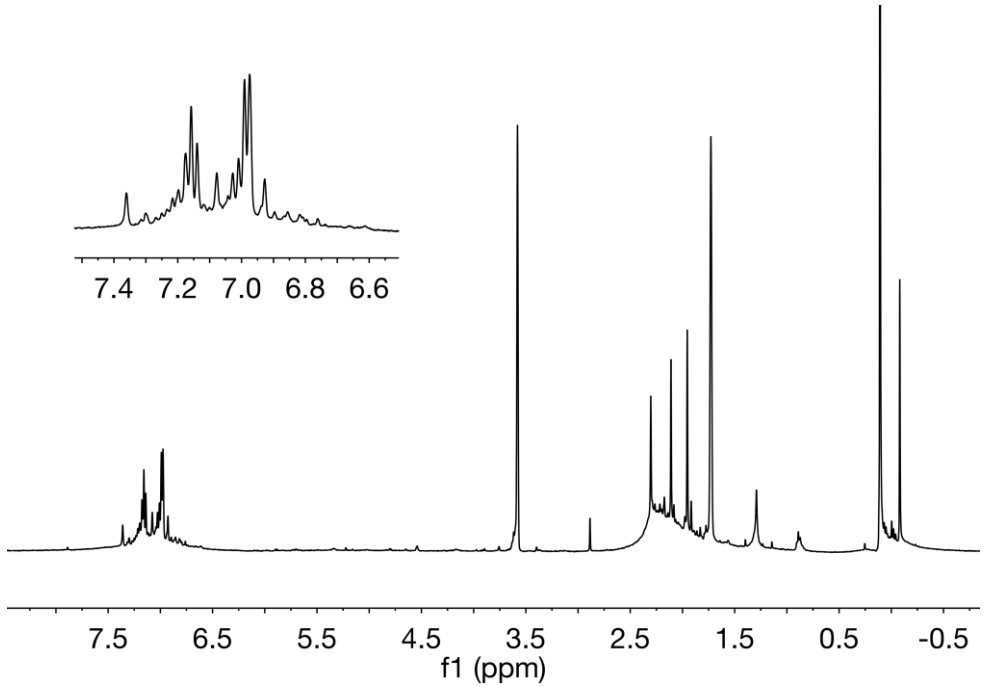

Figure 5.3.22. ^{1}H NMR spectrum of the crude product obtained in the reaction of **$H_3(L3^{Mes})Cl_2$** with *in situ* formed $ScBn_3$ in THF-d_8 at RT.

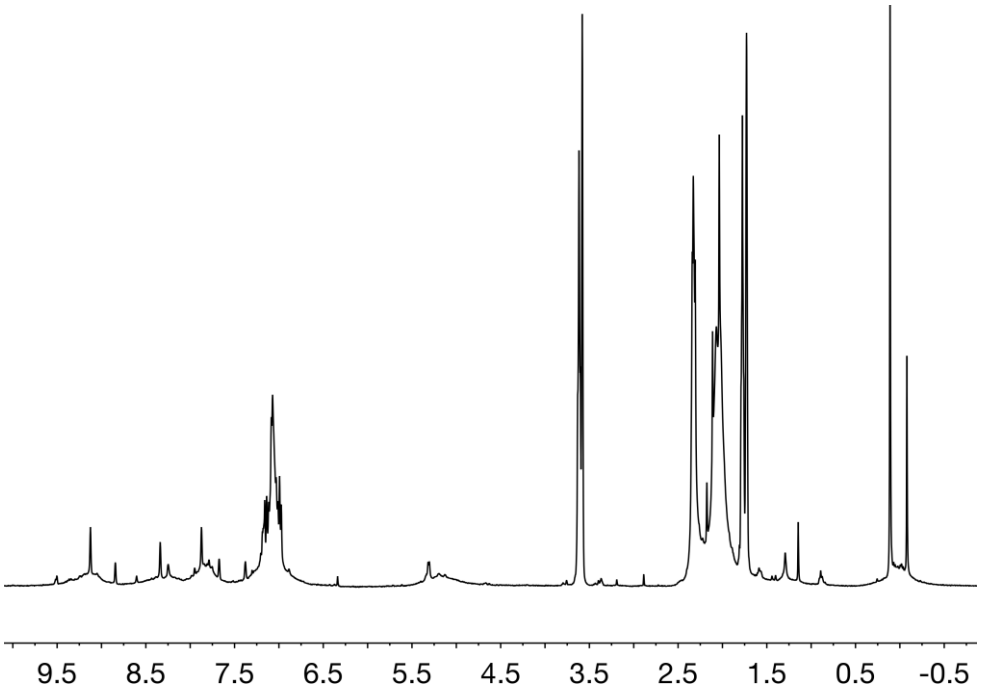

Figure 5.3.23. ^{1}H NMR spectrum of the crude product obtained in the reaction of **$H_3(L3^{Mes})(PF_6)_2$** with *in situ* formed $ScBn_3$ in THF-d_8 at RT.

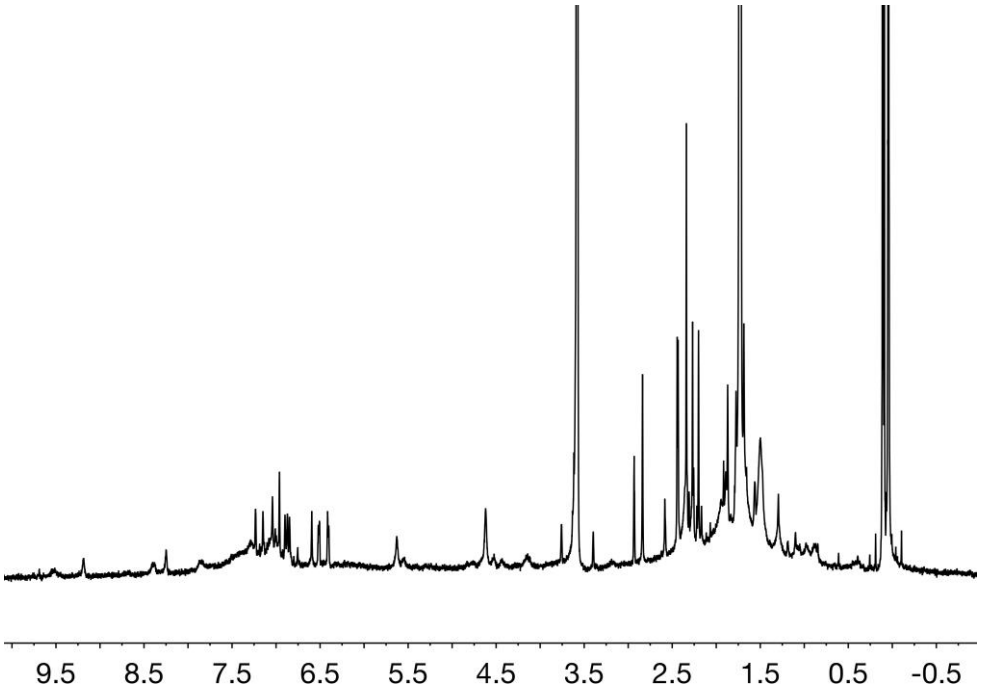

Figure 5.3.24. ^{1}H NMR spectrum of the crude product obtained in two-step reaction of **$H_3(L4^{Mes})Br_2$** with KN" and $CeCp_3$ in THF-d_8 at RT.

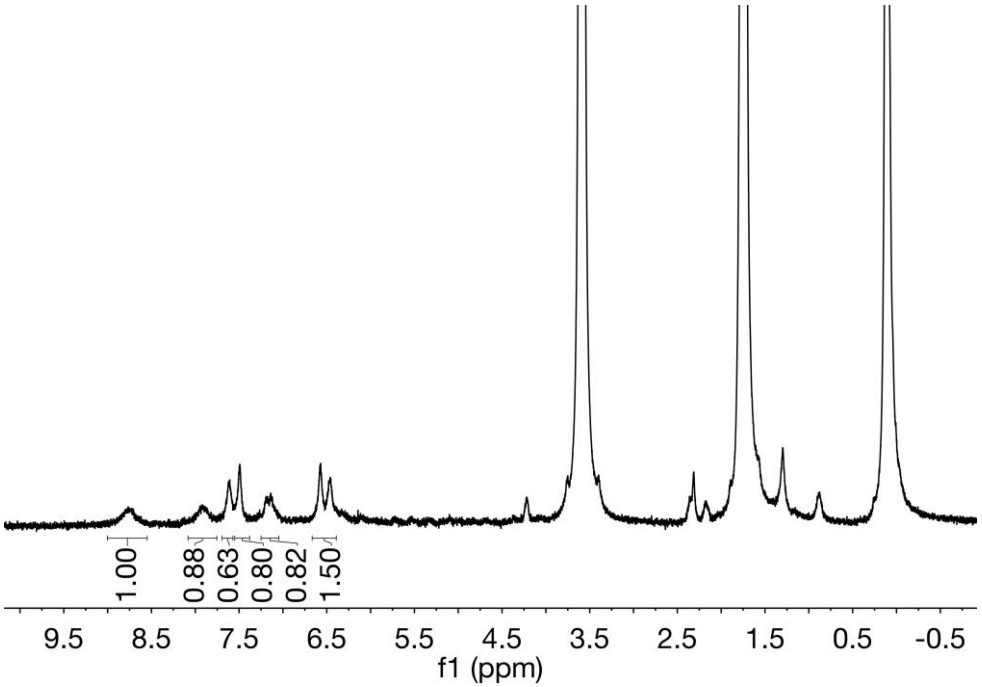

Figure 5.3.25. ^{1}H NMR spectrum of the crude product obtained in two-step reaction of **$H_2(L5^{Fu})Br_2$** with KN" and $CeCl_3(THF)_2$ in THF-d_8 at RT.

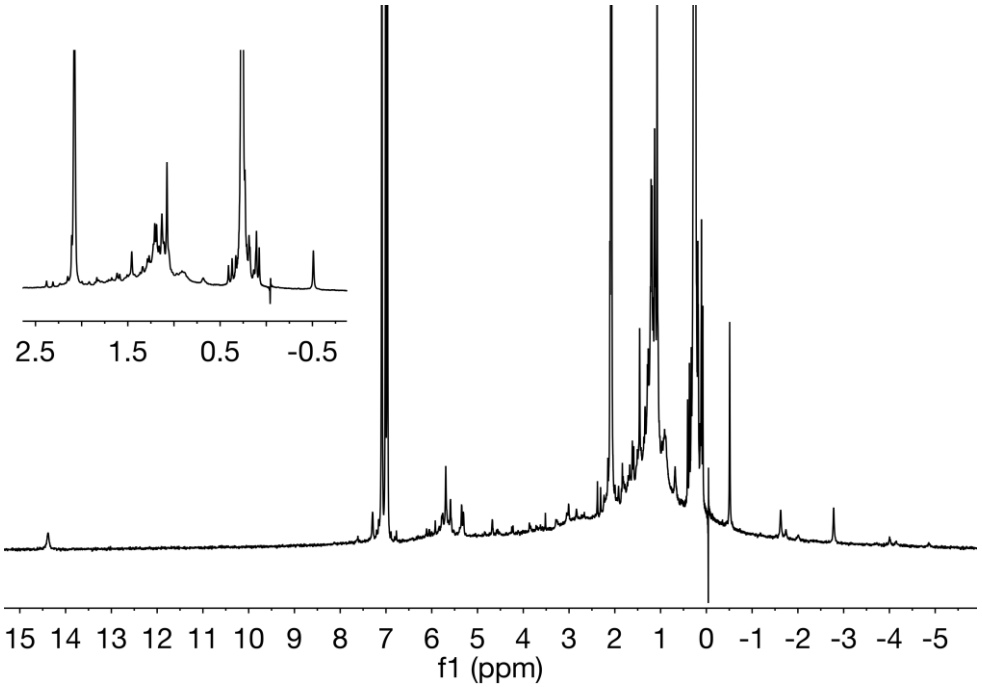

Figure 5.3.26. ^{1}H NMR spectrum of the crude product obtained in two-step reaction of **$H_2(L5^{Fu})Br_2$** with KN" and $Ce(BH_4)_3(THF)_4$ in touene-d_8 at RT.

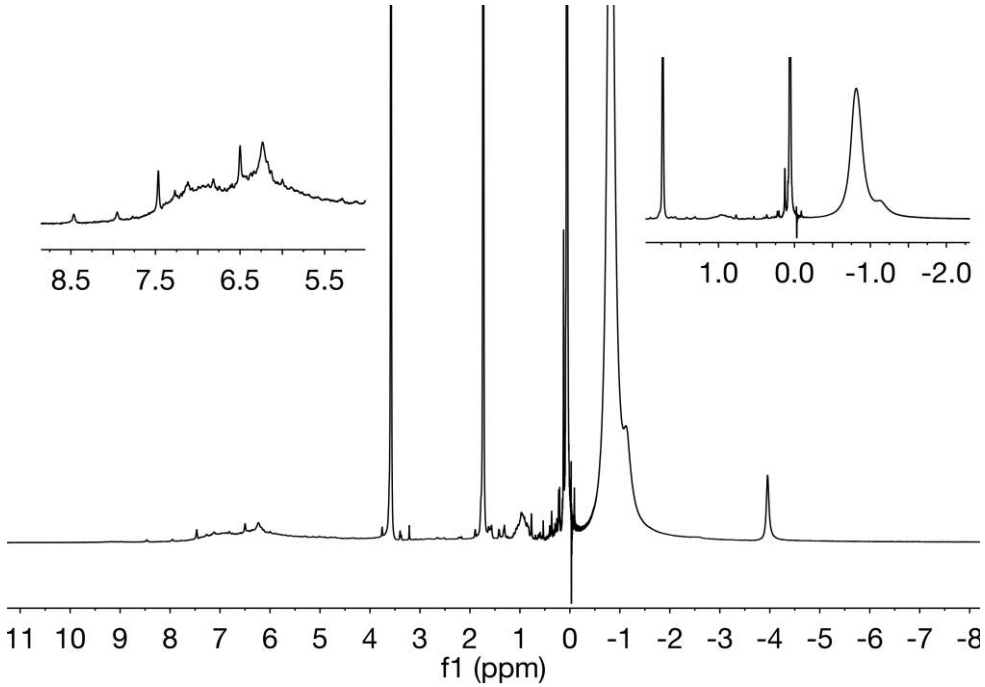

Figure 5.3.27. ^{1}H NMR spectrum of the crude product obtained in the reaction of **$H_2(L5^{Fu})Br_2$** with CeN"$_3$ in THF-d_8 at RT.

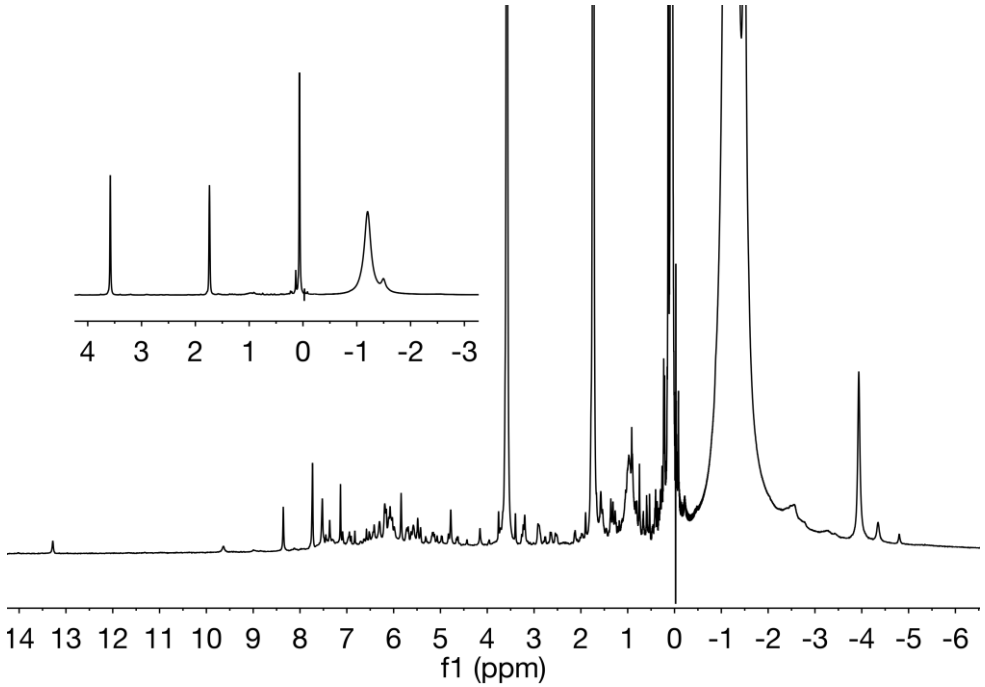

Figure 5.3.28. ^{1}H NMR spectrum of the crude product obtained in the reaction of **$H_2(L6^{Fu})Br_2$** with CeN"$_3$ in THF-d_8 at RT.

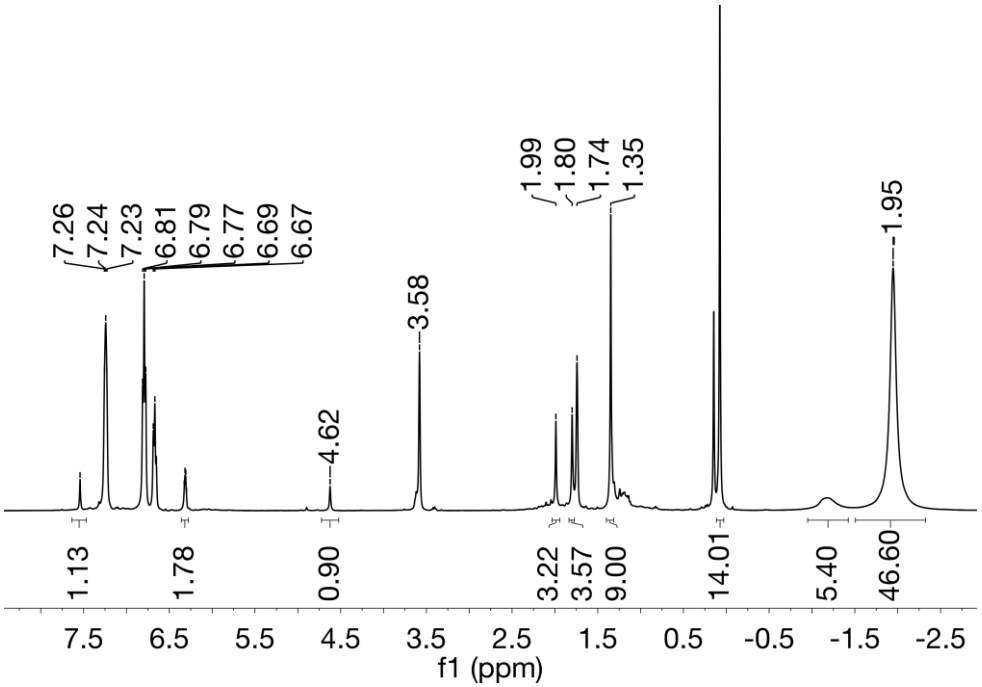

Figure 5.3.29. ^{1}H NMR spectrum of the crude product obtained in the reaction of **H_2(L5^{tFu})Br_2** with CeN"$_3$ in THF-d_8 at RT.

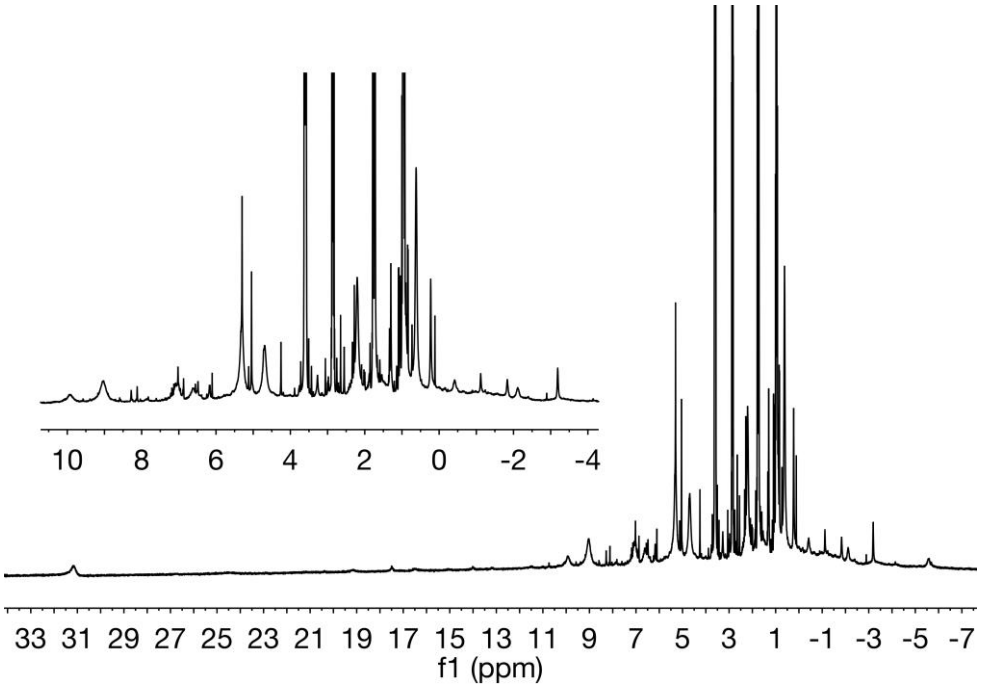

Figure 5.3.30. ^{1}H NMR spectrum of the crude product obtained in the reaction of **H_2(L7^{Mes})Br_2** with Li[Ce{N(*i*-Pr)$_2$}$_4$](THF) in THF-d_8 at RT.

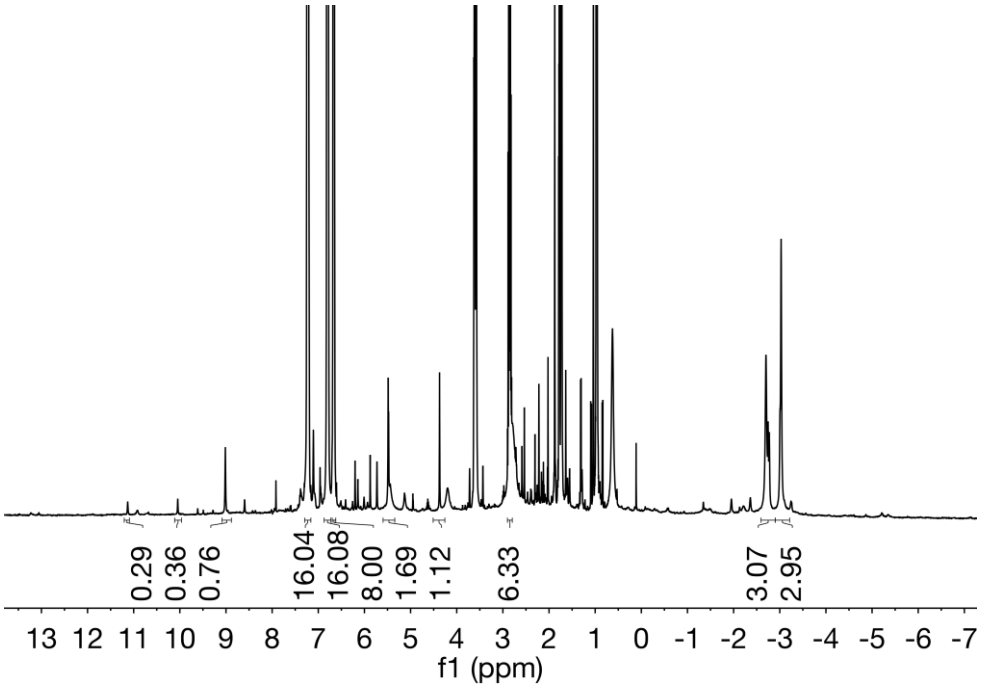

Figure 5.3.31. ^{1}H NMR spectrum of the crude product obtained in the reaction of **H_2(L7^{Mes})(BPh_4)$_2$** with Li[Ce{N(*i*-Pr)$_2$}$_4$](THF) in THF-*d*$_8$ at RT.

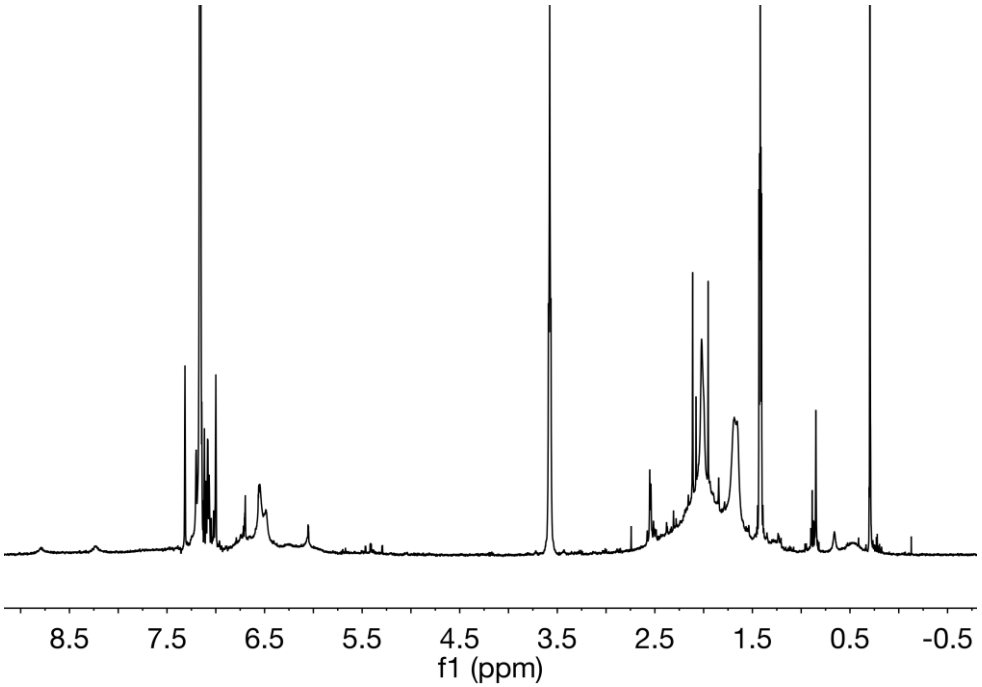

Figure 5.3.32. ^{1}H NMR spectrum of the crude product obtained after the treatment of **H_2(L7^{Mes})Br_2** with *in situ* formed $ScBn_3$ in C_6D_6 at RT.

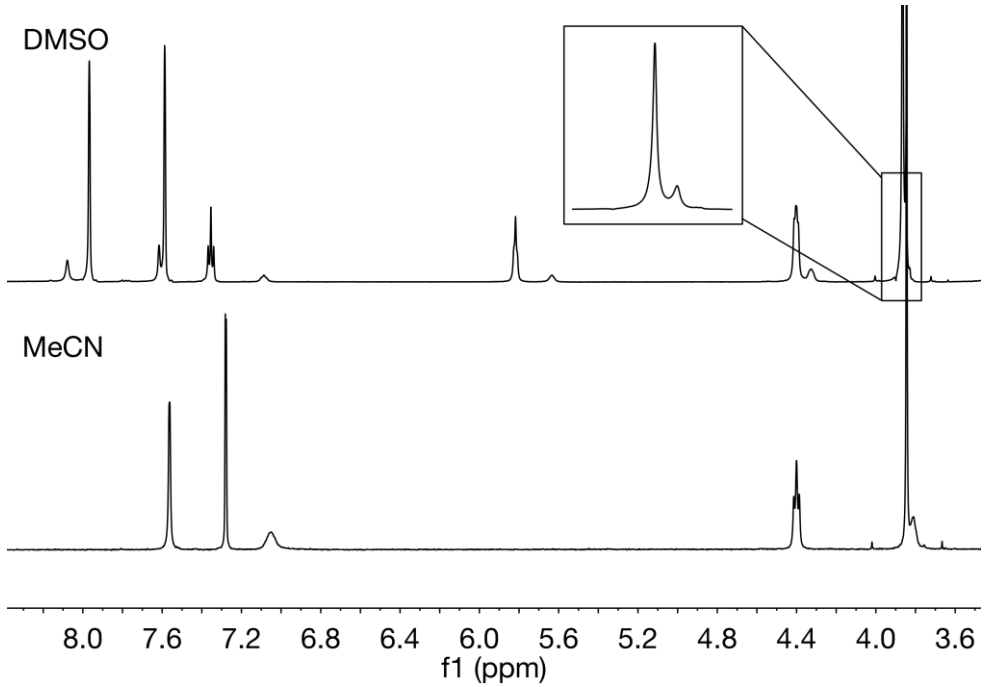

Figure 5.3.33. Comparison of the ^{1}H NMR spectra of **$Ag_2(HL3^{Me})_2(PF_6)_2$** in MeCN-d_3 (bottom) and DMSO-d_3 (top) at RT.

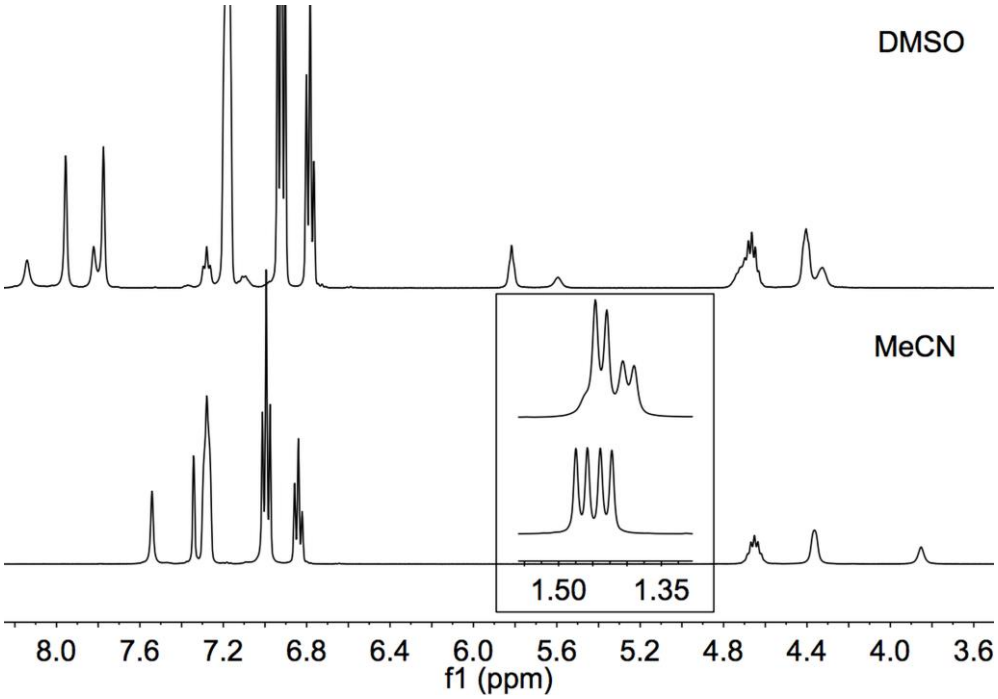

Figure 5.3.34. Comparison of the ^{1}H NMR spectra of **$Ag_2(HL3^{i\text{-}Pr})_2(PF_6)_2$** in MeCN-$d_3$ (bottom) and DMSO-d_3 (top) at RT.

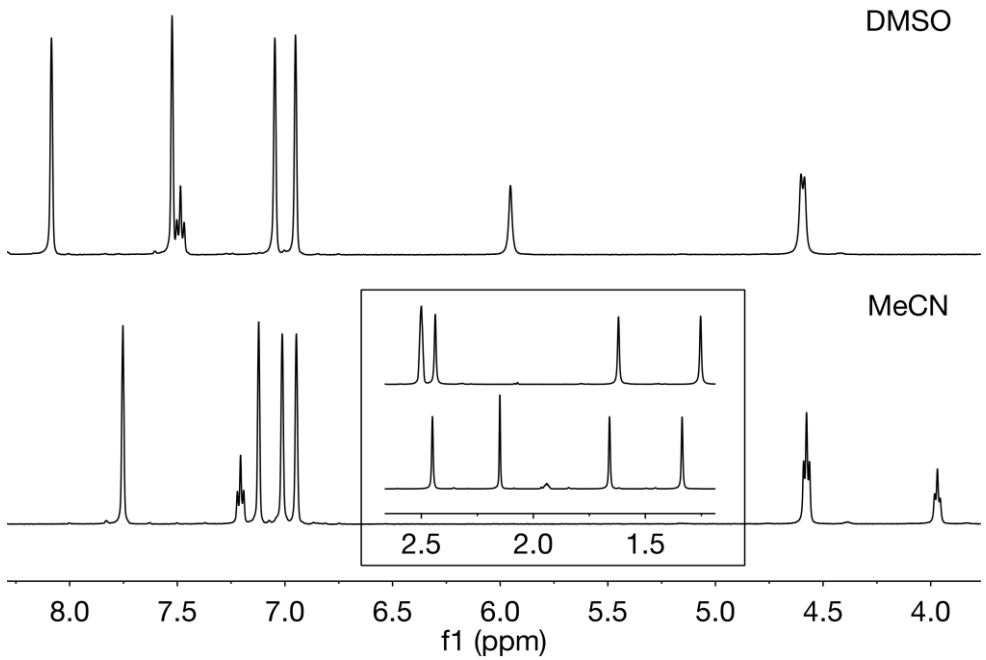

Figure 5.3.35. Comparison of ^{1}H NMR spectra of **$Ag_2(HL3^{Mes})_2(PF_6)_2$** in MeCN-$d_3$ (bottom) and DMSO-d_3 (top) at RT.

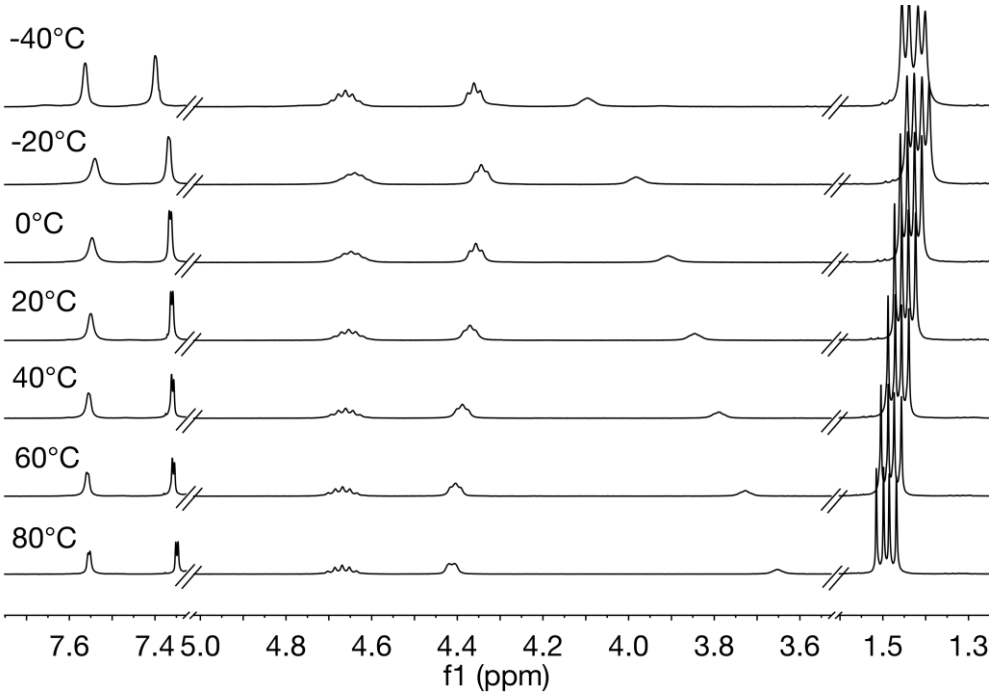

Figure 5.3.36. ^{1}H VT NMR spectra of **$Ag_2(HL3^{i\text{-}Pr})_2(BPh_4)_2$** in MeCN-$d_3$. The signals for BPh_4^- and solvent have been cut out for clarity.

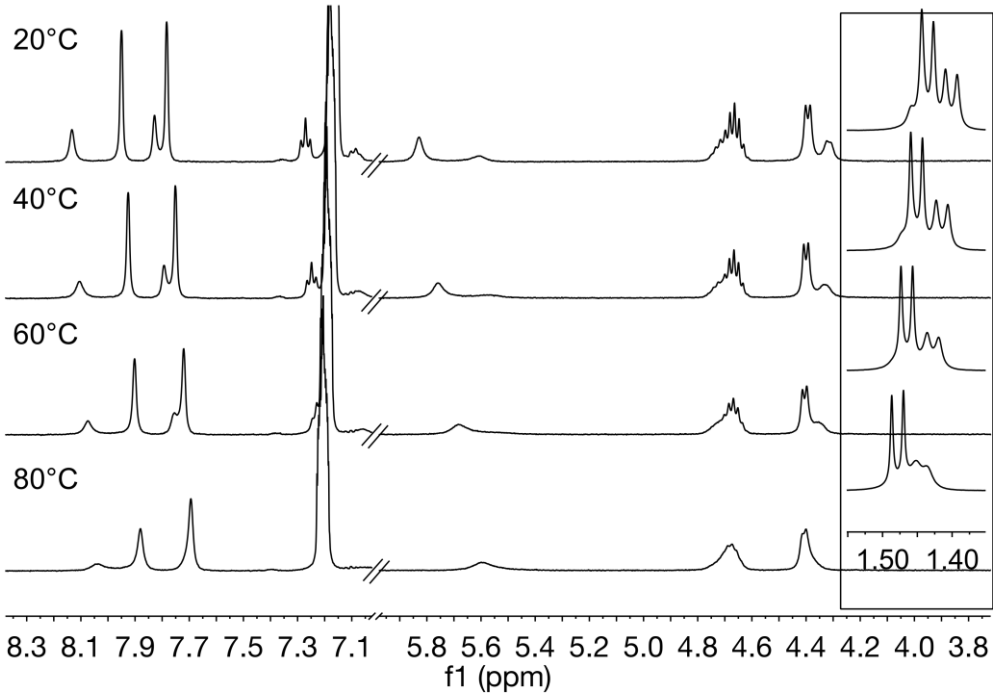

Figure 5.3.37. ^{1}H VT NMR spectra of **$Ag_2(HL3^{i\text{-}Pr})_2(BPh_4)_2$** in DMSO-$d_6$. The signals for BPh_4^- and solvent have been cut out for clarity.

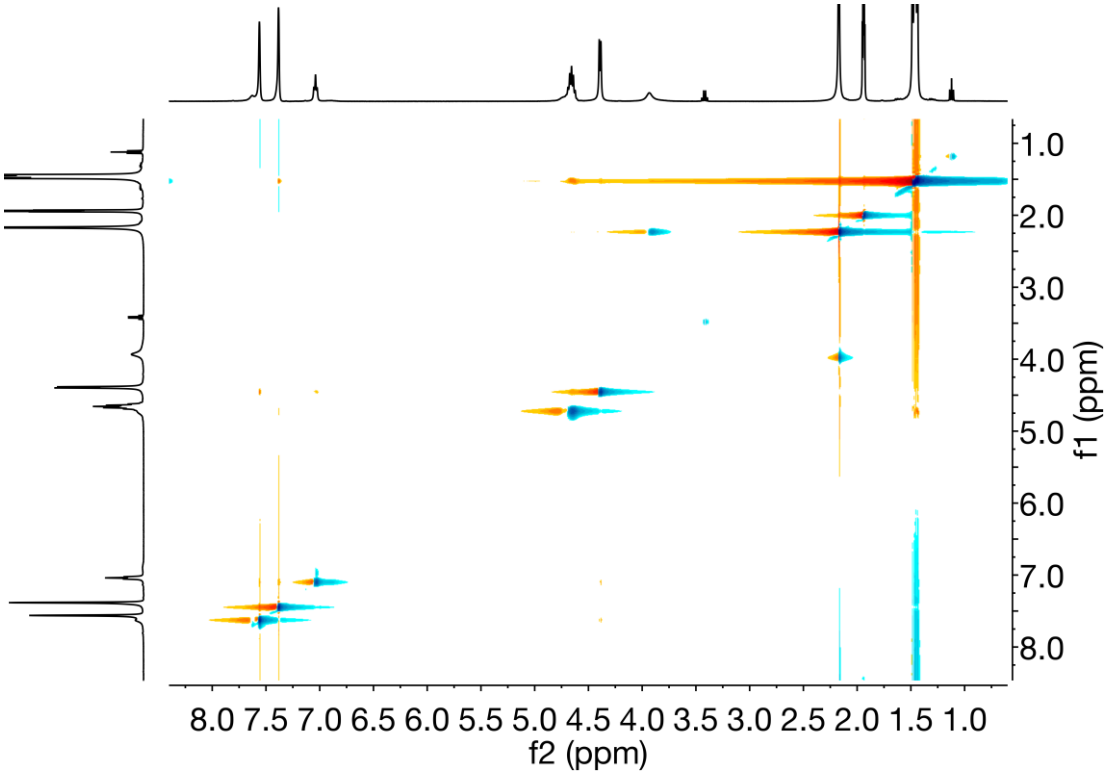

Figure 5.3.38. H,H-NOESY NMR spectrum of **$Ag_2(HL3^{i\text{-}Pr})_2(PF_6)_2$** in MeCN-$d_3$ at RT.

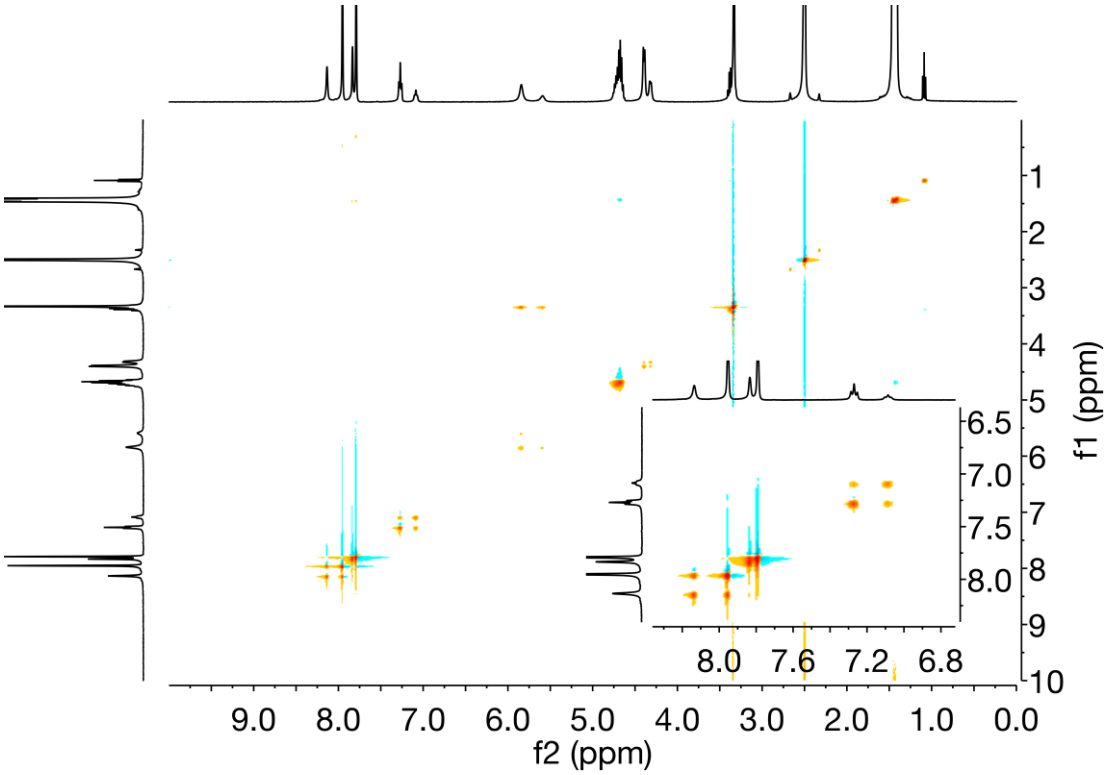

Figure 5.3.39. H,H-NOESY NMR spectrum of **$Ag_2(HL3^{i\text{-}Pr})_2(PF_6)_2$** in DMSO-*$d_6$* at RT.

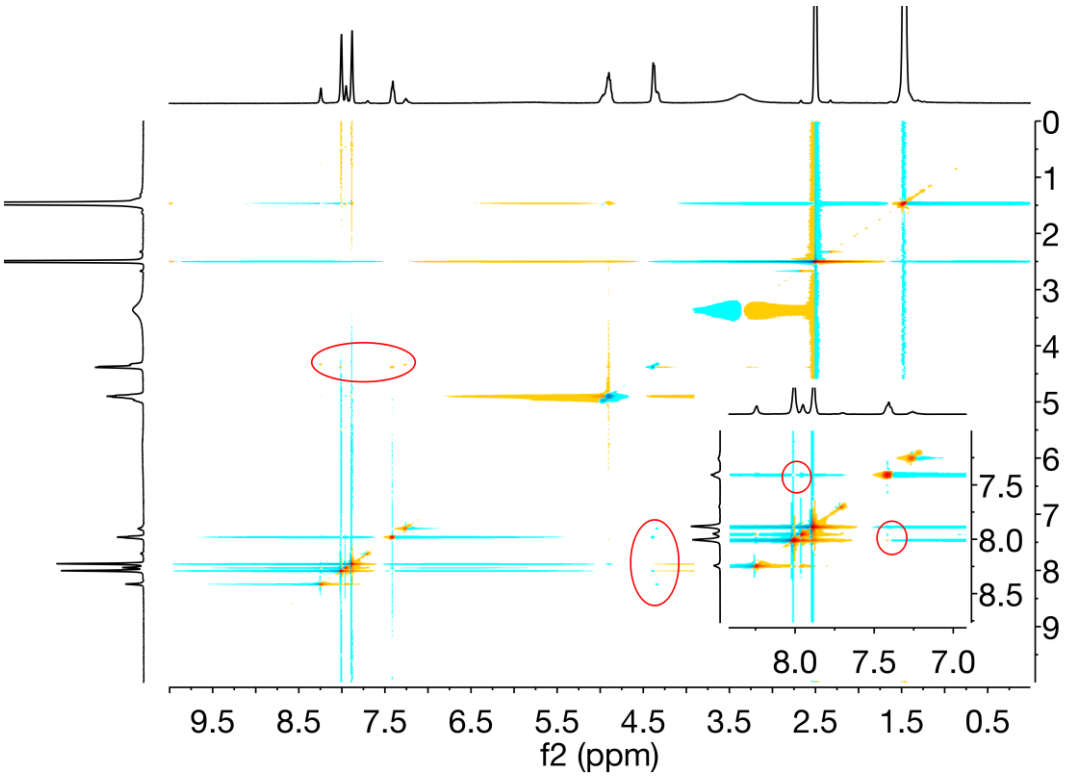

Figure 5.3.40. H,H-NOESY NMR spectrum of **$Au_2(HL3^{i\text{-}Pr})_2(PF_6)_2$** in DMSO-*$d_6$* at RT.

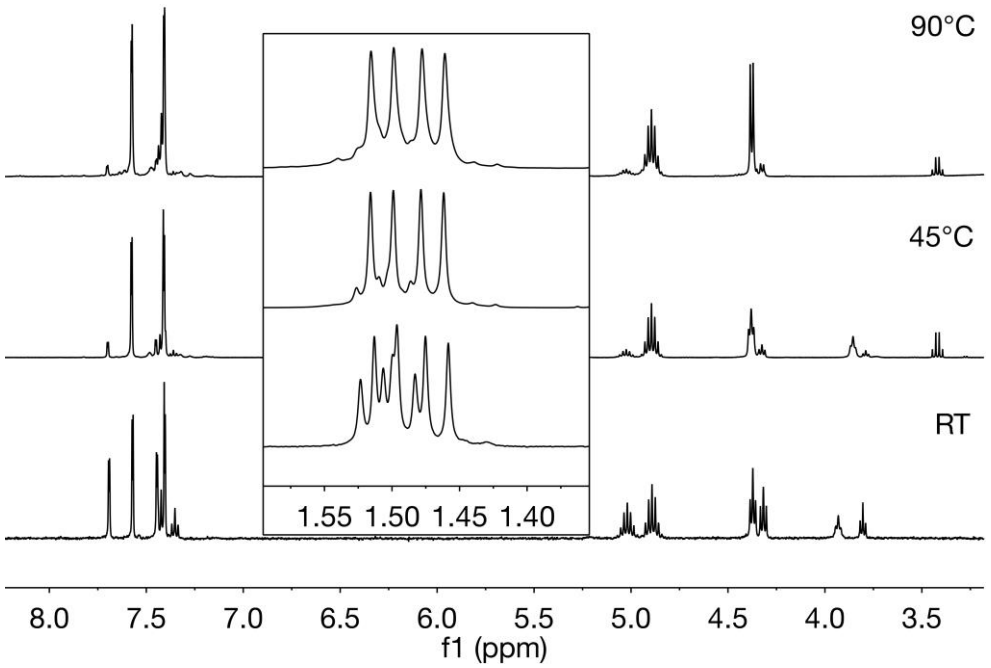

Figure 5.3.41. Formation of anti/syn isomers of **$Au_2(HL3^{i\text{-}Pr})_2(PF_6)_2$** in MeCN-$d_3$ at different temperatures.

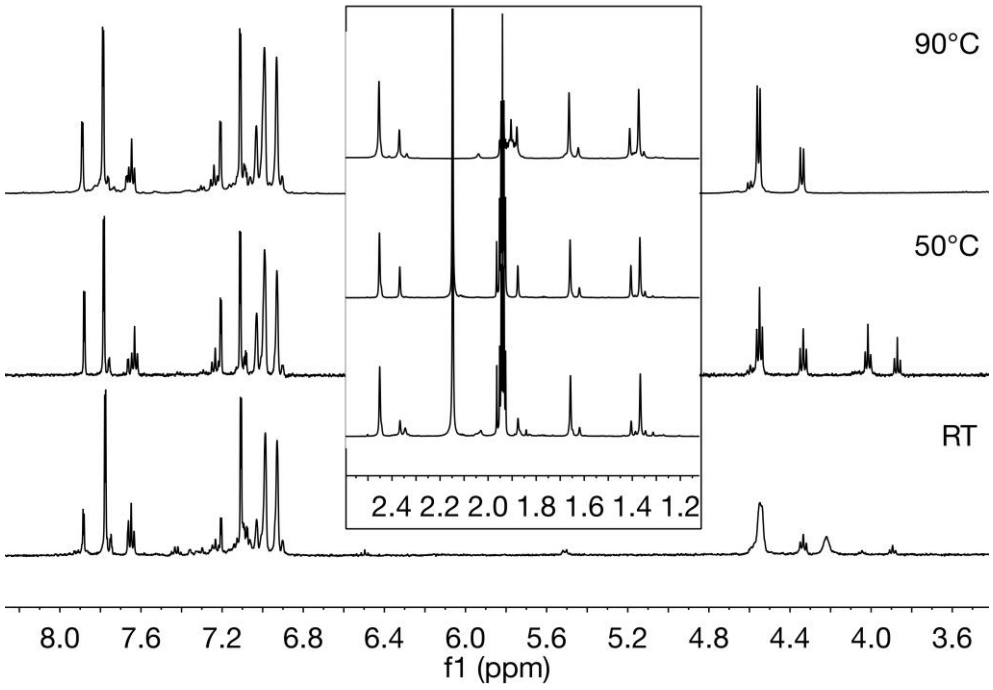

Figure 5.3.42. Formation of anti/syn isomers of **$Au_2(HL3^{Mes})_2(PF_6)_2$** in MeCN-$d_3$ at different temperatures.

5.3.2 MS Spectra

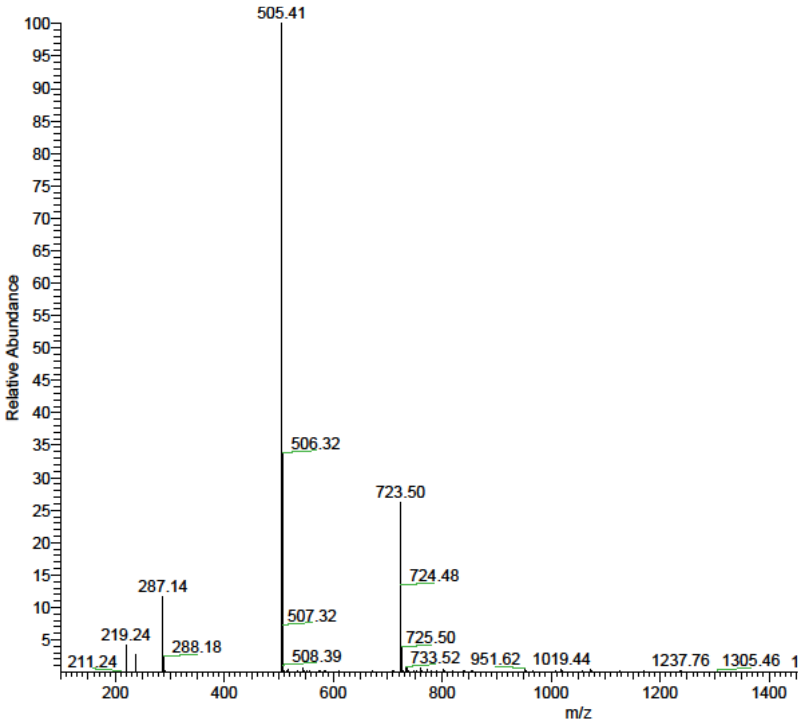

Figure 5.3.43. ESI MS spectrum of the crude product formed in a reaction of **H_3(L2)Br** with KN".

5.3.3 UV-VIS Spectra

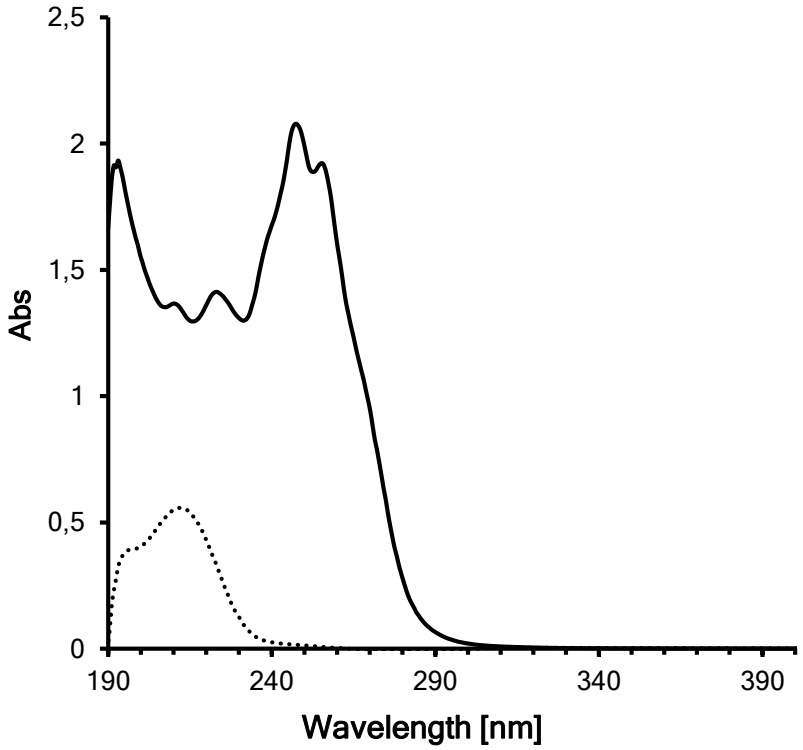

Figure 5.3.44. UV-VIS spectra of **$Au_2(HL3^{Me})_2(PF_6)_2$** (solid line) and **$H_2(L3^{Me})(PF_6)_2$** (dashed line) in acetonitrile ($6.5x10^{-5}$ mol/L).

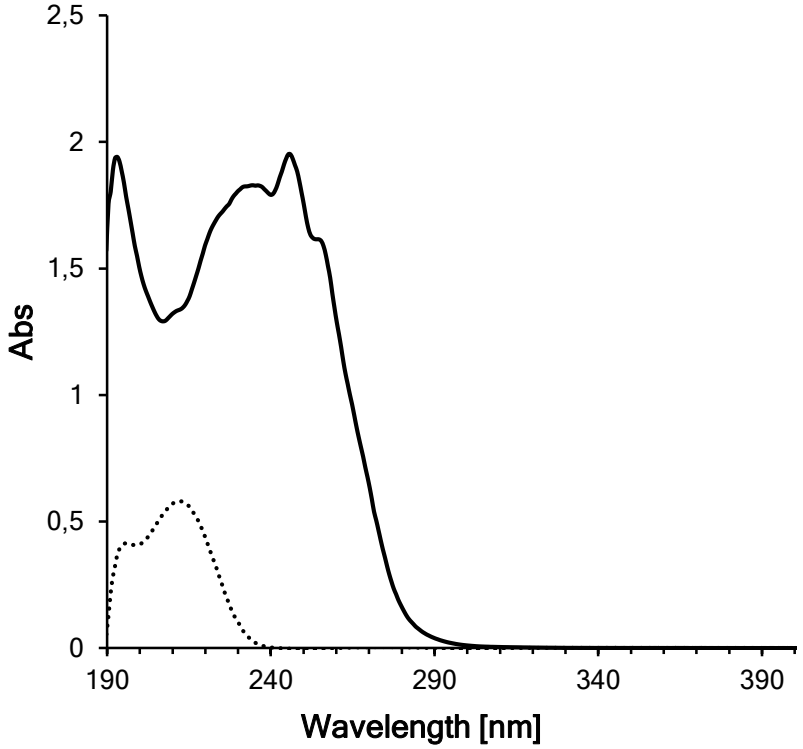

Figure 5.3.45. UV-VIS spectra of **$Au_2(HL3^{i\text{-}Pr})_2(PF_6)_2$** (solid line) and **$H_2(L3^{i\text{-}Pr})(PF_6)_2$** (dashed line) in acetonitrile ($6.5x10^{-5}$ mol/L).

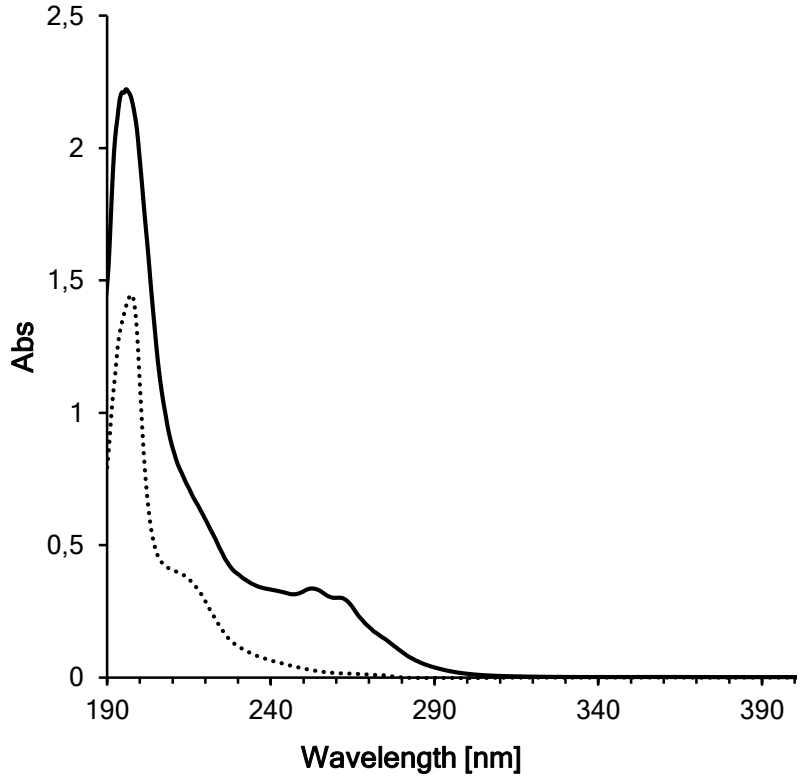

Figure 5.3.46. UV-VIS spectra of **$Au_2(HL3^{Mes})_2(PF_6)_2$** (solid line) and **$H_2(L3^{Mes})(PF_6)_2$** (dashed line) in acetonitrile ($6.5x10^{-5}$ mol/L).

5.3.4 Cytotoxicity Studies

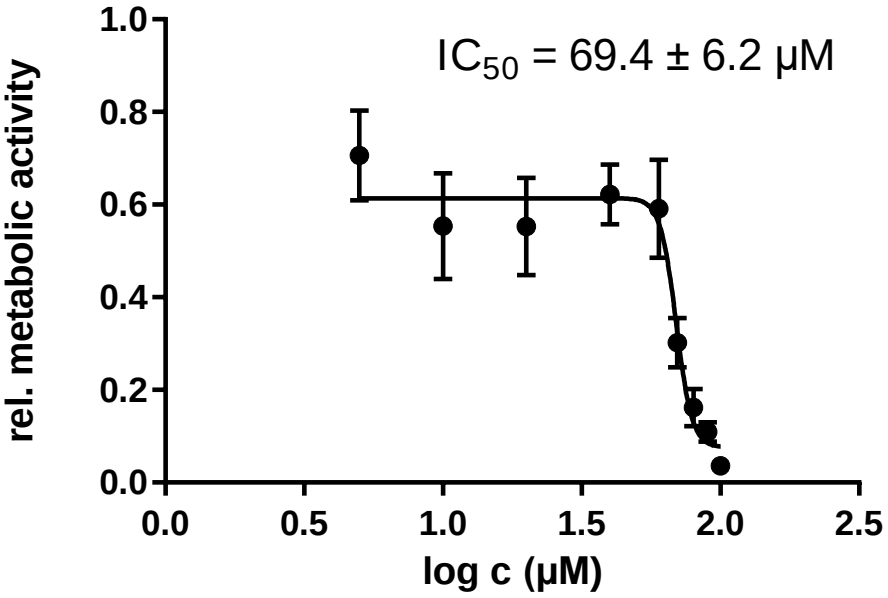

Figure 5.3.47. Metabolic activity of **$Au_2(HL3^{Me})_2(PF_6)_2$** in human liver cancer cell lines HepG2.

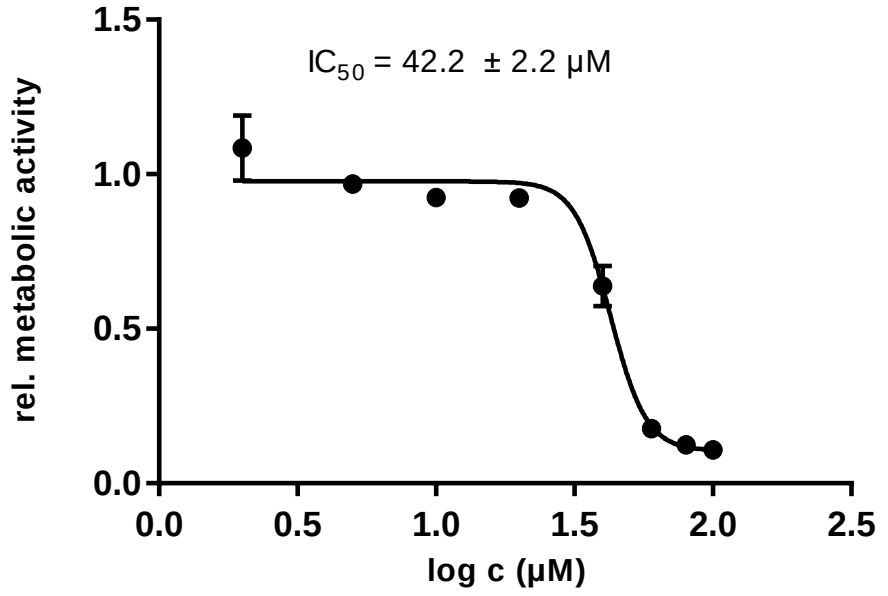

Figure 5.3.48. Metabolic activity of **$Au_2(HL3^{i\text{-}Pr})_2(PF_6)_2$** in human liver cancer cell lines HepG2.

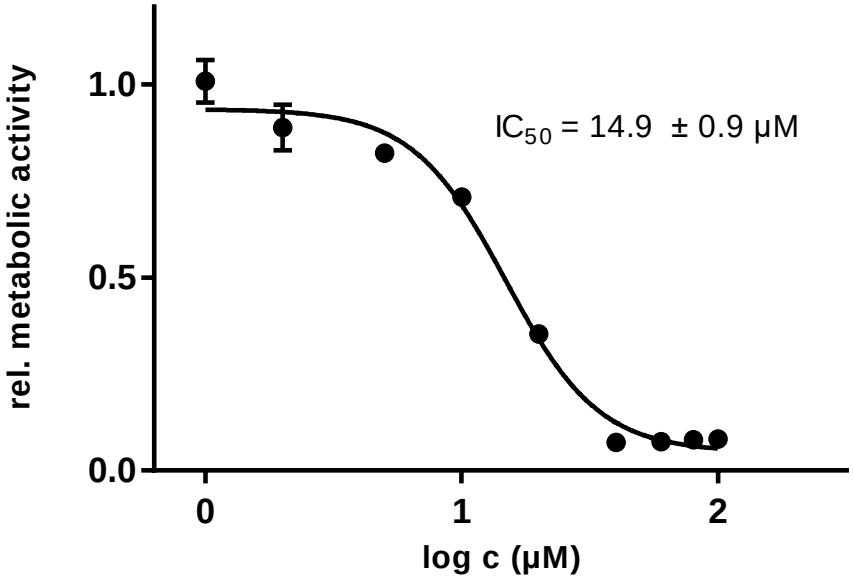

Figure 5.3.49. Metabolic activity of **$Au_2(HL3^{Mes})_2(PF_6)_2$** in human liver cancer cell lines HepG2.

5.3.5 DFT Calculations

Table 5.3.1. Atomic coordinates for the anti, exo isomer of **$[Ag_2(HL3^{i\text{-}Pr})_2]^{2+}$** in acetonitrile and the corresponding free enthalpy.

Ag-anti-exo (MeCN)							
Ag	-1.8407960	-0.2936430	-0.0188540	H	0.4177240	5.2533760	1.5038230
Ag	1.5323530	0.2348830	0.0111300	C	-3.4707380	1.9484710	-3.6515110
N	-2.0327890	-3.1440430	1.2996380	H	-2.4021320	1.7698010	-3.8075180
N	1.5719960	-2.7875670	-1.0755110	H	-4.0306060	1.3259300	-4.3560030
N	3.4227870	-2.2315740	-0.1580380	H	-3.6873850	2.9965910	-3.8859820
N	-0.6694630	-3.1860680	-0.3487570	C	-5.3622150	1.8280890	-1.9514900
N	-3.0614220	2.3408520	-1.2540810	H	-5.6072130	1.5855140	-0.9124820
N	0.5619810	3.1415580	0.9910540	H	-5.6487250	2.8681980	-2.1430960
N	2.5031830	3.1885360	0.0935250	H	-5.9634970	1.1895800	-2.6060230
N	-1.7171880	2.8113880	0.3423030	C	4.1702430	3.6950390	-1.6605460
C	-1.4846300	-2.3586510	0.3520480	H	3.3544390	3.8053330	-2.3817240
C	-0.7053670	-4.4722630	0.1607860	H	4.4595750	4.6879000	-1.2996320
C	0.1694020	-2.7413230	-1.4527620	H	5.0338250	3.2719790	-2.1823060
C	2.1832830	-1.7687690	-0.4162580	C	4.8568270	2.6358340	0.5470690

C	-3.0018070	-2.6834200	2.3099040	H	4.5559830	1.9283130	1.3263940
C	4.4760160	-1.4540970	0.5216970	H	5.7852580	2.2774530	0.0920870
C	-2.2375800	1.7701140	-0.3542840	H	5.0630580	3.6027530	1.0196140
C	-3.0565290	3.7186150	-1.1315540	C	5.0984190	-2.2620520	1.6549190
C	-2.2072990	4.0190380	-0.1226020	H	4.3297430	-2.6443990	2.3337990
C	-0.7387030	2.6483970	1.4071030	H	5.6891830	-3.1058490	1.2827710
C	1.4886760	2.3509900	0.3898970	H	5.7702160	-1.6170670	2.2291430
C	2.2254240	4.4797240	0.5026570	C	5.5018320	-0.9566690	-0.4910980
C	-3.8799650	1.5944420	-2.2257980	H	5.0242720	-0.3528020	-1.2694120
C	3.7753840	2.7634570	-0.5207540	H	6.2523390	-0.3418150	0.0148590
H	-0.0820410	-1.6941290	-1.6236780	H	6.0208500	-1.7923760	-0.9739950
H	-3.1228890	-1.6145620	2.1146390	C	-4.3446420	-3.3788130	2.1131150
H	3.9526330	-0.5969070	0.9540320	H	-5.0763100	-2.9684870	2.8160170
H	-3.6496300	4.3657320	-1.7584480	H	-4.7192760	-3.2246190	1.0963100
H	-1.9229100	4.9741030	0.2901840	H	-4.2708960	-4.4562550	2.2980940
H	-0.6356550	1.5736690	1.5615480	C	-2.4302390	-2.8689970	3.7117380
H	2.9125910	5.2999600	0.3688370	H	-2.2948120	-3.9287670	3.9549120
H	-3.6448420	0.5428710	-2.0390630	H	-1.4648530	-2.3625510	3.8103130
H	3.5646840	1.7753370	-0.9387860	H	-3.1197990	-2.4433460	4.4471690
C	3.5940430	-3.5125940	-0.6495280	C	-1.1996760	3.2770630	2.7178510

C	2.4240220	-3.8714640	-1.2235120	H	-0.3954650	3.1576900	3.4539510
C	-1.5682300	-4.4427930	1.2016370	H	-1.4048980	4.3484330	2.5996920
H	4.5197400	-4.0585080	-0.5588780	C	-0.1096520	-3.5152150	-2.7371360
H	2.1481010	-4.7862240	-1.7240050	H	0.5970760	-3.1745020	-3.5033710
H	-1.8828060	-5.2294910	1.8692620	H	0.0283720	-4.5941170	-2.5936670
H	-0.1276270	-5.2889520	-0.2422470	O	-2.3648840	2.5804800	3.0968140
C	0.9957690	4.4562440	1.0639050	O	-1.4428910	-3.2218850	-3.0877730
H	-2.7153090	2.9738290	3.9058110	H	-1.6770950	-3.7276210	-3.8761420
G[Hartree] = -1972.161345							

Table 5.3.2. Atomic coordinates for the anti, exo isomer of **$[Ag_2(HL3^{i\text{-}Pr})_2]^{2+}$** in dimethylsulfoxide and the corresponding free enthalpy.

Ag-anti-exo (DMSO)						
Ag	1.8412160	0.3020090	-0.0197670	H	-0.3980290	-5.2572200	1.4977460
Ag	-1.5255270	-0.2419340	0.0062280	C	3.4905290	-1.9319600	-3.6540690
N	2.0157890	3.1508880	1.3039200	H	2.4219460	-1.7587990	-3.8164610
N	-1.5793670	2.7811550	-1.0808090	H	4.0510020	-1.3075550	-4.3564760
N	-3.4268360	2.2134250	-0.1644360	H	3.7137020	-2.9791530	-3.8866510
N	0.6565850	3.1892800	-0.3473540	C	5.3714610	-1.7980570	-1.9441290
N	3.0715590	-2.3254780	-1.2591550	H	5.6088760	-1.5543320	-0.9035940
N	-0.5473450	-3.1456990	0.9849730	H	5.6660220	-2.8362490	-2.1340520

N	-2.4898260	-3.1969480	0.0908920	H	5.9731740	-1.1557390	-2.5945590
N	1.7299670	-2.8047840	0.3364480	C	-4.1711950	-3.7153760	-1.6460560
C	1.4785210	2.3659780	0.3500910	H	-3.3590590	-3.8428150	-2.3685610
C	0.6759970	4.4718270	0.1717270	H	-4.4697640	-4.7008290	-1.2726500
C	-0.1759160	2.7443650	-1.4560050	H	-5.0321200	-3.2905850	-2.1708350
C	-2.1846100	1.7585010	-0.4223650	C	-4.8381070	-2.6338400	0.5546820
C	2.9814900	2.6930350	2.3181040	H	-4.5329440	-1.9181960	1.3247840
C	-4.4747170	1.4302750	0.5165220	H	-5.7705120	-2.2818200	0.1028140
C	2.2468670	-1.7598350	-0.3571510	H	-5.0401740	-3.5957620	1.0392680
C	3.0704840	-3.7034500	-1.1413000	C	-5.0965930	2.2336550	1.6528440
C	2.2225590	-4.0094610	-0.1330290	H	-4.3273880	2.6178250	2.3301550
C	0.7514920	-2.6488370	1.4021790	H	-5.6918470	3.0759580	1.2843840
C	-1.4766850	-2.3573470	0.3855160	H	-5.7638770	1.5854590	2.2287850
C	-2.2088770	-4.4872680	0.5000790	C	-5.5015300	0.9315080	-0.4941120
C	3.8896940	-1.5740300	-2.2268460	H	-5.0248900	0.3291810	-1.2742370
C	-3.7645280	-2.7736720	-0.5191570	H	-6.2505010	0.3154450	0.0126470
H	0.0827090	1.6996800	-1.6315850	H	-6.0232480	1.7664690	-0.9755450
H	3.1461640	1.6360140	2.0922520	C	4.3006890	3.4428940	2.1710130
H	-3.9466870	0.5742710	0.9455480	H	5.0331100	3.0376630	2.8760520
H	3.6649070	-4.3471000	-1.7705010	H	4.7018520	3.3343840	1.1583070
H	1.9409480	-4.9667930	0.2763600	H	4.1851250	4.5108460	2.3871880
H	0.6446230	-1.5751200	1.5606130	C	2.3763800	2.8150360	3.7124790
H	-2.8944240	-5.3091730	0.3682710	H	2.1908480	3.8611100	3.9804920
H	3.6466440	-0.5239420	-2.0420870	H	1.4314190	2.2664270	3.7781000
H	-3.5539850	-1.7904480	-0.9487440	H	3.0686740	2.3985110	4.4506550
C	-3.6058130	3.4934790	-0.6550120	C	1.2140590	-3.2816950	2.7100290

C	-2.4379190	3.8598550	-1.2284560	H	0.4087510	-3.1685120	3.4459650
C	1.5362030	4.4446380	1.2146780	H	1.4222820	-4.3519990	2.5874620
H	-4.5346860	4.0338810	-0.5639600	C	0.1007110	3.5277860	-2.7349970
H	-2.1679520	4.7769630	-1.7278880	H	-0.6032980	3.1884110	-3.5043320
H	1.8398200	5.2300740	1.8888480	H	-0.0435920	4.6049250	-2.5848960
H	0.0902380	5.2848460	-0.2271790	O	2.3769780	-2.5845280	3.0948040
C	-0.9782030	-4.4611370	1.0588080	O	1.4358650	3.2455660	-3.0878460
H	2.7234810	-2.9812300	3.9038340	H	1.6641920	3.7591180	-3.8728250
G[Hartree] = -1972.156319							

Table 5.3.3. Atomic coordinates for the syn, meso isomer of **$[Ag_2(HL3^{i\text{-}Pr})_2]^{2+}$** in acetonitrile and the corresponding free enthalpy.

Ag-syn-meso (MeCN)							
O	-1.9821290	-3.9714400	-2.7453360	H	-4.2837320	-3.3774390	-1.2774590
N	-0.1685580	-2.1983550	2.4155130	H	-6.0142260	-1.2525520	-1.3583680
N	-2.8259210	-1.7851400	-1.0114370	Ag	-1.2965680	0.9174050	-0.4635180
N	-4.1791910	-0.1276510	-1.0888010	Ag	1.4400670	-0.9012800	0.0594740
N	-1.2239540	-2.5377980	0.5863010	C	-5.1162960	1.5800860	0.4107970
C	-0.0803010	-2.0046980	1.0836460	H	-5.9458330	0.9431520	0.7383020
C	-1.5832800	-2.5225140	-0.8244710	H	-4.2772130	1.4386660	1.0998520
C	-2.8758740	-0.4301460	-0.9466820	H	-5.4405130	2.6236420	0.4746670
C	0.8440130	-1.6990670	3.3700360	C	-5.8277340	1.4598750	-2.0287490
C	-1.6345940	-3.9489930	-1.3831690	H	-6.0806470	2.5236310	-2.0628400
H	-1.2303170	-3.6744340	-3.2756220	H	-5.5234990	1.1498510	-3.0334650

H	-0.7943490	-1.9683420	-1.3358380	H	-6.7378540	0.9166820	-1.7522290
H	1.8034710	-1.8245220	2.8598060	C	0.8610930	-2.5308900	4.6460100
H	-2.3770150	-4.5531730	-0.8548330	H	0.9559900	-3.5996080	4.4297360
N	4.3213490	-0.2823790	-0.9292210	H	1.7230020	-2.2319420	5.2496510
N	1.3774870	2.7069220	-0.4053340	H	-0.0349370	-2.3686890	5.2544590
N	0.1612870	2.9602600	1.3390430	C	0.6093580	-0.2154290	3.6434730
N	3.0912200	1.3833710	-1.4566260	H	0.6630280	0.3629910	2.7149190
C	3.0507670	0.1634190	-0.8612210	H	-0.3717000	-0.0531550	4.1042160
C	5.1458660	0.6312450	-1.5591070	H	1.3779450	0.1613400	4.3259490
C	4.3687970	1.6854530	-1.8938250	C	5.2959140	-2.4615180	-1.5298560
C	1.9535340	2.2766030	-1.6723370	H	6.2001730	-2.0473110	-1.9894670
C	0.2171770	2.2914540	0.1675140	H	5.5447470	-3.4514360	-1.1356070
C	1.2597010	3.7846330	1.5000410	H	4.5339860	-2.5810360	-2.3067690
C	2.0313260	3.6234210	0.4033990	C	5.8158930	-1.3576730	0.7041250
C	4.7846650	-1.5766340	-0.3978820	H	6.0723380	-2.3177880	1.1621490
H	6.1992930	0.4609530	-1.7147770	H	6.7386780	-0.9165710	0.3111140
H	4.6053120	2.6096030	-2.3981200	H	5.4199710	-0.6986790	1.4835580
H	1.4035500	4.4102110	2.3658380	C	-2.0954550	3.8252620	1.8140540
H	2.9752460	4.0700090	0.1313890	H	-2.9480900	3.7512620	2.4964640
H	3.8921480	-2.0357230	0.0363690	H	-1.7442600	4.8634990	1.8147140
C	-4.7042740	1.2506970	-1.0209880	H	-2.4401100	3.5766910	0.8052790
H	-3.8587320	1.8836160	-1.3053470	C	-0.5529310	3.1559080	3.7055950
C	-0.9856780	2.8815520	2.2701010	H	-0.3470280	4.2183860	3.8756310
H	-1.3382040	1.8474960	2.2039870	H	-1.3662180	2.8705290	4.3789600
C	-1.3542580	-2.8263410	2.7512480	H	0.3337410	2.5780660	3.9831170
C	-2.0219010	-3.0472120	1.5957080	H	-0.6542470	-4.4032980	-1.1990450

H	-1.6250250	-3.0707060	3.7654870	H	2.3733790	3.1724810	-2.1352200
H	-2.9804110	-3.5080760	1.4144780	C	0.9488280	1.6820910	-2.6689630
C	-4.9444740	-1.2720790	-1.2249950	H	0.6069490	0.6984790	-2.3397920
C	-4.0919640	-2.3216610	-1.1778220	H	0.0840000	2.3496520	-2.7497030
H	1.6272570	2.3209430	-4.3901870	O	1.5761220	1.4813280	-3.9140990
G[Hartree] = -1972.161716							

Table 5.3.4. Atomic coordinates for the syn-meso isomer of **$[Ag_2(HL3^{i\text{-}Pr})_2]^{2+}$** in dimethylsulfoxide and the corresponding free enthalpy.

Ag-syn-meso (DMSO)							
O	-1.9788940	-3.9656090	-2.7752870	H	-4.2884690	-3.3724600	-1.2786540
N	-0.1838170	-2.1980800	2.3972130	H	-6.0197820	-1.2471380	-1.3187770
N	-2.8256250	-1.7814430	-1.0333990	Ag	-1.2916120	0.9202190	-0.4957250
N	-4.1798750	-0.1237930	-1.0776850	Ag	1.4412520	-0.8990830	0.0570650
N	-1.2269990	-2.5400160	0.5616890	C	-5.1006480	1.5616680	0.4560850
C	-0.0875580	-2.0047300	1.0659000	H	-5.9262210	0.9194130	0.7834190
C	-1.5831510	-2.5196840	-0.8500930	H	-4.2545500	1.4111090	1.1346950
C	-2.8742400	-0.4270110	-0.9627400	H	-5.4255830	2.6036620	0.5387620
C	0.8202690	-1.6948270	3.3583360	C	-5.8375540	1.4761320	-1.9772260
C	-1.6348880	-3.9444630	-1.4123210	H	-6.0913430	2.5401790	-1.9939040
H	-1.2261730	-3.6629610	-3.3010270	H	-5.5437030	1.1806580	-2.9894390
H	-0.7935900	-1.9634910	-1.3582690	H	-6.7448770	0.9288870	-1.6993930
H	1.7842200	-1.8197100	2.8564800	C	0.8282170	-2.5233230	4.6361940
H	-2.3783480	-4.5493680	-0.8862990	H	0.9281390	-3.5923800	4.4236340

N	4.3382180	-0.2815020	-0.8874020	H	1.6840660	-2.2211380	5.2468130
N	1.3898300	2.7038460	-0.3911250	H	-0.0732290	-2.3624500	5.2369770
N	0.1423260	2.9470510	1.3319940	C	0.5801480	-0.2112890	3.6268460
N	3.1179640	1.3876210	-1.4257070	H	0.6452280	0.3666330	2.6987040
C	3.0672810	0.1653200	-0.8364040	H	-0.4067620	-0.0500280	4.0752960
C	5.1728590	0.6337230	-1.5012010	H	1.3396850	0.1672700	4.3184460
C	4.4019980	1.6903070	-1.8423950	C	5.3054730	-2.4642130	-1.4849950
C	1.9848720	2.2836090	-1.6524650	H	6.2121770	-2.0526030	-1.9421870
C	0.2172090	2.2893460	0.1555330	H	5.5503630	-3.4549480	-1.0902410
C	1.2413830	3.7640650	1.5218670	H	4.5459470	-2.5820960	-2.2645570
C	2.0330380	3.6090030	0.4385150	C	5.8190080	-1.3649700	0.7521550
C	4.7926270	-1.5782610	-0.3550470	H	6.0652640	-2.3259970	1.2138160
H	6.2283140	0.4634430	-1.6425500	H	6.7479580	-0.9317550	0.3648960
H	4.6471250	2.6164880	-2.3387850	H	5.4235610	-0.7016780	1.5282230
H	1.3721710	4.3807950	2.3960710	C	-2.1271600	3.8021160	1.7578520
H	2.9840570	4.0533410	0.1886120	H	-3.0043430	3.7074800	2.4057280
H	3.8963000	-2.0339380	0.0747870	H	-1.7874130	4.8437250	1.7881060
C	-4.7040060	1.2530460	-0.9845870	H	-2.4310380	3.5681290	0.7325500
H	-3.8615150	1.8901880	-1.2682950	C	-0.6237400	3.1367820	3.6820330
C	-1.0241340	2.8624900	2.2377290	H	-0.4230440	4.1994400	3.8569340
H	-1.3704460	1.8268600	2.1624370	H	-1.4508790	2.8503660	4.3379200
C	-1.3701810	-2.8281070	2.7258020	H	0.2576170	2.5603920	3.9790860
C	-2.0302240	-3.0503000	1.5663820	H	-0.6554070	-4.4001920	-1.2268410
H	-1.6473070	-3.0722900	3.7383530	H	2.4125250	3.1825680	-2.1020950
H	-2.9872860	-3.5122280	1.3804110	C	0.9927120	1.6972940	-2.6661170
C	-4.9477530	-1.2673230	-1.2050520	H	0.6405540	0.7143820	-2.3456760

C	-4.0946150	-2.3170960	-1.1782610	H	0.1324090	2.3694570	-2.7569510
H	1.7081720	2.3421960	-4.3684000	O	1.6344880	1.4977060	-3.9040590
G[Hartree] = -1972.156273							

Table 5.3.5. Atomic coordinates for the anti, exo isomer of **$[Au_2(HL3^{i\text{-}Pr})_2]^{2+}$** in acetonitrile and the corresponding free enthalpy.

Au-anti-exo (MeCN)							
N	-2.8828840	2.7744400	-0.7376200	H	-3.4062150	-3.1848090	3.3339980
N	1.2274000	2.9518970	0.6907780	H	-5.0175490	-2.4495440	3.3688740
N	3.0487440	2.7754080	-0.4324170	H	-4.7750030	-3.9677550	2.5053830
N	-1.1669530	2.9553950	0.5402700	C	-5.2150380	-2.0111080	0.5853950
N	-2.8836590	-2.7739050	0.7375910	H	-4.9664350	-1.3862070	-0.2789520
N	1.2265690	-2.9521620	-0.6904840	H	-5.5763880	-2.9798770	0.2224000
N	3.0480700	-2.7758910	0.4324810	H	-6.0278920	-1.5264450	1.1354200
N	-1.1678320	-2.9552400	-0.5403810	C	4.6687180	-3.0772220	2.2791330
C	-1.9497160	2.0483530	-0.0935340	H	3.8325910	-3.3202310	2.9421160
C	-1.6178140	4.2410940	0.2989430	H	5.1312070	-4.0085470	1.9356010
C	-0.0151720	2.5989020	1.3563120	H	5.4201880	-2.5378440	2.8629320
C	2.0307940	2.0505550	0.0712490	C	5.3305140	-1.9286680	0.1076470
C	-4.0046900	2.1849190	-1.4988380	H	4.9795340	-1.2627900	-0.6876270
C	4.2217170	2.1938060	-1.1210800	H	6.1813530	-1.4525890	0.6048290
C	-1.9502800	-2.0480310	0.0935720	H	5.6801160	-2.8620920	-0.3478550
C	-2.7006120	-4.1229380	0.5038480	C	4.6698630	3.0771220	-2.2785980
C	-1.6190950	-4.2408350	-0.2992060	H	3.8339870	3.3210970	-2.9415420

C	-0.0158500	-2.5989800	-1.3562250	H	5.1328510	4.0079290	-1.9343310
C	2.0302870	-2.0508780	-0.0712890	H	5.4211030	2.5377130	-2.8626610
C	2.8937390	-4.1145280	0.1301810	C	5.3306740	1.9266750	-0.1078490
C	-4.0053270	-2.1841200	1.4988220	H	4.9792140	1.2604780	0.6869420
C	4.2212690	-2.1944750	1.1209060	H	6.1812990	1.4504250	-0.6052310
H	-0.0269630	1.5121210	1.4465640	H	5.6807440	2.8595930	0.3483220
H	-3.6451300	1.2001280	-1.8092330	C	-5.2145780	2.0125800	-0.5855290
H	3.8668650	1.2429980	-1.5270270	H	-6.0275680	1.5281510	-1.1355600
H	-3.3436580	-4.8823180	0.9182540	H	-4.9663350	1.3877290	0.2789590
H	-1.1530380	-5.1219870	-0.7094610	H	-5.5755760	2.9815660	-0.2227790
H	-0.0274340	-1.5122000	-1.4464860	C	-4.3100320	3.0056990	-2.7454810
H	3.5996410	-4.8701810	0.4338270	H	-4.7735050	3.9686680	-2.5057410
H	-3.6453860	-1.1995490	1.8094910	H	-3.4049130	3.1850760	-3.3340620
H	3.8669000	-1.2431830	1.5261460	H	-5.0165460	2.4504490	-3.3691150
C	2.8948810	4.1139910	-0.1296470	C	-0.0911190	-3.1960590	-2.7576700
C	1.7468440	4.2305920	0.5739060	H	0.8132120	-2.8885590	-3.2967250
C	-2.6994170	4.1234430	-0.5040470	H	-0.1184200	-4.2927450	-2.7303420
H	3.6009770	4.8695270	-0.4331380	C	-0.0906030	3.1959880	2.7577310
H	1.2760910	5.1059140	0.9910160	H	0.8135640	2.8883560	3.2969850
H	-3.3422080	4.8830010	-0.9185320	H	-0.1177390	4.2926770	2.7303680
H	-1.1514880	5.1221560	0.7090970	O	-1.2592870	-2.6742700	-3.3464330
C	1.7456150	-4.2309860	-0.5732520	O	-1.2589810	2.6744050	3.3462570
H	1.2745530	-5.1062810	-0.9900700	H	-1.3570960	3.0482650	4.2310760
C	-4.3111640	-3.0050040	2.7452790	H	-1.3574910	-3.0483870	-4.2311320
Au	1.9030260	-0.0001500	-0.0001010	Au	-1.8725520	0.0001520	0.0000350

G[Hartree] = -1951.591571

Table 5.3.6. Atomic coordinates for the anti, exo isomer of **$[Au_2(HL3^{i\text{-}Pr})_2]^{2+}$** in dimethylsulfoxide and the corresponding free enthalpy.

Au-anti-exo (DMSO)							
N	-2.8995610	2.7718590	-0.6876110	H	-3.5196060	-3.2274860	3.2554940
N	1.2385920	2.9560660	0.6648240	H	-5.1169280	-2.4609000	3.2496720
N	3.0380180	2.7732750	-0.4915810	H	-4.8739240	-3.9664850	2.3644090
N	-1.1581840	2.9581110	0.5544370	C	-5.2106680	-1.9704090	0.4697640
N	-2.8991570	-2.7721650	0.6876530	H	-4.9207410	-1.3382010	-0.3761150
N	1.2389980	-2.9559060	-0.6649260	H	-5.5755770	-2.9273830	0.0797120
N	3.0384200	-2.7729930	0.4914700	H	-6.0342290	-1.4797730	0.9983050
N	-1.1577750	-2.9582070	-0.5544180	C	4.6090790	-3.0541070	2.3823010
C	-1.9463490	2.0490090	-0.0691010	H	3.7534190	-3.2910460	3.0223630
C	-1.6233410	4.2417370	0.3300620	H	5.0825000	-3.9885970	2.0630070
C	0.0073000	2.6047140	1.3518090	H	5.3416090	-2.5062380	2.9821180
C	2.0325180	2.0513020	0.0389390	C	5.3304670	-1.9313690	0.2169140
C	-4.0374740	2.1784430	-1.4217280	H	5.0013910	-1.2795230	-0.5990400
C	4.1938310	2.1852540	-1.2024680	H	6.1648640	-1.4436850	0.7307560
C	-1.9460540	-2.0491990	0.0691080	H	5.6963050	-2.8706510	-0.2132420
C	-2.7207070	-4.1208020	0.4496830	C	4.6085980	3.0543840	-2.3824750
C	-1.6227560	-4.2418920	-0.3300150	H	3.7528890	3.2911240	-3.0225440
C	0.0076340	-2.6046590	-1.3518330	H	5.0818940	3.9889800	-2.0633050
C	2.0328200	-2.0511000	-0.0389690	H	5.3411920	2.5065450	-2.9822420
C	2.8877300	-4.1138700	0.1980210	C	5.3301880	1.9320160	-0.2169610

C	-4.0371480	-2.1788900	1.4217630	H	5.0012110	1.2802320	0.5990840
C	4.1941620	-2.1848920	1.2024090	H	6.1646420	1.4443750	-0.7307530
H	-0.0018320	1.5182910	1.4451980	H	5.6959080	2.8714020	0.2130660
H	-3.6740050	1.2060250	-1.7647390	C	-5.2109520	1.9697650	-0.4697230
H	3.8291490	1.2288530	-1.5865060	H	-6.0344490	1.4790280	-0.9982700
H	-3.3775630	-4.8782570	0.8454480	H	-4.9209260	1.3375710	0.3761330
H	-1.1537170	-5.1247050	-0.7330740	H	-5.5759920	2.9266740	-0.0796360
H	-0.0016240	-1.5182330	-1.4451790	C	-4.4005110	3.0177510	-2.6397000
H	3.5871030	-4.8676200	0.5211460	H	-4.8745220	3.9659450	-2.3643110
H	-3.6738170	-1.2064090	1.7647410	H	-3.5201040	3.2271720	-3.2554330
H	3.8293530	-1.2285910	1.5865740	H	-5.1173150	2.4603510	-3.2496180
C	2.8871490	4.1141630	-0.1982760	C	-0.0459670	-3.2067400	-2.7520400
C	1.7526020	4.2346530	0.5266000	H	0.8701510	-2.9079580	-3.2757840
C	-2.7212980	4.1205150	-0.4496070	H	-0.0804860	-4.3030770	-2.7208680
H	3.5864140	4.8679750	-0.5214910	C	-0.0462980	3.2068440	2.7519950
H	1.2885060	5.1123620	0.9462380	H	0.8698690	2.9081660	3.2757130
H	-3.3782690	4.8778880	-0.8453380	H	-0.0809200	4.3031760	2.7207830
H	-1.1544140	5.1246060	0.7331300	O	-1.1997650	-2.6804480	-3.3650380
C	1.7531840	-4.2344390	-0.5268440	O	-1.2000240	2.6804690	3.3650590
H	1.2891980	-5.1121660	-0.9465650	H	-1.2861600	3.0637430	4.2469750
C	-4.4000490	-3.0182130	2.6397630	H	-1.2859770	-3.0637980	-4.2469120
Au	1.9106630	0.0000910	0.0001080	Au	-1.8577240	-0.0000900	-0.0000390
G[Hartree] = -1951.584257							

Table 5.3.7. Atomic coordinates for the syn, meso isomer of **$[Au_2(HL3^{i\text{-}Pr})_2]^{2+}$** in acetonitrile and the corresponding free enthalpy.

Au-syn-meso (MeCN)							
O	-1.4325120	-3.9242590	-2.7345570	H	-5.8091100	-1.9121890	-1.3132820
N	0.1908300	-2.1491660	2.4293640	C	-5.3554320	0.9125620	0.5973870
N	-2.5807130	-2.0189430	-0.9448260	H	-6.0757180	0.1354440	0.8763010
N	-4.1552390	-0.5579560	-0.9626290	H	-4.5149050	0.8778100	1.2985940
N	-0.8621270	-2.5782520	0.6114660	H	-5.8453730	1.8859950	0.6999990
C	0.2320930	-1.9427320	1.0991500	C	-6.0011830	0.8224980	-1.8611080
C	-1.2476120	-2.5924170	-0.7926090	H	-6.4043940	1.8391840	-1.8479130
C	-2.8254580	-0.6896170	-0.8163430	H	-5.6384980	0.6125820	-2.8720810
C	1.1481580	-1.5462860	3.3808110	H	-6.8278450	0.1409950	-1.6328240
C	-1.1276690	-4.0002850	-1.3619000	C	1.3540130	-2.4380960	4.5979560
H	-1.3330220	-4.8013040	-3.1267630	H	1.5872400	-3.4672880	4.3077380
H	-0.5468130	-1.9443040	-1.3192220	H	2.1970760	-2.0499440	5.1765580
H	2.0923940	-1.4808330	2.8334940	H	0.4813040	-2.4448140	5.2599530
H	-1.7886850	-4.7004040	-0.8334570	C	0.6832120	-0.1395810	3.7479770
N	4.2796040	0.1487330	-0.9661860	H	0.6196530	0.4888470	2.8534880
N	0.9574540	2.7469490	-0.4761730	H	-0.2992650	-0.1650410	4.2324910
N	-0.2253980	2.9746500	1.3029330	H	1.3978000	0.3179120	4.4393090
N	2.8053380	1.6061630	-1.5155610	C	5.5555520	-1.8814160	-1.5179980
C	2.9621620	0.4173700	-0.8764300	H	6.3768640	-1.3561240	-2.0178380
C	4.9442580	1.1445220	-1.6550220	H	5.9593840	-2.8074460	-1.0974430
C	4.0165970	2.0632080	-2.0022630	H	4.8011670	-2.1430420	-2.2665180
C	1.5544290	2.3341020	-1.7408450	C	5.9496680	-0.6282640	0.6657340

C	-0.1504090	2.2726150	0.1530600	H	6.3560130	-1.5218840	1.1491190
C	0.8117680	3.8824720	1.3961980	H	6.7894080	-0.0700920	0.2375930
C	1.5585510	3.7392890	0.2812150	H	5.4723250	-0.0095210	1.4322190
C	4.9433610	-1.0431680	-0.4018700	C	-2.5301620	3.6494180	1.8716470
H	6.0064060	1.1201820	-1.8389430	H	-3.3406420	3.5046400	2.5929240
H	4.1071070	2.9895030	-2.5477520	H	-2.2844180	4.7166850	1.8402100
H	0.9338050	4.5499080	2.2332380	H	-2.8946110	3.3465470	0.8847600
H	2.4560200	4.2456600	-0.0384480	C	-0.8395050	3.1776170	3.6963780
H	4.1406580	-1.6143450	0.0714160	H	-0.6993310	4.2563620	3.8249670
C	-4.8758480	0.7263740	-0.8384370	H	-1.6008010	2.8604730	4.4145620
H	-4.1288460	1.4904260	-1.0686590	H	0.0952350	2.6692330	3.9506440
C	-1.3176150	2.8242470	2.2931880	H	-0.0940940	-4.3229260	-1.1901940
H	-1.5774660	1.7618670	2.2709170	H	1.8482870	3.2537960	-2.2502770
C	-0.9231460	-2.8897760	2.7771700	C	0.6317060	1.5944940	-2.7043070
C	-1.5871660	-3.1660830	1.6319320	H	0.4227150	0.5781480	-2.3559100
H	-1.1500000	-3.1619610	3.7950110	H	-0.3098490	2.1485140	-2.7941160
H	-2.5014210	-3.7127580	1.4613710	O	1.3345480	1.5706450	-3.9297160
C	-4.7486080	-1.7895760	-1.1661280	H	0.8578900	1.0012730	-4.5468600
C	-3.7598740	-2.7122580	-1.1567520	Au	1.5825400	-0.7693950	0.0813000
H	-3.8024170	-3.7779950	-1.3083330	Au	-1.4806520	0.7907690	-0.3685320

G[Hartree] = -1951.591156

Table 5.3.8. Atomic coordinates for the syn, meso isomer of **$[Au_2(HL3^{i\text{-}Pr})_2]^{2+}$** in dimethylsulfoxide and the corresponding free enthalpy.

Au-syn-meso (DMSO)							
O	-1.5233190	-3.8420670	-2.8403330	H	-5.8646650	-1.8243760	-1.2214960
N	0.1640740	-2.2033370	2.3551800	C	-5.1376860	1.0128920	0.7856400
N	-2.6262590	-1.9724640	-0.9837590	H	-5.8306110	0.2583860	1.1750620
N	-4.1833840	-0.4945390	-0.9036830	H	-4.2065810	0.9581090	1.3593030
N	-0.8989020	-2.5935950	0.5343420	H	-5.5818460	2.0005650	0.9443690
C	0.2013340	-1.9742140	1.0286690	C	-6.1454820	0.8760330	-1.5400090
C	-1.2994490	-2.5680920	-0.8655600	H	-6.5410930	1.8941990	-1.4822310
C	-2.8498600	-0.6440140	-0.8178140	H	-5.9474640	0.6487890	-2.5921610
C	1.1283070	-1.6217550	3.3129130	H	-6.9272810	0.2034310	-1.1714830
C	-1.2091570	-3.9618570	-1.4727890	C	1.3218670	-2.5284790	4.5205970
H	-1.4456410	-4.7109950	-3.2546840	H	1.5412960	-3.5578550	4.2204300
H	-0.5959260	-1.9165660	-1.3842550	H	2.1704150	-2.1585480	5.1031970
H	2.0739630	-1.5625100	2.7671880	H	0.4496740	-2.5301650	5.1833650
H	-1.8786550	-4.6651160	-0.9593090	C	0.6796600	-0.2135420	3.6947470
N	4.2953690	0.1314850	-0.9083720	H	0.6325860	0.4284040	2.8087740
N	0.9901180	2.7477620	-0.4907410	H	-0.3071370	-0.2318370	4.1707640
N	-0.1913870	2.9623420	1.2902040	H	1.3946320	0.2248130	4.3981010
N	2.8404090	1.5925470	-1.4980790	C	5.8155310	-1.7636780	-1.3313510
C	2.9737200	0.3925240	-0.8758710	H	6.6920080	-1.1674080	-1.6079950
C	4.9869500	1.1476710	-1.5377450	H	6.1792160	-2.7021900	-0.9022610
C	4.0712880	2.0678380	-1.9120770	H	5.2507620	-1.9982330	-2.2390030
C	1.5982250	2.3267660	-1.7476080	C	5.6883050	-0.6542280	0.9575640

C	-0.1191540	2.2718450	0.1333470	H	6.1079360	-1.5463080	1.4327980
C	0.8478460	3.8664250	1.3919760	H	6.5139620	0.0308840	0.7352090
C	1.5943370	3.7312140	0.2757510	H	5.0155400	-0.1694110	1.6723430
C	4.9373860	-1.0544530	-0.3074600	C	-2.4905160	3.6380960	1.8728070
H	6.0568960	1.1342770	-1.6693750	H	-3.3041990	3.4828850	2.5881930
H	4.1834510	3.0050210	-2.4346330	H	-2.2408230	4.7049930	1.8642430
H	0.9716820	4.5258790	2.2351070	H	-2.8514760	3.3586070	0.8776870
H	2.4936690	4.2378840	-0.0382970	C	-0.7988200	3.1284870	3.6874030
H	4.1106810	-1.7156340	-0.0355400	H	-0.6523530	4.2041170	3.8339350
C	-4.8764320	0.7968440	-0.7023150	H	-1.5598320	2.8036880	4.4025230
H	-4.1731500	1.5536860	-1.0602760	H	0.1339400	2.6111300	3.9312390
C	-1.2817170	2.8009590	2.2800840	H	-0.1809380	-4.3093560	-1.3187000
H	-1.5449660	1.7397690	2.2412600	H	1.9054150	3.2415910	-2.2575970
C	-0.9523960	-2.9437150	2.6943790	C	0.6809220	1.5892200	-2.7170200
C	-1.6226810	-3.1955290	1.5473690	H	0.4594180	0.5762580	-2.3666830
H	-1.1769560	-3.2332830	3.7079110	H	-0.2554630	2.1499490	-2.8182450
H	-2.5399030	-3.7356850	1.3721470	O	1.3942320	1.5533520	-3.9363940
C	-4.7982860	-1.7146600	-1.1117170	H	0.9153650	0.9857060	-4.5533800
C	-3.8207740	-2.6477730	-1.1629280	Au	1.5686460	-0.8023520	0.0333700
H	-3.8818530	-3.7090470	-1.3375740	Au	-1.4699230	0.8103880	-0.3923280
G[Hartree] = -1951.584299							

5.3.6 Additional Crystallographic Information

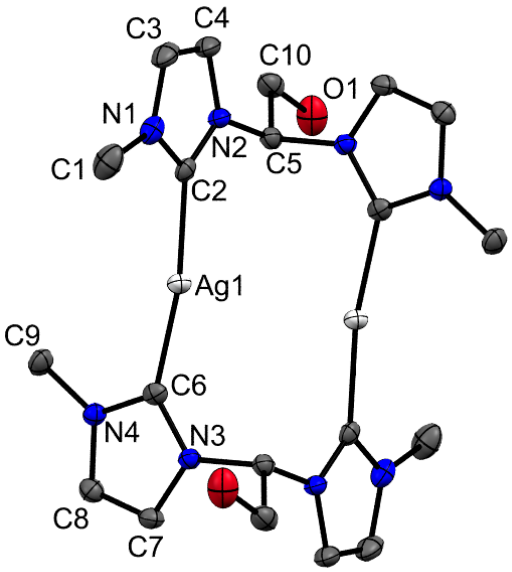

Figure 5.3.50. ORTEP style representation of the cation of **$Ag_2(HL3^{Me})_2(BPh_4)_2$** with ellipsoids at 50 % probability. Hydrogen atoms, BPh_4^- and co-crystallised acetonitrile molecules are omitted for clarity.

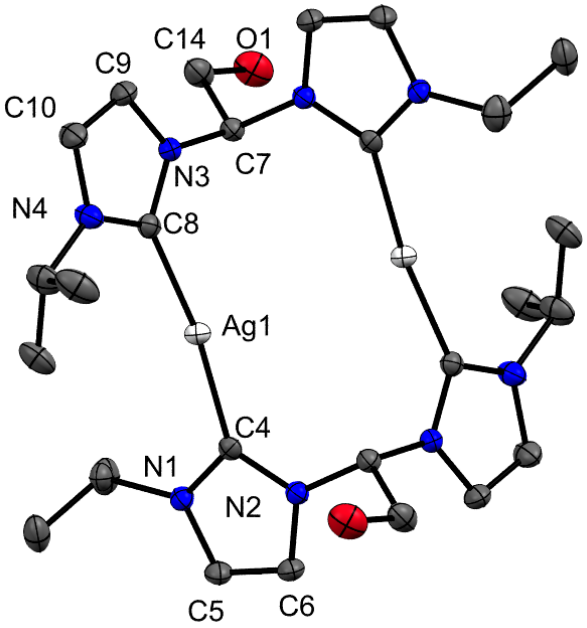

Figure 5.3.51. ORTEP style representation of the cation of **$Ag_2(HL3^{i\text{-}Pr})_2(BPh_4)_2$** with ellipsoids at 50 % probability. Hydrogen atoms and BPh_4^- are omitted for clarity.

Table 5.3.9. Crystallographic information for bis(imidazolium) salts and **L6^{tFu}**.

	$H_2(L3^{i\text{-}Pr})(BPh_4)_2$	**$H_2(L5^{tFu})(BPh_4)_2$**	**$H_2(L6^{tFu})Br_2$**	**$H_2(L6^{tFu})(PF_6)_2$**	**$L6^{tFu}$**	**$H_2(L7^{Mes})Br_2$**
Formula	$C_{62}H_{64}B_2N_4O\cdot 2(C_2H_6O)$	$2(C_{75}H_{78}B_2N_4O_2)\cdot C_4H_{10}O$	$C_{28}H_{40}Br_2N_4O_2$	$C_{28}H_{40}F_{12}N_4O_2P_2$	$C_{28}H_{38}N_4O_2$	$C_{27}H_{32}Br_2N_4$
Fw	1019.00	2252.18	624.46	754.58	462.64	572.39
color/habit	colorless/ fragment	colorless/ fragment	pale yellow/ fragment	colorless/ fragment	white/ fragment	pale yellow/ fragment
cryst dimens [mm^3]	0.55×0.41×0.36	0.22×0.45×0.49	0.15×0.26×0.29	0.25×0.26×0.37	0.32×0.36×0.48	0.12×0.26×0.40
cryst syst	Triclinic	triclinic	monoclinic	triclinic	monoclinic	monoclinic
space group	$P\bar{1}$	$P\bar{1}$	*C2/c*	$P\bar{1}$	*C2/c*	$P2_1/n$
a, [Å]	11.9017(4)	14.1987(10)	17.8721(5)	6.239(3)	16.1383(15)	15.7415(5)
b, [Å]	15.3089(5)	18.0447(13)	19.7762(6)	7.467(3)	12.0946(11)	11.0191(4)
c, [Å]	17.2755(5)	29.091(2)	9.7325(3)	19.985(7)	13.3917(13)	16.7198(6)
α, [deg]	102.960(1)	77.878(4)	90	90	90	90
β, [deg]	105.720(1)	76.745(3)	119.8230(10)	92.65(3)	102.218(5)	112.650(1)
γ, [deg]	98.213(1)	89.081(3)	90	110.98(3)	90	90

	$H_2(L3^{i\text{-}Pr})(BPh_4)_2$	$H_2(L5^{tFu})(BPh_4)_2$	$H_2(L6^{tFu})Br_2$	$H_2(L6^{tFu})(PF_6)_2$	$L6^{tFu}$	$H_2(L7^{Mes})Br_2$
V, [Å^3]	2882.32(16)	7089.1(9)	2984.32(16)	868.0(11)	2554.7(4)	2676.49(16)
Z	2	2	8	2	8	4
T, [K]	100(2)	123(2)	129(2)	100(2)	123(2)	123(2)
D_{calcd}, [g cm^{-3}]	1.174	1.055	1.390	1.441	1.203	1.420
μ, [mm^{-1}]	0.07	0.063	2.746	0.222	0.077	3.05
F(000)	1092	2412	1288	390	1000	1168
ϑ range, deg	1.82 to 25.35	0.74 to 25.35	2.06 to 28.46	2.04 to 2.35	2.12 to 28.28	2.27 to 25.40
index ranges (*h, k, l*)	±14, ±18, ±20	±17, ±21, ±35	–16≤ h ≥+23 –17≤ k ≥+26 –13≤ l ≥+12	±7, ±9, –24≤ l ≥+23	±21, ±16, ±17	±18, ±13, ±20
no. of reflns collected	107091	107680	55413	20894	55245	92590
no. of indep reflns/R_{int}	10538/0.0402	25915/0.0376	3742/0.0000	3164/0.0191	3182/0.0360	4919/0.073
no. of obsd reflns (I>2σ(I))	8559	21867	2910	2963	2936	3822
no. of data/restraints/params	10538/0/703	25915/0/1562	3742/0/168	3164/0/222	3182/0/169	4919/0/304
R1/wR2 ($I > 2\sigma(I)$)[a]	0.0446/0.0932	0.0506/0.1259	0.0350/0.0674	0.0298/0.0709	0.0406/0.1054	0.0324/0.0669
R1/wR2 (all data)[a]	0.0608/0.1008	0.0600/0.1320	0.0569/0.0716	0.0323/0.0725	0.0433/0.1077	0.0519/0.0738

	$H_2(L3^{i\text{-}Pr})(BPh_4)_2$	$H_2(L5^{tFu})(BPh_4)_2$	$H_2(L6^{tFu})Br_2$	$H_2(L6^{tFu})(PF_6)_2$	$L6^{tFu}$	$H_2(L7^{Mes})Br_2$
GOF (on F^2)[a]	1.068	1.041	1.081	1.029	1.066	1.023
largest diff peak and hole [e Å^{-3}]	+0.322/−0.301	+0.678/–0.428	+0.492/–0.388	+0.251/–0.210	+0.422/–0.351	+0.667/–0.430

[a] $R1 = \Sigma(||F_o| - |F_c||)/\Sigma|F_o|$; $wR2 = \{\Sigma[w(F_o^2 - F_c^2)^2]/\Sigma[w(F_o^2)^2]\}^{1/2}$; $GOF = \{\Sigma[w(F_o^2 - F_c^2)^2]/(n - p)\}^{1/2}$

Table 5.3.10. Crystallographic details for Ag(I) bis(NHC) complexes.

	$Ag_2(HL3^{Me})_2(BPh_4)_2$	$Ag_2(HL3^{i\text{-}Pr})_2(PF_6)_2$	$Ag_2(HL3^{i\text{-}Pr})_2(BPh_4)_2$	$Ag_2(HL3^{i\text{-}Pr})_2(BPh_4)_2$ ·DMSO	$Ag_2(HL3^{Mes})_2(PF_6)_2$	$Ag_2(L7^{Mes})_2(PF_6)_2$
formula	$C_{68}H_{68}Ag_2B_2N_8O_2$ ·2(C_2H_3N)	$C_{28}H_{44}Ag_2F_{12}N_8O_2P_2$ ·2($C_2H_{10}O$)	$C_{76}H_{84}Ag_2B_2N_8O_2$	$C_{76}H_{84}Ag_2B_2N_8O_2$ ·4(C_2H_6OS)	$C_{52}H_{60}Ag_2F_{12}N_8O_2P_2$ ·C_2H_3N·H_2O	$C_{54}H_{60}Ag_2F_{12}N_8P_2$ ·C_2H_3N
fw	1348.76	1178.63	1378.87	1691.38	1378.02	1367.83
color/habit	colorless/ fragment	colorless/shard	colorless/ fragment	colorless/ fragment	colorless/ fragment	colorless/ fragment
cryst dimens [mm^3]	0.31×0.44×0.50	0.27×0.26×0.14	0.23×0.16×0.13	0.22×0.21×0.17	0.42×0.30×0.19	0.06×0.11×0.63
cryst syst	Monoclinic	monoclinic	monoclinic	triclinic	monoclinic	orthorhombic

	$Ag_2(HL3^{Me})_2(BPh_4)_2$	$Ag_2(HL3^{i\text{-}Pr})_2(PF_6)_2$	$Ag_2(HL3^{i\text{-}Pr})_2(BPh_4)_2$	$Ag_2(HL3^{i\text{-}Pr})_2(BPh_4)_2$ ·DMSO	$Ag_2(HL3^{Mes})_2(PF_6)_2$	$Ag_2(L7^{Mes})_2(PF_6)_2$
space group	$P2_1/n$	$P2_1/c$	$P2_1/n$	$P\bar{1}$	$P2_1/c$	$Pbcn$
a, [Å]	10.3121(2)	8.2134(11)	9.9899(7)	10.980(2)	12.4267(9)	37.441(4)
b, [Å]	13.6734(3)	23.932(3)	14.7429(9)	14.280(3))	15.8703(11)	13.2906(14)
c, [Å]	22.9830(5)	12.3064(14)	22.6289(14)	14.447(3)	30.676(2)	24.427(3)
α, [deg]	90	90	90	102.950(11)	90	90
β, [deg]	99.6200(10)	90.035(7)	100.939(3)	98.253(11)	100.465(5)	90
γ, [deg]	90	90	90	109.318(11)	90	90
V, [Å^3]	3195.07(12)	2419.0(5)	3272.2 (4)	2024.1(7)	5949.2(7)	12154.8(2)
Z	4	2	2	1	4	8
T, [K]	123(2)	123(2)	123(2)	100(2)	100(2)	100(2)
D_{calcd}, [g cm^{-3}]	1.402	1.618	1.400	1.388	1.538	1.495
μ, [mm^{-1}]	0.668	0.97	0.65	0.65	0.80	0.78
F(000)	1392	1200	1432	893	2796	5552
ϑ range, deg	1.80 to 26.37	3.01 to 27.88	1.66 to 25.35	1.83 to 26.02	1.67 to 30.50	2.18 to 25.35

	$Ag_2(HL3^{Me})_2(BPh_4)_2$	$Ag_2(HL3^{i\text{-}Pr})_2(PF_6)_2$	$Ag_2(HL3^{i\text{-}Pr})_2(BPh_4)_2$	$Ag_2(HL3^{i\text{-}Pr})_2(BPh_4)_2$ ·DMSO	$Ag_2(HL3^{Mes})_2(PF_6)_2$	$Ag_2(L7^{Mes})_2(PF_6)_2$
index ranges (*h, k, l*)	±12, ±17, ±28	±10, ±31, ±16	±12, ±17, ±27	±13, ±17, ±17	–17≤ h ≤+16, –22≤ k ≤+21, –37≤ l ≤+43	±45 –13≤ k ≤+16, –27≤ l ≤+29
no. of reflns collected	42952	82069	77780	62925	41345	111671
no. of indep reflns/R_{int}	6526/0.0368	5754/0.056	5996/0.0528	7946/0.0690	16957/0.0502	11116/0.0927
no. of obsd reflns ($I>2\sigma(I)$)	5584	4961	5489	7186	12874	8159
no. of data/restraints/params	6526/0/402	5754/181/344	5996/0/411	7946/0/488	16957/1/757	11116/618/892
R1/wR2 ($I > 2\sigma(I)$)[a]	0.0258/0.0654	0.0244/0.0531	0.0286/0.0711	0.0267/0.0659	0.0451/0.0931	0.0463/0.0986
R1/wR2 (all data)[a]	0.0338/0.0687	0.0311/0.0559	0.0319/0.0735	0.0311/0.0682	0.0656/0.1015	0.0788/0.1158
GOF (on F^2)[a]	1.045	1.043	1.033	1.040	1.020	1.060
largest diff peak and hole [e Å^{-3}]	+0.504/–0.521	+0.701/−0.554	+1.362/−0.555	+0.428/−0.473	+751/−0.615	+0.932/–1.338

[a] $R1 = \Sigma(||F_o| - |F_c||)/\Sigma|F_o|$; $wR2 = \{\Sigma[w(F_o^2 - F_c^2)^2]/\Sigma[w(F_o^2)^2]\}^{1/2}$; $GOF = \{\Sigma[w(F_o^2 - F_c^2)^2]/(n - p)\}^{1/2}$

Table 5.3.11. Crystallographic details for Au(I) bis(NHC) complexes and **$Li_2[Ce_3(L1^{Me*})_3(N\{i\text{-}Pr\}_2)_5](THF)_2$**.

	$Au_2(HL3^{i\text{-}Pr})_2(PF_6)_2$	**$Au_2(HL3^{i\text{-}Pr})_2(BPh_4)_2$**	**$Au_2(HL3^{Mes})_2(PF_6)_2$**	**$Au_2(L7^{Mes})_2(PF_6)_2$**	**$Li_2[Ce_3(L1^{Me*})_3(N\{i\text{-}Pr\}_2)_5](THF)_2$**
Formula	$C_{28}H_{44}Au_2F_{12}N_8O_2P \cdot C_4H_{10}O$	$C_{76}H_{84}Au_2B_2N_8O_2$	$C_{52}H_{60}Au_2F_{12}N_8O_2P \cdot 3(C_4H_8O)$	$C_{54}H_{60}Au_2F_{12}N_8P_2 \cdot C_2H_3N$	$Ce_6Li_4C_{184}H_{316}N_{22}O_{10} \cdot 2(C_6H_6)$
Fw	1356.83	1557.07	1729.28	1546.02	4021.28
color/habit	colorless/fragment	colorless/fragment	colorless/fragment	colorless/fragment	yellow fragment
cryst dimens [mm^3]	0.55×0.20×0.11	0.23×0.17×0.15	0.52×0.20×0.18	0.12×0.17×0.21	0.23×0.29×0.67
cryst syst	Monoclinic	monoclinic	monoclinic	orthorhombic	triclinic
space group	$P2_1/c$	$P2_1/n$	$P2_1$	$Pbcn$	$P\bar{1}$
a, [Å]	8.1974(3)	10.0106(4)	12.7112(7)	37.808(8)	14.2898(16)
b, [Å]	23.8226(9)	14.8180(7)	22.4182(11)	13.138(3)	17.937(2)
c, [Å]	12.3123(4)	22.5591(10)	13.1902(7)	24.830(5)	21.837(2)
α, [deg]	90	90	90	90	100.428(2)
β, [deg]	90.292(1)	101.129(2)	106.3979(16)	90	94.826(3)
γ, [deg]	90	90	90	90	90.276(3)
V, [$Å^3$]	2404.36(15)	3283.4(3)	3605.8(3)	12334.0(4)	5484.1(11)

	$Au_2(HL3^{i\text{-}Pr})_2(PF_6)_2$	$Au_2(HL3^{i\text{-}Pr})_2(BPh_4)_2$	$Au_2(HL3^{Mes})_2(PF_6)_2$	$Au_2(L7^{Mes})_2(PF_6)_2$	$Li_2[Ce_3(L1^{Me*})_3(N\{i\text{-}Pr\}_2)_5](THF)_2$
Z	2	2	2	8	4
T, [K]	100(2)	123(2)	100(2)	123(2)	100(2)
D_{calcd}, [g cm^{-3}]	1.874	1.575	1.593	1.665	1.218
μ, [mm^{-1}]	6.25	4.52	4.19	4.88	1.27
F(000)	1328	1560	1720	6064	2098
ϑ range, deg	2.38 to 28.36	2.25 to 27.88	2.23 to 26.37	2.24 to 25.35	2.23 to 25.35
index ranges (*h, k, l*)	±10, ±31, ±16	±13, ±19, ±29	±15, ±28, ±16	±45, ±15, ±29	±17, ±21, ±26
no. of reflns collected	116889	74721	149399	112908	155945
no. of indep reflns/R_{int}	6009/0.0400	7833/0.0587	14749/0.0385	11245/0.0866	20083/0.0489
no. of obsd reflns ($I>2\sigma$(I))	5552	6372	14222	8930	15865
no. of data/restraints/params	6009/153/344	7833/113/461	14749/550/964	11245/279/807	20083/936/1340
R1/wR2 ($I > 2\sigma(I)$)[a]	0.0180/0.0346	0.0259/0.0453	0.0186/0.0365	0.0313/0.0626	0.0519/0.1134
R1/wR2 (all data)[a]	0.0216/0.0353	0.0394/0.0494	0.0205/0.0369	0.0494/0.0688	0.0745/0.1321
GOF (on F^2)[a]	1.131	1.025	1.111	1.014	1.061

largest diff peak and hole [e Å^{-3}]	+0.617/−1.321	+1.412/−1.856	+0.877/−1.414	+1.315/–0.790	+3.882/–2.416

References

[1] A. J. Arduengo, R. L. Harlow, M. Kline, *J. Am. Chem. Soc.* **1991**, *113*, 361-363.

[2] (a) W. A. Herrmann, *Angew. Chem. Int. Ed.* **2002**, *41*, 1290-1309; (b) S. Díez-González, N. Marion, S. P. Nolan, *Chem. Rev.* **2009**, *109*, 3612-3676; (c) L. Mercs, M. Albrecht, *Chem. Soc. Rev.* **2010**, *39*, 1903-1912; (d) K. M. Hindi, M. J. Panzner, C. A. Tessier, C. L. Cannon, W. J. Youngs, *Chem. Rev.* **2009**, *109*, 3859-3884.

[3] S. Meyer, I. Klawitter, S. Demeshko, E. Bill, F. Meyer, *Angew. Chem. Int. Ed.* **2013**, *52*, 901-905.

[4] S. T. Liddle, I. S. Edworthy, P. L. Arnold, *Chem. Soc. Rev.* **2007**, *36*, 1732-1744.

[5] (a) P. L. Arnold, Z. R. Turner, R. Bellabarba, R. P. Tooze, *J. Am. Chem. Soc.* **2011**, *133*, 11744-11756; (b) P. L. Arnold, T. Cadenbach, I. H. Marr, A. A. Fyfe, N. L. Bell, R. Bellabarba, R. P. Tooze, J. B. Love, *Dalton Trans* **2014**.

[6] P. L. Arnold, S. Pearson, *Coord. Chem. Rev.* **2007**, *251*, 596-609.

[7] P. L. Arnold, S. T. Liddle, *Organometallics* **2006**, *25*, 1485-1491.

[8] (a) J. Zheng, Y.-D. Yu, F.-F. Liu, B.-Y. Liu, G. Wei, X.-C. Huang, *Chem. Commun.* **2014**, *50*, 9000-9002; (b) A. Biffis, M. Baron, C. Tubaro, in *Adv. Organomet. Chem., Vol. Volume 63* (Ed.: J. P. Pedro), Academic Press, **2015**, pp. 203-288.

[9] (a) J. C. Garrison, W. J. Youngs, *Chem. Rev.* **2005**, *105*, 3978-4008; (b) A. Kascatan-Nebioglu, M. J. Panzner, C. A. Tessier, C. L. Cannon, W. J. Youngs, *Coord. Chem. Rev.* **2007**, *251*, 884-895; (c) A. Melaiye, Z. Sun, K. Hindi, A. Milsted, D. Ely, D. H. Reneker, C. A. Tessier, W. J. Youngs, *J. Am. Chem. Soc.* **2005**, *127*, 2285-2291.

[10] (a) P. J. Barnard, L. E. Wedlock, M. V. Baker, S. J. Berners-Price, D. A. Joyce, B. W. Skelton, J. H. Steer, *Angew. Chem. Int. Ed.* **2006**, *45*, 5966-5970; (b) M. Baron, C. Tubaro, A. Biffis, M. Basato, C. Graiff, A. Poater, L. Cavallo, N. Armaroli, G. Accorsi, *Inorg. Chem.* **2012**, *51*, 1778-1784.

[11] (a) N. Marion, S. P. Nolan, *Chem. Soc. Rev.* **2008**, *37*, 1776-1782; (b) S. P. Nolan, *Acc. Chem. Res.* **2011**, *44*, 91-100.

[12] (a) P. J. Barnard, S. J. Berners-Price, *Coord. Chem. Rev.* **2007**, *251*, 1889-1902; (b) B. Bertrand, A. Casini, *Dalton Trans.* **2014**, *43*, 4209-4219; (c) S. A. Patil, S. A. Patil, R. Patil, R. S. Keri, S. Budagumpi, G. R. Balakrishna, M. Tacke, *Future Med. Chem.* **2015**, *7*, 1305-1333.

[13] (a) M. Hermann, *Liebigs Ann. Chem.* **1855**, *95*, 211-225; (b) A. Geuther, *Liebigs Ann. Chem.* **1862**, *123*, 121-122; (c) J. U. Nef, *Liebigs Ann. Chem.* **1897**, *298*, 202-374.

[14] (a) W. von E. Doering, L. H. Knox, *J. Am. Chem. Soc.* **1953**, *75*, 297-303; (b) W. von E. Doering, A. K. Hoffmann, *J. Am. Chem. Soc.* **1954**, *76*, 6162-6165.

[15] E. O. Fischer, A. Maasböl, *Angew. Chem. Int. Ed.* **1964**, *3*, 580-581.

[16] A. Igau, H. Grutzmacher, A. Baceiredo, G. Bertrand, *J. Am. Chem. Soc.* **1988**, *110*, 6463-6466.

[17] H. W. Wanzlick, H. J. Schönherr, *Angew. Chem. Int. Ed.* **1968**, *7*, 141-142.

[18] K. Öfele, *J. Organomet. Chem.* **1968**, *12*, P42-P43.

[19] (a) D. Bourissou, O. Guerret, F. P. Gabbaï, G. Bertrand, *Chem. Rev.* **2000**, *100*, 39-92; (b) F. E. Hahn, M. C. Jahnke, *Angew. Chem. Int. Ed.* **2008**, *47*, 3122-3172; (c) P. L. Arnold, I. J. Casely, *Chem. Rev.* **2009**, *109*, 3599-3611; (d) J. C. Y. Lin, R. T. W. Huang, C. S. Lee, A. Bhattacharyya, W. S. Hwang, I. J. B. Lin, *Chem. Rev.* **2009**, *109*, 3561-3598; (e) S. Bellemin-Laponnaz, S. Dagorne, *Chem. Rev.* **2014**, *114*, 8747-8774.

[20] M. N. Hopkinson, C. Richter, M. Schedler, F. Glorius, *Nature* **2014**, *510*, 485-496.

[21] G. B. Schuster, in *Adv. Phys. Org. Chem., Vol. Volume 22* (Eds.: V. Gold, D. Bethell), Academic Press, **1986**, pp. 311-361.

[22] D. J. Nelson, S. P. Nolan, *Chem. Soc. Rev.* **2013**, *42*, 6723-6753.

[23] R. Hoffmann, G. D. Zeiss, G. W. Van Dine, *J. Am. Chem. Soc.* **1968**, *90*, 1485-1499.

[24] (a) C. W. Bauschlicher, H. F. Schaefer, P. S. Bagus, *J. Am. Chem. Soc.* **1977**, *99*, 7106-7110; (b) J. F. Harrison, R. C. Liedtke, J. F. Liebman, *J. Am. Chem. Soc.* **1979**, *101*, 7162-7168; (c) D. Feller, W. Thatcher Borden, E. R. Davidson, *Chem. Phys. Lett.* **1980**, *71*, 22-26.

[25] N. C. Baird, K. F. Taylor, *J. Am. Chem. Soc.* **1978**, *100*, 1333-1338.

[26] A. J. Arduengo, F. Davidson, H. V. R. Dias, J. R. Goerlich, D. Khasnis, W. J. Marshall, T. K. Prakasha, *J. Am. Chem. Soc.* **1997**, *119*, 12742-12749.

[27] C. Heinemann, T. Müller, Y. Apeloig, H. Schwarz, *J. Am. Chem. Soc.* **1996**, *118*, 2023-2038.

[28] (a) M. Melaimi, M. Soleilhavoup, G. Bertrand, *Angew. Chem. Int. Ed.* **2010**, *49*, 8810-8849; (b) V. Lavallo, Y. Canac, C. Präsang, B. Donnadieu, G. Bertrand, *Angew. Chem. Int. Ed.* **2005**, *44*, 5705-5709; (c) O. Schuster, L. Yang, H. G. Raubenheimer, M. Albrecht, *Chem. Rev.* **2009**, *109*, 3445-3478.

[29] E. Aldeco-Perez, A. J. Rosenthal, B. Donnadieu, P. Parameswaran, G. Frenking, G. Bertrand, *Science* **2009**, *326*, 556.

[30] (a) P. Fournari, P. de Cointet, E. Laviron, *Bull. Soc. Chim. Fr.* **1968**, 2438-2446; (b) B. K. M. Chan, N.-H. Chang, M. R. Grimmett, *Aust. J. Chem.* **1977**, *30*, 2005-2013.

[31] (a) W. A. Herrmann, C. Köcher, L. J. Gooßen, G. R. J. Artus, *Chem. Eur. J.* **1996**, *2*, 1627-1636; (b) V. P. W. Böhm, T. Weskamp, C. W. K. Gstöttmayr, W. A. Herrmann, *Angew. Chem. Int. Ed.* **2000**, *39*, 1602-1604.

[32] (a) A. A. Gridnev, I. M. Mihaltseva, *Synth. Commun.* **1994**, *24*, 1547-1555; (b) H. Zhang, J. Liu, J. Chen, J. Zhao, Y. Zhao, L. Li, *Synthesis* **2003**, 2661-2666; (c) W. A. Herrmann, L. J. Gooβen, M. Spiegler, *J. Organomet. Chem.* **1997**, *547*, 357-366.

[33] B. Bildstein, M. Malaun, H. Kopacka, K. Wurst, M. Mitterböck, K.-H. Ongania, G. Opromolla, P. Zanello, *Organometallics* **1999**, *18*, 4325-4336.

[34] (a) H.-J. Cristau, P. P. Cellier, J.-F. Spindler, M. Taillefer, *Chem. Eur. J.* **2004**, *10*, 5607-5622; (b) H. Zhang, Q. Cai, D. Ma, *J. Org. Chem.* **2005**, *70*, 5164-5173; (c) Y.-Z. Huang, H. Miao, Q.-H. Zhang, C. Chen, J. Xu, *Catal. Lett.* **2008**, *122*, 344-348.

[35] N. Kuhn, T. Kratz, *Synthesis* **1993**, *1993*, 561-562.

[36] (a) E. A. Carter, W. A. Goddard, *J. Phys. Chem.* **1986**, *90*, 998-1001; (b) G. Trinquier, J. P. Malrieu, *J. Am. Chem. Soc.* **1987**, *109*, 5303-5315; (c) J. P. Malrieu, G. Trinquier, *J. Am. Chem. Soc.* **1989**, *111*, 5916-5921; (d) H. Jacobsen, T. Ziegler, *J. Am. Chem. Soc.* **1994**, *116*, 3667-3679.

[37] G. Raabe, K. Breuer, D. Enders, J. H. Teles, *Z. Naturforsch. A* **1996**, *51*, 95–101.

[38] Y. T. Chen, F. Jordan, *J. Org. Chem.* **1991**, *56*, 5029-5038.

[39] (a) H. W. Wanzlick, E. Schikora, *Angew. Chem.* **1960**, *72*, 494-494; (b) H.-W. Wanzlick, E. Schikora, *Chem. Ber.* **1961**, *94*, 2389-2393; (c) H. W. Wanzlick, *Angew. Chem. Int. Ed.* **1962**, *1*, 75-80.

[40] J. A. Blush, H. Clauberg, D. W. Kohn, D. W. Minsek, X. Zhang, P. Chen, *Acc. Chem. Res.* **1992**, *25*, 385-392.

[41] C. Heinemann, W. Thiel, *Chem. Phys. Lett.* **1994**, *217*, 11-16.

[42] (a) T. Andrew Taton, P. Chen, *Angew. Chem.* **1996**, *108*, 1098-1100; (b) T. A. Taton, P. Chen, *Angew. Chem. Int. Ed.* **1996**, *35*, 1011-1013; (c) R. P. Thummel, V. Goulle, B. Chen, *J. Org. Chem.* **1989**, *54*, 3057-3061; (d) D. C. Graham, K. J. Cavell, B. F. Yates, *J. Phys. Org. Chem.* **2005**, *18*, 298-309.

[43] R. W. Alder, M. E. Blake, L. Chaker, J. N. Harvey, F. Paolini, J. Schütz, *Angew. Chem. Int. Ed.* **2004**, *43*, 5896-5911.

[44] (a) D. M. Lemal, R. A. Lovald, K. I. Kawano, *J. Am. Chem. Soc.* **1964**, *86*, 2518-2519; (b) H. E. Winberg, J. E. Carnahan, D. D. Coffman, M. Brown, *J. Am. Chem. Soc.* **1965**, *87*, 2055-2056.

[45] (a) Z. Shi, R. P. Thummel, *J. Org. Chem.* **1995**, *60*, 5935-5945; (b) J. R. Ames, M. A. Houghtaling, D. L. Terrian, T. P. Mitchell, *Can. J. Chem.* **1997**, *75*, 28-36.

[46] M. E. Jung, *Synlett* **1999**, *1999*, 843-846.

[47] P. I. Jolly, S. Zhou, D. W. Thomson, J. Garnier, J. A. Parkinson, T. Tuttle, J. A. Murphy, *Chem. Sci.* **2012**, *3*, 1675-1679.

[48] (a) A. Nickon, *Acc. Chem. Res.* **1993**, *26*, 84-89; (b) H. M. Sulzbach, M. S. Platz, H. F. Schaefer, C. M. Hadad, *J. Am. Chem. Soc.* **1997**, *119*, 5682-5689; (c) F. Ford, T. Yuzawa, M. S. Platz, S. Matzinger, M. Fülscher, *J. Am. Chem. Soc.* **1998**, *120*, 4430-4438; (d) A. E. Keating, M. A. Garcia-Garibay, K. N. Houk, *J. Am. Chem. Soc.* **1997**, *119*, 10805-10809.

[49] G. A. McGibbon, C. Heinemann, D. J. Lavorato, H. Schwarz, *Angew. Chem. Int. Ed.* **1997**, *36*, 1478-1481.

[50] (a) A. Wacker, H. Pritzkow, W. Siebert, *Eur. J. Inorg. Chem.* **1998**, *1998*, 843-849; (b) A. Wacker, H. Pritzkow, W. Siebert, *Eur. J. Inorg. Chem.* **1999**, *1999*, 789-793.

[51] S. Solé, H. Gornitzka, O. Guerret, G. Bertrand, *J. Am. Chem. Soc.* **1998**, *120*, 9100-9101.

[52] (a) D. Enders, O. Niemeier, A. Henseler, *Chem. Rev.* **2007**, *107*, 5606-5655; (b) P.-C. Chiang, J. W. Bode, in *N-Heterocyclic Carbenes: From Laboratory Curiosities to Efficient Synthetic Tools* (Ed.: S. Díez-González), RSC Publishing, Cambridge, **2010**, pp. 399-435.

[53] T. Weskamp, V. P. W. Böhm, W. A. Herrmann, *J. Organomet. Chem.* **2000**, *600*, 12-22.

[54] P. L. Arnold, S. T. Liddle, *Chem. Commun.* **2006**, 3959-3971.

[55] G. Boche, C. Hilf, K. Harms, M. Marsch, J. C. W. Lohrenz, *Angew. Chem. Int. Ed.* **1995**, *34*, 487-489.

[56] I. I. I. A. J. Arduengo, M. Tamm, J. C. Calabrese, F. Davidson, W. J. Marshall, *Chem. Lett.* **1999**, *28*, 1021-1022.

[57] R. W. Alder, M. E. Blake, C. Bortolotti, S. Bufali, C. P. Butts, E. Linehan, J. M. Oliva, A. Guy Orpen, M. J. Quayle, *Chem. Commun.* **1999**, 241-242.

[58] I. V. Shishkov, F. Rominger, P. Hofmann, *Organometallics* **2009**, *28*, 3532-3536.

[59] M. Brendel, J. Wenz, I. V. Shishkov, F. Rominger, P. Hofmann, *Organometallics* **2015**, *34*, 669-672.

[60] M. S. Hill, G. Kociok-Köhn, D. J. MacDougall, *Inorg. Chem.* **2011**, *50*, 5234-5241.

[61] L. C. H. Maddock, T. Cadenbach, A. R. Kennedy, I. Borilovic, G. Aromí, E. Hevia, *Inorg. Chem.* **2015**, *54*, 9201-9210.

[62] P. L. Arnold, S. A. Mungur, A. J. Blake, C. Wilson, *Angew. Chem. Int. Ed.* **2003**, *42*, 5981-5984.

[63] S. A. Mungur, S. T. Liddle, C. Wilson, M. J. Sarsfield, P. L. Arnold, *Chem. Commun.* **2004**, 2738-2739.

[64] I. S. Edworthy, A. J. Blake, C. Wilson, P. L. Arnold, *Organometallics* **2007**, *26*, 3684-3689.

[65] (a) P. L. Arnold, M. Rodden, K. M. Davis, A. C. Scarisbrick, A. J. Blake, C. Wilson, *Chem. Commun.* **2004**, 1612-1613; (b) P. L. Arnold, M. Rodden, C. Wilson, *Chem. Commun.* **2005**, 1743-1745.

[66] G. Steiner, A. Krajete, H. Kopacka, K.-H. Ongania, K. Wurst, P. Preishuber-Pflügl, B. Bildstein, *Eur. J. Inorg. Chem.* **2004**, *2004*, 2827-2836.

[67] S. P. Downing, A. A. Danopoulos, *Organometallics* **2006**, *25*, 1337-1340.

[68] (a) T. Simler, A. A. Danopoulos, P. Braunstein, *Chem. Commun.* **2015**, *51*, 10699-10702; (b) T. Simler, L. Karmazin, C. Bailly, P. Braunstein, A. A. Danopoulos, *Organometallics* **2016**, *35*, 903-912.

[69] A. Nasr, A. Winkler, M. Tamm, *Coord. Chem. Rev.* **2016**, *316*, 68-124.

[70] J. B. Waters, J. M. Goicoechea, *Coord. Chem. Rev.* **2015**, *293*, 80-94.

[71] A. A. Danopoulos, K. Y. Monakhov, P. Braunstein, *Chem. Eur. J.* **2013**, *19*, 449-454.

[72] (a) A. A. Danopoulos, P. Braunstein, *Chem. Commun.* **2014**, *50*, 3055-3057; (b) A. A. Danopoulos, P. Braunstein, E. Rezabal, G. Frison, *Chem. Commun.* **2015**, *51*, 3049-3052.

[73] Y. Wang, Y. Xie, M. Y. Abraham, P. Wei, H. F. Schaefer, P. v. R. Schleyer, G. H. Robinson, *J. Am. Chem. Soc.* **2010**, *132*, 14370-14372.

[74] (a) S. Kronig, E. Theuergarten, C. G. Daniliuc, P. G. Jones, M. Tamm, *Angew. Chem. Int. Ed.* **2012**, *51*, 3240-3244; (b) Y. Wang, Y. Xie, M. Y. Abraham, R. J. Gilliard, P. Wei, C. F. Campana, H. F. Schaefer, P. v. R. Schleyer, G. H. Robinson, *Angew. Chem. Int. Ed.* **2012**, *51*, 10173-10176; (c) Y. Wang, Y. Xie, M. Y. Abraham, P. Wei, H. F. Schaefer, P. v. R. Schleyer, G. H. Robinson, *Organometallics* **2011**, *30*, 1303-1306; (d)

M. Vogt, C. Wu, A. G. Oliver, C. J. Meyer, W. F. Schneider, B. L. Ashfeld, *Chem. Commun.* **2013**, *49*, 11527-11529; (e) Y. Wang, M. Y. Abraham, R. J. Gilliard, P. Wei, J. C. Smith, G. H. Robinson, *Organometallics* **2012**, *31*, 791-793.

[75] J. B. Waters, J. M. Goicoechea, *Dalton Trans.* **2014**, *43*, 14239-14248.

[76] (a) D. R. Armstrong, S. E. Baillie, V. L. Blair, N. G. Chabloz, J. Diez, J. Garcia-Alvarez, A. R. Kennedy, S. D. Robertson, E. Hevia, *Chem. Sci.* **2013**, *4*, 4259-4266; (b) A. J. Martinez-Martinez, M. A. Fuentes, A. Hernan-Gomez, E. Hevia, A. R. Kennedy, R. E. Mulvey, C. T. O'Hara, *Angew. Chem. Int. Ed.* **2015**, *54*, 14075-14079.

[77] (a) A. El-Hellani, V. Lavallo, *Angew. Chem. Int. Ed.* **2014**, *53*, 4489-4493; (b) M. J. Asay, S. P. Fisher, S. E. Lee, F. S. Tham, D. Borchardt, V. Lavallo, *Chem. Commun.* **2015**, *51*, 5359-5362.

[78] M. Otto, S. Conejero, Y. Canac, V. D. Romanenko, V. Rudzevitch, G. Bertrand, *J. Am. Chem. Soc.* **2004**, *126*, 1016-1017.

[79] (a) B. Cordero, V. Gomez, A. E. Platero-Prats, M. Reves, J. Echeverria, E. Cremades, F. Barragan, S. Alvarez, *Dalton Trans.* **2008**, 2832-2838; (b) P. Pyykkö, M. Atsumi, *Chem. Eur. J.* **2009**, *15*, 186-197.

[80] B. S. Van Gosen, P. L. Verplanck, K. R. Long, J. Gambogi, R. R. Seal, *U.S. Geological Survey Fact Sheet* **2014**, *3078*, 4.

[81] W. J. Evans, *Inorg. Chem.* **2007**, *46*, 3435-3449.

[82] (a) M. D. H. Fryzuk, T. S.; Berg David J.; Rettig Steven J. , *Pure Appl. Chem.* **1991**, *63*, 845-850; (b) L. H. Gade, *Chem. Commun.* **2000**, 173-181.

[83] R. H. Crabtree, *J. Organomet. Chem.* **2005**, *690*, 5451-5457.

[84] H. Jacobsen, A. Correa, A. Poater, C. Costabile, L. Cavallo, *Coord. Chem. Rev.* **2009**, *253*, 687-703.

[85] H. Schumann, M. Glanz, J. Winterfeld, H. Hemling, N. Kuhn, T. Kratz, *Angew. Chem. Int. Ed.* **1994**, *33*, 1733-1734.

[86] (a) H. Schumann, M. Glanz, J. Winterfeld, H. Hemling, N. Kuhn, T. Kratz, *Chem. Ber.* **1994**, *127*, 2369-2372; (b) H. G. Schumann, M.; Gottfriedsen, J.; Dechert, S.; Wolff, D., *Pure Appl. Chem.* **2001**, *73*, 279-282; (c) A. J. Arduengo, M. Tamm, S. J. McLain, J. C. Calabrese, F. Davidson, W. J. Marshall, *J. Am. Chem. Soc.* **1994**, *116*, 7927-7928; (d) T. Mehdoui, J. C. Berthet, P. Thuery, M. Ephritikhine, *Chem. Commun.* **2005**, 2860-2862; (e) D. Baudry-Barbier, N. Andre, A. Dormond, C. Pardes, P. Richard, M. Visseaux, C. J. Zhu, *Eur. J. Inorg. Chem.* **1998**, 1721-1727.

[87] W. A. Herrmann, F. C. Munck, G. R. J. Artus, O. Runte, R. Anwander, *Organometallics* **1997**, *16*, 682-688.

[88] H. Schumann, D. M. M. Freckmann, S. Schutte, S. Dechert, M. Hummert, *Z. Anorg. Allg. Chem.* **2007**, *633*, 888-892.

[89] G. M. Ferrence, A. J. Arduengo, A. Jockisch, H.-J. Kim, R. McDonald, J. Takats, *J. Alloys Compd.* **2006**, *418*, 184-188.

[90] (a) S. T. Liddle, P. L. Arnold, *Organometallics* **2005**, *24*, 2597-2605; (b) P. L. Arnold, S. T. Liddle, *Chem. Commun.* **2005**, 5638-5640.

[91] X. Gu, X. Zhu, Y. Wei, S. Wang, S. Zhou, G. Zhang, X. Mu, *Organometallics* **2014**, *33*, 2372-2379.

[92] X. X. Gu, L. J. Zhang, X. C. Zhu, S. W. Wang, S. L. Zhou, Y. Wei, G. C. Zhang, X. L. Mu, Z. M. Huang, D. J. Hong, F. Zhang, *Organometallics* **2015**, *34*, 4553-4559.

[93] (a) I. J. Casely, S. T. Liddle, A. J. Blake, C. Wilson, P. L. Arnold, *Chem. Commun.* **2007**, 5037-5039; (b) P. L. Arnold, I. A. Marr, S. Zlatogorsky, R. Bellabarba, R. P. Tooze, *Dalton Trans.* **2014**, *43*, 34-37; (c) P. L. Arnold, S. Zlatogorsky, N. A. Jones, C. D. Carmichael, S. T. Liddle, A. J. Blake, C. Wilson, *Inorg. Chem.* **2008**, *47*, 9042-9049.

[94] P. L. Arnold, I. J. Casely, Z. R. Turner, C. D. Carmichael, *Chem. Eur. J.* **2008**, *14*, 10415-10422.

[95] (a) Z. R. Turner, R. Bellabarba, R. P. Tooze, P. L. Arnold, *J. Am. Chem. Soc.* **2010**, *132*, 4050-4051; (b) P. L. Arnold, Z. R. Turner, A. I. Germeroth, I. J. Casely, R. Bellabarba, R. P. Tooze, *Dalton Trans.* **2010**, *39*, 6808-6814.

[96] Z. Li, M. Xue, H. Yao, H. Sun, Y. Zhang, Q. Shen, *J. Organomet. Chem.* **2012**, *713*, 27-34.

[97] Z.-G. Wang, H.-M. Sun, H.-S. Yao, Q. Shen, Y. Zhang, *Organometallics* **2006**, *25*, 4436-4438.

[98] Z.-G. Wang, H.-M. Sun, H.-S. Yao, Y.-M. Yao, Q. Shen, Y. Zhang, *J. Organomet. Chem.* **2006**, *691*, 3383-3390.

[99] H. S. Yao, Y. Zhang, H. M. Sun, Q. Shen, *Eur. J. Inorg. Chem.* **2009**, 1920-1925.

[100] (a) M. Zhang, X. Ni, Z. Shen, *Organometallics* **2014**, *33*, 6861-6867; (b) M. Zhang, J. Zhang, X. Ni, Z. Shen, *RSC Adv.* **2015**, *5*, 83295-83303.

[101] S. P. Downing, S. C. Guadaño, D. Pugh, A. A. Danopoulos, R. M. Bellabarba, M. Hanton, D. Smith, R. P. Tooze, *Organometallics* **2007**, *26*, 3762-3770.

[102] B. Wang, D. Wang, D. Cui, W. Gao, T. Tang, X. Chen, X. Jing, *Organometallics* **2007**, *26*, 3167-3172.

[103] (a) B. Wang, D. Cui, K. Lv, *Macromolecules* **2008**, *41*, 1983-1988; (b) Y. Hu, G. M. Miyake, B. Wang, D. Cui, E. Y. X. Chen, *Chem. Eur. J.* **2012**, *18*, 3345-3354; (c) C. Yao, C. Wu, B. Wang, D. Cui, *Organometallics* **2013**, *32*, 2204-2209.

[104] (a) W. Fegler, T. P. Spaniol, J. Okuda, *Dalton Trans.* **2010**, *39*, 6774-6779; (b) W. Fegler, T. Saito, K. Mashima, T. P. Spaniol, J. Okuda, *J. Organomet. Chem.* **2010**, *695*, 2794-2797.

[105] (a) K. Lv, D. M. Cui, *Organometallics* **2008**, *27*, 5438-5440; (b) K. Lv, D. M. Cui, *Organometallics* **2010**, *29*, 2987-2993.

[106] P. L. Arnold, Z. R. Turner, N. Kaltsoyannis, P. Pelekanaki, R. M. Bellabarba, R. P. Tooze, *Chem. Eur. J.* **2010**, *16*, 9623-9629.

[107] S. Diez-Gonzalez, S. P. Nolan, *Coord. Chem. Rev.* **2007**, *251*, 874-883.

[108] J. C. Green, B. J. Herbert, *Dalton Trans.* **2005**, 1214-1220.

[109] (a) N. A. Jones, S. T. Liddle, C. Wilson, P. L. Arnold, *Organometallics* **2007**, *26*, 755-757; (b) R. D. Shannon, *Acta Crystallogr. Sect. A* **1976**, *32*, 751-767.

[110] (a) C. D. Abernethy, G. M. Codd, M. D. Spicer, M. K. Taylor, *J. Am. Chem. Soc.* **2003**, *125*, 1128-1129; (b) L. Maron, D. Bourissou, *Organometallics* **2007**, *26*, 1100-1103.

[111] L. Maron, D. Bourissou, *Organometallics* **2009**, *28*, 3686-3690.

[112] P. L. Arnold, S. T. Liddle, *C. R. Chim.* **2008**, *11*, 603-611.

[113] (a) P. L. Arnold, S. T. Liddle, J. McMaster, C. Jones, D. P. Mills, *J. Am. Chem. Soc.* **2007**, *129*, 5360-+; (b) P. L. Arnold, J. McMaster, S. T. Liddle, *Chem. Commun.* **2009**, 818-820.

[114] P. L. Arnold, Z. R. Turner, A. I. Germeroth, I. J. Casely, G. S. Nichol, R. Bellabarba, R. P. Tooze, *Dalton Trans.* **2013**, *42*, 1333-1337.

[115] B. L. Wang, T. Tang, Y. S. Li, D. M. Cui, *Dalton Trans.* **2009**, 8963-8969.

[116] K. Lv, D. Cui, *Organometallics* **2010**, *29*, 2987-2993.

[117] D. Patel, S. T. Liddle, S. A. Mungur, M. Rodden, A. J. Blake, P. L. Arnold, *Chem. Commun.* **2006**, 1124-1126.

[118] M. Glanz, S. Dechert, H. Schumann, D. Wolff, D. Wolff, J. Springer, *Z. Anorg. Allg. Chem.* **2000**, *626*, 2467-2477.

[119] J. Yuan, H. F. Hu, C. M. Cui, *Chem. Eur. J.* **2016**, *22*, 5778-5785.

[120] W. Xie, H. Hu, C. Cui, *Angew. Chem. Int. Ed.* **2012**, *51*, 11141-11144.

[121] A. Pindwal, A. Ellern, A. D. Sadow, *Organometallics* **2016**, *35*, 1674-1683.

[122] H. G. Raubenheimer, S. Cronje, *Chem. Soc. Rev.* **2008**, *37*, 1998-2011.

[123] I. J. B. Lin, C. S. Vasam, *Coord. Chem. Rev.* **2007**, *251*, 642-670.

[124] S. K. Schneider, W. A. Herrmann, E. Herdtweck, *Z. Anorg. Allg. Chem.* **2003**, *629*, 2363-2370.

[125] P. J. Barnard, M. V. Baker, S. J. Berners-Price, B. W. Skelton, A. H. White, *Dalton Trans.* **2004**, 1038-1047.

[126] A. J. Arduengo, H. V. R. Dias, J. C. Calabrese, F. Davidson, *Organometallics* **1993**, *12*, 3405-3409.

[127] H. M. J. Wang, I. J. B. Lin, *Organometallics* **1998**, *17*, 972-975.

[128] A. A. D. Tulloch, A. A. Danopoulos, S. Winston, S. Kleinhenz, G. Eastham, *J. Chem. Soc., Dalton Trans.* **2000**, 4499-4506.

[129] O. Guerret, S. Solé, H. Gornitzka, M. Teichert, G. Trinquier, G. Bertrand, *J. Am. Chem. Soc.* **1997**, *119*, 6668-6669.

[130] P. L. Chiu, C. Y. Chen, J. Y. Zeng, C. Y. Lu, H. M. Lee, *J. Organomet. Chem.* **2005**, *690*, 1682-1687.

[131] J. M. Hayes, M. Viciano, E. Peris, G. Ujaque, A. Lledós, *Organometallics* **2007**, *26*, 6170-6183.

[132] (a) H.-L. Su, L. M. Pérez, S.-J. Lee, J. H. Reibenspies, H. S. Bazzi, D. E. Bergbreiter, *Organometallics* **2012**, *31*, 4063-4071; (b) T. Simler, P. Braunstein, A. A. Danopoulos, *Dalton Trans* **2016**, *45*, 5122-5139.

[133] (a) C. Boehme, G. Frenking, *Organometallics* **1998**, *17*, 5801-5809; (b) D. Nemcsok, K. Wichmann, G. Frenking, *Organometallics* **2004**, *23*, 3640-3646; (c) X. Hu, I. Castro-Rodriguez, K. Olsen, K. Meyer, *Organometallics* **2004**, *23*, 755-764.

[134] X. He, V. W.-W. Yam, *Coord. Chem. Rev.* **2011**, *255*, 2111-2123.

[135] (a) H. Schmidbaur, *Chem. Soc. Rev.* **1995**, *24*, 391-400; (b) H. Schmidbaur, A. Schier, *Chem. Soc. Rev.* **2008**, *37*, 1931-1951.

[136] P. Pyykkö, *Angew. Chem. Int. Ed.* **2004**, *43*, 4412-4456.

[137] J. Muñiz, C. Wang, P. Pyykkö, *Chem. Eur. J.* **2011**, *17*, 368-377.

[138] (a) C. Carcedo, J. C. Knight, S. J. A. Pope, I. A. Fallis, A. Dervisi, *Organometallics* **2011**, *30*, 2553-2562; (b) P. Marshall, R. L. Jenkins, W. Clegg, R. W. Harrington, S. K. Callear, S. J. Coles, I. A. Fallis, A. Dervisi, *Dalton Trans.* **2012**, *41*, 12839-12846.

[139] C. X. Lin, X. F. Kong, Q. S. Li, Z. Z. Zhang, Y. F. Yuan, F. B. Xu, *Crystengcomm* **2013**, *15*, 6948-6962.

[140] (a) A. Liu, X. Zhang, W. Chen, H. Qiu, *Inorg. Chem. Commun.* **2008**, *11*, 1128-1131; (b) X. M. Zhang, S. J. Gu, Q. Q. Xia, W. Z. Chen, *J. Organomet. Chem.* **2009**, *694*, 2359-2367.

[141] (a) A. Poethig, T. Strassner, *Organometallics* **2011**, *30*, 6674-6684; (b) A. Poethig, T. Strassner, *Organometallics* **2012**, *31*, 3431-3434.

[142] J. Vaughan, D. J. Carter, A. L. Rohl, M. I. Ogden, B. W. Skelton, P. V. Simpson, D. H. Brown, *Dalton Trans.* **2016**, *45*, 1484-1495.

[143] (a) D. J. Nielsen, K. J. Cavell, B. W. Skelton, A. H. White, *Inorg. Chim. Acta* **2003**, *352*, 143-150; (b) J.-W. Wang, H.-B. Song, Q.-S. Li, F.-B. Xu, Z.-Z. Zhang, *Inorg. Chim. Acta* **2005**, *358*, 3653-3658; (c) Q. X. Liu, J. Yu, X. J. Zhao, S. W. Liu, X. Q. Yang, K. Y. Li, X. G. Wang, *Crystengcomm* **2011**, *13*, 4086-4096; (d) Q.-X. Liu, Z.-Q. Yao, X.-J. Zhao, A.-H. Chen, X.-Q. Yang, S.-W. Liu, X.-G. Wang, *Organometallics* **2011**, *30*, 3732-3739.

[144] (a) A. Vellé, A. Cebollada, M. Iglesias, P. J. Sanz Miguel, *Inorg. Chem.* **2014**, *53*, 10654-10659; (b) A. Cebollada, A. Velle, M. Iglesias, L. B. Fullmer, S. Goberna-Ferron, M. Nyman, P. J. Sanz Miguel, *Angew. Chem. Int. Ed. Engl.* **2015**, *54*, 12762-12766.

[145] (a) S. Kobialka, C. Müller-Tautges, M. T. S. Schmidt, G. Schnakenburg, O. Hollóczki, B. Kirchner, M. Engeser, *Inorg. Chem.* **2015**, *54*, 6100-6111; (b) A. A. Penney, V. V. Sizov, E. V. Grachova, D. V. Krupenya, V. V. Gurzhiy, G. L. Starova, S. P. Tunik, *Inorg. Chem.* **2016**, *55*, 4720-4732.

[146] J. Gil-Rubio, V. Cámara, D. Bautista, J. Vicente, *Inorg. Chem.* **2013**, *52*, 4071-4083.

[147] F. Jean-Baptiste dit Dominique, H. Gornitzka, A. Sournia-Saquet, C. Hemmert, *Dalton Trans.* **2009**, 340-352.

[148] (a) C. Tubaro, M. Baron, M. Costante, M. Basato, A. Biffis, A. Gennaro, A. A. Isse, C. Graiff, G. Accorsi, *Dalton Trans.* **2013**, *42*, 10952-10963; (b) M. Monticelli, C. Tubaro, M. Baron, M. Basato, P. Sgarbossa, C. Graiff, G. Accorsi, T. P. Pell, D. J. D. Wilson, P. J. Barnard, *Dalton Trans.* **2016**, *45*, 9540-9552.

[149] L. E. Wedlock, J. B. Aitken, S. J. Berners-Price, P. J. Barnard, *Dalton Trans.* **2013**, *42*, 1259-1266.

[150] A. Rit, T. Pape, F. E. Hahn, *Organometallics* **2011**, *30*, 6393-6401.

[151] (a) A. n. Caballero, E. Díez-Barra*, F. A. Jalón, S. Merino, A. M. Rodríguez, J. Tejeda, *J. Organomet. Chem.* **2001**, *627*, 263-264; (b) D. H. Brown, G. L. Nealon, P. V. Simpson, B. W. Skelton, Z. S. Wang, *Organometallics* **2009**, *28*, 1965-1968; (c) F. Dominique, H. Gornitzka, A. Sournia-Saquet, C. Hemmert, *Dalton Trans.* **2009**, 340-352; (d) A. Herbst, C. Bronner, P. Dechambenoit, O. S. Wenger, *Organometallics* **2013**, *32*, 1807-1814; (e) T. P. Pell, D. J. D. Wilson, B. W. Skelton, J. L. Dutton, P. J. Barnard, *Inorg. Chem.* **2016**, *55*, 6882-6891; (f) T. Nakamura, S. Ogushi, Y. Arikawa, K. Umakoshi, *J. Organomet. Chem.* **2016**, *803*, 67-72.

[152] A. Biffis, M. Cipani, C. Tubaro, M. Basato, M. Costante, E. Bressan, A. Venzo, C. Graiff, *New J. Chem.* **2013**, *37*, 4176-4184.

[153] L. E. Wedlock, P. J. Barnard, A. Filipovska, B. W. Skelton, S. J. Berners-Price, M. V. Baker, *Dalton Trans.* **2016**, *45*, 12221-12236.

[154] (a) C. Radloff, H.-Y. Gong, C. Schulte to Brinke, T. Pape, V. M. Lynch, J. L. Sessler, F. E. Hahn, *Chem. Eur. J.* **2010**, *16*, 13077-13081; (b) R. E. Andrew, C. M. Storey, A. B. Chaplin, *Dalton Trans.* **2016**, *45*, 8937-8944.

[155] (a) V. Gierz, C. Maichle-Mössmer, D. Kunz, *Organometallics* **2012**, *31*, 739-747; (b) V. Gierz, A. Seybold, C. Maichle-Mossmer, K. W. Tornroos, M. T. Speidel, B. Speiser, K. Eichele, D. Kunz, *Organometallics* **2012**, *31*, 7893-7901.

[156] (a) N. J. Wheate, S. Walker, G. E. Craig, R. Oun, *Dalton Trans.* **2010**, *39*, 8113-8127; (b) D. Wang, S. J. Lippard, *Nat Rev Drug Discov* **2005**, *4*, 307-320.

[157] S. Nobili, E. Mini, I. Landini, C. Gabbiani, A. Casini, L. Messori, *Med. Res. Rev.* **2010**, *30*, 550-580.

[158] (a) A. Bindoli, M. P. Rigobello, G. Scutari, C. Gabbiani, A. Casini, L. Messori, *Coord. Chem. Rev.* **2009**, *253*, 1692-1707; (b) J. L. Hickey, R. A. Ruhayel, P. J. Barnard, M. V. Baker, S. J. Berners-Price, A. Filipovska, *J. Am. Chem. Soc.* **2008**, *130*, 12570-12571; (c) S. Gromer, S. Urig, K. Becker, *Med. Res. Rev.* **2004**, *24*, 40-89.

[159] T. Zou, C. T. Lum, C.-N. Lok, J.-J. Zhang, C.-M. Che, *Chem. Soc. Rev.* **2015**, *44*, 8786-8801.

[160] A. A. Mohamed, A. E. Bruce, M. R. M. Bruce, *Met.-Based Drugs* **1999**, *6*, 233-238.

[161] T. Zou, C. T. Lum, C.-N. Lok, W.-P. To, K.-H. Low, C.-M. Che, *Angew. Chem. Int. Ed.* **2014**, *53*, 5810-5814.

[162] (a) T. V. Serebryanskaya, A. A. Zolotarev, I. Ott, *MedChemComm* **2015**, *6*, 1186-1189; (b) B. Bertrand, L. Stefan, M. Pirrotta, D. Monchaud, E. Bodio, P. Richard, P. Le Gendre, E. Warmerdam, M. H. de Jager, G. M. M. Groothuis, M. Picquet, A. Casini,

Inorg. Chem. **2014**, *53*, 2296-2303; (c) C. Bazzicalupi, M. Ferraroni, F. Papi, L. Massai, B. Bertrand, L. Messori, P. Gratteri, A. Casini, *Angew. Chem. Int. Ed.* **2016**, *55*, 4256-4259.

[163] P. J. Barnard, M. V. Baker, S. J. Berners-Price, D. A. Day, *J. Inorg. Biochem.* **2004**, *98*, 1642-1647.

[164] J. W. Daly, *Cell. Mol. Life Sci.* **2007**, *64*, 2153-2169.

[165] I. Ott, *Coord. Chem. Rev.* **2009**, *253*, 1670-1681.

[166] P. L. Arnold, M. W. McMullon, J. Rieb, F. E. Kühn, *Angew. Chem. Int. Ed.* **2015**, *54*, 82-100.

[167] W. Liu, R. Gust, *Chem. Soc. Rev.* **2013**, *42*, 755-773.

[168] (a) G. Fukata, T. Itoh, M. Tashiro, *Heterocycles* **1981**, *16*, 549-554; (b) H. Ren, P. Yao, S. Xu, H. Song, B. Wang, *J. Organomet. Chem.* **2007**, *692*, 2092-2098.

[169] G. Fukata, T. Itoh, M. Tashiro, *J. Org. Chem.* **1981**, *46*, 4454-4458.

[170] H. Aihara, T. Matsuo, H. Kawaguchi, *Chem. Commun.* **2003**, 2204-2205.

[171] D. Zhang, H. Aihara, T. Watanabe, T. Matsuo, H. Kawaguchi, *J. Organomet. Chem.* **2007**, *692*, 234-242.

[172] G. Engelhardt, M. Mägi, E. Lippmaa, *J. Organomet. Chem.* **1973**, *54*, 115-122.

[173] (a) R. Zhong, A. Pöthig, S. Haslinger, B. Hofmann, G. Raudaschl-Sieber, E. Herdtweck, W. A. Herrmann, F. E. Kühn, *ChemPlusChem* **2014**, *79*, 1294-1303; (b) R. Zhong, A. Pöthig, D. C. Mayer, C. Jandl, P. J. Altmann, W. A. Herrmann, F. E. Kühn, *Organometallics* **2015**, *34*, 2573-2579.

[174] O. Holloczki, P. Terleczky, D. Szieberth, G. Mourgas, D. Gudat, L. Nyulaszi, *J. Am. Chem. Soc.* **2011**, *133*, 780-789.

[175] P. L. Arnold, C. Wilson, *Inorg. Chim. Acta* **2007**, *360*, 190-196.

[176] (a) N. B. Jokić, C. S. Straubinger, S. Li Min Goh, E. Herdtweck, W. A. Herrmann, F. E. Kühn, *Inorg. Chim. Acta* **2010**, *363*, 4181-4188; (b) C. S. Straubinger, N. B. Jokić, M. P. Högerl, E. Herdtweck, W. A. Herrmann, F. E. Kühn, *J. Organomet. Chem.* **2011**, *696*, 687-692.

[177] K. A. Thorn, D. W. Folan, J. B. Arterburn, M. A. Mikita, P. MacCarthy, *Sci. Total Environ.* **1989**, *81–82*, 209-218.

[178] J. Rieb, A. Raba, S. Haslinger, M. Kaspar, A. Pöthig, M. Cokoja, J.-M. Basset, F. E. Kühn, *Inorg. Chem.* **2014**, *53*, 9598-9606.

[179] (a) S. Meyer, S. Demeshko, S. Dechert, F. Meyer, *Inorg. Chim. Acta* **2010**, *363*, 3088-3092; (b) K. A. Kreisel, G. P. A. Yap, K. H. Theopold, *Organometallics* **2006**, *25*, 4670-4679; (c) S. Ahrens, T. Strassner, *Inorg. Chim. Acta* **2006**, *359*, 4789-4796.

[180] J. E. Fitzpatrick, D. J. Milner, P. White, *Synth. Commun.* **1982**, *12*, 489-494.

[181] H. Bredereck, G. Theilig, *Chem. Ber.* **1953**, *86*, 88-96.

[182] A. D'Sa, L. A. Cohen, *J. Heterocycl. Chem.* **1991**, *28*, 1819-1820.

[183] (a) T. L. Amyes, S. T. Diver, J. P. Richard, F. M. Rivas, K. Toth, *J. Am. Chem. Soc.* **2004**, *126*, 4366-4374; (b) H. Aihara, T. Matsuo, H. Kawaguchi, *Chem. Commun.* **2003**, 2204.

[184] H. W. Wanzlick, *Angew. Chem.* **1962**, *74*, 129-134.

[185] S. Haslinger, J. W. Kück, M. R. Anneser, M. Cokoja, A. Pöthig, F. E. Kühn, *Chem. Eur. J.* **2015**, *21*, 17860-17869.

[186] H. Tong, D. Bell, K. Tabei, M. M. Siegel, *J. Am. Soc. Mass. Spectrom.* **1999**, *10*, 1174-1187.

[187] (a) E. Doni, J. A. Murphy, *Chem. Commun.* **2014**, *50*, 6073-6087; (b) J. Broggi, T. Terme, P. Vanelle, *Angew. Chem.* **2014**, *126*, 392-423.

[188] J. A. Murphy, T. A. Khan, S.-z. Zhou, D. W. Thomson, M. Mahesh, *Angew. Chem. Int. Ed.* **2005**, *44*, 1356-1360.

[189] J. Broggi, M. Rollet, J.-L. Clément, G. Canard, T. Terme, D. Gigmes, P. Vanelle, *Angew. Chem. Int. Ed.* **2016**, *55*, 5994-5999.

[190] J. Gmeiner, M. Seibicke, C. Lang, U. Gärtner, O. Trapp, *Adv. Synth. Catal.* **2014**, *356*, 2081-2087.

[191] O. Eicher-Lorka, G. K. Kupetis, L. Rastenyté, A. Matijoka, *Synthesis* **1999**, *1999*, 2131-2137.

[192] J. Clayden, N. Greeves, S. Warren, *Organic chemistry*, 2nd ed., Oxford University Press Inc., New York, USA, **2012**.

[193] (a) R. Corberán, M. Sanaú, E. Peris, *Organometallics* **2007**, *26*, 3492-3498; (b) E. F. Hahn, B. Heidrich, A. Hepp, T. Pape, *J. Organomet. Chem.* **2007**, *692*, 4630-4638; (c) R. Gümüşada, N. Özdemir, M. E. Günay, M. Dinçer, M. S. Soylu, B. Çetinkaya, *Appl. Organomet. Chem.* **2014**, *28*, 324-331; (d) R. A. Haque, P. O. Asekunowo, M. R. Razali, *Transition Met. Chem.* **2014**, *39*, 281-290.

[194] L.-C. Song, X. Luo, Y.-Z. Wang, B. Gai, Q.-M. Hu, *J. Organomet. Chem.* **2009**, *694*, 103-112.

[195] (a) R. A. Musgrave, R. S. P. Turbervill, M. Irwin, R. Herchel, J. M. Goicoechea, *Dalton Trans.* **2014**, *43*, 4335-4344; (b) R. A. Musgrave, R. S. P. Turbervill, M. Irwin, J. M. Goicoechea, *Angew. Chem. Int. Ed.* **2012**, *51*, 10832-10835.

[196] A. J. Martínez-Martínez, M. Á. Fuentes, A. Hernán-Gómez, E. Hevia, A. R. Kennedy, R. E. Mulvey, C. T. O'Hara, *Angew. Chem. Int. Ed.* **2015**, *54*, 14075-14079.

[197] J. B. Waters, R. S. P. Turbervill, J. M. Goicoechea, *Organometallics* **2013**, *32*, 5190-5200.

[198] A. Krüger, E. Kluser, H. Müller-Bunz, A. Neels, M. Albrecht, *Eur. J. Inorg. Chem.* **2012**, *2012*, 1394-1402.

[199] (a) M. J. Bitzer, A. Pothig, C. Jandl, F. E. Kuhn, W. Baratta, *Dalton Trans.* **2015**, *44*, 11686-11689; (b) M. J. Bitzer, F. E. Kühn, W. Baratta, *J. Catal.* **2016**, *338*, 222-226.

[200] C. Romain, D. Specklin, K. Miqueu, J.-M. Sotiropoulos, C. Fliedel, S. Bellemin-Laponnaz, S. Dagorne, *Organometallics* **2015**, *34*, 4854-4863.

[201] R. L. Corey, D. T. Shane, R. C. Bowman, M. S. Conradi, *J. Phys. Chem. C* **2008**, *112*, 18706-18710.

[202] E. Despagnet-Ayoub, L. M. Henling, J. A. Labinger, J. E. Bercaw, *Organometallics* **2013**, *32*, 2934-2938.

[203] B. Dominelli, Master's thesis, Technische Universität München (Garching b. München), **2016**.

[204] D. P. Curran, A. Solovyev, M. M. Brahmi, L. Fensterbank, M. Malacria, E. Lacote, *Angew. Chem. Int. Ed.* **2011**, *50*, 10294-10317.

[205] D. Schneider, T. Spallek, C. Maichle-Mossmer, K. W. Tornroos, R. Anwander, *Chem Commun (Camb)* **2014**, *50*, 14763-14766.

[206] (a) W. J. Evans, C. A. Seibel, J. W. Ziller, *J. Am. Chem. Soc.* **1998**, *120*, 6745-6752; (b) M. R. MacDonald, J. W. Ziller, W. J. Evans, *Inorg. Chem.* **2011**, *50*, 4092-4106.

[207] (a) K. S. Kisel, G. Linti, G. L. Starova, V. V. Sizov, A. S. Melnikov, A. P. Pushkarev, M. N. Bochkarev, E. V. Grachova, S. P. Tunik, *Eur. J. Inorg. Chem.* **2015**, *2015*, 1734-1743; (b) F. Piccinelli, M. Bettinelli, A. Melchior, C. Grazioli, M. Tolazzi, *Dalton Trans.* **2015**, *44*, 182-192; (c) F. Piccinelli, M. Leonzio, M. Bettinelli, M. Monari, C. Grazioli, A. Melchior, M. Tolazzi, *Dalton Trans.* **2016**, *45*, 3310-3318.

[208] (a) T. Mitsudome, Y. Mikami, H. Mori, S. Arita, T. Mizugaki, K. Jitsukawa, K. Kaneda, *Chem. Commun.* **2009**, 3258-3260; (b) A. Y. Kim, H. S. Bae, S. Park, S. Park, K. H. Park, *Catal. Lett.* **2011**, *141*, 685-690.

[209] R.-S. Luo, X.-A. Mao, Z.-Q. Pan, Q.-H. Luo, *Spectrochim. Acta A, Mol. Biomol. Spectrosc.* **2000**, *56*, 1675-1680.

[210] (a) G. Venkatachalam, M. Heckenroth, A. Neels, M. Albrecht, *Helv. Chim. Acta* **2009**, *92*, 1034-1045; (b) C. A. Quezada, J. C. Garrison, M. J. Panzner, C. A. Tessier, W. J. Youngs, *Organometallics* **2004**, *23*, 4846-4848.

[211] (a) Y. Cohen, L. Avram, L. Frish, *Angew. Chem. Int. Ed.* **2005**, *44*, 520-554; (b) D. Li, G. Kagan, R. Hopson, P. G. Williard, *J. Am. Chem. Soc.* **2009**, *131*, 5627-5634.

[212] A. Bondi, *J. Phys. Chem.* **1964**, *68*, 441-451.

[213] S. B. Aher, P. N. Muskawar, K. Thenmozhi, P. R. Bhagat, *Eur. J. Med. Chem.* **2014**, *81*, 408-419.

[214] M. V. Baker, P. J. Barnard, S. J. Berners-Price, S. K. Brayshaw, J. L. Hickey, B. W. Skelton, A. H. White, *Dalton Trans.* **2006**, 3708-3715.

[215] (a) W. Liu, R. Gust, *Coord. Chem. Rev.* **2016**, *329*, 191-213; (b) J. Turek, Z. Růžičková, E. Tloušťová, H. Mertlíková-Kaiserová, J. Günterová, L. Rulíšek, A. Růžička, *Appl. Organomet. Chem.* **2016**, *30*, 318-322; (c) A. Citta, V. Scalcon, P. Gobel, B. Bertrand, M. Wenzel, A. Folda, M. P. Rigobello, E. Meggers, A. Casini, *RSC Adv.* **2016**, *6*, 79147-79152; (d) A. B. Mullick, Y. M. Chang, I. Ghiviriga, K. A. Abboud, W. Tan, A. S. Veige, *Dalton Trans.* **2013**, *42*, 7440-7446.

[216] M. C. Harris, X. Huang, S. L. Buchwald, *Org. Lett.* **2002**, *4*, 2885-2888.

[217] S. Ahrens, A. Zeller, M. Taige, T. Strassner, *Organometallics* **2006**, *25*, 5409-5415.

[218] M. J. Frisch, G. W. Trucks, H. B. Schlegel, G. E. Scuseria, M. A. Robb, J. R. Cheeseman, G. Scalmani, V. Barone, B. Mennucci, G. A. Petersson, H. Nakatsuji, M. Caricato, X. Li, H. P. Hratchian, A. F. Izmaylov, J. Bloino, G. Zheng, J. L. Sonnenberg, M. Hada, M. Ehara, K. Toyota, R. Fukuda, J. Hasegawa, M. Ishida, T. Nakajima, Y. Honda, O. Kitao, H. Nakai, T. Vreven, J. A. Montgomery Jr., J. E. Peralta, F. Ogliaro, M. J. Bearpark, J. Heyd, E. N. Brothers, K. N. Kudin, V. N. Staroverov, R. Kobayashi, J. Normand, K. Raghavachari, A. P. Rendell, J. C. Burant, S. S. Iyengar, J. Tomasi, M. Cossi, N. Rega, N. J. Millam, M. Klene, J. E. Knox, J. B. Cross, V. Bakken, C. Adamo, J. Jaramillo, R. Gomperts, R. E. Stratmann, O. Yazyev, A. J. Austin, R. Cammi, C. Pomelli, J. W. Ochterski, R. L. Martin, K. Morokuma, V. G. Zakrzewski, G. A. Voth, P. Salvador, J. J. Dannenberg, S. Dapprich, A. D. Daniels, Ö. Farkas, J. B. Foresman, J. V. Ortiz, J. Cioslowski, D. J. Fox, *Gaussian 09,* Gaussian Inc., Wallingford, CT, USA, **2009**.

[219] J.-D. Chai, M. Head-Gordon, *Phys. Chem. Chem. Phys.* **2008**, *10*, 6615-6620.

[220] J. J. P. Stewart, *J. Mol. Model.* **2007**, *13*, 1173-1213.

[221] (a) T. H. Dunning, Jr., P. J. Hay, *Mod. Theor. Chem.* **1977**, *3*, 1-27; (b) M. M. Francl, W. J. Pietro, W. J. Hehre, J. S. Binkley, M. S. Gordon, D. J. DeFrees, J. A. Pople, *J. Chem. Phys.* **1982**, *77*, 3654-3665; (c) P. C. Hariharan, J. A. Pople, *Theor. Chim. Acta* **1973**, *28*, 213-222.

[222] P. J. Hay, W. R. Wadt, *J. Chem. Phys.* **1985**, *82*, 270-283.

[223] (a) Z. Atieh, A. R. Allouche, D. Graveron-Demilly, F. Fauvelle, M. Aubert-Frécon, *Meas. Sci. Technol.* **2009**, *20*, 104024; (b) M. Clericuzio, G. Alagona, C. Ghio, L. Toma, *J. Org. Chem.* **2000**, *65*, 6910-6916; (c) A. Victora, H. M. Moeller, T. E. Exner, *Nucleic Acids Res.* **2014**, *42*, e173/171-e173/110.

[224] A. V. Marenich, C. J. Cramer, D. G. Truhlar, *J. Phys. Chem. B* **2009**, *113*, 6378-6396.

[225] (a) *APEX suite of crystallographic software, APEX 3 Version 2015-5.2,* Bruker AXS Inc., Bruker, Madison, Wisconsin, USA, **2015**; (b) *APEX suite of crystallographic software, APEX 2 Version 2014-9.0*, Bruker AXS Inc., Bruker, Madison, Wisconsin, USA, **2014**.

[226] *SAINT, Version 8.34A and SADABS, Version 2014/5,* Bruker AXS Inc., Bruker, Madison, Wisconsin, USA, **2014**.

[227] (a) G. Sheldrick, *Acta Crystallogr. Sect. C* **2015**, *71*, 3-8; (b) G. Sheldrick, *Acta Crystallogr. Sect. A* **2015**, *71*, 3-8; (c) C. B. Hubschle, G. M. Sheldrick, B. Dittrich, *J. Appl. Crystallogr.* **2011**, *44*, 1281-1284.

[228] A. J. C. Wilson (Ed.), *International Tables for Crystallography, Vol. C, Tables 6.1.1.4 (pp. 500-502), 4.2.6.8 (pp. 219-222), and 4.2.4.2 (pp. 193-199)*, Kluwer Academic Publishers, Dordrecht, The Netherlands, **1992**.

[229] A. Spek, *Acta Crystallogr. Sect. C* **2015**, *71*, 9-18.

[230] C. F. Macrae, P. R. Edgington, P. McCabe, E. Pidcock, G. P. Shields, R. Taylor, M. Towler, J. van de Streek, *J. Appl. Crystallogr.* **2006**, *39*, 453-457.

[231] O. V. Starikova, G. V. Dolgushin, L. I. Larina, P. E. Ushakov, T. N. Komarova, V. A. Lopyrev, *Russ. J. Org. Chem.*, *39*, 1467-1470.

[232] C. E. Sroog, H. M. Woodburn, *Org. Synth.* **1952**, *32*, 46.

[233] D. E. Pearson, S. D. Venkataramu, W. E. Childers, *Synth. Commun.* **1979**, *9*, 5-10.

[234] M. Konkol, M. Nabika, T. Kohno, T. Hino, T. Miyatake, *J. Organomet. Chem.* **2011**, *696*, 1792-1802.

[235] T. K. Panda, M. T. Gamer, P. W. Roesky, *Organometallics* **2003**, *22*, 877-878.

[236] P. J. Bailey, R. A. Coxall, C. M. Dick, S. Fabre, L. C. Henderson, C. Herber, S. T. Liddle, D. Lorono-Gonzalez, A. Parkin, S. Parsons, *Chemistry* **2003**, *9*, 4820-4828.

[237] W. J. Evans, R. E. Golden, J. W. Ziller, *Inorg. Chem.* **1991**, *30*, 4963-4968.

[238] M. Roger, T. Arliguie, P. Thuéry, M. Fourmigué, M. Ephritikhine, *Inorg. Chem.* **2005**, *44*, 584-593.

[239] G. Wilkinson, J. M. Birmingham, *J. Am. Chem. Soc.* **1954**, *76*, 6210-6210.

[240] N. Meyer, P. W. Roesky, S. Bambirra, A. Meetsma, B. Hessen, K. Saliu, J. Takats, *Organometallics* **2008**, *27*, 1501-1505.

[241] E. C. Alyea, D. C. Bradley, R. G. Copperthwaite, *J. Chem. Soc., Dalton Trans.* **1972**, 1580.

[242] R. Neufeld, M. John, D. Stalke, *Angew. Chem.* **2015**, *127*, 7100-7104.

[243] H. Kurata, Y. Oki, K. Matsumoto, T. Kawase, M. Oda, *Chem. Lett.* **2005**, *34*, 910-911.

[244] L. Zhu, P. Guo, G. Li, J. Lan, R. Xie, J. You, *J. Org. Chem.* **2007**, *72*, 8535-8538.